

## ABSTRACT

LEOPOLD, MICHAEL CHRISTOFI. Interfacial Investigations of a Biological Electron Transfer Model: Cytochrome c Adsorbed on Gold Electrodes Modified with Self-Assembled Monolayers. (Advised by Professor Edmond F. Bowden)

Interfacial investigations of a protein monolayer electrochemical system, cytochrome c (cyt c) adsorbed to a carboxylic acid (COOH) terminated self-assembled monolayer (SAM) were undertaken. Previous research suggested that anomalous peak broadening observed in the voltammetry of cyt c may be the manifestation of surface effects at the SAM/solution interface (heterogeneous adsorption sites). To examine this matter further, research was directed at 1) deciphering the role of the gold substrate's topography in both SAM formation and cyt c voltammetry; 2) understanding the protein binding interactions at the SAM/solution interface that influence cyt c adsorption and electrochemical response, and 3) investigating the microscopic properties of all the surfaces involved.

Electrochemical and scanning probe microscopy techniques were used to explore the influence of gold topography in cyt c / COOH SAM / Au systems. COOH SAMs (11-mercaptoundecanoic acid and 14-mercaptotetradecanoic acid) were prepared and characterized on a variety of gold surfaces including evaporated, bulk, single crystal, and epitaxially grown on mica gold substrates. Each type of gold surface exhibited specific topographical features and characteristic roughness. SAMs were found to have a decreasing number of defects as the topography of the gold became smoother, as evidenced by an increased ability to block solution probe molecules. As the SAMs become less defective on the smoother gold, the extent of adsorption and the magnitude of the electrochemical response of adsorbed cyt c decreased significantly. These results show cyt c adsorption and electrochemistry to be intimately related to the density of defects in the SAM, which, in turn, are heavily influenced by the gold topography.

Additionally, as the gold roughness decreased, the double layer capacitance of the films was observed to increase. A physical model was proposed in which the structure and properties of COOH SAMs are dictated by significant endgroup interactions in addition to chain-chain interactions. The model illustrates how gold topography plays an intricate role in determining the structure and application of COOH terminated SAMs.

Research was also performed on the SAM/solution interface by thermally healing SAMs on gold and utilizing SAMs on Ag-UPD modified gold. Thermal healing, by reducing the number of defects in the SAMs, was also found to affect both SAM structural properties and cyt c adsorption. SAMs that had been thermally healed exhibited a lower density of defects while, at the same time, supported lower electroactive cyt c coverage. Ag UPD layers were tested as a means of creating more stable, less defective COOH SAMs for cyt c immobilization and possibly allowing for more ideal voltammetry of the proteins. Preliminary research has shown that SAMs with Ag-UPD layers have fewer defects and greater inherent stability. Finally, scanning probe microscopy techniques were employed to investigate the structure of the gold substrate, the SAM/solution interface, and adsorbed cyt c.

In addition to cyt c / SAM / Au research, results from the following investigations are presented: electrochemistry of adsorbed cyt c at indium tin oxide electrodes and the electron transfer (ET) properties of iron-sulfur metallodendrimers. The metallodendrimers exhibited attenuated ET properties with increasing generations of dendritic ligands in a solventless, polymeric media. The electrochemistry of Cu(II) in physiological pathways that may be related to neurological and ocular diseases was also explored. Research on these systems revealed that the reduction of Cu(II) by certain peptides and catabolites may play a vital role in the development of these diseases.

**INTERFACIAL INVESTIGATIONS OF A  
BIOLOGICAL ELECTRON TRANSFER MODEL:  
CYTOCHROME C ADSORBED ON GOLD ELECTRODES MODIFIED WITH  
SELF-ASSEMBLED MONOLAYERS**

by

**MICHAEL CHRISTOFI LEOPOLD**

A Dissertation Submitted to the Graduate Faculty of  
North Carolina State University  
in Partial Fulfillment of the  
Requirements for the Degree of  
Doctor of Philosophy

Department of Chemistry  
Analytical Division

Raleigh, North Carolina  
June 27, 2000

Approved by:

---

Edmond F. Bowden, Chair of Advisory Committee

---

Christopher B. Gorman

---

James D. Martin

---

Charles B. Boss

---

Graduate School Representative

*This accomplishment is dedicated to my family -  
past, present, and future...*

*...but especially Mom & Dad.*

## **BIOGRAPHY**

Michael Christofi Leopold, the second of three children, was born on March 12, 1972, in Newport News, Virginia to Irene and Otto Leopold. With an older brother, John, and later a younger sister, Lauren, Michael grew up first in Newport News, later moving to Idaho Falls, Idaho, and eventually spending most of his time in Grafton, Virginia. In Grafton, a small town near Yorktown, Virginia, he received his primary education at Grafton Bethel Elementary School and his secondary education at Tabb High School, where he graduated in 1990. Michael then enrolled at James Madison University, where he would meet his longtime girlfriend and future wife, Tamara Kelsey. Michael, commonly referred to by the nickname “Leo,” graduated from James Madison in 1994 with a Bachelor of Science degree in Chemistry. In the summer of 1994, Michael moved to Raleigh, North Carolina to pursue a Doctor of Philosophy degree in analytical chemistry from North Carolina State University. Over the next five years, Michael worked on his degree, studying chemistry and performing research under professor Edmond Bowden. In early 1999, Michael proposed to Tammy Kelsey and married her in March of 2000. After completing his Ph.D., Michael headed to the University of North Carolina, Chapel Hill for a postdoctoral appointment with professor Royce Murray.

## ACKNOWLEDGEMENTS

This achievement is not mine alone and could have never been completed without the love and support of my family and friends throughout the years. The people that have helped me attain this goal are too numerous to name, but several deserve specific mention.

First and foremost, I must acknowledge my parents. My mother and father have been a constant source of encouragement and unconditional love during, not only my years in graduate school, but throughout my entire life. The values my parents instilled in me have enabled me to be successful at anything in life. You did a great job Mom and Dad, I love you and thank you. I have always been able to count on my family - Mom, Dad, John, and Lauren - you've always been there for me and it never went unnoticed.

Equally important, I must sincerely thank my best friend, teammate and newest member of my family, my long-time girlfriend and wife, Tamara Kelsey. Tammy and I met a long time ago at JMU and have been through a lot together. Tammy has always stuck with me, through the good, the bad and the ugly; she has had to put up with more than any woman should ever have to. Tammy, your love, support, and encouragement were an essential part of this achievement - I love you and I am excited about our future together.

Although they are not all still with me, my grandparents were a source of inspiration during my years in school. I miss them. Throughout my life, I have been blessed with a large and loving family - the part of my life for which I will always be most proud.

I must acknowledge Ed Bowden for his help, guidance, and many useful discussions about numerous topics over the year. I really enjoyed our meetings and bouncing scientific ideas off each other. Over the past several years, Dr. Bowden became Ed - not only my advisor, but also a trusted friend. I look forward to continuing our relationship long after I have left N.C. State.

I would also like to thank the other members of my committee. Dr. Chris Gorman was always supportive of my efforts and on more than one occasion gave me useful advice about graduate school and my research. I appreciated his input very much and have a great deal of respect for him. Dr. Gorman also has a great sense of humor which I enjoyed very much. I am equally grateful to Dr. Jim Martin. Dr. Martin's door was always open to me through the years. Jim was always willing to listen and has given me great advice both on scientific and non-scientific issues. No one can get you excited about science like Jim - he's simply a good man. Finally, I am extremely appreciative of Dr. Charles Boss for his friendship over the years and the many useful discussions about science, the department, and life in general. I very much enjoyed stopping by Dr. Boss's office, whether it be to talk about science, the department, the direction and voice of Phi Lamda

Upsilon, or just to simply sneak a piece of candy from his desk while his back was turned (damn that mirror!).

Aside from the members of my committee, I would also like to thank Jean Sigvaldsen, Joyce Dunn, Cynthia Martin, and the late Joyce Weatherspoon - their friendship, professionalism, and many useful discussions were greatly appreciated. I considered these people to be the “glue” of the department. These people always went out of their way to make things a little bit better and it meant a lot to me.

My list of acknowledgments would not complete without mentioning the faculty at JMU. They provided me with an unparalleled quality of scientific training that allowed me to be successful at graduate school. I would especially like to thank Dr. Frank Palocsay - a long standing friend and mentor from JMU; Dr. Downey - for first inspiring me to do something different and try going to NCSU; and Dr. Roddy Amenta - my first research advisor. I will always feel a great deal of gratitude and a fraternal bond with the people at JMU. I must also acknowledge my high school chemistry teacher, Ms. Ester Freeman for first inspiring me to pursue chemistry as a career.

Finally, I must thank the many friends I have made and kept over the years. Drew, Booker, Andy, and Kyle - thanks for being patient and understanding, you guys are the best. To the graduate school class that came in with me in 1994, (Russ, Jen, Stacy, Fabio, Mark, Kathleen, Jean, Karen, etc.) - it took awhile, but we all made it. Thanks for taking the edge off. I must specifically mention Russ – a good friend and long time roommate – thanks for the support and, of course, the computer. I would like to acknowledge specifically the support and friendship of my former roommates and long time friends from JMU, Andrew and Dana, as well as, my current roommate Chris who always manages to crack me up. I also appreciate the guys and gals of the “Saturday Basketball Crew” – for the last four years, competitive yet friendly basketball with fellow graduate students every Saturday morning really helped alleviate the stress of graduate school.

Lastly, I would like to especially thank Jill, my best friend here in graduate school - Jill made graduate school and life for that matter, fun - the way it should be.

## TABLE OF CONTENTS

<b>LIST OF TABLES.....</b>	<b>xi</b>
<b>LIST OF FIGURES.....</b>	<b>xiii</b>
<b>LISTS OF SYMBOLS, ABBREVIATIONS, SUBSCRIPTS, AND CONSTANTS.....</b>	<b>xx</b>
<b>PREFACE.....</b>	<b>xxiv</b>
<b>1. OVERVIEW AND SIGNIFICANCE OF RESEARCH.....</b>	<b>1</b>
1.1. COMMERCIAL BIOSENSORS.....	2
1.2. BIOCOMPATIBLE MATERIALS AND SURFACES.....	4
1.3. BIOSENSOR RESEARCH AND DEVELOPMENT.....	6
1.3.1. Elements of a Biosensor.....	6
1.3.2. Characteristics of an Ideal Biosensing Device.....	8
1.3.3. Complications of Biosensor Related Research.....	8
1.4. PROTEINS.....	9
1.4.1. Biological Electron Transfer and Proteins.....	9
1.4.2. Protein Adsorption Processes.....	12
1.5. ADDRESSING THE CHALLENGES OF BIOSENSOR RESEARCH.....	14
1.5.1. Electrochemistry.....	14
1.5.2. Scanning Probe Microscopy.....	15
1.5.3. Nanotechnology.....	16
1.5.4. Self-Assembled Monolayers.....	16
1.6. ELECTROCHEMICAL APPROACHES TO BIOSENSOR RESEARCH.....	17
1.6.1. Basic Electrochemical Biosensor Design.....	18
1.6.2. Direct ET Designs.....	21
1.7. SUMMARY AND PERSPECTIVE OF DISSERTATION RESEARCH.....	21
1.8. REFERENCES.....	24
<b>2. BACKGROUND, INTRODUCTION, AND OBJECTIVES OF RESEARCH.....</b>	<b>27</b>
2.1. BIOLOGICAL ET OF PROTEINS.....	28
2.1.1. Homogeneous ET of Proteins.....	28
2.1.2. Heterogeneous ET of Proteins.....	30
2.2. THE STRATEGY: PROTEIN MONOLAYER ELECTROCHEMISTRY.....	32
2.2.1. PME: Advantages and Disadvantages.....	34
2.2.2. Modified Electrodes and PME.....	37
2.3. THE CYT C / SAM / Au ELECTRODE SYSTEM.....	38
2.4. EQUINE (HORSE HEART) CYTOCHROME C.....	40
2.4.1. Physical and Structural Properties of Cyt c.....	40
2.4.2. Physiological Function of Cyt c.....	42
2.5. SELF-ASSEMBLED MONOLAYERS.....	45
2.5.1. General Characteristics.....	45
2.5.2. The Process of Self-Assembly.....	45
2.5.3. Alkane Chain Length.....	47
2.5.4. SAM Endgroups (Terminal Groups).....	49
2.5.5. SAM Applications.....	53
2.5.6. Cyt c / COOH SAM / Au System (Bowden Research).....	54

2.6.	ELECTROCHEMISTRY – VOLTAMMETRY OF AN ADSORBED SPECIES.....	55
2.6.1.	Laviron’s Kinetics of Adsorbed Species.....	57
2.7.	DOUBLE LAYER THEORY AND CAPACITANCE.....	59
2.7.1.	The Double Layer.....	59
2.7.2.	Parallel Plate Capacitors.....	60
2.7.3.	Dielectric Materials.....	63
2.7.4.	SAMs, Dielectrics, and Double Layer Capacitance.....	67
2.7.5.	Cyclic Voltammetry and Double Layer Capacitance.....	69
2.8.	ELECTROCHEMICAL BEHAVIOR OF CYT C / COOH SAM / Au SYSTEMS.....	72
2.8.1.	Electrochemical Properties of Cyt c.....	74
2.8.2.	Previous Research – Testing the Heterogeneous Adsorption Site Hypothesis.....	75
2.9.	FOCUS OF DISSERTATION RESEARCH.....	79
2.9.1.	Surfaces and Objectives of Research.....	79
2.9.2.	Methodology and Approach.....	81
2.9.3.	Organization of Dissertation.....	82
2.10.	REFERENCES .....	84

### **3. THE ROLE OF GOLD TOPOGRAPHY IN CYT C / SAM / GOLD ELECTROCHEMICAL SYSTEMS.....92**

3.1.	INTRODUCTION.....	93
3.1.1.	The Topography of Gold Substrates.....	95
3.1.2.	Previous Research Into Gold Topography.....	97
3.1.3.	Gold Topography and the Cyt c / SAM / Au System.....	98
3.2.	EXPERIMENTAL GOLD – GENERAL CHARACTERISTICS.....	99
3.2.1.	Evaporated Gold Thin Films.....	100
3.2.2.	Bulk Polycrystalline Gold.....	100
3.2.3.	Single Crystal Gold.....	102
3.2.4.	Au Epitaxially Grown on Mica.....	102
3.3.	EXP. GOLD CHARACTERIZATION – ROUGHNESS FACTORS.....	103
3.3.1.	Basis and Background of $R_f$ .....	104
3.3.2.	Experimental Results - $R_{f/E/C}$ .....	107
3.3.3.	$R_{f/E/C}$ Results – Comparison of Various Types of Gold Substrates.....	114
3.3.4.	SPM Roughness Factors - $R_{f-SPM}$ .....	117
3.4.	EXP. GOLD CHARACTERIZATION – CRYSTALLINITY.....	117
3.4.1.	Gold Oxide Formation and Crystallinity.....	117
3.4.2.	Lead Underpotential Deposition Experiments.....	119

#### ***MULTIPLE GOLD SUBSTRATE STUDY (PART I)***

3.5.	CYT C ELECTROCHEMICAL RESPONSE ON MODIFIED GOLD.....	122
3.6.	X-RAY PHOTOELECTRON SPECTROSCOPY .....	123
3.7.	EFFECT OF INTENTIONAL ROUGHENING ON CYT C RESPONSE.....	125
3.8.	SQUARE WAVE VOLTAMMETRY.....	126
3.9.	PROPERTIES AND STRUCTURE OF COOH SAMs.....	127
3.9.1.	Redox Probing of SAMs.....	128
3.9.2.	Hydroxymethyl Ferrocene Redox Probing of SAMs on Experimental Gold.....	129
3.10.	$C_{dl}$ OF THE CYT C / SAM / Au SYSTEMS.....	131
3.11.	MIXED SAMs.....	134
3.11.1.	The Structure of Mixed SAMs.....	135
3.11.2.	The Effect of Mixed SAMs on Smooth Topographies and Cyt c Response.....	138

3.11.3. XPS of the Mixed SAM / Cyt c System.....	141
3.11.4. Kinetic Analysis of Cyt c Adlayers on Mixed SAMs.....	141

***EVAPORATED GOLD STUDY (PART II)***

3.12. INITIAL RESEARCH – ROLE OF THE GOLD SUBSTRATE.....	144
3.12.1. Roughness of Evaporated Gold Substrates.....	144
3.12.2. SAM Desorption Linear Sweep Voltammetry.....	144
3.12.3. Capacitance of COOH SAMs on Evaporated Au Substrate.....	149
3.12.4. Hydroxymethyl ferrocene Redox Probing.....	150
3.12.5. Cyt c Response for Evaporated Gold Substrates.....	150
3.12.6. Effect of Intentional Roughening of Evaporated Au (HFA).....	152
3.12.7. Mixed SAMs on Annealed Evaporated Au.....	152
3.12.8. The Titanium Experience – A Comment on Annealing and Contamination.....	152
3.13. DISCUSSION.....	157
3.13.1. Carboxylic Acid SAM Structure and Gold Topography.....	157
3.13.2. Cyt c Adsorption/Electrochemistry and Gold Topography.....	159
3.14. FUTURE DIRECTIONS.....	163
3.15. SPECIAL ACKNOWLEDGEMENTS.....	164
3.16. EXPERIMENTAL DETAILS.....	165
3.16.1. Experimental Gold Substrates.....	165
3.16.2. General Materials – Solution Preparation.....	166
3.16.3. Electrochemistry (General – Equipment).....	167
3.16.4. Gold Substrate Pretreatments.....	168
3.16.5. Scanning Probe Microscopy Imaging.....	169
3.16.6. Roughness Factor Experiments.....	170
3.16.7. Lead UPD Experiments.....	170
3.16.8. SAM Deposition Procedure.....	171
3.16.9. SAM Characterization Procedure – Redox Probing.....	171
3.16.10. Cyt c Purification.....	172
3.16.11. Cyt c Adsorption and Electrochemistry.....	181
3.16.12. XPS Testing Analysis.....	182
3.16.13. Square Wave Voltammetry.....	183
3.16.14. Intentional Roughening Procedures and Mixed SAM Usage.....	183
3.16.15. SAM Deposition LSV Procedure.....	183
3.17. REFERENCES.....	184

**4. THE CYT C / SAM INTERFACE: PRELIMINARY INVESTIGATION OF SAM HEALING AND SILVER UPD.....191**

4.1. THERMAL HEALING OF SELF-ASSEMBLED MONOLAYERS.....	192
4.1.1. Mechanistic Aspects of Thermal Healing of SAMs.....	193
4.2. RESULTS AND DISCUSSION – THERMAL HEALING OF SAMS.....	196
4.2.1. Cyt c Response – Thermal Healing of SAMs.....	196
4.2.2. HMFc Redox Probing of Thermally Healed SAMs.....	198
4.2.3. SAM Desorption Studies of Thermally Healed SAMs.....	199
4.2.4. Conclusions and Future Directions for Thermal Healing.....	200
4.3. SILVER UNDERPOTENTIAL DEPOSITION BASED SAMS (Ag-UPD).....	201
4.3.1. Underpotential Deposition – General Discussion.....	201
4.3.2. Silver and Copper UPD Based SAMs on Gold.....	202

4.3.3.	Methods of Depositing UPD Layers.....	204
4.3.4.	Results and Discussion – Ag UPD Layers.....	205
4.3.5.	Piranha Cleaning vs. Electrochemical Cleaning – The Cyt c Response.....	210
4.3.6.	Future Directions – Ag/Cu UPD Layers on Au.....	212
4.4.	FUTURE DIRECTIONS FOR THE SAM/CYT C INTERFACE.....	213
4.5.	SPECIAL ACKNOWLEDGEMENTS.....	214
4.6.	EXPERIMENTAL DETAILS.....	214
4.6.1.	Thermal Healing Experiments.....	214
4.6.2.	Ag – UPD Experiments.....	215
4.7.	REFERENCES.....	217
<b>5.</b>	<b>THE CYT C/SAM/GOLD SYSTEM ON A MOLECULAR LEVEL: A SCANNING PROBE MICROSCOPY STUDY.....</b>	<b>219</b>
5.1.	SPM: THE GOLD SUBSTRATE.....	221
5.2.	SPM: SAM / SOLUTION INTERFACE.....	233
5.3.	SPM: PROTEINS (CYTOCHROME C).....	235
5.3.1.	SPM: Cytochrome c on Gold – Experimental Results.....	236
5.4.	SPM: THE CYT C / SAM / Au SYSTEM – CONCLUSIONS AND FUTURE DIRECTIONS.....	242
5.5.	SPECIAL ACKNOWLEDGEMENTS.....	252
5.6.	EXPERIMENTAL DETAILS.....	252
5.6.1.	STM Experiments.....	252
5.6.2.	AFM Experiments.....	253
5.7.	REFERENCES.....	254
<b>A.</b>	<b>APPENDIX A: SOLVENTLESS ELECTROCHEMISTRY OF METALLODENDRIMERS.....</b>	<b>259</b>
A.1.	INTRODUCTION – NANOTECHNOLOGY.....	260
A.2.	THE INFORMATION BEARING UNIT.....	260
A.3.	THE GORMAN RESEARCH PROJECT – METALLODENDRIMERS.....	261
A.3.1.	Fe-S Based Dendrimers.....	263
A.3.2.	Gorman / Bowden Collaboration Project.....	268
A.3.3.	Research Objectives.....	270
A.4.	PRELIMINARY EXPERIMENTS.....	270
A.4.1.	Exploratory Electrochemistry in Propylene Carbonate.....	272
A.5.	SOLVENTLESS ELECTROCHEMISTRY.....	275
A.5.1.	Polymer Salts.....	275
A.5.2.	Solventless Electrochemistry at Microelectrodes – Royce Murray Research.....	277
A.5.3.	Apparent Diffusion Coefficients ( $D_{app}$ ).....	278
A.5.4.	$D_{app}$ and Diffusion Geometry.....	279
A.5.5.	Relevant Experimental Results from the Murray Group.....	281
A.6.	SOLVENTLESS ELECTROCHEMISTRY – METALLODENDRIMERS.....	284
A.6.1.	N.C. State versus UNC.....	285
A.6.2.	Preliminary Results – Carboxylic Acid Ferrocene / MePEG(250).....	286
A.6.3.	Flexible IBUs / MePEG(250) Results.....	287
A.7.	DISCUSSION.....	288
A.8.	CONCLUSIONS AND FUTURE DIRECTIONS.....	295
A.9.	SPECIAL ACKNOWLEDGEMENTS.....	297
A.10.	EXPERIMENTAL DETAILS.....	297

A.10.1. Equipment / Materials / Procedures.....	297
A.10.2. SAM Experiments and LSV Desorption.....	298
A.10.3. Solventless Electrochemistry.....	299
A.11. REFERENCES.....	302

**B. APPENDIX B: INTERESTING ELECTROCHEMISTRY AT  
INDIUM OXIDE ELECTRODES.....306**

B.1. INTRODUCTION.....	307
B.2. NEUROLOGICAL DISEASE.....	307
B.3. METAL OXIDE ELECTRODES.....	308
B.4. THE KYNURENINE PATHWAY – A CATARACT STUDY.....	309
B.5. THE A $\beta$ PEPTIDE AND ALZHEIMER’S DISEASE.....	316
B.6. CYTOCHROME C AT ITO ELECTRODES.....	319
B.7. SPECIAL ACKNOWLEDGEMENTS.....	323
B.8. EXPERIMENTAL DETAILS.....	323
B.8.1. Kynurenine Pathway Experiments.....	323
B.8.2. A $\beta$ Experiments.....	324
B.8.3. Cyt c / ITO Experiments.....	324
B.9. REFERENCES.....	326

## LIST OF TABLES

Table 1-1. Examples of biological implants or biocompatible materials.....	5
Table 1-2. Protein classification and function.....	10
Table 1-3. Sampling of genetic diseases linked to proteins and enzymes.....	15
Table 2-1. Scientific advantages and limitations of PME.....	35
Table 2-2. Dielectric constants and dielectric strengths for various materials.....	64
Table 2-3. Electrochemical properties of cyt c voltammetry.....	76
Table 3-1. Summary of experimental gold substrate properties.....	101
Table 3-2. Estimated values – charge density passed for the reduction of an oxygen ad-atom monolayer of Au-oxide.....	107
Table 3-3. Electrochemical and SPM roughness factors - experimental gold substrates.....	116
Table 3-4. Categories of SAM defects.....	128
Table 3-5. HMFc SAM defect redox probe voltammetry results on various gold substrates.....	131
Table 3-6. Double layer capacitance measurements of SAMs on various gold substrates.....	132
Table 3-7. HMFc redox probing for SAM defects – mixed SAMs on evaporated gold.....	139
Table 3-8. Double layer capacitance results – mixed SAMs / various gold substrates.....	140
Table 3-9. Effect of roughening and mixed SAMs on cyt c voltammetric properites.....	140
Table 3-10. Electrochemical and SPM roughness factors – evaporated gold film substrates.....	145
Table 3-11. Linear scan voltammetry – SAM desorption results - evaporated gold film substrates.....	148
Table 3-12. SAM double layer capacitance - evaporated gold film substrates – chainlength and pretreatment dependence.....	149
Table 3-13. SAMs double layer capacitance of SAMs on evaporated gold – various pretreatments.....	153
Table 3-14. Chemicals, solutions, and equipment for horse heart cyt c purification.....	173
Table 4-1. Cyt c / C <sub>11</sub> OOH voltammetry – SAM thermal healing results.....	198
Table 4-2. Voltammetry cyt c / C <sub>11</sub> OOH SAM – electrochemical properties – piranha cleaning vs. Electrochemical cleaning.....	212
Table 5-1. Comparison of known protein dimensions to experimental SPM determined Dimensions.....	237
Table A-1. Electrochemical data previously obtained for metallodendrimers.....	267
Table A-2. Summary of solvent / electrolyte / potential window testing.....	272
Table A-3. Linear scan voltammetry – SAM desorption results.....	274
Table A-4. Techniques for measuring very small diffusional parameters.....	278

Table A-5. Solventless electrochemical properties of metallodendrimers.....	288
Table A-6a. IBU parameters and properties .....	294
Table A-6b. Microelectrode assembly parameters and properties.....	294
Table A-7. Dendrimer – polymer film – number of molecules electrolyzed.....	296
Table B-1. Cyt c / ITO voltammetry.....	321

## LIST OF FIGURES

Figure 1.1. Depiction of potential <i>in vivo</i> biosensors with biospecific.....	3
Figure 1.2. Common enzymes used in biosensors.....	4
Figure 1.3. Basic biosensor design.....	7
Figure 1.4. Diagrams of chloroplasts and photosynthesis chain.....	12
Figure 1.5. Protein adsorption processes.....	13
Figure 1.6. Generic model illustration of a self-assembled monolayer.....	17
Figure 1.7. Electrochemical designs of biosensors.....	19
Figure 1.8. Mediating species used in electrochemical based biosensor designs.....	20
Figure 1.9. Flowchart illustrating span and diversity of biosensor and biocompatible research.....	23
Figure 2.1. Illustrations and reactions schemes depicting the simplified strategy of PME versus traditional bimolecular reactions.....	33
Figure 2.2. Illustrations showing a hypothetical structure for cyt c molecules adsorbed at a gold electrode modified with a 16-MHDA SAM.....	39
Figure 2.3. Crystal and space filled structures of HH cyt c – rotated 90°.....	41
Figure 2.4. Simulated UV-Vis spectrum of oxidized and reduced forms of HH cyt c.....	41
Figure 2.5. Cross-sectional 3-D diagram of a eukaryotic cell.....	42
Figure 2.6. Mitochondrion structure (diagram and electron micrograph).....	44
Figure 2.7. Mitochondrial ET system with four major complexes including cyt c.....	44
Figure 2.8. Schematics of a SAM highlighting endgroups, headgroups, alkane chains, tilt angle, substrate, and lateral interactions.....	46
Figure 2.9. SAM structural property trends based on SAM chain length.....	48
Figure 2.10. Endgroup related trends of SAM properties.....	50
Figure 2.11. Cyclic voltammogram for an ideally adsorbed, reversible electrochemical system.....	56
Figure 2.12. A commonly accepted model for the electrode-solution interface known as the double layer.....	60
Figure 2.13. Parallel plate capacitor as an electronic component and in a simple circuit.....	61
Figure 2.14. Dielectric effect on voltage across a capacitor.....	63
Figure 2.15. Dielectric materials on a molecular level.....	66
Figure 2.16. Comparison of how a SAM modified electrode can be modeled as a parallel plate capacitor with a dielectric material.....	68
Figure 2.17. Determining $C_{dl}$ from cyclic voltammograms.....	70
Figure 2.18. Background voltammograms taken for diagnostic $C_{dl}$ measurements to track progress of electrochemical experiments with SAM modified electrodes.....	70

Figure 2.19. Reciprocal $C_{dl}$ of alkanethiolate SAMs as a function of chainlength and electrolyte....	72
Figure 2.20. Schematics of cyt c model system used in Bowden research: side and top view.....	73
Figure 2.21. Cyclic voltammogram of typical electrochemical behavior of cyt c adsorbed onto a carboxylic acid SAM.....	74
Figure 2.22. Generalized schematic diagrams depicting the experimental protocol for investigating sub-populations of adsorbed cyt c.....	77
Figure 2.23. Desorption plots of formal potential, full-width half maximum, and electron transfer rate constant as a function of electroactive surface coverage for a cyt c / 16-MHDA SAM / Au system.....	78
Figure 2.24. Illustration of the cyt c / SAM / Au system and the three major surfaces to be investigated.....	80
Figure 3.1. Examples of SAM defects attributable to gold topography.....	96
Figure 3.2. Cyclic voltammetry “roughness scan” in 0.1 M $H_2SO_4$ .....	105
Figure 3.3. Cyclic voltammetry of final electrochemical cleaning cycle and multiple cleaning cycle scans.....	109
Figure 3.4. Cyclic voltammetry roughness scans of evaporated gold as received and after electrochemical cleaning.....	110
Figure 3.5. Cyclic voltammetry roughness scans illustrating roughening effect of electrochemical cycling on smooth gold (bulk gold example).....	111
Figure 3.6. Illustrations of the three major stages of annealing.....	112
Figure 3.7. Photomicrographs showing the effect of annealing on grain size (brass example).....	112
Figure 3.8. Effect of annealing on the properties of a Zn-Cu alloy.....	113
Figure 3.9. Cyclic voltammetry roughness scans illustrating the smoothing effect of HFA on both bulk gold and evaporated gold.....	115
Figure 3.10. Cyclic voltammetry roughness scans of various types of gold substrates and pretreatments with corresponding roughness factors.....	116
Figure 3.11. Cyclic voltammetry roughness scans of evaporated gold illustrating the link between the surface crystallinity and the shape of Au-oxide formation peaks.....	118
Figure 3.12. Pb UPD stripping voltammetry showing the crystallinity of evaporated gold after various pretreatments.....	120
Figure 3.13. Pb UPD stripping voltammograms of bulk gold after etching in aqua regia, after oven annealing, and before/after HFA.....	121
Figure 3.14. Cyclic voltammetry of cyt c adsorbed at $C_{14}OOH$ SAMs on various gold substrates including evaporated gold, bulk gold, Au(111), and Au on mica.....	122

Figure 3.15. XPS spectra of the N(1s) region and corresponding cyclic voltammograms of cyt c adsorbed at C <sub>14</sub> OOH SAM modified bulk gold substrates that have been electrochemically cleaned and hydrogen flame annealed.....	124
Figure 3.16. Cyclic voltammetry of cyt c / C <sub>14</sub> OOH / bulk Au assemblies where the gold surface has been smoothed with HFA and roughened by electrochemical cycling.....	126
Figure 3.17. Square wave voltammetry of cyt c / C <sub>14</sub> OOH / Au / mica assemblies after initial protein adsorption and after exposure to several rinses with 1 M KCl.....	127
Figure 3.18. HMFC voltammetry at various gold substrates modified with HOOC(CH <sub>2</sub> ) <sub>13</sub> SH.....	131
Figure 3.19. Plot of double layer capacitance versus the overall roughness factor of various gold substrates.....	132
Figure 3.20. Proposed model to explain the observed trend in C <sub>dl</sub> for SAMs on the Au substrates of varying roughness.....	134
Figure 3.21. Illustration of the basic structure and surface distribution of a two component mixed SAM on gold.....	136
Figure 3.22. Schematics of two component mixed SAMs – hydrophobic/hydrophilic endgroup/chain interactions.....	137
Figure 3.23. Crystallinity of Type II mixed SAMs.....	138
Figure 3.24. Cyclic voltammetry of cyt c adsorbed to a single component C <sub>14</sub> acid SAM on annealed bulk Au compared to cyt c adsorbed to a mixed SAM on annealed bulk Au.....	139
Figure 3.25. XPS spectra and cyclic voltammetry of cyt c on C <sub>14</sub> OOH SAMs on smoothed, roughened, and mixed SAM modified bulk gold substrates.....	142
Figure 3.26. Cyclic voltammetry of cyt c adsorbed on C <sub>14</sub> OOH modified evaporated Au and on a mixed SAM (C <sub>14</sub> OOH & C <sub>10</sub> OH) modified evaporated Au – illustrates kinetic effect of mixed SAMs.....	143
Figure 3.27. Roughness scan voltammetry of evaporated Au as received, electrochemically cleaned, and hydrogen flame annealed.....	145
Figure 3.28. LSV-SAM desorption scans – electrochemically cleaned and hydrogen flame annealed evaporated gold – various chain length SAMs .....	146
Figure 3.29. LSV-SAM desorption scans electrochemically cleaned and hydrogen flame annealed evaporated gold – C <sub>14</sub> OOH SAMs.....	148
Figure 3.30. Plot of COOH SAM chainlength (total # of carbons in chain) versus C <sub>dl</sub> <sup>-1</sup> for electrochemically cleaned, oven annealed, and hydrogen flame annealed evaporated Au substrates.....	150
Figure 3.31. HMFC redox probe voltammetry at C <sub>14</sub> OOH SAMs on electrochemically cleaned evaporated gold, HFA evaporated gold, Au/mica, and at bare evaporated Au.....	151

Figure 3.32. Cyclic voltammetry of cyt c on C <sub>14</sub> OOH SAMs on electrochemically cleaned evaporated gold and HFA evaporated gold.....	151
Figure 3.33. Cyclic voltammetry with background signals illustrating the effect of surface roughening on the cyt c response (evaporated Au with C <sub>14</sub> OOH SAMs).....	153
Figure 3.34. Cyclic voltammetry of cyt c adsorbed onto a HFA evaporated gold substrate modified with a mixed SAM.....	154
Figure 3.35. XPS survey scans of evaporated gold as received, electrochemically cleaned, oven annealed, and hydrogen flame annealed.....	154
Figure 3.36. Cross sectional diagrams of evaporated Au film substrates as received and upon annealing.....	155
Figure 3.37. Computer simulations of cyt c adsorption onto SAMs.....	162
Figure 3.38. Schematic illustration of electrochemical cell used in this research.....	168
Figure 3.39. Apparatus for protein purification illustrating column/siphon system.....	175
Figure 3.40. Separation mechanism of the CM-52 column during ion exchange chromatographic purification of cytochrome c.....	177
Figure 3.41. Schematic diagram of Amicon filtration cell.....	179
Figure 3.42. Experimental UV-Vis spectrum of horse heart cyt c.....	181
Figure 4.1. STM images illustrating example of thermal healing of SAMs.....	195
Figure 4.2. Cyclic voltammetry of cyt c adsorbed to traditionally prepared and thermally healed SAMs.....	197
Figure 4.3. Cyclic voltammetry of HMFc redox probe at traditionally prepared and thermally healed SAMs.....	198
Figure 4.4. Cyclic voltammetry of HMFc redox probe at methyl terminated SAMs traditionally prepared and thermally healed.....	199
Figure 4.5. Linear sweep voltammetry scans of traditionally prepared and thermally healed C <sub>11</sub> OOH SAMs on evaporated gold.....	200
Figure 4.6. Schematic illustration of a gold / silver or copper UPD layer / alkanethiolate SAM assembly.....	202
Figure 4.7. LSV of various gold, gold-UPD, and gold-UPD-SAM systems.....	204
Figure 4.8. Survey cyclic voltammetry illustrating UPD and bulk silver processes.....	205
Figure 4.9. Waveform of the chronocoulometry experiment for depositing Ag UPD layers.....	206
Figure 4.10. Cyclic voltammetry example of Ag UPD deposition and stripping.....	207
Figure 4.11. Cyclic voltammetry of Ag-UPD experiment on piranha cleaned evaporated gold.....	207
Figure 4.12. HMFc redox probe voltammetry at a n-octanethiol SAM on evaporated gold and at a n-octanethiol SAM on Ag-UPD modified evaporated gold.....	208

Figure 4.13. LSV SAM desorption sweep of an octane thiol SAM on Ag-UPD modified evaporated gold.....	209
Figure 4.14. Stripping / depositing voltammetry of Ag-UPD layer on freshly prepared evaporated gold film.....	210
Figure 4.15. Cyclic voltammetry of cyt c adsorbed on SAMs formed on electrochemically cleaned and piranha cleaned evaporated gold substrates.....	211
Figure 4.16. Experimental apparatus for thermal healing of SAMs in the electrochemical cell.....	215
Figure 5.1. Contact mode AFM images of evaporated gold before and after electrochemical Cleaning.....	222
Figure 5.2. Roughness analysis of an STM image of electrochemically cleaned evaporated gold.....	223
Figure 5.3. Roughness analysis of an STM image of evaporated gold that has been HFA.....	224
Figure 5.4. Optical photomicrographs of bulk gold substrates after etching in dilute aqua regia.....	225
Figure 5.5. Scanning electron microscope images of bulk gold electrodes after being etched in aqua regia.....	226
Figure 5.6. STM images and corresponding cross sectional analyses of evaporated gold compared to bulk gold .....	227
Figure 5.7. STM images and cross sectional analyses of a Au(111) substrate.....	228
Figure 5.8. STM image of Au epitaxially grown on mica substrates.....	229
Figure 5.9. Roughness analysis of an STM image of Au grown on mica.....	230
Figure 5.10. Sectional analysis of a gold step edge on a gold on mica substrate.....	231
Figure 5.11. Sectional analysis of another gold step edge on a gold on mica substrate.....	232
Figure 5.12. STM image and cross-sectional analysis illustrating the atomic step plateau topography of gold on mica.....	232
Figure 5.13. Illustration of how SPM techniques can skew the apparent dimensions of imaged adsorbates.....	236
Figure 5.14. STM image (survey scan) of cyt c proteins on gold on mica.....	238
Figure 5.15. STM image of apparent single molecules of cyt c protein adsorbed onto a gold on mica surface.....	239
Figure 5.16. Sectional-analysis of two apparent cyt c molecules from an STM image.....	240
Figure 5.17. STM images of individual cyt c molecules on gold on mica – top and three dimensional views.....	241
Figure 5.18. Schematic of resonant tunneling ECSTM experiment by Tao.....	244
Figure 5.19. STM images of Fe-protoporphyrin embedded in an array of protoporphyrin reference molecules.....	245

Figure 5.20. Sample and reference molecules from Tao's resonant tunneling experiment.....	246
Figure 5.21. STM images and corresponding cyclic voltammetry of Fe-protoporphyrin and protoporphyrin adsorbed on graphite during resonant tunneling experiments.....	246
Figure 5.22. Apparent height of imaged Fe-protoporphyrin molecules during STM resonant tunneling experiments.....	247
Figure 5.23. Hypothetical ECSTM resonant tunneling experiments on cyt c molecules.....	249
Figure 5.24. Hypothetical sketches of potential-current plots for a two electrode resonant tunneling experiment.....	249
Figure 5.25. Yeast cyt c covalently bonded to a SAM via a disulfide bond between the SAM and a cysteine amino acid group in position 102.....	251
Figure 5.26. Microperoxidase may be used in future experiments for initial tests of resonant tunneling of proteins.....	251
Figure A.1. Plot showing the miniaturization of electronic devices – past, present, and future.....	260
Figure A.2. Main classes of macromolecular architectures.....	262
Figure A.3. Dendritic encapsulation prevents facile ET between redox centers.....	263
Figure A.4. The tertiary butyl thiolated iron-sulfur core – the redox center for metallodendrimers synthesized in the Gorman Research Group.....	264
Figure A.5. Flexible IBU metallodendrimer with varying generations.....	265
Figure A.6. Fourth generation rigid type metallodendrimer.....	266
Figure A.7. Data illustrating the effective encapsulation of the metallodendrimers and its effect on the ET rate constant.....	267
Figure A.8. Illustrative models showing the similarities between the ET systems being researched in the Bowden and Gorman research groups.....	269
Figure A.9. LSV desorption scan of a tetradecanethiol SAM on Au in propylene carbonate.....	274
Figure A.10. Experimental apparatus used by Royce Murray Group for performing solventless electrochemistry at a platform microelectrode.....	278
Figure A.11. Solventless electrochemistry at microelectrodes – background voltammograms using a variety of polymer melts.....	282
Figure A.12. Cyclic voltammetry of 5 mM carboxylic acid ferrocene / Me <sub>2</sub> PEG films at the microelectrode assembly.....	283
Figure A.13. Cyclic voltammogram of background signal of Me <sub>2</sub> PEG(250)/LiClO <sub>4</sub> .....	285
Figure A.14. Cyclic voltammogram of carboxylic acid ferrocene in Me <sub>2</sub> PEG(250) / LiClO <sub>4</sub> at varying scan rates.....	287
Figure A.15. Cyclic voltammograms of first three generations of flexible IBU molecules in Me <sub>2</sub> PEG(250) with LiClO <sub>4</sub> .....	289

Figure A.16. Cyclic voltammetry results comparing GO, G1, and G2 flexible IBUs.....	290
Figure A.17. Cyclic voltammogram at various scan rates of GO-flex in Me <sub>2</sub> PEG(250)/LiClO <sub>4</sub> .....	291
Figure A.18. Scan rate dependence plots of GO-flex IBU in Me <sub>2</sub> PEG(250)/LiClO <sub>4</sub> .....	292
Figure A.19. Hypothetical model used for charge calculations aimed at determining the number of IBUs being electrolyzed.....	294
Figure A.20. In-house built experimental apparatus used for solventless electrochemistry of the metallodendrimers.....	300
Figure B.1. Tryptophan metabolism – kynurenine pathway.....	310
Figure B.2. Electrochemical analysis by cyclic voltammetry of kynurenine pathway catabolites in the presence of Cu(II).....	312
Figure B.3. Cyclic voltammetry of PBS background and PBS background with added H <sub>2</sub> O <sub>2</sub> .....	312
Figure B.4. Cyclic voltammetry of copper (II) chloride in the presence of 3-HAA – varying potential windows.....	314
Figure B.5. Cyclic voltammetry copper chloride in PBS scanned in different potential windows...	315
Figure B.6. Illustration of how Alzheimer’s attacks the brain.....	316
Figure B.7. Model for the generation of reduced metal ions by Aβ peptides.....	317
Figure B.8. Electrochemical characterization of a complex formed between Aβ1-42 and copper...	318
Figure B.9. Cyclic voltammetry of HH cyt c adsorbed to indium tin oxide electrode.....	321
Figure B.10. Plot of scan rate versus electron transfer rate constant for HH cyt c / ITO assemblies.....	322
Figure B.11. Plot of scan rate versus peak splitting for HH Cyt c / ITO systems.....	322

## LISTS OF SYMBOLS, ABBREVIATIONS, SUBSCRIPTS, AND CONSTANTS

( in approximate alphabetical order)

### Standard Subscripts

a	anodic
ads	adsorbed
b	backward
c	cathodic
des	desorbed
dl	double layer
et	electron transfer
exp	experimental
f	forward
Ox	oxidized species (oxidant)
p	peak
r	reverse
Red	reduced species (reductant)
rxn	reaction
soln	solution
surf	surface
theor	theoretical
$\infty$	bulk solution

### Greek Symbols

Symbol	Meaning	Units
$\alpha$	transfer coefficient	none
$\beta$	adsorption coefficient	none
	distance decay factor	$\text{CH}_2^{-1}$
$\epsilon$	extinction coefficient (molar absorbtivity)	$\text{M}^{-1} \text{cm}^{-1}$
	dielectric constant	none
$\Gamma$	electroactive surface concentration	$\text{mol}/\text{cm}^2, \text{pmol}/\text{cm}^2$
$\Gamma_{\text{mono}}$	thiolate concentration comprising SAM	$\text{pmol}/\text{cm}^2$
$\lambda$	wavelength	nm
	activation energy	kJ/mol
$\mu$	ionic strength	M, mM
$\nu$	scan rate (sweep rate)	V/s, mV/s
	frequency	$\text{s}^{-1}$
$\sigma$	charge density	$\text{Coul}/\text{cm}^2$
$\xi$	average redox center-to-center distance	$\text{\AA}, \text{nm}, \text{cm}$

## Standard Symbols

Symbol	Meaning	Units
a, b, c	crystallographic dimensions	nm, Å
A	electrode area	cm <sup>2</sup>
C	concentration	M, mM
	capacitance	F, μF
C <sub>dl</sub>	double layer capacitance	F/cm <sup>2</sup> , μF/cm <sup>2</sup>
C <sub>M</sub>	capacitance of monolayer	F, μF
C <sub>T</sub>	total capacitance of system	F, μF
d	distance	cm
	diameter	nm, Å
D <sub>app</sub>	apparent diffusion coefficient	cm <sup>2</sup> /sec
D <sub>coeff</sub>	diffusion coefficient	cm <sup>2</sup> /sec
D <sub>phys</sub>	physical diffusion coefficient	cm <sup>2</sup> /sec
E	electrochemical potential (applied potential)	V, mV
E <sup>o'</sup>	standard redox potential (formal potential)	V, mV
E <sup>o'</sup> <sub>surf</sub>	surface or adsorbed formal potential	V, mV
E <sub>f</sub>	electric field (applied)	mV, V
E <sub>p</sub>	peak potential	V, mV
ΔE <sub>p</sub>	difference between anodic and cathodic peak;  E <sub>p,a</sub> - E <sub>p,c</sub>	V, mV
E <sub>p,a</sub>	anodic peak potential	V, mV
E <sub>p,c</sub>	cathodic peak potential	V, mV
FWHM	half-wave potential of the anodic or cathodic peak	V, mV
GG	grain growth stage of annealing	none
ΔG <sup>o</sup>	Gibbs free energy	kJ/mol
I <sub>total</sub>	sum of anodic and cathodic current;  I <sub>a</sub> + I <sub>c</sub>	A, μA
I or i	current	A, μA
i <sub>p</sub>	peak current	A, μA
i <sub>p,a</sub>	anodic peak current	A, μA
i <sub>p,c</sub>	cathodic peak current	A, μA
I <sub>t</sub>	tunneling current between tip and substrate (SPM experiments)	pA
k	rate constant for a homogeneous or heterogeneous reaction	depends upon order
k <sub>a</sub> or d	rate constant of association or dissociation steps	cm/sec
k <sup>o</sup> <sub>et</sub>	standard electron transfer rate constant	s <sup>-1</sup>
k <sub>ads</sub> or des	rate constant for the adsorption step or desorption step	cm/s
k <sub>et</sub>	rate constant for the electron transfer step	s <sup>-1</sup>
k <sub>ex</sub>	electron exchange rate constant	M <sup>-1</sup> s <sup>-1</sup>
MW	molecular weight	g/mol
n	number of electrons involved in the redox reaction	none
	number of methylene units (-CH <sub>2</sub> -) in SAM	none
Q or q	charge	C
Q <sub>o</sub>	initial charge	Coul
R <sup>2</sup>	coefficient of determination	none
R1	recovery stage of annealing	none
R2	recrystallization stage of annealing	none
R <sub>a</sub>	mean roughness determined by SPM techniques	nm
R <sub>f</sub>	general roughness factor	none

$R_{f-E/C}$	electrochemically determined roughness factor	none
$R_{f-SPM}$	roughness factor determined by microscopy techniques	none
$R_q$	RMS roughness	nm
$t$	time	sec
$T$	absolute temperature	K
$V_b$	voltage bias between tip and substrate in SPM experiment	mV, V
$V_{DI}$	voltage applied across a dielectric material	mV, V
$V_s$	spatial volume	$\text{\AA}^3$
$X$	times	none

### Fundamental Physical Constants

$F$	Faraday constant	96485 C/mol
$R$	gas constant	8.31451 J/K·mol
$h$	Planck's constant	$6.6261 \times 10^{-34}$ joule-sec
$\epsilon_0$	permittivity of free space constant	$8.854187817 \text{ C}^2/\text{Nm}^2$

### Main Abbreviations

A	acceptor protein species
AE	auxiliary electrode
AFM	atomic force microscopy
ATP	adenosine triphosphate
CAG	contact angle goniometry
CM	carboxymethyl
CV	cyclic voltammetry
cyt <i>c</i>	cytochrome <i>c</i>
D	donor protein species
	dendritic ligand
DNA	deoxyribose nucleic acid
e-	electron
E/C	electrochemistry or electrochemical
ECSPM	electrochemical scanning probe microscopy
ECSTM	electrochemical scanning tunneling microscopy
EIS	electrochemical impedance spectroscopy
ER	electroreflectance spectroscopy
ET	electron transfer
$\text{Fe}(\text{CN}_6)^{3-}$	ferricyanide
FWHM	full width half maximum
GG	globular domains of vWf
G1,G2...	generation designation for IBU metallodendrimers
HFA	hydrogen flame annealed or hydrogen flame annealing
HH	horse heart
HMFc	hydroxymethyl ferrocene redox probe
HOMO	highest occupied molecular orbital
IBU	independent binary unit
IHP	inner Helmholtz plane

IR	infrared spectroscopy
IP	ionization potential
ITO	indium tin oxide
KE	kinetic energy
KPB	potassium phosphate buffer
LSV	linear scan voltammetry
LUMO	lowest unoccupied molecular orbital
Me <sub>2</sub> PEG	dimethyl terminated polyethylene glycol
16-MHDA	16-mercaptohexadecanoic acid
14-MUDA	14-mercaptoundecanoic acid
6-MHA	6-mercaptohexanoic acid
MS	mass spectrometry
MW	molecular weight
MX	metallic salt
OHP	outer Helmholtz plane
PAR	Princeton applied research
PBS	phosphate buffered saline solution
PC	propylene carbonate
Pcyt c	porphyrin cytochrome c
PEG	polyethylene glycol
PEO	polyethylene oxide
PES	photoelectron spectroscopy
PK	Pelletier – Kraut ET model for cyt c and its redox partner
PME	protein monolayer electrochemistry
PR	piranha cleaned (cleaning)
QCM	quartz crystal microbalance
RE	reference electrode
RMS	root mean square
RR	fibrillar domains of vWf
RT	resonant tunneling
-RY-	polymer repeat unit
SAM	self-assembled monolayer
SCE	saturated calomel electrode
SDH	succinate dehydrogenase
SEM	scanning electron microscopy
SPM	scanning probe microscopy
STM	scanning tunneling microscopy
SWV	square wave voltammetry
UPD	underpotential deposition
UV-Vis	ultraviolet – visible spectroscopy
VWf	von Willebrand factor protein
WE	working electrode
YCC	yeast cytochrome c

## PREFACE

As far as my life is concerned, this dissertation represents the culmination of six years of hard work and a variety of invaluable learning experiences. Hard work is something I believe in - hard work and dedication. Upon undertaking any endeavor, it is these two concepts that I apply in the hope of making a difference. A person trying to make a difference can accomplish great things. For me, being a dedicated and hard working individual in everything that I do will always be more valuable than sheer intelligence or natural ability. If something is worth doing, it's worth doing right. I am not the smartest chemist or even the most gifted researcher - I simply apply myself and work hard with the understanding that anyone can learn to do anything if they simply dedicate themselves to the objective and work at it. This is the attitude and approach with which I came to North Carolina State University - properties of my character that were instilled in me by my parents and in them by their parents. My ancestors were blue-collar workers and immigrants who started with very little and gradually built good lives for themselves and their families. Hard work and dedication of this nature have now brought me to this point in my life - the culmination of the last six years of work in the form of a research dissertation and a Doctorate of Philosophy in Chemistry.

Research of this magnitude and on this level is not only a substantial challenge, but is also an invaluable experience for future endeavors. The process of becoming an independent scientist means, for me, that I can solve problems. In my opinion, a Ph.D. is really an independent problem solver - a person capable of dedicating themselves to a problem and adept at working toward logical solutions to that problem. The ability to do this process well is beneficial, not only for scientific research, but also in many other aspects of life, from personal situations to society and government. For this specific reason, I believe that Ph.D. scientists are well suited for numerous types of jobs. What my fellow colleagues and I have been taught here at NCSU is the process of problem solving. The research described in this dissertation addresses my experiences at learning how to solve problems. Unfortunately, a vast amount of my learning experience here at NCSU was independent of the work presented in this dissertation. Many other activities have helped me to this point in my life - each with a unique importance to the overall knowledge I have gained from my time here at NCSU.

When I first entertained thoughts of joining a graduate program in chemistry, I was given the opportunity to attend more prestigious institutions than NCSU. Upon visiting other universities, however, it became evident that NCSU Chemistry was different. The chemistry department at NCSU represented a dynamic, changing, atmosphere. NCSU was a program on the rise with brilliant ideas of intermixing the different disciplines of chemistry and unique research ideas. For me, it was much more exciting to be a part of that change rather than simply join an established program with the best

apparent "reputation." I viewed the chemistry department at NCSU as a team - an underdog - and I always root for the underdog. The opportunity to be part of something like that was appealing and so I went for it. After six years, I believe the decision to come to NCSU has been rewarding, with a variety of experiences that would have never been available to me in other places.

My research experience and Ph.D. project, under the guidance of Professor Edmond Bowden, was fruitful with learning experiences. Along with my main Ph.D. project, I was allowed to get involved with several other research collaborations, both with Dr. Chris Gorman of NCSU's chemistry department, and with Dr. Ashley Bush's group at the Harvard Medical School and Massachusetts General Hospital. Cross discipline collaborations such as these really raised my level of exposure to other areas of science. Within my own group, I was able to serve as an REU (Research Experience for Undergraduates) mentor and have further benefited from directing two other undergraduate researchers in projects as well. Another great opportunity for learning was Dr. Bowden allowing me to contribute to the writing of a NSF research proposal, which was ultimately accepted for funding. All in all, the positive research experiences over the last few years have been extremely beneficial toward my development as a scientist and as a person.

As far as the research, graduate school in the core sciences is a unique experience, one that is not easily understood by people outside the field. It's hard and requires a level of dedication and self-motivation that even medical and law graduate students cannot identify with. Over the last several years many people (family and friends) have asked about what I do, the difficulties of graduate school in chemistry and what it is like to do basic, fundamental research. I've always had trouble with those sorts of questions, never really being able to convey to others the experience as it really is. Fortunately, an article in the New York Times Magazine summed up the experience as accurately as I've ever seen and it bears mentioning here.

*Graduate study in the sciences is a very unsentimental education. It requires the intellectual evolution from an undergraduate who can ace tests of textbook knowledge to original thinker who can execute research about which the textbooks have yet to be written...At this level of achievement, there are no more A's for effort. As a sign in on lab had it 'Don't Try. Do.'...The life of a graduate student is so uncertain...there's no guarantee that you're going to be able to find a job. And then you add the self-imposed pressures of the students themselves...You're dealing with people during a very difficult transition in their lives...Once they choose a research project, graduate students essentially fend for themselves - there are no courses, no tests, no timecards, no guardrails. In scientific, the graduate student's journey from ignorance to expertise is like a trip without a compass...it's completely self-motivated, and there are no landmarks in the landscape...There are no rewards along the way, no stages when you get evaluated. It feels like there's a long period where you don't have any landmark to see where you are.*

Strangely, it is this concept of graduate school that makes it so hard and, at the same time, so rewarding and great. It is that much sweeter when you accomplish your task, aware of how difficult it was and knowing that only a small minority of the people in the world have done likewise.

Aside from the excellent research related experiences, I have also had an opportunity to develop interpersonal and leadership skills during my NCSU years. As a major officer in the honorary chemical society in the department, Phi Lambda Upsilon, for three years, I gained valuable experience with organizational skills, working with departmental personnel and faculty members, generating substantial funding, assisting in the creation of a graduate student authored solutions manual for a general chemistry textbook, initiating beneficial programs for fellow graduate students, such as the thesis and travel funds that provides graduate students with financial assistance to participate in conferences and in printing their dissertations. Eventually, in my role with Phi Lambda Upsilon, space was secured for the Joyce Weatherspoon Graduate Student Facility, a much needed area where graduate students can meet, enjoy their lunch, and, most importantly, interact with other graduate students, thereby establishing the vital bond between graduates students that is essential to any successful graduate program.

On the university level, I represented the graduate students of the chemistry department as their Graduate Student Association representative. During my time with the GSA, I rewrote the department's GSA constitution to allow chemistry graduate students, with their hectic schedules, to maintain an equal representation at GSA meetings, thereby improving the chances of chemistry graduate students getting GSA benefits. As a teaching assistant at NCSU, I gained valuable experience teaching chemistry laboratories, effectively communicating chemistry-related ideas to large groups of people. As an analytical teaching assistant, I was also involved in the creation and writing of new experiments for the laboratory sessions.

Through personal initiation, I was able to develop my leadership skills. Leadership, in my opinion, is an important quality to have as a Ph.D., a person likely to lead fellow researchers, a research group, meetings, a business or classes at a university. NCSU's Student Leadership Center was able to supplement my scientific education-taking place in the Chemistry Department with courses in the Leadership Development Series. Through attending many different seminars, I achieved the Leadership Certificate and valuable training to assist me at being an effective leader.

The foundation of a good department is its students and graduate students. I have always believed it is important for graduate students to remain active in student organizations in order to maintain a voice in departmental and university matters. To this end, I have served as the graduate student member of several departmental committees aimed at improving the department in a variety

of ways. All of this non-research-related experience were invaluable and have shaped the type of Ph.D. I will be in the future. They are as much a part of me as the research discussed in this dissertation.

As far as this dissertation itself is concerned, I tried to have fun with it. It is a serious attempt at research but is written here in an original, somewhat entertaining format. Science, after all, should be somewhat fun and interesting. Because I have this belief and based on some personal experience with non-scientific people, like my family and friends, I have written this dissertation with novice scientists in mind. Professors might find this style of writing, with a great deal of explanation and detail, to be too tedious and simplistic. Graduate students and undergraduate students may find it somewhat more informative and interesting. This is the intent. This dissertation is intended to be a tool for future scientists doing research in this area of science. Thus, some sections have been written with a greater degree of detail than is completely necessary. Additionally, it is written in this manner because I was tired of coworkers responding to questions about our research and why we do certain things with statements like, "I don't know, we just do it that way because we've always done it that way." For my dissertation, I chose to actually explain some of these things. Much of the detail included in these explanations was spurred on by questions and discussions I frequently found myself having with undergraduate researchers, fellow graduate students, friends and even members of my graduate committee during my preliminary report on this research. One such question is "why do this research?" or "why should the general public be interested in this work?" As an answer, the first chapter of this dissertation is dedicated to addressing this point and placing the research in perspective with the world. In fact, before presenting the bulk of my results, the first two chapters first delve into the background information of this research. These chapters are useful for inexperienced researchers but may be quite boring for people with a good understanding of the concepts involved. In this case, the person should skim these sections and begin focusing on Chapter 3. In any event, this dissertation tells a story, as any good research effort should. There is a beginning, middle, end, and future to this research. It is intended to be useful and, for the most part, entertaining - I hope you find it that way.

One other thought on this dissertation that should be noted is that it is mine. I tried to have fun with it in my own way. I realize that the traditional way for most graduate students to approach a dissertation or thesis is to virtually copy the style and writing techniques of former graduate students. For my dissertation, however, I did not do that. I conceived of the organization and style of this dissertation by myself using a mental outline created only by me. Several quotes find themselves in these pages. Some of the quotes help summarize my entire experience in graduate school, some

reflect my feelings on a particular moment during my time here at NCSU, some were inspiring during long nights in the laboratory, and some are just for fun. For now, I present you with one that summarizes one of the more valuable lessons I have learned in graduate school:

#### *ATTITUDE*

*The longer I live, the more I realize the impact of attitude in life. Attitude, to me, is more important than facts. It is more important than education, than money, than circumstances, than failures, than successes, than what people think, or say, or do. It's more important than appearance, giftedness, or skill. It will make or break a company ...a church...a home...I am convinced that life is 10 percent of what happens to me and 90 percent how I react to it. -- Charles Swindoll*

When I first joined Dr. Bowden's group in the summer of 1995, he said to me, "I want you to get what you want out of your education here at State..." - I believe I have.

As I stated earlier, I hold myself to a standard of hard work, dedication, and making a difference - it is my hope and belief that I have indeed made a difference here at North Carolina State University.

Michael C. Leopold

June 2000

## **OVERVIEW AND SIGNIFICANCE OF RESEARCH**

### **CHAPTER ONE**

*“Some men see things as they are and say why. I dream things that never were and say why not.” – Robert Kennedy*

## 1. OVERVIEW

One of the main objectives of recent bioanalytical research is the development of versatile and clinically useful biosensors. The medical and environmental communities view the development of useful biosensors as an achievable and essential goal of the research world. Current interest in this type of bioanalytical research stems from the intriguing notion that biosensors can be created, in theory, for almost any specific biological target molecule.<sup>1</sup> The potential applications of such scientific advancement would be extremely useful, especially the ability to monitor specific biological chemicals linked to pathogenesis. As biotechnology advances, it is conceivable that biosensors will evolve from being useful *in vitro* devices that are connected to the body externally, to self-sufficient *in vivo* sensors that are integrated into physiological systems (Figure 1.1).<sup>2</sup> Although the research contained in this thesis is related to biosensors only on a fundamental level, a discussion of biosensors and their technological background is in order to provide the reader with an idea of how the research evolved and the significance of the work that will be presented.

### 1.1 COMMERCIAL BIOSENSORS

Commercial biosensors presently available for clinical or industrial use are limited in number and application. Much of the biosensor “consumer” market revolves around glucose sensors for diabetic patients. Currently, devices for self-monitoring of glucose levels are available as a type of biochemical sensor which utilizes blood samples drawn from diabetic people.<sup>3</sup> In spite of the dominance of glucose monitoring in the biosensor field, there has also been substantial development of sensors based on lactate, pesticides, phenols, heavy metals such as lead and copper, environmentally harmful gases like carbon monoxide and nitrous oxide, and many others.<sup>4</sup>

Unfortunately, consumer need is not always the main consideration in the development of biosensors. Glucose oxidase, the primary component of glucose sensing devices, is one of the most abundant enzymes available. Thus, the preponderance of work on glucose biosensors in the scientific literature is not surprising. There exists, however a severe lack of reports involving sensors for cholesterol related enzymes.

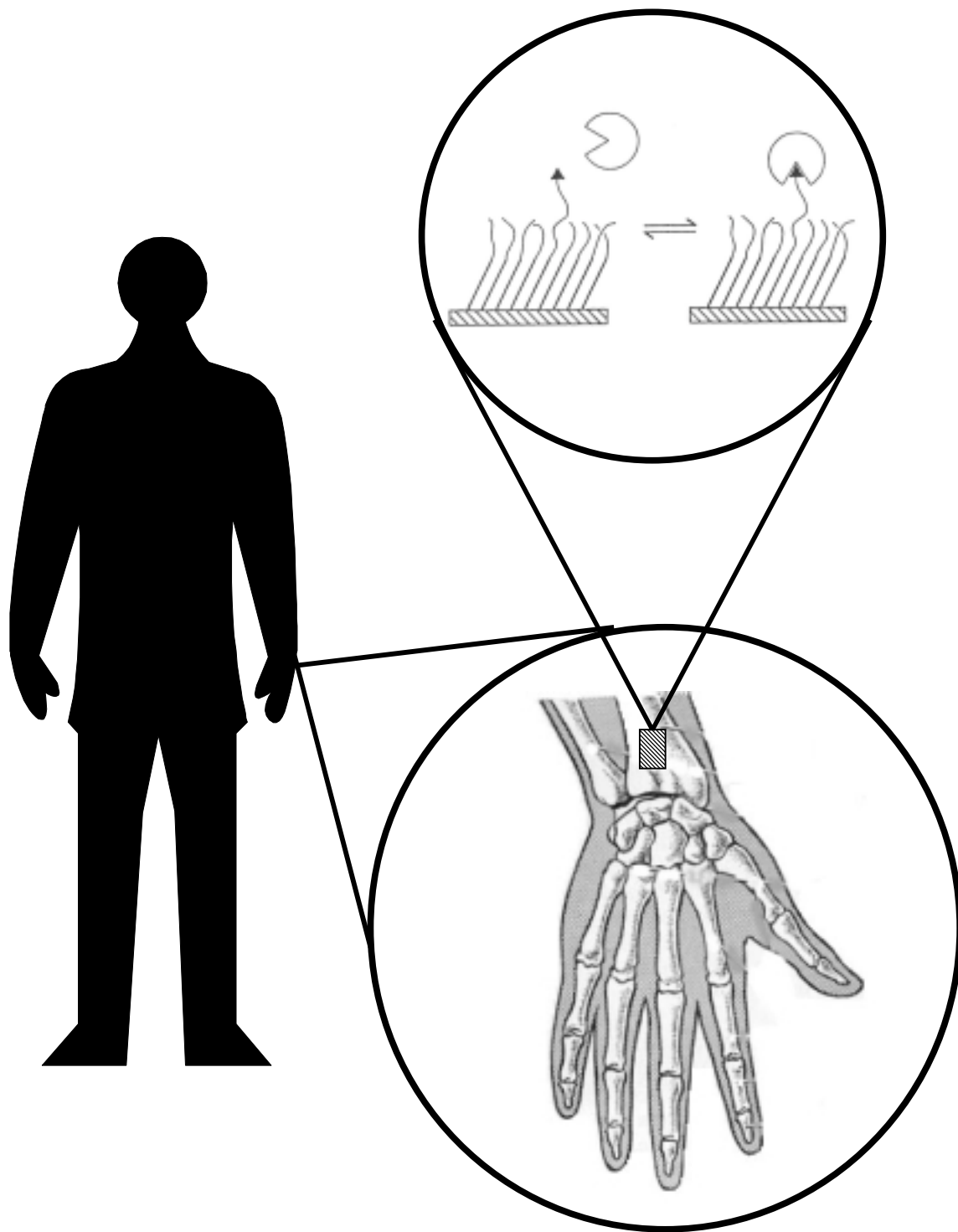


**Figure 1.1.** Depiction of potential *in vivo* biosensor with biospecific adsorption. Integrated devices such as this are desired to be completely bio-compatible, self-sufficient, and miniscule in size. (adapted from a figure in Ref. 2).

Figure 1.2 displays the common enzymes being used in biosensor research today. Cholesterol biosensors have an arguably greater potential to benefit medicine and a huge market of consumers, but are only represented in about 1% of the biosensor research activity.<sup>4</sup>

The high cost and difficulty of fabricating clinically useful biosensors is intimately related to uncovering successful biomaterials. The material is considered successful if it can be used in the construction of a reliable biosensor that can accurately assess a specific biological response while maintaining mechanical stability. The material must have all of these qualities and still be produced at a relatively low cost. Biosensor research, in essence, is basically about the science of biocompatibility.

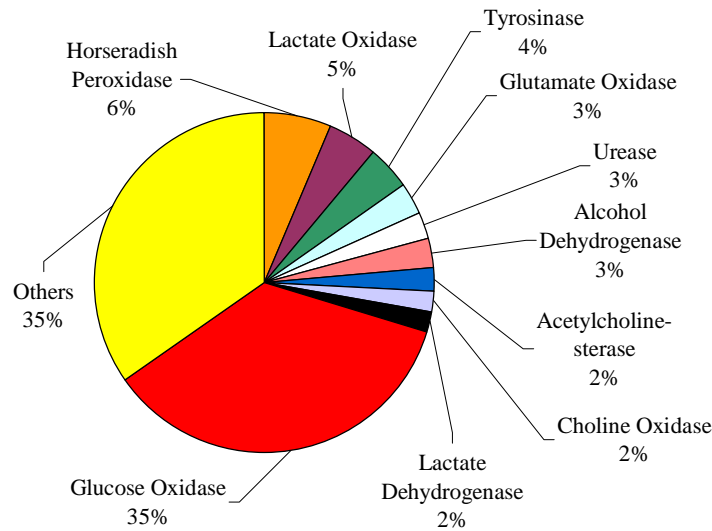


**Figure 1.2.** Common enzymes utilized in biosensor related research.<sup>4</sup>

## 1.2 BIOCOMPATIBLE MATERIALS & SURFACES

Biosensor research really involves a scientific examination of how biological matter interacts with man-made materials - the biocompatibility of a material. Interestingly, interfacing synthetic substances into biological systems to restore, complement, or replace some form of biofunction in the human body is already a common practice. Medical science, as well as the fundamental physical sciences, have already been utilizing somewhat successful forms of biocompatible devices. Each example, shown in Table 1-1, represents a situation where materials science and biology are united.<sup>2,5</sup>

The actual materials used for implants include metals like stainless steel and titanium, other substances like synthetic polymers and silicone implants, as well as, ceramics that are used to replace bone.<sup>5</sup> In all cases, the idea is to mimic the biological entity being replaced as closely as possible.

Historically, this technology has fallen short because most of the biomaterials

being used were developed based on mechanical and physical properties, weighed with financial considerations and little concern for the biological aspects of the implant.<sup>5</sup> These materials, when placed in a biological environment, are recognized by the body as foreign objects and, in most cases, the body will react to try to destroy the implant through phagocytosis. If not destroyed, the body will reject the implant by other means, enveloping

***“...as far as the biology is concerned, these materials are all foreign objects, not very different from a bullet, or a splinter.”***

*-Dr. Buddy D. Ratner<sup>5</sup>  
University of Washington (UWEB)*

this type of synergy between synthetic and natural materials is dependent on the surface science involved.

The surface of a material comprising a biosensor will largely determine the body’s reaction to it. Whether or not the body rejects the substance, either declaring it a trespasser and attacking it, or accepting it as compatible and integrating it, will be dictated based on how the surface of the implant presents itself to the body. When biological cells come into contact with a foreign surface, the membranes of those cells actively search for surface

**Table 1-1.** Examples of Biological Implants or Biocompatible Materials<sup>2,5</sup>

<b>Medical Science</b>	Heart valves Hip/knee replacements Pacemakers Dental implants Intraocular lenses Blood vessel prostheses Drug delivery devices Coatings for catheters Contact lenses Glucose sensors Protein storage
<b>Physical Sciences</b>	Chromatography

the foreign body in a layer of fibrous, denatured protein in an attempt to cut off communication between the body and the implant.<sup>5</sup> The real key to biomaterial research then, is to create materials that are so completely compatible with the biological systems that the living organism accepts the object as its own. Successfully achieving

characteristics or signals that communicate whether or not the surface chemistry of the material is compatible with the cell's surface chemistry. Clearly, the surface of materials and how specific biomolecules react and, in some cases, interact with it is of extreme importance to the study of biocompatible materials and, in turn, biosensor development.

### **1.3 BIOSENSOR RESEARCH & DEVELOPMENT**

What exactly is a biosensor? Simply put, a biosensor is an analytical device that utilizes biological molecules that have been immobilized on a surface. The surface is positioned near a transducer that can detect specific analyte interactions with the immobilized biomolecules. The interaction between the bio-substrate and the analyte results in some type of chemical signal which can be harnessed and converted to an electronic signal (Figure 1.3).<sup>1</sup>

#### **1.3.1. Elements of a biosensor**

In many cases, the elements of a biosensor are most easily described as the following: a substrate housing a sensing element, a transducer, and a specific method of analysis.<sup>4</sup> In some instances, as in the research that will be presented in this dissertation, the substrate is synthetically designed to mimic a desired biological surface rather than employing expensive biomolecules for immobilization on the surface.<sup>2,6</sup> Because biological entities interacting with the sensor will never “feel” the bulk of the sensor itself, it is clearly evident that the interface between the target macromolecule and the receptor surface is of utmost importance in this type of work. The mechanical and physical properties of the biosensor will reside within the device and only the surface of the biosensor will be presented. Thus, the way the sensing element interacts with the analyte and how the mediator element communicates the analyte's chemical signal are extremely important aspects of this technology and take place in much the same way that receptor-ligand interactions occur.

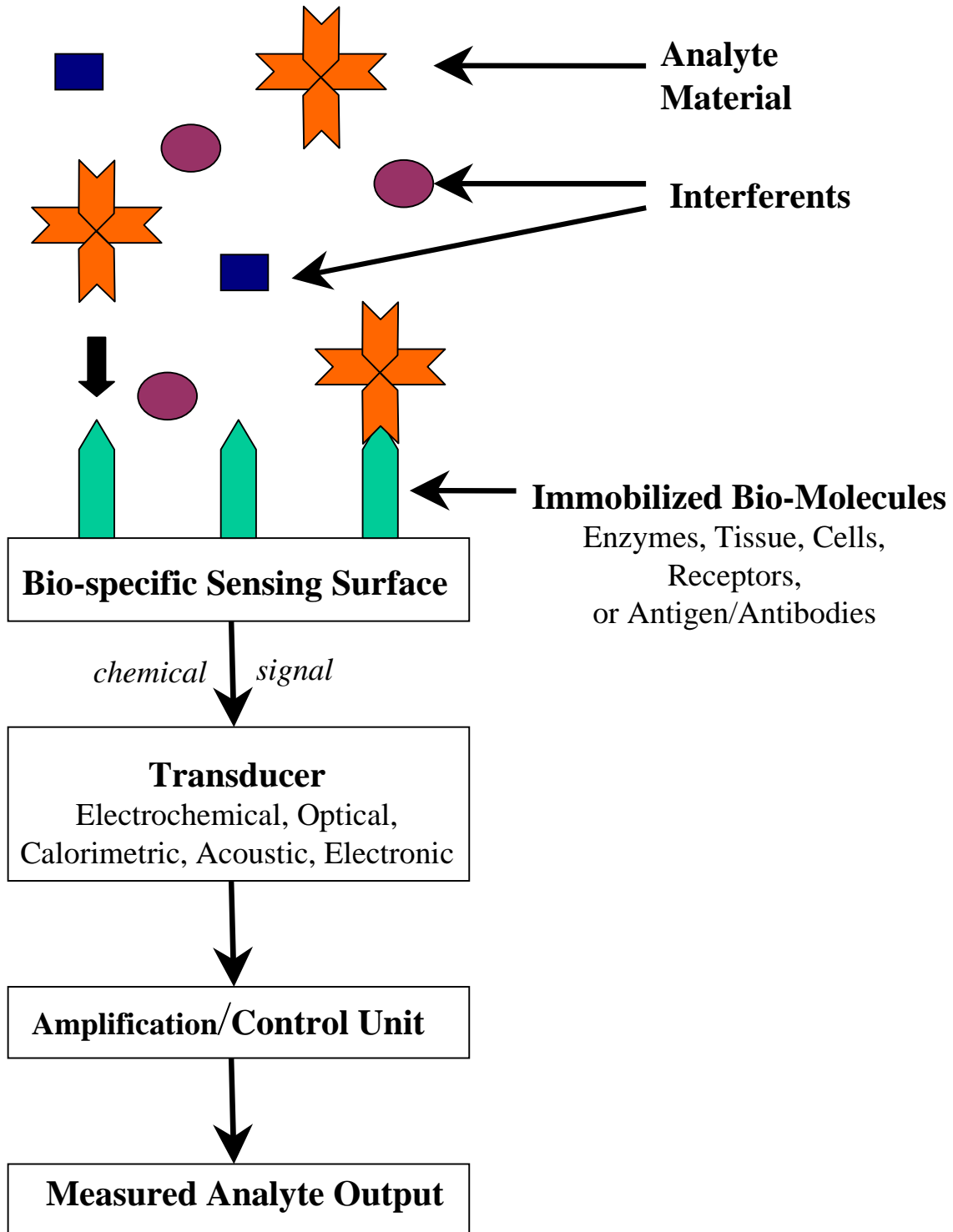


**Figure 1.3.** Illustration of basic biosensor design (adapted from a figure in Ref. 1).

In an attempt to simplify the interactions between the elements of the biosensor, methods of establishing direct communication with immobilized probe molecules have been explored. Effectively, this research is focused on sensors where the biomolecules of interest adsorb to a surface and transmit a chemical signal that can be easily analyzed. The ability to design a surface that effectively mimics normal tissue but that can also be selective toward specific analytes is a crucial challenge for biosensor researchers interested in creating new biocompatible materials targeting specific drug interactions and studying cellular communication.<sup>4,5</sup> Much of the research into this technology involves trying to understand biological events on surfaces that have been chemically designed and engineered for specific biological recognition.

### **1.3.2. Characteristics of an Ideal Biosensing Device**

The main characteristics of an ideal biosensor are miniaturization for potential *in vivo* applications, real time and selective monitoring of analyte signals, and cost efficient production. In addition, it is desired that the analytical signal generated by the device be large enough to accurately measure and consistent enough to be stable over a long period of time. Real time measurements would truly benefit the current medical world which is already highly dependent on time consuming, tedious, and very expensive laboratory procedures that almost always involve multi-step spectroscopic and chromatographic analyses.<sup>4</sup> Having described what is desired and needed in bioanalytical research to this point, it is now time to examine some of the complications that are involved with the development of this type of biotechnology.

### **1.3.3. Complications of Biosensor Related Research**

In general, recent work in this area of bioanalytical chemistry displays a lack of reproducibility and has generated concern over how the orientation of the macromolecule affects results. Mastering the ability to immobilize biomolecules to specific sites while preserving stability and functionality may lead to more effective biosensor designs. Clearly, however, the most significant challenge, as well as the largest drawback of biosensors and biocompatible implants, is their inadequate selectivity.

Overall, biosensor prototypes and models being used for fundamental research suffer greatly from extremely poor selectivity. More specifically, these devices are severely limited

in their ability to quantitatively determine a specific analyte in an untreated biological matrix. Molecular recognition and subsequent selectivity of target molecules over other molecules is the ultimate goal of analytical scientists in this field. For example, with sensors designed to be biospecific for proteins, the surface must possess a selectivity for a particular protein while simultaneously resisting the nonspecific adsorption of other, unwanted proteins. An obvious part of research into this type of system is the need to understand the protein adsorption process.

## **1.4 PROTEINS**

Of all the biomolecules that exist in a living organism, proteins are probably the most important macromolecules. Proteins perform a plethora of tasks for living organisms. Numbering in the thousands, proteins play essential roles in the many different biological processes from a cellular level to a direct functional role in vital life sustaining events. Some of the variety of tasks that proteins perform are summarized in Table 1-2. Amazingly, all of these proteins, with distinctive properties and functions, are formed from the same group of twenty, naturally occurring amino acid residues. Each specific protein is its own unique sequence of these amino acids, differing only in the order that they are joined through peptide bonds.<sup>8</sup> Almost all cellular activity involves at least one or more proteins to properly operate. Many biological processes of interest involve the use of many proteins performing specific functions in a chain of events.

### **1.4.1. Biological Electron Transfer & Proteins**

Biological electron transfer (ET) reactions are an intrinsic part of certain biological processes including photosynthesis, respiration, and intermediary metabolism.<sup>9</sup> There are two basic kinds of biological ET reactions. The first involves the redox reactions of organic metabolites and usually incorporates short range, multiple electron movements related to chemical bond formation and dissipation. This type of ET is sometimes referred to as inner sphere ET because the electron donor and the electron acceptor, through altering their coordination spheres, form a direct chemical bond between each other. The second form of ET reaction in biology, and the eventual focus of the research that will be discussed here, takes place over longer distances, sometimes tens of Angstroms (Å), and involves the transfer

of only a single electron.<sup>8</sup> This ET is fittingly referred to as outer sphere ET, owing to the fact that the donor and acceptor species only slightly change their coordination spheres during the process.<sup>8</sup> In these type of ET processes, certain proteins exist whose sole function is to deliver or transport an electron from one cellular location to another. These proteins are referred to as ET proteins.

**Table 1-2. Protein Classification and Function**<sup>7,8</sup>

<b>Classification</b>	<b>Function or Bio-role</b>	<b>Examples</b>
Enzymes	Catalysts for organic biomolecules undergoing chemical reactions in cells	<i>Luciferin</i> - part of the chemical reaction to make fireflies glow
Transport / Carrier proteins	Bind and carry specific molecules, ions, or electrons from one place to another in a cell or blood plasma	<i>Cytochrome c</i> - ET transfer reactions in respiration chain <i>Plastocyanin</i> - ET transfer reactions in photosynthesis <i>Hemoglobin</i> - O <sub>2</sub> transport
Nutrient / Storage proteins	Store vital nutrients for living organisms	<i>Ferritin</i> - storage of iron for living organisms
Contractile proteins	Enable cells to contract, change shape, or move	<i>Actin</i> - skeletal muscles
Structural proteins	Give biological structures strength, stability, and protection	<i>Collagen</i> - tendons; cartilage <i>Elastin</i> - ligaments <i>Keratin</i> - hair; fingernails <i>Fibroin</i> - spider webs <i>Resilin</i> - insect wings
Defense proteins	Defend organisms against attack and invasion of foreign matter	Immunoglobins (antibodies): - <i>Fibrinogen</i> - <i>Thrombin</i>
Regulatory proteins	Regulate cellular or physiological activity	Hormones <i>Insulin</i> - sugar metabolism <i>Cytochrome c</i> - intracellular communication

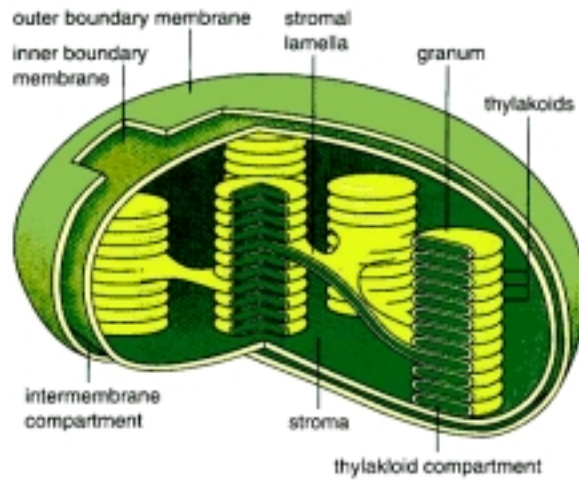
An example of where ET proteins contribute to an important biological function is photosynthesis. Green plants, algae, and some bacteria perform photosynthesis, making carbohydrates needed for their survival. In overly simplistic terms, the process of photosynthesis is initiated by sunlight and involves a chain of events where inorganic substances are converted to cellular energy in the form of ATP. The chemistry involved with

this process takes place inside the chloroplasts of the plant and uses carbon dioxide, water, and the aforementioned energy from sunlight, to create carbohydrates, water, and, most importantly for human beings, oxygen.<sup>10,11</sup> Inside the chloroplasts are tiny compartments called thylakoids. It is in these thylakoid compartments that the electron transport reactions take place (Figure 1.4). For the purpose of this thesis, the focus of this discussion about photosynthesis, a rather complicated process in itself, will revolve around the ET proteins involved in the chain.

Both plastocyanin and ferredoxin are proteins that bear the simple, but extremely important responsibility of delivering an electron to various locations in the thylakoid. Ferredoxin is an iron-sulfur protein with some form of an Fe-S cage as its redox center. Its function in the photosynthesis chain is to accept electrons from photosystem I and donate them to another enzyme. Plastocyanin is a “blue” protein, meaning it contains a copper atom at its center that varies between the +2 and +1 oxidation states. As shown in Figure 1.4, plastocyanin is effectively a freely moving electron shuttle between the b<sub>6</sub>/f complex found in the cell membrane, and photosystem I, also housed in the cell’s membrane.<sup>8,10</sup> Through some unknown mechanism, these freely moving proteins know where to deliver their packages of electrons. This type of protein/surface interaction is an example of the type of selective recognition of a functional protein by a biocompatible surface. To understand such biological interfaces and derive useful information from them, it is of great interest for biosensor and biomaterials research to focus on the specific interactions of proteins with synthetic surfaces that attempt to imitate biological interfaces.

With each passing year, more and more genetic diseases are being linked to proteins and enzymes. More than 1400 human genetic diseases are now known to be directly related to defective proteins (Table 1-3).<sup>7</sup> Biosensors that can detect, monitor, or serve as models to study the interactions of these proteins could be of immeasurable value in understanding the physiological aspects of such diseases. We next turn to some of the current fundamental research aspects that underlie the development of biosensors and protein adsorption model systems.

a.



b.

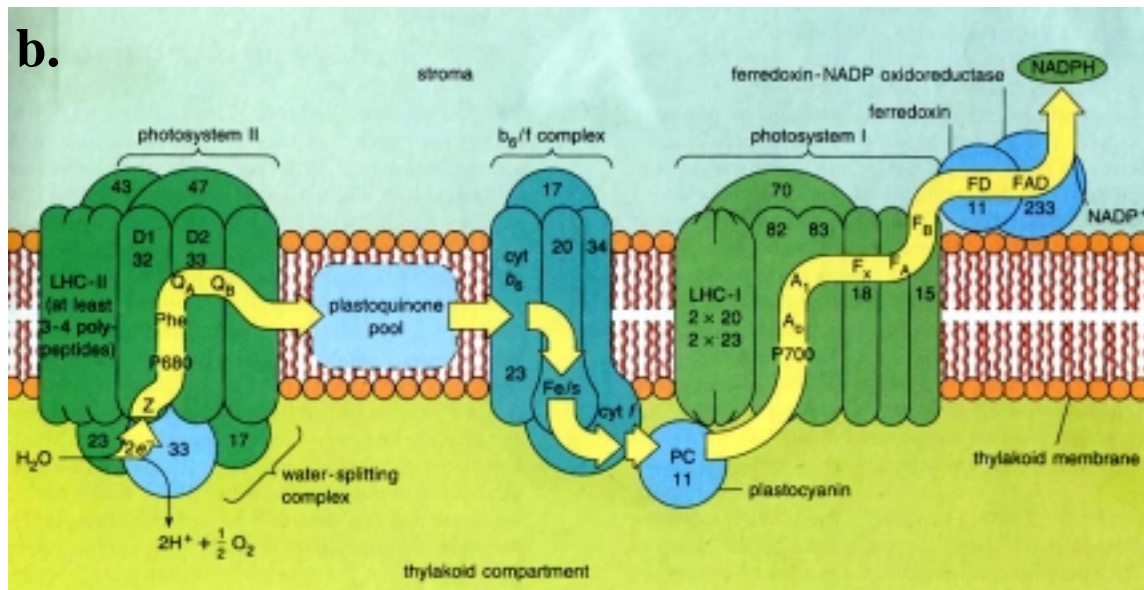


**Figure 1.4.** a) The membranes and compartments of chloroplasts. Chloroplasts enable plant cells to perform photosynthesis in the thylakoids; b) Photosystems and electron transport carriers of the photosynthesis chain in the thylakoid membranes (Figures from Ref. 10).

### 1.4.2. Protein Adsorption Processes

For over three decades, we have struggled to understand how proteins interact with each other and with biocompatible man-made surfaces.<sup>2</sup> Many of the biological processes of interest involve or are dependent upon proteins adsorbing to surfaces in very particular ways. The actual adsorption process of a protein onto a surface can be a very complicated scenario<sup>2,6</sup> (see Figure 1.5) - one which can either be beneficial or detrimental to the process

at hand or the experiment being conducted. In light of this, many researchers focus on trying to decipher protein-surface interactions on a mechanistic level. Accomplishing this means gaining an understanding of the factors that govern the adsorption process, including the complex nature of a protein's outer shell chemistry and surface structure of the substrate or biological interface. After all, defining that chemistry and being able to predict the interaction between the two components of the system is at the very heart of bioanalytical research.

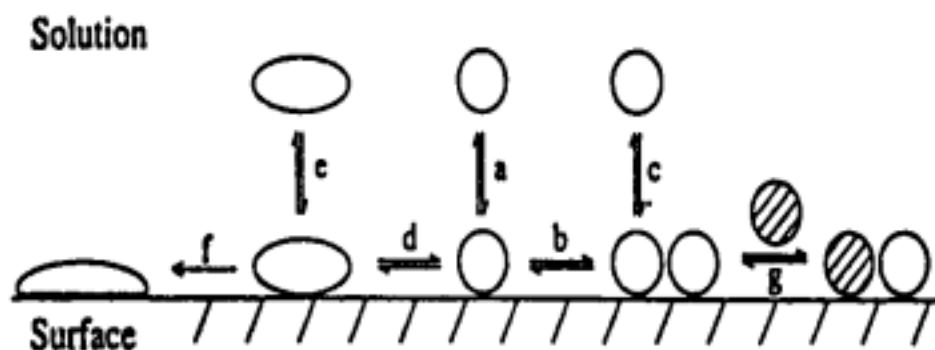


**Figure 1.5.** The complexities of protein adsorption - Several equilibrium processes must be considered upon (a) adsorption of a protein to a surface; (b) lateral mobility of the protein; (c) dissociation of the protein from the surface; (d) reversible denaturation and changes in conformation of the protein; (e) dissociation of the altered protein species; (f) irreversible denaturation coupled with permanent adsorption; and (g) exchange of surface bound protein with protein from solution. All of these processes are further complicated by the many different conformations and chemical environments that exist where the protein exists (Figure from Ref. 2).

A traditional method of studying protein adsorption processes is to create a model system involving an actual protein and a specifically tailored synthetic surface that effectively mimics the protein's natural binding partner. The use of a model system has the advantages of simplicity and, in some cases, allowing for the study of the protein in its natural state. Unfortunately, these experimental models are often highly dependent on solution conditions (pH, temperature, solvents, etc.) and, as stated earlier, suffer from poor selectivity.<sup>6</sup> Until recently, another major disadvantage of these models was their lack of molecular or atomic level detail of the interactions taking place. Gradually, through technological developments in instrumentation and innovative experimentation, research on protein adsorption models is revealing the molecular level detail needed to provide a fundamental basis for understanding

protein adsorption. It is a model system of this nature that will eventually be the focus of the research presented here.

## **1.5 ADDRESSING THE CHALLENGES OF BIOSENSOR RESEARCH**

Having stated the desired needs and problems of this field, it is important to recognize that plausible and fruitful techniques and scientific discoveries exist to meet each challenge. In addition to the information presented below, fundamental research review articles on biosensors and analytical electrochemistry are available.<sup>12</sup>

### **1.5.1. Electrochemistry**

Electrochemistry, for reasons that will be described, lends itself as an excellent technique to be used in this type of bioanalytical research. First of all, electrochemistry is very inexpensive and relatively simple in practice. These are important benefits when dealing with such potentially expensive materials and complex biological processes to understand. Furthermore, within the realm of electrochemistry exists a technique, called amperometry, that is capable of monitoring real time current signals. Current signals, even of very small magnitude, are relatively easy to detect, amplify, and measure. Electrochemical instrumentation used in amperometry is sensitive over a large range of concentrations and would be useful in certain situations where spectroscopic techniques are ineffective. In addition, the usage of an electrode as the substrate material in a sensor, allows the experimenter to control the energy applied to the system. The predominance of electron transfer reactions in biology and the demonstrated ability of electrochemistry to measure the direct redox activity of an immobilized, electroactive enzyme are major benefits of using this

**Table 1-3.** Sampling of Genetic Diseases Linked to Proteins or Enzymes<sup>7</sup>

<b>Disease</b>	<b>Physiological Effects</b>	<b>Related Enzyme / Protein</b>
Sickle-cell anemia	pain; swelling in hands; severe bone and joint pain; death	Hemoglobin
Tay-Sachs disease	motor deficiency; mental deterioration; death by age 3	Hexosaminidase
Familial hypercholesterolemia	atherosclerosis; early death from heart failure	Low density lipoprotein receptor
Rickets (Vit. D- dependent)	short stature; convulsions	25-Hydroxycholecalciferol-1-hydroxylase
Gout	overproduction of uric acid; acute arthritis	Phosphoribosyl pyrophosphate synthetase
Gaucher's disease	erosion of bones, hips, joints; brain damage	Glucocerebrosidase
Immunodeficiency disease	severe loss of immune system (bubble children)	Adenosine deaminase
Immunodeficiency disease	severe loss of immune response	Purine nucleoside phosphorylase
Lesch-Nyhan syndrome	neurological defects; self-mutilation; mental retardation	Hypoxanthine-guanine phosphoribosyl transferase
Cystic fibrosis	abnormal lung, pancreas, sweat glands secretions; chronic pulmonary disease; death	Chloride channel
Cell apoptosis	systematic cell death	Cytochrome c †

† Research is ongoing but a direct link has not been identified.<sup>18</sup>

tool to perform research of this nature. In the context of some type of bio-sensitive device, electrochemistry is a powerful tool for evaluating the overall operation of a system by divulging statistically averaged information about a population of sample molecules. It is important to keep in mind, however, that electrochemistry yields information strictly about electroactive molecules and lacks the selectivity needed to learn about the specific adsorption properties being considered when dealing with a protein/surface interface.

### 1.5.2. Scanning Probe Microscopy

In recent years, scanning probe microscopy (SPM) has enjoyed a great deal of research attention.<sup>13,14</sup> Unlike electrochemistry, SPM provides the opportunity to gain a more detailed understanding of protein/electrode interfaces on a molecular level. For evaluating

surface structure, SPM is ideal for probing localized electronic states as well as essential topographical information. Moreover, SPM offers some exciting possibilities in the realm of *in situ* studies of individual biomolecules. Through the molecular level information and imaging, especially at solid/fluid interfaces, the potential of SPM is truly unparalleled.

### 1.5.3. Nanotechnology

Electrochemistry and SPM have prospered greatly from recent scientific discoveries taking place in electronic technology. Electronics are being miniaturized and nanotechnology research is developing molecular scale, functional

***“Commercial success of any sensor will depend on the nature, size, and expense of the device.”***

*-Dr. H. Vaughan<sup>4</sup>  
University of Paisley, UK*

electrical components like information storage units, capacitors, and wires.<sup>15,16</sup> Not only is hardware being made on the nanoscale, the ability of researchers to manipulate such molecular devices is increasing.<sup>17</sup> This type of microfabrication and control means faster response times for transient signals, as well as, potentially very small biocompatible devices. Size will be extremely vital if *in vivo* biological implants are to be realized.

### 1.5.4. Self-Assembled Monolayers

When considering direct contact of biomolecules with a sensing element, the nature of the surface becomes very important. Depending on the surface characteristics, the protein might denature or unfold upon its interaction with a substrate. Controlling the properties of a surface has been simplified with the use of self-assembled monolayers (SAMs).<sup>2,19</sup> SAMs (Figure 1.6), particularly of alkanethiolates, are ideally suited for the study of biointerfacial chemistry and they will be discussed in depth later. The advantages of SAMs in this type of research reside in the fact that one can control the surface environment by manipulating the components that comprise the monolayer and, thus, the surface characteristics exposed to the incoming biomolecule. Controlling the surface to this degree allows for the study of molecular scale interactions between the protein and a specifically tailored surface. Since the structure and functionality of SAM can be easily manipulated, SAMs provide a marked increase in our ability to design a surface for specific molecular recognition, a key aspect of potential biosensing devices.<sup>20</sup> Usually supported on coinage metals (Au, Ag, Cu) or

mercury substrates, SAM modification of electrodes is advantageous to bioanalytical research for several reasons: 1) SAMs are optically transparent, 2) one can maintain electrical contact to the system through the conductive metal supporting the SAM, 3) SAMs are highly compatible with many analytical techniques, 4) SAMs are very stable over time 5) they are resistant to chemical attack, and 5) SAMs offer a wide variety of chemical and functional diversity at an interface. At this point, SAMs represent the best known surface available for the fundamental investigation into mechanistic aspects of the coupling between a biological macromolecule and a surface created specifically to mimic a biological interface.<sup>2</sup>

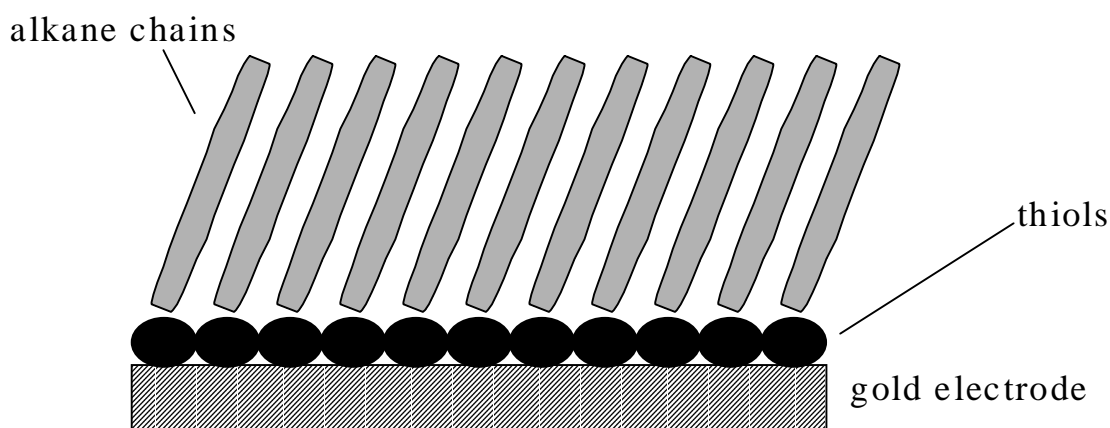


**Figure 1.6.** Generic model illustration of an ideal self-assembled monolayer (SAM); alkanethiolates are highly organized with a common orientation on the surface of a gold substrate, anchored by a thiol-Au bond.

## 1.6 ELECTROCHEMICAL APPROACHES TO BIOSENSOR RESEARCH

When considering electrochemical approaches to biosensor related research, it is desirable to achieve reproducible electronic communication between immobilized biomolecules and a bulk electrode material. Four basic approaches to this problem have been used and are depicted in Figure 1.7. These sorts of designs are based either on the redox chemistry of enzymatic products and/or reactants at the electrode surface or on the use of ET mediators. As will be briefly discussed in the following paragraphs, each method is burdened with its share of problems, and all of the methods suffer from a relatively high limit of detection for the targeted analytes.<sup>4</sup>

### 1.6.1. Basic Electrochemical Biosensor Designs

The simplest approach (Figure 1.7a) involves measuring the consumption of molecular oxygen by the enzymes or immobilized biomolecules. This process is beneficial in that, for many enzymes, oxygen is a naturally occurring electron acceptor. However, this type of analysis suffers from several limitations including slow response times and a dependence on oxygen content in the solution. Oxygen dependence in any of the methods presented here has the capability to drastically reduce the accuracy and reproducibility of a device.<sup>4</sup>

An alternative to oxygen consumption methods is to measure the redox signal of the byproduct hydrogen peroxide (Figure 1.7a). This method addresses the problem of response time, but is still too dependent on oxygen levels in the testing medium. In addition, high positive potentials are required to oxidize hydrogen peroxide. In spite of this, peroxide detection biosensor designs are very popular and common in recent literature reports.<sup>4</sup> A third method of analysis and the least common approach used by scientists is the use of bienzymatic systems (Figure 1.7b). In these set-ups, one couples the sensing enzyme with a second enzyme. Many enzymes are capable of catalyzing the oxidation of hydrogen peroxide and, thus, accommodate the complications associated with direct oxidation of hydrogen peroxide needed for the second method of analysis. Research on this type of system is progressing, especially with the use of horseradish peroxidase, and many scientists are advancing into incorporating enzymes into exotic media such as carbon paste electrodes<sup>21</sup> and polymeric media.<sup>3,22</sup> In spite of this progress, the added complexity of bienzymatic systems is still a major deterrent to using this type of biosensor design.<sup>4</sup>

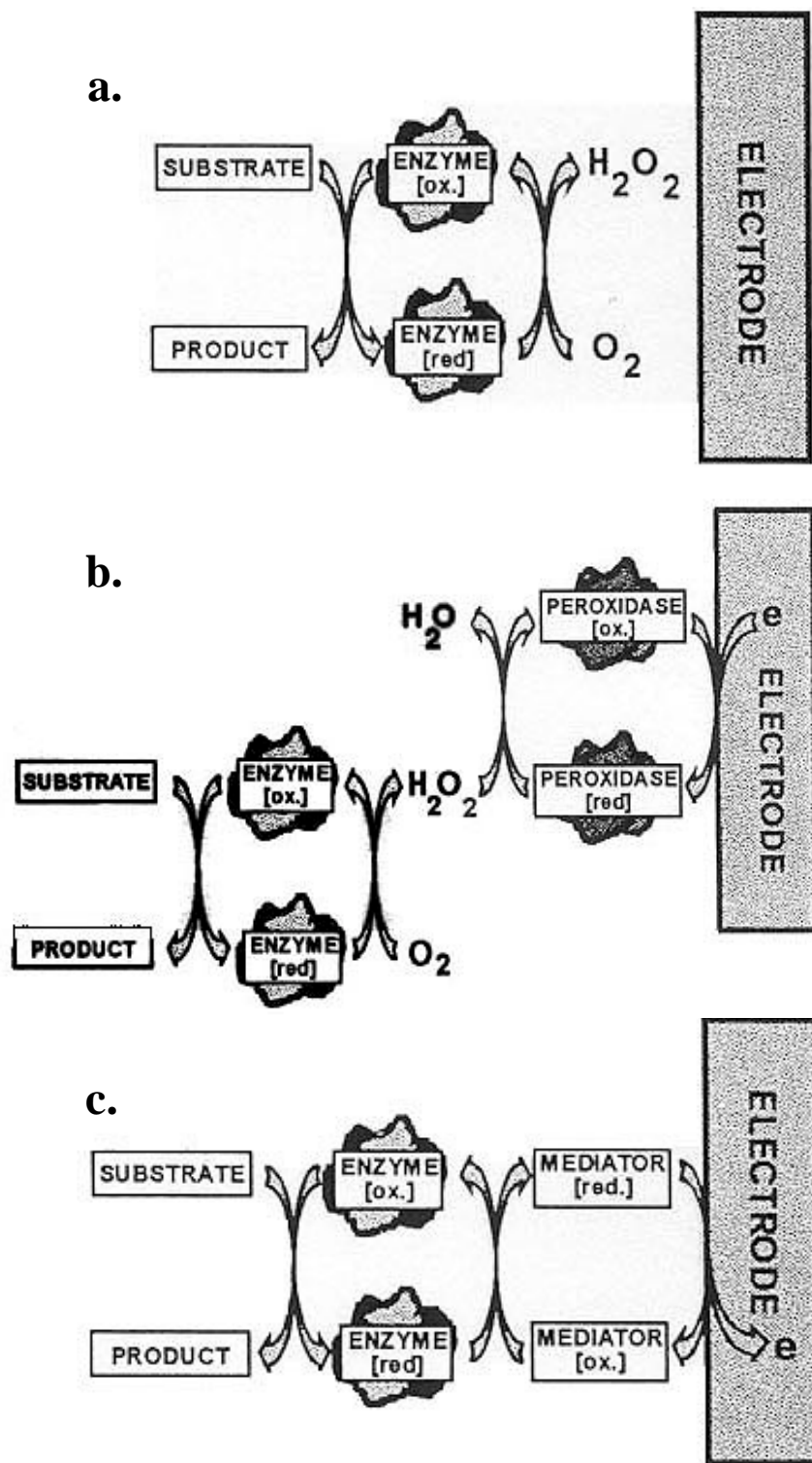


**Figure 1.7.** Popular approaches to electrochemical biosensor designs: a) oxygen consumption (8%) and hydrogen peroxide generation (62.5%) techniques; b) bienzymatic design (1.4%); and c) mediated enzyme techniques (28.1%). Percentages reflect each technique's usage in biosensor related electrochemical research (Figure from Ref. 4).

Using an artificial replacement, called an ET mediator, to substitute for an enzyme's natural electron acceptor is a fourth approach to biosensor models (Figure 1.7c). The mediator shuttles electrons between the electrode and the target enzymes. In addition to increasing the reproducibility and decreasing the dependence of oxygen on the system, the use of a mediator also assists with interfering substances. When oxidized at the electrode surface, ascorbic and uric acids are common fouling agents for electrochemical biosensors. Mediators, acting as electron shuttles, can eliminate this problem because they can be selected by the researcher to have a redox potential where contaminant oxidation of ascorbic/uric acid does not occur. As seen in Figure 1.8, a wide variety of mediators is available for research needs.

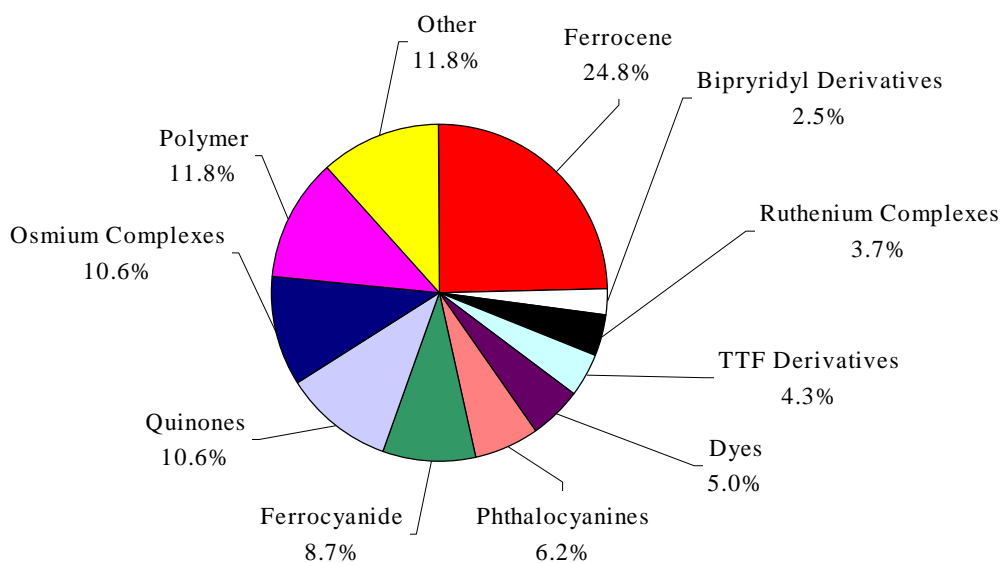


**Figure 1.8.** Mediating species used in mediator based electrochemical sensor designs.<sup>4</sup>

Unfortunately, the use of a mediating redox species complicates any potential use of this type of system for *in vivo* studies although prototype DNA sensors of this sort are already in development.<sup>23</sup> Inside a living organism, the diffusing mediating element would have to be controlled, most likely by immobilizing it along with the enzyme or protein onto the electrode surface. Scientists are attempting to incorporate the mediating component into a polymer film that coats the electrode surface. Metal complexes are already being electrostatically entrapped within polymer films, such as ethylene glycols<sup>24</sup> and polypyrroles,<sup>3,4</sup> but the research is still at a basic stage and is ongoing.

### 1.6.2. Direct ET Designs

Directly linking enzymes to electrode assemblies is yet another approach that, until recent technological advancements and innovative research, was not a major focus of electrochemists studying biosensor designs. Recent reports summarize the research activity involving direct electrochemical communication with enzymes.<sup>13,25</sup> This is an attractive methodology due to its mechanistic simplicity - direct ET connection between enzyme and electrode. With no diffusional elements involved, the mass transport of charge and other complications that arise with such diffusing systems are eliminated. As the result of this “direct wiring,” there is maximum coupling between the components at the electrode/solution interface making extremely fast response times achievable.<sup>1,13</sup> It is this type of configuration that is attractive for fundamental research into microamperometric biosensors and protein adsorption models.

***“Direct electrical communication between unmodified biological molecules and electrodes does not normally occur, because the redox active site is surrounded by an insulating protein shell.”***  
-Dr. H. Vaughan<sup>4</sup>  
University of Paisley, UK

### 1.7 SUMMARY AND PERSPECTIVE OF THESIS RESEARCH

In summary, models of biological systems that are to be used for research purposes in the bioanalytical field should incorporate three major components: 1) a protein or enzyme whose properties, structure, and function are highly understood; 2) a surface with specific and structurally well defined properties that can be easily altered and controlled to allow for relevant biochemical interactions (electrostatic; hydrophobic, etc.); and 3) an analytical technique that can measure protein adsorption in real time and potentially *in situ*.<sup>2</sup> In light of these requirements, the biological ET model that is the focus of the research presented within this thesis is introduced. Cytochrome *c* (cyt *c*), an important ET protein, is chosen based on its unique and well documented structure and properties. The protein will be directly immobilized on a surface through the use of a specific kind of SAM. Electrochemistry will

be used to delineate thermodynamic, kinetic, and mechanistic information about proteins adsorbed on self-assembled monolayers. SPM will be used to complement this approach with an overall motivation of gaining a molecular understanding of the electronic coupling at the protein/electrode interface. As alluded to earlier, understanding surface interactions in biological systems is vitally important, not only to biosensor and biocompatibility research, but also to delineating the basic process of how proteins adsorb to surfaces. Therefore, the specific focus of this research will be on the interfaces (surfaces) involved in this model. With the direct coupling aspect of the protein adsorbed on the self-assembled monolayer, careful attention must be given to the surface chemistry of the interfaces. By examining the ET kinetics and the adsorption properties of cyt *c*, as well as microscopic images of each surface, this research seeks to provide a deeper understanding of how proteins bind to surfaces and establish the interfacial electronic coupling. Thus, this dissertation, entitled “Interfacial Investigations of a Biological Electron Transfer Model: Cytochrome *c* Adsorbed on Self-Assembled Monolayers” is presented.

To place this discussion in perspective, it is important to mention here that the research in this thesis, while related to biosensors and biocompatible devices, is of a fundamental nature. The preceding discussions of this chapter serve only as a prelude to the work presented here. The research within this thesis is not aimed at developing an operational biosensor. As depicted in Figure 1.9, this research is completely fundamental, with immediate goals of providing information about the biological processes of ET and protein adsorption.

As with any research and development effort, fundamental studies, although not immediately applicable to society, are a necessary and important part of scientific

***“Lacking the necessary biological perspective, we have been miserable failures in mimicking the structure and function of natural tissue.”-Dr. David Grainger<sup>5</sup>***  
*Colorado State University*

advancements. Moreover, with the recent flux of new information about biological systems, the time is ripe for basic research to continue investigating the junction of man-made materials with biomolecules. It

is the hope of this researcher that this work will one day benefit in the development of operational and clinically useful biosensors or biocompatible materials.

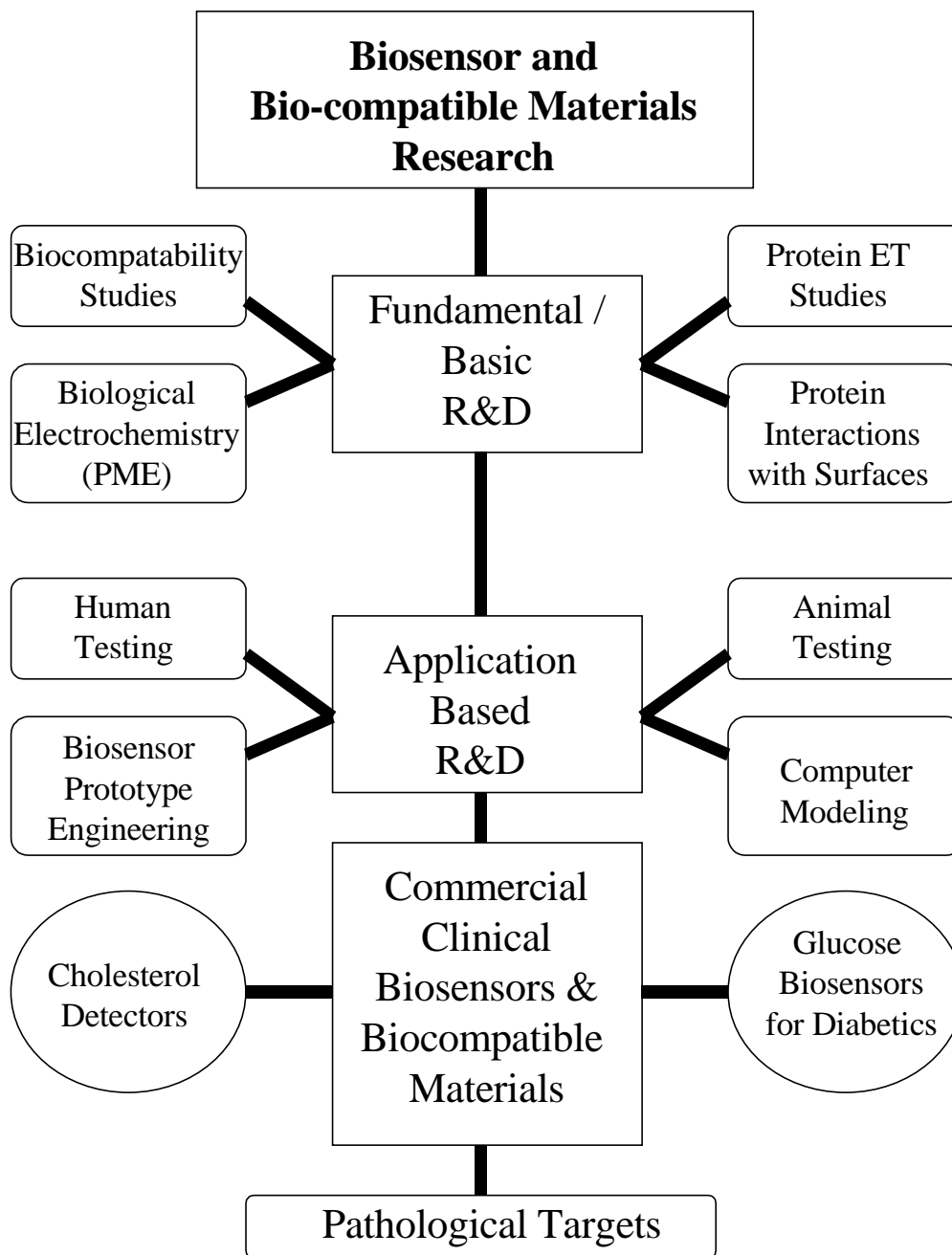


**Figure 1.9.** Flowchart illustrating the span of research in the areas of biosensor and biocompatible research. The research comprising this dissertation is basic, fundamental research – part of the early stages of the overall scheme.

## 1.8 REFERENCES

1. W.H. Scouten, J.H.T. Luong, and R.S. Brown, "Enzyme or protein immobilization techniques for applications in biosensor design," *Trends in Biotechnology*, **1995**, *13*, 178-185.
2. Mrksich and G.M. Whitesides, "Using self-assembled monolayers to understand the interactions of man made surfaces with proteins and cells," *Annual Review of Biophysics and Biomolecular Structure*, **1996**, *25*, 55-78.
3. A. Heller, "Electrical Connection of Enzyme Redox Centers to Electrodes," *J. Phys. Chem.*, **1992**, *96*, 3579-3587.
4. J. Davis, D.H. Vaughan, and M.F. Cardosi, "Elements of biosensor construction," *Enzyme Microb. Technol.*, **1995**, *17*, 1030-1035.
5. A. M. Rouhi, "Contemporary Biomaterials - Understanding surfaces is key to the design of clinically useful materials," *C&E News*, January 18, **1999**, 51-59.
6. M. Wahlgren and T. Arnebrant, "Protein adsorption to solid surfaces," *Trends in Biotechnology*, **1991**, *9*, 201-208.
7. A.L. Lehninger, D.L. Nelson, and M.M. Cox, *Principles of Biochemistry*, Worth Publishers: New York, New York, 1993.
8. J.J.R. Frausto da Silva and R.J.P. Williams, *The Biological Chemistry of the Elements - The Inorganic Chemistry of Life*, Clarendon Press: Oxford, 1991.
9. F.S. Millei, "Minireview Series: Biological Electron Transfer - Introduction," *Journal of Bioenergetics and Biomembranes*, **1995**, *27*(3), 261-351.
10. S.L. Wolfe, *Molecular and Cellular Biology*, Wadsworth Publishing Company: Belmont, California, 1993.
11. P. Barnes-Svarney, "Chapter 5 - The Human Body and Biomedical Science," *The New York Public Library Science Desk Reference*, Stonesong Press: New York, New York, 1995.
12. a) J. Janata, M. Josowicz, P. Vanysek, and D.M. DeVaney, "Chemical Sensors," *Anal. Chem.*, **1998**, *70*, 179R-208R. b) J.L. Anderson, L.A. Coury, and J. Leddy, "Dynamic Electrochemistry: Methodology and Application," **1998**, *70*, 519R-589R. c) J.L. Anderson, E.F. Bowden, and P.G. Pickup, "Dynamic Electrochemistry: Methodology and Application," *Anal. Chem.* **1996**, *68*, 379R-444R.
13. a) Proposal to the National Science Foundation by Edmond F. Bowden, "Protein Monolayer Electrochemistry," 1998. b) Proposal to the National Science Foundation by Edmond F. Bowden, "Protein Monolayer Electrochemistry," 1993.
14. a) O. Marti and M. Amrein, *STM and AFM in Biology*, Academic Press Inc.: New York, 1993. b) H.J. Guntherodt and R. Wiesendanger, Eds., *Scanning Tunneling Microscopy I - Springer Series in Surface Sciences 20*, Springer-Verlag: Berlin, 1992. c) H.J. Guntherodt and R. Wiesendanger,

- Eds., *Scanning Tunneling Microscopy II* - Springer Series in Surface Sciences 28, Springer-Verlag: Berlin, 1992. d) C. Bai, *Scanning Tunneling Microscopy and Its Application* - Springer Series in Surface Sciences 32, Springer-Verlag: Berlin, 1995. e) S. Magonov and M.H. Whangbo, *Surface Analysis with STM and AFM: Experimental and Theoretical Aspects of Image Analysis*, VCH: New York, 1996. f) L.A. Bottomley, J.E. Coury, and P.N. First, *Anal. Chem.* **1996**, *68*, 185R-230R. g) L.A. Bottomley, "Scanning Probe Microscopy," *Anal. Chem.*, **1998**, *70*, 425R-475R. h) R.J. Hamers, *J. Phys. Chem.* **1996**, *100*, 13103-13120. i) M.D. Ward and H.S. White, In *Modern Techniques in Electroanalysis*, P. Vanysck (Ed.), Chemical Analysis Series, John Wiley and Sons, Inc.: **1996**, *139*, Ch 3.
15. a) C.B. Gorman, "Encapsulated Electroactive Molecules," *Advanced Materials*, **1997**, *9*(14), 1117. b) C.B. Gorman, "Metallo dendrimers: Structural Diversity and Functional Behavior," *Advanced Materials*, **1998**, *10*(4), 295. c) C.B. Gorman, B.L. Parkhurst, W.Y. Su, K-Y. Chen, M.W. Hager, and I. Touzov, "A Model for Single-Molecule Information Storage," *Forth International Conference on Frontiers of Polymers and Advanced Materials*.
16. a) D.L. Feldheim and C.D. Keating, "Self-assembly of single e- transmitters and related devices," *Chemical Society Reviews*, **1998**, *27*, 1. b) M. Kastner, "Technology and the single electron," *Nature*, October, 16, **1997**, 389. c) "Making Devices Smaller, Brighter, and More Bendy," *Science*, **1998**, *282*, 2179.
17. R. Dagani, "Putting the Nano Finger on Atoms," *Chemical and Engineering News*, Dec. 2, **1996**, 20.
18. a) R.S. Cotran, V. Kumar, and S.L. Robbins; F.J. Schoen (Ed.), *Robbins - Pathologic Basis of Disease*, W.B. Saunders Co.: Philadelphia, Pennsylvania, 1994. b) Z. Zaheri and J.L. Tilly; R.A. Lockshin (Ed.), *When Cells Die: A Comprehensive Evaluation of Apoptosis and Programmed Cell Death*, Wiley-Liss Publishing: New York, New York, 1998. c) D. Watters; M. Lavin (Ed.), *Programmed Cell Death: the Cellular and Molecular Biology of Apoptosis*, Harwood Academic Publishers: Switzerland, 1993; d) I. Martinou, S. Desagher, J.-C. Martinou, "The release of cyt c from mitochondria during apoptosis of NGF-deprived sympathetic neurons is a reversible event," *Journal of Cell Biology*, **1999**, *144*(5), 883; e) E.P. Holinger, T. Chittenden, R.J. Luiz, "Bak BH<sub>3</sub> peptides antagonize Bcl-XL function and induce apoptosis through cyt c independent activation of caspases," *Journal of Biological Chemistry*, **1999**, *274*(19), 13298; f) M. Leist, B. Sirgler, and P. Nicotora, "Nitric oxide inhibits execution of apoptosis at two distinct ATP - dependent steps upstream and downstream of mitochondrial cyt c release," *Biochemical and Biophysical Research Comm.*, **1999**, *258*(1), 215; g) P. Jouvret, P. Rustin, and H. Mehmet, *Trans. of Biochemical Society*, **1998**, *26*(4), S341; h) J. Cai, J. Yang, D.P. Jones, "Mitochondrial control of apoptosis: the role of cyt c," *Biochimica et Biophysica Acta Bioenergetics*, **1998**, *1366*(1/2), 139; i) R.M. Kluch, E. Bossy-Wetzel, D.D. Newmeyer, "Release of cyt c from mitochondria: a primary site for Bcl-2 regulation of apoptosis," *Science*, **1997**, *275*(5303), 1132.
19. H. O. Finklea, "Electrochemistry of Organized Monolayers of Thiols and Related Molecules on Electrodes," A.J. Bard and I. Rubinstein (Eds.), *Electroanalytical Chemistry - A Series of Advances*, Vol. 19, 108-335, Marcel Dekker: New York, New York, 1996.
20. D. Mandler and I. Turyan, "Applications of Self-Assembled Monolayers in Electroanalytical Chemistry," *Electroanalysis* **1996**, *8*(3), 207-213.

21. a) J.Wang, Q. Chen, and M. Pedrero, "Highly selective biosensing of lactate at lactate oxidase containing rhodium-dispersed carbon paste electrodes," *Anal. Chim. Acta*, **1995**, *304*, 41-46. b) J. Wang, G. Rivas, and M. Cicharro, "Iridium-dispersed carbon paste enzyme electrodes," *Electroanalysis*, **1996**, *9*, 434-437.
22. G. Kenausis, Q. Chen, and A. Heller, "Electrochemical Glucose and Lactate Sensors Based on 'Wired' Thermostable Soybean Peroxidase Operating Continuously and Stably at 37° C," *Anal. Chem.*, **1997**, *69*, 1054-1060.
23. a) D.H. Johnston and H.H. Thorpe, "Cyclic Voltammetry Studies of Polynucleotide Binding and Oxidation by Metal Complexes: Homogeneous Electron-Transfer Kinetics," *J. Phys. Chem.*, **1996**, *100*, 13837-13843; b) M.E. Napier, C.R. Loomis, M.F. Sistare, J. Kim, A.E. Eckhardt, and H.H. Thorpe, "Probing Biomolecule Recognition with Electron Transfer: Electrochemical Sensors for DNA Hybridization," *Bioconjugate Chem.*, **1997**, *8*, 906-913; c) M.E. Napier and H.H. Thorpe, "Modification of Electrodes with Dicarboxylate Self-Assembled Monolayers for Attachment and Detection of Nucleic Acids," *Langmuir*, **1997**, *13*, 6342-6344.
24. a) T. Hatazawa, R.H. Terrill, and R.W. Murray, "Microelectrode Voltammetry and Electron Transport in an Undiluted Room Temperature Melt of an Oligo(ethylene glycol) - Tailed Viologen," *Anal. Chem.*, **1996**, *68*, 597-603. b) M.L. Longmire, M. Watanabe, H. Zhang, T.T. Wooster, and R.W. Murray, "Voltammetric Measurement of Ultraslow Diffusion Rates in Polymeric Media with Microdisk Electrodes," *Anal. Chem.*, **1990**, *62*, 747-752.
25. L.H. Guo and H.A.O. Hill, *Adv. Inorg. Chem.* **1991**, *36*, 341-375.

## **BACKGROUND, INTRODUCTION, AND OBJECTIVES OF RESEARCH**

### **CHAPTER TWO**

*“Good judgement comes from  
experience, and experience comes from  
bad judgement.” – Barry LePatner*

## **2. BACKGROUND, INTRODUCTION, AND OBJECTIVES OF RESEARCH**

### **2.1 BIOLOGICAL ELECTRON TRANSFER OF PROTEINS**

Biological electron transfer (ET) reactions and adsorption processes involving proteins play a critical role in certain vital physiological functions. For decades, chemical, physical, and biological scientists have focused their attention on understanding these ET reactions that are such a crucial part of life sustaining processes in living organisms, most notably photosynthesis and mitochondrial respiration. The rate and mechanistic aspects of the ET known to occur between certain proteins, as well as, the need for an effective strategy to study these complex reactions are at the heart of this type of research.<sup>1</sup>

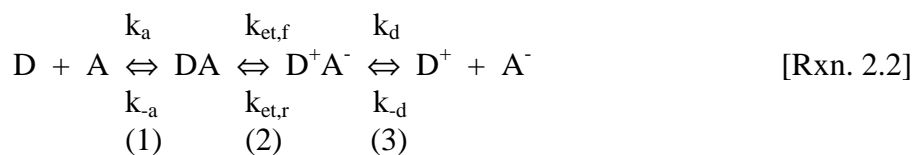
During the 1980's, research into biological ET reactions saw a significant and unprecedented advancement in both the experimental and theoretical treatment of this phenomenon. Of these advancements, two of the most noteworthy were the improvement of crystallographic methods concerning the structural characterization of biological molecules<sup>2</sup> and the theories developed based on donor-acceptor (D-A) chemistry for describing ET reactions.<sup>3</sup> By designating each redox partner or protein in an ET scheme as either an electron donor (D) or as an electron acceptor (A), the door was opened for the development of various strategies to probe ET reactions. The following sections, based on articles by Bowden and coworkers,<sup>1,4</sup> summarize this development and provide seminal examples of each strategy. Strategies for studying ET reactions can be divided into two types: homogeneous ET, where the ET occurs between two species in solution, or heterogeneous ET, where a single redox species undergoes ET at an electrode.

#### **2.1.1. Homogeneous Electron Transfer of Proteins**

Before the 1980's, homogeneous biomolecular strategies were the prevalent methodology for studying ET reactions between proteins. This strategy revolved around the intermolecular ET reaction of two independently diffusing redox proteins or redox molecules. The ET process, as depicted in the reaction below (Rxn. 2.1), involves the reduction of the acceptor redox partner (A) and the simultaneous oxidation of the donor partner (D). Assuming only simple one-electron transfers, the typical net reaction taking place is as follows:



Examining this type of reaction in greater detail, one can classify it as a diffusional ET reaction. That is, the reaction is dependent upon redox species diffusing up to one another and undergoing an electron exchange. Therefore, Rxn. 2.1 can be written more descriptively as Rxn. 2.2 below, which includes several distinct steps: the association ( $\pm a$ ) of D and A to form the D-A complex, the ET within that complex that forms the  $D^+A^-$  complex, and the subsequent dissociation ( $\pm d$ ) of the  $D^+A^-$  complex:<sup>5</sup>



Although this approach has been used to study the ET kinetics of the ET protein cytochrome *c* (cyt *c*) with a variety of redox partners, including other biomolecules as well as inorganic and organic redox species,<sup>6</sup> this strategy is not without its complications.

Kinetic analysis of the ET step (step 2) of this type of reaction (Rxn. 2.2) can be extremely complicated due to the complexity of this three step scheme. In addition to the forward and reverse rate constants ( $k_{\text{et,f}}$ ;  $k_{\text{et,r}}$ ) relating to the fundamental ET, the rate of the overall reaction can be controlled by the rate of association or dissociation ( $k_{a/-a}$ ;  $k_{b/-b}$ ).<sup>5</sup> With this in mind, researchers turned to the development of diffusionless strategies as a means of simplifying the kinetic analysis of ET reactions.

The first diffusionless strategies incorporated stable D-A complexes or protein/protein complexes. By utilizing these kind of complexes, the complicated kinetics of Rxn. 2.2 are dramatically simplified with the elimination of the diffusional aspects of the reaction scheme (steps 1 & 3 in Rxn. 2.2). Thus, the ET process is rendered completely intramolecular:



This significant change in approaching fundamental ET studies laid the foundation for many successful research efforts. Research into homogeneous intramolecular ET focused on covalently altering proteins, metal substitutions into proteins, and stable protein/protein complexes.<sup>3a,7</sup> Respective examples of each endeavor include work with ruthenated cyt *c* and cyt *b5* ET proteins,<sup>8</sup> Fe-Zn hybrids of hemoglobin,<sup>3a,7</sup> and cyt *c*/cyt *c* peroxidase or cyt *c*/cyt

*b5* protein complexes.<sup>9</sup> It was during this phase of protein ET research that a remarkable level of understanding concerning the distance dependence of ET, the importance of the orientation of D-A docking sites, and the role of thermodynamic driving force and reorganization energies was ultimately achieved.<sup>3a,7,10</sup>

### **2.1.2. Heterogeneous Electron Transfer of Proteins**

Typical heterogeneous ET experiments are performed using a protein or enzyme as either the electron acceptor (A) or as the electron donor (D), depending on the direction of the reaction. The other redox partner is an electrode, which contributes or receives the electron in the reaction. The ET of this reaction is direct, from protein to electrode, and does not require the presence of a mediating species.<sup>11</sup> Solid electrodes used to study heterogeneous ET include metal oxides<sup>12a</sup> and pyrolytic graphite.<sup>12b</sup> This strategy came into prominence during the 1980's but originated in the 1970's through research done in the laboratories of Hill,<sup>13</sup> Hawkrige,<sup>14</sup> and Kuwana.<sup>12a</sup> More recently, researchers have been successful using heterogeneous techniques to perform direct electrochemistry on complex biological systems.<sup>4</sup>

Researchers in Armstrong's group used electrochemistry to delineate mechanistic aspects, previously unknown to the scientific community, of succinate dehydrogenase (SDH).<sup>15</sup> SDH is involved in the mitochondrial respiration chain and is a rather large biomolecule with a molecular mass of approximately 97,000 Daltons which has several redox centers. Armstrong successfully immobilized SDH by adsorbing it onto a pyrolytic graphite electrode. The graphite surface facilitates the binding of the enzyme through adsorption sites that maintain the electroactivity of the SDH enzyme, an important aspect of heterogeneous ET studies. SDH is part of an enzyme complex known as Complex II and is an important part of the mitochondrial oxidative phosphorylation chain. Bound in a membrane, Complex II functions by oxidizing succinate to fumarate and passing electrons on to quinones that are also membrane-bound. In the laboratory, the hydrophilic and functional portion of the complex can be isolated and accessed on an electrode, allowing Armstrong to study the direct catalysis of succinate oxidation, as well as, the reverse reaction. Cyclic voltammetry on this system allowed for an unprecedented understanding of the molecular role of SDH in this complex biological process.<sup>4</sup>

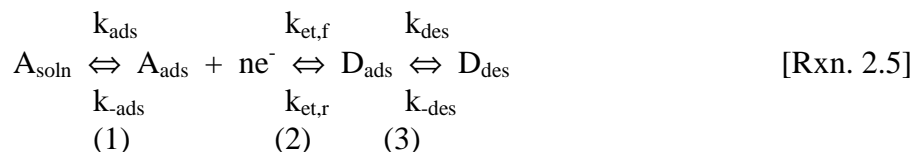
Another example of the potential of electrochemistry being used for the study intricate biological events emerged from the Hawkrigde research group.<sup>16</sup> Researchers in this lab immobilized cytochrome oxidase, another member of the respiration chain in the mitochondrion, known as Complex IV, in a fabricated bilayer that was intended to simulate the natural location of the complex in the cell membrane. Being extremely large, approaching 200,000 Daltons, and very complicated, housing multiple redox sites, the functional immobilization of this biomolecule on an electrode surface was, in itself, a formidable accomplishment. Its biological function is to catalyze the reduction of dioxygen and involves cytochrome oxidase exchanging electrons with its redox partner, cytochrome *c*. Through his electrochemical experiments, Hawkrigde was able to study the reversible ET occurring between immobilized cyt *c* oxidase in this membrane and freely diffusing cyt *c* in solution. This experimental arrangement bears a remarkable resemblance to what actually takes place inside the cell, and therefore may be an excellent model for studying the process.

These two examples serve to display the immense possibilities of electrochemistry as a tool for scientists to learn about complex biological processes. Electrochemistry, as will be shown in this research, is especially effective on simpler ET proteins and systems. In any event, it is clearly evident that heterogeneous ET strategies are significant and effective means for learning about the fundamental processes of protein adsorption and ET kinetics and thermodynamics.

Analogous to the homogeneous ET reaction scheme, mechanistic aspects of heterogeneous ET in proteins can be written in D-A terminology. The overall net reaction taking place during heterogeneous ET reactions is shown:



More specifically, the reaction is best described by including the adsorption and desorption processes of the protein on the electrode surface:



where the subscripts “soln,” “ads,” and “des” designate the status of the electroactive species in solution, adsorbed to the electrode surface, or desorbed from the electrode’s surface,

respectively.<sup>17</sup> As with the homogeneous ET scheme, clear evaluation of the ET step in this type of reaction is not easy due to the coexisting and complicating rates of protein adsorption and desorption. Again, the overall rate of reaction is subject to control by processes other than the ET, rendering a fundamental ET study difficult to accomplish with any degree of certainty. A strategy that simplifies the reaction and isolates the ET step is needed.

## 2.2. THE STRATEGY: PROTEIN MONOLAYER ELECTROCHEMISTRY

Over the years, various strategies have been developed to create a simplified model for heterogeneous ET studies. Early in the 1980's, researchers such as Niki<sup>18</sup> and Armstrong<sup>19-22</sup> concentrated their efforts into establishing an electrochemical model for this process that would alleviate the complicated kinetic analysis involved with heterogeneous ET.<sup>1</sup> Their work resulted in an approach known as protein monolayer electrochemistry (PME), a diffusionless heterogeneous technique where the protein is confined to the electrode surface. The direct adsorption of the protein to the electrode effectively eliminates the previously competitive processes of adsorption and desorption, and provides the necessary simplification to study fundamental ET. Adjusting Rxn. 2.5 to this simplification results in a reaction scheme similar to the diffusionless homogeneous reaction (Rxn. 2.3) and synonymous to the second step of Rxn. 2.5:



Thus, the ET step is totally isolated, resulting in a diffusionless, heterogeneous reaction mechanism governed by only one rate constant, the ET rate constant ( $k_{\text{et, f\&b}}$ ). The beneficial simplification provided by the use of PME as a strategy for studying biological ET reactions is depicted in Figure 2.1. It is thought that these protein/electrode systems can be utilized to simulate the important protein/protein complexes in living organisms.<sup>20</sup> A key obstacle to employing this strategy is the successful immobilization of a protein onto a solid metal electrode. Thus, much of the PME research being performed devotes attention to an effective means of accomplishing the adsorption of the protein. Through studying the direct electronic interactions taking place between the metal electrode and the protein in this type of model, a

deeper understanding of the biological ET process, as well as protein interfacing processes, can be achieved.

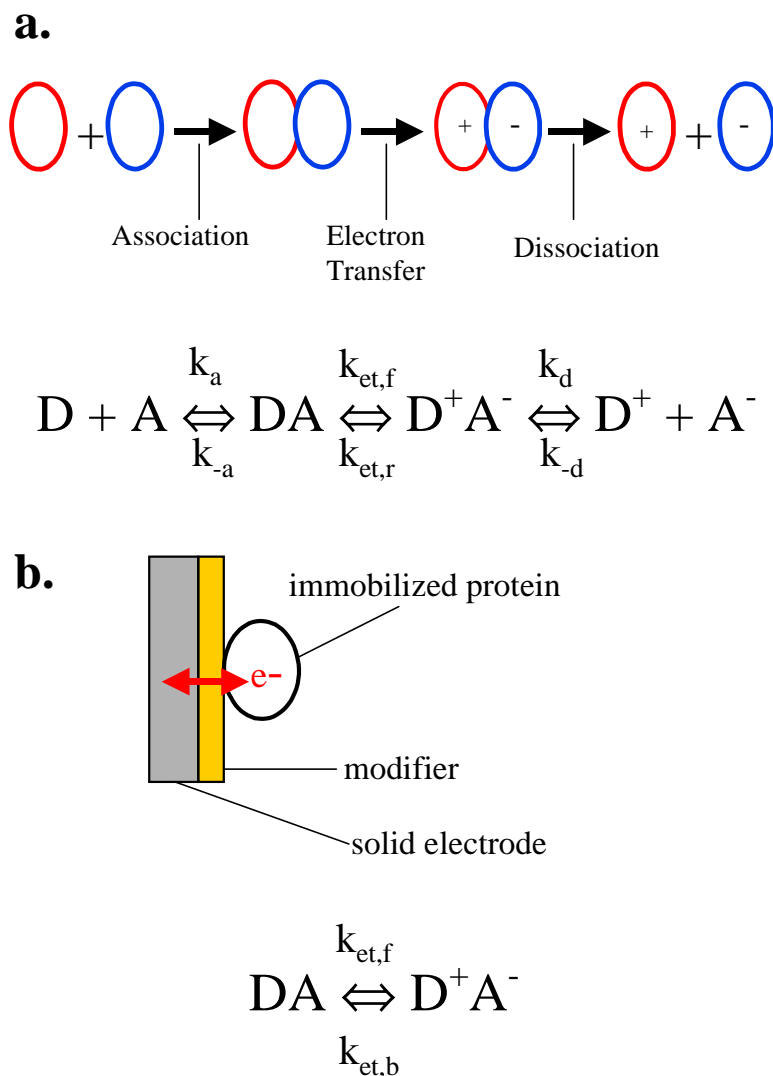


**Figure 2.1.** Illustrations and reaction schemes depicting the simplified strategy of protein monolayer electrochemistry or PME (b) versus traditional bimolecular reactions (a). Note that the immobilized protein in PME, (b), can serve as either the electron donor or the electron acceptor, with the electrode itself serving as the complementary redox partner.

PME has progressed through the years as an effective strategy for ET studies. Most notably, Niki has used PME in conjunction with spectroscopy to study the ET and conformations of cyt c and cyt c<sub>3</sub>.<sup>18</sup> In Armstrong's laboratory PME has been employed to elucidate the inorganic chemistry of ferredoxin, a prominent member of the Fe-S family of proteins.<sup>19-22</sup> Bowden and coworkers successfully utilized PME as a means of gaining an

unprecedented understanding of ET kinetics. In summary, PME has become an established technique for fundamental studies of biological ET in proteins.

### **2.2.1. PME: Advantages & Disadvantages**

What advantages does PME offer that make it so useful for studying biological ET? Performing PME allows researchers to acquire thermodynamic and kinetic data that, when used in conjunction with the crystal structure of the protein, prove to be extremely valuable in efforts to understand protein ET and adsorption. The advantages and limitations of PME as a method are briefly described here. Many advantages of this strategy have already been mentioned and are summarized, along with additional benefits and limitations of PME, in Table 2-1. When using PME, redox thermodynamics are readily obtained from simple cyclic voltammetry (CV) experiments, making the technique a popular tool for biochemists wishing to determine formal potentials of biomolecules in a variety of environments. In addition to thermodynamic measurements, PME is also effective at illuminating a more detailed understanding of interfacial interactions, such as the kinetics of ET and adsorption properties, between electrodes and proteins.<sup>4</sup>

As discussed earlier, the predominant benefit PME offers in terms of kinetic analysis is simplification. The ET is both heterogeneous and diffusionless, thus simplifying the kinetics by excluding any possible rate limitations arising from mass transfer (diffusion) and adsorption processes.<sup>4,23</sup> When PME is performed on simple ET proteins, as is the case in this thesis, the kinetic analysis is further simplified by the existence of a single redox site. This simplification allows the PME experiment to resemble self-exchange reactions which also have only one redox center. In self-exchange reactions, however, the electroactivity of this redox site is traditionally difficult to measure, whereas the electrochemical determination of heterogeneous ET rate constants are comparatively very easy. Moreover, the rate at which an electron travels from electrode to protein or vice versa is highly dependent on two important variables: the distance between donor and acceptor sites and the nature of the medium between the sites.<sup>24</sup>

PME addresses these two variables nicely, considering that in some instances, the modifying species on the electrode surfaces, such as self-assembled monolayers (SAMs), can act as an adjustable spacer that controls the distance between electrode (D/A #1) and protein

(D/A #2). Using a iterative series as a type of spacer, for which SAMs are an ideal example, one can use distance to manipulate ET rates without altering the activation barrier of the surface confined protein.<sup>1</sup> This kind of control in PME experiments offers the potential to study the distance dependence of ET.<sup>25</sup>

**Table 2-1.** Scientific Advantages and Limitations of PME<sup>1</sup>

	<b>PME Characteristic</b>	<b>Notes</b>
<b>Advantages</b>	Diffusionless ET	-Simpler kinetic analysis -Isolation of ET step -Diffusion is eliminated
	Controllable $\Delta G_{rxn}$	-Free energy of reaction variable via potentiostat control -Provides basis for determining reorganization energy
	$k_{et}^{\circ}$ at Zero Driving Force <sup>*</sup>	-A key parameter difficult to measure in homogeneous ET reactions
	Activationless Reaction Partner	-Electrode is activationless -Activation barrier is restricted to that of the protein itself (single site activation)
	Variable Distance / Timescale of ET	-Electrodes can be modified with different sized organic spacers (SAMs) -Allows for kinetic control without altering activation property of protein
	Electric Field Effects	-Enables investigation into the influence of electric fields on ET
<b>Limitations</b>	Non-ideal behaviors	-Electrochemical properties
	Signal to Noise Ratio (Faradaic vs. Nonfaradaic)	-Signal limited to a monolayer or less of protein -Background signals can be large -SAM technology beneficial -E/C techniques specifically designed to discriminate against charging current (background)
	Structural Characterization	-Two dimensional dispersion of protein on electrode -Interfacial characterization on the molecular scale is challenging -Spectroscopy / Microscopy developments
	Unknown Interfacial and Electric Field Complications	-Interfacial nature of system raises questions: -charge compensation? -Potential profiles across interfaces?

\* $k_{et}^{\circ}$  = standard electron transfer rate constant.

As far as the nature of the medium between the two reaction sites is concerned, PME experiments are usually performed in aqueous solutions with supporting electrolyte. Therefore, the environment surrounding the adsorbed protein can be altered at will and made to simulate physiological conditions. This is especially important when attempting to study biological molecules in their native forms. Furthermore, results obtained in physiological environments can be directly related to the overall goal of this research, bioanalytical devices.

An additional advantage of using PME is that the driving force behind the ET reactions, the free energy of the reaction, is infinitely variable via potentiostatic control of the electrode. This type of experimental manipulation is not available with solution D-A complexes, whose free energy only changes when the redox site is actually chemically altered.<sup>26</sup> The potentiostat controls the free energy of the electrons associated with the working electrode, allowing the experimenter to simultaneously control the direction of the ET reaction through an applied voltage and measure the current flow between the two reactants (electrode and electroactive molecules).

With heterogeneous ET reactions, such as those taking place in PME, the electrode exhibits no reorganization energy of its own and can be considered to be an activationless ( $\lambda_{\text{electrode}} = 0$ ) entity. The only activation barrier to contend with in PME is that of the proteins. This feature of PME allows the experimental results obtained to be directly attributable to a protein's specific characteristics or adsorption state, analogous to self-exchange reactions.<sup>1</sup>

The first of several limitations involved with PME deals with signal to noise issues. The magnitude of the current response, the analytical signal of the adsorbed ET proteins, is limited to the amount of material actually adsorbed on the surface, usually only a monolayer or submonolayer. The signal produced by this monolayer of proteins, sometimes called the faradaic current, can be obscured by the non-faradaic or background signal, also called the charging current (nonfaradaic current). When experimenting with such small signals, a large background current can render quantitative electrochemical measurements on the system very difficult.<sup>18a,b,e,20e,27</sup> To combat this problem, electrochemists sought electrode modifiers that are not only compatible and successful in confining specific proteins to a surface, but that are also effective at differentiating between faradaic and non-faradaic current, usually by

attenuating the charging current. One such modifier, which will be discussed in greater detail in a later section, is alkanethiolate self-assembled monolayers (SAMs). In addition to altering the systems interfacial characteristics to battle this problem, techniques have been developed that are specifically designed to address low signal to background current ratios. Pulsed voltammetry<sup>28,29,30</sup> and spectroelectrochemical techniques<sup>18a,b,e,31</sup> are examples of methods being used for this purpose.<sup>1</sup>

Another limitation found in PME is the lack of structural characterization of the system on the molecular scale. Being a surface bound model involving minute amounts of protein, the interfacial structures involved with PME are difficult to define. In comparison, homogeneous solutions and solid crystals are readily characterized by a variety of techniques. Therefore, most PME experiments are limited to proteins that have already been well characterized and are structurally defined. It is hopeful, however, that continuing developments in spectroscopy and especially scanning probe microscopy (SPM) will offer a promising outlook for this particular limitation of PME.

A related problem, and a major aspect of this research, is the inherent non-ideal properties that exist in PME results. Ideally, every protein on the surface would be adsorbed in the exact same manner with identical orientation, stability, and binding interactions. However, as will be discussed later, this is seldom the case. As a result, the redox properties of the proteins, such as formal potential and rate constants, are dispersed and classically non-ideal.<sup>1,32</sup> This broadened distribution of electrochemical properties is the focus of much research and will be very important in future sections.

Two positive aspects of PME is that it is a very promising strategy for obtaining ET data and that all of its limitations can be addressed, circumvented, or minimized. Much of the research done on PME revolves around controlling and/or understanding its limitations. The future of the PME strategy to study biological ET will be largely dictated by how successful the research is at overcoming these disadvantages. Success will be primarily rooted in fundamental thermodynamic and kinetic analysis of well understood proteins, an example of which is the research presented in this dissertation.

### **2.2.2. Modified Electrodes and PME**

A key component of PME is the successful development and prominent use of modified electrodes. Early biological measurements were performed using *cyt c* adsorbed on indium oxide<sup>33</sup> and tin oxide<sup>1,27b</sup> electrodes. However, the electrochemical response on these metal oxide films was difficult to interpret and was degenerative over time, a condition induced by the semi-conducting properties of these substrates. Non-biological kinetic testing on diffusionless electrochemical systems was conducted by Weaver and coworkers.<sup>23a,27b</sup> These systems displayed irreversible chemical behavior at the electrode surface. By 1984, researchers in Niki's laboratory used electroreflectance (ER) techniques to show the irreversible adsorption of *cyt c* on bare Au electrodes.<sup>18a</sup> It became apparent from studies like these that the irreversible adsorption of proteins onto bare metal electrodes would be problematic. Conventional electrodes typically generate poor responses from proteins which adsorb strongly to the metal surface and subsequently suffer from a loss of native ET function, commonly referred to as denaturation or protein unfolding.<sup>4,11,34</sup> The goal then is to modify the electrode surface in a way that can sustain the protein's ET function and natural structure.

Modified electrodes that permit PME without subsequent denaturation are of major interest to studying protein adsorption and fundamental ET. Gold electrodes have been modified with numerous compounds; two examples of modifiers are methyl viologen<sup>14</sup> and 4-4'-bipyridyl.<sup>13</sup> However, probably the most significant advancement in modification of electrodes for this purpose came from Taniguchi and coworkers. In 1982, Taniguchi introduced a novel technique involving the modification of gold electrodes with organosulfur compounds.<sup>35</sup> By maintaining the integrity and thus the native state of the protein while adsorbed on the surface, organosulfur modifications of electrodes make the comparison of these protein/electrode complexes to naturally occurring protein/protein complexes a more viable analogy. The use of self-assembled monolayers (SAMs) to modify electrodes has been a successful part of the biological electron transfer model being studied in the Bowden Research Group.

### **2.3. THE CYT C / SAM / Au ELECTRODE SYSTEM**

During the past several years, research in the Bowden group has been primarily focused on the PME of cytochrome c (cyt c) ET proteins adsorbed onto a gold electrode that has been modified with a self-assembled monolayer (SAM).<sup>27d,36,37</sup> A hypothetical depiction of this system is shown in Figure 2.2. Several years ago, researchers in the Bowden Group, along with collaborator Mike Tarlov of the National Institute of Standards and Technology (NIST), established that stable monolayers of equine (horse heart, HH) cyt c could be strongly adsorbed to a certain type of SAM.<sup>36c</sup> In this case, the SAM is terminated with an carboxylate functional group, which extend out into solution and create a negatively charged or acidic surface, ideal for the immobilization of such basic proteins as cyt c. This protein's natural binding partners, cytochrome c oxidase and cytochrome b5, exhibit anionic surface domains.<sup>37</sup> Thus, a negatively charged modified electrode surface provides an excellent model for studying the ET process between two such physiological partners. Using this system, fundamental knowledge of the electronic coupling between the electrode and the cyt c protein is desired to be able to design and understand effective models for studying ET.

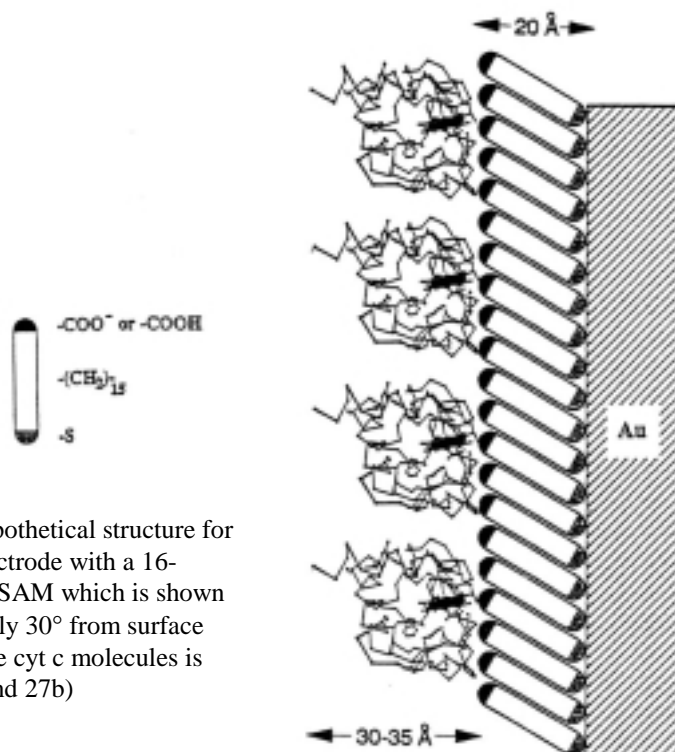


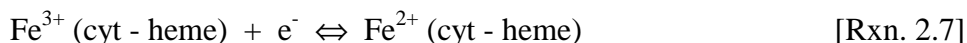
**Figure 2.2.** Illustration showing a hypothetical structure for cyt c molecules adsorbed at a gold electrode with a 16-mercaptohexanoic acid (16-MHDA) SAM which is shown ideally ordered and tilted approximately 30° from surface normal. Spacing and orientation of the cyt c molecules is speculative (Figures from Refs. 1,4, and 27b)

The following two sections of this thesis involve a more detailed and in depth look at the primary components that comprise this system: the protein, cyt c and the modifier or SAMs. A fundamental understanding of both components is critical to realizing how and why this model system is composed and the way it functions.

## 2.4 EQUINE (HORSE HEART) CYTOCHROME C

### 2.4.1. Physical and Structural Properties of Cyt c

Equine cytochrome c is an ideal prospect for use in PME. This highly characterized, water soluble protein, is one of the simplest and best understood proteins that exists. The crystal structure of horse heart (HH) cyt c has been known for quite some time and is displayed in Figure 2.3.<sup>38</sup> Cyt c is a globular protein, somewhat ellipsoidal in shape, with approximate dimensions of 34Å x 34Å x 30Å, and a molecular weight of approximately 12,500 Daltons. Within cyt c's polypeptide shell is an off-centered and embedded heme redox group whose edge (~ 5%) is exposed to solution (See Figure 2.3).<sup>39</sup> It is believed that this face of the protein is the functional end, where docking with redox partners occurs.<sup>4</sup> The heme's electroactivity is comprised of a simple outer-sphere ET reaction:<sup>4,40</sup>



The heme group resides in the protein in a porphyrin core that is covalently linked to the polypeptide backbone through bonds to cysteine residues at all four equatorial positions. The iron itself is low spin and six coordinate, possessing an octahedral geometry with axial ligands to histidine and methionine (See Figure 2.3). Additionally, cyt c possesses excellent chromophoric properties, a useful commodity for physical characterization, quantification, and spectroelectrochemical applications.<sup>27b,c</sup> A theoretical UV-Vis spectrum of the oxidized and reduced forms of cyt c is shown in Figure 2.4.

As is the case with many ET proteins, cyt c possesses an asymmetric charge distribution on its surface. The exposed heme edge is surrounded, predominantly, with positively charged lysine and arginine amino acid residues. These residues are uncompensated on this side of the protein, lacking negatively charged aspartate and glutamate residues, thus giving the protein a net asymmetric charge across its surface. This charge distribution is depicted in Figure 2.3. This phenomenon is believed to be biologically

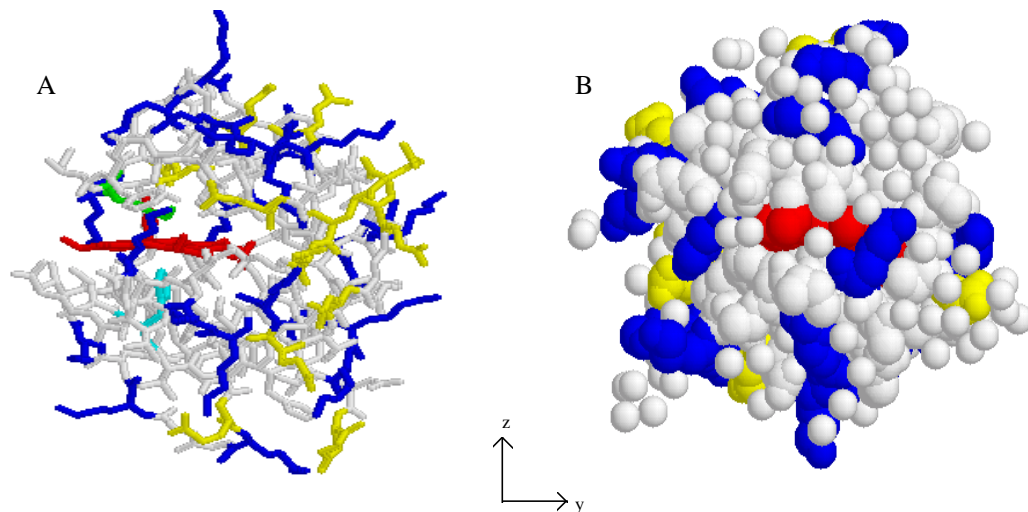


**Figure 2.3.** The ET protein equine (horse heart) cyt c (MW ~ 12,000 Da; Diameter ~ 3.0 - 3.5 nm). A) Crystal structure of cyt c depicting the asymmetric charge distribution around the heme group, an Fe core embedded in a porphyrin ring (shown in red). Positively charged amino acid groups (lysines and arginines) are shown in blue; negatively charged amino acid groups (aspartates and glutamates) are shown in yellow. Axial ligands to the iron heme, histidine, and methionine are shown as aqua and green, respectively. B) Protein is rotated 90° about the z axis and space filled to show the predominant uncompensated positive charge surrounding the embedded heme edge.

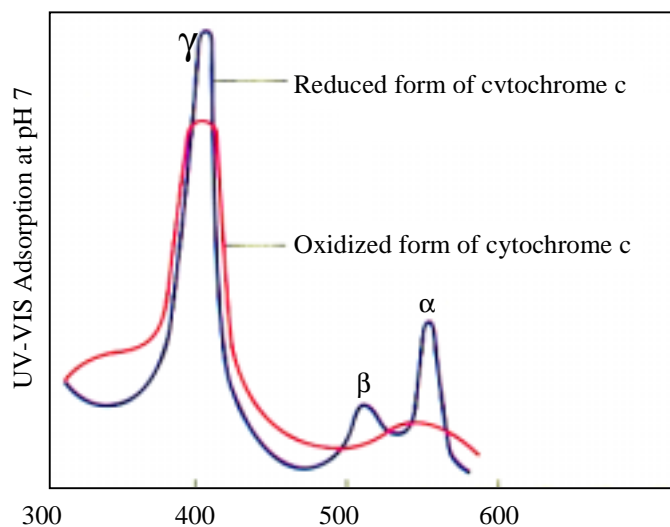


**Figure 2.4.** Simulated UV-VIS spectrum of the oxidized and reduced forms of HH cyt c; characteristic  $\alpha$ ,  $\beta$ , and  $\gamma$  bands of the reduced are labeled (Figure from Ref. 42).

relevant and purposeful by design, considering the protein binds to its natural redox partners primarily through electrostatic interactions.<sup>41</sup> It is this excess positive charge, in the form of lysine and arginine residues around the heme crevice, that make cyt c an ideal candidate for immobilization on a negatively charged surface, such as that of a carboxylic acid terminated SAM.

#### 2.4.2. Physiological Function of Cyt c

Besides being structurally well suited for PME applications, cyt c is a vital part of cellular respiration and therefore interesting on a physiological level as well. Cellular respiration or oxidative phosphorylation takes place in the mitochondrion of eukaryotic cells (See Figure 2.5). In aerobic cells, the mitochondrion is the principal producer of

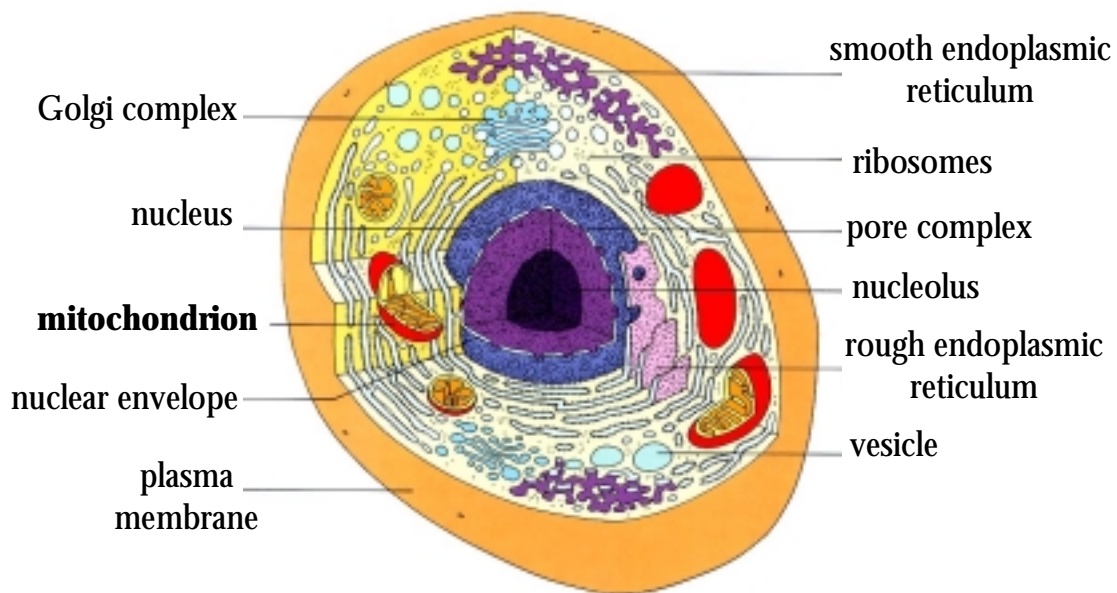


**Figure 2.5.** Cross sectional 3-D diagram of a eukaryotic cell; oxidative phosphorylation (cellular respiration) takes place in the mitochondria of eukaryotic cells (Figure from Ref. 42).

ATP, the chemical energy of living organisms, required for cellular functioning.

Mitochondria vary in size, but are typically about one micron in diameter, and can number from several hundred to one thousand per plant or animal cell. In general, the population of mitochondria in a cell is dependent upon that particular cell's function and metabolic activity. Each mitochondrion is composed of two major membranes: an outer membrane, a smooth

continuous covering which encases the entire structure but is permeable to small ions/molecules, and an inner membrane, made up of numerous folds and projections called cristae (Figure 2.6). These cristae, which are largely impermeable to most ion/molecules, possess a large surface area and house an inner compartment in the mitochondria called the matrix. The matrix is a concentrated solution of enzymes and chemicals involved in energy synthesis reactions or energy metabolism. Thus, the mitochondria are often referred to as the cell's "power plants."<sup>42</sup>

Cyt c is located between the inner membrane and the outer membrane of the mitochondrion. Its primary function within these membranes is to act as an electron shuttle between two locations in the mitochondrial electron transport system, shown in Figure 2.7. As seen in this figure, the inner membrane is home to the four major complexes, known as Complexes I-IV, which comprise the cell's electron transport system. Cyt c occupies a position in this chain that is analogous to the previously mentioned role of plastocyanin in the photosynthesis chain (Chapter 1).<sup>42</sup> Cyt c, a mobile electron carrier, delivers an electron from Complex III, also known as cyt c reductase, to Complex IV, or cytochrome oxidase. It is clear that the protein adsorption process and, of course, the ET process are major steps in this cycle and warrant study, if for no other reason, than to expand our understanding of these simple biological events. Thus, cyt c is a not only a vital biological molecule, but is by its very nature, an excellent selection for ET models.

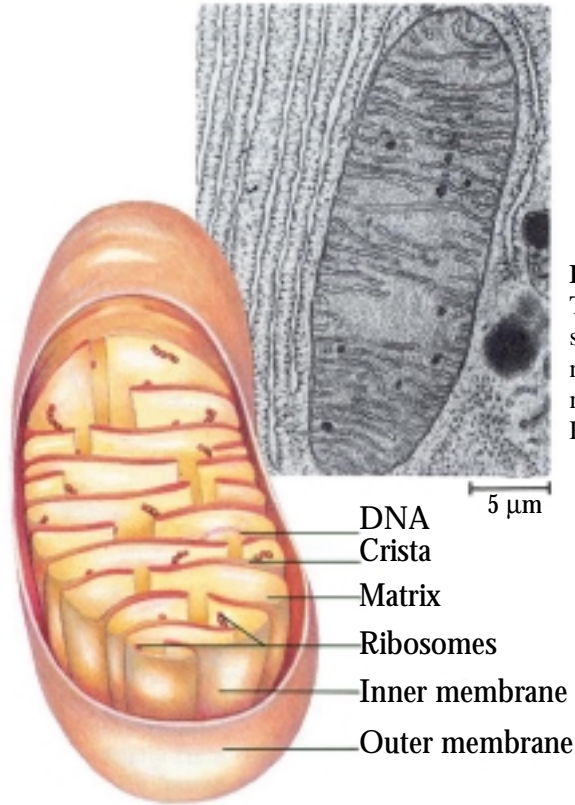


**Figure 2.6.** Mitochondrion structure. The electron micrograph verifies the smooth outer membrane and the numerous infoldings of the inner membrane, called cristae (Figure from Ref. 42).

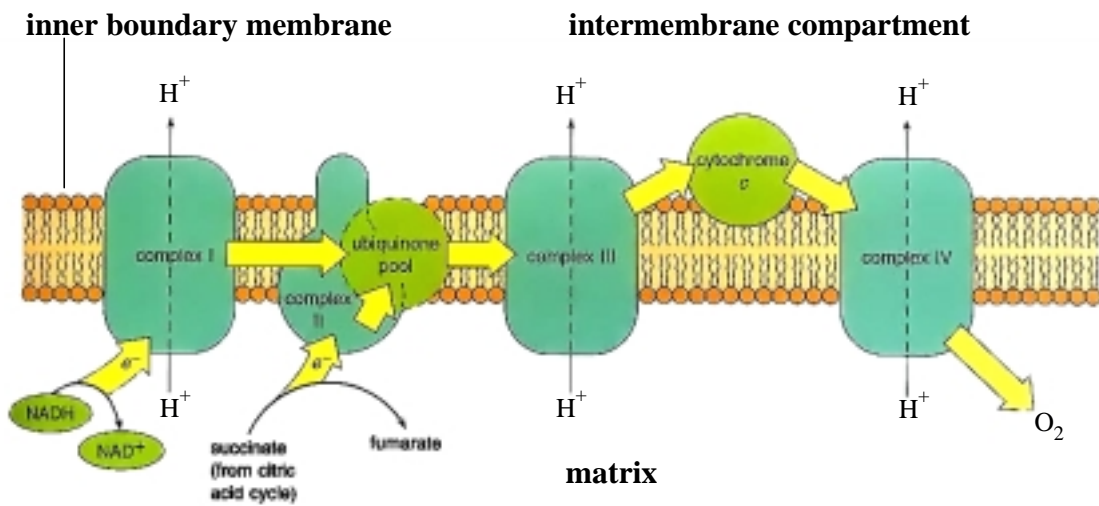


**Figure 2.7.** The mitochondrial electron transport system with four major complexes imbedded in the cell membrane and two smaller electron carrier species, ubiquinone and cytochrome c. Electron flow is shown as yellow arrows; hydrogen movement as dashed, black arrows. Note that cyt c is the only mobile electron carrier, freely moving in the intermembrane compartment (Figure from Ref. 42).

## **2.5 SELF-ASSEMBLED MONOLAYERS (SAMs)**

### **2.5.1. General Characteristics**

Alkane based SAMs are a type of spontaneously formed, highly organized molecular adlayer whose singular members share a common orientation. A generic picture of a SAM, showing the four major components of the molecules involved in the self-assembly process and their corresponding terminology, is shown in Figure 2.8. Each component, the metal substrate, the headgroup, the alkane chain, and the terminal group, plays a specific role in the formation and subsequent structure of a SAM. Therefore, this specific terminology is vital to understanding the ensuing discussion of SAMs and their use in subsequent research studies. The interplay of all these components give SAMs and the materials they modify certain characteristics that make them attractive for many research purposes. The structure and properties of SAMs have been and continue to be well characterized with a variety techniques including the following examples: electrochemistry,<sup>43</sup> ellipsometry (wetting), contact angle goniometry (CAG), infrared spectroscopy,<sup>44</sup> x-ray photoelectron spectroscopy (XPS),<sup>45</sup> and mass spectrometry (MS).<sup>46</sup> The following discussion attempts to convey the results of many of these research studies and summarize some of their major conclusions about the structure of SAMs in aqueous solution. Here, we limit the discussion to SAMs where water serves as the solvent, keeping in mind that any solvent, including water, can affect the properties of a SAM. As will be seen, SAMs essentially provide scientists with a well defined and controllable surface, an extreme advantage for surface related research. First, however, the process of self-assembly and the roles of each component of the SAM will be examined, starting with the interaction between the metal substrate and the headgroup.

### **2.5.2. The Process of Self-Assembly**

The high degree of organization that is inherent in SAMs is initiated by the affinity of the headgroup for the substrate. A major class of SAMs is derived from molecules with sulfur based headgroups such as thiols, disulfides, and sulfides. This family of headgroups have a high affinity to form metal-S bonds with the coinage metals (Au, Ag, Cu)<sup>47</sup> as well as with other metals such as platinum and mercury.<sup>48</sup> Gold, however, is the most effective substrate for SAM formation, and is the predominant metal seen in SAM literature.<sup>43</sup> Several

literature reviews on Au-alkanethiolate based SAMs are available,<sup>43,49</sup> but research involving SAMs in recent years is rather expansive.

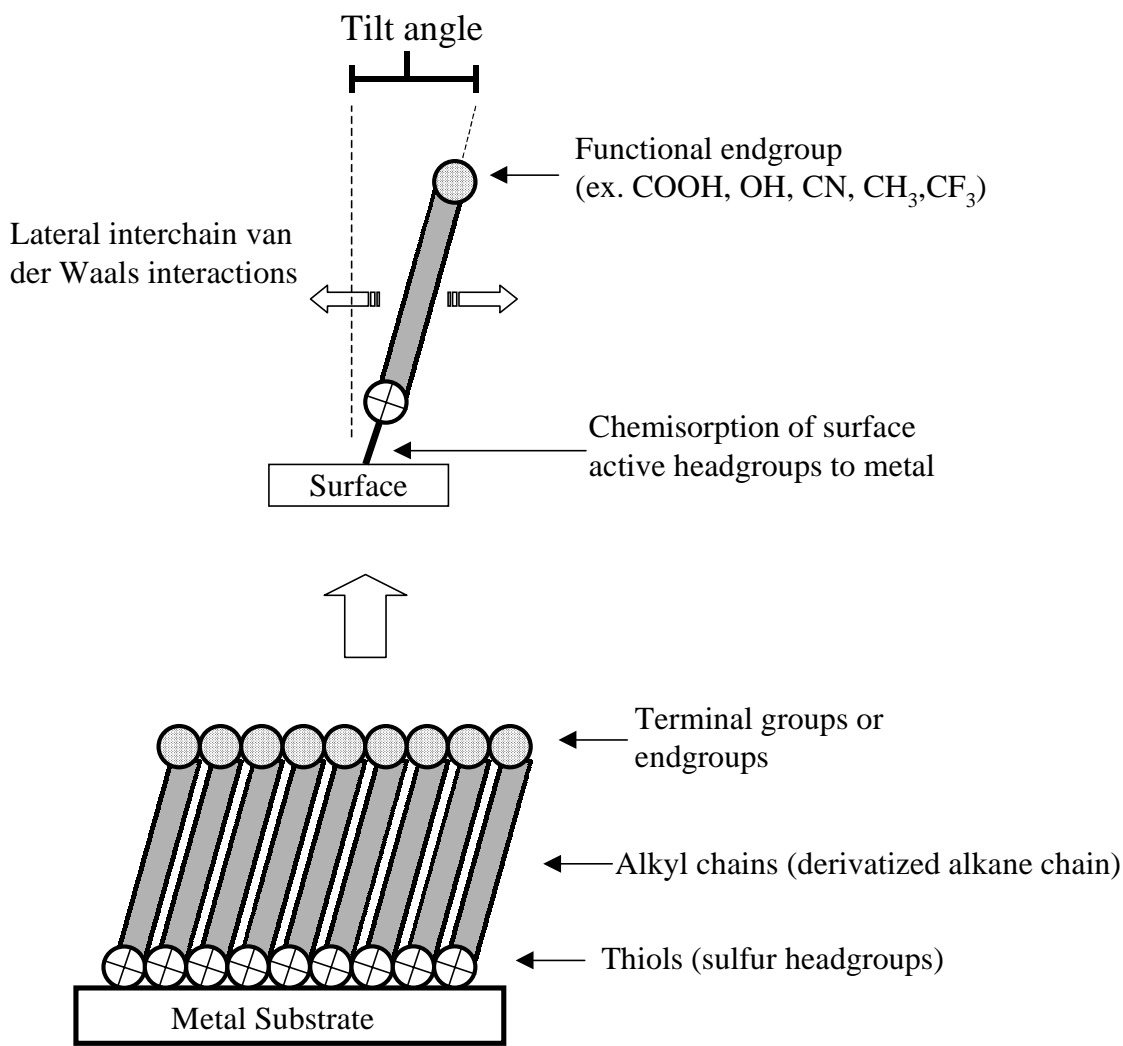


**Figure 2.8.** Schematics of a self-assembled monolayer highlighting important aspects of the system: endgroups, headgroups, alkane chains, tilt angle, substrate, and lateral interactions between the components that comprise the SAM.

Using Au as an example, the self-assembly process begins with the sulfur headgroups being chemisorbed to the Au surface from a homogeneous thiol solution. Subsequently, the high density of Au-S bond formation brings the alkyl chains of the molecules into van der Waals contact. The tails of the anchored molecules then seek to maximize the intermolecular van der Waals interactions. If in aqueous solution, the alkanethiolates experience

hydrophobic interactions among the alkane tails. The chains, being predominantly hydrophobic hydrocarbons, will try to achieve the most energetically favorable situation by isolating themselves and minimizing their exposure to the aqueous or polar layer.<sup>50</sup> To accomplish this, the chains will actually bend, adopting a tilt angle of 28-40° from the surface normal; the tilt angle variability being directly attributable to different terminal groups SAMs can have, as well as, other specific experimental conditions.<sup>43,51</sup> Ellipsometry of SAM modified Au substrates has shown that the initial chemisorption of the headgroups occurs very rapidly, covering the gold surface with thiolate material almost immediately. Over a longer period of time, however, the alkane chains undergo rearrangement as they maneuver to maximize their lateral interactions with other chains.<sup>52</sup> Therefore, a substantial degree of order in the monolayer is achieved quickly but can increase if the self-assembly process is allowed to continue over time. The manifestation of the self-assembly process is an organic film composed of a compact layer of hydrocarbon which creates a substantial barrier at the metal/solution interface. The properties of this barrier are influenced by two variables: the thickness of the SAM and the endgroup used at the SAM/solution interface.

### **2.5.3. Alkane Chain Length**

Depending on the number of methylene groups (-nCH<sub>2</sub>-) in the alkane chains of a SAM, the nature of the packing density can vary from highly crystalline, extremely ordered monolayers to less ordered, “liquid-like” films (See Figure 2.9). This property of SAMs is somewhat influenced by temperature and by the choice of terminal group employed, but is generally considered to be a definitive trend.<sup>43,44,53</sup> At room temperature, SAMs comprised of longer chains (nCH<sub>2</sub> > 6-8) tend to be extremely impermeable to both solvent and electrolyte ions.<sup>43,54</sup> Effectively, the strong lateral interactions previously discussed cause the monolayer to be a virtually impenetrable layer, void of solvent molecules or ions from the contact solution. In fact, SAMs comprised of alkane chains of twelve or more methylene units in contact with an aqueous solution, barring any other influences, is considered to be an effective solid-liquid interface.<sup>54b</sup>

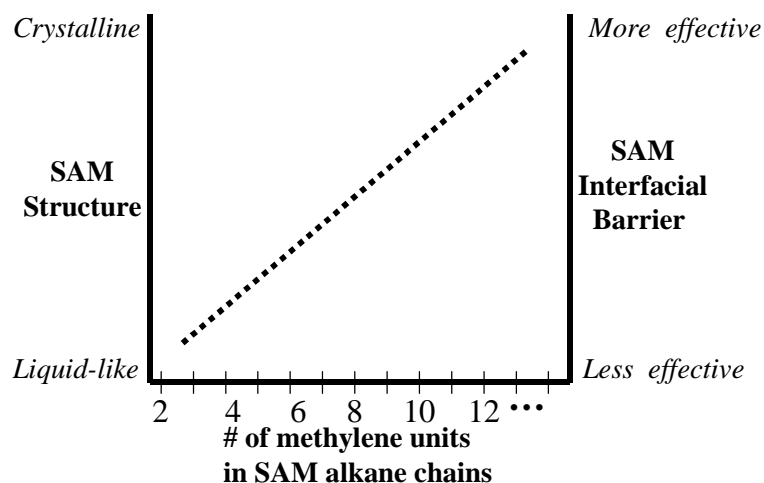


**Figure 2.9.** SAM structural property trends based only on alkane chain length in SAM. Note: Figure is designed to illustrate to the reader the general trends involved with SAMs as derived from literature reports<sup>43</sup> and is not based on actual data collected in this research. More accurately, the relationship shown is not linear. Also, the illustration ignores any effect from endgroups (discussed later).

The reasons for this phenomenon relate to the aforementioned lateral interactions taking place within the SAM during the self-assembly process. Longer alkane tails will have a greater propensity to accommodate significant van der Waals interactions with other chains. This is borne out with infrared spectroscopy (IR) studies which indicate that SAMs made of longer alkanethiols are predominantly hydrocarbons in *all-trans* conformations,<sup>44a,51</sup> meaning that the alkane chains are all as close to possible, leaning into each other at an angle to maximize their interaction. This type of film is extremely ordered, an achievement only possible if solvent and ionic species are energetically excluded from the alkane medium. On the other hand, IR results on shorter alkanethiolates reveal films with a higher density of gauche defects,<sup>44a,55</sup> an indication that random chain orientation exists. This result is a reflection of the shorter chains lack of an alkyl tail long enough to dictate the dominant lateral interactions. The inherent motion of the shorter SAMs results in a more mobile (“liquid-like”) state on the surface and is a less effective barrier at the interface.

An important caveat of these films is that as they become thicker, their ability to passivate the electrode surface is greater. That is, if the film is substantially thick enough to create a barrier at the interface, it can prevent redox species in the solution above the film from making contact with the metal substrate. This passivation has two effects: 1) it decreases the current response of an electroactive species in solution by severely hampering the rate of ET, allowing current to flow only at defect sites in the film or forcing it to tunnel

through the hydrocarbon layer<sup>51</sup> and 2) it decreases the background signal or charging current of the electrode.<sup>43</sup> The first effect is the reason that SAM research is at the heart of many corrosion studies,<sup>56</sup> effectively “protecting” metal surfaces from chemical attack. Many scientist use redox active molecules in solution to detect the presence of defect sites in the SAMs. This is a popular way of studying SAM structure and is called redox probing of SAMs.<sup>57</sup> The second effect, involving charging current, is brought into focus later in this chapter. While chain length provides a definite variable that controls SAM structure, the endgroups of the SAM can be extremely influential on the overall properties of the SAM.

#### **2.5.4. SAM Endgroups (Terminal Groups)**

The terminal group or endgroup of the SAM is probably the most important component of a SAM, primarily because it is the component that is exposed on the surface. Up to this point in the discussion, it has been assumed that the endgroups of the SAM were simply methyl groups. There are however, many other possibilities. Numerous synthetic manipulations of alkanethiolates allow for SAMs to be created with a variety of terminal groups. These functionalities can alter the packing order, as well as the hydrophobicity and, in some cases, the charge density of the SAM/solution interface. Thiols manipulated for SAM purposes are often referred to as  $\omega$ -substituted alkanethiolates. Examples of common  $\omega$ -substituted alkanethiols include molecules that have been terminated with methyl, hydroxyl, carboxyl, amine, fluorinated hydrocarbons and cyano functional groups. SAMs with more exotic endgroups, such as succinate,<sup>54b</sup> or electroactive moieties, such as ferrocene,<sup>58</sup> have also been used. Instead of composed of only  $\omega$ -substituted alkanethiols, aromatic based SAMs have also been explored.<sup>57a,b</sup> The variety of  $\omega$ -substituted alkanethiols utilized in SAM studies is staggering, but for the purposes of this dissertation, this discussion will limit itself to some of the more common, nonelectroactive functional groups just mentioned (-CH<sub>3</sub>, CF<sub>3</sub>, -OH, -COOH, -CN, etc.).

There have been many research studies based on the characterization of SAMs with different terminal functional groups. Ellipsometry, CAG, IR spectroscopy, XPS, and electrochemical redox probing and capacitance measurements have all been employed at one time or another to delineate specific SAM properties related to different endgroups.<sup>43,51,59</sup> The following discussion attempts to summarize the major conclusions from these various

literature reports. Figure 2.10 also displays the results of this work and the major trends concerning SAMs with different endgroups.

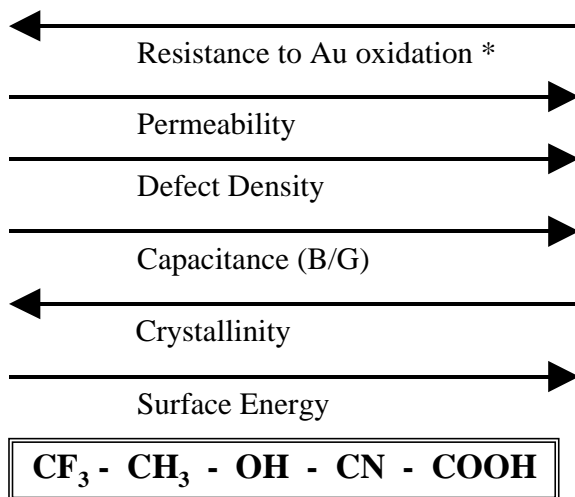


**Figure 2.10.** Endgroup related trends of SAM properties.<sup>43,51</sup> (\* Resistance to Au oxidation showed the specific trend of CF<sub>3</sub> - CH<sub>3</sub> - OH - COOH - CN.)<sup>51</sup>

Ion penetration into the SAM or SAM permeability has been extensively investigated by many of the techniques mentioned in the preceding paragraph. Normally, invasion of ions into the film occurs at defect sites in the monolayer. SAMs with larger defect densities tend to be more permeable toward solvent and/or ions, and are not as effective as an interfacial barrier. Consequently, electrochemical current suppression at the metal electrode is more difficult and the background signal for the modified Au substrate is larger. Of the functional groups tested as SAM endgroups in the specific literature examined, the permeability of the films in aqueous solution were as follows:<sup>43,51</sup>



The same trend was found for background capacitance and defect density, adhering to the previous discussion. Ellipsometry measurements on these SAMs revealed that the surface energy of these films also increased in the same order. The opposite trend, however, was seen for IR studies focusing on the crystalline nature of the different SAMs:



From these trends one can derive that ion penetration is not highly dependent on the wetting properties (hydrophobicity) of the SAMs. Instead, it appears that the barrier properties of the SAM are impacted more by the crystallinity and packing order of the hydrocarbon portion of the film. This conclusion is drawn because the hydrophobic cyano terminated SAMs fall in the trends between the alcohol and carboxylic acid terminated SAMs, whose wettabilities are both very hydrophilic. Thus, these trends suggest that the terminal can exert influence on the packing order and density of the SAM.<sup>43</sup>

A common procedure for testing the stability of a SAM modifying a Au substrate is to electrochemically measure the film's ability to inhibit Au oxidation.<sup>43,51</sup> For the Au surface to be oxidized, electrolyte solution must physically penetrate the SAM and contact the metal surface.<sup>43</sup> On a well formed SAM, this type of penetration usually occurs only at pinholes and defect sites in the SAM. Therefore, the extent to which a SAM passivates the Au oxidation process can be used as a measure of SAM structure and stability. The ability of the different terminated SAMs to block the oxidation of Au was as follows:<sup>51</sup>



According to all of these observed trends, SAMs composed of fluorinated alkanethiolates provide the best barrier properties and have superior overall stability. This observation is corroborated by both IR and contact angle results on fluorinated films which show an extremely crystalline structure coupled with very little tilt angle. Alcohol and methyl terminated SAMs, in comparison, also have a high degree of crystallinity but possess much more significant tilt angle in the packed chains. Nitrile SAMs have crystalline packing to a degree but suffer from several complications that alter these SAM's stability. The nitrile terminated SAMs exhibited very sporadic wetting characteristics and very poor electrochemical properties concerning the inhibition of Au oxidation and redox probing. It is believed that these cyano based SAMs may undergo significant rearrangement when in contact with aqueous solution and that measurements made on these films are severely impacted by variable chain conformations inherent in these particular SAMs.<sup>51</sup>

Clearly, the  $\omega$ -substituted alkanethiol based SAM with the worst blocking characteristics is the carboxylic acid terminated SAM. All measurements made on the acid terminated films revealed a very liquid-like structure and a very porous barrier property with

regard to electrolyte ions and solvent. Data collected for the COOH SAMs suggests that the mere presence of the carboxyl group may actually disrupt the alkane packing of the SAM, thereby severely hampering its ability to act as a barrier. The acid group at the interface of the SAM effectively negates the lateral interactions of several methylene units. Therefore, to achieve the same blocking characteristics as SAMs terminated with other functional groups, carboxylic acid terminated SAMs require a significant increase in the number of methylene units in their alkane chains. It is believed that with long enough chains, carboxylic acid terminated SAMs can be created that are more impermeable.<sup>51</sup>

It should be noted that if the tail groups are charged species, the situation changes. Introducing charged groups as endgroups will have the same effect as ions penetrating the SAM interface and decrease the SAM's effective hydrocarbon thickness. Furthermore, the influence of the endgroups can be altered by the solvent being used. All of the previous comparisons were done in aqueous solution where hydrophilic endgroups will be more susceptible to invasion of both solvent and supporting electrolyte ions.<sup>51</sup> Likewise, hydrophobic terminated SAMs will provide a much greater barrier toward permeation in aqueous solutions, but will be less effective at the task in organic, nonpolar solvents. This type of solvent can literally intermix with the hydrophobic SAM and loosen the chain packing making it more vulnerable to ions in the solvent.<sup>60</sup> Manipulating the compositions of solvent mixtures by varying the percentages of organic and aqueous phases has been used to study SAM structure.<sup>50</sup>

It has been proposed that the size of the endgroups plays a role in the spacing of the alkane chains of a SAM.<sup>51,61</sup> Consider, for example, the bulky functional group of a carboxylic acid (COOH). The analogy has been made that a carboxylic acid terminated SAM is like having beach balls on a beach of pebbles, where the acid groups are represented by the balls and the Au atoms of the substrate are the pebbles on the beach.<sup>54b</sup> To a molecule in solution, the surface of the SAM is dominated by the properties of the bulky endgroups. The idea is that the endgroup-endgroup interactions, which can range from steric/electrostatic repulsions to hydrogen bonding, are vital to the packing structure of the SAM. Even SAM/solvent interactions, such as H-bonding between water molecules and the carboxylic acid endgroups, can alter the properties of the SAM/solution interface. These interactions

can instigate different levels of order/disorder and, as previously mentioned, alter the inherent tilt angle of the SAM chains. Hydrogen bonding among both alcohol and acid terminated SAMs has recently been reported as a stabilizing influence on SAMs.<sup>62,59b</sup>

The ability to alter both the terminal group of the SAM and the length of the alkane chains, thereby changing the very structural nature and interfacial properties of the film, allows for enormous versatility in designing SAMs with tailored surfaces and specific purposes. To summarize, the ability of molecules to form a compact and subsequently stable SAM is dependent on three factors: 1) the strength of the binding between the headgroup and substrate; 2) the interactive forces at work between adsorbed molecules forming the SAM and; 3) the interaction of the molecules terminal groups with each other and with the surrounding environment. A stable SAM will maximize all of these interactions<sup>59b,c</sup> and, as a result, create a useful surface for a wide range of chemical applications.

### **2.5.5. SAM Applications**

SAMs have found widespread use in a variety of applications due to their unique properties and the relative ease with which their structural and topographical characteristics can be altered. The insulating nature of alkanethiolates on metals makes them resistive to chemical attack, a protective coating on the surface they modify. Thus, SAMs are used in many corrosion related studies.<sup>56</sup> This property of SAMs has also encouraged their use in electrochemistry where alkanethiolate modified electrodes have a drastically reduced magnitude of charging current, allowing for an accentuation of the electroanalytical signal.<sup>43</sup> Furthermore, SAMs have been applied to nanotechnology research, both as a coating for molecular electrical components,<sup>63</sup> and as a template for well defined scanning probe microscopy (SPM) experiments.<sup>64</sup> On a larger scale, the ability of a SAM to quickly and effectively coat a large area of substrate in a very specific nature, has captured the interests of scientists studying adhesion and lubrication.<sup>54a,65</sup> Perhaps, however, the greatest application of SAMs resides in their ability to provide a manageable surface that can easily withstand physiological conditions, making them attractive surfaces for bioanalytical and biocompatibility research.<sup>66</sup>

Indeed, SAMs offer exciting possibilities for both chemical sensors and biological studies. The use of SAMs as a primary component in biosensors is already the target of many

researchers.<sup>4,49a,b</sup> The ability to alter the functionality at the SAM/solution interface introduces a level of controlled selectivity to any potential sensing surface, a much desired quality in such devices. Additionally, SAM technology can be employed in biological models to help simulate biological entities like the lipid bilayers of cell walls.<sup>67</sup> Because SAMs can be specifically functionalized at their outer surface, where electron donor/acceptors can be directly attached, SAMs are used in the construction of novel ET models<sup>4,51</sup> and as platforms for specific interactions with proteins.<sup>68</sup> It is in this capacity that SAMs are a major part of the research effort in the Bowden Group.

#### **2.5.6. Cyt c / COOH SAM / Au System (Bowden Research)**

As previously noted, carboxylic acid terminated SAMs are utilized in the biological ET model being investigated. Carboxylic acid terminated SAMs are anchored to the Au surface via Au-S bonds with their alkyl chains and their acid terminus extending out into solution. As with other SAMs terminated with a single functionality, longer alkyl chains yield more organized alkane packing and subsequent improved SAM stability. However, as alluded to previously, COOH terminated SAMs are one of the most permeable films in aqueous solution, possessing a higher density of defects than other SAMs.<sup>43</sup> Their use in this case stems from the fact that the carboxylic acid groups, depending on the pH of the environment, can be largely unprotonated, creating a negatively charged surface. This acidic surface is ideal for the immobilization and subsequent ET study of such basic proteins as cytochrome c.

In the early 1990s, Bowden and researchers first reported the successful use of carboxylic acid terminated SAMs on Au substrates as a binding partner for the cytochrome c protein.<sup>36c</sup> Since that time, extensive characterization of the cytochrome c / SAM (COOH) / Au system has been performed using both electrochemical and spectroscopic (electrochemical impedance spectroscopy (EIS) and XPS) methods. Subsequent studies have employed the same methodology on the system for specific kinetic and thermodynamic analysis of the system's biological ET.<sup>25-27d,36a,37,69</sup> In recent years, research by the Bowden Group has focused on defining specific interfacial aspects of the system, such as the electronic coupling between the protein and SAM,<sup>36b</sup> and on examining the inherent surface effects observed in electrochemical results.<sup>32,70</sup>

The acid/base properties of the carboxylic acid SAMs obviously are a major factor in the model. Most of the electrochemistry performed on the cytochrome system is performed at a physiological pH of 7. At this pH value, the acid groups are largely unprotonated, facilitating the electrostatic adsorption of positively charged species. Research into the acid/base properties of these SAMs has shown that the carboxylic acids, which normally have a pKa value of 4-5, exhibit a considerably more basic surface pKa in the SAM. Values from these reports show the range of the surface pKa to be between 6-8.<sup>71</sup> Results from electrochemical experiments on acid terminated SAMs show their background signal is noticeably higher when they are in a neutral or basic environment.<sup>51</sup> This reiterates that electrostatic repulsions between negatively charged headgroups may indeed play an important role in the packing of the SAMs and reinforces the thought that, in acidic solutions, hydrogen bonding may be a factor. In any event, the cyt / SAM / Au electron transfer model represents an excellent example of how SAMs interact favorably with certain proteins and, on a broader scale, how SAMs can be tailored for specific scientific endeavors.

## **2.6 ELECTROCHEMISTRY – VOLTAMMETRY OF ADSORBED SPECIES**

More relevant to the research in the Bowden research group and to the work presented here, is the electrochemistry of adsorbed systems. Cyclic voltammetry on adsorbed molecules is an example of diffusionless electrochemistry. An electroactive molecule is considered adsorbed when it is immobilized on the electrode surface, either directly or through some type of modifier such as a SAM. Compared to diffusing voltammetry, the voltammograms of adsorbed systems are distinctive because of their specific peak shape. Since the diffusional aspect of the electrochemistry is eliminated from adsorbed systems, the response is a curve where the current proceeds back to the baseline after peaking. In an ideally adsorbed system, both the oxidative and reductive peaks are usually symmetrical and positioned directly on top of each other. That is, for an ideal, reversible (Nernstian) adsorbed response,  $E_{p,a} = E_{p,c} = E_p$ . The cyclic voltammogram of an adsorbed molecule is illustrated in Figure 2.11.

The adsorbed system, being fundamentally different than the typical diffusing electrochemical situation, possesses its own set of equations pertaining to peak current and

peak potential, as well as several other exclusive properties. For an adsorbed cyclic voltammogram, the peak current ( $i_p$ ) and the peak potential ( $E_p$ ) are given by:

$$i_p = \frac{n^2 F^2 \nu A \Gamma_o^*}{4RT} \quad [\text{Eqn. 2.1}]$$

$$E_p = E^{o'} - \frac{RT}{nF} \ln \left( \frac{\beta_{ox} \Gamma_{ox}}{\beta_{red} \Gamma_{red}} \right) \quad [\text{Eqn. 2.2}]$$

where  $n$  = number of electrons transferred

$\nu$  = scan rate (V/sec)

$A$  = area of the working electrode ( $\text{cm}^2$ )

$\Gamma$  = surface concentration of oxidized (Ox) or reduced (Red) species ( $\text{mol}/\text{cm}^2$ )

$\beta$  = adsorption coefficient

$T$  = temperature (K)

and  $R$  and  $F$  are the gas constant and Faraday constant respectively.

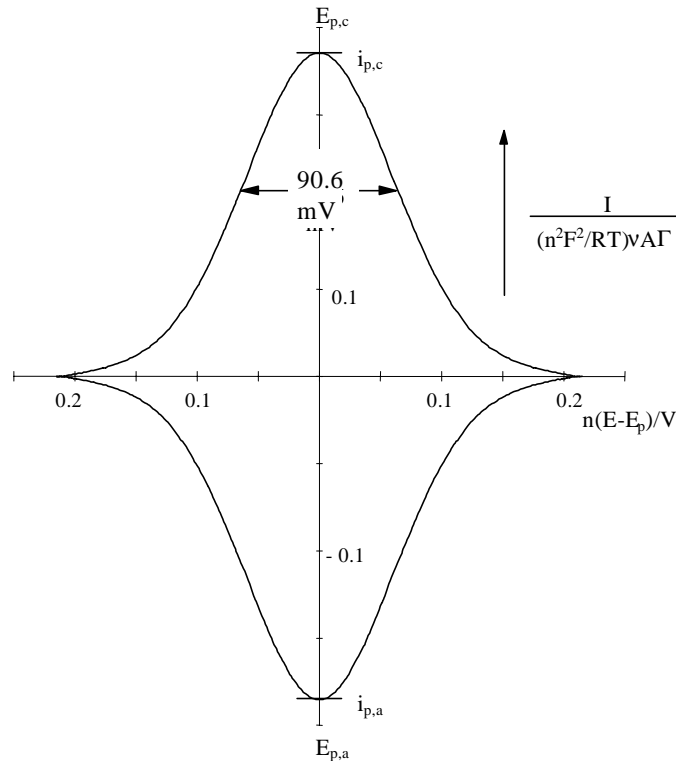


**Figure 2.11.** Cyclic voltammogram for an ideally adsorbed, reversible electrochemical system.

An indication that the voltammetric response is truly adsorbed is the direct linear relationship between peak current and sweep rate ( $i_p \propto \nu$ ) as dictated by Eqn. 2.1.

The formal potential of an adsorbed molecule is defined as the surface formal potential ( $E^{\circ}_{\text{surf}}$ ) and is given by the following:

$$E^{\circ}_{\text{surf}} = \frac{E_{\text{p,a}} + E_{\text{p,c}}}{2} \quad [\text{Eqn. 2.3}]$$

For the purposes of this dissertation  $E^{\circ}_{\text{surf}}$  will be referred to as simply  $E^{\circ}$ .

Another electrochemical parameter typically used in the analysis of adsorbed voltammetry is the full width at half maximum (FWHM) value, essentially a measure of the breadth of the cathodic and anodic voltammetric peaks (See Figure 2.11). For an ideal, reversible adsorbed system, the FWHM value for either peak should be approximately 90.6/n mV or 62.5/ $\alpha$  mV for an irreversible process at 25°C (where  $\alpha$  is the transfer coefficient).<sup>73</sup> The FWHM parameter of adsorbed cyclic voltammograms will be of extreme importance to understanding the reasoning for performing the research presented in future chapters.

The charge (Q) passed during a cathodic or anodic wave of a cyclic voltammetry experiment is a useful parameter for an adsorbed system. The area under a voltammetric peak, once corrected for charging current, can be integrated to obtain a measurement of the charge passed during an oxidation or reduction:

$$\int (\text{area under peak}) = \text{charge passed during redox process} \quad [\text{Eqn. 2.4}]$$

This charge, measured in coulombs, corresponds to the redox activity of a layer of adsorbed electroactive molecules according to the following equation:

$$Q = nFA\Gamma_{\text{surf}} \quad [\text{Eqn. 2.5}]$$

where: n = number of electrons transferred,

F = Faraday constant

A = area of the working electrode

$\Gamma_{\text{surf}}$  = the surface coverage of electroactive molecules (mol/cm<sup>2</sup>).

Therefore, by using the above expression, a measurement of the surface concentration or surface coverage of electroactive molecules can be derived.

### 2.6.1. Laviron's Kinetics of Adsorbed Species

In general, the rate of ET for an adsorbed species is much greater than the rate of the same species in solution.<sup>28</sup> Moreover, because of the adsorbed nature of the analyte, traditional kinetic analysis is unsatisfactory, requiring an alternative method for extracting kinetic information. To calculate the ET rate constant ( $k_{\text{et}}^{\circ}$ ) of adsorbed species, a model

based on CV and Butler-Volmer kinetics was developed by Laviron.<sup>1,73</sup> Using Laviron's simplest model for an adsorbed system, a mathematical expression is derived capable of measuring  $k_{et}^0$  at zero overpotential. Laviron incorporated several important assumptions into his model: 1) both the oxidized and reduced forms of the electroactive species are inherently stable and are strongly adsorbed to the electrode; 2) the system under consideration is completely diffusionless, and therefore diffusional aspects of the molecules can be excluded from the mathematical expression; and 3) the system obeys a Langmuir adsorption isotherm. An adsorption isotherm is a predicted relationship that exists between the amount of an adsorbed substance on a surface and its pressure or concentration at a constant temperature.<sup>74</sup> A chemical system adhering to a Langmuir isotherm assumes that there are no lateral interactions between the adsorbed species, that the surface of the electrode is completely homogeneous with no topographical structure (smooth), and that surface saturation eventually occurs, resulting in a monolayer coverage of highly active, adsorbed molecules. Laviron's mathematical representation of  $k_{et}^0$  is based on peak splitting ( $\Delta E_p$ ) and, for irreversible CV responses (where  $\Delta E_p \geq 200$  mV), is calculated with the following expression:

$$\log k_{et}^0 = \alpha \log(1-\alpha) + (1-\alpha) \log \alpha - \log \left( \frac{RT}{nFv} \right) - \frac{(\alpha(1-\alpha)nF\Delta E_p}{2.3RT} \quad [\text{Eqn. 2.6}]$$

where:  $k_{et}^0$  = electron transfer rate constant ( $\text{sec}^{-1}$ ),  
 $\alpha$  = transfer coefficient,  
 $T$  = temperature (K),  
 $v$  = scan rate (mV/sec),  
 $n$  = number of electrons transferred,  
 $\Delta E_p$  = peak splitting between the anodic and cathodic peak potentials (mV)  
and  $R$  and  $F$  are the gas constant and Faraday constant, respectively.

To change the CV signal of a reversible adsorbed species so that its  $\Delta E_p$  is  $\geq 200$  mV, allowing the use of the above equation, the voltammetry is run at continually higher sweep rates to increase the degree of peak splitting. This type of ET rate constant is known as the irreversible ET rate constant but, unless otherwise denoted, will be simply referred to as  $k_{et}^0$ .

The transfer coefficient ( $\alpha$ ) may also be calculated with this method by creating a Tafel plot of the data, a plot of peak potential ( $E_p$ ) versus the log of the scan rate ( $\log v$ ).<sup>73</sup>

Theoretically, this plot should yield two straight lines with slopes equal to the following expressions:

$$\frac{-2.3RT}{\alpha nF} \text{ for the cathodic peak,} \quad [\text{Eqn. 2.7}]$$

$$\frac{-2.3RT}{(1-\alpha)nF} \text{ for the anodic peak,} \quad [\text{Eqn. 2.8}]$$

allowing a value for  $\alpha$  to be calculated.

As stated previously, the preceding kinetic analysis is only applicable to an irreversible response ( $\Delta E_p \geq 200$  mV), but Laviron's model can also be applied to quasi-reversible voltammetry ( $\Delta E_p < 200$  mV) via a curve fitting algorithm.<sup>31b</sup> Unlike the irreversible case, the quasi-reversible model does not provide for an independent measurement of  $\alpha$ . Therefore, when this algorithm is employed to determine  $k_{et}^0$ ,  $\alpha$  is assumed to be a value close to 0.5.<sup>73</sup> Unless specifically noted, the kinetic analysis of this research was performed according to the irreversible model. In situations where the quasi-reversible model was used, the ET rate constant will be denoted as  $k_{et(Q/R)}^0$ . Laviron's models can also be applied, under certain restrictions, to linear sweep voltammetry, thin-layer voltammetry, and coulometry.<sup>75</sup>

## 2.7 DOUBLE LAYER THEORY AND CAPACITANCE

A substantial part of the research contained herein will deal with the concept of double layer capacitance as it relates to electrochemical systems and therefore a somewhat detailed discussion of this property is warranted. Capacitance measurements are used in this research as background quality checks, an experimental marker for the systematic progress of an experiment, and also as an analytical measurement to learn about surface structure of the system.

### 2.7.1. The Double Layer

When an electrode is placed in a solution of electrolyte and a voltage is applied to it, the electrode will bear either a positive or negative charge, depending on the polarization of the voltage applied to the electrode. For instance, if a negative potential is applied to the electrode, it will have an excess negative charge at its surface. To maintain electroneutrality

at the electrode/solution interface, ions from solution (the supporting electrolyte) will compensate the charge on the electrode with opposite charged ions. When this occurs, the region at the electrode surface is referred to as the electric double layer. The current required to charge the electrode and thus form this electric double layer is referred to as nonfaradaic or charging current. In voltammetry, this current flow commonly viewed as the background signal and is sometimes subtracted off the analytical signal. Many physical models have been created to describe the double layer and excellent reviews of double layer theory exist in the literature.<sup>28</sup> Depicted in Figure 2.12 is a commonly accepted model of the double layer that will be utilized for the purpose of this discussion.

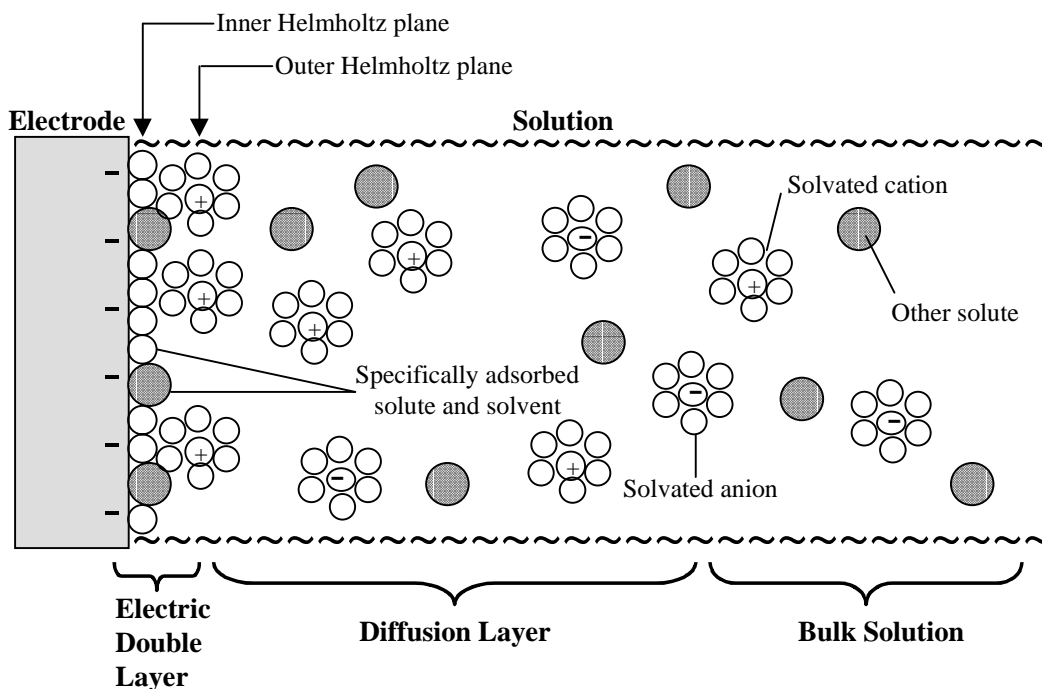


**Figure 2.12.** A commonly accepted model for the electrode-solution interface known as the electric double layer. The plane going through the center of the directly adsorbed species is called the inner Helmholtz plane (IHP); the plane passing through the layer of nonspecifically adsorbed ions is called the outer Helmholtz plane (OHP). The charge build-up at the OHP along with the charge build-up at the surface of the metallic electrode comprises the electric double layer which can be modeled as a parallel plate capacitor.

### 2.7.2. Parallel Plate Capacitors

One double layer theory, the Helmholtz model, makes the comparison of the electric double layer structure acting as a parallel plate capacitor in an electronic circuit. A capacitor

in a simple circuit is shown in Figure 2.13, where the plates on the capacitor represent planes of opposite charges separated by a distance. The analogous situation in

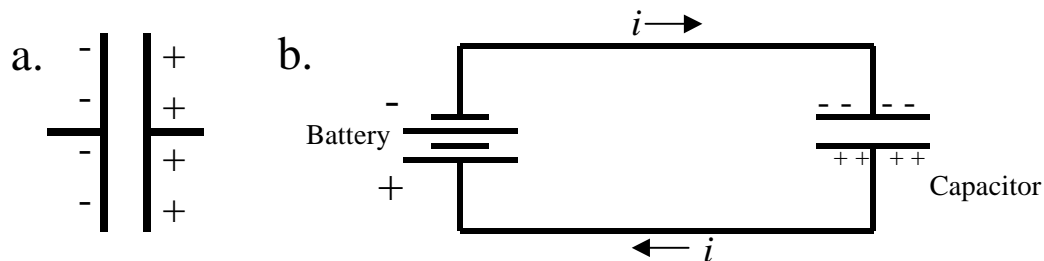


**Figure 2.13.** Parallel plate capacitor: a) electronic component and b) in a simple circuit with a voltage source (battery) where the capacitor builds up charge (current flow is indicated by arrows).

electrochemical systems is that the contact surface of the metal electrode with the solution is one of the plates and the ions of opposite charge from solution, when rigidly linked to the electrode through electrostatic attraction, represents the other parallel plate. Thus, the electrode/solution interface can be modeled with a basic circuit component, a simplification used by many electrochemists to describe various physical aspects of electrochemical systems. Known as equivalent circuitry, electronic circuits are used to represent specific electrochemical scenarios.

In electronics, a capacitor is basically two metal plates, separated by a dielectric material, that functions as a charge storage device. As shown in the equation below, the charge ( $q$ ) stored in a capacitor is dependent on two variables: the voltage ( $E$ ) applied across the capacitor, measured in volts (V) and the capacitance ( $C$ ) of the capacitor, measured in Farads:

$$q = C * E_{app} \quad [\text{Eqn. 2.9}]$$

With a certain applied potential or voltage across the capacitor, current will flow and charge will accumulate on the metal plates until the equation above is satisfied.<sup>29</sup> Excess charge (electrons) will build up on one plate, while a deficiency of electrons will exist on the other plate (See Figure 2.13). The current that flows until the condition dictated by Eqn. 2.9 above is met, when  $q_{\text{metal}} = -q_{\text{soln}}$ , is known as the charging current.

In general, the capacitance of a capacitor is defined as the ratio of the amount of charge on either plate to the magnitude of the potential applied:<sup>76</sup>

$$C \equiv \frac{Q}{E_{\text{applied}}} \quad [\text{Eqn. 2.10}]$$

where C is the capacitance measured in Farads (F) or charge per volt units (coul/V), Q is the charge, measured in coulombs, and  $E_{\text{app}}$  is the applied voltage in volts (V). Capacitance, by definition, is always a positive measurement and the quantity of Q/V is constant for a given capacitor.

For a parallel plate capacitor with plates of similar geometry and dimensions, an expression for capacitance can be derived as follows. Consider  $\sigma$  to be the charge (Q) per unit area of the parallel plate or  $\sigma = Q/A$  where A is the area of the parallel plates. The electric field ( $E_f$ ) between the plates can then be described as follows:

$$E_f = \frac{\sigma}{\epsilon_0} = \frac{Q}{\epsilon_0 A} \quad [\text{Eqn. 2.11}]$$

where  $\epsilon_0$  is the permittivity of free space constant ( $8.854187817 \times 10^{-12} \text{ C}^2/(\text{N m}^2)$ ).<sup>76</sup> The potential difference (V) between the two plates of the capacitor will be a function of this electric field and the distance it transpires:

$$V = E_f d \quad [\text{Eqn. 2.12}]$$

where d is the distance between the parallel plates. If Eqn. 2.11 is substituted for  $E_f$  in Eqn. 2.12, the following expression is yielded:

$$V = \frac{Qd}{\epsilon_0 A} \quad [\text{Eqn. 2.13}]$$

where d is the distance between the parallel plates. Furthermore, if this expression is used in conjunction with the relationship of Eqn. 2.10, a general mathematical expression of capacitance is derived for parallel plate capacitors:

$$C = \frac{Q}{V} = \frac{Q}{\left( \frac{Qd}{\epsilon_0 A} \right)} = \frac{\epsilon_0 A}{d} \quad [\text{Eqn. 2.14}]$$

It is easily noted from this expression that the capacitance value for a system is highly dependent on both the area of the plates or electrodes (directly proportional) and on the

distance separating the plates of the capacitor (inversely proportional). If the expression is being applied to an electrochemical interface adhering to the Helmholtz double layer theory, the capacitance is referred to as the double layer capacitance and, as will be seen, is usually reported per unit area ( $C/A$ ).

### 2.7.3. Dielectric Materials

An important aspect of the parallel plate capacitor model is now added to this discussion, the dielectric material. As previously mentioned, a parallel plate capacitor possesses two plates of charge separated by a distance. Occupying the space between the plates, is a dielectric material. The dielectric material is usually an insulating (nonconductive) material such as rubber, glass, or wax. Placing an insulating material between the two parallel plates of a capacitor results in an increase in the overall capacitance value for that particular capacitor. If the dielectric material completely fills the gap between the two plates, the capacitance is increased by a factor of  $\epsilon$ , the dielectric constant, a dimensionless value dependent on the nature of the material in the gap.<sup>76a</sup> A list of dielectric constants for various materials is provided as Table 2-2.

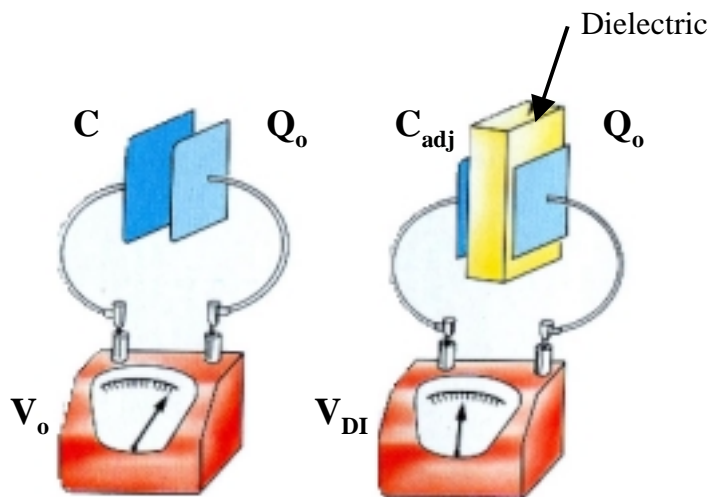


**Figure 2.14.** Dielectric effect on voltage across a capacitor. When a dielectric is inserted between the plates of a capacitor, the charge on the plates remains unchanged ( $Q_0$ ), but the potential difference with and without the dielectric ( $V_{DI}$  vs.  $V_0$ ) is effectively reduced by a factor equal to the dielectric constant ( $V=V_0/\epsilon$ ). As a result, the capacitance of the system is increased by a factor equal to  $\epsilon$ .<sup>76</sup> (Figure from Ref. 76a).

**Table 2-2.** Dielectric Constants and Dielectric Strengths for Various Materials<sup>a, 43,76</sup>

Material	Dielectric Constant, $\epsilon$	Dielectric Strength <sup>b</sup> (V/m)
Vacuum	1.00000	---
Air	1.000059	$3 \times 10^6$
Bakelite	4.9	$24 \times 10^6$
Fused Quartz	3.78	$8 \times 10^6$
Pyrex Glass	5.6	$14 \times 10^6$
Polystyrene	2.56	$24 \times 10^6$
Teflon	2.1	$60 \times 10^6$
Neoprene Rubber	6.7	$12 \times 10^6$
Nylon	3.4	$14 \times 10^6$
Paper	3.7	$16 \times 10^6$
Strontium titanate	233	$8 \times 10^6$
Water	80	---
Silicone oil	2.5	$15 \times 10^6$
<b>Alkanethiol SAM<sup>c</sup></b>	<b><math>2.6 - 6^d</math></b>	---
Carbon Disulfide	2.64	---
Carbon Tetrachloride	2.24	---

<sup>a</sup> Measurements made at room temperature (temperature can affect values).<sup>72</sup>

<sup>b</sup> Dielectric strength equals the maximum electric field that can be applied to the dielectric material before electrical breakdown.<sup>72</sup>

<sup>c</sup> Methyl-terminated alkanethiolate SAMs -  $\text{CH}_3(\text{CH}_2)_n\text{S}$ - where  $n > 8$ .<sup>43</sup>

<sup>d</sup> Value is based on the slope of a plot of SAM chain length,  $n$ , versus reciprocal capacitance, assuming *trans* chain conformations and a tilt angle of  $30^\circ$ , and is dependent on the nature of the substrate and the solvent being used.<sup>43</sup>

The traditional increase of capacitance when an insulating material is used as a dielectric ( $\epsilon > 1$ ) is easily explained by the fact that the capacitor possesses the same amount of charge but with a lower value of effective potential across the capacitor. As seen in Figure 2.14, the charge remains unchanged while the potential difference is reduced:

$$V_{\text{DI}} = V_o/\epsilon \quad [\text{Eqn. 2.15}]$$

where  $V_{\text{DI}}$  is the voltage considering the dielectric material,  $\epsilon$  is the dielectric constant of the material ( $\epsilon > 1$ ), and  $V_o$  is the original potential difference (ignoring the existence of the dielectric material). Referring back to the fundamental equation for capacitance (Eqn. 2.10) and adjusting its variables for this particular discussion by noting  $Q_o$  as the original amount of charge on the capacitor, the expression becomes as follows:

$$C = \frac{Q_o}{V} \text{ before considering the dielectric.} \quad [\text{Eqn. 2.16}]$$

Substituting Eqn. 2.15 into the above expression to account for the applied voltage adjusted for the dielectric material:

$$C_{\text{adj}} = \frac{Q_o}{\left(\frac{V_o}{\epsilon}\right)} = \frac{Q_o \epsilon}{V_o} \quad [\text{Eqn. 2.17}]$$

for the capacitance of a capacitor containing a dielectric material. Thus, the original capacitance is effectively increased by a factor equivalent to the dielectric constant ( $C_{\text{adj}} = C_o \epsilon$ ). Therefore, considering Eqn. 2.15 in conjunction with Eqn. 2.13 and its transduction to Eqn. 2.14, a more comprehensive expression for double layer capacitance that also incorporates the influence of the dielectric material, can be achieved:<sup>29,76a</sup>

$$C = \frac{\epsilon \epsilon_o A}{d} \quad [\text{Eqn. 2.18}]$$

or per unit area as,

$$C = \frac{C}{A} = \frac{\epsilon \epsilon_o}{d} \quad [\text{Eqn. 2.19}]$$

This is the equation that will be used throughout this work to describe the double layer capacitance of the electric double layer at the electrode surface.<sup>29</sup>

From Eqn. 2.19, it would seem that the  $C_{\text{dl}}$  could be made very large by simply decreasing the distance ( $d$ ) between the plates of the capacitor. In actuality, the lowest value of  $d$  is limited by the dielectric material's potential to electrically discharge. That is, for a certain distance between two plates of a capacitor, there is a maximum voltage that can be applied to the capacitor before the dielectric material ceases to be insulating and begins to conduct. Once this voltage is surpassed, the dielectric witnesses electrical discharge across the plates and the capacitor fails. This voltage threshold is known as the dielectric strength of the material. Several examples of materials and their dielectric strengths are included as part of Table 2-2.<sup>76</sup>

Why is the applied electric field reduced by a factor of  $\epsilon$  ( $V = V_o/\epsilon$ )? To answer this question, an in depth look at dielectric materials on a molecular level is necessary (See Figure 2.15).<sup>76</sup> This phenomenon is most easily understood if one considers that the molecules composing the dielectric material are polarizable. That is, they can be made so that their positive and negative charges or regions of electron density, can be separated and aligned in even the slightest amount. The degree to which the dielectric molecules align is dependent on the dipole moment of the molecules, as well as, the temperature and magnitude of the

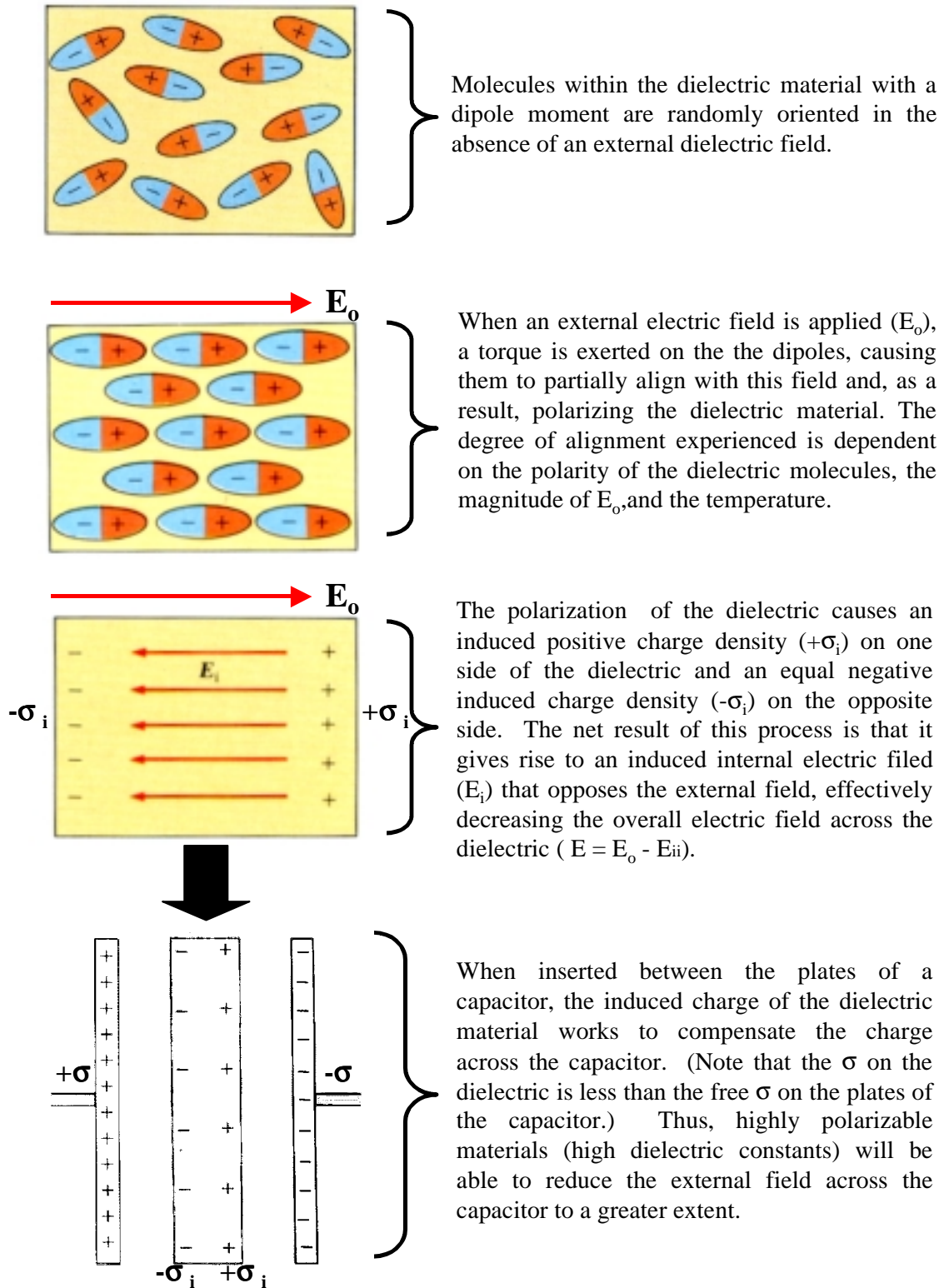


**Figure 2.15.** Dielectric materials on a molecular level (Figures from Ref. 76a).

applied electric field. Alignment and charge separation within the dielectric increases with decreasing temperature and with increasing field strength. Most importantly, these partially aligned dipoles produce an internal electric field that opposes the external electric field and thus effectively reduces the applied potential felt by the capacitor (See Figure 2.15). Thus, it makes sense that more polarizable substances, such as water, will reduce the electric field to a greater extent and possess a high dielectric constant.<sup>76</sup>

In summary, dielectric materials, when placed in a parallel plate capacitor can pose several important advantages: 1) a dielectric increases the capacitance of a capacitor; 2) a dielectric increases the maximum operating voltage of a capacitor; and 3) a dielectric may provide mechanical support between the conducting plates.<sup>76</sup>

#### **2.7.4. SAMs, Dielectrics, and Double Layer Capacitance ( $C_{dl}$ )**

A SAM modified electrode produces a profound effect in double layer capacitance values. The SAM serves two functions toward altering the  $C_{dl}$ : 1) the SAM acts as a spacer, increasing the distance between the capacitor plates of opposite charge and 2) the SAM, being composed of primarily organic alkane chains, changes the dielectric constant of the capacitor to a very low value. The alkane chains will fill the space between the parallel plates and are the predominant dielectric material for the parallel plate capacitor model.

Considering Eqn. 2.19 and illustrated in Figure 2.16, both these effects serve to drastically lower the  $C_{dl}$  of a SAM modified electrode. Methyl terminated SAMs with ten or more methylene units have shown  $C_{dl}$  values in the 1-5  $\mu\text{F}/\text{cm}^2$  range.<sup>43</sup> Moreover, research has shown that reciprocal capacitance ( $C_{dl}^{-1}$ ) varies linearly with SAM chain length ( $n\text{CH}_2$ ), where  $n$  is the number of methylene units that comprise the chain.

Plots of  $n$  versus  $C_{dl}^{-1}$  have yielded capacitance values per methylene unit on the order of 0.055  $\mu\text{F}/\text{cm}^2$  per  $\text{CH}_2$  group and a dielectric constant value of 2-3 (unitless quantity) for SAMs composed of methyl terminated alkane thiols with more than eight methylene units.<sup>43</sup> Experimental determinations of these values are highly dependent on the specifics of the physical system: the gold substrate, the electrolyte components, and especially on the structure and properties of the SAM, including the specific tail group being used. In any event, the values of the  $C_{dl}$  reported for SAMs tend to be justified considering the crystalline nature, low dielectric constant, and spacer properties of the alkane chains comprising the thin

films. The dielectric constant is made considerable lower by the fact that SAMs of this type possess extremely low permeability for water molecules, which are very polar, and ions from solution. Penetration of the film by such species usually occurs only at pinhole sites and defects in the SAM structure. The greater the extent of this penetration, the larger the degradation of the dielectric barrier. As a result, the dielectric constant will be higher, subsequently raising the value of the double layer capacitance. In this manner, the double layer capacitance of a system can be used to make a statement about the structure and packing completeness (defect density) of the SAM.<sup>77</sup>

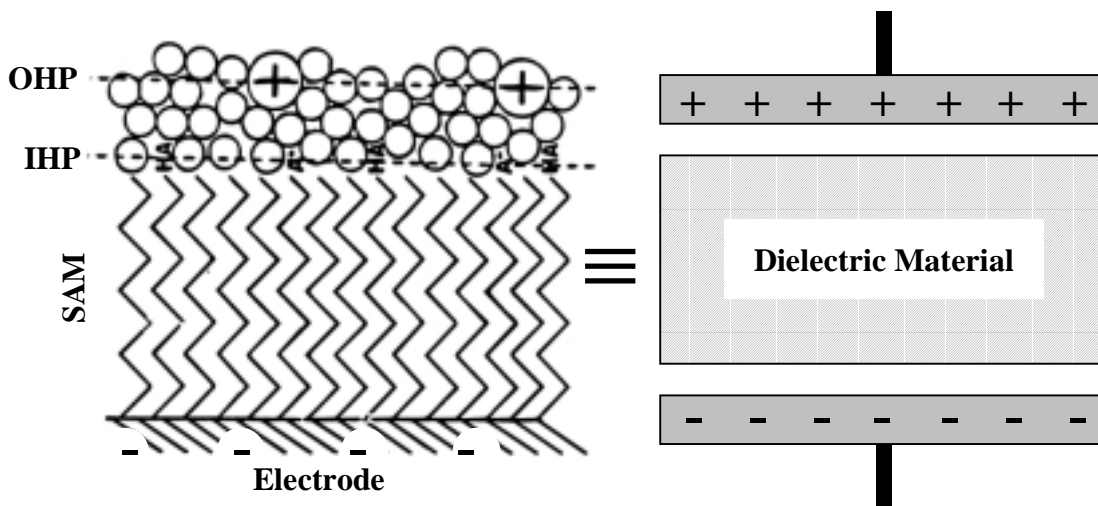


**Figure 2.16.** Comparison showing how a SAM modified electrode can be approximately modeled as a simple parallel plate capacitor with a dielectric. The  $C_{dl}$  of the SAM system is drastically lowered by both the increased distance between the planes of charge that is created by the alkane chain spacers, and by the low dielectric constant provided by the alkane chain density between the plates that acts as the capacitor's dielectric material (See Eqn. 2.32) (Adapted from a figure in Ref. 43).

Double layer capacitance theories exist that propose that certain types of SAMs may induce two capacitances that contribute to the overall capacitance of the system, the total capacitance ( $C_T$ ). These two sources of capacitance are the previously discussed double layer capacitance ( $C_{dl}$ ), and the capacitance of the monolayer itself ( $C_M$ ); equivalent to two parallel plate capacitors in series.<sup>43</sup> Using the electronic law for adding capacitors in series, the result for  $C_T$  is as follows:

$$\frac{1}{C_T} = \frac{1}{C_{dl}} + \frac{1}{C_M} \text{ or } C_T = \frac{C_{dl} C_M}{(C_{dl} + C_M)} \quad [\text{Eqn. 2.20}]$$

For simplicity, electrochemical systems with SAMs that adhere to this situation are usually treated with Eqn. 2.19 for the overall capacitance, which is usually dominated by  $C_M$  anyway ( $\therefore C_M \approx C_T$ ).

### 2.7.5. Cyclic Voltammetry and Double Layer Capacitance

During CV experiments,  $C_{dl}$  is measured by performing a scan in a potential window where the magnitude of the charging current is independent of the applied voltage and where no redox activity is occurring (i.e. the CV is flat). This is usually accomplished by running the scan in only supporting electrolyte solution, with no redox species present, so that only charging current can exist. The thickness or total current of the cyclic voltammogram is then measured at a potential that is specifically chosen for comparison purposes. The following equation is applied to calculate  $C_{dl}$  from CV scans:

$$C_{dl} (\mu\text{F}/\text{cm}^2) = \frac{I_{\text{total}}}{(2\nu A) \times 10^{-6}} \quad [\text{Eqn. 2.21}]$$

where  $I_{\text{total}} = |i_a + i_c|$  in amps,  $\nu$  is the sweep rate (V/s), and  $A$  is the area of the WE in  $\text{cm}^2$ . This measurement is demonstrated in Figure 2.17. Being sensitive to the breakdown of the parallel plate capacitor concept,  $C_{dl}$  measurements made with CV are advantageous in that the technique is relatively slow allowing the detection of ion penetration to be observable for a longer period of time.

For the experiments performed in the research presented here,  $C_{dl}$  is used as a diagnostic check on the preparation of the cyt c/SAM/Au system and as an analytical tool for measuring global information about the structure and stability of the SAM. As a diagnostic check, a voltammogram of the background is taken at each step of assembling the cyt c/SAM/Au system. Shown in Figure 2.18 (red scan), the original scan of the Au gives a certain background signal. Once the Au is electrochemically cleaned, the charge separation is minimal, existing right at the electrode surface and possessing a very high, aqueous in nature, dielectric property. Thus, the  $C_{dl}$  of the system is very high after a cleaning procedure is applied to the Au surface (Figure 2.18 – blue scan). Once the SAM is adsorbed and allowed to self-assemble, the  $C_{dl}$  is lowered drastically (Fig. 2.18 – black scan) due to the huge increase in the separation distance and the drastic decrease in the dielectric constant value. In this manner, the progress of assembling this system can be monitored.

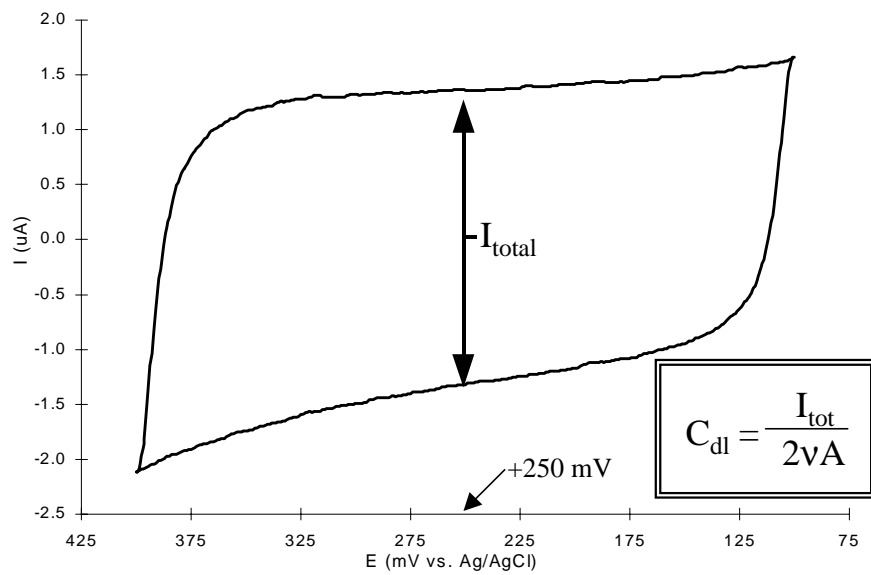


**Figure 2.17.** Double layer capacitance ( $C_{\text{dl}}$ ) is determined from cyclic voltammograms by measuring the total current at +250 mV and applying the value of that current measurement in the equation shown (Eqn. 2.34).

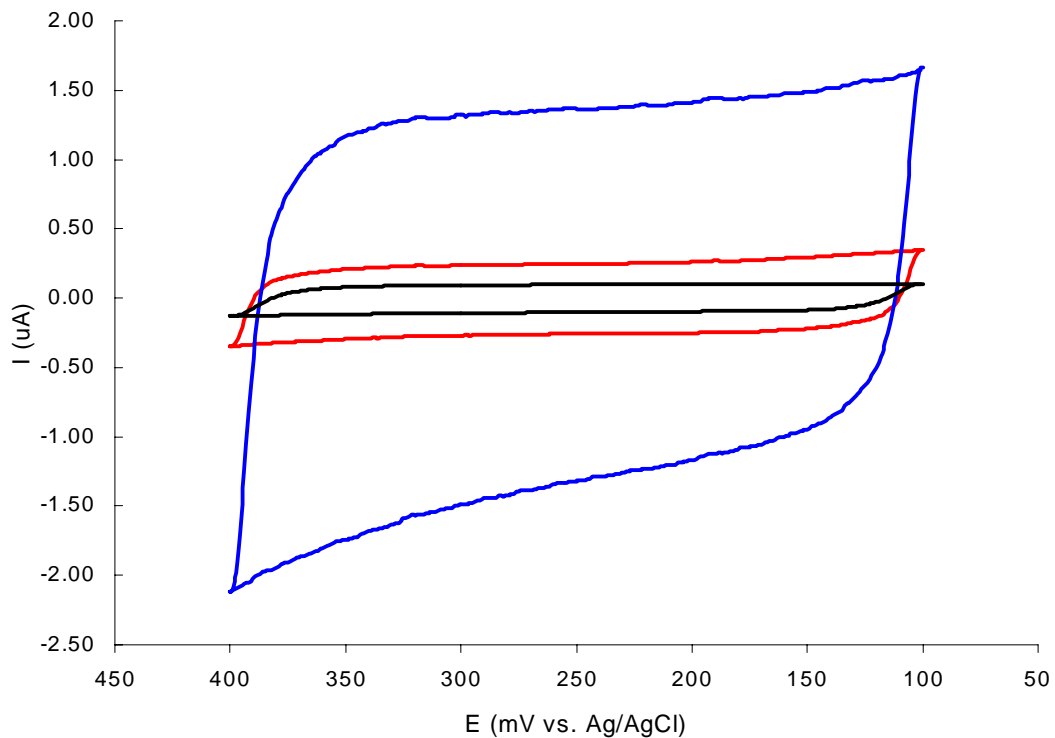


**Figure 2.18.** Background voltammograms taken for diagnostic  $C_{\text{dl}}$  measurements of an evaporated Au substrate initially or as received (red), after electrochemical cleaning in 0.1 M  $\text{H}_2\text{SO}_4$  and 0.01 M KCl (blue) and after being modified with a 11-MUDA or  $\text{HS}(\text{CH}_2)_{10}\text{COOH}$  SAM (black).

The drastic decrease in  $C_{dl}$  with the SAM actually represents a critical experimental advantage for electrochemical experiments involving ET of adsorbates on SAMs. Because the magnitude of the charging current is so markedly lower with the SAM than with bare Au, the signal to noise ratio of any faradaic current is significantly improved. The SAM actually helps to suppress the background signal and simultaneously provides a biocompatible surface for protein adsorption and immobilization. This is a substantial benefit of using SAM modified electrodes in PME, considering the cyt c voltammetry is limited to a low electroactive surface coverage, in this case, a single monolayer or less of adsorbed cyt c.

As an analytical tool,  $C_{dl}$  values can elucidate properties about the structure of the SAM. Alluded to earlier, the effect of defects and pinholes on the structure of SAMs can be profound and their effect is subsequently observed in the value of the SAM's  $C_{dl}$ .<sup>43,49,50,59,78,79</sup> Defects in the SAM allow aqueous solution and electrolyte components to “seep” into the SAM, disrupting the packing of the alkane chains and decreasing the effective separation of the charged planes. Both effects, lowering the separation and increasing the dielectric constant value, will cause the  $C_{dl}$  of the system to be higher than that of a system with an intact, defect-free, stable SAM.  $C_{dl}$  values for short chain SAMs, which have liquid-like structural properties, are sporadic and are always comparatively higher than values for long chain SAMs, which possess a more rigid, crystalline structure (See Figure 2.19). Thus, by making comparisons of  $C_{dl}$  measurements on different systems, conclusions can be derived about the structure of the SAM. This type of analysis will be used extensively throughout the presented work.

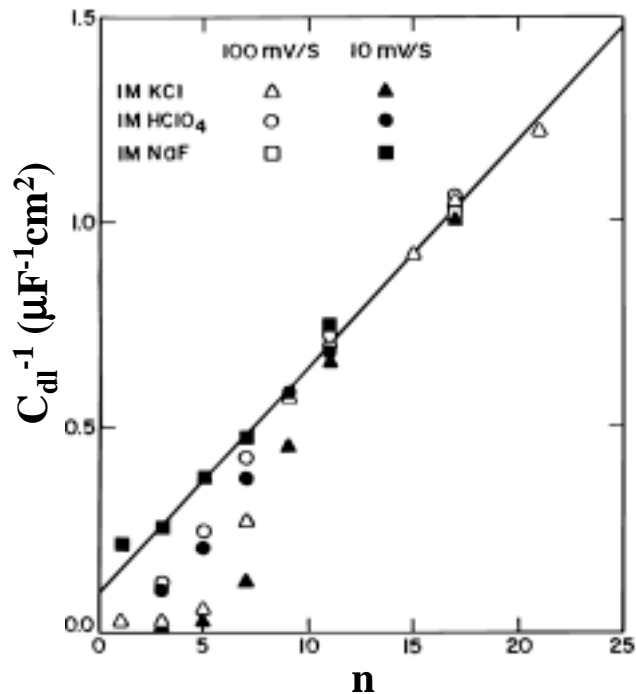


**Figure 2.19.** Reciprocal capacitance of alkanethiol modified gold electrodes as a function of alkane chain length,  $n$ , and electrolyte. Note the increase in the scatter of data points as the chain length gets smaller - a consequence of the inherent disorder and defect density of short chain SAMs where solution can penetrate the SAM layer more easily and cause a fundamental breakdown of the parallel plate capacitor model. The slope of a plot such as the one shown above represents the dielectric constant of the system. (Figure from Ref. 43).

## 2.8 ELECTROCHEMICAL BEHAVIOR OF CYT C / SAM / AU SYSTEM

It is now time to revisit the biological electron transfer model used in the Bowden Research Group, cyt c adsorbed on carboxylic acid terminated SAMs (See Figure 2.20). This system is used as an electrochemical model for biological electron transfer within protein/protein complexes, using the SAM modified electrode to simulate one of the proteins in the redox reaction.<sup>16,18f,36a,c</sup> Typical cyclic voltammetry of this system is shown in Figure 2.21. During this type of experiment, the adsorbed cyt c is electrochemically oxidized and reduced. Upon reduction of the cyt c, an electron is transferred from the electrode, through the alkyl chain layer of the SAM, across a SAM/protein interface, and finally through the polypeptide shell of the protein to the redox center, a heme group centered in a porphyrin ring. The reverse process occurs when the cytochrome is oxidized.<sup>18a,36a</sup>

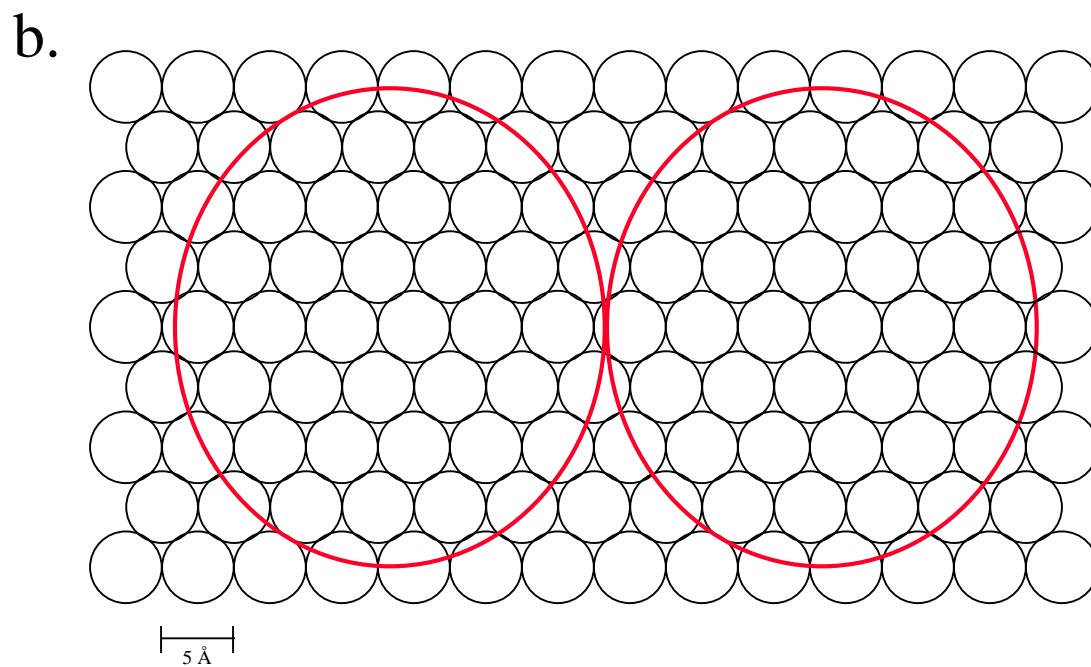
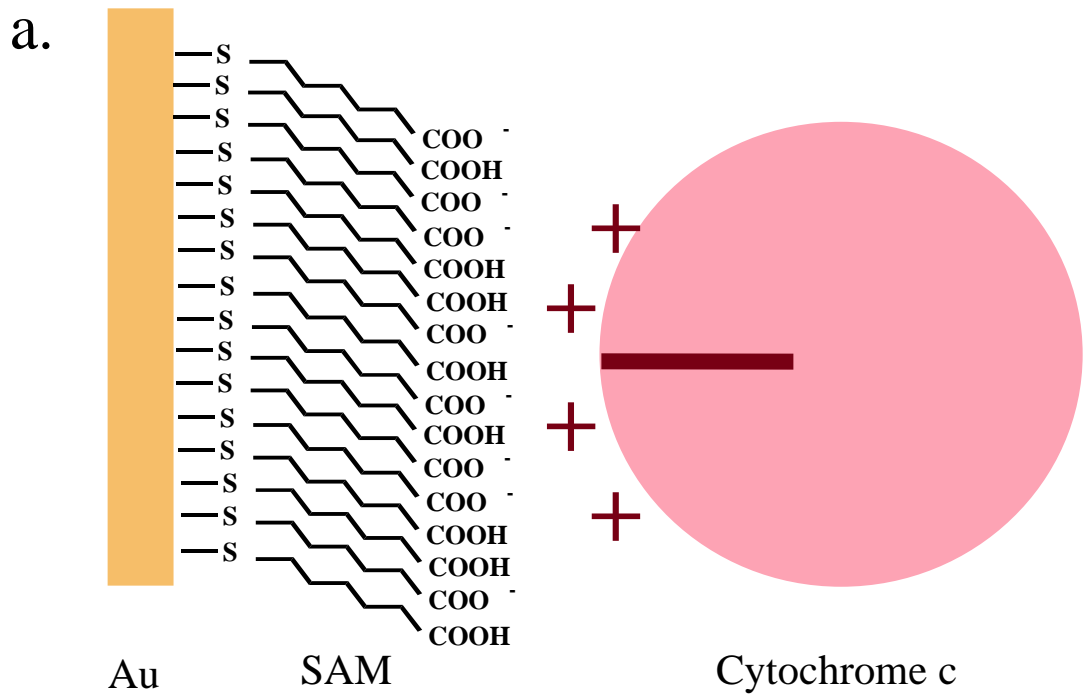
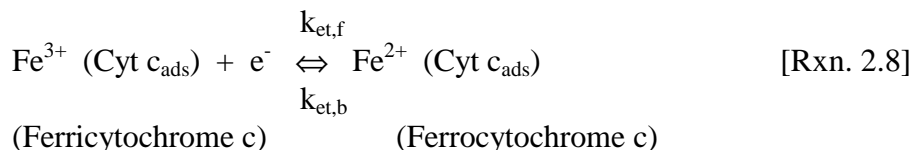


**Figure 2.20.** Side view of the cyt c / SAM / Au model system used in the Bowden Research Laboratory to study biological ET (a); top view of the system illustrating the relative dimensions of cyt c (red) to carboxylic acid terminal groups of the SAM (black). Cyt c is expected to have dimensions of 30Å x 35Å.



This system, in conjunction with the electrochemical technique of CV, allows for extensive studies of the thermodynamic and kinetic electrochemical properties of cyt c in an adsorbed state.

### 2.8.1. Electrochemical Properties of Cyt c

Although the voltammetric response of cyt c, shown in Figure 2.21, is highly stable and repeatable, it deviates significantly from the expected response of an ideally behaved adsorbed system (Sect. 2.6). The shape of the voltammogram itself differs from that of the adsorbed voltammogram shown in Figure 2.11. The peaks are not directly on top of each other but are rather offset from each other. This is a kinetic effect of the SAMs presence in the system. Because the ET must occur through the SAM, an extra kinetic variable is introduced which slows the reaction down and causes the peaks to split apart. The offset is greater with SAMs composed of longer alkyl chains and less with SAMs of shorter chain lengths.

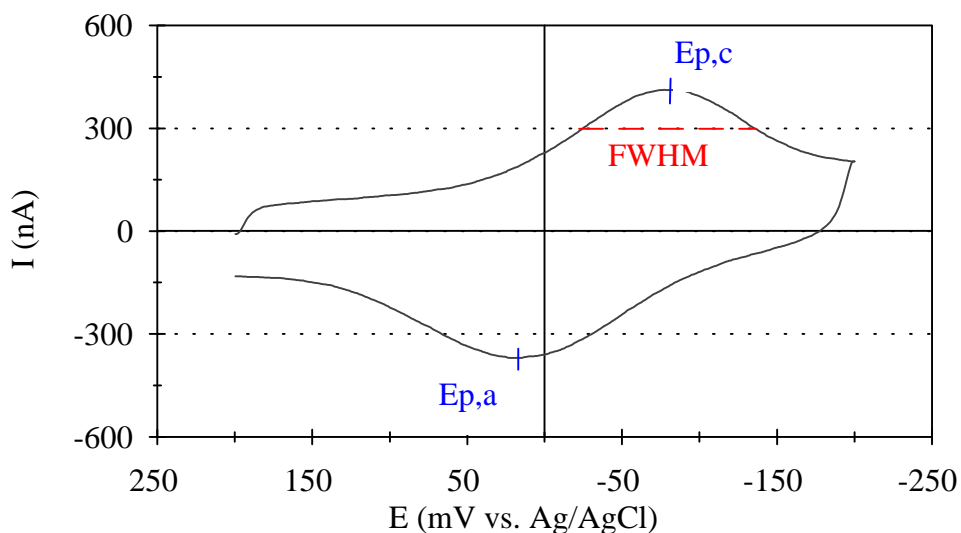


**Figure 2.21.** Cyclic voltammogram illustrating typical electrochemical behavior of cyt c adsorbed onto a Au surface modified with a carboxylic acid terminated SAM (14-MTDA or HS(CH<sub>2</sub>)<sub>13</sub>COOH). Peak broadening is seen with a deviation of the FWHM, which is typically measured in this system to be ~120-150 mV instead of the ideal value for adsorbed behavior (~90 mV).

Of the deviations from an ideal behavior, the most notable is the anomalous peak broadening seen with HH cyt c. The broadening of the voltammetric peaks is most easily illustrated by examining the full width at half maximum height (FWHM) measurements. Ideal adsorbed behavior would result in a CV which has a FWHM of 90 mV.<sup>28,29</sup> Commonly observed values of FWHM for cyt c experiments, where the protein is adsorbed to SAM and cyclic voltammetry is performed, are much larger in magnitude, sometimes ranging from 135 to 175 mV. The reason for this peak broadening is thought to be a consequence of a dispersion of electrochemical properties such as formal potential ( $E^{\circ'}$ ) and ET rate constants ( $k^{\circ_{et}}$ ) for the adsorbed cyt c coverage.<sup>32</sup> Typical values of cyt c electrochemical properties, including the FWHM measurements, at several different sized SAMs are provided as Table 2-3. Understanding this voltammetric peak broadening is a fundamental research objective of the Bowden Research Group.

### **2.8.2. Previous Research - Testing the Heterogeneous Adsorption Site Hypothesis**

It has been hypothesized that these inherently non-ideal electrochemical properties are caused by the existence of a heterogeneous adsorption surface, which, in turn, gives rise to a variation in cyt c adsorption energies. Therefore, the voltammetric behavior displayed by cyt c in this system can be thought of as the collective response of different subpopulations of adsorbed proteins which, depending on their interfacial microenvironments, may exhibit non-ideal electrochemical properties ( $E^{\circ'}$  and  $k^{\circ_{et}}$ ) and culminate in broadened voltammetry peaks.<sup>32</sup>

The heterogeneous adsorption site hypothesis was tested by a former researcher in the Bowden group, Rose Clark. Her research into the existence of heterogeneous adsorption sites was based on the assumption that the surface was composed of “strong” and “weak” adsorption sites only. It was believed that this simplification would show the more strongly retained cytochromes to exhibit specific electrochemical properties: more negative formal potentials, faster ET rate constants, and narrow FWHM values. All of these characteristics are highly indicative of cytochrome c molecules with excellent electronic coupling to the surface. The weakly bound cytochromes, on the other hand, were expected to show the opposite trend. To separately examine the electrochemical properties of the cytochromes

residing in each type of site, experiments had to be designed that could isolate and measure each population separately.

**Table 2-3.** Electrochemical Properties of Cyt c Voltammetry

SAM	Property	Monolayer Coverage <sup>a</sup>	Monolayer Coverage <sup>b</sup>	Electroactive submonolayer <sup>a</sup>	
				“Strong” sites	“Weak” sites
16-MHDA	E°(mV)	-32(± 4)	---	-52(± 3)	-27(± 3)
	Γ, pmol/cm <sup>2</sup>	13(± 3)	---	4.0(± 1.7)	6(± 1.5)
	FWHM, V	0.17(± 0.01)	---	0.14(± 0.01)	0.16(± 0.01)
	k <sub>et</sub> <sup>o</sup> , s <sup>-1</sup>	0.4(± 0.1)	---	0.4(± 0.1)	0.08(± 0.03)
14-MTDA	E°(mV)	---	-26(± 5)	---	---
	Γ, pmol/cm <sup>2</sup>	---	6.3(± 1.6)	---	---
	FWHM, V	---	0.12(± 0.01)	---	---
	k <sub>et</sub> <sup>o</sup> , s <sup>-1</sup>	---	0.9(± 0.1)	---	---
11-MUDA	E°(mV)	-32(± 4)	-17.6(± 9.2)	-58(± 2)	-23
	Γ, pmol/cm <sup>2</sup>	15.3(± 1)	13.1(± 5.2)	3(± 1)	5
	FWHM, V	0.135(± 0.004)	0.14 <sub>2</sub> (± 18)	0.115(± 0.005)	0.13
	k <sub>et</sub> <sup>o</sup> , s <sup>-1</sup>	---	5.7(± 6.6)	---	---
6-MHA	E°(mV)	-23(± 1)	-37	-40	-16(± 2)
	Γ, pmol/cm <sup>2</sup>	17.5(± 1)	---	6	9(± 3)
	FWHM, V	0.152(± 0.006)	0.10	0.125	0.130(± 0.008)

<sup>a</sup> Data collection by Rose Clark.<sup>32</sup> <sup>b</sup> Data collection by Michael Leopold.

E° ≡ Formal potential of redox reaction.

Γ ≡ Surface concentration of adsorbed cyt c.

FWHM ≡ Full width at half maximum of a voltammetric peak.

k<sub>et</sub><sup>o</sup> ≡ Electron transfer kinetic rate constant (calculated using Laviron's theorem )

16-MHDA = 16-mercaptohexadecanoic acid; 14-MTDA = 14-mercaptotetradecanoic acid;

11-MUDA = 11-mercaptoundecanoic acid; 6-MHA = 6-mercaptohexanoic acid.

The strongly bound cyt c molecules were investigated using a series of ionic strength based desorption experiments. By treating (rinsing) the monolayer of adsorbed cyt c with successively higher ionic strength buffers than the original buffer that the protein was adsorbed in, the electrostatic attraction between the SAM and the protein is gradually diminished and the protein tends to desorb from the surface. Thus, ionic strength experiments, as shown in Figure 2.22, are designed to progressively remove the weakly bound cyt c molecules, eventually leaving only the very strongly bound cytochromes on the surface and available for electrochemical analysis. Experimental results, shown in Figure 2.23, show the more strongly adsorbed cyt c subpopulation does indeed display a more negative formal potential, faster ET rate constants, and narrower FWHM, with each parameter converging toward nearly ideal voltammetric behavior for an adsorbed species.

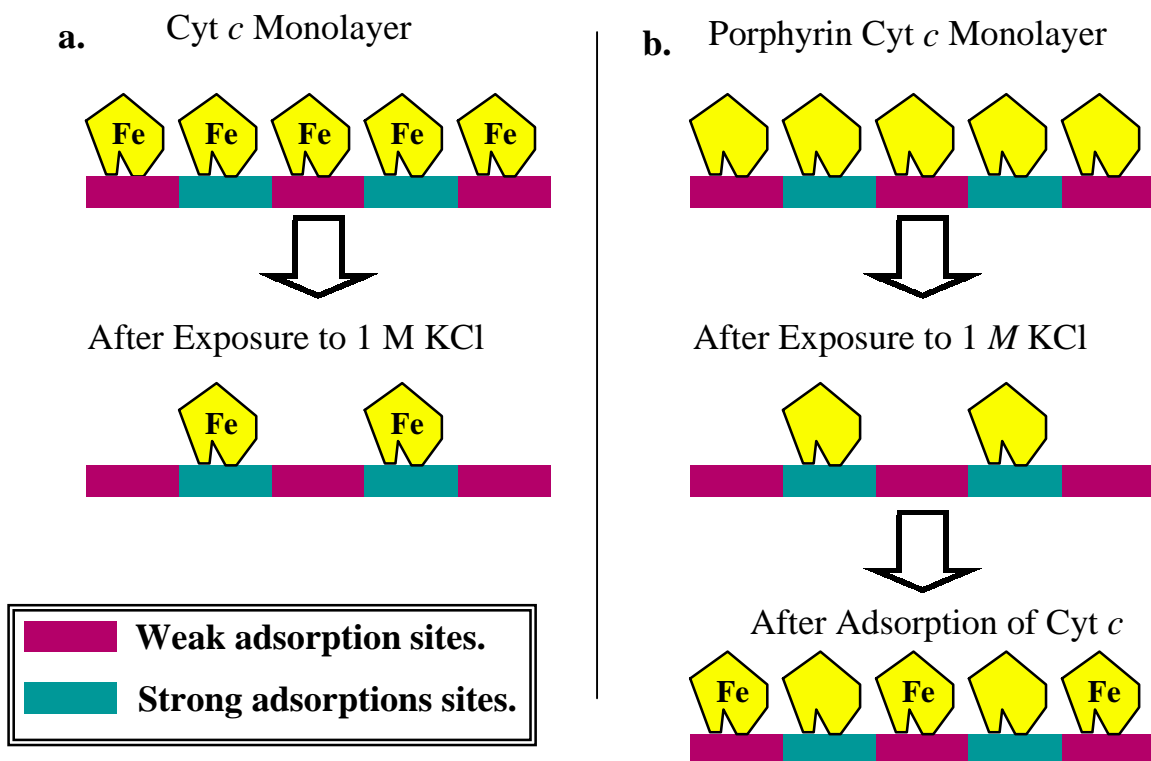


**Figure 2.22.** Generalized schematic diagram depicting the experimental methods used to separately investigate sub-populations of electroactive cyt *c* on a heterogeneous "two site" surface: a) strongly adsorbed cyt *c*; b) weakly adsorbed cyt *c* (Adapted from a Figure in Ref. 32)

"Weaker" sites were then examined by excluding the cyt *c* adsorption from the "stronger" sites. To do this, porphyrin cyt *c* (Pcyt *c*) was utilized. Pcyt *c* is structurally very similar to native cyt *c* except for the fact that it has been rendered electroinactive by the removal of its iron redox core. Experiments involving Pcyt *c* were advantageous for this type of study because the molecule possesses a larger affinity to bind to with the acid surface and will quantitatively displace any bound cyt *c*.<sup>80</sup> Once the Pcyt *c* had blocked all the adsorption sites, the weaker sites were opened up for subsequent adsorption of the native HH cyt *c* by exposing the adsorbed layer of Pcyt *c* to a high ionic strength buffer. A schematic diagram of this experimental phase of the testing is also shown in Figure 2.22. With electroactive protein now occupying the weak adsorption sites, and electroinactive Pcyt *c* adsorbed in all the other adsorption sites, electrochemical

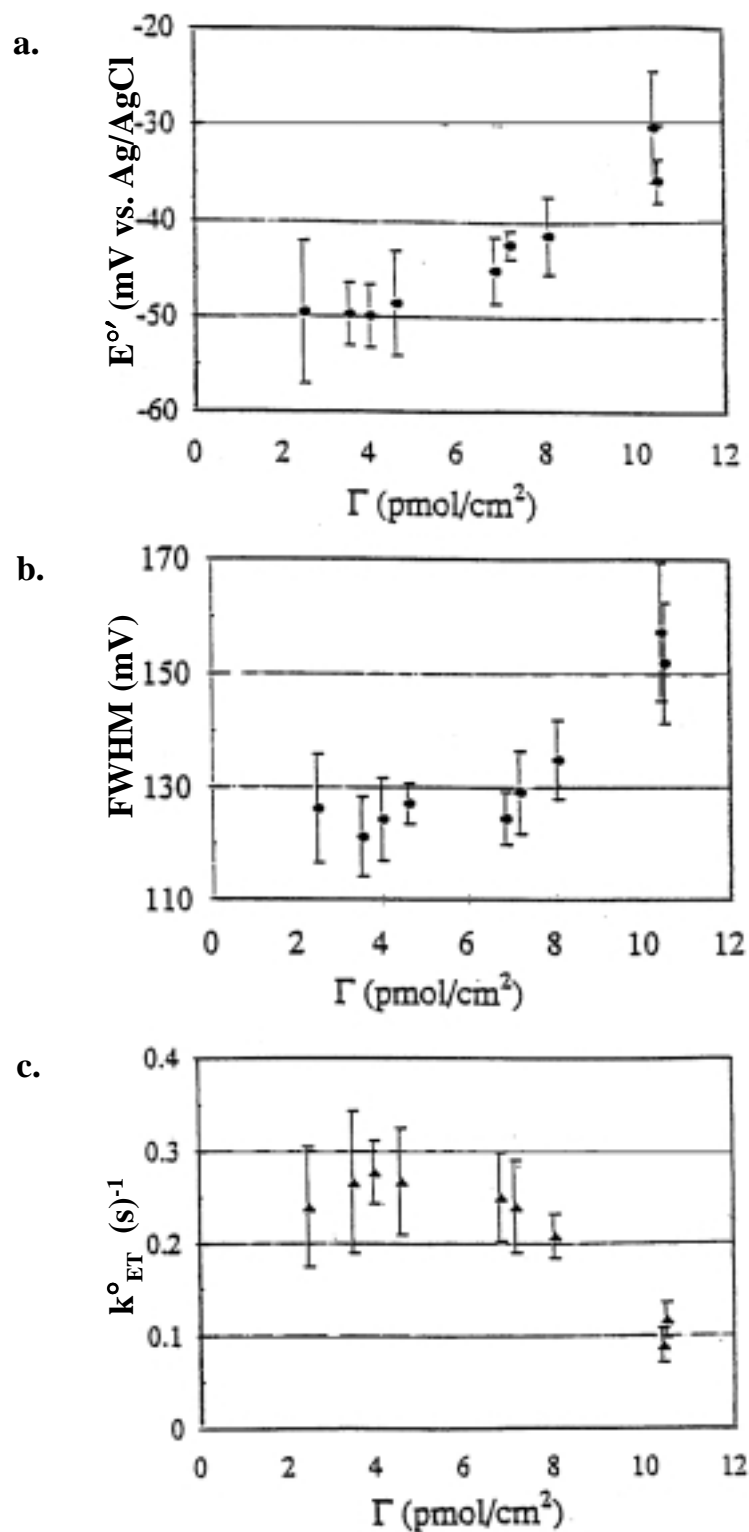


**Figure 2.23.** Desorption plots of a) formal potential ( $E^{\circ'}$ ), b) FWHM, and c) ET rate constant ( $k_{ET}^{\circ}$ ) as a function of electroactive surface coverage ( $\Gamma$ ) for a cyt c/16-MHDA SAM/Au. The ionic strength of the desorption buffers was increased (10→80 mM) from left to right across the plots, eventually only exposing “strongly” bound cyt c (Figure from Ref. 32).

measurements accounting solely for the weakly bound cyt c could be performed. A direct comparison of the results from these experiments is included as part of Table 2-3. The results of these experiments support the hypothesis that heterogeneous adsorption sites exist and may be a major reason for the observed peak broadening seen in cyt c voltammetry. Furthermore, these results suggest that surface aspects of the cyt c adsorption process, specifically the sources of the heterogeneity found in adsorption sites, require further examination to better understand this system.

## **2.9. FOCUS OF DISSERTATION RESEARCH**

Previously obtained electrochemical results, discussed in the preceding section, have suggested that surface related phenomena may play an intrinsic role in the ET and adsorption properties of cyt c.<sup>32</sup> The research composing this dissertation will focus on the notion that the sources and reasons accounting for these surface effects lie in the physical characteristics of the surfaces involved and can be specifically identified, controlled, and understood through strategic experimentation. Therefore, the basis of the research presented in this dissertation is to characterize these effects and delineate their contributions to the electrochemical response of cyt c. By gaining a thorough comprehension of the surface structure involved with the cyt c ET system, this research may, on a molecular level, begin to substantiate an accurate physical model for the study of biological redox chemistry.

### **2.9.1. Surfaces and Objectives of Research**

When presented with surface studies of a system such as the cyt/SAM/Au model, three surfaces must be considered. Depicted in Figure 2.24, these three surfaces consist of the surface of the gold substrate itself, the surface presented by the terminal groups of the SAM at the SAM/solution interface, and the surface of the overall system when a monolayer of protein is adsorbed onto the SAM modified Au substrate. Each of these surfaces must be evaluated because they all can easily exert an influence on the adsorption behavior of cyt c.

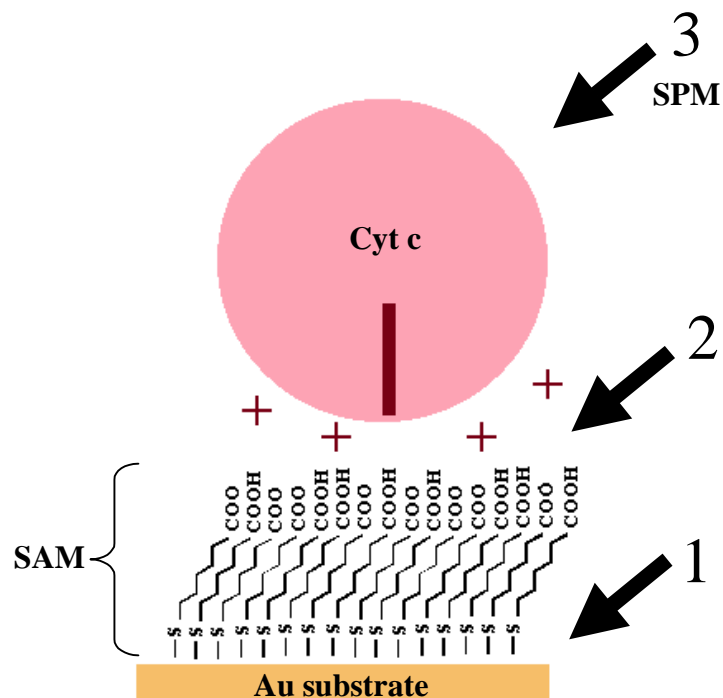


**Figure 2.24.** Illustration of the cyt c/SAM/Au system and the three major surfaces to be investigated: the gold substrate (Chapter 3), the SAM/solution interface (Chapter 4), and the surface of the overall system (Chapter 5). Chapter 5 is primarily a SPM study of the system.

The objectives of the research presented here somewhat coincide with these three surfaces. The specific objectives of this research are as follows:

**1. Determine the role of the Au substrate in cyt c voltammetry;**

A primary goal will be to gain a deeper understanding of how the surface characteristics and topographical features of the gold substrate influence the formation and structure of the SAM and, ultimately, the adsorption and subsequent ET properties of cyt c. Correlating specific surface characteristics of Au to voltammetry is desired to fulfill this objective. Examining the influence of the Au substrate in the voltammetry of cyt c adsorbed on carboxylic acid terminated SAMs is the focus of Chapter 3.

**2. Determine the specific nature of the SAM/cyt c interface;**

The interaction between cyt c and the SAM is an integral aspect of this system. Specific experiments will be used to elucidate the nature of the bonding between cyt c and the acid terminated SAM. Believed to be largely electrostatic, the interaction between the two components needs to be better understood, especially on a molecular level. Adjunct to this objective is an assessment of defect density in the monolayer and an evaluation of their

impact on protein adsorption. SAM defect sites have the potential to play a major role in the electrochemistry of this system. This research objective is addressed in greater detail and is the subject matter of Chapter 4.

**3. *Physically characterize all of the interfaces between substrates, SAMs, and cytochrome c on a molecular level;***

Scanning probe microscopy (SPM) is used to explore the molecular aspects of the surfaces of each component: the Au substrate topography, the SAM surface structure, and the adsorbed cyt c molecules. Specifically, the distribution of adsorbed cyt c molecules and a more accurate physical picture of the cyt c coverage is sought. Eventually, SPM will also be used to explore the specific adsorption sites on the SAM. This type of exploration would possibly allow for the direct comparison of adsorption and electrochemical properties of cyt c adsorbed on highly ordered regions of the SAM to those proteins localized at defect sites. Moreover, it is hopeful that SPM will be utilized to identify or differentiate between individually adsorbed, electroactive or electroinactive cytochrome molecules. SPM and its application to the cyt/SAM/Au system is the basis for Chapter 5.

While all three of these objectives have been addressed to some degree in this body of work, all of them were not completely achieved. However, certain aspects of these objectives remain part of the projected research in the Bowden Group and will be addressed in this dissertation with a discussion about possible experiments and research directions for the future. Accomplishing all three of these objectives to a substantial degree, should elucidate important aspects of the surfaces involved; aspects which must be understood and applied to PME strategies if the potential of these systems as a model for ET is to be realized.

**2.9.2. Methodology and Approach**

Electrochemistry (E/C) and scanning probe microscopy (SPM) are the primary modes of experimentation that are utilized for the surface studies to be discussed. E/C is a powerful tool for evaluating the overall operation of a system by divulging statistically averaged information about a population of sample molecules. However, E/C yields information strictly about the electroactive molecules and lacks the sensitivity needed to learn about the specific surface adsorption properties being considered. SPM, on the other hand, provides the opportunity to gain a more detailed understanding of such surface bound assemblies.

SPM is ideal for probing localized electronic states as well as topographical information that is imperative to any surface science. With the recent advancements in the SPM field, one can envision using SPM techniques to selectively probe the electrochemical behavior of individual adsorbed molecules or, as in this case, specifically adsorbed proteins. All of the research contained herein is conducted using this complimentary dual approach. Additionally, other techniques are used to supplement the bulk E/C and SPM results.

A lengthy discussion about SPM and specific information about the electroanalytical techniques is unnecessary at this point. Within each chapter, however, the techniques employed and the experiments performed are described as needed, usually as part of the experimental details section found at the end of each chapter.

### **2.9.3. Organization of Dissertation**

The subsequent chapters of this dissertation focus on each of these surfaces. Beginning with Chapter 3, where the role of the Au substrate in cyt c voltammetry is examined in detail, there is essentially a chapter of work dedicated to each of the surfaces involved: the Au substrate, the SAM/solution interface, and the overall system. Each chapter begins with an introduction, experimental data and results, a discussion of those results. Each chapter ends with experimental details, author's notes, and finally an offering of future directions for the research. More specifically, Chapter 3 contains two major sections: one dedicated to preliminary results and a section devoted to more substantiated results. Chapter 4 will focus on the SAM/solution interface, where experiments were designed to specifically alter this interface with respect to controlling how the cyt c voltammetry will respond. Finally, SPM and the molecular scale evaluation of all aspects of the cyt c/SAM/Au system will be the directive of Chapter 5. As alluded to earlier, not all of these surfaces and chapters are developed to the same extent. Largely due to time and money constraints, some topics are covered in greater detail, and some require further investigations, perhaps an opportunity for another aspiring scientist in the Bowden Research Group.

Two appendices are included as part of this dissertation. The subject matter of the appendices are based on research done as a collaborative effort between Professor Bowden's group and others. Although, for the most part, these side projects are unrelated to surface studies of the cyt c/SAM/Au system, they represent new avenues of discovery for the Bowden

research group and an overall expansion of the application of electrochemistry into new areas of research. The first appendix focuses on a materials science/nanotechnology study done in collaboration with Professor Chris Gorman (NCSU). This project consisted of studying the ET of dendritic polymer encapsulated molecules, precursors for viable molecular information storage units. The second appendix consists of experiments involving the substrate indium tin oxide (ITO). Related to the primary research system of the Bowden Group, cytochrome c/SAM/Au, the electrochemistry of cytochrome c adsorbed on these metal oxide films and the electrochemical properties of these substrates was examined. In conjunction with Dr. Ashley Bush (Harvard Medical School/Massachusetts General Hospital), electrochemistry at ITO electrodes was investigated with respect to its potential usefulness in delineating drug pathways and neurological diseases.

In summary, the research presented in this dissertation addresses a specific adsorbed protein system that can be used to understand fundamental aspects of protein adsorption and ET processes. The very nature of this work lends itself to being directly significant to the advancement of protein monolayer electrochemistry as a means of simplifying complex ET kinetic analysis. This strategy allows for extensive investigations into normally complex redox protein behavior. Exploration of these types of processes, will not only assist in the development of advanced ET theory, but will help lay the foundation of knowledge required for the creation of useful bioanalytical technologies like real time amperometric biosensors and biocompatible implants.

## 2.10 REFERENCES

1. E.F. Bowden, R.A. Clark, J.L. Willit, and S. Song, "Protein Monolayer Electrochemistry: A Strategy for Probing Biological Electron Transfer Kinetics," In *Proceedings of the Fifth International Symposium on Redox Mechanisms and Interfacial Properties*, F. Shultz and I. Taniguchi, Eds., The Electrochemical Society: Pennington, New Jersey, 1993, 34-45.
2. a) J. Deisenhofer and H. Michel, *Science*, **1989**, *245*, 1463-1474; b) J. Deisenhofer and H. Michel, *Chemica Scripta*, **1989**, *29*, 205-220; c) G. Feher, J.P. Allen, M.Y. Okamura, and D.C. Rees, *Nature*, **1989**, *339*, 111-116.
3. a) J.R. Bolton, N. Mataga, and G. McLendon, "Electron Transfer in Inorganic, Organic, and Biological Systems," In *Advances in Chemistry Series 228*, American Chemical Society: Washington D.C., 1991; b) B.E. Bowler, A.L. Raphael, and H.B. Gray, *Progr. Inorg. Chem.*, **1990**, *38*, 259-322; c) C.C. Moser, J.M. Keske, K. Warncke, R.S. Farid, and P.L. Dutton, *Nature*, **1992**, *355*, 796-802.
4. E.F. Bowden, "Wiring Mother Nature: Interfacial Electrochemistry of Proteins," *The Electrochemical Society: Interface*, **1997**, *6*, 40-44.
5. a) R.A. Scott, A.G. Mauk, and H.B. Gray, *J. Chem. Edu.*, **1985**, *62* 932-938; b) R. Marcus and N. Sutin, *Biochim. Biophys. Acta*, **1985**, *811*, 265-322; c) J.R. Bolton, and M.D. Archer, *Adv. Chem. Ser.*, **1991**, *228*, 7.
6. a) S. Ferguson-Miller, D.L. Brautigan, and E. Margoliash, In *The Porphyrins*, Vol. 7B, D. Dolphin, Ed., Academic Press: New York, 1979; b) N. Sutin, *Adv. Chem. Ser.*, **1977**, *162*, 156.
7. G. Palmer, Ed., "Long-Range Electron Transfer in Biology," In *Structure and Bonding Series*, Vol. 75, Springer-Verlag: Berlin, 1991, pp. 160-174.
8. a) J.R. Winkler, H.B. Gray, *Chem. Rev.*, **1992**, *92*, 369-379; b) J.R. Scott, A. Willie, M. McLean, P.S. Stayton, S.G. Sligar, B. Durham, and F. Millett, *J. Am. Chem. Soc.*, **1993**, *115*, 6820-6824.
9. a) R. Seetharaman, S.P. White, and M. Rivera, *Biochemistry*, **1996**, *35*, 12455-12463; b) S.M. Andrew, K.A. Thomasson, and S.H. Northrup, *J. Am. Chem. Soc.*, **1993**, *115*, 5516-5521; c) M.R. Mauk, L.S. Reid, A.G. Mauk, *Biochemistry*, **1982**, *21*, 1943-1846; d) F.R. Salemme, *J. Mol. Biol.*, **1976**, *102*, 563-568.
10. a) A.G. Mauk, M.K. Mauk, G.R. Moore, Sh.H. Northrup, *J. Bioenerg. Biomembr.*, **1995**, *27*, 311-330; b) B. Durham, J.L. Fairris, M. McLean, F. Millett, J.R. Scott, S.G. Sligar, and A. Willie, *J. Bioenergetics Biomembranes*, **1995**, *27*, 331-340.
11. a) E.F. Bowden, F.M. Hawkrigde, and H.N. Blount in *Comprehensive Treatise of Electrochemistry*, Volume 10, S. Srinivasan, Y.A. Chizmadzhev, J.O.M. Bockris, B.E. Conway, and E. Yeager, Eds. Plenum Press: New York, 1985, p. 297; b) F.A. Armstrong, H.A.O. Hill, and N.J. Walton, *Acc. Chem. Res.* **1988**, *21*, 407-413.

12. a) P. Yeh, and T. Kuwana, *Chem. Lett.* **1977**, 1145-1148. b) F.A. Armstrong, H.A.O. Hill, P.A. Cox, V.J. Lowe, and B.N. Oliver, *J. Electroanal. Chem.* **1987**, 217, 331-366.
13. M.J. Eddowes and H.A.O. Hill, *J. Chem. Soc. Chem. Commun.* **1977**, 771-772.
14. H.L. Landrum, R.T. Salmon, and F.M. Hawkridge, *J. Am. Chem. Soc.* **1977**, 99, 3154-3158.
15. J. Hirst, A. Sucheta, B.A. C. Ackrell, and F.A. Armstrong, "Electrocatalytic Voltammetry of Succinate Dehydrogenase: Direct Quantification of the Catalytic Properties of a Complex Electron-Transport Enzyme," *J. Am. Chem. Soc.* **1996**, 118, 5031-5038.
16. J.K. Cullison, F.M. Hawkridge, N. Nakashima, and S. Yoshikawa, "A study of cytochrome c oxidase in lipid bilayer membranes on electrode surfaces," *Langmuir* **1994**, 10, 877-882.
17. W.J. Albery, M.J. Eddowes, H.A.O. Hill, and A.R. Hillman, *J. Am. Chem. Soc.* **1981**, 103, 3904.
18. a) T. Sagara, K. Niwa, A. Sone, C. Hinnin, and K. Niki, "Redox Mechanism of Cytochrome c at Modified Gold Electrodes," *Langmuir* **1990**, 6, 254-262; b) C. Hinnin, and K. Niki, *J. Electroanal. Chem.* **1989**, 264, 157-165; c) K. Niwa, M. Furukawa, and K. Niki, *J. Electroanal. Chem.* **1988**, 254, 275-285; d) K. Niki, Y. Kawasaki, Y. Kimuma, Y. Higuchi, and N. Yasuoki, *Langmuir* **1987**, 3, 982-986; e) C. Hinnen, R. Parsons, K. Niki, *J. Electroanal. Chem.* **1983**, 147, 329-337; f) D. Zhang, G.S. Wilson, and K. Niki, *Anal. Chem.* **1994**, 66, 3873-3881.
19. a) Butt, S.J. George, E.C. Hatchikian, A.J. Thompson, J. Breton, and F.A. Armstrong, *J. Am. Chem. Soc.* **1991**, 113, 6663-6670; b) F.A. Armstrong, J.N. Butt, S.J. George, E.C. Hatchikian, and A.J. Thompson, *FEBS Lett.* **1989**, 258, 15-18.
20. a) E.A.E. Garber, E. Margoliash, *Biochim. Biophys. Acta* **1990**, 1015, 279-287; b) J.T. Hazzard, G. McLendon, M.A. Cusanovich, and G. Tollin, *Biochem. Biophys. Res. Commun.* **1988**, 151, 429-453; c) S.H. Northrup, J.O. Boles, J.C.L. Reynolds, *Science* **1988**, 241, 67-70; d) J.J. Wendolfski, J.B. Mathew, P.C. Wever, F.R. Salemme, *Science* **1987**, 238, 794-797; e) J. Willit and E.F. Bowden, *J. Electroanal. Chem.* **1987**, 221, 265-274.
21. a) F.A. Armstrong, S.J. George, R. Cammack, E.C. Hatchikian, and A.J. Thomson, *Biochem. J.* **1989**, 264, 265-273; b) J.N. Butt, A. Sucheta, E.C. Hatchikian, A.J. Thompson, J. Breton, and F.A. Armstrong, *J. Am. Chem. Soc.* **1991**, 113, 8948-8950.
22. J.J.R. Frausto da Silva and R.J.P. Williams, *The Biological Chemistry of the Elements - The Inorganic Chemistry of Life*, Clarendon Press: Oxford, 1991.
23. a) J.T. Hupp and M.J. Weaver, *J. Electroanal. Chem.* **1983**, 145, 43-51; b) J.T. Hupp and M.J. Weaver, *J. Phys. Chem.* **1985**, 89, 2795-2804.
24. G. McLendon, *Acc. Chem. Res.* **1988**, 21, 160-167; b) D.W. Dixon, X. Hong, S.E. Woehler, G.A. Mauk, B.P. Sishita, *J. Am. Chem. Soc.* **1990**, 112, 1082-1088.
25. T.M. Nahir, J.M. Wallace, and E.F. Bowden, results unpublished.

26. Proposal to the National Science Foundation by Edmond F. Bowden, "Protein Monolayer Electrochemistry," 1993.
27. a) J. Willit and E.F. Bowden, in *Redox Chemistry and Interfacial Behavior of Biological Molecules*, G. Dryhurst and K. Niki, Eds., Plenum Press: New York, 1988, p. 63; b) J.L. Willit and E.F. Bowden, "Adsorption and Redox Thermodynamics of Strongly Adsorbed Cytochrome c on Tin Oxide Electrodes," *J. Phys. Chem.* **1990**, *94*, 8241; c) M. Collinson and E.F. Bowden, *Anal. Chem.* **1992**, *64*, 1470; d) M. Collinson, M.J. Tarlov and E.F. Bowden, "Voltammetry of Covalently Immobilized Cytochrome c on Self-Assembled Monolayer Electrodes," *Langmuir* **1992**, *8*, 1247-1250; e) T.T. Li and M.J. Weaver, *J. Am. Chem. Soc.* **1984**, *106*, 6107.
28. C.M.A. Brett and A.M.O. Brett, *Electrochemistry - Principles, Methods, and Applications*, Oxford University Press: Oxford, 1993.
29. A.J. Bard and L.R. Faulkner, *Electrochemical Methods - Fundamentals and Applications*, John Wiley and Sons, Inc.: New York, 1980.
30. a) J.H. Reeves, S. Song, and E.F. Bowden, *Anal. Chem.* **1993**, *65*, 683; b) J. Osteryoung, *Acc. Chem. Res.* **1993**, *26*, 77.
31. a) S. Burris and E.F. Bowden, results unpublished; b) J.L. Willit, Ph.D. thesis, p. 74.
32. R.A. Clark and E.F. Bowden, "Voltammetric Peak Broadening for Cytochrome c/Alkanethiolate Monolayer Structures: Dispersion of Formal Potentials," *Langmuir* **1996**, *13*, 559-565.
33. E.F. Bowden, F.M. Hawkridge, and H.N. Blount, *J. Electroanal. Chem.* **1984**, *61*, 355-376.
34. F.A. Armstrong, *Struct. Bonding (Berlin)* **1990**, *72*, 137-221.
35. a) I. Taniguchi, K. Toyosawa, H. Yamaguchi, and K. Yasukouchi, *J. Chem. Soc. Chem. Commun.* **1982**, 1032-1033; b) I. Taniguchi, H. Yamaguchi, and K. Yasukouchi and M. Iseki, *J. Electroanal. Chem.* **1984**, *175*, 341-348; c) I. Taniguchi, H. Yamaguchi, and K. Yasukouchi and M. Iseki, *J. Electroanal. Chem.* **1985**, *186*, 299-307.
36. a) S. Song, R.A. Clark, M.J. Tarlov and E.F. Bowden, "Characterization of Cytochrome c / Alkanethiolate Structures Prepared by Self-Assembly on Gold," *J. Phys. Chem.* **1993**, *97*, 6564-6572; b) A.E. Kasmir, J.M. Wallace, E.F. Bowden, S.M. Binet, and R.J. Linderman, "Controlling Interfacial ET Kinetics of Cyt c with Mixed SAMs," *J. Am. Chem. Soc. Comm.* **1998**, *120*, 225-226; c) M.J. Tarlov and E.F. Bowden, "Electron-Transfer Reaction of Cytochrome c Adsorbed on Carboxylic Acid Terminated Alkanethiol Monolayer Electrodes," *J. Am. Chem. Soc.* **1991**, *113*, 1847-1849.
37. Proposal to the National Science Foundation by Edmond F. Bowden, "Protein Monolayer Electrochemistry," 1998.
38. a) R.E. Dickerson, T. Takano, D. Eisenberg, O.B. Kallai, L. Samson, A. Cooper, and E. Margoliash, *J. Biol. Chem.* **1971**, *246*, 1511; b) R.E. Dickerson and R. Timkovich, In *The Enzymes*, P.D. Boyer, Ed., Academic Press: New York, Vol. XIA, 1975, pp. 397-547; c) S.

Ferguson-Miller, D.L. Brautigan, and E. Margoliash, In *The Porphyrins*, D. Dolphin, Ed., Academic Press: New York, Vol. VIIB, 1979, pp. 149-240.

39. E. Stellwagen, *Nature* **1978**, 275, 73-74.
40. G.W. Pettigrew, G.R. Moore, *Cytochromes c: Biological Aspects*, Springer Verlag: Heidelberg, 1990.
41. D.M. Tiede, A.C. Vashista, and M.R. Gunner, *Biochemistry* **1993**, 32, 4515-4531.
42. S.L. Wolfe, *Molecular and Cellular Biology*, Wadsworth Publishing Company: Belmont, California, 1993.
43. H. O. Finklea, "Electrochemistry of Organized Monolayers of Thiols and Related Molecules on Electrodes," A.J. Bard and I. Rubinstein (Eds.), *Electroanalytical Chemistry - A Series of Advances*, Vol. 19, 108-335, Marcel Dekker: New York, New York, 1996.
44. a) M.D. Porter, T.B. Bright, D.L. Allara, and C.E.D. Chidsey, "Spontaneously Organized Molecular Assemblies. 4. Structural Characterization of n-Alkyl Thiol Monolayers on Gold by Optical Ellipsometry, Infrared Spectroscopy, and Electrochemistry," *J. Am. Chem. Soc.* **1987**, 109, 3559-3568; b) R.G. Nuzzo, L.H. Dubois, and D.L. Allara, "Fundamental Studies of Microscopic Wetting on Organic Surfaces. 1. Formation and Structural Characterization of a Self-Consistent Series," *J. Am. Chem. Soc.* **1990**, 112, 558-569; c) L.H. Dubois, B.R. Zegarski, and R. Nuzzo, "Fundamental Studies of Microscopic Wetting on Organic Surfaces. 2. Interaction of Secondary Adsorbates with Chemically Textured Organic Monolayers," *J. Am. Chem. Soc.* 1990, 112, 570-579.
45. a) T. Ishida, M. Hara, I. Kojima, S. Tsuneda, N. Nishida, H. Sasabe, and W. Knoll, "High Resolution X-ray Photoelectron Spectroscopy Measurements of Octanethiol Self-Assembled Monolayers on Au(111)," *Langmuir* **1998**, 14, 2092-2096; b) T. Ishida, M. Hara, S. Tsuneda, N. Nishida, H. Sasabe, and W. Knoll, "Surface-Conditioning Effect of Gold Substrates on Octadecanethiol Self-Assembled Monolayer Growth," *Langmuir* **1997**, 13(17), 4638-4643.
46. J.H. Griffin, et. al., *Langmuir* 1994, 10, 883-889.
47. a) P.E. Laibinis, G.M. Whitesides, D.L. Allara, Y-T. Tao, Atul N. Parikh, and R.G. Nuzzo, "Comparison of the Structures and Wetting Properties of Self-Assembled Monolayers of n-Alkanethiols on the Coinage Metal Surfaces, Cu, Ag, Au," *J. Am. Chem. Soc.* **1991**, 113, 7152-7167; b) P.E. Laibinis and G.M. Whitesides, " $\omega$ -Terminated Alkanethiolate Monolayers on Surfaces of Copper, Silver, and Gold Have Similar Wettabilities," *J. Am. Chem. Soc.* **1992**, 114, 1990-1995.
48. A. Demoz and D.J. Harrison, "Characterization of Extremely Low Defect Density Hexadecanethiol Monolayers on Hg Surfaces," *Langmuir* **1993**, 9, 1046-1050.
49. a) M. Mrksich and G.W. Whitesides, "Using Self-Assembled Monolayers to Understand the Interactions of Man-Made Surfaces with Proteins and Cells," *Annual Review of Biophysics and Biomolecular Structure*, **1996**, 25, 55-78. b) D. Mandler and I. Turyan, "Applications of Self-Assembled Monolayers in Electroanalytical Chemistry," *Electroanalysis* **1996**, 8(3), 207-213; c)

- C.B. Gorman and G.M. Whitesides, "Self-Assembled Monolayers: Models for Organic Surface Chemistry," *In Handbook of Surface Imaging and Visualization*, A.T. Hubbard, Ed., CRC Press: NY, 1995.
50. a) H.O. Finklea, S. Avery, M. Lynch, "Blocked Oriented Monolayers of Alkyl Mercaptans on Gold Electrodes," *Langmuir* **1987**, *3*, 409-413; b) H.M. Schessler, D.S. Karpovich, and G.J. Blanchard, "Quantitating the Balance Between Enthalpic and Entropic Forces in Alkanethiol/Gold Monolayer Self Assembly," *J. Am. Chem. Soc.* **1996**, *118*, 9645-9651.
  51. a) C.E.D. Chidsey and Dominic Loiacono, "Chemical Functionality in Self-Assembled Monolayers: Structural and Electrochemical Properties," *Langmuir* **1990**, *6*, 682-691; b) M.H. Schoenfisch and J.E. Pemberton, "Air Stability of Alkanethiol Self-Assembled Monolayers on Silver and Gold Surfaces," *J. Am. Chem. Soc.*, submitted.
  52. C.D. Bain, E.B. Troughton, Y.T. Tao, J. Evall, G.M. Whitesides, and R.G. Nuzzo, "Formation of Monolayer Films by the Spontaneous Assembly of Organic Thiols from Solution onto Gold," *J. Am. Chem. Soc.* **1989**, *111*, 321-335.
  53. a) E. Delamarche, et al., *Science* **1997**, *276*, 2021; b) P. Fenter, A. Eberhardt, K.S. Liang, and P. Eisenberger, "Epitaxy and Chainlength Dependent Strain in Self-Assembled Monolayers," *J. Chem. Phys.* **1997**, *106*(4), 1600-1607;
  54. a) E.L. Smith, C.A. Alves, J.W. Anderegg, M.D. Porter, L.M. Siperko, *Langmuir* **1992**, *8*, 2707-2714; b) E. Delamarche and H.A. Biebuyck, *Advanced Materials* **1996**, *8*(9), 719-729.
  55. G.M. Whitesides, R.G. Nuzzo, and P.E. Laibinis, *J. Phys. Chem.* **1992**, *96*, 5097-5105.
  56. G.K. Jennings and P.E. Laibinis, "Underpotentially Deposited Metal Layers of Silver Provide Enhanced Stability to Self-Assembled Alkanethiol Monolayers on Gold," *Langmuir* **1996**, *12*, 6173-6175.
  57. a) E. Sabatani, J. Cohen-Boulakia, M. Bruening, and I. Rubinstein, "Thioaromatic Monolayers on Gold: A New Family of Self-Assembling Monolayers," *Langmuir* **1993**, *9*, 2974-2981; b) Y-Q. Wang, H-Z. Yu, J-Z. Cheng, J-W. Zhao, S-M. Cai, and Z-F. Liu, "End-Group-Dominated Electrochemical Kinetics of Axobenzene Self-Assembled Monolayers on Gold," *Langmuir* **1996**, *12*, 5466-5471; c) M. French and S.E. Creager, "Enhanced Barrier Properties of Alkanethiolate-Coated Gold Electrodes By 1-Octanol in Solution," *Langmuir* **1998**, *14*, 2129-2133.
  58. a) S.E. Creager, L.A. Hockett, and G.K. Rowe, "Consequences of Microscopic Surface Roughness for Molecular Self-Assembly," *Langmuir* **1992**, *8*, 854-861; b) E. Katz and I. Willner, "Kinetic Separation of Amperometric Responses of Composite Redox-Active Monolayers Assembled onto a Au Electrode: Implications to the Monolayer's Structure and Composition," *Langmuir* **1997**, *13*, 3364-3373.
  59. a) P. Tengrall, B. Leidberg, and M. Lestelius, *Langmuir* **1997**, *13*, 5900-5908; b) C. Miller, et. al. *J. Phys. Chem.* **1991**, *95*, 877-886; c) H.O. Finklea, D.A. Snider, and John Fedyk, "Characterization of Octadecanethiol-Coated Gold Electrodes as Microarray Electrodes by Cyclic Voltammetry and AC Impedance Spectroscopy," *Langmuir* **1993**, *9*, 3660-3667.

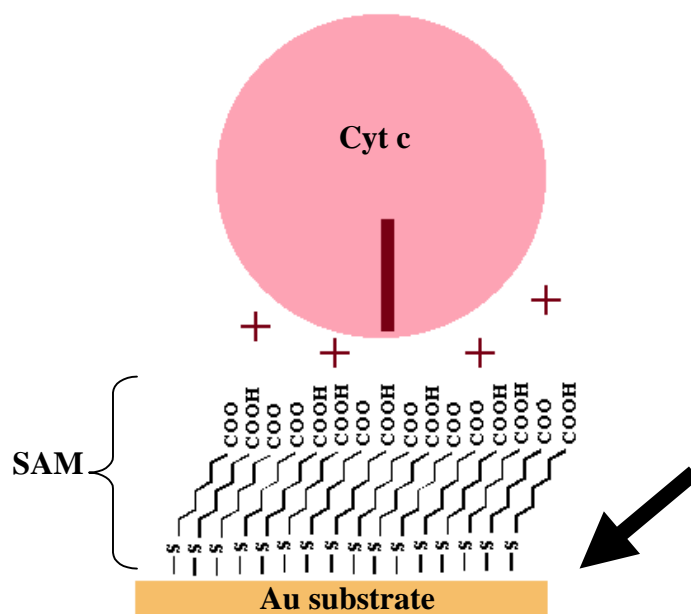
60. a) M.R. Anderson, M.N. Evaniak, and M. Zhang, "Influence of Solvent on the Interfacial Structure of Self-Assembled Alkanethiol Monolayers," *Langmuir* **1996**, *12*(10), 2327-2331; b) O. Dannenberger, J.J. Wolff, and M. Buck, "Solvent Dependence of the Self-Assembly Process of an Endgroup-Modified Alkanethiol," *Langmuir* **1998**, *14*, 4679-4682.
61. E. Delamarche and B. Michel, "Structure and Stability of Self-Assembled Monolayers," *Thin Solid Films* **1996**, *273*, 54-60.
62. a) E. Cooper and G.J. Leggett, "Influence of Tail-Group Hydrogen Bonding on the Stabilities of Self-Assembled Monolayers of Alkylthiols on Gold," *Langmuir* **1999**, *15*, 1024-1032; b) R.S. Clegg and J.E. Hutchison, "Hydrogen Bonding, Self-Assembled Monolayers: Ordered Molecular Films for Study of Through Peptide Electron Transfer," *Langmuir* **1996**, *12*(22), 5239-5243; c) E. Delamarche, M. Sprik, B. Michel, U. Rothlisberger, M.L. Klein, H. Wolf, and H. Ringsdorf, "Structure of Hydrophilic Self-Assembled Monolayers: A Combined Scanning Tunneling Microscopy and Computer Simulation Study," *Langmuir* **1994**, *10*, 4116-4130;
63. S. Chen, R.S. Ingram, M.J. Hostetler, J.J. Pietron, R.W. Murray, T.G. Schaaff, J.T. Khoury, M.M. Alvarez, and R.L. Whetten, "Gold Nanoelectrodes of Varied Size: Transition to Molecule-Like Charging," *Science* **1998**, *280*, June 26, 2098-2101.
64. a) I. Touzov and C.B. Gorman, "Tip Induced Structural Rearrangements of Alkanethiolate Self-Assembled Monolayers on Gold," *J. Phys. Chem. B* **1997**, *101*(27), 5263-5276; b) I. Touzov and C.B. Gorman, "A Scanning Tunneling Microscopy Study of the Interaction of H<sub>2</sub>S with a Au(III) Surface: Characterization of Corrosion and Monolayer Structure," *Langmuir* **1997**, *13*(18), 4850-4854.
65. T.R. Lee, R.I. Carey, H.A. Biebuyck, and G.M. Whitesides, *Langmuir* **1994**, *10*, 741-749.
66. a) J. Spinke, M. Liley, H.J. Guder, L. Angermaier, and W. Knoll, *Langmuir* **1993**, *9*, 1821; b) I. Willner, E. Katz, A. Riklin, R. Kasher, *J. Am. Chem. Soc.* **1992**, *114*, 10965-10966; c) H.A.O. Hill, G.A. Lawrance, *J. Electroanal. Chem.* **1989**, *270*, 309-318; d) E. Katz, T. Lotzbeyer, D.D. Schlereth, W. Schuhmann, and H.L. Schmidt, *Electroanal. Chem.* **1994**, *373*, 189-200; e) K.L. Prime and G.M. Whitesides, *Science* **1991**, *252*, 1164-1167; f) I. Willner, S. Rubin, and Y. Cohen, *J. Am. Chem. Soc.* **1993**, *115*, 4937-4938; g) K. Takehara, H. Takemura, and Y. Ide, *J. Electroanal. Chem.* **1991**, *308*, 345-350; h) K.T. Kinnear and H.G. Monbouquette, *Langmuir* **1993**, *9*, 2255; i) K.L. Prime and G.M. Whitesides, *J. Am. Chem. Soc.* **1993**, *115*, 10714-10721.
67. J.D. Burgess, V.W. Jones, M.D. Porter, M.C. Rhoten, and F.M. Hawkrige, "Scanning Force Microscopy Images of Cyt c Oxidase Immobilized in an Electrode Supported Lipid Bilayer Membrane," *Langmuir* **1998**, *14*(23), 6628-6631.
68. a) D.J. Tobias, W. Mar, J.K. Blasie, and M.L. Klein, "Molecular Dynamics Simulations of a Protein on Hydrophobic and Hydrophilic Surfaces," *Biophysical Journal* **1996**, *71*, 2933-2941; b) M. Lestelius, B. Liedberg, and P. Tengvall, "In Vitro Plasma Protein Adsorption on ω-Functionalized Alkanethiolate Self-Assembled Monolayers," *Langmuir* **1997**, *13*, 5900-5908; c) G.B. Sigal, C. Bamdad, A. Barberis, J. Stominger, and G.M. Whitesides, *Anal. Chem.* **1996**, *68*, 490-497; d) M. Mrksich, G.B. Sigal, and G.M. Whitesides, "Surface Plasmon Resonance Permits *in Situ* Measurement of Protein Adsorption on Self-Assembled Monolayers of Alkanethiolates on Gold," *Langmuir* **1995**, *11*, 4383-4385; e) C.D. Tidwell, S.I. Ertel, and B.D. Ratner, "Endothelial

- Cell Growth and Protein Adsorption on Terminally Functionalized Self-Assembled Monolayers of Alkanethiolates on Gold,” *Langmuir* **1997**, *13*, 3404-3413; f) A.K. Gaigalas and G. Niaura, “Measurement of Electron Transfer Rates between Adsorbed Azurin and a Gold Electrode Modified with a Hexanethiol Layer,” *J. Colloid and Interface Science* **1997**, *193*, 60-70.
69. a) T.M. Nahir, R.A. Clark, and E.F. Bowden, “Linear Sweep Voltammetry of Irreversible Electron Transfer in Surface Confined Species Using the Marcus Theory,” *Anal. Chem.* **1994**, *66*, 2595-2598; b) T.M. Nahir and E.F. Bowden, “The Distribution of Standard Rate Constants for ET Between Thiol-Modified Gold Electrodes and Adsorbed Cyt c,” *J. Electroanal. Chem.* **1996**, *410*, 9-13; c) T.M. Nahir and E.F. Bowden, “Impedance Spectroscopy of Electroinactive Thiolate Films Adsorbed on Gold,” *Electrochim. Acta* **1994**, *39*, 2347-2352.
70. M.C. Leopold, J.A. Black, and E.F. Bowden, “Cyt c Voltammetry - The Role of the Au Substrate,” manuscript in preparation.
71. a) J. Wang, L.M. Frostman, and M.D. Ward, *J. Phys. Chem.* **1992**, *96*, 5224-5228; b) C.D. Bain and G.M. Whitesides, *Langmuir* **1989**, *5*, 1370-1378; c) S.E. Creager and J. Clarke, *Langmuir* **1994**, *10*, 3675-3683; d) C.P. Smith and H.S. White, *Langmuir* **1993**, *9*, 1-3; W.R. Fawcett, *J. Electroanal. Chem.* **1994**, *378*, 117-124; e) K. Hu and A. Bard, “Use of Atomic Force Microscopy for the Study of Surface Acid-Base Properties of Carboxylic Acid-Terminated Self-Assembled Monolayers,” *Langmuir* **1997**, *13*, 5114-5119; f) .
72. P.T. Kissinger and W.H. Heineman, Eds., In *Laboratory Techniques in Electroanalytical Chemistry*, 2<sup>nd</sup> Ed., Marcel Dekker Inc.: New York, 1996.
73. E Laviron, “General Expression of the Linear Potential Sweep Voltammogram in the Case of Diffusionless Electrochemical Systems,” *J. Electroanal. Chem.* **1979**, *101*, 19-28.
74. The Wordsworth *Dictionary of Science and Technology*, Wordsworth Editions Ltd.: Denmark, 1995.
75. a) E. Laviron, “Theoretical Study of a Reversible Reaction Followed by a Chemical Reaction in Thin Layer Linear Potential Sweep Voltammetry,” *J. Electroanal. Chem.* **1972**, *39*, 1-23; b) E. Laviron, “Adsorption, Autoinhibition, and Autocatalysis in Polarography and in Linear Potential Sweep Voltammetry,” *J. Electroanal. Chem.* **1974**, *52*, 355-393; c) E. Laviron, “A Critical Study of the Factors Causing the Appearance of Brdicka’s Adsorption Currents - Influence of the Interactions Between the Adsorbed Molecules,” *J. Electroanal. Chem.* **1975**, *63*, 245-261.
76. a) R.A. Serway, *Physics for Scientists and Engineers*, 3<sup>rd</sup> Edition, Saunders College Publishing: Philadelphia, 1990; b) R.P. Feynman, R.B. Leighton, and M. Sands, *The Feynman Lectures on Physics, Mainly Electromagnetism and Matter*, Volume II, Addison-Wesley Publishing Co.: Reading, Massachusetts, 1964.
77. C. Krause, V. Mirsky, and K.D. Heckmann, “Capacitive Detection of Surfactant Adsorption on Hydrophobized Gold Electrodes,” *Langmuir* **1996**, *12*, 6059-6064.
78. H.O. Finklea, D.A. Snider and J. Fedyk, “Passivation of Pinholes in Octadecanethiol Monolayers on Gold Electrodes by Electrochemical Polymerization of Phenol,” *Langmuir* **1990**, *6*, 371-376.

79. a) L. Sun and R.M. Crooks, "Indirect Visualization of Defect Structures Contained Within Self-Assembled Organomercaptan Monolayers: Combined Use of Electrochemistry and Scanning Tunneling Microscopy," *Langmuir* **1993**, *9*, 1951-1954 b) S. Creager and K.A. Groat, "Self-Assembled Monolayers in Organic Solvents: Electrochemistry at Alkanethiolate-Coated Gold in Propylene Carbonate," *Langmuir* **1993**, *9*, 3668-3675; c) P. Krysinski and M. Brzostowska-Smolka, "Three Probe Voltammetric Characterization of Octadecanethiol Self-Assembled Monolayer Integrity on Gold Electrodes," *J. Electroanal. Chem.* **1997**, *424*, 61-67; d) E. Saabatani and I. Rubinstein, "Organized Self-Assembling Monolayers on Electrodes. 2. Monolayer-Based Ultramicroelectrodes for the Study of Very Rapid Electrode Kinetics," *J. Phys. Chem.* **1987**, *91*, 6663-6669.
80. J. Lyklema, *Colloids Surf.* **1984**, *10*, 33-42.

# THE ROLE OF THE GOLD SUBSTRATE IN CYT C/SAM/GOLD ELECTROCHEMICAL SYSTEMS

## CHAPTER THREE



*“It doesn’t matter what he does, he will never amount to anything.” – Albert Einstein’s teacher giving his opinion on Einstein’s future to Einstein’s father.*

### **3. THE ROLE OF THE GOLD SUBSTRATE IN CYT C/SAM/GOLD ELECTROCHEMICAL SYSTEMS**

#### **3.1. INTRODUCTION**

The guiding objective of this research is to gain a detailed knowledge of the ET and adsorption processes occurring in the cyt c/SAM/Au system. One important requirement is the identification and understanding of the specific interactions that occur between the protein and modified electrode to best promote both cyt c adsorption and ET. As previously mentioned, the electrochemistry of cyt c molecules adsorbed on carboxylic acid terminated SAMs is non-ideal, displaying broadened voltammetric peaks. Based on previous research, there is strong evidence suggesting that this phenomenon is the manifestation of specific surface effects.<sup>1</sup> Moreover, results support the hypothesis that adsorption sites on the surface of the SAM exhibit a significant degree of heterogeneity arising from a distribution of interfacial surface environments and resulting in a heterogeneous population of adsorbed cyt c molecules. Because of this, the adsorbed protein displays dispersed thermodynamic properties, in particular its formal potential. There is also a dispersion of electron transfer rate constants for the system as well.<sup>10</sup> It is believed that this dispersion of electrochemical properties is the underlying basis for the observed non-ideal cyclic voltammetry.<sup>1</sup>

The specific causes of surface heterogeneity and the specific nature of the adsorption sites remains elusive and unidentified. Since surface effects are suspected as playing the major role in creating these heterogeneous adsorption sites, fundamental research into the surfaces involved in this system was undertaken to identify, understand, and minimize the sources of the non ideal electrochemical behavior of cyt c. Defining this ET system to a high degree of detail should provide a means to optimize the protein's voltammetric response, a key aspect of the overall research goals. Accordingly, the first surface to be examined is that of the gold substrate itself.

A long standing goal of the Bowden Research Group is to establish a deeper understanding of the role played by the gold substrate in the voltammetry of cyt c.<sup>2</sup> Thus, the first objective of this research effort was to define the influence of the gold substrate's topography and how it affects the structure and stability of the cyt c/SAM/Au system, as well as, how it correlates with the voltammetric behavior of cyt c. It is believed that the

topography of the gold exerts a strong influence on the eventual structure of a SAM formed on that surface. Gold surface features are sometimes characteristic of the type of gold being employed and have been known to dictate the defectiveness, consistency, and stability of a SAM.<sup>3</sup> Therefore, included in this objective is an assessment of different gold substrates and their propensity for forming SAMs with defects. The topographical features of the gold surfaces and their impact on SAM formation, protein adsorption, and the electrochemical response of cytochrome c is the primary focus of evaluating the surface effects on this system.

To address this issue, experiments have been performed on the cyt c/SAM systems with various types of gold substrates. A previous researcher performed experiments to generally characterize different types of gold substrates as a means of assessing their use in electrochemical experiments involving cyt c. The results of those experiments, however, were never specifically correlated with cyt c electrochemical behavior and left the exact role of the gold substrate largely undefined.<sup>4</sup> Therefore, the experiments comprising this research effort are more specifically aimed at relating specific gold surface structure to the observed voltammetry of the cyt c.

This chapter consists of two major, independent research efforts into the role of the gold substrate in cyt c voltammetry. The first set of experiments focused entirely on evaporated gold substrates whereas a subsequent investigation involved multiple types of gold surfaces covering a wide range of topography. Both endeavors produced consistent results but are presented here as separate parts in the chapter. As will be discussed later, the second study involving multiple types of gold was undertaken because of potential contamination complications issues that arose from pretreatment of evaporated gold substrates. The more recent work involving multiple substrate types and a wider range of topography is presented first, followed by results from the earlier study of evaporated gold.

The gold substrates used in this study were specifically chosen or prepared to provide a range of crystallinity, roughness, and topographical features, including gold with extremely flat, plateau-like regions. After modification with a carboxylic acid terminated SAMs, cyt c was adsorbed to each of these modified gold substrates and the electrochemical response was monitored. Each of the gold substrate surfaces was also characterized with both

electrochemistry and microscopy techniques. The structure and defectiveness of the SAMs formed on the different gold substrates were evaluated using electrochemical experiments.

At the time this work was undertaken, the prevailing view of the SAM community was that atomically smooth surfaces make the most effective templates for creating very ordered, low defect monolayers.<sup>5</sup> Considering the widespread use of inherently rough substrates in most of the cyt c electrochemistry performed in the Bowden Research Group, the experiments discussed here were initially carried out with the idea that flat gold surfaces that allow for the formation of low defect SAMs may minimize or eliminate the non-ideal aspects of the voltammetry of cyt c. Extremely flat gold surfaces could possibly lead to decreased adsorption of cyt c molecules at defect sites, thereby minimizing the ubiquitous peak broadening. Therefore, a considerable effort was focused on the use of atomically flat gold substrates or the alteration of existing rough gold to a smoother state.

### **3.1.1. The Topography of Gold Substrates**

Typical topographical features of gold surfaces can be categorized according to two prominent properties: the overall roughness of the surface and the crystal grain composition of the surface. The roughness of a gold surface is largely influenced by how the substrate was created and, in some cases, pretreated. Many gold substrates are created by the formation of a gold layer on a template material, whose roughness can largely dictate the eventual roughness of the gold overlayer. Some template materials are extremely smooth, even atomically flat, over most of their surface, allowing for a flat gold surface to be created whose roughness consists of only gold step edges. A gold step edge is a topographical feature of gold where the surface “steps up” one gold atom high and, on a larger scale, can create atomically flat plateaus. The opposite extreme of roughness occurs when the gold surface is formed on an inherently rough template and results in a rougher terrain across the surface, usually consisting of rolling hills and sharp peaks of gold.

The second property to consider when dealing with gold substrates is the crystallinity of the gold at the surface. Gold can exist with one of three low index crystal planes at a surface: Au(111), Au(110), and Au(100). The lowest energy, and therefore the most stable, surface is the Au(111) orientation. The Au(100) orientation, on the other hand, is very unstable and usually exhibits a predisposition to undergo a structural reconstruction to achieve a lower energy.<sup>6</sup> Gold surfaces can be either single crystal in nature, where there is a

predominant crystal grain across the majority of the surface, or polycrystalline, where the gold surface is comprised of a combination of the different crystal grains. Again, like the roughness of the gold substrate, the type of crystal grains found on a gold surface is highly influenced by the way the gold was deposited on the template material and pretreated prior to experimentation. The existence of two different crystal grains on a surface creates grain boundaries in the gold's surface architecture. As will be seen, the existence and number of these grain boundaries can have a substantial impact on the structure of a SAM.

SAMs formed on substrates can possess a variety of defects partially attributable to the surface characteristics of the gold. As shown in Figure 3.1, rough terrain, step edges, and grain boundaries can all affect the defect density of a SAM. Moreover, certain gold substrates tend to form SAMs with pinhole defect sites. In the SAM literature, the term "pinhole defect" has been used with a variety of meanings. In this dissertation, SAM pinholes will be defined as defect sites where electrolyte can effectively penetrate the SAM and contact the metal electrode. Non-pinhole defect sites, on the other hand, will be defined as any location in the film where ions or analyte molecules can approach the electrode surface at a distance shorter than the thickness of the SAM<sup>5</sup>

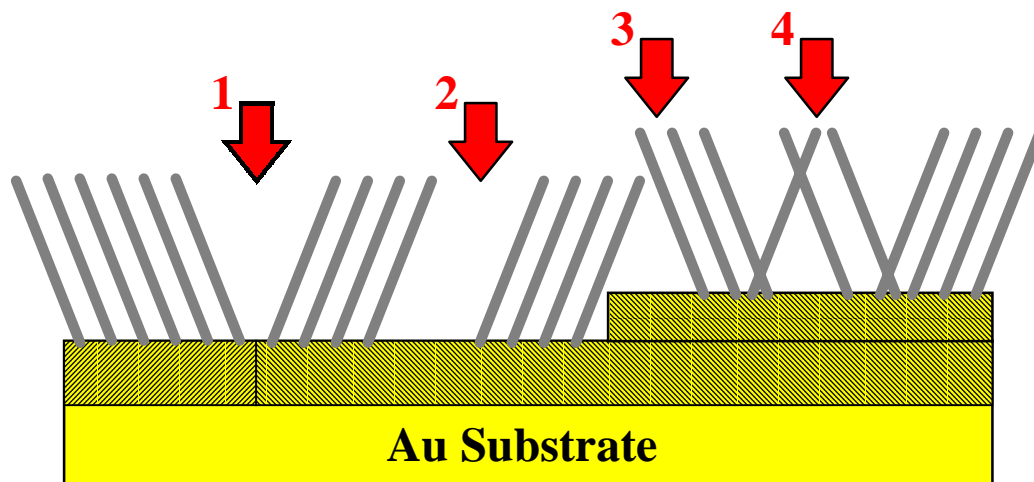


**Figure 3.1.** Examples of SAM defects attributable to gold topography: 1) grain boundaries, 2) pinholes, 3) step edges, 4) general regions of disorder in the SAM structure.

Fortunately, techniques exist that allow researchers to gain a semi-quantitative understanding of all of these surface characteristics. Scanning probe microscopy (SPM) provides a means to characterize gold surfaces and SAM modified gold substrates at the

molecular level. SPM techniques can assess specific topographical features such as step edges and SAM pinholes as well as assist in delineating the overall terrain of a surface. Likewise, specific electrochemical experiments can be designed to identify the crystallinity of a gold surface, as well as the defectiveness of a SAM formed on a specific gold substrate. As will be shown in subsequent sections of this chapter, the use of both electrochemistry and microscopy techniques to substantiate the expected topographical and morphological features of the different gold substrates is an effective approach to characterization.

### **3.1.2. Previous Research Into Gold Topography**

In spite of the availability of an array of powerful characterization techniques, in-depth analyses dedicated to comparative studies of gold topography are rare. Some SPM reports do compare the microscopic features of a variety of different gold substrates and are the subject of microscopy based reviews.<sup>7</sup> SPM literature, however, usually addresses the topography of gold substrates from a standpoint of what is most beneficial for microscopy experiments. Gold preparations resulting in flat surfaces with large atomically smooth plateaus are typically sought for imaging the atomic level surface packing of the gold itself or for adsorbates residing on the gold surface. While research found in the literature involving gold substrates often includes a substantial degree of surface characterization, it usually is limited to only the specific type of gold substrate being used for that particular experiment. A comparison of the same experiment on several different gold substrates to see if the topography or pretreatment of the gold influences the results is rarely done. The reasons for this lack of comparison-based studies appears to be two fold: 1) the high cost of working with many of the specialized types of gold and 2) the notion of experimental simplicity. Researchers often tend to settle on a type of gold substrate and surface pretreatment that is successful for their specific systems and experiments.

Several literature reports have focused on the assembly and structure of self-assembled monolayers on different types of gold or on gold subjected to different types of pretreatment procedures.<sup>5</sup> Creager and coworkers utilized polycrystalline bulk gold that was annealed and chemically etched with aqua regia solution. Their research, which involved studying the inhibition of interfacial ET from redox-active solute at SAMs on gold substrates of varying roughness, lends support to the notion that SAMs with excellent blocking characteristics can be formed on polycrystalline gold. Polycrystalline gold, it was

determined, is a surface that is rough on the micron scale but is also composed of smoother planes on a smaller scale. (macroscopically rough vs. microscopically smooth). From this work, Creager concluded that defectiveness in SAMs correlates strongly to the method used to prepare the gold substrate for self-assembly and established the importance of surface roughness and grain boundaries to the quality of the SAMs.<sup>3a</sup> Likewise, experiments performed by Guo *et al.* with long chain methyl-terminated SAMs (HS(CH<sub>2</sub>)<sub>16</sub>CH<sub>3</sub>) on evaporated gold on mica suggested that SAMs formed on rougher substrates had better blocking characteristics than those on smoother gold.<sup>3b</sup> Researchers in Golan's laboratory,<sup>3g</sup> as well as those with Crooks<sup>3d</sup> created apparent pinhole-free SAMs with superior blocking behavior on sputtered and evaporated films on glass and mica. Porter's group traditionally thermally anneals gold-on-mica films to create well ordered, low defect, SAMs and have suggested that roughness may be less important for dictating SAM permeability than other topographical features such as crystallinity.<sup>3c</sup> Clearly the debate on the influence of gold topography and morphology on SAM structure is ongoing. Taking this one step further and studying the effect that gold topography has on the SAM and subsequent adsorbates is a unique and largely unexplored prospect for research.

### **3.1.3. Gold Topography and the Cyt c / SAM / Au System**

In the case of the cyt c/COOH-SAM/Au system, the Bowden Research Group established two hypotheses for the role of gold topography in the non-ideal electrochemical response of cyt c. The first hypothesis was that grains with different crystal faces exposed resulted in different types of adsorption sites in the SAM itself. This thought is supported by work of Creager and coworkers that showed in microscopy images that chemically etched gold surfaces display roughly equal proportions of Au(111) and Au(110).<sup>3a</sup> Similar results were obtained for sputter deposited gold film electrodes used in our laboratory prior to 1994.<sup>2,4</sup> Thus, the excessive broadness of the cyt c voltammetric peaks may represent the collective signal of two or more unique populations of protein adsorbed on different crystal planes. If this hypothesis proved to be correct, more ideal cyt c voltammetry should result from the use of single crystal gold substrates.

In the second hypothesis, defect sites in the SAM were proposed to give rise to heterogeneous adsorption and subsequent dispersion of electrochemical properties. The source of the surface heterogeneity causing the broadened cyt c voltammetry peaks, may be

the manifestation of having some cyt c molecules adsorb at defects sites and others adsorb at highly ordered, non-defective regions of the SAM. Researchers in Chidsey's laboratory successfully minimized the non-ideal aspects of the voltammetry of ferrocene-terminated SAMs by purportedly exchanging electroactive molecules at defect regions with nonelectroactive methyl-terminated alkanethiols.<sup>8</sup> This was done by immersing the ferrocene-terminated SAM in a solution of methyl-terminated thiol and taking advantage of the apparently favorable thiol exchange kinetics that exist at defect sites.<sup>8,9</sup> This hypothesis is related to the first in that polycrystalline gold will have a larger contingency of grain boundaries at the surface and, therefore, a greater propensity for SAM defects. It follows then, that the defect density of a SAM may indeed have a profound effect on the electrochemistry of adsorbed cyt c.

### **3.2 EXPERIMENTAL GOLD – GENERAL CHARACTERISTICS**

The gold substrates selected for this study include evaporated gold films, bulk polycrystalline gold, single crystal gold, and gold epitaxially grown on mica, each of which is expected to possess unique surface characteristics. Each substrate's surface characteristics (topography, crystallinity, etc.), as well as, the typical pretreatment methods applied to them are described in subsequent sections. Several techniques used to characterize the surfaces are introduced in the following paragraph.

The overall roughness of each surface, a measurement describing a large area of the surface, was characterized by an electrochemically determined roughness factor ( $R_f$ ) and by a more specific, small surface area, sampled measurement using SPM. Lead underpotential deposition (Pb - UPD) experiments were performed to evaluate the exposed surface crystallinity of the gold substrates. Further qualitative evidence for the crystallinity of the substrates was obtained by evaluating the formation patterns of gold oxide during voltammetry experiments. Each type of gold surface was also investigated with SPM to obtain a visual description of the surface. These techniques and the results obtained will be discussed in greater detail in future sections. The major characteristics and properties of the four gold substrates, ranging from the molecular level terrain on the surface, to the mechanical stability and cost of the materials, are summarized in Table 3-1.

The results from the SPM experiments are an important part of the description of the gold substrate's topography (see Table 3-1) but they are not specifically discussed in this chapter. SPM imaging of the gold surface and other explorations into the microscopy of the cyt c/SAM/Au system are the subject of Chapter 5.

### **3.2.1. Evaporated Gold Thin Films**

Evaporated gold substrates have been the predominant electrode material used in the Bowden Research Group and are used extensively throughout electrochemistry. Polycrystalline in nature, they are manufactured by evaporating high purity gold onto a glass mount covered by an adhesive layer of titanium or chromium. Evaporated gold films, as well as sputter deposited films, are known to have a strong Au(111) character when deposited on a heated mount of glass, silicon, or mica. Therefore, scientists wishing to perform "single crystal" experiments sometimes use evaporated gold film substrates as a cheap alternative to actual bulk Au(111) samples.<sup>5</sup> In this lab, electrochemical pretreatment of these mirror finished gold surfaces has been found to drastically improve the reproducibility of cyt c/SAM/Au based experiments.<sup>10</sup> Literature reports of SPM characterization have described evaporated gold substrates as inherently rough with "sand-dune" topography prevalent over most of the surface.<sup>7</sup> This is a commonly accepted description of evaporated gold and, because of this rough terrain, these substrates are seldom used for SPM applications, which require large, flat areas for imaging. Evaporated gold on glass is relatively inexpensive, but possesses poor mechanical stability. The thin layer of gold can be easily damaged with abrasive pretreatment and can be chemically eroded away without much effort. Therefore, the number and nature of pretreatment methods applicable to these evaporated gold films is limited. Evaporated gold is usually employed for a single experiment and then discarded.

### **3.2.2. Bulk Polycrystalline Gold.**

This polycrystalline gold material is often referred to as simply bulk gold, gold foil, or gold wire. For this study, we limit the discussion to traditional gold foil substrates. The use of this type of bulk gold in both electrochemistry and microscopy is not unfounded,<sup>3a,11</sup> but is a rather expensive substrate to purchase. The most common pretreatments for bulk gold foil found in the literature are polishing and/or abrasive chemical etching in a solution such as aqua regia (HCl & HNO<sub>3</sub> – see Experimental Details). The roughness of these etched substrates has been described as macroscopically rough and microscopically smooth.

**Table 3-1.** Summary of Experimental Gold Substrate Properties

<b>Property</b>	<b>Evaporated Gold Films</b>	<b>Bulk Gold (Gold Foil)</b>	<b>Single Crystal Gold - Au(111)</b>	<b>Au Epitaxially Grown on Mica</b>
<i>Physical Description</i>	1000 Å Au / 50 Å Ti / Glass	12 x 12 x 1 mm solid gold (99.9985%)	2 mm thick gold discs	1.4 x 1.1 cm mica w/ 1500 Å of Au covering 1 x 1.1 cm
<i>General Topographical Characteristics<sup>a</sup></i>	"Sand-dune" topography	"Partical board" topography -Macroscopically rough -Microscopically smooth	"Plateau" topography  -low degree of rough terrain	"Plateau" topography  -Extremely flat Au islands -Lower density of Au step edges
<i>Crystallinity<sup>b</sup></i>	Polycrystalline Au(111) / Au(110)	Polycrystalline Au(111) / Au(110)	Predominantly Au(111)	Predominantly Au(111)
<i>Potential Defect Surface Structure<sup>a</sup></i>	-Crystal grain boundaries  -Rough terrain	-Crystal grain boundaries  -Rough terrain	High density of Au step edges	Low density of Au step edges
<i>Annealing Possibilities</i>	Annealing can be used to lower overall roughness and create a predominantly Au(111) surface	Overall roughness can be significantly lowered using chemical etching, polishing, and annealing techniques	Usually pretreated before use with a light HFA to revitalize the surface structure of the Au(111) plateaus	Usually pretreated before use with a light HFA to revitalize the surface structure of the Au(111) plateaus
<i>Mechanical Stability</i>	Good	Superior	Good - delicate surface structure	Poor
<i>Cost</i>	Inexpensive	Expensive	Extremely Expensive	Expensive

Notes:

<sup>a</sup> Determined through SPM; <sup>b</sup> Determined through electrochemical experiments (Au oxidation & Pb-UPD)

Both optical microscopy and scanning electron microscopy (SEM) show the surface of bulk gold to be like “particle board,” in that the surface is made up of a number of different patches or grains of gold. Collectively, these grains present a very rough surface, but individually, each grain exhibits a molecularly flat, possibly angled, facet of specific crystal orientation.<sup>3a</sup> Perhaps the greatest attribute of bulk gold, however, is its mechanical stability. These substrates can withstand chemical etching and mechanical polishing, and are thus reusable. For this research, bulk gold substrates were usually etched in dilute aqua regia to remove a few layers of gold, polished with alumina slurries, and either etched again or pretreated electrochemically or by hydrogen flame annealing (See Experimental Details Section). Essentially, bulk gold presents a surface with a high density of crystal grain boundaries and a roughness that can be systematically altered. Thus, bulk gold substrates are extremely attractive for research addressing topographical issues.

### **3.2.3. Single Crystal Gold.**

Quality gold substrates of single crystal orientations [ Au(111), Au(110) or Au(100) ] that are acceptable for electrochemical experiments of this magnitude are expensive and thus, there are fewer SAM studies found incorporating these substrates.<sup>5</sup> The obvious benefit to using a single crystal gold substrate is the fact that the substrate is devoid of crystal grain boundaries. With high quality Au(111) single crystal gold, SPM experiments have shown the surface to be mostly flat with a high density of gold step edges.<sup>4,12</sup> The primary single crystal used in this research, Au(111), has excellent durability and can be polished and/or annealed under a hydrogen flame to regenerate the gold step topography. A common view is that Au(111) samples promote the formation of highly ordered, pinhole free SAMs, whose structure is not influenced by grain boundaries. There is, however, no consistent evidence in the literature that these type of SAMs require the use of Au(111) single crystals.<sup>5</sup>

### **3.2.4. Au Epitaxially Grown on Mica.**

Gold on mica substrates are known for their extremely smooth surfaces and are the preeminent gold substrate for microscopy studies. Mica is atomically smooth, providing an excellent surface for the eventual gold structure. The gold, when grown on heated mica, tends to form extremely large, flat, plateau-like regions known as gold terraces that are essentially 100% Au(111). Au on mica usually possesses a lower density of step edges than the single crystal substrates, especially when pretreated with a gentle hydrogen flame (See

Experimental Details). The “Achilles heal” of using Au on mica is its poor mechanical stability. Au/mica substrates are extremely fragile and can only be placed in the electrochemical cell a single time. The gold layer tends to crack and peel away from the brittle mica backing if removed from the cell. Thus, many comparisons of before/after effects on Au on mica cannot be made. Additionally, Au/mica is expensive when purchased from a supplier and, as witnessed in our own SPM experiments, usually suffers from a significant degree of substrate-to-substrate topographical reproducibility, an artifact of the gold deposition procedure used.<sup>25</sup> The following section summarizes the in-house characterization and pretreatment methods performed on these substrates.

### **3.3. EXP. GOLD CHARACTERIZATION - ROUGHNESS FACTORS**

A general characteristic that can account for the broad spectrum of topographical and morphological features possible on these gold surfaces is overall roughness. In this case, roughness is defined as the ratio of the real surface area to the geometric surface area<sup>13</sup> and can be used to relate these unique substrates to each other. Even though the surface geometry of an electrode, as visible to the naked eye, defines an electrode area, the actual or real surface area may be greater due to specific topographical features (i.e. step edges, rough terrain, etc.). Only when the real surface is perfectly flat will its area correspond exactly to the geometric area, a ratio of one. In order to quantify the surface roughness of each type of gold or the effect of a pretreatment, the roughness factors ( $R_f$ ) of the substrates were measured using an electrochemical technique ( $R_{f, E/C}$ ). The  $R_{f, E/C}$  is not a molecularly well-defined property but is instead an averaged surface property useful for comparative studies. Additionally, it should be noted that electrochemistry is a population technique, measuring a specific property over an entire surface area. Because this research is concerned with gold topography as it relates to SAM formation and eventual cyt c adsorption and ET behavior, the roughness of a smaller, sampled area of the surface is also of major interest. To provide this type of information, SPM based roughness factors ( $R_{f, SPM}$ ) were also obtained. Each type of roughness factor and the experimental results of roughness experiments are described in the following sections.

### 3.3.1. Basis and Background of $R_{f-E/C}$

Many different electrochemical methods exist for determining the  $R_f$  of a gold substrate, including the use of diffusional electrochemistry,<sup>14</sup> differential double layer capacitance,<sup>15a,b,e,13a</sup> and measurement of charge density passed during the reduction of a monolayer of a specific gold oxide (Au-oxide).<sup>13</sup> All current electrochemical methods, including these three, are subject to certain complications and pitfalls, including interpretation. Such considerations are not the focus of this research and are not discussed here in detail; they are, however, clearly outlined, along with other electrochemical methods for determining  $R_f$ , in a review by Trasatti and Petrii.<sup>16</sup>

In the present work, we have used the Au-oxide reduction charge density method to determine  $R_{f-E/C}$  for the gold substrates. Our implementation is derived from work by Oesch and Janata<sup>13</sup> and Arvia *et al.*,<sup>17</sup> in which a monolayer of Au-oxide is electrochemically formed and then reduced by cyclic voltammetry. In spite of its shortcomings, this technique has been broadly employed to obtain  $R_{f-E/C}$ , for which there is presently no clear, more accurate, or better alternative method.<sup>3h,i,4,18</sup> To obtain the  $R_{f-E/C}$ , the charge density passed during the reduction of Au-oxide, as determined by integrating the voltammetric peak area of the reduction wave, is ratioed to a theoretical value of charge density for the reduction of a monolayer of Au-oxide on an atomically flat surface:

$$R_{f-E/C} = \frac{Q_{\text{red(exp)}}}{Q_{\text{red(theor)}}} \quad [\text{Eqn. 3.1}]$$

where  $Q$  is the charge density ( $\mu\text{C}/\text{cm}^2$ ). The charge passed is assumed to be proportional to the actual area of the electrode.<sup>13a</sup>

Stable and reproducible Au-oxide formation and stripping peaks are indicative of a clean, well defined gold surface.<sup>5</sup> Figure 3.2 shows the voltammetry of what is referred to as a “roughness scan” in dilute (0.1 M)  $\text{H}_2\text{SO}_4$ . As indicated by this figure, the stripping peak, with its well-defined baseline, can be easily integrated to obtain the experimental charge density. Before integrating the stripping peaks, their relative sizes can provide a good indication of which surface is inherently smoother or rougher. This technique can be applied to any gold surface after any pretreatment as long as the system isn’t compromised by the presence of chloride ions which can cause distortion of the baseline in the roughness scans.

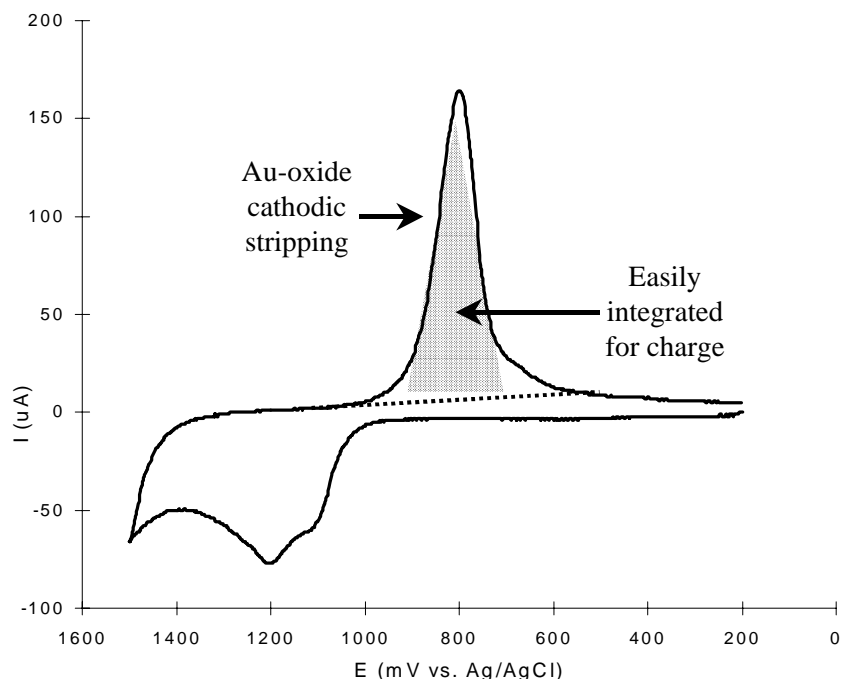


**Figure 3.2.** Cyclic voltammetry “roughness scan” in 0.1 M  $\text{H}_2\text{SO}_4$ . Note that the Au-oxide reduction peak is well defined with a very flat background and is easily integrated for charge passed. The value of the charge passed can be used to determine an electrochemical roughness factor.

Problems associated with this technique arise from the method’s dependence on specific, controlled Au-oxide formation and on the assumptions and estimations that must be made to predict a theoretical value for the reduction of a monolayer of Au-oxide. Although a large amount of research has been done on oxides of gold, their conclusions often disagree.<sup>13a</sup> The following discussion attempts to summarize the pertinent considerations of these arguments as they relate to electrochemically determined  $R_f$  and is largely based on the work of Janata and coworkers.<sup>13</sup>

During the anodic polarization of a gold electrode, three types of gold oxides can form: Oxide I, Oxide II, and Oxide III. Oxide I is thought to be the primary surface oxide,  $\text{Au}_2\text{O}_3$ , a compact, anhydrous layer that grows to a limiting amount of only a few molecular layers. At slightly higher oxidation potentials, Oxide II grows in, its specific nature largely unknown. Finally, at even more positive potentials, Oxide III forms, considered to be the bulk oxide layer, a thicker film ( $\leq 100$  monolayers) of  $\text{Au}(\text{OH})_3$  or hydrated  $\text{Au}_2\text{O}_3$ . Both the II and III oxide layers are thought to be porous, permitting the oxidation/reduction of the inner gold oxide (I) without significant disruption to the outer oxides (II & III). Of course,

all of these oxides and the potential and extent at which they form are dependent on solution conditions (pH, electrolyte, etc.).<sup>13</sup> In general, an anodic sweep on a gold electrode will first result in the formation of Au oxide (I). The anodic current will reach a maximum and then proceed to a minimum. This minimum is believed to signal the completion of a monolayer of gold oxide where the atomic ratio of gold to oxygen is one. It is thought that at this potential, just before the onset of the type II oxide, the type I oxide has not yet rearranged to the Au<sub>2</sub>O<sub>3</sub> structure. The size and shape of these oxidation waves are not well defined, largely because they are influenced by the composition of the supporting electrolyte, particularly anions, and the specific condition of the gold surface structure.<sup>13</sup> The shape of the oxide reduction wave, however, is unaffected by these same factors and yields the well-defined peak utilized for R<sub>f</sub> determinations. The charge density passed for the reduction of this oxygen adatom layer has been used by several workers to estimate surface roughness.<sup>19</sup>

The relevance of this discussion of gold oxides to roughness factors is that the presence of the different types of oxides complicates the measurement of Au-oxide monolayer reduction during roughness scans. Care must be taken to have the switching potential occur at the minimum discussed earlier, before the onset of the type II oxide. This minimum is not always well expressed and sometimes must be estimated. Oxidation of the gold beyond this point may inflate the Au oxide reductive current on the reverse scan because the Au-O ratio on the surface will no longer be one. In this manner a degree of error can be introduced into the experimental determination of Q<sub>red(exp)</sub>.<sup>13</sup>

A second major source of possible error is the theoretical estimation of charge density passed for an oxygen adlayer, Q<sub>red(theor)</sub>. As alluded to earlier, this theoretical determination is dependent upon the nature of the Au oxide layer being reduced. That is, the ratio of Au to oxygen for a perfectly flat oxide monolayer must be estimated for a particular surface in order to calculate the theoretical charge density (usually estimated to be 1:1). The actual composition of the Au-oxide layer at any point, however, depends on the extent of oxidation and is difficult to analyze.

An additional complication to using this type of R<sub>f-E/C</sub> is the fact that the surface concentration of Au atoms varies with the exposed crystallographic planes of the surface.<sup>13a</sup> Surfaces are not comprised of only perfect crystal planes. It is unknown how the density of topographical features, such as step edges, grain boundaries, etching pits, or regions of

contamination would affect both the concentration of Au atoms available for oxidation and the structure of the oxide adlayer. Therefore, in calculating the theoretical charge density for the reduction of a Au-oxide monolayer, these variables must also be somewhat approximated with assumptions about the surface being used. To this end, a variety of theories for Au-oxide formation have been developed, and, as a result, a wide range of  $Q_{\text{red-theor}}$  values appear in the literature. Table 3-2 is a sampling of some of these values, each derived with different assumptions about the surface of the gold or about the nature of the oxide layer.

### 3.3.2. Experimental Results - $R_{f-E/C}$

For the proposed experiments in this dissertation, a value of  $Q_{\text{red(theor)}}$  was developed with the help of Dr. Tal Nahir. Evidence presented later is consistent with the experimental gold surfaces being mostly, if not completely, Au(111). Therefore, using the atomic density for Au(111),<sup>18b</sup> and an oxygen to gold ratio of one when the switching potential is set to +1.5 (vs. Ag/AgCl),<sup>13a</sup> the following calculation yields  $Q_{\text{red(theor)}}$ :

$$1.4E^{15} \text{ Au atoms/cm}^2 \times 1 \text{ O atom/1 Au atom} \times 2e^-/1 \text{ O atom} \times 1.6E^{-19} \text{ coul/1e}^- \\ = \mathbf{448 \mu\text{Coul} / \text{cm}^2}$$

This value is in excellent agreement with literature values (See Table 3-2) and was used in the determination of all the electrochemical roughness factors in this dissertation.

**Table 3-2.** Estimated Values - Charge Density Passed for the Reduction of an Oxygen Ad-atom monolayer of Au-oxide ( $Q_{\text{red (theor)}}$ ):

$Q_{\text{red (theor)}}$ Estimations ( $\mu\text{C}/\text{cm}^2$ )	References
482	Oesch and coworkers, 1983 <sup>13a</sup>
450	Oesch and coworkers, 1983 <sup>13b</sup>
400	Burshtein and coworkers, 1972 <sup>18a</sup>
420	Arvia and coworkers, 1989 <sup>17</sup>
400	Manne and coworkers 1991 <sup>11</sup>
448	Leopold and Nahir, 1996 <sup>a</sup>

<sup>a</sup> Value is based on a theoretical surface with a predominantly Au(111) surface - a surface estimated to have a mean thickness of 2.6 Å and a Au atomic density of  $1.4 \times 10^{15}$  Au atoms/cm.<sup>2</sup>

### **-The Effect of Electrochemical Cleaning Pretreatment on $R_{f-EC}$**

In order to test the influence of gold topography on the cyt c / SAM / Au system, it was imperative to first understand how specific gold pretreatments affected their overall roughness. The two primary pretreatments used in this research, electrochemical cycling (EC) and hydrogen flame annealing (HFA), are presented next.

Electrochemical pretreatment of the gold substrate, developed by a previous researcher in the Bowden Group, Dr. Tal Nahir (currently at California State University, Chico), consists of potential cycling the potential in acidic chloride solution (0.1 M  $H_2SO_4$  with 0.01 M KCl). An example of this voltammetry is shown as Figure 3.3. Oxidative potential excursions of Au in an acidic chloride environment causes the dissolution of the gold surface via formation of chloro-aurate complexes. The voltammetry clearly shows the oxidation and reduction of these complexes (+1200 mV and +650mV, respectively), as well as, the reduction of Au-oxide at 825 mV. The corresponding Au-oxide formation (Au oxidation) peak is obscured by the large gold dissolution signal, the oxidation of the chloro-aurate. Eliminating the chloride source (KCl) from an otherwise identical scan results in a well-defined Au-oxide cathodic stripping peak in a voltammogram that that is synonymous with the “roughness scan” presented in Figure 3.2. This type of electrochemical cycling dissolves gold from the surface and effectively “cleans” by simply exposing new gold and redepositing fresh gold.<sup>13</sup> This type of chloride based etching is a permanent alteration of the surface as opposed to more temporary surface changes such as that induced by oxide layers.<sup>13,20</sup> Thus, the effect of this electrochemical pretreatment on the roughness factor of the gold was evaluated.

Figure 3.4 displays typical roughness scans of evaporated gold films before and after electrochemical pretreatment. As indicated by the size of the Au-oxide stripping peaks, the  $R_{f-EC}$  of this surface was not altered dramatically by the electrochemical pretreatment. Statistical analysis showed a statistically insignificant difference in  $R_{f-EC}$  between as received films and electrochemically cleaned films (Results and calculation not shown). At first glance, these results might suggest that evaporated gold substrates are not very rough (See Table 3-1). However, as revealed by SPM imaging (Chapter 5), they actually possess a very rough surface on a smaller scale.

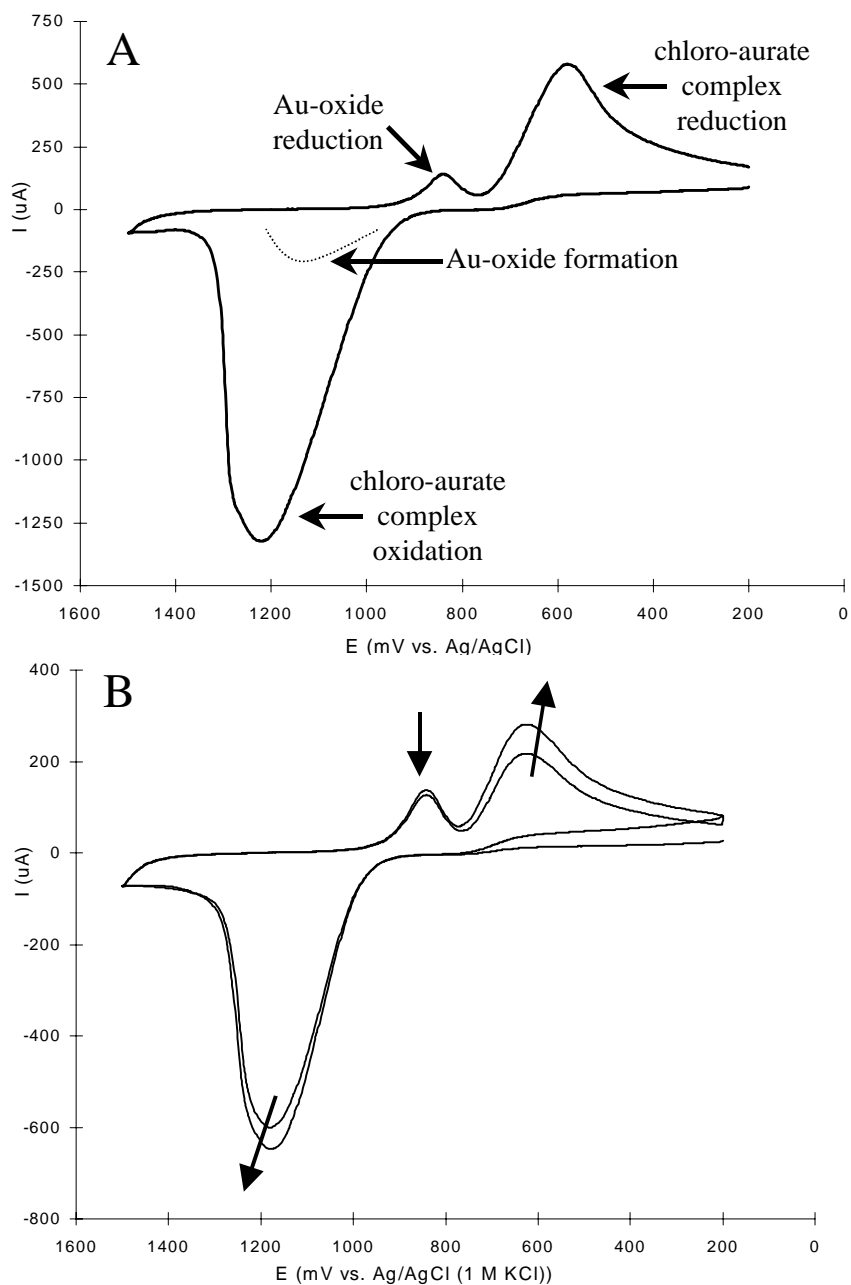


**Figure 3.3.** A) Cyclic voltammetry of the final electrochemical cleaning cycle (0.1 M  $\text{H}_2\text{SO}_4$  and 0.01 M KCl); B) During the cleaning cycles, the peaks corresponding to the oxidation and reduction of the chloro-aurate complex, at +1200 and +600 mV, respectively, continuously grow with each cycle. This peak growth is a sign that the gold surface is being consumed during the cleaning process, eventually exposing new, clean gold. The peak corresponding to Au-oxide reduction does not change substantially during cycling (the Au-oxide formation peak is masked by the large chloro-aurate oxidation signal).

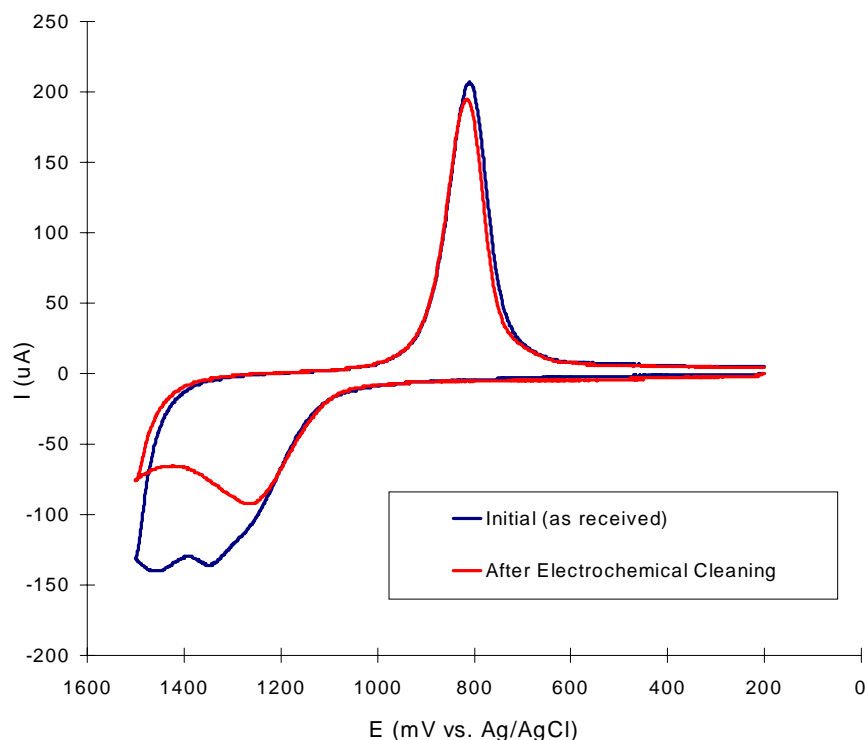


**Figure 3.4.** Cyclic voltammety roughness scans of evaporated gold substrates in 0.1 M H<sub>2</sub>SO<sub>4</sub> and 0.01 M KCl.

For smoother gold surfaces, on the other hand, increases in  $R_{f-EC}$  were observed as a result of electrochemical pretreatment. For example, in Figure 3.5, the Au-oxide reduction peak for HFA bulk gold (peak b) clearly grows following electrochemical cleaning (peak c). In general, smoother gold substrates exhibited an increase in  $R_f$  of 24-38% after the electrochemical pretreatment, a value consistent with literature reports of a 20-30% increase.<sup>13a</sup>

Thus, it was concluded that the electrochemical cleaning pretreatment tends to significantly roughen smoother surfaces but has little effect on the  $R_{f-EC}$  of evaporated gold. In both cases, however, it is clear that electrochemical pretreatment effectively cleans the surface as evidenced by a marked increase in double layer capacitance. Furthermore the electrochemical pretreatment seems to create a reproducible, albeit rough, surface. This phenomenon has been witnessed in our laboratory and has been reported in the literature as well.<sup>10,13a</sup>

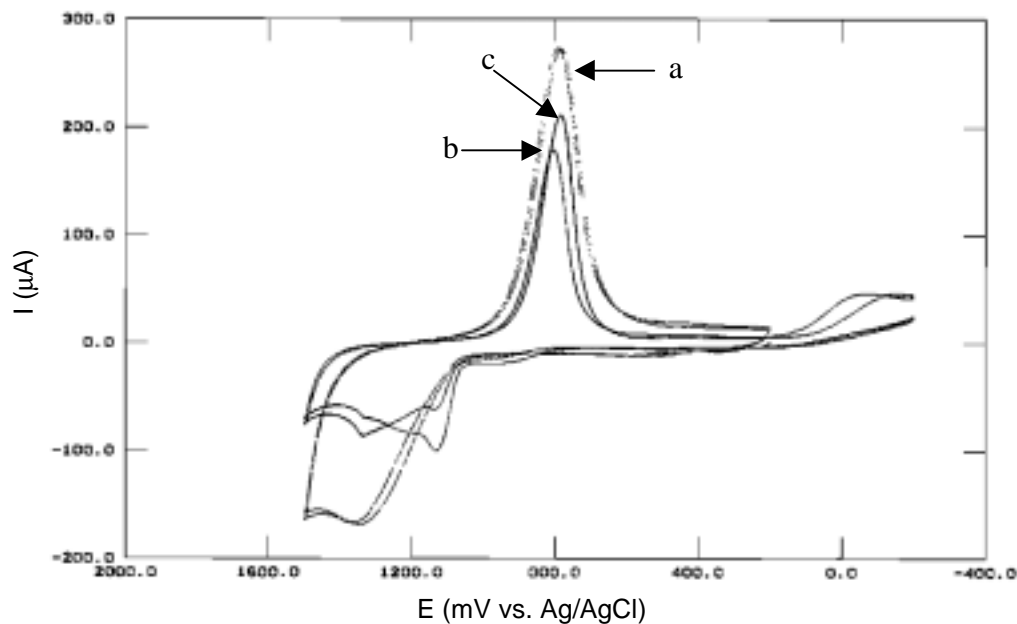


**Figure 3.5.** Cyclic voltammetry roughness scans in 0.1 M H<sub>2</sub>SO<sub>4</sub> illustrating the gold surface roughening effect of electrochemical cycling in 0.1 M H<sub>2</sub>SO<sub>4</sub> and 0.01 M KCl: a) initial bulk gold, b) bulk gold after HFA, and c) annealed bulk gold after electrochemical cleaning.

#### **-Effect of Annealing on $R_{f-E/C}$**

Annealing is a type of heat pretreatment employed to minimize strain and defects from a metallic surface. Annealing also restores a metal's ductility, improves the metal's corrosive resistance, and allows the metal to adopt well defined crystal facets.<sup>21</sup> The process of annealing typically leads to a more stable and smoother surface. Flames, ovens, and plasma chambers are all common means for heating substrates.

Annealing is most effective when performed at high temperatures for a prolonged amount of time. Annealing progresses through three major stages: 1) recovery (R1), 2) recrystallization (R2), and finally 3) grain growth (GG). These three stages of annealing and their effects on a metal surface are illustrated in Figure 3.6. The first stage, R1, occurs at lower temperature and is also known as the stress relief anneal stage. At this temperature, the additional thermal energy provided by the flame or other heat source allows dislocations(defects) in the surface to move. The dislocations move, but their density remains unchanged, forming a surface structure known as polygonized subgrain structure (Figure 3.6a→b). As the temperature is raised, the R2 stage is initiated and the surface experiences nucleation and growth of new crystal grains (Figure 3.6b→c). During this process, dislocation defects and stress sites are effectively eliminated. At even higher

temperatures the GG stage commences and the R1 and R2 stages occur simultaneously and more rapidly, causing favored grains to consume smaller grains. The culmination of the GG stage is the creation of larger, more consistent, and less defective grains at the surface of the metal (Figure 3.6c→d).<sup>21</sup> A real example of the annealing process of a brass alloy, exhibiting the result of each stage as a photomicrograph, is shown as Figure 3.7.

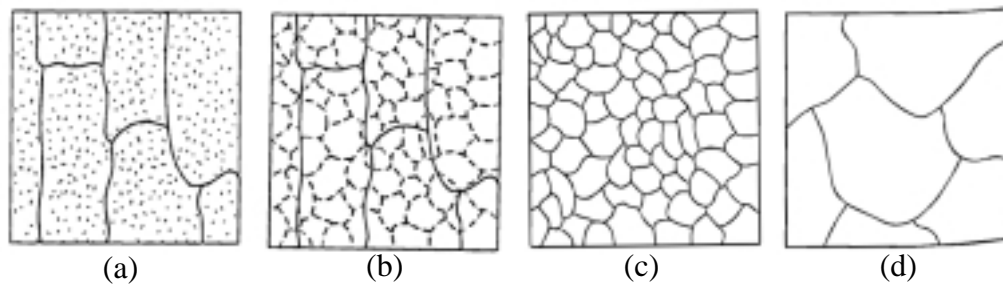


**Figure 3.6.** The three major stages of annealing. During the recovery stage (R1) (a→b), thermal energy causes dislocations in the material (shown as small dots) to move and form boundaries of a polygonized subgrain structure (b). At higher temperatures, the annealing proceeds to the recrystallization stage (R2) where the surface experiences nucleation and growth of new grains with fewer dislocation defects (b→c). The final stage of annealing, called grain growth (GG), allows for existing grains to grow and consume smaller grains (c→d). (Figure from Ref. 21)

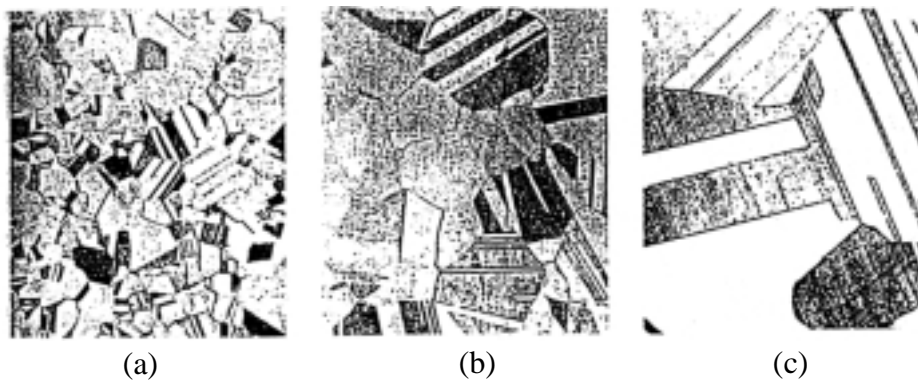


**Figure 3.7.** Photomicrographs showing the effect of annealing temperature on grain size in brass: a) annealed at 400°C, b) annealed at 650°C, c) annealed at 800°C. Imaged magnified 75X (Figure from Ref. 21).

Temperature is a key parameter when annealing for roughness and grain size purposes. As shown in the annealing graph, Figure 3.8, the grain size of the metal grows substantially at higher temperatures. Additionally, the total annealing time is critical for effective results of the heat pretreatment. If possible then, the substrate should be kept at an elevated temperature for as long as possible, allowing it to progress through the three stages

of annealing. Reducing the annealing time will cause the resultant grain size of the anneal to be smaller by minimizing the opportunity for grain growth.<sup>21</sup>

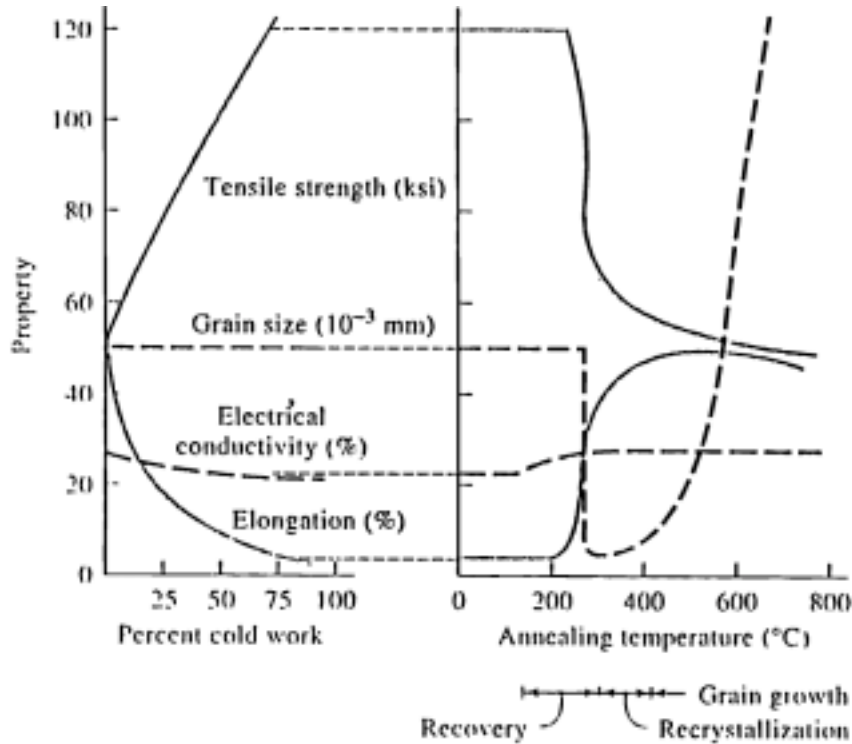


**Figure 3.8.** Effect of annealing of several properties of Cu-Zn alloy. Note the substantial increase in grain size at higher annealing temperatures (right). The three stages of the annealing process are noted beneath the graph (Figure from Ref. 21).

Flame annealing is a simple and effective heat treatment and has been utilized as a capable method for preparing very smooth, single crystal, surfaces of high quality on Pt, Ir, Ag, and Au.<sup>6a,23</sup> Different types of flames have been utilized for annealing, ranging from common Bunsen burner flames (gas-oxygen flames)<sup>22</sup> to specialized hydrogen flames.<sup>24</sup>

The topographical effects of annealing gold surfaces are well known. Annealing creates atomically flat terraces, sometimes tens of nanometers in width and predominantly of Au(111) orientation, separated by gold mono-atomic steps.<sup>6a</sup> To investigate the role of temperature, Mosher and coworkers<sup>3b</sup> recently used atomic force microscopy (AFM) to measure the roughness of gold evaporated onto cleaved mica before and after annealing at various temperatures. As expected from prior work, the results indicated that higher

temperatures lead to smoother surfaces.<sup>3b</sup> Also using microscopy techniques, Golan's group verified that large crystallites of gold occur when the metal is deposited via evaporation onto mica or "cleaned" glass. Furthermore, they reported an increase in grain size with prolonged exposure (several hours) to elevated annealing temperatures.<sup>3g</sup> Chailapakul and Crooks<sup>3d</sup> reported that, on rougher gold, surface atom mobility increases drastically at temperatures just below the melting point of gold, allowing surface defects on the gold to anneal.

The primary mode of annealing used for the present work is hydrogen flame annealing (HFA). HFA is used almost exclusively by microscopists to anneal gold and was recommended for this work by Molecular Imaging, Inc.<sup>25</sup> The exact procedure is fully described in the Experimental Details section of this chapter. HFA supplies a slow, clean, high temperature flame, advantageous for the thermal pretreatment of annealing.

The effect of hydrogen flame annealing on the  $R_f$  of gold is shown in Figure 3.9. The decrease in Au-oxide stripping peak area, after the gold has been annealed, results in a significantly lower roughness factor. Similar results were achieved with the annealing of other types of gold substrates as well. The smoothing effect of annealing on the gold was confirmed with SPM results (Chapter 5).

### 3.3.3. $R_{f-EC}$ Results – Comparison of Various Types of Gold

Roughness scans were performed on the following substrates: evaporated gold films that have been electrochemically cleaned, hydrogen flame annealed bulk gold samples, Au(111) single crystal, and gold epitaxially grown on mica. The roughness factors determined for the various substrates, shown in Table 3-3, reveal a clear trend. Examples of the roughness scans on each type of substrate are shown in Figure 3.10. It should be noted at this point that the roughness factors are used for relative comparisons only. Theoretically,  $R_{f-E/C}$  values less than one are, by definition, impossible to achieve. It is thought that  $R_{f-E/C}$  values less than unity reflect the approximations made in calculating the theoretical value for charge passed during the reduction of a monolayer of gold oxide, as previously discussed. The higher values of  $R_{f-E/C}$  ( $>1$ ) in Table 3-3 are in agreement with other reports.<sup>3l,4</sup> In any event, the overall roughness of these gold surfaces, from smoothest to roughest is as follows:

**Au/mica < Au(111) < Bulk Au < evaporated Au.**

Roughness, however, is just one of the many important gold surface characteristics that must be considered.

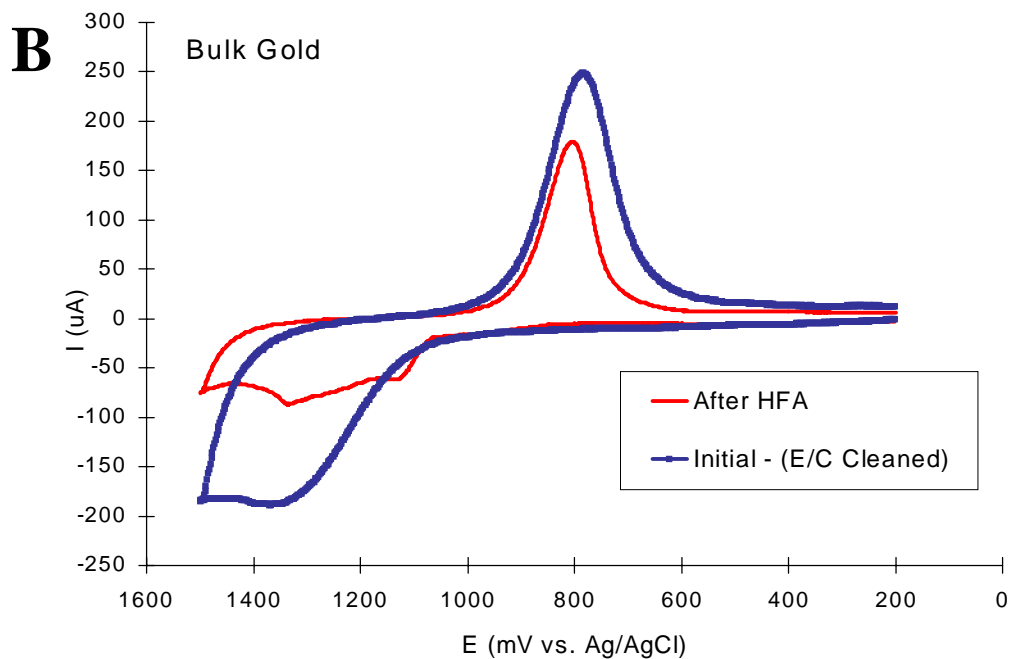
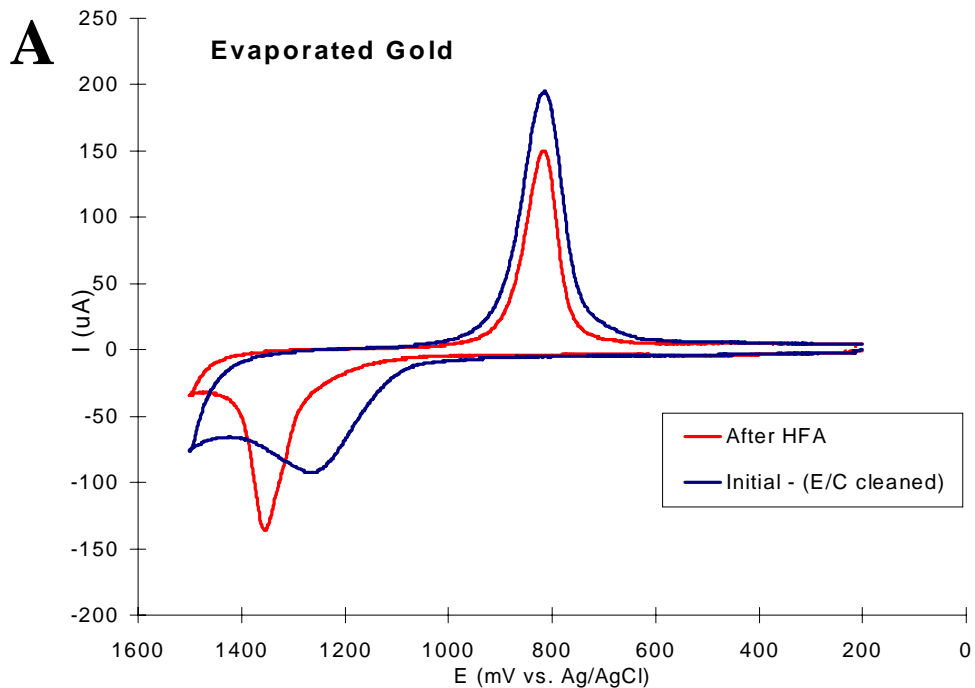


**Figure 3.9.** Cyclic voltammetry roughness scans of 0.1 M  $\text{H}_2\text{SO}_4$  on A) electrochemically cleaned versus HFA evaporated gold and B) electrochemically cleaned versus HFA bulk gold samples. Note the corresponding decrease in peak area (charge passed) for the Au-oxide reduction after the surfaces have been annealed.

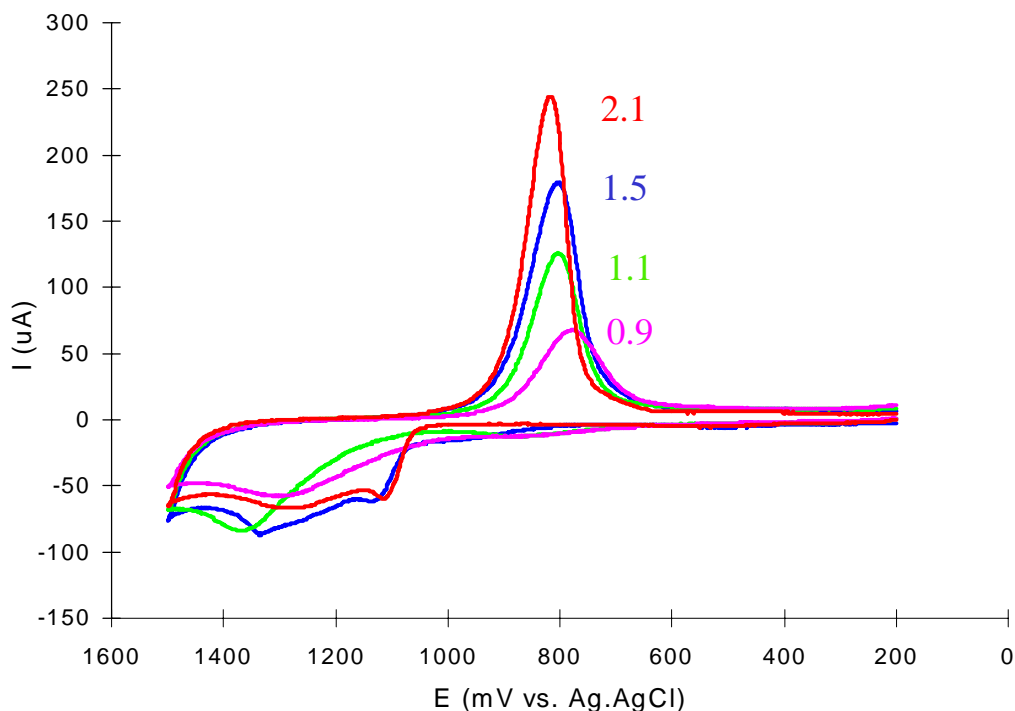


**Figure 3.10.** Cyclic voltammetry roughness scans in 0.1 M H<sub>2</sub>SO<sub>4</sub> of various types of gold substrates and pretreatments, shown with corresponding electrochemical roughness factors ( $R_{f-E/C}^*$ ). Repeated  $R_f$  measurements generally varied < 3%.  $R_f$  calculations are based on a predominantly Au(111) gold surface to achieve  $Q_{red-theor}$  and normalized to experimental Au/mica surfaces.  $R_f$  estimations of surfaces with a dominant exposed crystallinity other than Au(111), such as the Au(110) shown in this figure, are not justifiably comparable to other surfaces. For this reason, the  $R_f$  is unusually low (<1) and is included here for comparison but is not used again for the purposes of this research.

**Table 3-3.** Electrochemical and SPM Roughness Factors (Experimental Gold Substrates)

Gold Substrate	$R_{f-E/C}^a$	$R_{f-E/C}^*$	$R_{SPM}^b$ (nm)
Evaporated Gold (E/C)	1.7( $\pm$ 0.02)	2.1( $\pm$ 0.02)	1.8
Bulk Gold (HFA)	1.2( $\pm$ 0.1)	1.5( $\pm$ 0.1)	1.3
Single Crystal Au(111)	0.9( $\pm$ 0.04)	1.1( $\pm$ 0.05)	0.9
Gold Grown on Mica	0.8( $\pm$ 0.1)	1.0( $\pm$ 0.1)	0.3

<sup>a</sup> Determined from electrochemical roughness scans using 448  $\mu\text{C}/\text{cm}^2$ .

<sup>b</sup> Determined from RMS roughness calculation performed by the Nanoscope software ( $R_q$ ).

$-R_{f-E/C}^*$  normalized to the flattest experimental gold substrate (Au/mica) in the following manner:

$$Q_{red-theor} / Q_{red-exp} (Au/mica) = 448 \mu\text{C}/\text{cm}^2 / 358 \mu\text{C}/\text{cm}^2 = 1.25$$

Therefore, each  $R_{f-E/C}$  value was multiplied by 1.25 to obtain an adjusted/normalized value.

### 3.3.4. SPM Roughness Factors ( $R_{f\text{-SPM}}$ )

Roughness factors based on microscopy images of the experimental gold surfaces are derived from the actual current feedback of the SPM experiments. For a designated area of the surface, the Nanoscope software will calculate a root mean square (RMS) roughness known as  $R_q$ . RMS is a measure of the vertical standard deviation (z direction) of a plane from the mean of that plane based on the values of each point's z coordinate. RMS roughness is further described by an equation for  $R_q$  given in the Experimental Details of this chapter. For the purposes of this work,  $R_q$  is referred to as  $R_{f\text{-SPM}}$ . Areas of approximately 200-400 square nanometers were selected for mean roughness calculations. Examples of some of the images and the selected areas of the surfaces used for the determination of  $R_{f\text{-SPM}}$  can be found in Chapter 5. The results of these SPM based roughness factors are shown in Table 3-3 for various gold substrates and are in agreement with the trend found for  $R_{f\text{-EC}}$ .

## 3.4 EXPERIMENTAL GOLD CHARACTERIZATION - CRYSTALLINITY

As previously mentioned, gold typically exists in crystalline grains of three low index surface structures: Au(111), Au(110), and Au(100). If the gold is polycrystalline, the surface will have a significant population of grain boundaries. Grain boundaries, in turn, can serve as loci for potential defect sites in SAMs formed on the gold. Therefore, experiments were performed to characterize the crystallinity of the gold substrates.

### 3.4.1. Gold Oxide Formation and Crystallinity

Roughness scans in dilute sulfuric acid can provide a qualitative assessment of the exposed crystal planes on the gold surface. Gold oxide forms distinctly on the three different crystal faces of gold.<sup>17</sup> Therefore, Au-oxide formation yields multiple peaks, it can be inferred that the surface is polycrystalline. On the other hand, if Au oxidation yields a single, sharp oxidation peak, a single crystal orientation dominates the surface. An example of this behavior is shown in Figure 3.11 where multiple Au-oxide peaks appear for a polycrystalline electrode but are replaced by a single sharp peak after annealing. Annealing is a common technique used to induce gold rearrangement to the Au(111) orientation and, therefore, a sharpening of the Au oxidation peak is expected. One exception to this trend, however, was the annealed bulk gold which was resistant to a complete rearrangement to Au(111) upon annealing (compare the Au oxidation peaks in Figure 3.11 to those of Figure 3.9). Extended

exposure of annealed bulk gold to electrochemical cycling eventually removed the annealed surface layers and re-exposed the bulk polycrystalline gold.

In contrast to thermal annealing, electrochemical cleaning tended to not alter the crystallinity of the surface. An example of this can be seen in figure 3.11 where the roughness scan of evaporated gold after electrochemical pretreatment is shown. Compared to as received evaporated gold, shown in Figure 3.9A, the Au oxidation peaks undergo very little change as a result of electrochemical pretreatment, indicating there is little effect on the crystallinity of untreated gold surfaces.

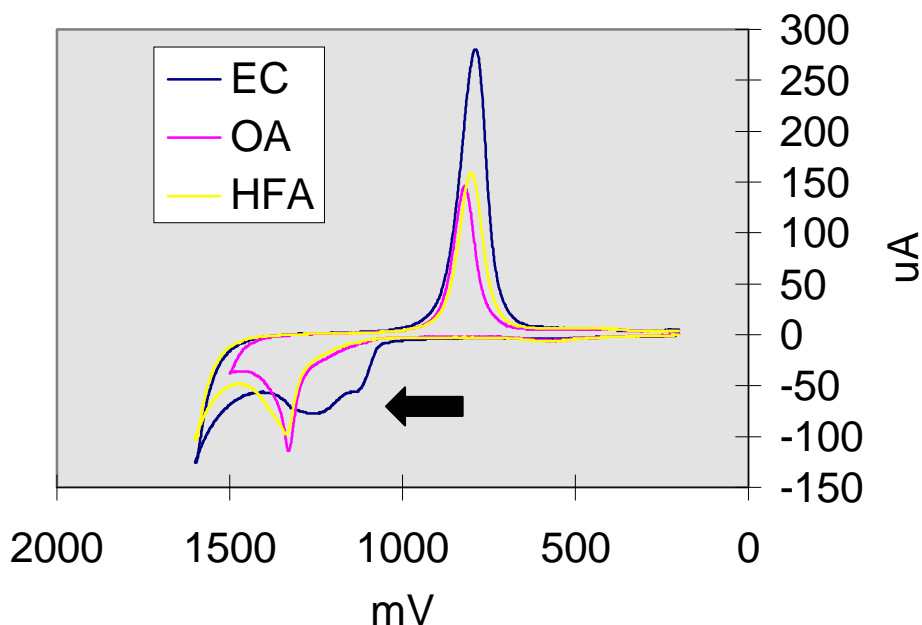


**Figure 3.11.** During roughness scans in 0.1 M  $\text{H}_2\text{SO}_4$ , the voltammetry of the Au-oxide formation (see arrow) can be characteristic of the gold's surface crystallinity. Here, the Au-oxide peaks reflect the changes in crystallinity of an evaporated Au substrate after electrochemically cleaning (EC), after oven annealing (OA), and after hydrogen flame annealing (HFA). Notice the multiple Au-oxide peaks (Au oxidation) after electrochemically cleaning, indicative of a polycrystalline surface. The sharpening of these peaks after some type of annealing treatment is believed to be the result of a predominantly Au(111) surface (Data collected by Joseph A. Black).

### 3.4.2. Lead Underpotential Deposition Experiments

A more quantitative technique for analyzing the crystallinity of gold surfaces is lead underpotential deposition (Pb UPD). A dissolved metal in solution will typically electrodeposit in limiting monolayer and submonolayer amounts onto a foreign metal surface when the electrochemical potential is moved to a value, sufficiently negative, yet still positive of the reversible Nernst potential where bulk deposition occurs. This region is known as the underpotential region.<sup>27</sup>

The amount of deposited metal, which can be up to a monolayer in the underpotential region, is dependent on the magnitude of the negative potential and the length of time that the substrate (working electrode) is held at that potential. The specific amount of metal in the UPD layer can be determined by sweeping the potential back in the positive direction after the deposition and oxidatively stripping the UPD layer off the surface. The stripping peaks can then be integrated for charge and subsequently converted to an amount. For quantitative determinations, it is essential to discriminate against the charging current by subtracting a background signal of the same scan in only electrolyte.<sup>27</sup>

Whereas numerous metal combinations form UPD layers,<sup>27</sup> of particular interest to the characterization of gold surfaces is Pb UPD. Pb UPD layers give rise to stripping voltammetry that is sensitive to different crystal faces of gold.<sup>28</sup> Prior Pb UPD experiments on gold have revealed that oxidative stripping peaks at approximately -0.25 V and -0.07 V (vs. Ag/AgCl RE) are indicative of Pb on Au(111) and Au(110) respectively.<sup>3a,4,29</sup>

Typical Pb UPD stripping voltammograms for some evaporated gold films are shown in Figure 3.12. The “blue” scan indicates that electrochemical cleaning maintains the polycrystalline nature of this surface, with sizeable Pb stripping peaks at both  $\sim -0.25$  V and  $-0.07$  V. Thermal annealing causes gold surfaces to become smoother and to rearrange to the Au(111) orientation.<sup>21</sup> This expectation is clearly shown by the Pb UPD results (Figure 3.12 – red and green scans) where the oven annealed, as well as, the hydrogen flame annealed evaporated gold substrate have significantly reduced Au(110) signals accompanied with an accentuated Au(111) signal. This result is an excellent example of how the relative percentages of crystal grains on a gold surface can be highlighted.

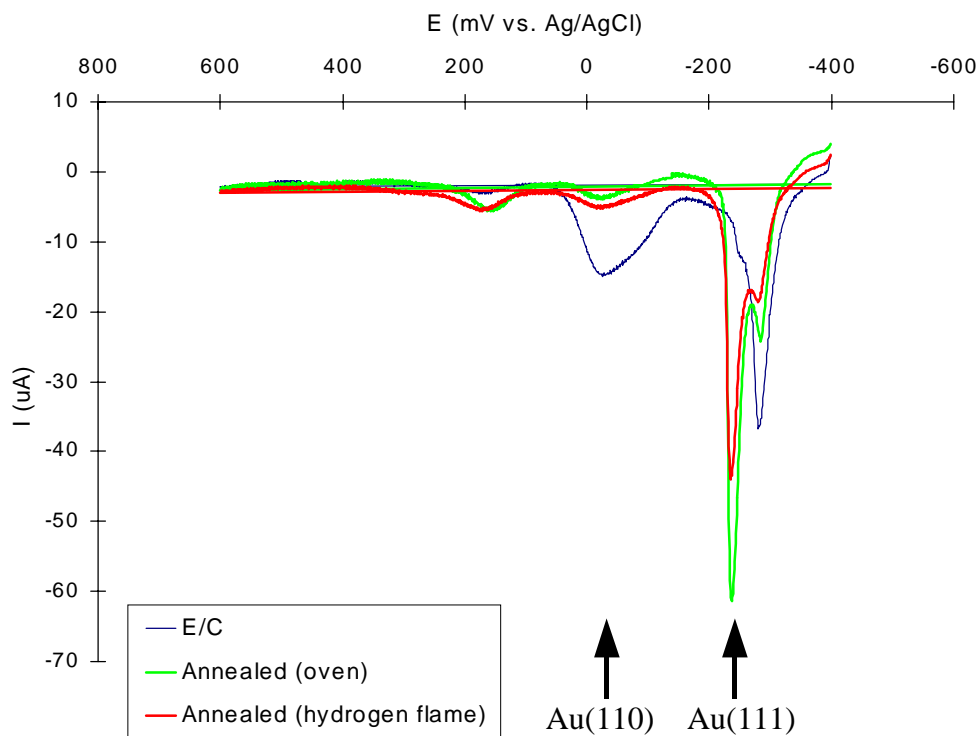


**Figure 3.12.** Pb UPD stripping voltammetry designed to illuminate the crystallinity of the evaporated gold surfaces that have been electrochemically cleaned, oven annealed, and HFA. Stripping peaks at approximately  $-0.070$  V and  $-0.250$  V are expected to be due to Au(110) and Au(111), respectively. Notice the increase in the Au(111) based stripping peak and a simultaneous decrease in Au(110) after annealing procedures have been performed.

Pb UPD also revealed, however, that polycrystalline bulk Au was resistant to thermally induced surface reorientation. Figure 3.13A shows Pb UPD stripping peaks for the bulk Au immediately after chemical etching, when the freshest gold has just been exposed. The multiple stripping peaks indicate an almost equal distribution of Au(111) and Au(110). After annealing in a tube furnace at  $\sim 968^{\circ}\text{C}$  for one hour, the crystal properties of the surface show little change (Figure 3.13B). In comparison, oven annealing of evaporated Au usually resulted in a largely Au(111) character. Only after treating the bulk gold with a hydrogen flame, which possesses a much higher annealing temperature, does the Au(110) character of the surface start to diminish (Figure 3.13C).

Pb UPD experiments were used to gain insight into the exposed crystal planes of all four of the experimental gold substrates (not all results shown). Roughness characterization (both electrochemical and microscopic), analysis of the Au-oxide peak shape and pattern, and SPM imaging were also used for characterization, as described earlier. A summary of the characterization of each type of Au surface is presented in Table 3-1.

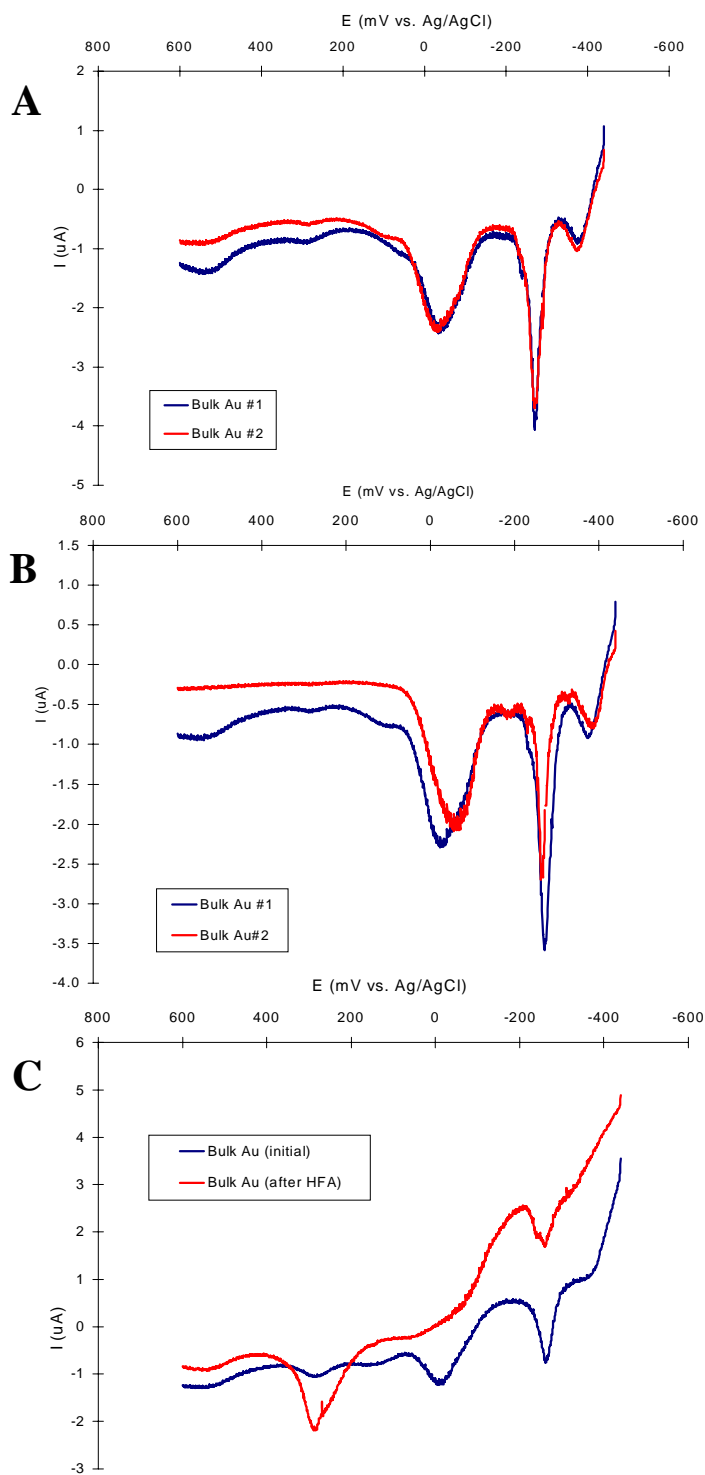


**Figure 3.13.** Pb UPD stripping voltammetry of (A) bulk gold samples immediately after chemical etching in aqua regia, (B) after oven annealing for one hour at  $\sim 968^\circ\text{C}$ , and (C) before and after HFA. Peaks at  $-0.070$  V and  $-0.250$  V are indicative of Au(110) and Au(111), respectively.

## PART I – MULTIPLE GOLD SUBSTRATE STUDY

### 3.5 CYT C ELECTROCHEMICAL RESPONSE ON MODIFIED GOLD

Considering that the original intent of this research was to elucidate the role of the Au substrate's topography in cyt c voltammetry, the different gold substrates were thus modified with COOH terminated SAMs and cyt c was adsorbed. It was expected that the flatter gold substrates would support SAMs of substantially lower defect density compared to the traditional evaporated Au films. Furthermore, it was anticipated that a significant reduction in FWHM might be observed for the cyt c voltammetry on these smoother surfaces. Such a result would support the hypothesis that peak broadening was due primarily to heterogeneous protein adsorption sites on the surface arising from defects in the SAM.

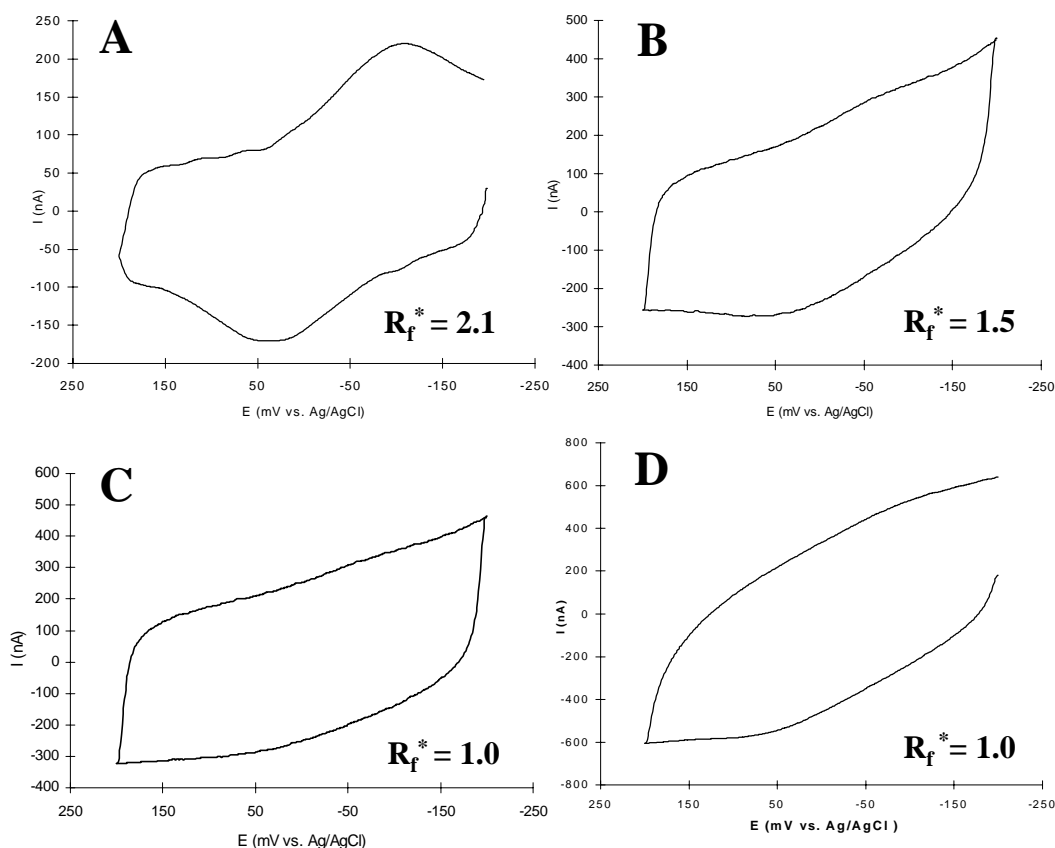


**Figure 3.14.** Cyclic voltammetry of cyt c adsorbed at  $C_{14}OOH$  SAMs on various gold substrates: A) Cyt c/  $C_{14}OOH$  SAM / Evaporated Au (E/C); B) Cyt c/  $C_{14}OOH$  SAM / Bulk Au (HFA); C) Cyt c/  $C_{14}OOH$  SAM / Au(111); D) Cyt c/  $C_{14}OOH$  SAM / Au / mica. Roughness factor trend of gold topographies:  $A > B > C > D$ ;  $\{C_{14}OOH = HOOC(CH_2)_{13}SH\}$ . Solution conditions: 4.4 mM KPB ( $\mu = 10$  mM, pH = 7, 100 mV/sec).

Interestingly, the cyt c response on these different SAM modified gold substrates varied significantly and unexpectedly. Examples of cyclic voltammograms of horse cyt c adsorbed onto each of the four experimental substrates are shown in Figure 3.14. There is a definite trend that emerges, but it is not the expected narrowing of the cyt c voltammetric peaks. Instead, as the Au surface becomes smoother and the SAM presumably less defective, as evidenced by the roughness and redox probe experiments, respectively, the faradaic current response of cyt c disappears. This surprising result was highly repeatable, and comprehending the reasons behind it became the focus of this work.

The results just described clearly show that gold substrate topography plays a significant role in the electrochemistry of adsorbed cyt c. To account for the surprising absence of electroactive cyt c on smoother Au substrates, two possibilities must be considered: 1) cyt c is adsorbed on the SAM but in an electroinactive state, possibly from improper orientation or denaturation; or 2) cyt c is not present on the surface, indicating that the low defect SAM resists adsorption of the protein. Furthermore, a combination of these two effects cannot be ruled out. To investigate this matter, a series of electrochemical and spectroscopic experiments were undertaken, as described in the following sections.

### **3.6 X-RAY PHOTOELECTRON SPECTROSCOPY**

A useful technique for determining the elemental composition of a surface and the presence of adsorbates is x-ray photoelectron spectroscopy (XPS), which is briefly discussed in this chapter's Experimental Details section. Previous research from this laboratory utilized XPS to detect the presence of cyt c adsorbed on carboxylic acid SAMs on evaporated Au substrates. By monitoring the N(1s) signal from the amino acids comprising the cytochrome's protein shell, XPS revealed that a substantial amount of protein was present on the surfaces of these SAMs.<sup>34</sup> In that study, XPS was also used to compare the amount of protein adsorbed to HOOC(CH<sub>2</sub>)<sub>n</sub>S- SAMs where n = 5, 10, and 15. XPS results revealed similar cyt c coverages on all three SAMs surfaces in spite of the fact that electrochemical experiments indicated lower values for electroactive cyt c coverage on the SAMs with smaller chainlengths.<sup>34</sup> In much the same manner, XPS was used in this research to

determine if the cyt c was indeed adsorbed to SAMs that had been formed on the smoother gold substrates.

For these experiments, a series of SAMs,  $\text{HS}(\text{CH}_2)_{13}\text{COOH}$ , were formed using identical deposition procedures on bulk Au samples whose surface roughness had been systematically altered. HFA was used to lower the surface roughness whereas electrochemical cleaning was used to promote rougher topography. As a blank, a modified ( $\text{C}_{14}\text{OOH}$  SAM), electrochemically cleaned gold substrate was used.

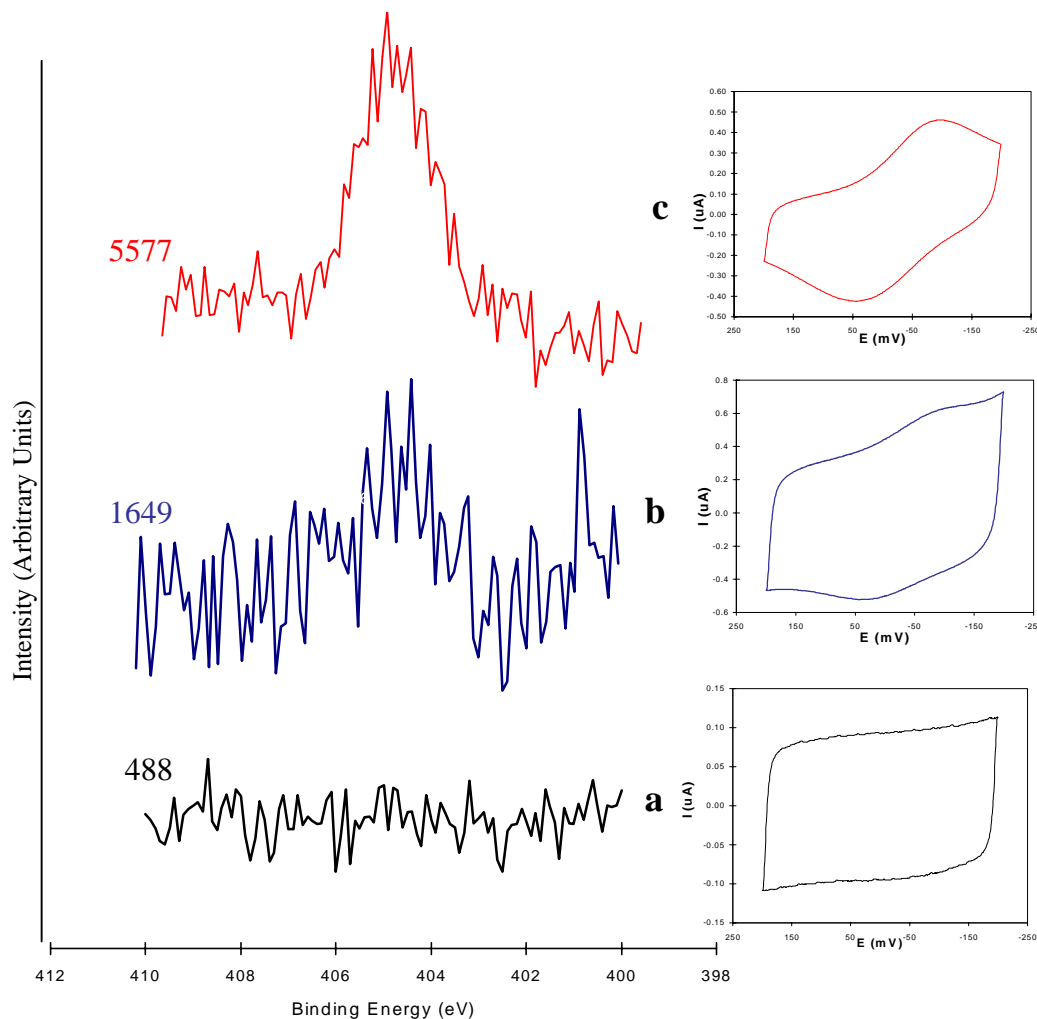


**Figure 3.15.** XPS spectra of the N(1s) region and corresponding cyclic voltammograms of a)  $\text{C}_{14}\text{OOH}$  SAM / evaporated Au (blank), b) cyt c /  $\text{C}_{14}\text{OOH}$  SAM / bulk Au (smoothed with HFA), and c) cyt c /  $\text{C}_{14}\text{OOH}$  SAM / bulk Au (roughened with electrochemical cleaning). The N(1s) signal (@405 eV) directly corresponds to adsorbed protein on the surfaces, measuring the N present in the amino acids of the protein shells. The numbers to the left of the figure correspond to the relative areas of the N(1s) XPS peaks shown and are provided for a semi-quantitative comparison of adsorbed protein.

Figure 3.15 illustrates the results of the XPS testing. The XPS N(1s) signal of these samples, when compared to the blank, clearly shows the existence of amino acids on both surfaces. However, there seems to be a substantially larger N(1s) signal and therefore higher coverage for cyt c adsorbed on the SAMs on rougher substrates. This result lends support to the hypothesis that cyt c adsorption is intimately related to the density of defect sites in the SAM. In this case, the presence of cyt c was clearly diminished on the gold surfaces that had been pretreated with HFA.

### **3.7 EFFECT OF INTENTIONAL GOLD ROUGHENING ON CYT C RESPONSE**

To further define the role of surface topography, experiments were designed to assess whether intentional roughening of smooth electrodes, which had consistently yielded poor cyt c voltammetry, would give rise to an improved response. If roughening the surface improved the cyt c response, it would lend support to the idea that rough substrates are better suited for protein adsorption and voltammetry.

Intentional roughening experiments were first performed on bulk Au due to its mechanical stability and renewable surface. Bulk gold samples were first smoothed using HFA, and the  $R_f$  value was measured. The surface was then modified with a COOH SAM and tested for cyt c response. Subsequent electrodes were smoothed in the same manner, the  $R_f$  value was measured, and they were then subjected to electrochemical pretreatment, which roughens the surface as described earlier. The roughening effect was then verified by remeasuring  $R_f$ . The new surface was then modified with a SAM, exposed to a deposition solution of cyt c, and subsequently tested for adsorbed cyt c response. Similar experiments were subsequently performed with other types of gold.

Figure 3.16 illustrates a typical example of how intentional roughening of a smoothed Au surface substantially improves the adsorption and voltammetry of cyt c. The improvement in the cyt c response was substantial enough that all electrochemical parameters, normally measured with cyclic voltammetry, were accessible. This result was highly repeatable and similar results were found for all of the other substrates, the results of which are not shown for the sake of space. These results thus provide further evidence that

the topography of the Au is a critical component in the voltammetry of adsorbed cyt c and indicate the preference of the system for rougher surfaces.

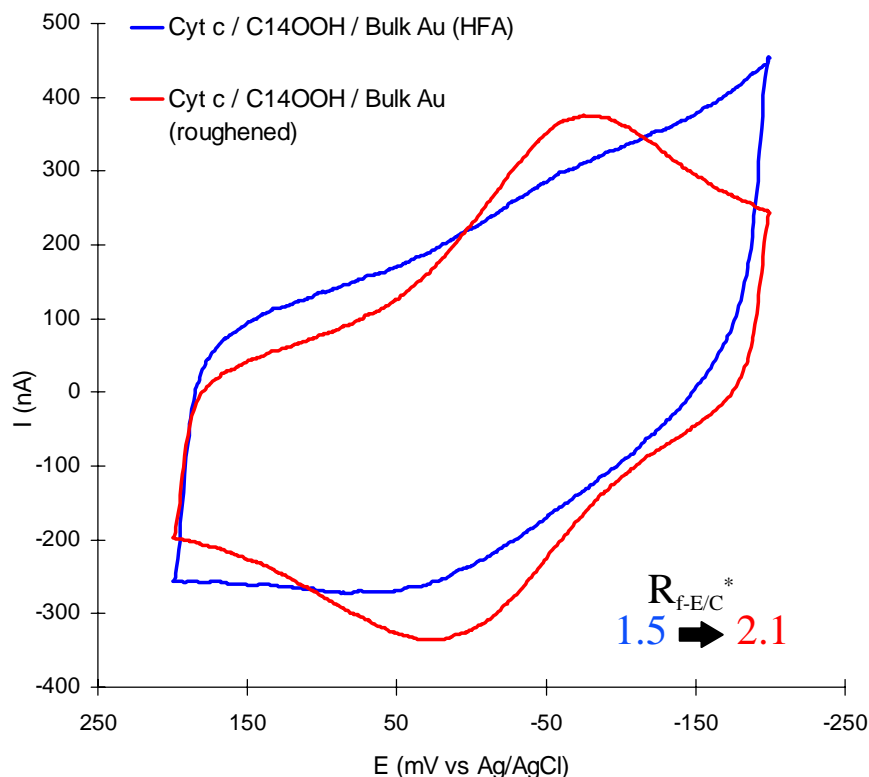


**Figure 3.16.** Cyclic voltammetry of cyt c / C<sub>14</sub>OOH SAM / bulk Au assemblies where the gold surface was smoothed through HFA and roughened by electrochemical cycling. The increase in  $R_f$  correlates with the regeneration of a well-defined cyt c voltammetric response. Similar results were obtained on other gold surfaces as well (results not shown). Solution conditions: 4.4 mM KPB ( $\mu = 10$  mM) at pH=7; 100 mV/sec.

### 3.8 SQUARE WAVE VOLTAMMETRY

Square wave voltammetry (SWV) was used in an effort to detect whether any electroactive cyt c was present on the surfaces of the more “ideal” SAMs on flat Au/mica substrates. Recall from Figure 3.14 that the Au/mica system gave rise to large  $C_{dl}$  values and weak to nonexistent faradaic current in cyclic voltammograms. SWV is a pulsed voltammetry technique that discriminates effectively against charging current. The method utilizes a staircase potential waveform with a superimposed square wave<sup>35,36</sup> and has been used successfully in prior work on adsorbed cyt c.<sup>36b</sup>

SWV was applied to the cyt c/C<sub>14</sub>OOH/Au/mica assembly and the results are shown in Figure 3.17. Based on prior work,<sup>36b</sup> the peak at 0-25 mV can be attributed to the presence

of adsorbed cyt c. Additionally, the SWV response after exposure to 1 M KCl solution is shown. A wash with high salt solution is known to desorb a significant portion of adsorbed cyt c, which is primarily electrostatically adsorbed.<sup>1</sup> The diminished SWV response after the wash shows this to be the case and provides further support that the observed peak results from adsorbed cyt c. The signal in both of these cases, however, is much less than that obtained using evaporated Au assemblies (result not shown). This result offers further voltammetric evidence for a very low electroactive cyt c coverage, which is consistent with the notion that SAMs formed on smoother Au surfaces are more resistant to adsorption.

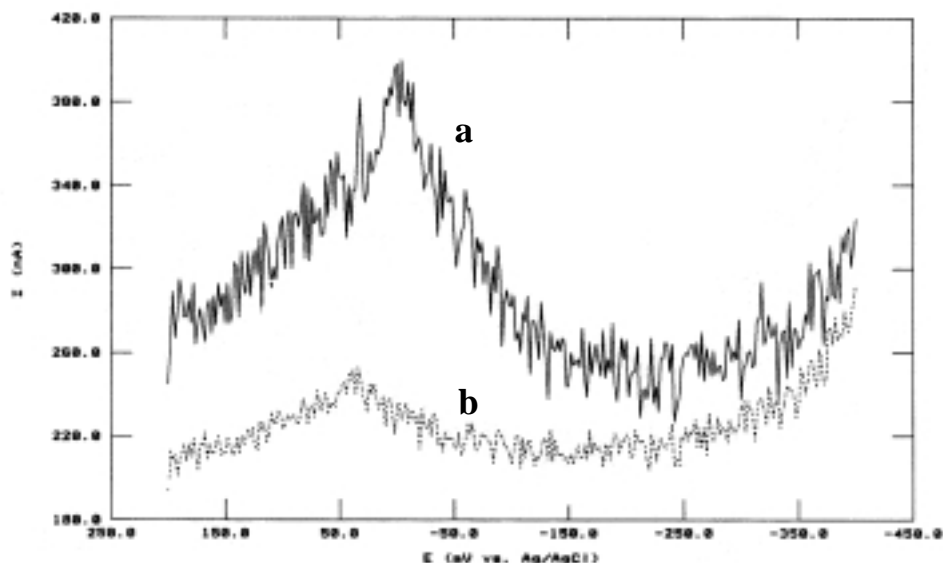


**Figure 3.17.** Square wave voltammetry (SWV) of cyt c / C<sub>14</sub>OOH SAM / Au / mica assemblies after initial protein adsorption (a) and after exposure to several rinses with 1 M KCl. Independent SWV experiments (results not shown) on cyt c / C<sub>6</sub>OOH SAMs / evaporated Au assemblies supported that the peak at 0-25 mV was indeed from adsorbed cyt c. Additionally, the cyt c signal was larger on the evaporated gold surfaces with C<sub>6</sub>OOH.

### 3.9 PROPERTIES AND STRUCTURE OF COOH SAMs

The results described to this point indicate that the topography of the gold substrate has a substantial effect on the electrochemical response of adsorbed cyt c. We now turn to results dealing with the structure and properties of the COOH SAM modifiers formed on the different types of gold surfaces. Eventually, a model for the structure of these SAMs will be proposed to help explain some of the results.

A primary concern with the variety of different topographies displayed by these unique gold substrates is how a SAM would form on the surface and the structure and

stability the monolayer would ultimately possess. The density of defects in the SAMs formed on these gold substrates is of major interest. Table 3-4 summarizes the types of defects possible in SAMs formed on gold. Each type of defect has been observed and described in the literature using both SPM and electrochemical methods.<sup>5</sup>

**Table 3-4.** Categories of SAM Defects<sup>5</sup>

<b>Defect Name</b>	<b>Description</b>
Point	Individual missing thiols
Line	Missing rows of thiols
Domain Boundary	Areas bordering two domains differing in rotational or translational symmetry
Grain Boundary	Areas between two different crystal grains
Low Order	Areas of loosely packed or disordered regions with more liquid-like properties (reason for low order defects range from contamination to insufficient deposition times for self-assembly)
Step Edge	Defects created at gold atomic step edges
Pinhole	Areas of bare gold - electrolyte solution is allowed to make contact with gold surface

Densely packed SAMs are capable of passivating the gold surface toward a variety of electrochemical processes including: oxidation of the Au itself, the underpotential deposition of metals, and the redox activity of electrochemically reversible solution species. Since all of these processes require solution species, in the form of redox molecules or the electrolyte itself, being able to penetrate the SAM and approach the electrode surface, they all can be used to qualitatively assess the defect site density in a SAM. Of particular interest in this study is the SAMs ability to inhibit a diffusing molecule's electrochemistry, a technique called redox probing.

### **3.9.1. Redox Probing of SAMs**

The voltammetry of a redox probe that is reversible at a bare metal electrode and suppressed by a SAM modified electrode can provide information about the SAM's structure. The degree of suppression is an indication of the defect and/or pinhole density in the SAM.

For example, if a redox probe at a SAM modified electrode exhibits reversible, mass transfer (MT) controlled behavior, the SAM is most likely riddled with pinhole defect sites, allowing the probe ready access to the underlying metal.

On the other hand, if the SAM has a sufficiently low level of defects, it will obstruct the approach of the probe to the electrode and the redox reaction will be significantly inhibited. The voltammetry, if any, will exhibit attenuated faradaic currents and slower kinetics due to unfavorable energetics associated with polar molecules diffusing through a layer of densely packed alkane chains. Thus, the redox probe will only gain access to the electrode at energetically favorable defects sites in the SAM. Many experimental factors can affect the results of redox probing experiments: solvent, electrolyte, and redox probe hydrophobicity, charge, and mechanism of ET (inner vs. outer sphere ET).<sup>5</sup>

A major advantage of redox probing for evaluating defect density in SAMs is the versatility provided by the method. This versatility stems from the numerous redox molecules, with a variety of properties, that can be employed as redox probes. Redox probes that have been utilized in SAM defect studies range from simple metal ions to more complicated organometallic complexes. Commonly used redox probes include: iron ( $\text{Fe}^{2+/3+}$ ),<sup>30a</sup> ferricyanide ( $\text{Fe}(\text{CN})_6^{4-}$ ),<sup>30e,f,g</sup> ruthenium hexamine ( $\text{Ru}(\text{NH}_3)_6^{3+/2+}$ ),<sup>30a-c,e-g</sup> phenol ( $(\text{C}_6\text{H}_5)\text{-OH}$ ),<sup>30b</sup> benzoquinone ( $\text{O}=(\text{C}_6\text{H}_4)=\text{O}$ ),<sup>30f</sup> and ferrocene or derivatives of ferrocene.<sup>30c,d</sup>

### 3.9.2. Hydroxymethyl ferrocene Redox Probing of SAMs on Experimental Gold

Carboxylic acid SAMs were first probed with both ferricyanide and ruthenium hexamine (results not shown), but these redox probes proved to be inadequate. The voltammetric response of the negatively charged ferricyanide ion was essentially nonexistent on all SAM/Au substrates, most likely due to electrostatic repulsion. Thus, ferricyanide is not a very sensitive redox probe for COOH SAMs. Likewise, electrostatic complications with ruthenium hexamine (RuHex) rendered it useless as a redox probe for acid terminated SAMs. With a charge of +3, RuHex strongly adsorbed to the negatively charged surfaces and, in fact, seemed to cause irreversible damage to the SAMs.

Of much greater usefulness is the redox probe hydroxymethyl ferrocene (HMFc), first described in work by Creager and coworkers.<sup>3a</sup> HMFc is a sensitive redox probe for

detecting SAM defects. It is a small, water soluble molecule that undergoes a rapid, outer sphere, chemically reversible redox reaction. Additionally, HMFC is neutral and possesses a hydrophobicity that makes it extremely sensitive to defects in the SAM. Creager observed that the oxidation of HMFC:



can be blocked by a low defect monolayer. In this case, the cyclic voltammetry will exhibit a severe attenuation of diffusion controlled current, usually apparent as a significantly smaller and positively shifted oxidation wave that is sometimes accompanied with no corresponding return signal (reduction wave). This voltammetric behavior is indicative of a kinetically challenged ET process. On the other hand, as SAMs become more defective, the reaction proceeds more readily and a conventional, MT-controlled voltammogram results. If the SAM is very defective and cannot block the probe molecule at all (a poor barrier), the voltammogram will reflect the redox activity of HMFC at a bare gold electrode.<sup>3a</sup>

For the HMFC probe experiments, carboxylic acid terminated SAMs of two chainlengths, C<sub>14</sub>OOH and C<sub>11</sub>OOH, were formed on the various gold substrates, as described in the Experimental Details section of this chapter. All SAMs were allowed to deposit for over three days to promote maximum packing.<sup>5</sup> SAMs with alkane chains of 10 and especially 13 methylene (-CH<sub>2</sub>) units were chosen because thicker films are more likely to exhibit a higher degree of crystallinity, presumably making the SAM structure more sensitive to the surface topography of the gold substrates than SAMs composed of shorter chain thiols.<sup>5</sup>

Figure 3.18 and Table 3-5 summarize the results of the HMFC redox probe experiments with C<sub>14</sub>OOH SAMs. As the overall roughness of the gold decreases, the blocking characteristics of the SAMs are enhanced, as evidenced by a positive shift of the oxidation peak (E<sub>p,a</sub>) and a significant decrease in the anodic and especially cathodic currents compared to HMFC at a bare Au surface. These results support the conventional notion that as the surface becomes smoother, with fewer grain boundaries, step edges, and the like, the SAM formed on the surface appears to be more well ordered with fewer defects.

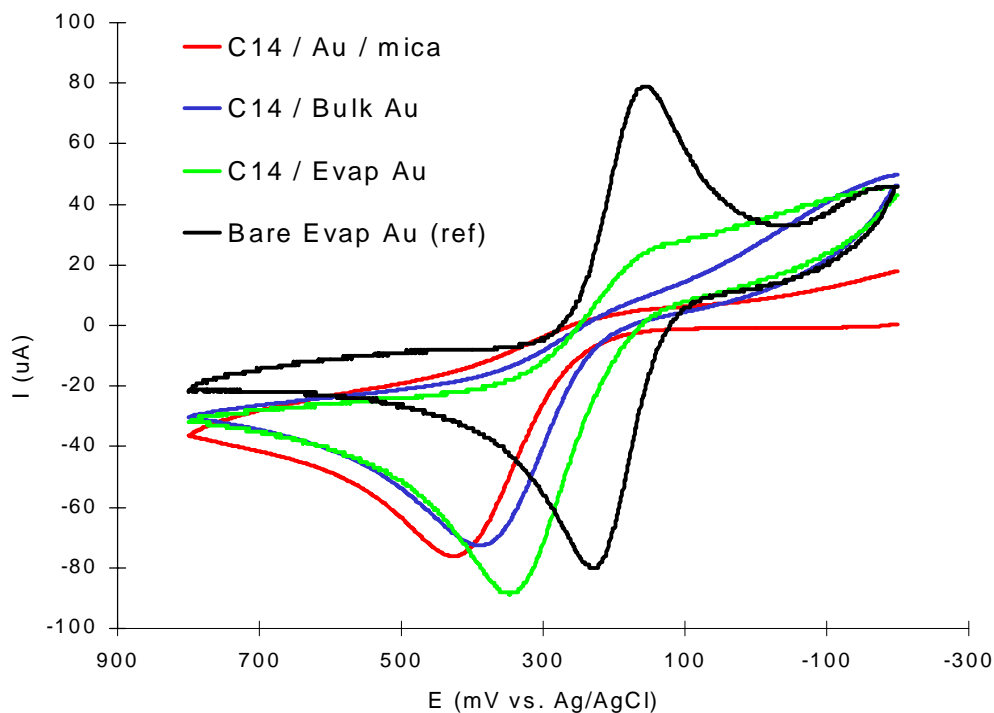


**Figure 3.18.** HMFc voltammetry at various gold substrates modified with  $\text{HOOC}(\text{CH}_2)_{13}\text{SH}$  (or  $\text{C}_{14}$  acid SAM). Note the positive shift in  $E_{p,a}$  of the voltammograms shown. The shift is more positive for the flatter gold substrates. Solution conditions: 0.2 mM HMFc in 0.1 M  $\text{HClO}_4$ ; scanned at 100 mV/sec.

**Table 3-5.** HMFc SAM Defect Redox Probe Voltammetry Results (  $\text{HOOC}(\text{CH}_2)_{14}\text{SH}$  SAMs on Various Gold Substrates)

System	$E_{p,a}$ (mV)	$E^{\circ}$ (mV)
Evaporated Gold (ref.)	230	193
$\text{C}_{14}$ SAM / Evap. Au (E/C)	348	n/a
$\text{C}_{14}$ SAM / Bulk Au (HFA)	388	n/a
$\text{C}_{14}$ SAM / Au(111)	384	n/a
$\text{C}_{14}$ SAM / Au / mica	419	n/a

Note: n/a indicates that the voltmmetry lacked a HMFc reduction wave, making an estimation of the formal potential impossible. The relative standard deviation in  $E_{p,a}$  and  $E^{\circ}$  was approximately 2%.

### 3.10 $C_{dl}$ OF THE CYT C / SAM / Au SYSTEMS

Upon closer inspection of the cyt c responses on each substrate, Figure 3.14, an interesting trend in the double layer capacitance ( $C_{dl}$ ) emerges. The  $C_{dl}$  values for SAMs on smoother gold are significantly higher than for SAMs on rougher gold surfaces. This trend is

confirmed by Figure 3.19 and Table 3-6, which collect capacitance results obtained using two different methods, CV and EIS.

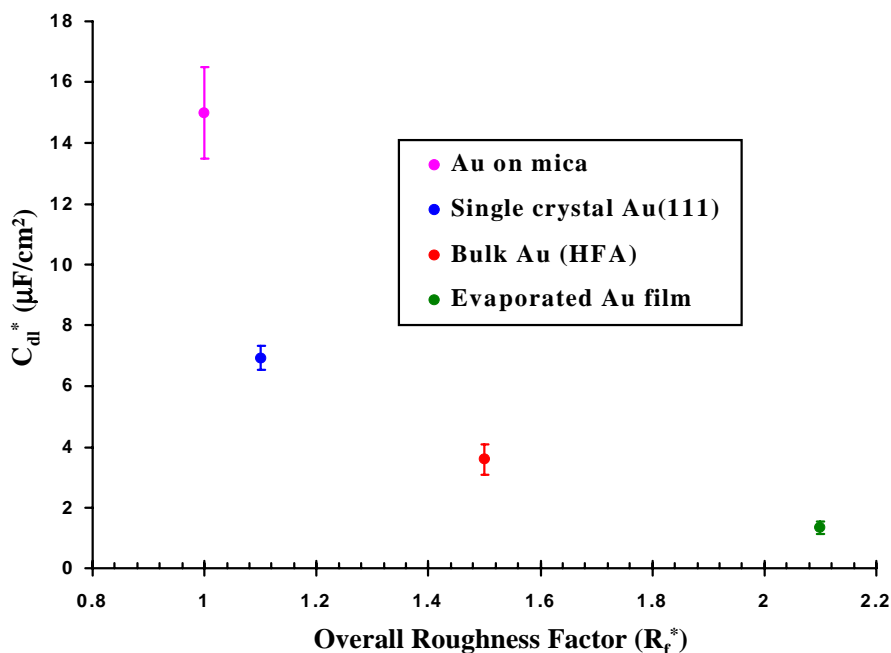


**Figure 3.19.** Plot of double layer capacitance ( $C_{dl}^*$ ) versus the overall roughness factor ( $R_{f-E/C}^*$ ) of the various gold substrates.  $C_{dl}$  measurements were made using EIS and CV and have been adjusted to incorporate the *real* surface area of the electrodes.  $R_f$  values are normalized to the flattest gold substrate (Au/mica) as previously described.

**Table 3-6.** Double Layer Capacitance Measurements of  $\text{HOOC}(\text{CH}_2)_{13}\text{SH}$  SAMs on Various Gold Substrates

Gold Substrate / $\text{C}_{14}\text{OOH}$ SAM	$R_{f-E/C}^*$ <sup>a</sup> (unitless)	$C_{dl}$ (CV) <sup>b</sup> ( $\mu\text{F}/\text{cm}^2$ )	$C_{dl}$ (EIS) <sup>c</sup> ( $\mu\text{F}/\text{cm}^2$ )	$C_{dl}^*$ (CV) <sup>d</sup> ( $\mu\text{F}/\text{cm}^2$ )	$C_{dl}^*$ (EIS) <sup>d</sup> ( $\mu\text{F}/\text{cm}^2$ )
Evap. Au (E/C)	2.1( $\pm 0.02$ )	2.8( $\pm 0.4$ )	1.9( $\pm 0.2$ )	1.3( $\pm 0.2$ )	0.90( $\pm 0.1$ )
Bulk Au (HFA)	1.5( $\pm 0.1$ )	5.4( $\pm 0.6$ )	3.9( $\pm 0.1$ )	3.6( $\pm 0.5$ )	2.6( $\pm 0.2$ )
Au(111)	1.1( $\pm 0.05$ )	7.6( $\pm 0.2$ )	5.5( $\pm 0.4$ )	6.9( $\pm 0.4$ )	5.0( $\pm 0.4$ )
Au / mica	1.0( $\pm 0.1$ )	15.0( $\pm 0.4$ )	13.5( $\pm 0.4$ )	15.0( $\pm 1.5$ )	13.5( $\pm 1.4$ )

<sup>a</sup>  $R_f$  measured electrochemically and verified using SPM;  $R_f$  have been normalized by designating the flattest substrate (Au/mica) as having a  $R_f = 1.0$  as previously described ( $R_f^*$ ).

<sup>b</sup>  $C_{dl}$  was determined from CV as  $(i_{\text{cath}} + i_{\text{anod}})/2 = i_{\text{charging}} = \nu C_{dl} A$  at 100 mV/sec in KPB (4.4 mM;  $\mu = 10$  mM, pH = 7), where A is the geometric area of the working electrode (0.32  $\text{cm}^2$ ).

<sup>c</sup> EIS was used as an alternative means of measuring  $C_{dl}$  by taking the central intersection of the x-axis in Cole-Cole plot of the data.

<sup>d</sup>  $C_{dl}$  values were adjusted to reflect the *real* surface area ( $C_{dl}^*$ ) of the electrodes by dividing each measurement by the  $R_{f-E/C}^*$  and propagating the error.

The observation that  $C_{dl}$  increases as  $R_f$  decreases is a striking result, especially in view of the HMFC probe results, which do not support increased  $C_{dl}$  as resulting from higher pinhole defect density in the SAM. Previous work by Chidsey and Loiacono<sup>30e</sup> examined the effects of chainlength and functional groups on  $C_{dl}$ , but not in conjunction with  $R_f$ . They found that  $C_{dl}$  for alkythiol SAMs decreases with increasing chainlength, as would be expected for a dielectric layer. The dependence of  $C_{dl}$  on functional end group was found to obey the following trend:



In light of the present study, it should be noted that all of Chidsey and Loiacono's experiments were performed on only one type of gold substrate, evaporated gold on silicon wafers.<sup>30e</sup> Considering this trend, higher relative values of  $C_{dl}$  with acid terminated SAMs, in and of itself, is not surprising. The apparent dependence of  $C_{dl}$  on  $R_f$  shown in Figure 3.19, however, is a newfound aspect of COOH-terminated SAMs.

Additional  $C_{dl}$  measurements on COOH SAMs were taken during those experiments involving intentional roughening of gold substrates (See Section 3.7). Those results are consistent with the  $C_{dl}$ - $R_f$  trend just described, that is, rougher gold surfaces modified with COOH SAMs consistently displayed lower  $C_{dl}$  values than those on smoother surfaces.

A proposed model to account for this result is introduced in Figure 3.20. It is proposed that when the carboxylic acid groups are forced into a more uniform plane as the gold surface becomes smoother, increased interactions among the COOH groups, i.e., hydrogen bonding and/or electrostatic repulsion, will increasingly dictate the overall structure of the SAM. Thus, the alkyl chains could be restricted from dense crystalline packing if the energy density associated with surface COOH interactions exceeded that due to chain-chain van der Waals interactions. The consequence of this would be an increase in the average dielectric constant of the SAM film, thus increasing  $C_{dl}$ :

$$C_{dl} = \frac{\epsilon\epsilon_o}{d} \quad [\text{Eqn. 3.2}]$$

On rougher surfaces, the COOH groups would tend to be more offset from each other normal to the surface, thus leading to decreased lateral interaction among the acid headgroups and, for a number of the components, greater conformational freedom. In this case, the energy associated with COOH interactions would decrease, allowing the alkane

chains to pack more densely in a lower energy state and subsequently lowering the dielectric constant ( $\epsilon$ ). A more detailed discussion of this model will be given later in this chapter (Section 3.13) after first presenting some additional results on mixed SAMs and the original evaporated gold study.

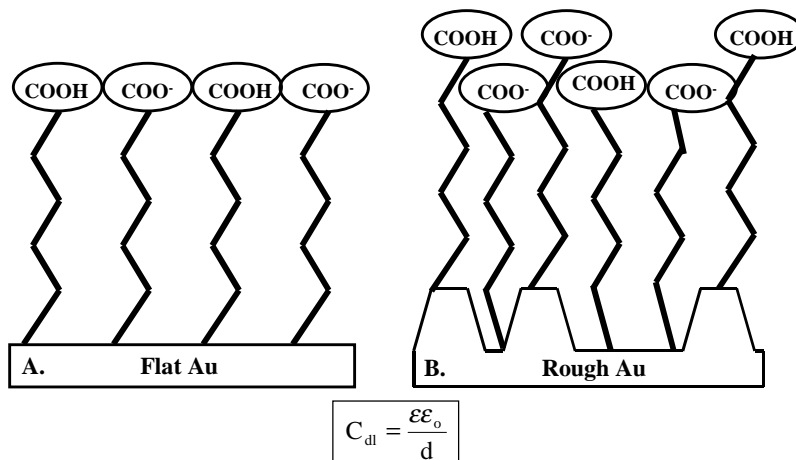


**Figure 3.20.** Proposed model to explain the observed trend in  $C_{dl}$  for SAMs on the Au substrates of varying roughness with smoother gold substrates supporting SAMs with significantly higher  $C_{dl}$  values for SAMs that are less defective. On smoother Au surfaces the alkane packing is dictated by the bulky terminal groups (COOH) spacing/interaction (A) whereas on rougher surfaces, the SAM will tend to have a higher degree of flexibility allowing the packing to better compensate endgroup-endgroup interactions. Thus, on rougher surfaces, the SAMs tend to have a higher alkane chain density which, in turn, directly impacts (lowers) the dielectric constant ( $\epsilon$ ) in the equation above and lowers the  $C_{dl}$  of the system.

### 3.11 MIXED SAMS

Mixed SAMs, or SAMs composed of  $\omega$ -substituted alkanethiols of two different chainlengths and/or terminal groups, have become an important part of the research effort in this group. In light of the cyt c results above, especially the positive effect of intentional gold roughening and the emergence of the hypothesis that cyt c adsorption/ET may be a strong function of the density of defects in the SAM, it was of interest to see how a mixed SAM on a smooth surface would behave toward cyt c adsorption and ET. The major motivation of this type of experiment arises from the view that certain mixed SAMs exhibit surfaces comprised essentially of molecular defects. Mixed SAMs of this type may be able to mimic the positive effect that roughening a smooth Au surface has on a pure COOH SAM, i.e., disruption of the COOH plane. Before presenting these experiments, it is important to have

an understanding of the general structure of mixed SAMs. Therefore, a brief synopsis of mixed SAMs and the structures they adopt is in order.

### 3.11.1. The Structure of Mixed SAMs

The structure of mixed SAMs is a popular topic and the literature dealing with this subject is extensive and varied. From this literature, however, several major trends have emerged, as described below. A variety of techniques have been employed to characterize the structure and composition of mixed SAMs including electrochemistry, ellipsometry, CAG, EIS, IR spectroscopy, MS, SPM, and others. Overall, this extensive characterization has created reasonably detailed descriptions of the structure of a number of mixed SAMs. The following discussion is limited to two-component mixed SAMs.

The literature on mixed SAMs, as well as the structures of mixed SAMs, can be generally divided into two major categories: Type I and Type II. Most literature reports deal exclusively with either Type I<sup>37</sup> or Type II<sup>38</sup> mixed SAMs. There are, however, articles that discuss both types and offer useful comparative analyses.<sup>39</sup>

The major difference between Type I and Type II mixed SAMs is derived from the different alkane chain lengths of the two thiol components, as depicted in Figure 3.21. If the chain length difference between the two components is small ( $< \sim (\text{CH}_2)_4$ ), making the length of the two components similar, the SAM is most likely to conform to the structural characteristics of Type I mixed monolayers, which tend to exhibit a random distribution of thiols across the gold surface (Fig. 3.21). As the chain length difference becomes greater ( $> 4$   $\text{CH}_2$  units), the SAM is considered Type II and will possess a characteristic domain segregation (Figure 3.21). It is believed that this structural arrangement is primarily driven by the van der Waals interactions of the alkane portions of the SAMs, resulting in the longer components clustering together. Thus, separate, nanometer-sized domains of both longer chain and shorter chain component are a characteristic property of Type II mixed SAMs. Another key aspect of mixed SAMs, both Type I and Type II, is the terminal group, which can exert a significant influence on the overall structure.

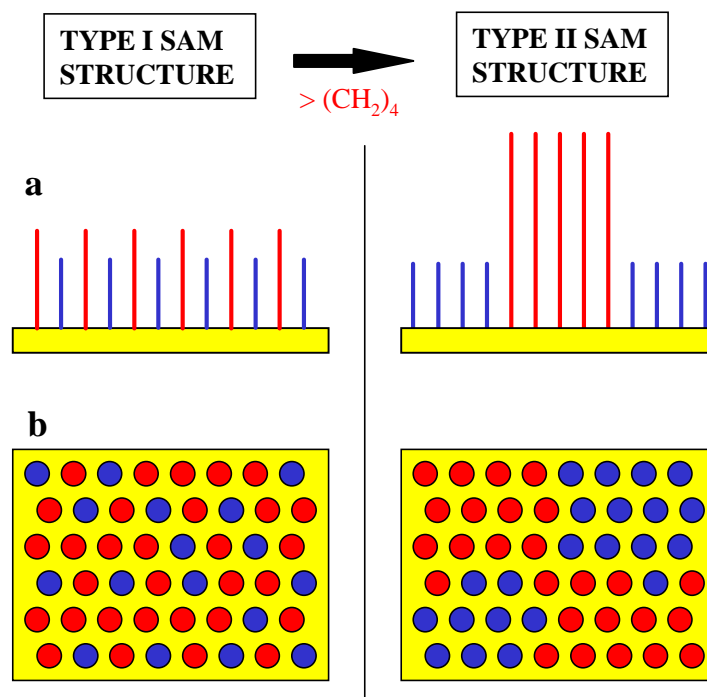


**Figure 3.21.** Illustration of the basic structure and distribution of a two component (red and blue) mixed SAM on gold: a) side view cross section; b) view from below. Note that as the difference in chainlength becomes greater than 3-4 methylene units, the distribution of the two components is expected to go from a random distribution (left) to a more phase segregated distribution with nanometer sized domains (right).<sup>39</sup>

A major advantage of two-component mixed SAMs is the ability to engineer surface chemistry by using different terminal groups. Charged groups can be mixed with neutral groups, hydrophobic termini can be mixed with hydrophilic termini, and numerous other combinations of functionality, including electroactive endgroups, are possible. It is important to remember, however, that the types of terminal group can have a significant impact on the structure of the mixed SAM. This is especially true of the Type II mixed SAMs. Figure 3.22 portrays how terminal groups can affect the structure of a Type II mixed SAM containing methyl and hydroxyl termini. In general, hydrophilic end groups avoid contact with hydrophobic entities, whether they be other endgroups or the hydrophobic alkane chains of the other component.<sup>39</sup>

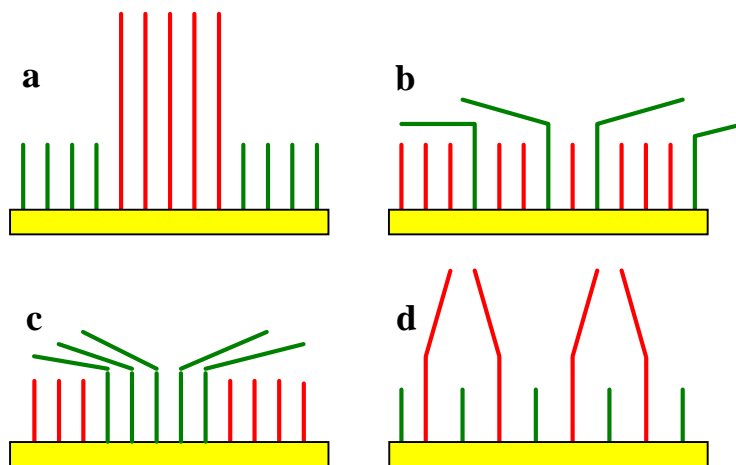


**Figure 3.22.** Two component mixed SAMs of both types (I & II) are sensitive to the influence of endgroups and will always arrange themselves to maximize favorable interactions. Hydrophobic/hydrophilic interactions are expected to play a role in the mixed SAM structure. Several examples of how hydrophobic interactions may affect the structure of these mixed SAMs are illustrated above with a two component SAM comprised of hydrophobic, methyl terminated thiols (red) and hydrophilic, hydroxy terminated thiols (green). Depending on which component is longer, it may be energetically favorable for the larger components to cluster together in an ordered fashion (a) avoiding unfavorable interactions between hydrophobic methylene chains and the alcohol endgroups. If, instead, the longer component is hydrophilically terminated (c), the longer chains may still be phase segregated, but may also bend over to maximize methylene chain interactions with the shorter methyl terminal groups. If the distribution is more random, there may be different types of bending in the components (b & d).<sup>39a</sup>

The crystallinity (degree of order) in the alkane portion of mixed SAMs can also vary. Type I mixed SAMs tend to have alkane packing similar to uniform SAMs of similar length. Again, however, the end groups can affect this property significantly. Longer chain Type I SAMs will usually be more ordered and crystalline in nature whereas shorter Type I SAMs will be more liquid-like. Both long and short Type I SAMs terminated with hydrophilic end groups typically exhibit some degree of liquid-like structure at the SAM/solution interface.

Type II mixed SAMs, on the other hand, can have a range of crystalline order within the film. This concept is illustrated in Figure 3.23. In fact, IR spectroscopy data suggest that the presence of the longer chain components in the Type II mixed SAM sometimes causes the inner crystalline region to be more ordered than if it were a uniform SAM composed only of the shorter  $\omega$ -substituted thiol. The larger the difference between the lengths of the components, the greater the effect appears to be.<sup>39</sup> Type II mixed SAMs are largely unexplored in the context of cyt c electrochemistry and are not the focus of the research at hand. Nonetheless, there are many intriguing aspects of using Type II SAMs in this work that can be envisioned.

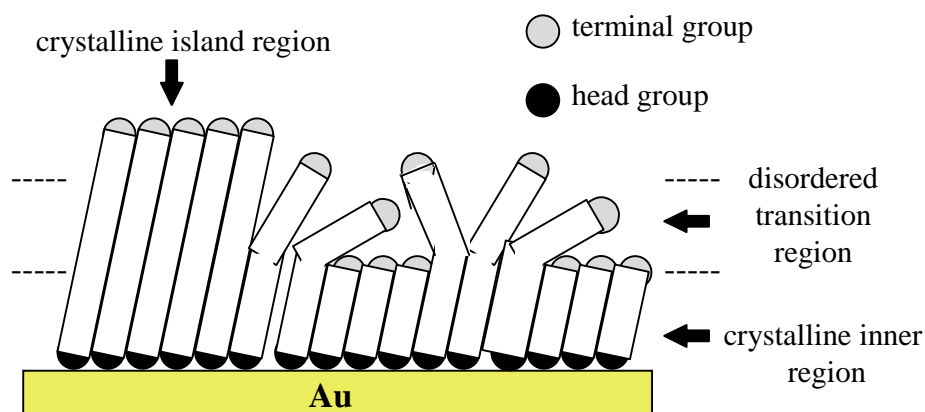


**Figure 3.23.** Crystallinity of Type II mixed SAMs.<sup>38a</sup>

### 3.11.2. The Effect of Mixed SAMs on Smooth Au Topographies and Cyt c Response

A Type I mixed SAM comprised of shorter hydroxyl-terminated alkane thiols and longer carboxylic acid terminated alkane thiols was employed for this research. This choice retains the electrostatic protein/surface attraction of the pure COOH SAM and, at the same time, maintains a hydrophilic interface. More importantly, the mixed SAM is an inherently defective film and should provide an irregular molecular texture when formed on a smooth gold surface which, according to the previously presented research, should be more conducive toward cyt c adsorption and ET. For these experiments, the annealed bulk Au was again initially used, modified with the mixed SAM, and subsequently exposed to a solution of cyt c. The cyt c/mixed SAM/smooth Au system displayed excellent cyt c electrochemistry, as shown in Figure 3.24, compared to the pure COOH SAM on this same substrate. This improvement is attributed to both the improved electronic coupling of the protein at the SAM interface and to a seemingly larger overall amount of electroactive protein being adsorbed to the surface. Similar results were observed on all of the other types of “smooth” gold surfaces as well.

HMFC redox probing experiments, the results of which are given in Table 3-7, reveal that this type of mixed SAM appears to be somewhat more defective when compared to pure acid SAMs, although testing was limited to only evaporated gold. Furthermore, double layer capacitance data, shown in Table 3-8, shows that the  $C_{dl}$  of these mixed SAMs falls consistently lower than for pure COOH SAMs.

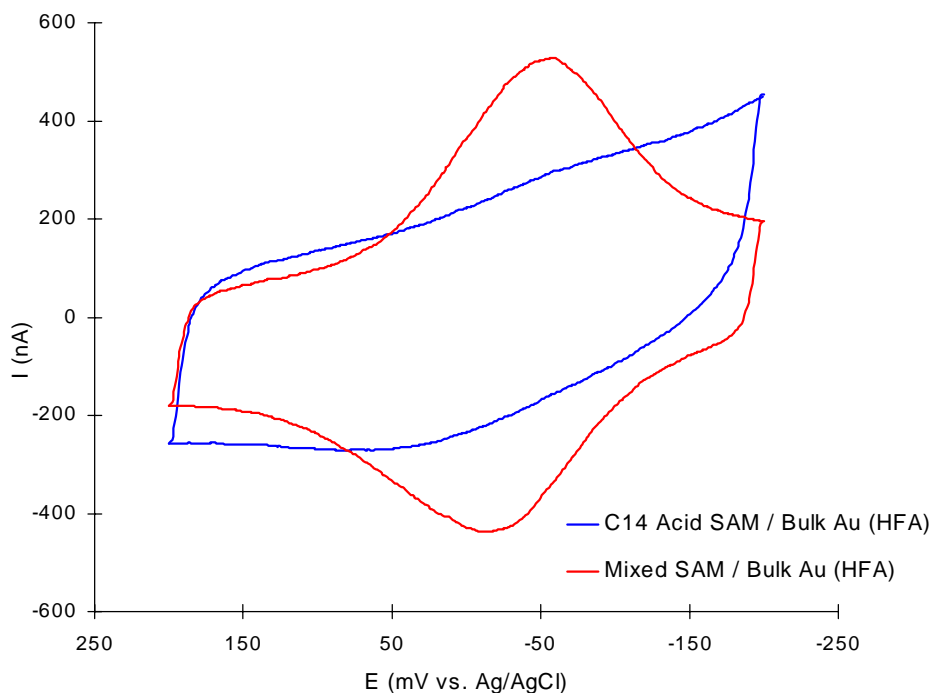


**Figure 3.24.** Cyclic voltammetry of cyt c adsorbed to a single component C<sub>14</sub> acid SAM on annealed bulk Au compared to a mixed SAM (C<sub>14</sub> acid with C<sub>10</sub> alcohol). The mixed SAM clearly produces an excellent cyt c response with well-resolved peaks, higher apparent electroactive coverage, and faster ET kinetics. The mixed SAM system also exhibits substantially lower double layer capacitance.

**Table 3-7.** HMFC Redox Probing for SAM Defects - Mixed SAM Experiments on Evaporated Gold

System <sup>a</sup>	E <sub>p,a</sub> (mV)	E <sup>o'</sup> (mV)
Bare Evaporated Au (Ref.)	230 <sub>(±2)</sub>	193 <sub>(±1)</sub>
C <sub>14</sub> OOH SAM / Evap. Au	348 <sub>(±9)</sub>	--- <sup>c</sup>
Mixed SAM <sup>b</sup> / Evap. Au	322 <sub>(±2)</sub>	161 <sub>(±8)</sub>

<sup>a</sup> Evaporated Au substrates were electrochemically cleaned prior to experiments.

<sup>b</sup> Mixed SAM = C<sub>14</sub>OOH & C<sub>10</sub>OH.

<sup>c</sup> Result unavailable because voltammetry lacks a HMFC reduction wave and no estimation of formal potential can be made.

These results create an interesting paradox that parallels the earlier topographical results. The mixed COOH/OH SAM seems more defective than pure COOH, and yet, its capacitance is lower. Conventionally, however, one would expect the more defective film (the mixed SAM) to have a higher capacitance due to increased breakdown of the parallel plate capacitor model. This unique property of these SAMs, a lower capacitance in spite of a higher density of defects, is key to establishing an accurate picture of these systems and will be examined further in the Discussion Section.

**Table 3-8.** Double Layer Capacitance Results - Mixed SAMs  
(Uniform SAMs vs. Mixed SAMs on Various Gold Substrates)<sup>a</sup>

System	$\Delta C_{dl}$ (CV) <sup>b</sup> $\mu\text{F}/\text{cm}^2$	$\Delta C_{dl}$ (EIS) <sup>b</sup> $\mu\text{F}/\text{cm}^2$
Mixed SAM / Evap. Au (E/C)	2.8→2.8	2.0→1.9
Mixed SAM / Bulk Au (HFA)	5.3→3.7	3.9→2.9
Mixed SAM / Au(111)	7.6→5.9	5.5→4.6
Mixed SAM / Au(110)	3.7→2.2	2.3→1.7

Note: Mixed SAM = C<sub>14</sub>OOH & C<sub>10</sub>OH.

<sup>a</sup> C<sub>dl</sub> values based on geometric area of electrode but can be adjusted for *real* surface area as previously shown.

<sup>b</sup> C<sub>dl</sub> values show the change in capacitance of a uniform SAM vs. a mixed SAM:  
{ C<sub>14</sub>OOH → C<sub>14</sub>OOH/C<sub>10</sub>OH }

In summary, the creation of an irregular binding surface appears to be essential for obtaining cyt c adlayers with good electrochemical properties. Either roughening the underlying gold or using a mixed SAM on smoother gold appear to be suitable means for achieving such surfaces. Table 3-9 provides a summary of results obtained on bulk gold systems to illustrate the dramatic nature of these effects on the electrochemical properties of cyt c. Smoother gold substrates, such as the HFA bulk gold substrate in this example, support quality cyt c electrochemistry only when modified with a mixed SAM or when the gold surface is roughened.

**Table 3-9.** Effect of Roughening and Mixed SAMs on Cyt c Voltammetric Properties  
(Bulk Au (HFA) Example)

SAM	R <sub>f</sub> <sup>*</sup> (unitless)	E <sup>o'</sup> (mV)	k <sub>et</sub> <sup>o</sup> (s <sup>-1</sup> )	k <sub>et</sub> <sup>o a</sup> (s <sup>-1</sup> )	Γ <sup>b</sup> (pmol/cm <sup>2</sup> )	Γ <sup>a</sup> (pmol/cm <sup>2</sup> )	FWHM (mV)	ΔE <sub>p</sub> (mV)	C <sub>dl</sub> <sup>*</sup> (CV/EIS <sup>a</sup> ) (μF/cm <sup>2</sup> )
C <sub>14</sub> OOH (smooth)	1.5 (±0.1)	⊗	⊗	⊗	⊗	⊗	⊗	⊗	3.5 / 2.6 (±0.3 / ±0.3)
C <sub>14</sub> OOH (Roughened)	2.1 (±0.02)	-14 (±1)	2.0 (±0.2)	0.4 (±0.2)	14.2 / 15.4 (±0.4 / ±0.2)	18.3 (±0.5)	127 (±5)	104 (±3)	1.5 / 1.2 (±0.1 / ±0.1)
Mixed SAM (C <sub>14</sub> OOH / C <sub>10</sub> OH) (smooth)	1.5 (±0.1)	-20.0 (±1)	13.0 (±0.1)	16.2 (±0.2)	16.0 / 15.5 (±0.2 / ±0.4)	12.0 (±0.3)	122 (±4)	40 (±3)	2.5 / 1.9 (±0.2 / ±0.2)

⊗ = Poor voltammetry rendered these properties impossible to measure;

<sup>a</sup> Properties measured using EIS; <sup>b</sup> Values determined for both cathodic and anodic peaks (cath. / anod.).

### 3.11.3. XPS of the Mixed SAM/Cyt c System

XPS analysis was performed for cyt c adsorbed at HFA bulk gold that had been modified with a Type I, two component mixed SAM ( $C_{10}OH$  &  $C_{14}OOH$ ). Voltammetry results on such systems, as seen in Figure 3.24, show, not only the regeneration of cyt c response, but a clearly superior voltammetric signal. In most cases, the coverage of the protein on the SAM appears to be greater when a mixed SAM of this type is used as the modifier compared to the single component SAM on a smoothed surface. Figure 3.25 repeats the XPS results for pure COOH SAMs (Fig. 3.15) with the addition of the N(1s) spectrum for the mixed SAM system. The use of a mixed SAM (Fig. 3.25d) appears to substantially increase total cyt c coverage relative to the pure SAM formed on a smooth gold surface (Fig. 3.25b), a result in agreement with the electrochemistry.

### 3.11.4. Kinetic Analysis of Cyt c Adlayers on Mixed SAMs

In parallel with this research, others in the Bowden Group were examining the impact of mixed SAMs on the ET rate of adsorbed yeast cyt c (YCC).<sup>40</sup> Those studies revealed a substantial increase of ET rate for YCC on mixed COOH/OH SAMs relative to pure COOH SAMs. On a Type I mixed SAM of  $C_{10}COOH$  and  $C_7OH$ , a 2500 fold increase in the ET rate constant was observed relative to a pure  $C_{10}COOH$  SAM. The Pelletier-Kraut (PK) model for YCC binding to cyt c peroxidase was proposed as a possible explanation of the results.<sup>40</sup> The PK model invokes the presence of a well-defined ET pathway between the two heme groups when they are electrostatically bound together. Using this model as a basis, El Kasmii et al. proposed that direct contact of extended chain termini of the SAM with the YCC's exposed heme edge could account for the enhanced ET rate. Thus, it seems clear that mixed SAMs can provide the appropriate interfacial properties for optimal binding and electronic coupling, whereas single component SAMs make this prospect a less likely possibility.<sup>40</sup>

Similar experiments on HH cyt c revealed the same general trend, although not as substantial.<sup>40</sup> HH cyt c ET rate constants show a 5-10 fold increase when adsorbed on a COOH/OH SAM as compared to a similar pure COOH SAM. An example of this comparison is shown in Figure 3.26. The change in  $k_{et}^{\circ}$  was consistent with that found in the previous study<sup>40</sup> and confirms that superior electronic coupling between SAM and protein occurs when a mixed SAM (Type I) is used. These results, coupled with the gold topography

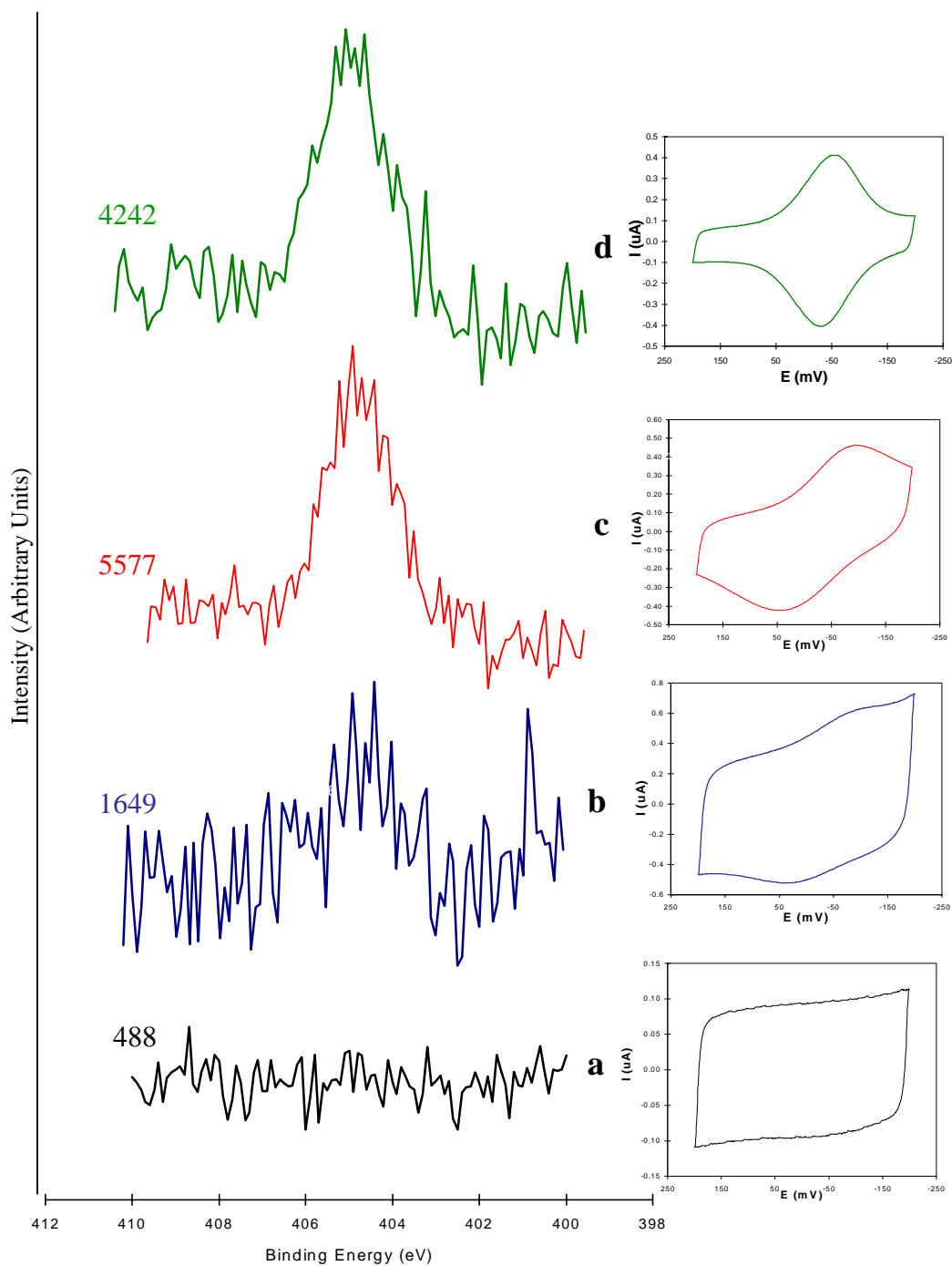


**Figure 3.25.** XPS and cyclic voltammetry of a)  $C_{14}OOH$  SAM / evap. Au (blank), b) cyt c /  $C_{14}OOH$  SAM / bulk Au (HFA), c) cyt c /  $C_{14}OOH$  SAM / bulk Au (electrochemically cleaned), and d) cyt c /  $C_{14}OOH$  &  $C_{10}OH$  - Mixed SAM / bulk Au (HFA). The numbers to the left of the figure represent the relative area of each XPS N(1s) peak (@450 eV) and is a unitless quantity provided for semi-quantitative comparison of protein on each surface.

results already presented, collectively support the idea that cyt c adsorption and ET are very much dependent on the density of defects the SAM presents.

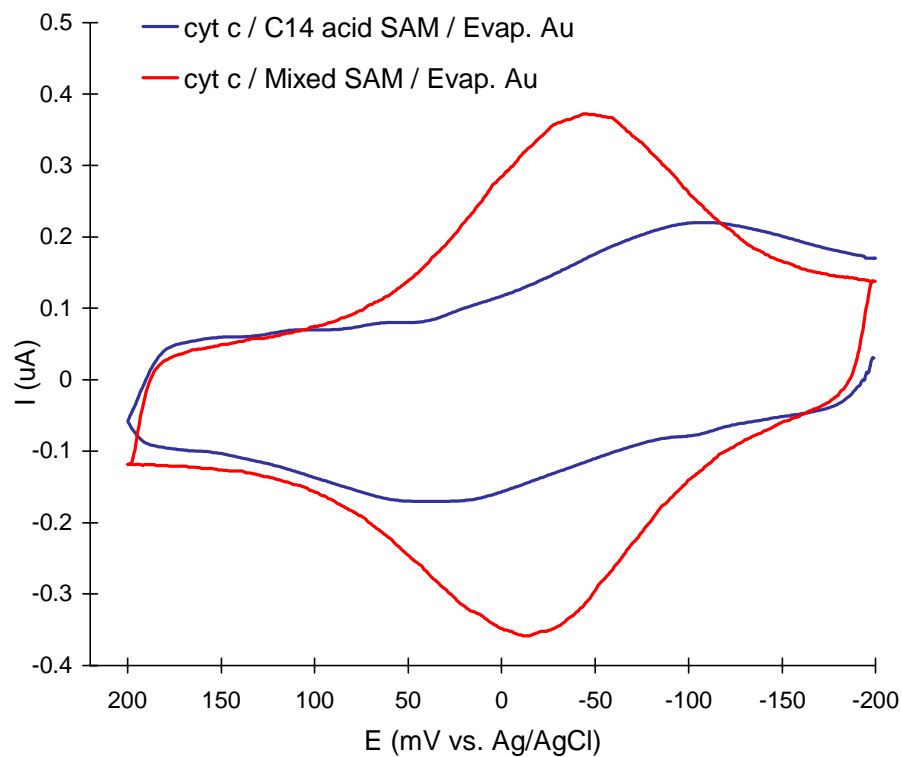


**Figure 3.26.** Cyclic voltammetry of cyt c adsorbed on a  $C_{14}$ OOH SAM on evaporated Au versus cyt c adsorbed on a mixed SAM ( $C_{14}$ OOH &  $C_{10}$ OH SAM) on evaporated gold. It is believed that the dramatic change in the voltammetry with cyt c on mixed SAMs is the result of superior electronic coupling.<sup>40</sup>

## ***PART II – EVAPORATED GOLD STUDY***

### **3.12 INITIAL RESEARCH – ROLE OF THE GOLD SUBSTRATE**

The research described to this point represents the most recent results concerning the role of the gold substrate topography. Those results followed an initial study on evaporated gold substrates that was possibly tainted by surface contamination artifacts. Nonetheless, the recent work has validated the earlier results, which are presented here in a consolidated section. The reader can skip ahead, if desired, to the Discussion (Section 3.13) without losing continuity. The present section describes annealing/roughening, SAM characterization, and cyclic voltammetry experiments similar to those described earlier, but limited to evaporated films. Furthermore, the results and conclusions mimic those obtained using a variety of gold substrates.

#### **3.12.1. Roughness of Evaporated Gold Substrates**

Figure 3.27 displays roughness scans of evaporated Au as received, after electrochemical pretreatment, and after HFA. Table 3-10 summarizes the roughness factors determined electrochemically and by SPM for these gold surfaces. As expected, the annealing appears to have a smoothing effect, whereas after electrochemical cleaning, the roughness of the gold is largely unchanged from the initial scan. Another noteworthy aspect of Figure 3.27 is the sharpening of the Au oxidation peaks after flame annealing which indicates that this pretreatment drives the polycrystalline gold surface to a predominantly single crystal state. Similar roughness scans, shown previously in Figure 3.11, indicate that the same topographical and crystallinity changes can be instigated by other annealing techniques. How lower levels of roughness affected the formation and structure of SAMs on evaporated Au was evaluated using several types of experiments: SAM desorption voltammetry, capacitance measurements, and HMFC redox probing. These results are described in the following sections.

#### **3.12.2. SAM Desorption Linear Sweep Voltammetry**

SAM desorption techniques developed by Porter *et al.*<sup>41</sup> can be used to gain a semi-quantitative assessment of thiolate concentration ( $\Gamma_{\text{mono}}$ ) in the monolayer. Application of a linear voltage sweep toward negative potentials to a SAM-modified gold electrode in a basic solution produces a cathodic wave with voltammetric peak(s) due to the reductive desorption

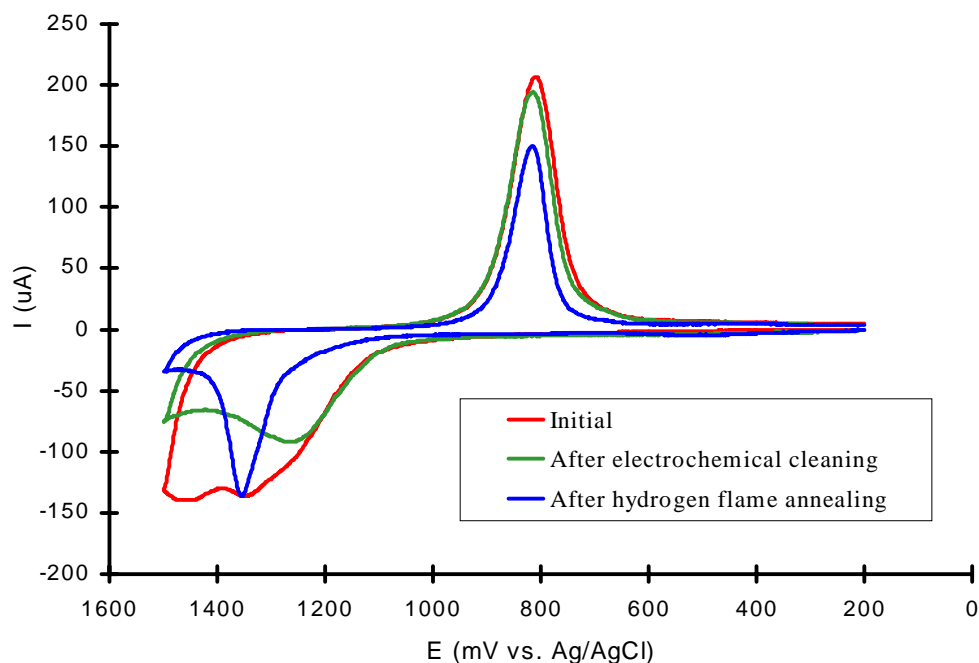


**Figure 3.27.** Roughness scan voltammetry in 0.1 M H<sub>2</sub>SO<sub>4</sub> of evaporated Au as received (initial), electrochemically cleaned, and hydrogen flame annealed. In addition to the change in the Au-oxide reduction peaks that correspond to changes in overall roughness, note the sharpening of the Au-oxidation peaks upon annealing that correspond to the changing crystallinity of the surface.

**Table 3-10.** Electrochemical and SPM Roughness Factors  
Evaporated Gold Film Substrates

Evap. Au Substrate	$R_{f-E/C}^a$	$R_{f-SPM}^b$ (nm)
Initial	1.5 <sub>(±0.1)</sub>	1.8
After E/C Cleaning	1.5 <sub>6(±0.1)</sub>	1.8
After HFA	1.0 <sub>2(±0.06)</sub>	0.9

<sup>a</sup> Determined from electrochemical roughness scans (not adjusted/normalized)

<sup>b</sup> Determined from RMS roughness calculation performed by the Nanoscope software ( $R_a$ )

of the thiolate adlayer. The following reaction has been proposed to account for this reductive desorption of the SAM:<sup>41</sup>



The potential at which this reaction becomes energetically possible depends upon at least three factors: 1) the strength of the Au-S bonds in the SAM; 2) the extent of intermolecular interactions among adjacent alkane thiol adsorbates; and 3) the terminal groups. An experimental example illustrating the second factor is shown in Figure 3.28, where C<sub>6</sub>OOH

SAMs are seen to desorb at more positive potentials, requiring less energy than the longer chain, more stable, C<sub>14</sub>OOH SAMs, which desorb at more negative potentials.

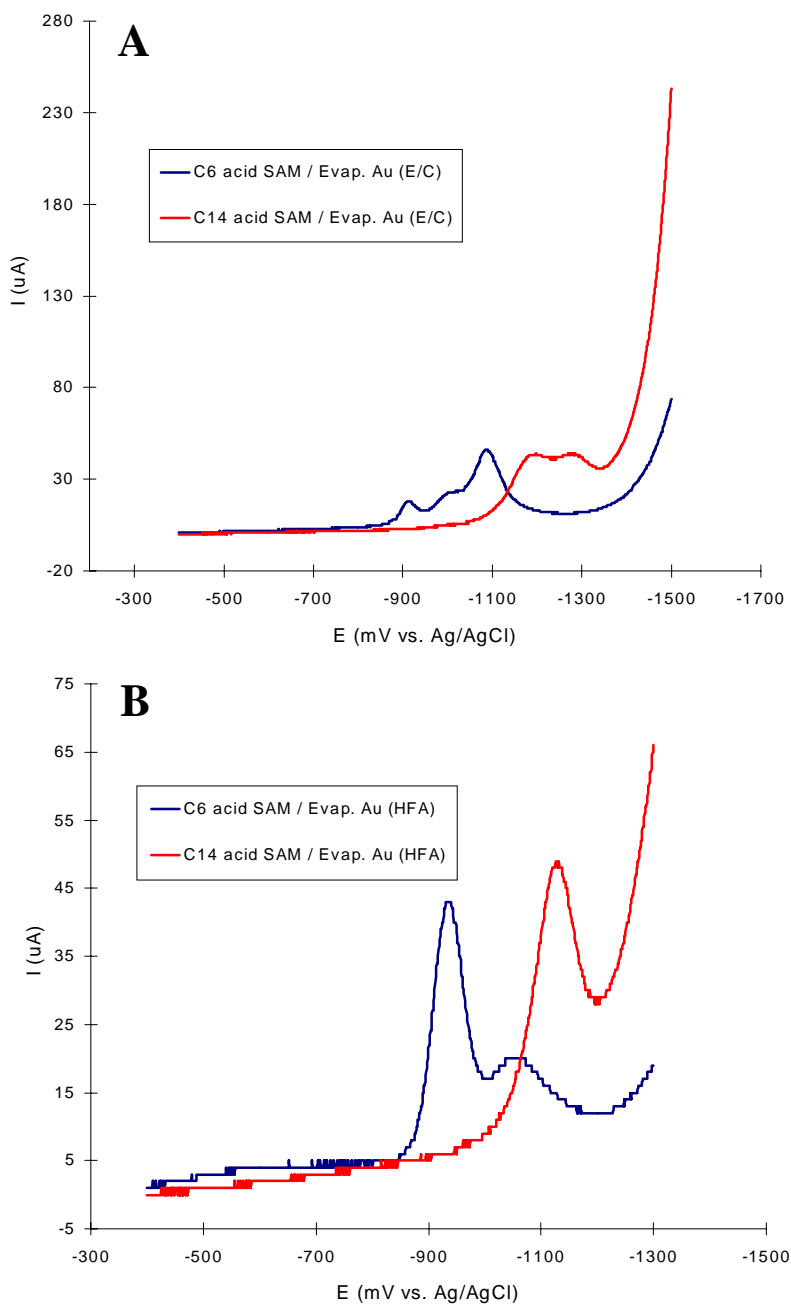


**Figure 3.28.** LSV – SAM desorption scans in 0.1 M KOH of A) electrochemically cleaned and B) HFA evaporated Au substrates modified with HS(CH<sub>2</sub>)<sub>5</sub>COOH SAMs (blue) and HS(CH<sub>2</sub>)<sub>13</sub>COOH (red).

Although only one reductive peak would be expected for a homogeneous SAM, sometimes, as in Figure 3.28A, multiple peaks are observed. Considering the polycrystalline

nature of the evaporated Au films, it is believed that the multiple peaks represent desorption of thiols from different crystal faces. This view is supported by the results shown in Figure 3.28B for HFA-treated gold, which is expected to exhibit predominantly the Au(111) crystal face. Desorption follows the same trend with alkane chain length, but the peaks are now singular and sharp.

The charge passed during reductive desorption of a SAM can be used in Faraday's Law:

$$Q = nFA\Gamma_{\text{mono}} \quad [\text{Eqn. 3.3}]$$

to calculate a value for surface concentration ( $\Gamma_{\text{mono}}$ ) of thiol. Comparison to theoretical determinations of  $\Gamma_{\text{mono}}$  for a well ordered SAM on Au(111) can allow inferences to be drawn about the SAM's density, packing, order, and, in the case of this research, how the results relate to the change in surface roughness. This approach has been used successfully for adsorbates on gold<sup>41</sup> and platinum,<sup>42</sup> including electrodes modified for the facilitation of cyt c ET reactions.<sup>43</sup>

Examples of SAM desorption sweeps are shown in Figure 3.29 for C<sub>14</sub>OOH SAMs on electrochemically cleaned evaporated Au and HFA evaporated Au. Calculations of  $\Gamma_{\text{mono}}$  are tabulated in Table 3-11. The results are consistent with the surface of the gold becoming flatter upon being pretreated with HFA. In comparison to the theoretical value for a densely packed monolayer of methyl terminated SAM, the experimental value of  $\Gamma_{\text{mono}}$ , 713 pmol/cm<sup>2</sup>, is slightly low (See Table 3-11). However, considering that the terminal group may influence monolayer packing,<sup>41</sup> the lower number may simply reflect the bulkier nature of the acid terminal groups and their inability to pack as densely as methyl terminated thiols.

In Figure 3.29, there is an additional point to be addressed regarding stability, namely, SAMs formed on HFA treated gold desorb approximately 100-200 mV more positive than those on electrochemically cleaned evaporated gold, an indication of a less stable film. As stated previously, the potential of desorption is dependent on lateral interactions among adsorbates, including chain-to-chain interactions. Earlier it was suggested that COOH SAMs on flatter gold substrates are less dense, as evidenced by higher C<sub>dl</sub> values, and presumably possess a higher dielectric constant. If this is indeed the case, COOH SAMs on flatter gold should exhibit weaker chain-to-chain interactions. These weaker interactions may originate

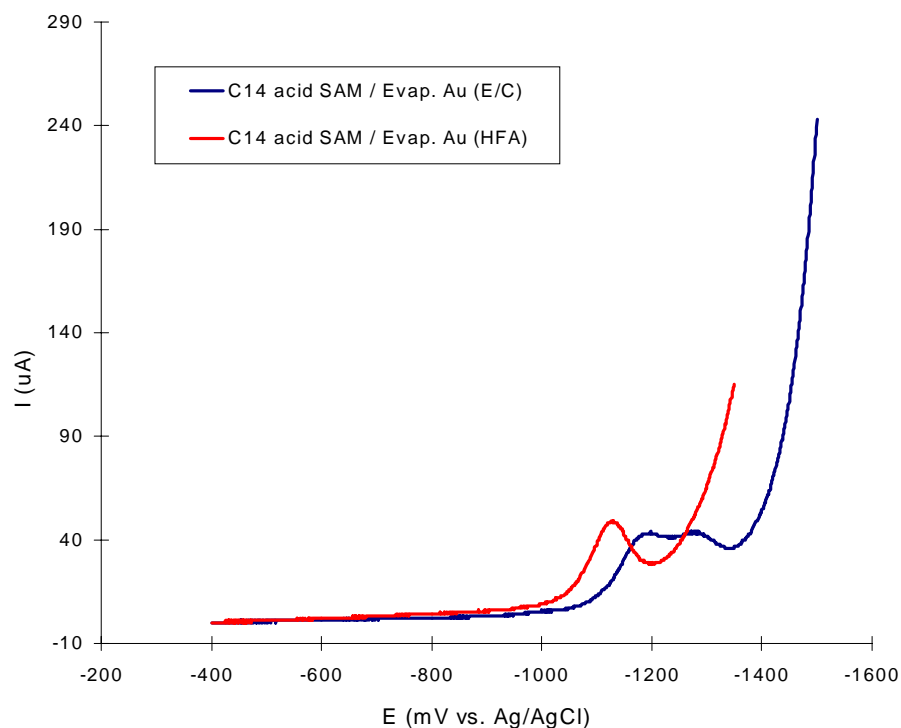
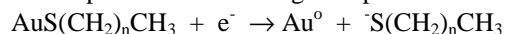


**Figure 3.29.** LSV-SAM desorption scans in 0.1 M KOH of HS(CH<sub>2</sub>)<sub>13</sub>COOH SAMs on electrochemically cleaned (E/C) and hydrogen flame annealed (HFA) evaporated gold.

**Table 3-11.** Linear Scan Voltammetry - SAM Desorption Results

Gold Substrate	$\Gamma_{\text{mono}}$ (pmol/cm <sup>2</sup> ) C <sub>6</sub> OOH SAM	$\Gamma_{\text{mono}}$ (pmol/cm <sup>2</sup> ) C <sub>14</sub> OOH SAM
Evaporated Gold (E/C)	1550	1050
Evaporated Gold (HFA)	1000	713
Highly ordered SAM <sup>a</sup>	760 - 870	

<sup>a</sup> Values for  $\Gamma_{\text{mono}}$  for a highly ordered SAM are based on values reported in the literature based on the following thiol desorption reaction at negative potentials:



where  $n = 3-17$  and is consistent with a Au(111) overlayer.<sup>41</sup>

-Note: variation in  $\Gamma_{\text{mono}}$  was approximately 10%.

from dominant terminal group influences. More specifically, the highly basic environment present during reductive desorption experiments will deprotonate all of the COOH functionalities in the SAM and cause a destabilizing electrostatic repulsion between the terminal groups. On flatter gold, the carboxylates will find themselves more crowded than on

a rougher surface, resulting in larger coulombic interactions. Coulombic interactions of this nature usually dominate weaker chemical interactions.

Flat baselines are necessary for accurate peak integration during LSV but can be difficult to achieve in some SAM desorption experiments, preventing the technique from being more quantitative. Longer chain SAMs, such as those considered here, don't desorb from gold until very negative potentials are reached. At these potentials, the LSV is often obscured by the reduction of oxygen, even after extensive degassing, as well as solvent reduction. Because of these complications, the SAM desorption experiments were eventually discontinued. Nevertheless, the results for evaporated gold presented here do offer some useful insight as well as impetus for future work. Furthermore, this is a potentially useful technique for mixed SAMs, which were found to exhibit distinct, yet not well resolved, reductive desorption peaks for each separate component of the SAM (Results not shown).

### 3.12.3. Capacitance of COOH SAMs on Evaporated Au Substrates

A  $C_{dl}$ -roughness trend was observed for COOH SAMs on evaporated gold films subjected to various pretreatments. The trend was similar to that obtained in the multi-substrate study, i.e., the capacitance increases as surface roughness decreases. COOH SAMs were prepared using thiols of various chain lengths on both annealed and electrochemically cleaned evaporated gold substrates. The results of these experiments are shown in Table 3-12 and Figure 3.30. Clearly, the capacitance is significantly higher for SAMs on the smoother, annealed gold than on the rougher electrochemically treated gold. The data of this graph converges as the alkanethiolates become shorter because the SAMs impact on the  $C_{dl}$  is significantly less at shorter chainlengths, i.e., smaller capacitors with higher dielectrics are less effective at building up charge.

**Table 3-12.** SAM Double Layer Capacitance - Evaporated Gold  
(Chainlength and Pretreatment Dependence)<sup>a,b</sup>

Pretreatment	$C_6\text{OOH}$ ( $\mu\text{F}/\text{cm}^2$ )	$C_{11}\text{OOH}$ ( $\mu\text{F}/\text{cm}^2$ )	$C_{14}\text{OOH}$ ( $\mu\text{F}/\text{cm}^2$ )
Electrochemically Cleaned	10.6( $\pm$ 0.2)	3.8( $\pm$ 0.1)	2.9( $\pm$ 0.8)
Hydrogen Flame Annealed	21.4( $\pm$ 1.0)	18.9( $\pm$ 3.3)	15.3( $\pm$ 3.8)
Oven Annealed	20.0( $\pm$ 4.3)	14.5( $\pm$ 1.2)	10.2( $\pm$ 1.3)

<sup>a</sup> Data collected by Joe A. Black; <sup>b</sup>  $C_{dl}$  values based on geometric area of electrode but can be adjusted to real surface area using  $R_f^*$  as previously described.

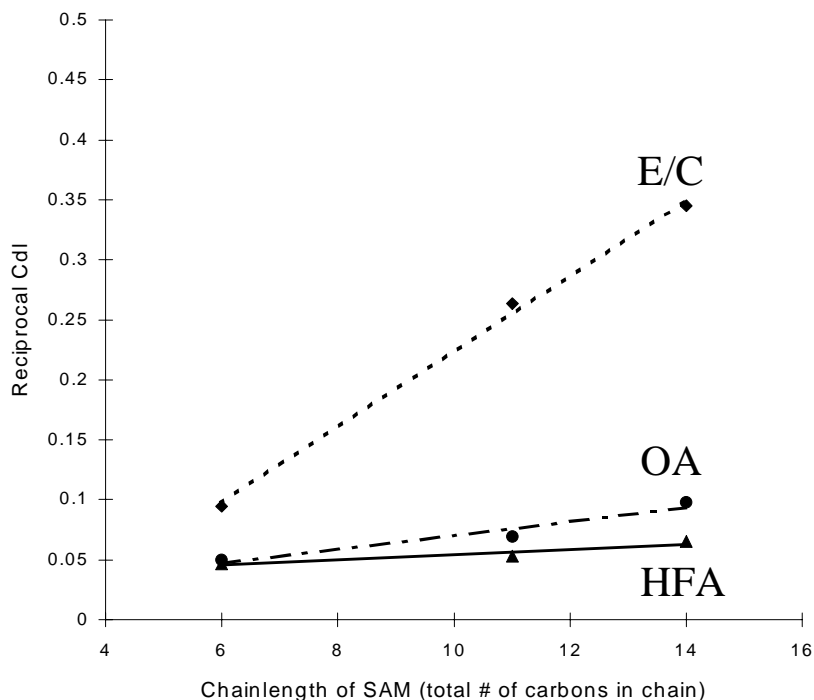


**Figure 3.30.** Plot of COOH SAM chainlength (total number of carbons in chain) versus  $C_{dl}^{-1}$  for electrochemically cleaned (E/C), oven annealed (OA), and hydrogen flame annealed (HFA) evaporated gold substrates (Data collected by Joseph A. Black). Note:  $C_{dl}$  values are based on geometric area of electrode but can be adjusted to *real* surface area using  $R_f^*$  as previously described.

#### 3.12.4. Hydroxymethyl ferrocene Redox Probing

Figure 3.31 shows the results of HMFc probing for defects in COOH SAMs on annealed and electrochemically treated Au films. For comparison purposes, the voltammetric responses of HMFc at a gold/mica based SAM, a low defect density film, and at bare Au are included. These results, while not as dramatic as those obtained in the multi-substrate study, still indicate a lower permeability, perhaps due to lower defect density for the SAM on the annealed gold.

#### 3.12.5. Cyt c Response for Evaporated Gold Substrates

Representative CVs for adsorbed cyt c on electrochemically cleaned and annealed evaporated gold electrodes are shown as Figures 3.32. The response in panel A is typical of this substrate, revealing well-defined, stable voltammetry. On the other hand, the voltammetry of cyt c adsorbed on the SAM modified annealed gold surface is poor (Panel B).. The smoother surface gives rise to a higher capacitance and weaker voltammetric signal from the protein.

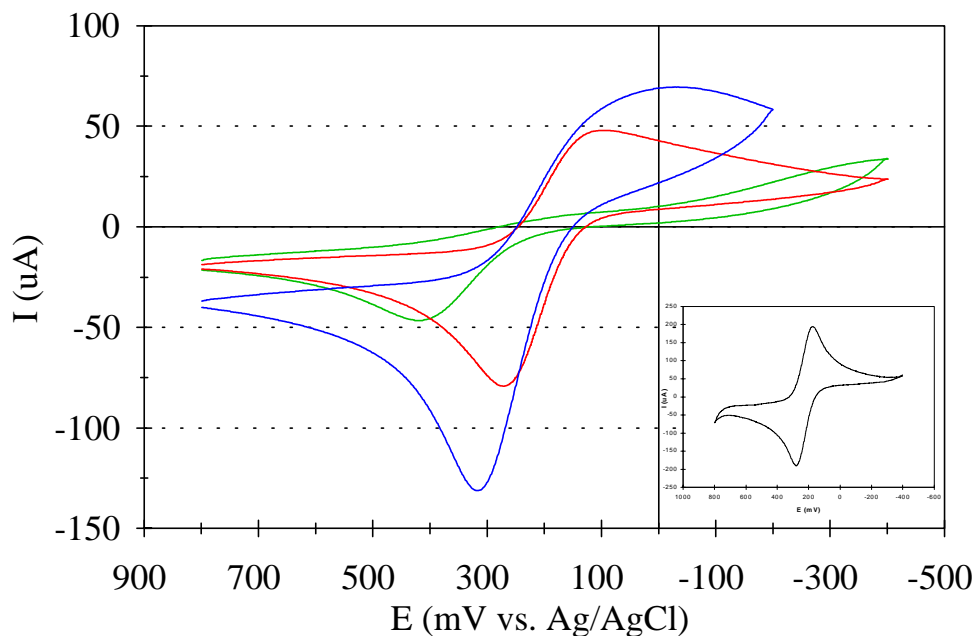


**Figure 3.31.** HMFc redox probe voltammetry at HS(CH<sub>2</sub>)<sub>13</sub>COOH SAMs on electrochemically cleaned evaporated Au (blue), HFA evaporated Au (red), and Au/mica (green). For comparison, figure inset (bottom right – black) displays HMFc voltammetry at an unmodified bare gold electrode.

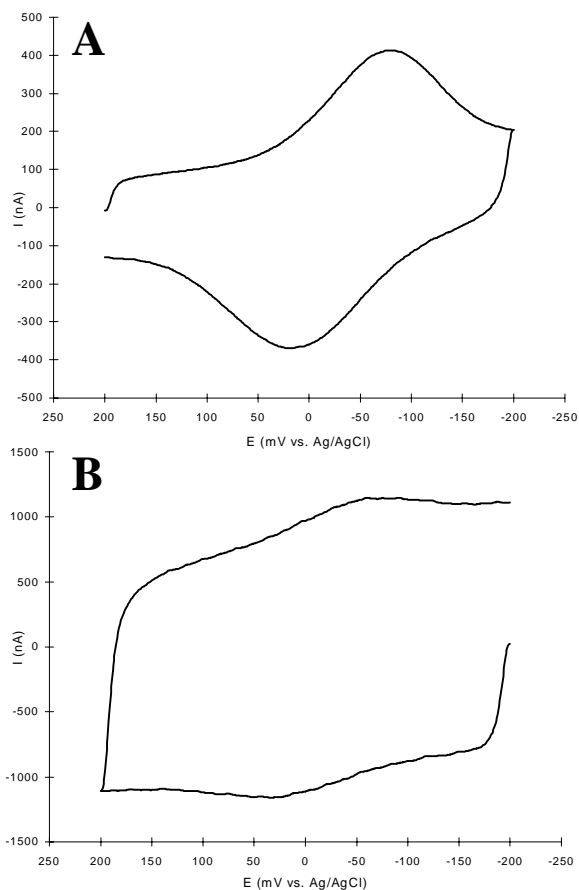


**Figure 3.32.** Cyclic voltammetry of cyt c on C<sub>14</sub>OOH SAMs on A) electrochemically cleaned evaporated Au and B) HFA evaporated Au. Solution conditions: 4.4 mM KPB;  $\nu$  = 10 mM; pH = 7; 100 mV/sec.

These results are highly reproducible and compare favorably with those obtained in the multi-substrate study. Similarly, adsorbed cyt c behavior was examined for COOH SAMs on intentionally roughened, pre-annealed evaporated gold and for mixed SAMs on annealed evaporated gold. These results are presented next.

### **3.12.6 Effect of Intentional Roughening of Evap. Au (HFA)**

Normally, the HFA evaporated Au electrode, when modified with a COOH SAM, yields a very poor cyt c response as seen in Figure 3.32B. Upon electrochemical cleaning of the HFA pretreated gold, which roughens the surface, an improved cyt c response was obtained. This result is shown in Figure 3.33, which also reveals a substantial drop in capacitance after the treatment. Table 3-13 summarizes the  $C_{dl}$  changes observed when evaporated gold substrates are treated with a combination of annealing and electrochemical cleaning compared to electrodes that have only been either annealed or electrochemically cleaned. Electrochemical roughening of the annealed gold decreases  $C_{dl}$  significantly but not to the low values observed for as-received substrates that have been subjected to a single electrochemical cleaning. This result reinforces the vital role that surface roughness plays in the attainment of cyt c adsorption and electrochemical signal.

### **3.12.7. Mixed SAMs on Annealed Evaporated Au**

Adsorbed cyt c was examined on smoothed HFA-treated evaporated gold surfaces modified with Type I mixed SAMs. A representative result is shown in Figure 3.34 where a greatly improved cyt c response can be seen compared to that in Figure 3.32B. In comparing the two voltammograms, note the significant difference in peak resolution, as well as, the apparent kinetic effect of using a mixed SAM of this nature. This result reinforces the idea that a highly irregular SAM, either originating from a rough gold substrate or a mixed SAM on a smooth surface, is advantageous for cyt c adsorption and electrochemistry.

### **3.12.8. The Titanium Experience - A Comment on Annealing and Contamination**

At a certain point well into this study, concern arose over the possibility of thermally induced titanium diffusion from the adhesion layer to the gold surface. XPS experiments did indeed reveal the presence of titanium on the surface of thermally annealed Au films. The XPS results, displayed as Figure 3.35, show that both flame and oven annealed films exhibit a signal at  $\sim 450$  eV binding energy, indicative of Ti. The as-received and electrochemically

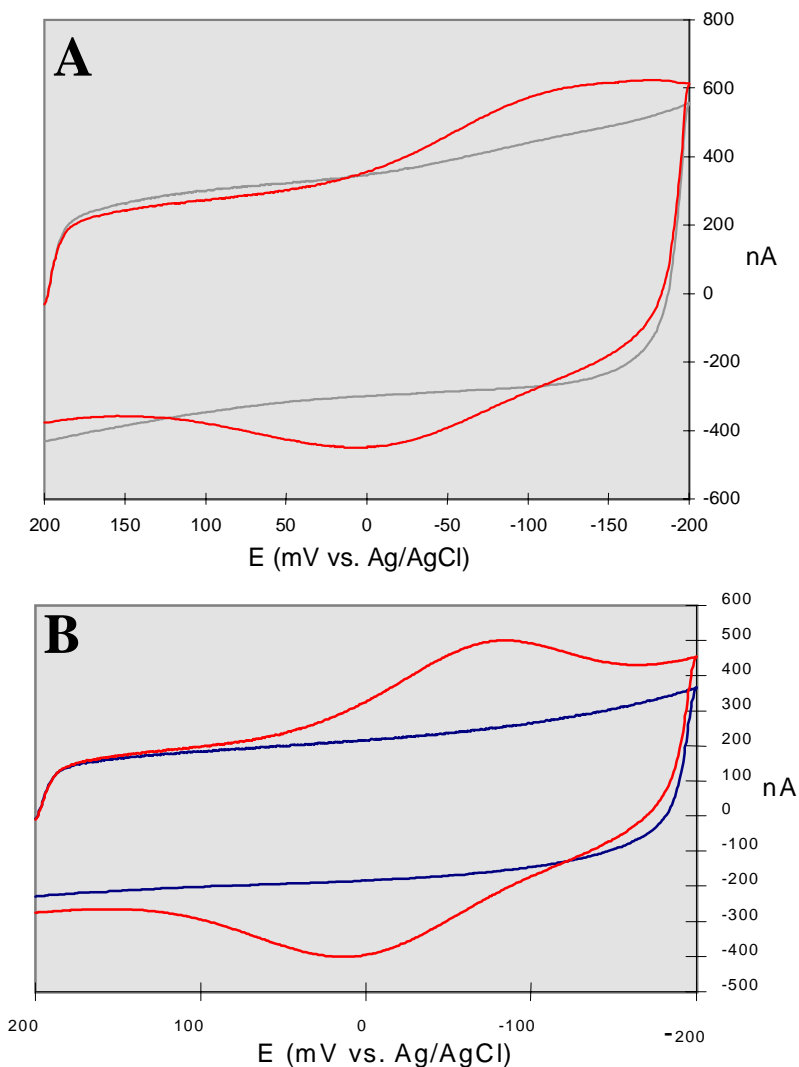


**Figure 3.33.** Cyclic voltammetry with background signals illustrating the effect of surface roughening on the cyt c response: A) cyt c / C<sub>14</sub> acid SAM / evaporated Au (HFA) and B) cyt c / C<sub>14</sub> acid SAM / evaporated Au (HFA and subsequently roughened with electrochemical cycling in 0.1 M H<sub>2</sub>SO<sub>4</sub> / 0.01 M KCl (Data collected by Joseph A. Black).

**Table 3-13.** SAMs Double Layer Capacitance Results  
C<sub>dl</sub> of SAMs on Evap. Au w/ various pretreatments<sup>a,b</sup>

Pretreatment of Gold in C <sub>14</sub> OOH SAM / Evap. Au System	C <sub>dl</sub> (μF/cm <sup>2</sup> )
E/C Cleaned	2.9(±0.8)
HFA	15.3(±3.8)
HFA then E/C Cleaned	5.2(±0.7)

<sup>a</sup> Data collected by Joe A. Black; <sup>b</sup> C<sub>dl</sub> values based on geometric area of electrode but can be adjusted to *real* surface area using R<sub>f</sub> as previously described

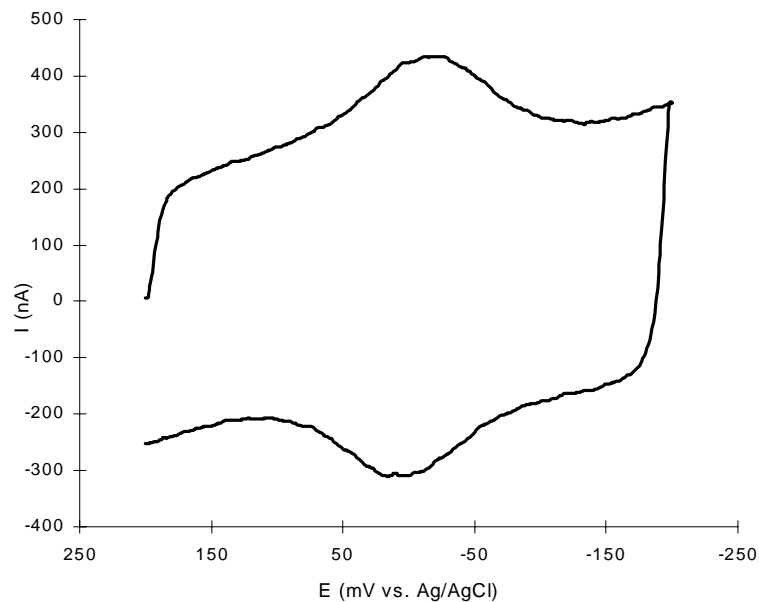


**Figure 3.34.** Cyclic voltammetry of cyt c adsorbed onto a HFA evap. Au substrate modified with a mixed SAM ( $C_{11}OOH$  &  $C_7OH$ ). As seen in a previous figure (Figure 3.32) the HFA evap. Au yields a poor cyt c response when modified with a single component SAM. The mixed SAM, however, regenerates a more defined response with lower  $C_{dl}$  and faster kinetics on the same HFA surface.

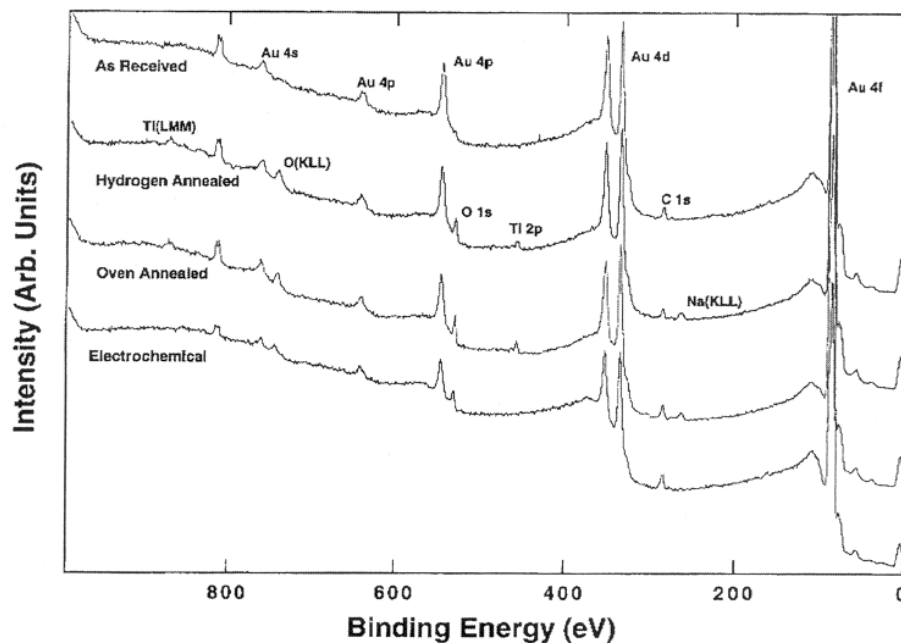


**Figure 3.35.** XPS survey scans of evaporated gold as received, electrochemically cleaned, oven annealed, and hydrogen flame annealed. Note the Ti (2p) signal at ~ 450 eV after the gold has been annealed.

cleaned gold films did not yield a Ti signal. Therefore, it was concluded that thermal annealing caused Ti to migrate from the adhesion layer to the surface of the gold films.

A cross-section of the evaporated Au film electrodes used in this research is shown in Figure 3.36. Chromium and titanium are often used as adhesion layers to bond gold to glass for improved mechanical stability of the gold film. The results presented here indicate that Ti will migrate through 2000 Å thick gold layers when subjected the flame annealing procedures described in the Experimental Details section of this chapter. It is believed that inorganic contaminants, such as the oxides of adhesion metal contaminants, can serve as loci for pinholes in SAMs on such substrates.<sup>5</sup> This possibility raised the question of whether or not the presence of Ti contamination seriously impacted the SAM and cyt c results that had been obtained.

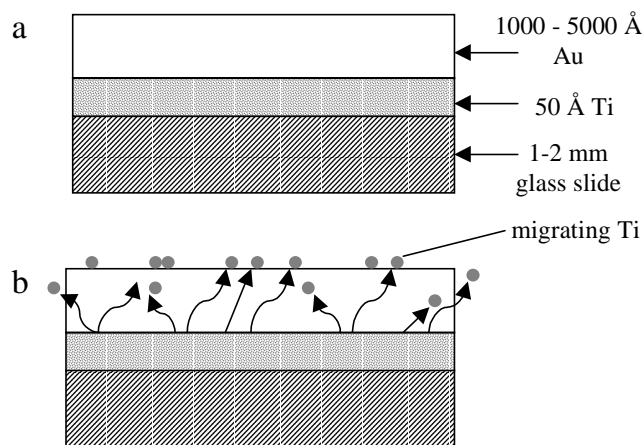


**Figure 3.36.** Cross-section diagrams of evaporated Au film substrates a) as received and b) upon annealing. It is hypothesized from the previous XPS data that the thermal energy provided by annealing enables Ti atoms to migrate through the gold lattice and become exposed on the surface.

Upon completing the multi-substrate study (Section 3.5), it was possible to compare the results of these two studies, a process which concluded that the initial results obtained with annealed evaporated gold films were most likely not an artifact of contaminated gold surfaces. Both studies basically yielded the same trends and phenomena. The following paragraph summarizes multiple reasons that rule out a significant role for Ti in the experimental results obtained with annealed evaporated gold films.

The first reason that discredits detrimental Ti effects has already been stated, namely, the similarity of results obtained for the separate study involving four different gold

substrates. The results were consistent among the four substrates as well as for individual substrates subjected to annealing/roughening treatments. The evaporated Au substrates possess an extremely potent source for possible Ti contamination, an approximately 50 Å thick layer directly beneath the gold film. The other gold substrates, which can be safely annealed, lack an adhesion layer of any kind. Thus, these substrates have a drastically reduced capacity for contamination because the source of potential contaminants is drastically reduced. Furthermore, all four types of gold substrates were of high purity (See Experimental Details); annealing would be expected to cause negligible surface contamination by trace metals. Even if a minute amount of inorganic contamination did reside on the surface, electrochemistry is a surface population technique, meaning that such minute amounts would have to exert an unusually potent impact to be apparent. Additionally, some metal oxides, including TiO<sub>2</sub> and Au<sub>2</sub>O<sub>3</sub> are known to form thiol linkages and therefore may simply be buried in the alkane layer. Perhaps the best evidence against the contamination issue is some of the experimental results themselves. Redox probing with HMFc on annealed gold based SAMs clearly suggested a resultant loss of defect density after the thermal annealing - a finding inconsistent with inorganic contaminants causing pinhole defects in SAMs. Furthermore, if surface contamination due to annealing was responsible for poor cyt c response, then why does the cyt c response regenerate so well when the same contaminated surface is modified with a mixed SAM? A grossly contaminated surface should show ill effects upon both uniform and mixed SAM formation, especially since the nature of the self-assembly process is identical for both. Considering the excellent cyt c response obtained with mixed SAMs on annealed Au surfaces, along with the reasons above, it is concluded that the Ti contamination has minor effect on the results obtained for annealed evaporated gold films.

An interesting corollary to this discovery of Ti on annealed Au films is the potential significance for SAM and SPM studies. There are many examples in the literature for which gold films are thermally annealed without mention of possible adhesion metal contamination of the surface.<sup>7,38g,46</sup> Most of these reports describe the annealing of Au films for use in SPM experiments- a forum where even small amounts of surface contamination can be misleading toward imaging. The fact that one could be imaging contamination becomes a concern

because SPM techniques are generally incapable of species identification. One paper using annealed evaporated Au substrates with adhesion layers even states the following: “Au films that were coated onto a quartz slide with an underlayer of Cr were much more stable following annealing.”<sup>7</sup>

### **3.13. DISCUSSION**

The major finding of the research can be summarized as follows: the topography of gold electrodes plays a very significant role in the structural properties of COOH SAMs, which, in turn, has a substantial impact on the adsorption and electrochemistry of cyt c. Acidic SAMs having a significant degree of defect density, arising from either rough gold topography or from a mixed SAM, exhibit a surface texture that appears more optimal for cyt c adsorption and electrochemical response. Additionally, the COOH SAMs with higher defect density gave rise to consistently lower double-layer capacitance ( $C_{dl}$ ) while at the same time exhibiting greater permeability to diffusing redox probes. In this discussion, we will address the major conclusions by first considering SAM structure and properties before turning to the cyt c electrochemistry.

#### **3.13.1. Carboxylic Acid SAM Structure and Gold Topography**

A significant part of this study and a key aspect of SAM structure as a function of gold topography is the redox probe results which define the permeability of the SAMs on various types of gold. Expectedly, the density of defects decreases as the topography becomes smoother and increasingly void of physical surface features that typically cause defects in SAMs. The voltammetry of the probe molecule HMFc becomes increasingly more restricted from access to the gold surface as the gold becomes smoother, a clear indication that fewer defects exist in the films. At the same time, however, the SAMs on these surfaces exhibit increasingly higher  $C_{dl}$  values. This paradoxical relationship is the first focus of this discussion.

The redox probe voltammetry results and the  $C_{dl}$  measurements of the SAMs formed on various gold substrates inspired the proposed model introduced in Figure 3.20 and Section 3.10. The model explains the high  $C_{dl}$  values found for SAMs on flatter gold in terms of a dielectric effect caused by the unique packing found with COOH SAMs. It was proposed that the acid termini are spatially restricted by the smoother topography to a more planar

arrangement which, in turn, gives rise to surface interactions that increasingly influence the packing structure of the SAM by decreasing the relative contribution of chain-chain van der Waals interactions. This scenario could lead to a SAM whose alkane region, while positioned more uniformly and devoid of many major defects, is less dense, resulting in an increased dielectric constant, which would elevate the  $C_{dl}$ .

Our SAM model is based on the concept that the acid termini interact attractively, most likely through hydrogen bonding (H-bonding), to form a stabilized and more cohesive interface that exerts substantial control over the structural properties of the SAM. The general importance of electrostatic and steric endgroup interactions in the packing structure of SAMs has been noted in prior work by Chidsey and Loiacono.<sup>30e</sup> Additionally, Poirier and coworkers recently concluded that H-bonding amongst hydroxyl termini play a vital role in determining the overall structural properties of mercaptohexanol SAMs on Au(111).<sup>49b,d</sup> Also in support of this model, a lateral force microscopy (LFM) study of various  $\omega$ -substituted alkane thiol SAMs found acid terminated SAMs to be “stiffer” than methyl terminated SAMs.<sup>33b</sup> If the terminal groups are attractively interacting to a significant degree, this is not a surprising result.

The major attractive interaction between COOH end groups is undoubtedly H-bonding. H-bonding appears to be strong enough to direct the packing and structure of the SAM and alter its overall properties. Using SIMS, Cooper and Leggett showed that COOH SAMs were more stable toward displacement by methyl terminated thiols and were equally as effective in displacing methyl terminated thiols at defect sites in existing SAMs. These tendencies were found to occur even when the methyl terminated thiols possessed substantially longer alkane chains. Their work predicted that for an alkylthiol on gold (SAM), the methylene chain-to-chain interactions contributes about 0.8 kcal/mol for each methylene group in the chain whereas the carboxylic acid endgroups contribute at least 7.2 kcal/mol, the equivalent of nine methylene groups, to the enthalpy of adsorption.<sup>49b</sup> Cooper and Leggett proposed interchain H-bonding as the primary cause of both phenomena.<sup>49b</sup> From our results, we furthermore propose that on smoother gold, H-bonding interactions are maximized whereas on rougher gold or with mixed SAMs, they are minimized due to disruption of the “plane” of H-bonding. With weaker H-bonding, the SAM components

would have greater conformational freedom and would be expected to pack with greater dependence on van der Waals interactions between alkane chains. With stronger H-bonding in the COOH “plane,” the surface will exhibit a cohesiveness or surface tension. Because the attractive energy between endgroups (H-bonding) must be overcome to disrupt or penetrate the SAM, increased H-bonding should inhibit defect formation and minimize film permeability.

The model proposed here may also help explain the inconsistency of pKa values that have been reported in the literature for COOH terminated SAMs, which range from 5.2 to 11.5.<sup>57</sup> It is proposed that the macroscopic pKa value of a COOH SAM is a gold substrate dependent property. The work described here has shown that the surface of the gold substantially impacts the properties and the structure of a SAM including the microenvironment associated with individual COOH groups. COOH groups engaged in H-bonding should be more difficult to deprotonate whereas less hindered groups that extend further into solution should be easier to deprotonate. Likewise, COOH groups more imbedded within the film reside in a more hydrophobic environment and will be more resistant to deprotonation, causing higher microscopic pKa values. The latter phenomenon has already been documented by Creager and coworkers in an investigation of mixed SAMs composed of COOH and CH<sub>3</sub> terminated thiols of different chainlengths. As the length of the methyl-terminated component was progressively increased from being shorter than the acid-terminated thiol to longer, the pKa of the COOH groups increased from 6.2 to 11.5.<sup>57a</sup> In summary, rougher gold is predicted to yield lower pKa values for COOH SAMs and smoother surfaces should exhibit higher pKa values in accordance with the proposed model.

### **3.13.2. Cyt c Adsorption/Electrochemistry and Gold Topography**

The adsorption and electrochemistry of cyt c seems intimately related to the density of defects in acidic SAMs. Topographically smoother, flatter gold substrates with fewer defect features such as grain boundaries and step edges, should give rise to more uniform SAMs with a lower overall density of defects. Such “ideal” surfaces have proven to be poor platforms for cyt c adsorption and electrochemistry. On the contrary, rougher, polycrystalline gold surfaces, supporting SAMs with a higher degree of defectiveness and disorder, have been found to be most suitable for cyt c adsorption and electrochemistry. It is concluded that

SAMs with significant defect density provide an irregularly textured, disordered surface, offering greater interfacial flexibility and conformational freedom that subsequently is better able to promote protein adsorption and electrochemistry. Such a surface would be more similar to that of a real protein.

Although not directly addressed by this research, it can be speculated that the cyt c adsorption is more favorable at specific types of defect sites. That is, non-pinhole defect sites in the SAM, such as defects formed at grain boundaries and step edges in the gold, may serve as more favorable sites for cyt c adsorption than other types of defects, at least from an electrochemical standpoint. Non-pinhole defects, it would seem, provide the protein with a more optimal binding site - an irregularly textured surface that also maintains substantial alkane density between the electrolytic solution and gold electrode, thereby lowering the overall  $C_{dl}$  of the system. This type of scenario is perhaps best exemplified by the mixed SAMs and by those assemblies prepared on intentionally roughened substrates. It may also explain the small amounts of electroactive cyt c found on the flatter gold substrates modified with COOH SAMs. Whereas redox probing showed these films to have very few pinhole-type defects, they most likely still possess step edge and/or grain boundary based defects which would be difficult to completely eliminate. Again, this concept has not yet been specifically tested and is included here as a hypothesis to better explain the intricacies of these systems.

One further issue to be kept in mind when visually assessing the quality of a diffusionless protein voltammogram is the ability of these different COOH SAM modified gold substrates to discriminate against charging current or  $C_{dl}$ . Cyt c voltammetry appears most well-defined when adsorption takes place on a SAM that has a high level of defectiveness, which, at the same time, effectively discriminates against charging current. This situation is most evident in experiments described earlier involving mixed SAMs composed of COOH thiols and slightly shorter OH thiols. Cyt c is most ill-defined on the flatter SAM modified substrates which, as shown earlier, is primarily the result of lower coverage of the protein. In addition, however, the appearance of the voltammogram is worsened by the SAM's inability to effectively depress charging current. Larger values of  $C_{dl}$  observed for SAMs on flatter gold thus help to mask the electrochemical signal from already

depleted amounts of adsorbed protein. From both the XPS and SWV results, there is always some protein adsorbed at these SAMs on flatter gold, albeit a much smaller amount than on the higher defect density SAMs. The large charging currents on these surfaces make peak identification and analysis more difficult than would otherwise be the case.

The results of this study clearly invalidate the “ideal” ET model system - proteins adsorbed on highly ordered, defect free, “perfect” SAMs, as commonly depicted in literature schematics or cartoons.<sup>34,58</sup> Protein desorption experiments performed in our laboratory using evaporated gold substrates have shown that there is an ionic strength dependence of protein adsorption indicative of a predominantly electrostatic adsorption. The idea that a highly ordered, charged, planar surface is not the optimal interface for the electrostatic adsorption of an oppositely charged sphere has been supported on a very basic level by the theoretical work of Stahlberg and Jonsson on a severely simplified system similar to the one examined in this study.<sup>31</sup> In light of the results presented here, however, other interfacial interactions may contribute to the adsorption and ET processes as well. For instance, Klein and coworkers have proposed from modeling studies that cyt c may partially penetrate the surface of the COOH SAMs upon adsorption, as depicted in Figure 3.37,<sup>32</sup> giving rise to the possibility of hydrophobic interactions. Such an adsorption process may occur exclusively at defects sites in the SAM and where the likelihood of additional interactive forces, such as hydrophobic effects, may be substantial in certain microenvironments. Considering the results presented here, however, it is also feasible that the topography influenced structure of COOH SAMs induces a significant change in the surface pKa of the acid endgroups, raising it to 9-10 and subsequently creating an essentially uncharged surface at the pH of the working buffer (physiological pH = 7). Thus, the protein would have a decreased electrostatic attraction to bind at the surface.

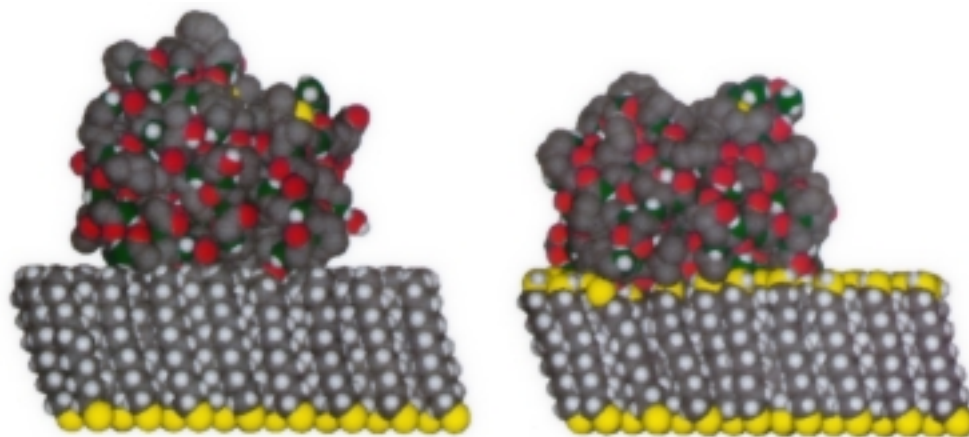


**Figure 3.37.** Computer simulation of a cyt c protein adsorbed onto SAMs as is believed to happen if the immobilization process of the protein is predominantly electrostatically driven (left). Cyt c may, however, also penetrate the SAM upon adsorption, altering the SAM structure and increasing the probability of significant hydrophobic interactions (right).<sup>32</sup>

The idea of disorder instigating beneficial effects on chemical systems is not unprecedented. Ringsdorf and coworkers,<sup>47</sup> for example, introduced an element of disorder into a biological system not completely dissimilar to that described here, namely, the binding of streptavidin to a biotinylated SAM ( $\text{HS}(\text{CH}_2)_{11}[\text{biotin}]$ ). Normally, streptavidin engulfs its biological partner, biotin, when they bind. On a uniform biotinylated SAM, however, this process cannot be easily duplicated because the streptavidin, due to steric hinderance and limited mobility, has difficulty binding tightly to the immobilized biotin groups. Ringsdorf and coworkers remedied this situation by introducing a mixed SAM with hydrophilic spacers ( $\text{HS}(\text{CH}_2)_{11}\text{OH}$ ) that position the biotin moieties further from the surface in a less hindered environment. The result was a greater degree of streptavidin binding at the SAM surface. They concluded the higher packing density and order of their initial model surface resulted in less effective immobilization of target molecules (streptavidin).<sup>47b</sup> This is one of the more pertinent examples from scattered reports in which disorder in a SAM based assembly was found to be beneficial to an adsorption process.<sup>47,48</sup>

In retrospect, it is probably not too terribly surprising that the rougher, defect-riddled surface would be more effective at immobilizing cyt c, considering that the natural binding partners of cyt c in biological systems are also irregularly textured both chemically and topographically. It follows then that the physiological binding partners of cyt c can be mimicked by a uniform SAM only to a very limited degree.<sup>40</sup> A more realistic model of a

protein binding partner would require an irregular binding surface with more appropriate interactive forces. In any event, this research effort is viewed as having achieved its goal of establishing a more defined role of the gold substrate in cyt c voltammetry. Surface effects directly attributable to the topography of the gold substrate and their impact on SAM formation may indeed account for the distribution of electrochemical properties and inherent peak broadening commonly seen in cyt c voltammetry. In light of the research that has been presented, the topography of the gold substrate must be carefully considered when comparing SAM based experiments as it can substantially affect both the structure and application of a SAM.

As a final observation, it is noted that the results of these gold topography experiments were highly reproducible on a variety of gold substrates and by multiple researchers in our laboratory. In addition to the results on 14-mercaptotetradecanoic acid SAMs, the same trends have also been observed for gold substrates that were modified with 11-mercaptopundecanoic acid. The trends noted were more prominent, however, with longer chainlengths, perhaps because the longer SAMs are more structurally sensitive, having greater packing order than the C<sub>11</sub>OOH SAMs which, being shorter, have a greater probability of having a more liquid-like structure, especially at the interface of the film.

### **3.14 FUTURE DIRECTIONS**

To further elucidate the role of gold in the electrochemistry of cyt c/SAM/Au assemblies, there is an obvious need to better define the structures and interfacial interactions that result from different surfaces. Several examples of these type of experiments are presented here.

An investigation of the dependence of H-bonding in COOH SAMs on the roughness of the Au substrate is needed. As these Au surfaces become smoother, bringing carboxylate groups into the same plane, does H-bonding between the endgroups become a significant factor in the self-assembly process? There are literature examples dedicated to this subject that strongly suggest that there is significant H-bonding between headgroups of acid and alcohol terminated SAMs.<sup>49</sup> Also, it is unknown whether there is substantial H-bonding

present within the mixed SAMs as well. IR measurements are commonly used to detect H-bonding in such systems.<sup>49c,d</sup>

IR spectroscopy can also be used to help delineate the internal structure of SAMs. This is a common practice found in the literature.<sup>50</sup> IR measurements can provide information about the density and packing order of the alkane chains in the SAMs. Since results have suggested that smoother gold gives rise to better blocking SAMs but with higher dielectric constants, it would be desirable to obtain specific chemical structural information to further assess the model.

Another important goal is to better comprehend the structure of mixed SAMs, which are playing an increasingly important role in this type of chemistry. IR, CAG, and SPM should all be used to gain a better understanding of the mixed SAM structure and characterize the distribution of thiol components across the surface and within those films.

As previously mentioned, hydrophobic interfacial interactions may play a role in the adsorption and ET properties of cyt c on SAMs. It would be most interesting to assess the hydrophobicity of each SAM interface as the gold surface roughness and topography are varied. CAG may make these types of measurements feasible as a step toward better defining the nature of these different interfaces, although the changes may be too subtle for the method and be effective only in microenvironments at the interface.

### **3.15 SPECIAL ACKNOWLEDGEMENTS**

I must sincerely thank Dr. Tal Nahir (currently at California State University, Chico) for much encouragement and many useful conversations throughout the early stages of this work. Tal also taught me a very important and, for me, difficult to learn, key to doing successful research – don't be afraid to spend money. My experience with Tal and his support in the time he was here was invaluable.

I would also like to give a special acknowledgment to Mr. Joseph Andrew Black, an REU student who worked in our group during the summer of 1997. Joe was a great worker – dedicated and smart – too bad he was a Detroit Tigers fan (Go Yankees!). Joe did extensive work on the evaporated Au films prior to the discovery of Ti on the surface. His work helped to eliminate many of the contamination possibilities being considered.

I would like to thank Dr. Mike Tarlov of NIST and John Phillips, the microscopist in the Analytical Instrument Facility, NCSU Centennial Campus, for performing the XPS measurements in this study.

### 3.16 EXPERIMENTAL DETAILS

#### 3.16.1. Experimental Gold Substrates

**-Evaporated Gold Films.** Evaporated gold film electrodes were purchased from Evaporated Metal Films, EMF (Ithaca, NY). Each electrode is comprised of 1000 to 5000 Å of Au evaporated on a glass slide over a 50 Å thick Ti adhesion layer. Electrodes received were individually wrapped and usually electrochemically cleaned via the procedure outlined below.

**-Bulk Polycrystalline Gold (Au Foil).** Bulk polycrystalline gold foil (Premion, 99.9985%) was purchased from Alpha Aesar/Johnson Matthey (Ward Hill, MA). Purchased as a 25 x 25 x 1 mm piece, the gold foil was machine cut into four square pieces with approximate dimensions of 11-12 x 11-12 x 1 mm. The bulk gold samples were usually chemically etched for ten minutes in dilute aqua regia, a solution of concentrated HCl, concentrated HNO<sub>3</sub>, and H<sub>2</sub>O in a 3:1:6 ratio.<sup>3a,b</sup> CAUTION: Aqua regia is a strong acidic solution and should be handled with extreme caution. The chemical etching with dilute aqua regia acts to remove surface gold. The bulk gold samples were polished via a Minimet polisher/grinder by Buehler (Lake Bluff, IL) using a polishing cloth (Buehler) and alumina pastes (Buehler) of 5, 1, 0.3, and 0.05 μm. Each gold substrate was mechanically polished with successively smaller alumina particles with the Minimet polisher (Instrument Settings: speed = 3; time = 7; half load). After each polishing sequence, the sample and the polishing cloth were rinsed with copious amounts of M/Q H<sub>2</sub>O. After the final polish with the smallest sized alumina paste, the gold samples were rinsed thoroughly with M/Q H<sub>2</sub>O and sonicated in both Alconox (Fisher Scientific) and M/Q H<sub>2</sub>O for 10 minutes before further treatment. At this point the samples were either electrochemically cleaned for rougher topography or annealed for a lower degree of roughness. After the completion of an experimental sequence with the bulk gold samples, the samples were reused by chemical etching and repolishing.

**-Single Crystal Gold { Au(111), Au(110).** Single crystal gold samples were previously purchased from Cornell University (Dept. of Materials Science and Engineering), Ithaca, NY. These samples were used repeatedly in conjunction with repeated annealing in a hydrogen flame. According to sources, a gentle anneal of these substrates after being used in an experiment causes the surface of these single crystals to completely regenerate.<sup>25</sup> On occasion, especially after extensive use, the annealing of the single crystal substrate was preceded by the mechanical polishing procedure previously discussed.

**-Gold Epitaxially Grown on Mica.** Gold grown on mica was purchased as Pico-Substrates from Molecular Imaging Corporation (Phoenix, AZ). They were specially ordered to be without an adhesion layer of Ti or Cr. The substrates has approximate dimensions of 1.4 cm x 1.1 cm with about 1500 Å of high purity gold covering an area of about 1.0 cm x 1.1 cm. Upon fabrication at Molecular Imaging, these substrates commonly showed atomically flat terraces that were typically several hundred nanometers in diameter. The recommended pretreatment was HFA which should result in even larger, atomically flat, gold terraces on the surface. Each substrate was HFA'd at Molecular Imaging and then packed in nitrogen for shipping. These substrates were usually HFA'd before use.

### **3.16.2 General Materials - Solution Preparation**

Several solutions were used throughout the research project for specific experiments and measurements (most were prepared volumetrically using chemicals purchased from Fisher Scientific): 1.0 M KCl for the reference electrode and for high ionic strength desorption of protein; 0.5 M NaF was used for most early measurements of double layer capacitance/background measurements (Note: this solution was ultimately eliminated in favor of testing double layer capacitance in the potassium phosphate buffer - see below); dilute (0.05 M) H<sub>2</sub>SO<sub>4</sub> was prepared by dilution from 18 M H<sub>2</sub>SO<sub>4</sub> and used for R<sub>f</sub> voltammetry; 0.1 M H<sub>2</sub>SO<sub>4</sub> with 0.01 M KCl served as the electrochemical cleaning solution and was constantly remade.

Various concentrations of potassium phosphate buffers (KPBs) with a variety of ionic strengths were prepared by combining calculated amounts of both monobasic (NaH<sub>2</sub>PO<sub>4</sub>) and dibasic phosphate (Na<sub>2</sub>HPO<sub>4</sub>) buffers solutions according to the following equation:

$$C_{\text{ph}} = 0.437\mu \quad [\text{Eqn. 3.4}]$$

where  $C_{\text{ph}}$  is total phosphate concentration and  $\mu$  is the ionic strength. Thus, buffers of specific ionic strength were prepared from solutions of individual phosphate components (mono and di), each at a concentration of  $0.437\mu$ , by combining them to a pH of 7.<sup>51</sup> The pH was monitored as all of the dibasic phosphate is added to a mixing flask and the monobasic is added until the pH is buffered at 7. The amount of monobasic sodium phosphate remaining (unmixed) was recorded for exact ionic strength calculations. All KPBs were prepared in this manner.

To calculate the exact  $\mu$  of a buffer, the number of moles of each phosphate component, determined experimentally, were used in the following equation:

$$\mu = \frac{1}{2} \sum C_i Z_i^2 \quad [\text{Eqn. 3.5}]$$

### 3.16.3. Electrochemistry (General - Equipment)

Voltammetry experiments were performed at room temperature ( $22 \pm 2^\circ\text{C}$ ) using an EG&G PAR potentiostat, Model 273 or Model 263, controlled by M270 PAR Software. Potentiostats were typically operated in Ramp Mode, generating a potential staircase waveform with a 0.25 mV step height and, in most cases, a 1 mV scan increment. Potential windows varied with the particular experiment being conducted, with larger potential windows sometimes warranting a 2 mV step increment. When operated at low scan rates ( $< 200 \text{ mV/sec}$ ), the current response from the potentiostat was passed through a 5.3 Hz low pass filter; at higher scan rates the low pass filter was turned off. A minimum of three cycles were collected for each scan, ensuring the stability of the electrochemical response. The last cycle of each experiment was saved for display. Unless specifically stated, all electrochemical experiments were performed at a sweep rate of 100 mV/sec. All potential and current peak values, peak splitting, as well as surface coverage, FWHM, and formal potentials were measured using the PAR software. Electron transfer rate constants were calculated using other software discussed below (See Cyt c Electrochemistry Section).

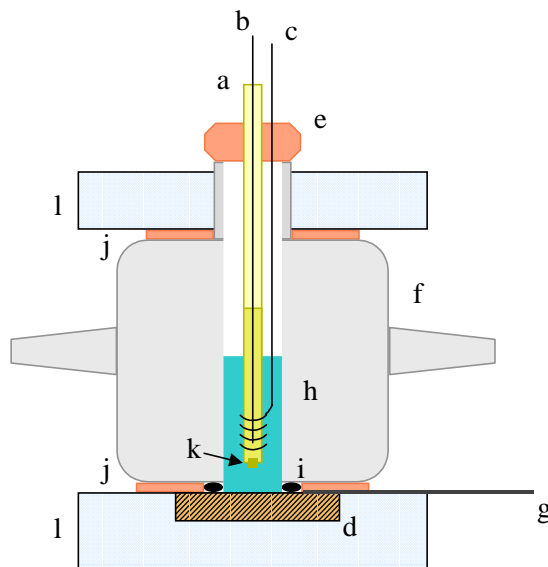


**Figure 3.38.** Schematic illustration of the electrochemical cell used in this research: a) reference electrode housing (glass barrel filled with 1 M KCl), b) Ag/AgCl reference wire, c) a Pt auxiliary electrode wire, d) SAM modified gold working electrode, e) rubber stopper fitted to hold both the glass reference barrel and the Pt counter electrode, f) glass cell body, g) brass electrical contact to gold working electrode, h) buffered electrolyte solution, i) Viton o-ring, j) rubber gaskets, k) a glass frit acting as a salt bridge, l) glass body's arms for attachment to a water bath for temperature controlled experiments, and m) Lucite retainer plates. The entire cell is held together with threaded rods and wing nuts (not shown).<sup>52</sup>

Gold WEs were assembled into the electrochemical cell shown in Figure 3.38. The basic design of this electrochemical cell was first described by Koller and Hawkrige and was subsequently modified for this work.<sup>50</sup> In addition to the gold working electrode which has an electrochemically active area of  $0.32 \text{ cm}^2$ , this cell also features a platinum wire auxiliary electrode (AE), and a Ag/AgCl (1M KCl) reference electrode (RE) (Microelectrodes Inc.). Both the AE and the RE were positioned in close proximity to the WE to reduce solution resistance. The Ag/AgCl RE was periodically calibrated against a saturated calomel electrode (SCE) and drift in the reference potential varied by only  $\pm 5 \text{ mV}$  (data not shown).

### 3.16.4. Gold Substrate Pretreatments

#### -Electrochemical Cleaning

Cell mounted gold substrates were electrochemically cleaned by adding several milliliters of a freshly prepared solution of  $0.1 \text{ M H}_2\text{SO}_4$  and  $0.01 \text{ M KCl}$  and cycling the potential for 5 cycles in each of the following potential windows:  $0.2 \rightarrow 0.75 \text{ V}$ ,  $0.2 \rightarrow 1.0 \text{ V}$ ,  $0.2 \rightarrow 1.25 \text{ V}$ , and  $0.2 \rightarrow 1.5 \text{ V}$ .<sup>10,13a</sup> The cell was immediately rinsed with copious amounts

of M/Q H<sub>2</sub>O before proceeding. WARNING: The procedure actually etches the gold during the potential cycling and can completely remove the gold film if not careful. This is especially a concern regarding the Au/mica and evaporated Au samples.

### **-Hydrogen Flame Annealing**

Hydrogen flame annealing (HFA) was performed via the procedure suggested by Molecular Imaging. The Au sample was mounted on a quartz slide on a fire brick where an additional quartz slide was sometimes required to anchor down one side of the gold substrate. The hydrogen gas was connected with Teflon tubing directly to a quartz tube that had been drawn to a small point and severed, i.e. a torch. The direct connection is beneficial because the hydrogen flame produced is very clean. The hydrogen gas flow through the quartz tube was increased until barely audible. The hydrogen torch was then ignited (usually making a loud pop). With the lights off, the hydrogen flame was adjusted so that it was burning mostly blue and was approximately 4 cm long. Care should be used when working with a hydrogen flame as it can reach temperatures in the 2000-2100°C range and has a maximum burning velocity of 300-440 cm/s.<sup>26</sup> The quartz plate holding the gold substrate was gently heated around the substrate to ensure even heating. This process was continued until water vapor no longer condensed on the quartz plate. The tip of the flame was then brought into contact with the gold surface at a 30° angle from surface normal and swept back and forth across the gold substrate (at ~ 1 Hz) for 30 to 60 seconds. The small flame spot on the gold was maintained as a slightly orange color, although the brightness of this orange glow may vary depending on the room light. In a normally lit room, the spot may not appear to glow at all. Care was taken not to overheat the sample.<sup>25</sup>

### **-Oven Annealing**

Samples were oven annealed in Lindberg Mini-Mite Tube Furnace (Watertown, WS) using a quartz tube and a set point temperature of ~950°C, which resulted in a chamber temperature between 980-1000°C and a tube temperature of ~968° C. Care was taken to control the temperature inside the tube, avoiding the melting point of gold (1064°C). Samples were usually oven annealed for one to several hours.

### **3.16.5. Scanning Probe Microscopy Imaging**

The specific procedure and equipment of the SPM imaging of these gold substrates is included as part of the Experimental Details section of Chapter 5.

### 3.16.6. Roughness Factor Experiments

#### -Electrochemical ( $R_{f-E/C}$ )

Electrochemical  $R_{f-s}$  were determined with a single cyclic voltammetry scan in the potential window of 0.2 to 1.5 V. Cells were filled with dilute sulfuric acid solutions (0.05 M  $H_2SO_4$ ) and scanned in this potential window at 100 mV/sec. Once the gold surface was in contact with the  $H_2SO_4$ , roughness scans were performed as quickly as possible because of concern over chloride contamination from the Ag/AgCl (1 M KCl) RE. Over time and during continuous roughness scan potential cycling, chloride from the RE can infest the experiment, allowing for chloroaurate complex voltammetry and obscuring the voltammetric peak used for roughness determinations (the roughness voltammetry resembles the electrochemical cleaning voltammetry after continuous cycling). In the future, this complication should be avoided by using a double junction or “S” shaped RE, where the flow of chloride contamination toward the WE can be better controlled and minimized.

#### -Microscopy Roughness Factors ( $R_{f-SPM}$ )

Microscopically determined  $R_{f-s}$  were a product of a RMS roughness calculation determination that is part of the Digital Instrument’s software package for the Nanoscope III Microscope.  $R_{f-SPM}$  or  $R_q$  is calculated by the following equation:

$$R_q = \left( \frac{\sum (z_i - z_{avg})^2}{N} \right)^{1/2} \quad [\text{Eqn. 3.6}]$$

where  $Z_i$  is each individual point’s distance from the mean surface level ( $Z_{avg}$ ) and N is the total number points in the population.

### 3.16.7. Lead UPD Experiments

Lead UPD experiments to determine the crystallinity of the gold substrates were performed via the following procedure. The electrochemical cell was filled with 0.1-0.17 mM  $Pb(NO_3)_2$  in an electrolyte solution of 0.10 M  $NaClO_4$  and 0.10  $HClO_4$ . The potential of the gold WE was held at -0.4 V or -0.44 V for 5 minutes, depositing Pb onto the gold surface, and then swept positive at 5 or 50 mV/sec to 0.6 V to oxidize the Pb UPD layer off the surface.

### 3.16.8. SAM Deposition Procedure

Following the electrochemical cleaning cycle or other pretreatment, a background scan was acquired in 4.4 mM potassium phosphate buffer (KPB) solution (pH = 7;  $\mu$ = 10 mM). Backgrounds were acquired in both the 0.1 to 0.4 V potential window and in the 0.2 to -0.2 or similar potential window. The double layer capacitance of the background scan was measured at +250 mV for comparison purposes. The Au substrates were prepared for SAM modification by rinsing 10X with H<sub>2</sub>O and 10X with 95% ethanol and then repeated. Immediately after the last rinse with EtOH, 200-250  $\mu$ L of thiol in ethanol solution (~5 mM) was added via microsyringe to the cell. In most cases, the SAM solution remained in contact with the gold for ~72 hours (3 days) to maximize self-assembly and thiol rearrangement on the surface. After modification, the cells were emptied and rinsed 10X with EtOH, 10X with M/Q H<sub>2</sub>O, 10X with EtOH, and 10X with M/Q H<sub>2</sub>O again. The cells were then subsequently filled with KPB solution, and background scans, known as monolayer checks, were acquired in the same potential window as the background signal for bare Au.

The thiols used were previously synthesized, purified, and characterized by Linderman and co-workers<sup>53</sup> (i.e. 14-mercaptotetradecanoic acid) or used as received from Aldrich Chemical Company (St. Louis, MO) (i.e. 11-mercaptoundecanoic acid). Solutions (4 mL) of 5 mM thiol were prepared volumetrically and mixed thoroughly using a vortex mixer.

### 3.16.9. SAM Characterization Procedure - Redox Probing

Redox probing of the SAMs with hydroxymethyl ferrocene (HMFC) was based on a procedure by Creager and coworkers.<sup>3a</sup> A solution of 2.0 mM HMFC (Strem Chemical Company) in acetone was prepared. The assembled cell was filled with 0.75 mL of 0.1 M HClO<sub>4</sub> and after which 50  $\mu$ L of the 2.0 mM HMFC/acetone solution was injected via microsyringe. The cell was capped and inverted several times to insure adequate mixing and solubilization of the HMFC in the aqueous environment. Note: It is important to do this step quickly to avoid concentration gradients substantial enough to cause the HMFC precipitation on the electrode. After some initial failures, solubilization of HMFC was always achieved by the procedure just described.

The HMFc probe was examined using cyclic voltammetry in the nominal potential window of 0.8 V to -0.4 V. HMFc in HClO<sub>4</sub> has an approximate formal potential of +0.15 V vs. Ag/AgCl RE. The scan rate used for HMFc redox probing was always 100 mV/sec.

Redox probing with potassium ferricyanide, the results of which are not presented in this chapter, was performed with a solution of 2.5 mM K<sub>3</sub>Fe(CN)<sub>6</sub> in 0.5 M KCl supporting electrolyte. The nominal potential window for ferricyanide redox probing was -0.4 V to 0.8 V and was also scanned at 100 mV/sec. The approximate formal potential for ferricyanide in this environment is at approximately 0.227 V vs. Ag/AgCl.

### **3.16.10. Cyt c Purification**

Horse heart (HH) or equine cyt c (Type VI) was purchased from Sigma Chemical Company and purified via column chromatography. The procedure for this purification step is presented here in detail for future use by researchers in the Bowden group. The entire procedure should take place in a refrigerator at ~4°C. A listing of all the chemicals, solutions, and equipment required for this purification procedure is provided as Table 3-14. Beforehand, approximately 50g of “preswollen” carboxymethyl cellulose (CM52, Whatman, Clifton, NJ) was hydrated over a 48 hour period in an excess (~200 mL) of potassium phosphate buffer (KPB) { C = 40 mM; μ = 90mM; pH = 7 }. Proteins are often separated using ion-exchange gels, such as cellulose, because they contain very small pores which cannot be infiltrated by the proteins. The hydrated gel should be gently stirred on occasion. Never use a glass stir bar to mix the gel, as this damages the gel beads and creates small fragments called “fines.” These small fragments must be removed because, if packed into the column, they can slow down the flow rate of the column and decrease the efficiency of the separation. “Fines” should be removed by decanting the supernatant liquid and rehydrating the gel several times. If the gel is being regenerated after use in a column, any brownish colored gel beads should be removed from the mixture. This removal can be accomplished

**Table 3-14.** Chemicals, Solutions, and Equipment for Horse Heart Cyt c Purification

<b>Chemicals</b>	-HH Cyt c (Sigma C7752) -K <sub>2</sub> HPO <sub>4</sub> (MW = 174.18 g/mol) -KH <sub>2</sub> PO <sub>4</sub> (MW = 136.09 g/mol) -Whatman CM-52 carboxymethyl cellulose cation exchange column gel -Bio-Rad Biogel P6DG size exclusion column resin
<b>Glassware / Plasticware</b>	-Multiple volumetric flasks: 1000 mLs (2) and 500 mLs (≤6) -Beakers: 1000-2000 mL range (several) -Plastic bottles: 1000 mLs (5); 250 mLs (2) -Glass vial (~ 4 mL) -Graduated cylinder (100 mL) -Magnetic stir bar -Teflon tubing and syringe for siphon system -Glass pipettes
<b>Solutions</b> (sample measurements included - individual results may vary)	<p><b>70 mM Potassium Phosphate Buffer (KPB); pH 7; <math>\mu \cong 160</math> mM</b></p> <ul style="list-style-type: none"> <li>• 12.19 g K<sub>2</sub>HPO<sub>4</sub> (Dibasic or Di) dissolved in 1000 mL volumetric flask</li> <li>• 9.53 g KH<sub>2</sub>PO<sub>4</sub> (Monobasic or Mono) dissolved in 1000 mL volumetric flask</li> <li>• Pour all of Di into a 2000 mL beaker with a magnetic stir bar; while monitoring the pH of this solution, add Mono until the pH reaches 7.0 (~600 mLs)</li> <li>• Be sure to record the amount of mono left over (not added) for exact <math>\mu</math> calcs.</li> <li>• Store in two plastic 1000 mL plastic bottles and store in the refrigerator.</li> </ul> <p><b>40 mM KPB; pH 7; <math>\mu \cong 90</math> mM</b></p> <ul style="list-style-type: none"> <li>• 3.48 g K<sub>2</sub>HPO<sub>4</sub> dissolved in 500 mL volumetric flask</li> <li>• 2.72 g KH<sub>2</sub>PO<sub>4</sub> dissolved in 500 mL volumetric flask</li> <li>• Prepare in the same manner as the 70 mM KPB (described above).</li> </ul> <p><b>4.4 mM KPB; pH 7; <math>\mu \cong 10</math> mM</b></p> <ul style="list-style-type: none"> <li>• 0.38 g K<sub>2</sub>HPO<sub>4</sub> dissolved in 500 mL volumetric flask</li> <li>• 0.30 g KH<sub>2</sub>PO<sub>4</sub> dissolved in 500 mL volumetric flask</li> <li>• Prepare in the same manner as the 70 mM KPB (described above).</li> </ul> <p><b>500 mM KPB with 0.04% NaN<sub>3</sub>; pH 7; <math>\mu \cong 1140</math> mM</b></p> <ul style="list-style-type: none"> <li>• 43.55 g K<sub>2</sub>HPO<sub>4</sub> dissolved in 500 mL volumetric flask</li> <li>• 34.02 g KH<sub>2</sub>PO<sub>4</sub> dissolved in 500 mL volumetric flask</li> <li>• Add 0.20 g NaN<sub>3</sub> to each flask before mixing.</li> <li>• Prepare in the same manner as the 70 mM KPB (described above).</li> </ul> <p><b>0.2 mM HH Cyt c</b></p> <ul style="list-style-type: none"> <li>• 5 mg HH Cyt c dissolved in 2 mL of 40 mM KPB (pH 7) in a glass vial</li> </ul>
<b>Miscellaneous Equipment</b>	-pH meter -UV-VIS spectrometer -Amicon cell with YM-10 or YM-3 membrane -Nitrogen tank

by decanting the supernatant liquid, or using a glass pipette attached to an aspirator as a vacuum. Once the gel is ready, approximately 10 mL of KPB (C = 40 mM;  $\mu$  = 90mM; pH =

7) should be added to a chromatographic column having a height of 30 cm and an internal diameter of 1.5 cm. The slurry of hydrated gel is then poured into the chromatographic column. If the total volume of the slurry is greater than the overall volume of the column (~53 mL), add the slurry slowly while the bottom of the column is left open to drain. Occasionally the sides of the column should be rinsed with buffer. Once the entire slurry has been added, the column should be allowed to settle. A rubber hose may be used to gently tap the sides of the column to produce better packing. The column should then be equilibrated by passing approximately three bed volumes of 40 mM KPB or until the gel bed has reached a constant height. The height of the equilibrated gel bed should be at least 25 cm. After equilibration, the flow rate of the column should be calculated and recorded, as well as the void volume of the column. The void volume is the amount of space in the column not occupied by gel material. The total volume of the column is the summation of the void volume and the gel volume. Usually the void volume is approximately 35% of the total volume. The void volume can be determined using a 1 mL solution of approximately 1 mg/mL Blue Dextran (Chemical Company). This is a highly visible molecule that should not be retained by the gel at all. The volume it takes to elute this compound is equivalent to the void volume of the gel bed.

### **Chromatographic Procedure (Ion Exchange Chromatography):**

#### *-THE SIPHON*

A siphon is used throughout this procedure as a means of delivering a constant flow of mobile phase from the buffer reservoir (See Figure 3.39). Teflon tubing is connected as shown in this figure. The siphon is established by placing the weighted end of the Teflon tubing in the buffer reservoir above the apparatus. The tubing is secured to the reservoir bottle with a rubber band. To initiate the siphon flow, the opposite end of the tubing is removed from the top of the column and temporarily attached to a 10 mL syringe. Using the syringe, buffer is drawn through the tubing from the reservoir container and will start dripping out of the end of the tubing. Once flow is established through the column, the tubing may be reattached to the top of the column. The bottom of the column should also be checked to make sure that the eluent is coming out of the column as a slow, steady drip.

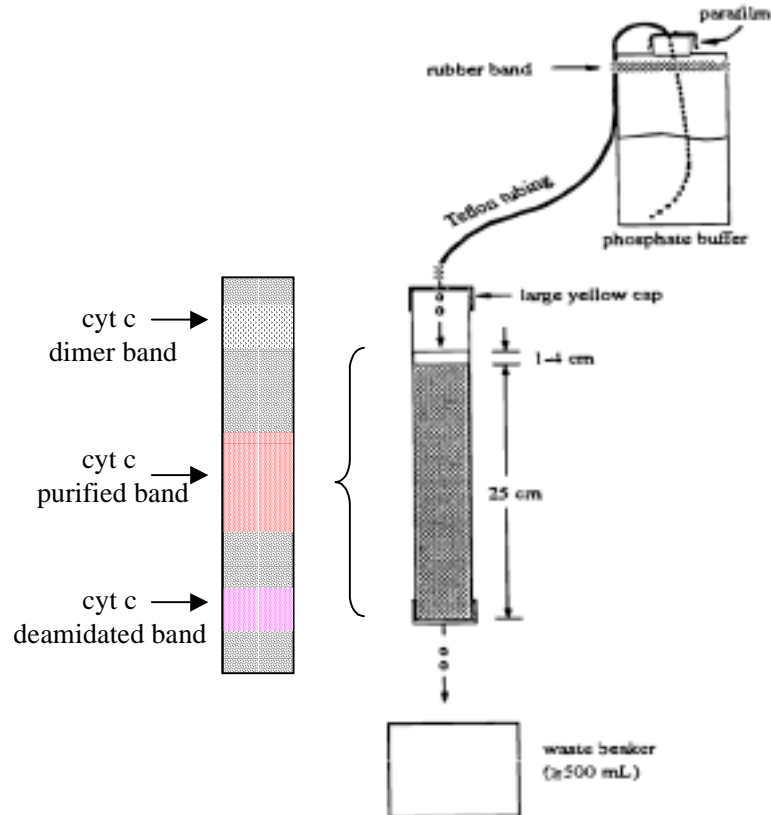


**Figure 3.39.** Apparatus for protein purification illustrating the column/siphon system used for cyt c purification. The three elution bands of cyt c are shown to the left of the figure.

### STEP 1- PREPARING THE COLUMN

The first step of the procedure is flush the column with several bed volumes of 40 mM KPb. This cleanses the column, removing contaminants and storage solution, and equilibrates it with the working buffer. This should be done by continuously running the column overnight. *Extra care should be taken to provide enough buffer in the reservoir so that the column does not run dry during this step.*

### STEP 2- CHROMATOGRAPHIC SEPARATION

When ready to place the cyt c solution on the column, the siphon should first be stopped and the level of buffer in the column, above the gel bed, should be allowed to drop to approximately 1 mm above the bed. It is best to do this step late in the day because the cyt c will take approximately 15 or more hours to elute from the column. Again, proper timing is essential to prevent the column from running dry and to collect the cyt c band coming off the column. The cyt c solution (0.2 mM HH cyt c in 40 mM KPb) should be placed on the column via a glass pipette, taking extra precaution to minimize disturbance of the column

bed. Gently adding the cyt c solution on the column is best done by allowing the solution to drip down the sides of the column rather than dropping the solution from the pipette. The cyt c solution should be spread across the top of the gel bed as evenly as possible to create a plug of cyt c that will move through the column. Again, the column should be allowed to drip until the cyt c band is well into the gel bed, with approximately 1 mm of solution above the bed. At this point, the pipette should be used to deliver several mLs of the buffer that will carry the cyt c down through the column, also called the eluent buffer (70 mM KPB;  $\mu$ = 160 mM; pH = 7). Use care when pipetting solution onto the column bed. The user should get as close to the top of the bed with the pipette tip without disturbing the resin/gel itself.

Dropping solution from the pipette at any significant height tends to have a “dive bombing” effect on the column bed. After the liquid level is 2-3 cm above the bed, discontinue buffer addition with a pipette and restart the siphon of the eluent buffer (70 mM KPB;  $\mu$ = 160 mM; pH = 7). A dark red band of cyt c should be seen at the very top of the white gel bed, and the solution above the bed should be clear and colorless. Over the course of the next 15-24 hours (older columns tend to take longer because of gel compression and a higher level of “fines”) the protein will typically separate into three bands: 1) deaminated cyt c, 2) purified cyt c, and 3) cyt c dimer (Figure 3.39). The deaminated protein elutes first, appearing as a very light red band, and is followed by a dark red band which is comprised of purified cyt c. The third band, or dimer band, will not elute from the column and may not be readily visible to the naked eye. This band is removed during a later step with sodium azide in high ionic strength buffer.

The separation process for cyt c is primarily ion-exchange chromatography. The cyt c separation proceeds because of the protein's partitioning between the solvent (mobile phase), and the fixed charge sites on the gel (stationary phase). In this case, the cellulose based stationary phase is made up of derivatized polymers made from the sugar glucose. The derivitization of the stationary phase for this separation is a weak acid, a carboxymethyl group (-OCH<sub>2</sub>CO<sub>2</sub>H), prompting the gel to be called CM-52.<sup>54</sup> For this particular gel, cationic solute material in the mobile phase will have an affinity for the anionic sites of the stationary phase. This separation process is allowed to proceed because of the molecular exclusion of cyt c from the gel. The pores of the gel are too small for the cationic cyt c to

penetrate and will elute from the column faster than molecules that are able to penetrate the gel. Being positively charged, if the protein could penetrate the gel pores, it would be held too tightly and not proceed down the column. This separation process is depicted in Figure 3.40. Care should be taken to make sure this part of the purification proceeds without interruption. Capping the bottom of the column and stopping the siphon can be done in an emergency, but the risk of detrimental band broadening increases if the column is left in this state for a significant amount of time.

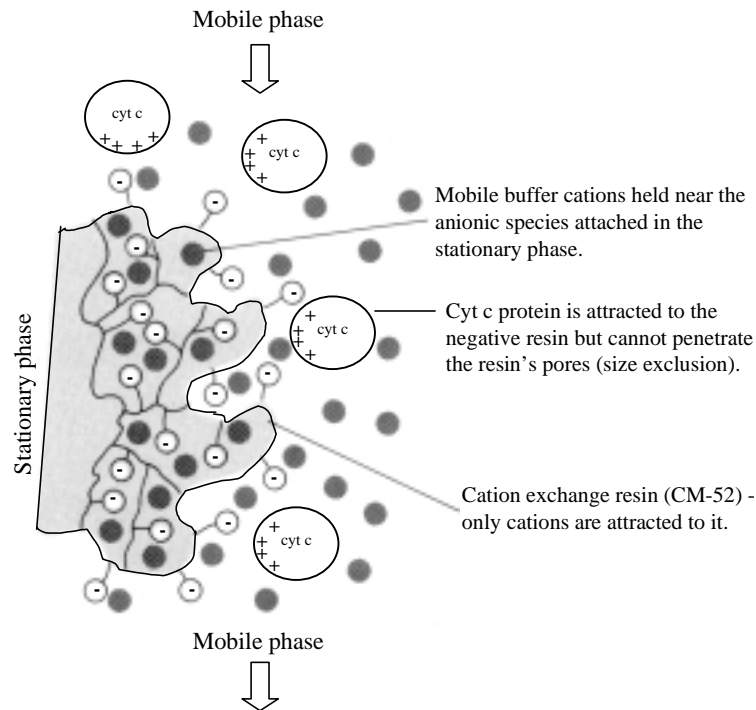


**Figure 3.40.** Separation mechanism of the CM-52 column during the ion-exchange chromatographic purification procedure for cyt c (Figure adapted from a figure in Ref. 54).

When the purified band begins to come off the column, begin collecting the eluate in a 250 mL bottle. Continue collecting eluate until most of the cyt c band has been removed from the column. This should take several hours and the bottom of the column can be capped during this step if necessary. Once the cyt c is collected, stop the siphon and change the buffer reservoir to the cleaning and storage buffer, 500mM KPB { $\mu= 1140$  mM; pH = 7} with 0.04% NaN<sub>3</sub>. Allow this solution to run through the column at least overnight. After running this buffer, laced with sodium azide, through the column, the column may be capped until the next usage.

### *STEP 3 - AMICON FILTRATION*

The collected cyt c eluate must now be concentrated by reducing the volume. This is done with an Amicon filtration cell and a membrane filter, shown in Figure 3.41. The concept of the Amicon cell is that gas pressure supplied by a N<sub>2</sub> tank will pressurize the chamber holding the cyt c solution and force solution through the pores in the membrane at the bottom of the cell. The membrane is size selective, allowing solvent and electrolyte to pass through the pores, while retaining the large proteins from. Two sizes of membranes have been used for this part of the procedure, the YM-10 membrane and the YM-3 membrane (Diaflo - Ultrafiltration Membranes, Amicon Inc., Beverly, MA). Both are equally successful, but the YM-3, having smaller pores takes significantly longer to filter cyt c solutions.

The membranes are stored in 10% EtOH solutions with their “glossy side” down. The “glossy side” of the membrane is identifiable by its glossy or wet appearance and by the observation that the filter usually curls toward the glossy side. Care should be taken not to handle the membrane too much. Gloves should be worn while handling the filter by its edges. If the filter is brand new, the filter should be soaked for three successive, 20 minute cycles in Milli-Q (M/Q) ultrapure water with the glossy side down. If it is a previously used filter, it can be removed from its storage solution and simply rinsed off with M/Q H<sub>2</sub>O. In any event, the filter is then placed in the Amicon cell with its glossy side up. Note that this is the only point where the filter’s glossy membrane is up. The o-rings used to seal the Amicon cell assembly should also be wetted or soaked in M/Q H<sub>2</sub>O before use.

The cyt c eluate should be quantitatively transferred to the assembled Amicon cell, which is then enclosed in a protective metal casing positioned on a magnetic stir plate in the refrigerator. The stir bar should be rotated slowly to prevent frothing and bubbling of the solution. The gas line should be connected to the top of the cell, and a clear glass container should be set up to receive the waste. Before engaging the gas tank, the small lever at the top

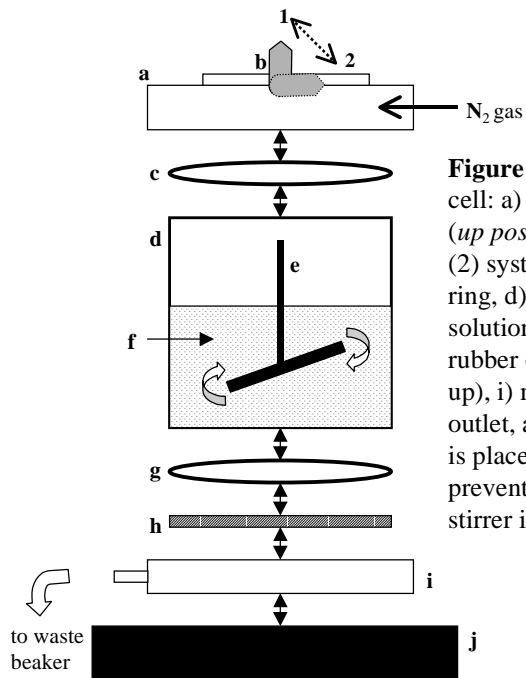


**Figure 3.41.** Schematic diagram of the Amicon filtration cell: a) cell top with gas intake valve, b) pressure lever – (up position (1) – system is sealed and pressurized; down (2) system open and not pressurized), c) larger rubber o-ring, d) plastic cell body, e) magnetic stir bar, f) cyt c solution being filtered (buffer exchanged), g) smaller rubber o-ring, h) YM-3 or YM-10 membrane (glossy side up), i) membrane holder with draining ridges and waste outlet, and j) base of assembly. Note: the entire assembly is placed in a protective metal casing (not shown) to prevent pressure explosions and is used on a magnetic stirrer in a refrigerator at 4-10° C.

of the cell should be checked to make sure it is in the “down” position (See Figure 3.41). The N<sub>2</sub> pressure should be increased gradually until the regulator reads approximately 55 psi. Prior to reaching 55 psi, a hissing sound will be heard, at which time the small lever should be moved to the “up” position, which closes off the system and prevents anymore gas from escaping. If the hissing sound persists while the system is sealed, it means that there is a leak in the cell and it must be reassembled. The threshold pressure to maintain the cell’s structural integrity is 75 psi; therefore, **never pressurize above 70 psi**. *NOTE: The Amicon cell is a pressurized system and eye protection should be worn at all times.* Continue the filtration process until the volume of the cyt c solution being concentrated in the cell is less than 2 mL.

One potential pitfall of this concentrating procedure is noteworthy. If the filtration process proceeds very quickly and/or the waste solution becomes colored (a white piece of paper under the waste flask is useful here), then the filter may be upside down. Should this occur, reassemble the cell with the glossy side of the filter facing up. If the problem persists, there is most likely a tear in the membrane and it must be discarded.

#### **STEP 4A - EXCHANGING THE BUFFER VIA THE AMICON CELL**

If the Amicon cell is being used to exchange the cyt c buffer to 4.4 mM KP<sub>B</sub> ( $\mu=10$  mM; pH = 7), add approximately 60 mL of the new buffer to the concentrated cyt c solution in the cell. Following the procedure described in step 3, reduce the volume to concentrate the cyt c again. Repeat this process three more times to ensure that the buffer has been effectively exchanged. Using great care, remove the cyt c solution from the Amicon cell using a hand held glass pipet and rubber bulb. Tilt the cell, using the glass pipet to draw the solution out while taking care not to puncture the membrane. When finished, disassemble the cell and remove the filter ( the plate holding the membrane with an o-ring may have to be soaked in a large beaker of M/Q H<sub>2</sub>O and “floated” out). Avoid grabbing or pinching the filter to get it out. Rinse the removed filter with M/Q H<sub>2</sub>O and soak it, glossy side down, in M/Q H<sub>2</sub>O for at least an hour before placing it in storage solution (10% EtOH in M/Q H<sub>2</sub>O). [Go to Step 5]

#### *STEP 4B - EXCHANGING THE BUFFER VIA A DESALTING COLUMN*

If a desalting column is used to exchange the buffer, transfer the 2 mL of concentrated cyt c solution from the Amicon cell to the desalting column as described in step 2. The desalting column (ht. = 50 cm; i.d.= 1 cm; bed ht.= 34 cm) should contain a approximately 40 mL of BioRad P6DG desalting gel (BioRad, Richmond, CA). The column is packed via the procedure described above, starting with about 7 grams of the dry gel (7 mLs/g). In removing the cyt c solution from the Amicon cell use great care not to damage the membrane. The cell may be tilted and a glass pipette can be used to remove the cyt c solution out of the cell.

The desalting column is relatively quick compared to the CM-52 column. Once the cyt band has been collected from the column, it will again have to be concentrated down in the Amicon cell. When finished, disassemble the cell and remove the filter ( the plate holding the membrane with an o-ring may have to be soaked in a large beaker of M/Q H<sub>2</sub>O and “floated” out). Avoid grabbing or pinching the filter to get it out. Rinse the removed filter with M/Q H<sub>2</sub>O and soak it, glossy side down, in M/Q H<sub>2</sub>O for at least an hour before placing it in storage solution (10% EtOH in M/Q H<sub>2</sub>O). [Go to Step 5]

#### *STEP 5 - UV-VIS SPECTROSCOPIC DETERMINATION OF CYT C CONC.*

To measure the concentration of the cyt c solution, UV-Vis spectroscopy is used. Allow the instrument’s light source to warm up for approximately 20 minutes before

commencing with measurements. Using a 1 mm cuvette, being careful not to touch the sides of the cuvette with ungloved hands, measure a background scan in the 4.4 mM KPB. Empty the cuvette and refill it with the cyt c solution. An example of an experimental adsorption spectrum is given in Figure 3.42. To calculate the concentration of cyt c, the Soret band at approximately 410 nm can be used in conjunction with the Beer-Lambert law:

$$A = \epsilon bc \quad [\text{Eqn. 3.7}]$$

where  $c$  is the unknown concentration (M),  $b$  is the cuvette's path length of 0.1 cm, and  $\epsilon$  is the molar absorptivity or extinction coefficient of cyt c ( $106,100 \text{ M}^{-1} \text{ cm}^{-1}$ ).<sup>55</sup> After the UV-Vis measurement, the cuvette should be sonicated in M/Q H<sub>2</sub>O to remove the protein from its walls. Once the concentration of this stock cyt c solution is known, it may be diluted to make working solutions of varying concentrations.

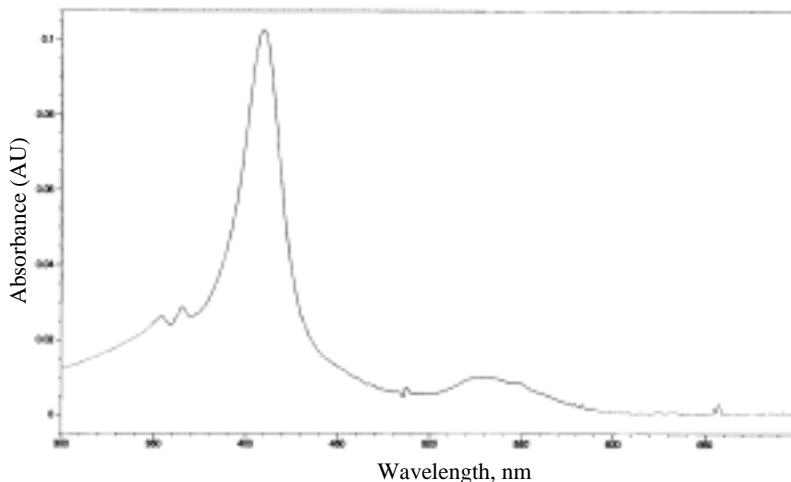


**Figure 3.42.** Experimental UV-VIS spectrum of HH cyt c.

### 3.16.11. Cyt c Adsorption and Electrochemistry

After a carboxylic SAM is formed on a Au substrate, the thiol solution is removed from the cell followed by copious rinsing with EtOH and H<sub>2</sub>O (10X EtOH; 10X H<sub>2</sub>O; 10X EtOH; and 10X H<sub>2</sub>O). The cell is then filled with KPB (4.4 mM;  $\mu=10$  mM; pH = 7) and background voltammograms are acquired. The cell is then rinsed 3X with 4.4 mM KPB and refilled with a solution of 10-25  $\mu\text{M}$  HH cyt c solution in KPB (4.4 mM;  $\mu=10$  mM; pH = 7). The cyt c is allowed to adsorb to the SAM for 45 minutes to 1 hour. The cytochrome adsorption was performed at room temperature and in a 5-8°C refrigerator, with no noticeable difference in the behavior observed. After adsorption, the cell is rinsed 5X with KPB (4.4

mM;  $\mu=10$  mM; pH = 7) and refilled with the same buffer. At this point the solution was sometimes purged for 5-10 minutes with H<sub>2</sub>O-saturated Ar to remove oxygen. Cyt c cyclic voltammetry experiments were typically performed using the following potential windows: +0.2 V to -0.2 V, +0.25 V to -0.25 V, and +0.3 V to -0.3 V. Formal potentials and cyt c surface coverage were usually determined from CVs collected at slower scan rates 1-100 mV/sec; FWHM values were determined using 100 mV/sec scans, and the ET rate constants were primarily determined from CVs acquired at scan rates giving rise to peak splitting  $\geq 200$  mV. ET rate constants were calculated according to Laviron's simplest theory for adsorbed species using software written by former Bowden Group research Jim Willit, "CV3091."<sup>50</sup> Cyt c signals were stable, if the cells were refrigerated, for several days, but data were usually collected on the same day as the cyt c was adsorbed.

### 3.16.12. XPS Testing Analysis

X-ray photoelectron spectroscopy (XPS) is a form of photoelectron spectroscopy (PES) which, in general, is focused on electronic transitions involving the ejection of a single electron out of a molecular state to a vacuum level. In PES, a sample is struck with photons of high enough energy to displace electrons out of molecular or atomic orbitals:



The energy used to eject the electron from the species is known as the binding energy of the electron or its ionization potential (IP). During this process the system obeys a conservation of energy known as the photoelectric effect. That is, after some of the energy of the photon is used to displace an electron from the species, the rest of the energy becomes kinetic energy (KE) of the ejected electron:

$$\text{KE} = h\nu - \text{IP}(e^-) \quad [\text{Eqn. 3.8}]$$

The KE of these ejected electrons, when measured, can be directly correlated to specific atomic and molecular species. Each specific type of atom will require a signature amount of energy to release an electron from its orbitals. In this manner, PES can be used to identify and verify materials. More tightly held electrons, those in lower orbitals, will require more energy to eject and therefore result in ejected electrons with less KE.

More specifically, XPS involves bombarding a sample with x-ray photons energetic enough to eject core electrons, whose kinetic energies are then measured. Because

photoelectrons can only transverse several angstroms of material, XPS is predominantly a surface analysis technique.<sup>56</sup>

For this research XPS testing was performed by either Mike Tarlov of NIST or by John Phillips, the residential microscopist at the Analytical Instrumentation Facility at the Engineering Graduate Research Center at North Carolina State University's Centennial Campus. Both Mr. Phillips and Dr. Tarlov performed survey scans of the surfaces being tested. Additionally, Mr. Phillips also ran high resolution scans for N(1s), C(1s), and O(1s) evaluation. Dr. Tarlov's testing was aimed at determining if Ti contamination existed on the thermally annealed gold surfaces whereas the main focus of the testing by Mr. Phillips was the presence of nitrogen, an indication of adsorbed protein.

### **3.16.13. Square Wave Voltammetry**

Square wave voltammetry (SWV) was performed between +0.2 V and -0.4 V with a pulse height of 10 mV, a frequency of 5 Hz, and a scan increment of 2 mV. SWV was performed on monolayers of cyt c as well as submonolayers that persisted following treatment with 1 M KCl.

### **3.16.14. Intentional Roughening Procedures and Mixed SAM Usage**

Some gold substrates were intentionally roughened by electrochemical cycling in 0.1M H<sub>2</sub>SO<sub>4</sub> and 0.01 M KCl. Roughness scans in dilute H<sub>2</sub>SO<sub>4</sub> were performed both before and after the intentional roughening to verify the change in roughness factor.

Mixed SAMs were applied to the gold surfaces in the same manner as uniform SAMs. Deposition time and concentration of the thiol solution was the same as when uniform SAMs were utilized.

### **3.16.15. SAM Desorption LSV Procedure**

SAM desorption experiments were performed in 0.5 M KOH according to procedures described by Porter and coworkers.<sup>41</sup> Typically a SAM desorption scan employed LSV initiated at -0.2 or -0.4 V and scanned negatively until either solvent reduction current or SAM desorption peaks were observed. The scans were run at 100 mV/sec. Care should be taken to select a current range adequate for scaling the expected current since LSV SAM desorption scans can only be performed once on each sample.

### 3.17 REFERENCES

1. R.A. Clark and E.F. Bowden, "Voltammetric Peak Broadening for Cytochrome *c*/Alkanethiolate Monolayer Structures: Dispersion of Formal Potentials," *Langmuir* **1996**, *13*, 559-565.
2. Proposal to the National Science Foundation by Edmond F. Bowden, "Protein Monolayer Electrochemistry," 1993.
3. a) S.E. Creager, L.A. Hockett, and G.K. Rowe, "Consequences of Microscopic Surface Roughness for Molecular Self-Assembly," *Langmuir* **1992**, *8*, 854-861; b) L.H. Guo, J.S. Facci, G. McLendon, and R. Mosher, "Effect of Gold Topography and Surface Pretreatment on the Self-Assembly of Alkanethiol Monolayers," *Langmuir* **1994**, *10*, 4588-4593; c) C.A. Widrig, C. Chung, and M.D. Porter, *J. Electroanal. Chem.* **1991**, *310*, 335; d) O. Chailapakul and R.M. Crooks, *Langmuir* **1993**, *9*, 884; e) S. Steinberg, Y. Tor, E. Sabatani, and I. Rubinstein, *J. Am. Chem. Soc.* **1991**, *113*, 5176; f) S. Steinberg and I. Rubinstein, *Langmuir* **1992**, *8*, 1183; g) Y. Golan, L. Margulis, and I. Rubinstein, *Surface Science* **1992**, *264*, 312; h) R. Subramanian and V. Lakshminarayanan, "Effect of Surface Roughness on the Self-Assembly of Octadecanethiol Monolayers Onto Polycrystalline Noble Metal Surfaces," *Current Science* **1999**, *76*(5), 665-669; and i) J.C. Hoogvliet, M. Dijkstra, B. Kamp, and W.P. van Bennekom, "Electrochemical Pretreatment of Gold Electrode Surfaces for Molecular Self-Assembly: A Study of Bulk Polycrystalline Gold in Phosphate Buffer pH 7.4," submitted to *Analytical Chemistry*, 1999.
4. Rose Anne Clark, Ph.D. Thesis, Appendix.
5. H. O. Finklea, "Electrochemistry of Organized Monolayers of Thiols and Related Molecules on Electrodes," A.J. Bard and I. Rubinstein (Eds.), *Electroanalytical Chemistry - A Series of Advances*, Vol. 19, 108-335, Marcel Dekker: New York, New York, 1996.
6. a) D.M. Kolb, "Reconstruction Phenomena at Metal-Electrolyte Interfaces," *Progress in Surface Science* **1996**, *51*(2), 109-173; b) O.M. Magnussen, J. Hotlos, R.J. Behm, N. Batina, and D.M. Kolb, "An In-Situ Scanning Tunneling Microscopy Study of Electrochemically Induced "Hex"  $\leftrightarrow$  (1x1) Transitions on Au(100) Electrodes," *Surface Science* **1993**, *296*, 310-332; c) O.M. Magnussen, J. Hotlos, R.J. Behm, R.J. Nichols, T. Twomey, and D.M. Kolb, "An In-Situ STM Study of Potential-Induced Changes in the Surface Topography of Au(100) Electrodes," *J. Electroanal. Chem.* **1990**, *290*, 21-31.
7. C.R. Clemmer and T.P. Beebe, "A Review of Graphite and Gold Surface Studies for Use as Substrates in Biological Scanning Tunneling Microscopy Studies," *Scanning Microscopy* **1992**, *6*(2), 319-333.
8. C.E.D. Chidsey, C.R. Bertozzi, T.M. Putvinski, and A.M. Muijsce, *J. Am. Chem. Soc.* **1990**, *112*, 4301-4306.
9. D.M. Collard and M.A. Fox, *Langmuir* **1991**, *7*, 1192-1197.
10. T. Nahir and E.F. Bowden, "The Distribution of Standard Rate Constants for Electron Transfer Between Thiol Modified Gold Electrodes and Adsorbed Cyt *c*," *J. Electroanal. Chem.* **1996**, *410*(1), 9-13.

11. S. Manne, J. Massie, V.B. Elings, P.K. Hansma, and A.A. Gewirth, "Electrochemistry on a Gold Surface Observed With the Atomic Force Microscope," *J. Vac. Sci. Technol. B* **1991**, 9(2), 950-954.
12. a) J. Wiechers, T. Twomey, R.J. Behm and D.M. Kolb, "An *In-Situ* Scanning Tunneling Microscopy Study of Au(111) with Atomic Scale Resolution," *J. Electroanal. Chem.* **1988**, 248, 451-460; b) C. Vitus and A.J. Davenport, "*In-Situ* Scanning Tunneling Microscopy Studies of the Formation and Reduction of a Gold Oxide Monolayer on Au(111)," *J. Electrochem. Soc.* **1994**, 141(5), 1291-1298; c) D.J. Trevor, C.E.D. Chidsey, and D.N. Loiacono, "*In Situ* Scanning-Tunneling- Microscope Observation of Roughening, Annealing, and Dissolution of Gold (111) in an Electrochemical Cell," *Physical Review Letters* **1989**, 62(8), 929-932.
13. a) U. Oesch and J. Janata, "Electrochemical Study of Gold Electrodes with Anodic Oxide Films - I. Formation and Reduction Behavior of Anodic Oxides on Gold," *Electrochimica Acta* **1983**, 28(9), 1237-1246; b) U. Oesch and J. Janata, "Electrochemical Study of Gold Electrodes with Anodic Oxide Films - II. Inhibition of Electrochemical Redox Reactions By Monolayers of Surface Oxides," *Electrochimica Acta* **1983**, 28(9), 1247-1253.
14. a) R.S. Nicholson and I. Shain, *Analyst. Chem.* **1964**, 36, 706; b) D.W. Kirk, F.R. Foulkes, and W.F. Graydon, *J. Electrochemical Society* **1980**, 127, 1069.
15. a) J.W. Shultze and K.J. Vetter, *Ber. Bunsenges. Phys. Chem.* **1975**, 71, 470; b) J. Clavilier and C.N. Van Huong, *Acad. Sci. Paris* **1969**, 269, 736 c) A. Capon and R. Parsons, *J. Electroanal. Chem.* **1973**, 44, 1 & 239, 45, 205; d) A.H. Taylor, R.D. Pearce, and S.B. Brummer, *Trans. Faraday Soc.* **1971**, 67, 801; C. Hinnen, *J. Electroanal. Chem.* **1979**, 95, 131.
16. S. Trasatti and O.A. Petrii, International Union of Pure and Applied Chemistry - Physical Chemistry Division - Commission on Electrochemistry - Chaired by K. Niki and L.R. Faulkner, "Real Surface Area Measurements in Electrochemistry," *Pure and Applied Chemistry* **1991**, 63(5), 711-734.
17. M.E. Vela, R.C. Salvarezza, and A.J. Arvia, "The Electroreduction Kinetics of the Hydrous Gold Oxide Layers and Growth Modes and Roughness of the Electroreduced Gold Overlayers," *Electrochimica Acta* **1990**, 35(1), 117-125.
18. a) A.A. Michri, A.G. Pshchenichnikov, and R.Kh. Burshtein, "Determining the Actual Area of Smooth Gold Electrodes," *Elektrokhimiya* **1972**, 8(3), 364-366; b) Z. Samec and J. Weber, "Study of the Oxidation of SO<sub>2</sub> Dissolved in 0.5M H<sub>2</sub>SO<sub>4</sub> on a Gold Electrode - I Stationary Electrode," *Electrochimica Acta* **1975**, 20, 403-412; c) S.B. Brummer and A.C. Makrides, "Surface Oxidation of Gold Electrodes," *J. Electrochemical Society* **1964**, 111(10), 1122-1128; d) D.A.J. Rand and R. Woods, "The Nature of Adsorbed Oxygen on Rh, Pd, and Au Electrodes," *J. Electroanal. Chem.* **1971**, 31, 29-38; e) D.A.J. Rand and R. Woods, "A Study of the Dissolution of Pt, Pd, Rh, and Au Electrodes in 1M H<sub>2</sub>SO<sub>4</sub> by Cyclic Voltammetry," *J. Electroanal. Chem.* **1972**, 35, 209-218; f) S.H. Cadle and Stanley Bruckenstein, "Ring-Disk Electrode Study of the Anodic Behavior of Gold in 0.2M Sulfuric Acid," *Anal. Chem.* **1974**, 46(1), 16-20.
19. a) A.A. Michri, *Soviet Electrochem.* **1972**, 8, 351; b) J. Weber, Z. Samec, and V. Marecek, *J. Electroanal. Chem.* **1978**, 89, 271; c) J.O. Besenhard, R. Parsons, and R.M. Reeves, *J.*

- Electroanal. Chem.* **1979**, *96*, 57; d) L.D. Burke and M. McRann, *J. Electroanal. Chem.* **1981**, *125*, 387.
20. M. Hyland, J.A. McLaughlin, D-M. Zhou, and E.T. McAdams, "Surface Modification of Thin Film Gold Electrodes for Improved *In Vivo* Performance," *Analyst* **1996**, *121*, 705-709.
21. D. Ashland, *The Science and Engineering of Materials*, 3<sup>rd</sup> Edition, 1989.
22. J. Clavilier, R. Faure, G. Guinet, and R. Durand, "Preparation of Monocrystalline Pt Microelectrodes and Electrochemical Study of the Plane Surfaces Cut in the Direction of the (111) and (110) Planes," *J. Electroanal. Chem.* **1980**, *107*, 205-209.
23. a) J. Clavilier, K.E. Achi, M. Petit, A. Rodes, and M.A. Zamakhchari, *J. Electroanal. Chem.* **1990**, *295*, 333; b) S. Motoo, and N. Furuya, *J. Electroanal. Chem.* **1984**, *172*; *167*; *181*, 339; *309*; *301* (resp.); c) A. Hamelin, L. Doubova, D. Wagner, and H. Schirmer, *J. Electroanal. Chem.* **1987**, *220*, 155; d) N. Batina, A.S. Dakkouri, and D.M. Kolb, *J. Electroanal. Chem.* **1994**, *370*, 87.
24. M. Dietterle, T. Will, and D.M. Kolb, "Step Dynamics at the Ag(111)-Electrolyte Interface," *Surface Science Letters* **1995**, *327*, L495-L500.
25. Personal communication with technical support at Molecular Imaging Corporation.
26. D.A. Skoog and J.J. Leary, *Principles of Instrumental Analysis*, 4<sup>th</sup> Ed., Saunders College Publishing: Fort Worth, Texas, 1992.
27. D.M. Kolb, "Physical and Electrochemical Properties of Metal Monolayer on Metallic Substrates," in *Advances in Electrochemistry and Electrochemical Engineering*, Vol. 11, H. Gerischer and C.W. Tobias, Eds., 125-271, John Wiley & Sons: New York, 1978.
28. J.W. Schultze and D. Dickertmann, *Surface Science* **1976**, *54*, 489.
29. K. Engelsmann, W.J. Lorenz, E. Schmidt, *J. Electroanal. Chem.* **1980**, *114*, 1-10.
30. a) H.O. Finklea, S. Avery, M. Lynch, T. Furtch, "Blocking Oriented Monolayers of Alkyl Mercaptans on Gold Electrodes," *Langmuir* **1987**, *3*, 409-413; b) H.O. Finklea, D.A. Snider and J. Fedyk, "Passivation of Pinholes in Octadecanethiol Monolayers on Gold Electrodes by Electrochemical Polymerization of Phenol," *Langmuir* **1990**, *6*, 371-376; c) H.O. Finklea, D.A. Snider, and John Fedyk, "Characterization of Octadecanethiol-Coated Gold Electrodes as Microarray Electrodes by Cyclic Voltammetry and AC Impedance Spectroscopy," *Langmuir* **1993**, *9*, 3660-3667; d) S. Creager and K.A. Groat, "Self-Assembled Monolayers in Organic Solvents: Electrochemistry at Alkanethiolate-Coated Gold in Propylene Carbonate," *Langmuir* **1993**, *9*, 3668-3675; e) C.E.D. Chidsey and Dominic Loiacono, "Chemical Functionality in Self-Assembled Monolayers: Structural and Electrochemical Properties," *Langmuir* **1990**, *6*, 682-691; f) P. Krysinski and M. Brzostowska-Smolka, "Three Probe Voltammetric Characterization of Octadecanethiol Self-Assembled Monolayer Integrity on Gold Electrodes," *J. Electroanal. Chem.* **1997**, *424*, 61-67; g) E. Saabatani and I. Rubinstein, "Organized Self-Assembling Monolayers on Electrodes. 2. Monolayer-Based Ultramicroelectrodes for the Study of Very Rapid Electrode Kinetics," *J. Phys. Chem.* **1987**, *91*, 6663-6669.

31. a) C.M. Roth and A.M. Lenhoff, "Electrostatic and van der Waals Contributions to Protein Adsorption: Computation of Equilibrium Constants," *Langmuir* **1993**, *9*, 962-972; b) J. Stahlberg, U. Appelgren, and B. Jonsson, "Electrostatic Interactions between a Charged Sphere and a Charged Planar Surface in an Electrolyte Solution," *J. Colloid and Interfacial Science* **1995**, *176*, 1-11; c) J. Stahlberg, "Electrostatic Retention Model for Ion-Exchange Chromatography," *Anal. Chem.* **1994**, *66*, 440-449.
32. D.J. Tobias, W. Mar, J.K. Blasie, and M.L. Klein, "Molecular Dynamics Simulations of a Protein on Hydrophobic and Hydrophilic Surfaces," *Biophysical Journal* **1996**, *71*, 2933-2941.
33. a) G. Bar, S. Rubin T.N. Taylor, B.I. Swanson, T.A. Zawodzinski, J.T. Chow, and J.P. Ferraris, "Patterned Self-Assembled Monolayers of Ferrocene and Methyl Terminated Alkanethiols on Gold: A Combined Electrochemical, Scanning Probe Microscopy, and Surface Science Study," *J. Vac. Sci. Tech. A* **1996**, *14*(3), 1794-1800; b) J.L. Wilbur, H.A. Biebuyck, J.C. MacDonald, and G.M. Whitesides, "Scanning Force Microscopies Can Image Patterned Self-Assembled Monolayers," *Langmuir* **1995**, *11*, 825-831.
34. S. Song, R.A. Clark, M.J. Tarlov, and E.F. Bowden, "Characterization of Cytochrome c/Alkanethiolate Structures Prepared by Self-Assembly on Gold," *J. Phys. Chem.* **1993**, *97*, 6564-6572.
35. C.M.A. Brett and A.M.O. Brett, *Electrochemistry - Principles, Methods, and Applications*, Oxford University Press: Oxford, 1993.
36. a) Z. Stojek and Janet Osteryoung, "Linear Scan and Staircase Voltammetry of Adsorbed Species," *Anal. Chem.* **1991**, *63*(8), 839-841; b) J.H. Reeves, S. Song, and E.F. Bowden, "Application of Square Wave Voltammetry to Strongly Adsorbed Quasireversible Redox Molecules," *Anal. Chem.* **1993**, *65*, 683-688.
37. a) C.D. Bain, J. Evall, G.M. Whitesides, "Formation of Monolayers by the Coadsorption of Thiols on Gold: Variation in the Head Group, Tail Group, and Solvent," *J. Am. Chem. Soc.* **1989**, *111*, 7155-7164; b) L. Bertilsson and B. Liedberg, "Infrared Study of Thiol Monolayer Assemblies on Gold: Preparation, Characterization, and Functionalization of Mixed Monolayers," *Langmuir* **1993**, *9*, 141-149; c) S.J. Stanick, A.N. Parikh, Y.-T. Tao, D.L. Allara, and P.S. Weiss, "Phase Separation of Mixed-Composition Self-Assembled Monolayers into Nanometer Scale Molecular Domains," *J. Phys. Chem.* **1994**, *98*, 7636-7646; d) G.K. Rowe and S.E. Creager, "Redox and Ion Pairing Thermodynamics in Self-Assembled Monolayers," *Langmuir* **1991**, *7*, 2307-2312; e) K.L. Prime and G.M. Whitesides, "Self-Assembled Organic Monolayers: Model Systems for Studying Adsorption of Proteins at Surfaces," *Science* **1991**, *252*, 1164-1167; f) C.E.D. Chidsey, C.R. Bertozzi, T.M. Putvinski, and A.M. Muzsca, "Coadsorption of Ferrocene-Terminated and Unsubstituted Alkanethiols on Gold: Electroactive Self-Assembled Monolayers," *J. Am. Chem. Soc.* **1990**, *112*, 4301-4306.
38. a) P.E. Laibinis, R.G. Nuzzo, and G.M. Whitesides, "Structure of Monolayers Formed by Coadsorption of Two n-Alkanethiols of Different Chain Lengths on Gold and Its Relation to Wetting," *J. Phys. Chem.* **1992**, *96*, 5097-5105; b) C.D. Bain and G.M. Whitesides, "Correlations Between Wettability and Structure in Monolayers of Alkanethiols Adsorbed on Gold," *J. Am. Chem. Soc.* **1988**, *110*, 3665-3666; c) J.P. Folkers, P.E. Laibinis, J. Deutch and G.M. Whitesides,

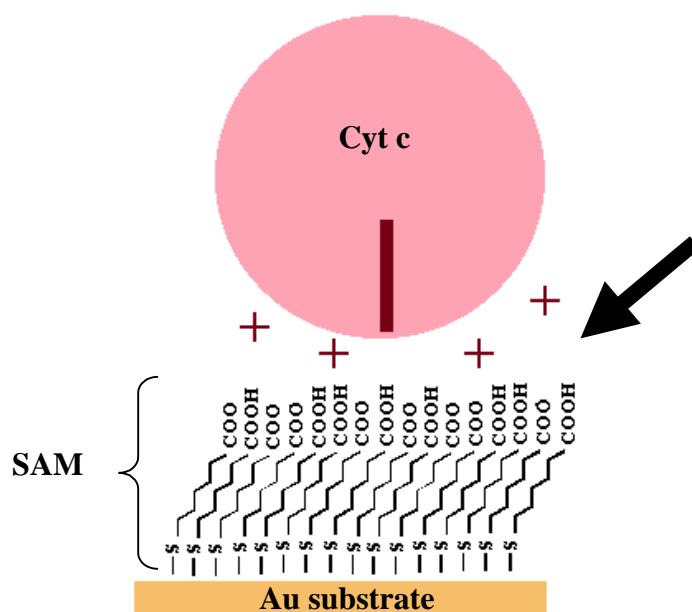
- “Phase Behavior of Two-Component Self-Assembled Monolayers of Alkanethiolates on Gold,” *J. Phys. Chem.* **1994**, *98*, 563-571; d) C.D. Bain and G.M. Whitesides, “Formation of Monolayers by the Coadsorption of Thiols on Gold: Variation in the Length of the Alkyl Chain,” *J. Am. Chem. Soc.* **1989**, *111*, 7164-7175; e) J.P. Folkers, P.E. Laibinis, and G.M. Whitesides, “Self-Assembled Monolayers of Alkanethiols on Gold: Comparisons of Monolayers Containing Mixtures of Short- and Long- Chain Constituents with CH<sub>3</sub> and CH<sub>2</sub>OH Terminal Groups,” *Langmuir* **1992**, *8*, 1330-1341; f) O. Chailapakul and R.M. Crooks, “Synthesis and Characterization of Simple Self-Assembling, Nanoporous Monolayer Assemblies: A New Strategy for Molecular Recognition,” *Langmuir* **1993**, *9*, 884-888; g) C. Miller, P. Cuendet, and M. Gratzel, “Adsorbed ω-Hydroxy Thiol Monolayers on Gold Electrodes: Evidence for Electron Tunneling To Redox Species in Solution,” *J. Phys. Chem.* **1991**, *95*, 877-886; h) D.A. Offord, C.M. John, and J.H. Griffin, “Contact Angle Goniometry, Ellipsometry, XPS, and TOF-SIMS Analysis of Gold-Supported, Mixed Self-Assembled Monolayers Formed From Mixed Dialkyl Disulfides,” *Langmuir* **1994**, *10*, 761-766; i) D.A. Offord, C.M. John, M.R. Linford and J.H. Griffin, “Contact Angle Goniometry, Ellipsometry, and TOF-SIMS Analysis of Gold-Supported, Mixed Self-Assembled Monolayers Formed From Alkyl Mercaptans,” *Langmuir* **1994**, *10*, 883-889.
39. a) S. Atre, B. Liedberg, and D.L. Allara, “Chain Length Dependence of the Structure and Wetting Properties in Binary Composition Monolayers of OH- and CH<sub>3</sub>- Terminated Alkanethiolates on Gold,” *Langmuir* **1995**, *11*, 3883-3893; b) K. Tamada, M. Hara, H. Sasabe, and W. Knoll, “Surface Phase Behavior of n-Alkanethiol Self-Assembled Monolayers Adsorbed on Au(111): An Atomic Force Microscope Study,” *Langmuir* **1997**, *13*, 1558-1566.
40. A.E. Kasmi, J.M. Wallace, E.F. Bowden, S.M. Binet, and R.J. Linderman, “Controlling Interfacial Electron-Transfer Kinetics of Cytochrome c with Mixed Self-Assembled Monolayers,” *J. Am. Chem. Soc.* **1998**, *120*, 225-226.
41. a) M.M. Walczak, D.D. Popenoe, R.S. Deinhammer, B.D. Lamp, C. Chung, and M.D. Porter, “Reductive Desorption of Alkanethiolate Monolayers at Gold: A Measure of Surface Coverage,” *Langmuir* **1991**, *7*, 2687-2693; b) M.M. Walczak, D.E. Weisshaar, and M.D. Porter, “Electrochemically Induced Transformations of Monolayers Formed by Self-Assembly of Mercaptoethanol at Gold,” *Langmuir* **1993**, *9*, 323-329.
42. a) J.Y. Gui, D.A. Stern, D.G. Frank, F. Lu, D.C. Zapien, and A.T. Hubbard, “Adsorption and Surface Structural Chemistry of Thiophenol, Benzyl Mercaptan, and Alkyl Mercaptans. Comparative Studies at Ag(111) and Pt(111) Electrodes by Means of Auger Spectroscopy, Electron Energy Loss Spectroscopy, Low-Energy Electron Diffraction, and Electrochemistry,” *Langmuir* **1991**, *7*, 955-963; b) J.Y. Gui, D.A. Stern, C-H. Lin, P. Gao, and A.T. Hubbard, “Potential-Dependent Surface Chemistry of Hydroxypyridines Adsorbed at a Pt(111) Electrode Studied by Electron Energy Loss Spectroscopy, Low Energy Electron Diffraction, Auger Electron Spectroscopy, and Electrochemistry,” *Langmuir* **1991**, *7*, 3183-3189.
43. B.D. Lamp, D. Hobara, M.D. Porter, K. Niki, and T.M. Cotton, “Correlation of Structure and Performance of Pyridinethiolate Surface Modifiers at Gold Electrodes for the Facilitation of Cyt c Heterogeneous ET Reactions,” *Langmuir* **1997**, *13*(4), 736-741.
44. E. Sabatani, J. Cohen-Boulakia, M. Bruening, and I. Rubinstein, “Thioaromatic Monolayers on Gold: A New Family of Self-Assembling Monolayers,” *Langmuir* **1993**, *9*, 2974-2981.

45. A. Mosca, R. Paleari, P. Arosio, A. Cricenti, M.A. Scarselli, R. Generosi, S. Selci, and E. Rovida, "Direct Observation of Human Liver Ferritin By Scanning Tunneling Microscopy," *J. Vac. Sci. Technol. B* **1994**, *12*(3), 1486-1489.
46. a) J. Vancea, G. Reiss, F. Schneider, K. Bauer, and H. Hoffmann, "Substrate Effects on the Surface Topography of Evaporated Au Films - An STM Investigation," *Surface Science* **1989**, *218*, 108-126; b) J. Ulstrup, *Surface Science* **1995**, *325*, 193-205.
47. a) L. Haussling, F.J. Schmitt, W. Knoll, and H. Ringsdorf, "Biotin-Functionalized Self-Assembled Monolayers on Gold: Surface Plasmon Optical Studies of Specific Recognition Reactions," *Langmuir* **1991**, *7*(9), 1837-1840; b) L. Haussling, B. Michel, H. Rohrer, and H. Ringsdorf, "Direct Observation of Streptavidin Specifically Adsorbed on Biotin-Functionalized Self-Assembled Monolayers with the Scanning Tunneling Microscope," *Angew. Chem. Int. Engl.* **1991**, *30*(5), 569-572.
48. a) M. Niwa, T. Mori, E. Nishio, H. Nishimura, and N. Higashi, "Specific Binding of Concanavalin A to Glycolipid Monolayers on Gold Electrodes," *J. Chem. Soc. Chem. Commun.* **1992**, 547-549; b) D. Mandler and I. Turyan, "Applications of Self-Assembled Monolayers in Electroanalytical Chemistry," *Electroanalysis* **1996**, *8*(3), 207-213.
49. a) E. Delamarche, M. Sprik, B. Michel, U. Rothlisberger, M.L. Klein, H. Wolf, and H. Ringsdorf, "Structure of Hydrophilic Self-Assembled Monolayers: A Combined Scanning Tunneling Microscopy and Computer Simulation Study," *Langmuir* **1994**, *10*, 4116-4130; b) E. Cooper and G.J. Leggett, "Influence of Tail-Group Hydrogen Bonding on the Stabilities of Self-Assembled Monolayers of Alkylthiols on Gold," *Langmuir* **1999**, *15*, 1024-1032; c) R.S. Clegg and J.E. Hutchison, "Hydrogen Bonding, Self-Assembled Monolayers: Ordered Molecular Films for Study of Through Peptide Electron Transfer," *Langmuir* **1996**, *12*(22), 5239-5243; d) G.E. Poirier, E.D. Pylant, J. White, *J. Chem. Phys.* **1996**, *105*, 2089; e) P. Tengrall, B. Liedberg, and N. Lestelius, *Langmuir* **1997**, *13*, 5900-5908.
50. a) M.D. Porter, T.B. Bright, D.L. Allara, and C.E.D. Chidsey, "Spontaneously Organized Molecular Assemblies. 4. Structural Characterization of n-Alkyl Thiol Monolayers on Gold by Optical Ellipsometry, Infrared Spectroscopy, and Electrochemistry," *J. Am. Chem. Soc.* **1987**, *109*, 3559-3568; b) R.G. Nuzzo, L.H. Dubois, and D.L. Allara, "Fundamental Studies of Microscopic Wetting on Organic Surfaces. 1. Formation and Structural Characterization of a Self-Consistent Series," *J. Am. Chem. Soc.* **1990**, *112*, 558-569; c) L.H. Dubois, B.R. Zegarski, and R. Nuzzo, "Fundamental Studies of Microscopic Wetting on Organic Surfaces. 2. Interaction of Secondary Adsorbates with Chemically Textured Organic Monolayers," *J. Am. Chem. Soc.* **1990**, *112*, 570-579.
51. E.F. Bowden Thesis, Virginia Commonwealth University - Appendix II.
52. J. Willit, Ph.D. Thesis, North Carolina State University, 1990.
53. T.M. Nahir, D. Tiani, D. Miller, R.J. Linderman, and E.F. Bowden, manuscript in preparation.
54. D.C. Harris, *Quantitative Chemical Analysis*, 3<sup>rd</sup> Ed., W.H. Freeman and Company: New York, 1991.

55. E. Margoliash and N. Frohwirt, *Biochem. J.* **1959**, *71*, 570.
56. Professor Chris Gorman's class notes from CH525 - Physical Methods in Organic Chemistry, 1996.
57. a) S.E. Creager and J. Clarke, "Contact-Angle Titrations of Mixed  $\omega$ -Mercaptoalkanoic Acid/Alkanethiol Monolayers on Gold. Reactive vs. Nonreactive Spreading, and Chain Length Effects on Surface  $pK_a$  Values," *Langmuir* **1994**, *10*, 3675-3683; b) E.W. van der Vegte and G. Hadziioannou, "Acid-Base Properties and the Chemical Imaging of Surface-Bound Functional Groups Studied with Scanning Force Microscopy," *J. Phys. Chem. B* **1997**, *101*, 9563-9569; c) H.S. White, J.D. Peterson, Q. Cui, and K.J. Stevenson, "Voltammetric Measurement of Interfacial Acid/Base Reactions," *J. Phys. Chem. B* **1998**, *102*, 2930-2934; d) T.R. Lee, R.I. Carey, H.A. Biebuyck, and G.M. Whitesides, *Langmuir* **1994**, *10*, 741; e) C.D. Bain and G.M. Whitesides, *Langmuir* **1988**, *5*, 1370; f) Y. Mo, M. Sandifer, C. Sukenik, R.J. Barriga, M.P. Soriaga, and D. Scherson, "In Situ QCM Studies of Molecular Adsorbates Containing Thiol and Hydroquinone Moieties Bound to Au(111) Surfaces in Aqueous Electrolytes," *Langmuir* **1995**, *11*, 4626-4628.
58. a) E.F. Bowden, R.A. Clark, J.L. Willit, and S. Song, "Protein Monolayer Electrochemistry: A Strategy for Probing Biological Electron Transfer Kinetics," In *Proceedings of the Fifth International Symposium on Redox Mechanisms and Interfacial Properties*, F. Shultz and I. Taniguchi, Eds., The Electrochemical Society: Pennington, New Jersey, 1993, 34-45; b) E.F. Bowden, "Wiring Mother Nature: Interfacial Electrochemistry of Proteins," *The Electrochemical Society:Interface*, **1997**, *6*, 40-44; c) J.D.H. Glenn and E.F. Bowden, "Diffusionless Electrochemistry of Cyt  $b_5$  Adsorbed on a Multilayer Film Electrode," *Chemistry Letters* **1996**, 399-400.

**THE CYT C / SAM INTERFACE:  
PRELIMINARY INVESTIGATIONS OF SAM HEALING  
AND  
SILVER UPD**

**CHAPTER FOUR**



*“Basic research is when I’m doing what I don’t know what I’m doing.” - Wernher von Braun*

#### **4. PRELIMINARY INVESTIGATIONS OF SAM HEALING AND SILVER UPD**

The next surface to address in the cyt c/SAM/Au system is the interface of the SAM and the protein. More specifically, this chapter deals with the surface of the SAM and how it relates to the adsorption and ET properties of cyt c. In contrast to the previous chapter, the research described or proposed in this chapter will explore this interface while maintaining the initial gold surface topography as a constant. There are numerous options for manipulating the SAM/solution interface. In light of the results of the experiments on the influence of the gold substrate and the conclusions made about the importance of SAM defect density on the adsorption and ET properties of cyt c, the research in this chapter primarily involves alternative testing of the same concepts addressed in Chapter 3. Here however, experiments are designed to affect the density of defects in the SAM by means other than altering the Au surface topography. Instead, physical manipulation of the SAM is incorporated as a way of varying SAM structure by either blocking or minimizing the occurrence of defect sites in the SAM. The SAMs are then subsequently characterized by many of the same techniques previously described, including their responsiveness to cyt c adsorption and ET.

Two types of experiments, in particular, comprise the bulk of this chapter. Both of these experimental concepts involve interesting SAM manipulations, as well as, address the need for altering the defect density of the SAM structure. Thermal healing of SAMs and SAMs assembled on Ag UPD layers on Au both seem to serve this project well and are included here because it is believed they would benefit the understanding of this system greatly if pursued further. The research on these subjects in the following sections are simply examples of the potential that these concept hold for delineating information about the cyt c/SAM/Au ET system.

##### **4.1 THERMAL HEALING OF SELF-ASSEMBLED MONOLAYERS**

In the literature are examples of the use of temperature to dramatically reduce the density of defects in thiol SAMs.<sup>1-3</sup> Elevated temperatures are typically applied during the self-assembly process, allowing for a form of thermal annealing referred to as thermal healing. During this heat treatment, the adsorbates comprising the SAM are energetically

activated to rearrange and diffuse laterally across the surface for optimal positioning, effectively “healing” many defects sites. In light of the results presented in Chapter 3, a decrease in SAM defect density should have a negative effect on cyt c’s adsorption and/or its electrochemical response. In addition to its obvious application to the cyt c system, low defect monolayers are of interest to many researchers involved in corrosion studies, nanolithography, and high quality dielectric materials for microelectronics.<sup>2</sup>

#### **4.1.1. Mechanistic Aspects of Thermal Healing of SAMs**

From the detailed work of Weiss, Allara and coworkers in a recent publication and references within that paper,<sup>2</sup> some of the mechanistic aspects of the thermal healing process have been elucidated. The overall effect of thermal healing of SAMs is the manifestation of several processes that occur while the SAM is kept immersed in the self-assembly solution at an elevated temperature for an extended amount of time. The temperature where the thermal healing of methyl-terminated SAMs of chain lengths of 10 and 12 occurs is suggested to be approximately 78° C.<sup>2</sup> However, increasing the temperature to this level causes several other events to take place. Initially, the temperature rises above room temperature where IR spectroscopy has revealed that alkyl chain gauche defects increase substantially. At 60° C, thiolate desorption becomes significant and X-ray diffraction studies have shown that a melting transition occurs in the film at 50 to 70°C. Therefore, at 70° C the degree of thermally induced disorder in the SAM is expected to be quite high. This disorder in the film allows for greater access of the solution to the gold surface through thermally induced defect sites.<sup>2</sup>

Because the self-assembly process is taking place during the thermal healing process, the exchange of thiols from solution at these defect sites is presumably enhanced. Organothiols exchange kinetics at defect regions are known to be much faster than at ordered domains of SAMs.<sup>4</sup> It is expected that the desorption of alkanethiols at defect sites is accelerated by the elevated temperatures and the increased solvation of the thiolates and thiolate-Au complexes. Chemical analysis of the thiol/ethanol solution during thermal healing revealed a continuously increasing gold content with assembly time.<sup>1</sup> It is hypothesized in the article by Weiss et al. that the desorption of alkanethiolates from the surface occurs primarily at the edges of ordered SAM domains and at other lower coverage

regions and is not favored at highly ordered domains.<sup>2</sup> Furthermore, the higher temperatures encourage increased lateral diffusion of anchored thiols as well as the Au itself. All of these processes result in for Ostwald ripening, where the size of highly ordered SAM terraces are ultimately limited only by the properties of the underlying substrate.

The effects of thermal healing on SAMs is most evident in SPM imaging of these surfaces.<sup>2</sup> Most SPM images of SAMs contain topographical depressions in the self-assembled films, or dark pits.<sup>5</sup> There is some controversy about the exact nature of these pits as they have been attributed to being caused by the accumulation of gauche defects in the thiol layer, a ramification of the topography of the Au substrate, or by the chemical erosion of gold atoms during the self-assembly process.<sup>1,5</sup> These pits are usually circular in nature, 2-6 nm in diameter, and tend to be 0.2-1.1 nm deep. In many instances the depth of the pits corresponds to the height of a Au step edge, approximately 0.29 nm. Depending on the experimental conditions of self-assembly, the pits can comprise 5-30% of the surface<sup>5d</sup> and are often lined with thiolate material rather than exposing bare gold. Pitting is considered to be a sign of significant defect density in SAMs.

An example of a SAM with this type of pitting from Weiss and coworkers is shown in Figure 4.1(top).<sup>2</sup> Dark pits are evident throughout this STM image of a n-mercaptododecane (C12) SAM formed on Au(111) grown on mica. The contrast within the SAM domains in this image is indicative of defects in the SAM. In an identical manner, separate SAMs were formed on gold by immersing the thiol deposition solution of approximately 1 mM in a water bath held at 78°C for 1 hour during the self-assembly process. The image of this thermally healed SAM is shown as Figure 4.1 (bottom). The dark depressions are no longer present in the image, suggesting that areas of disorder and defect density has have been drastically minimized. Similar experiments performed at various time increments during the thermal healing process revealed that the pits seem to mobilize and coalesce, moving to the edge of ordered domains or to step edges and grain boundaries.<sup>1</sup> These examples, while subject to certain criticisms inherent to the imaging process itself, suggest that thermal healing of SAMs may be a legitimate method to be considered for controlling the defect density of the SAMs used in cyt c electrochemistry.

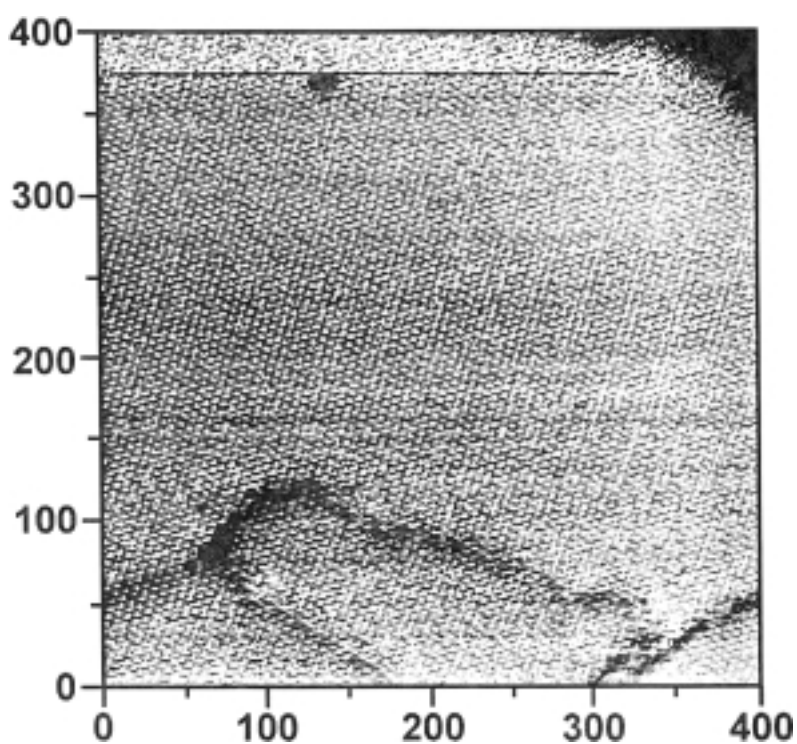
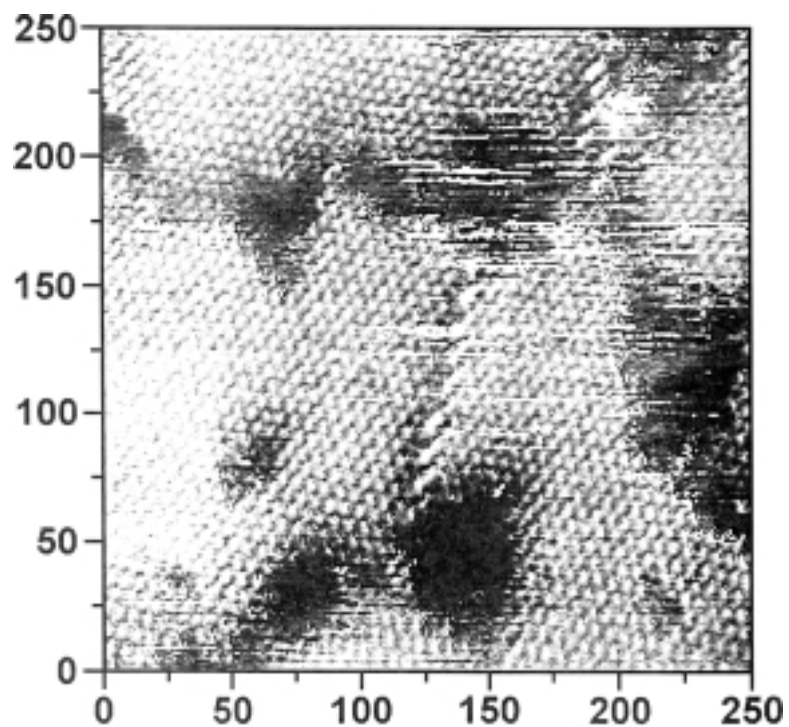


**Figure 4.1.** Example of SAM thermal healing effects: (*top*) STM image of n-dodecanethiol ( $\text{H}_3\text{C}(\text{CH}_2)_{11}\text{SH}$ ) SAM on gold; (*bottom*) STM image of the same type of SAM after thermal healing at  $78^\circ\text{C}$  for 1 hour in 1 mM n-dodecanethiol/ethanol solution. Images were obtained with a tip bias of +1.0 V and a tunneling current of 10 pA [axis marked in Angstroms] (Figure from Ref. 2).

## 4.2 RESULTS AND DISCUSSION -- THERMAL HEALING OF SAMs

Single component COOH SAMs were prepared on electrochemically cleaned Au substrates and subjected to thermal healing as described in the Experimental Details section of this chapter. Temperature was controlled using a water bath and jacketed electrochemical cell, an experimental set-up that seems to be superior to those described in the literature<sup>1-3</sup> because it minimizes many of the SAM and solution manipulations. Plus, one is able to monitor the film's electrochemical properties during the actual thermal healing process. The temperature of the thiol/ethanol deposition solution was carefully elevated to 77°C and held at that temperature for approximately one hour. The thermally healed SAMs were then compared to control SAMs formed using traditional preparation procedures involving a three day deposition period at room temperature. Characterization by redox probing and reductive SAM desorption were performed along with cyt c adsorption and voltammetry.

### 4.2.1. Cyt c Response -- Thermal Healing of SAMs

Figure 4.2 displays typical cyclic voltammetry of cyt c adsorbed on COOH SAMs prepared both traditionally and with thermal healing. Background subtracted voltammetry is included for further comparison. The thermally healed SAMs appear to have lower electroactive surface concentrations of adsorbed cyt c molecules. Table 4-1 summarizes the electrochemical properties of cyt c adsorbed on both thermally healed and control SAMs. Most notably, there seems to be significant changes in the aforementioned surface coverage ( $\Gamma$ ) as well as in the peak width (FWHM). On the other hand, there appears to be no significant change in ET kinetics as evidenced by the  $\Delta E_p$  and  $k_{et}^\circ$  parameters. The decrease in  $\Gamma$  and FWHM values for C<sub>11</sub>OOH SAMs due to thermal healing was present, but not as pronounced at longer chain lengths (C<sub>14</sub>OOH) (Results not shown).

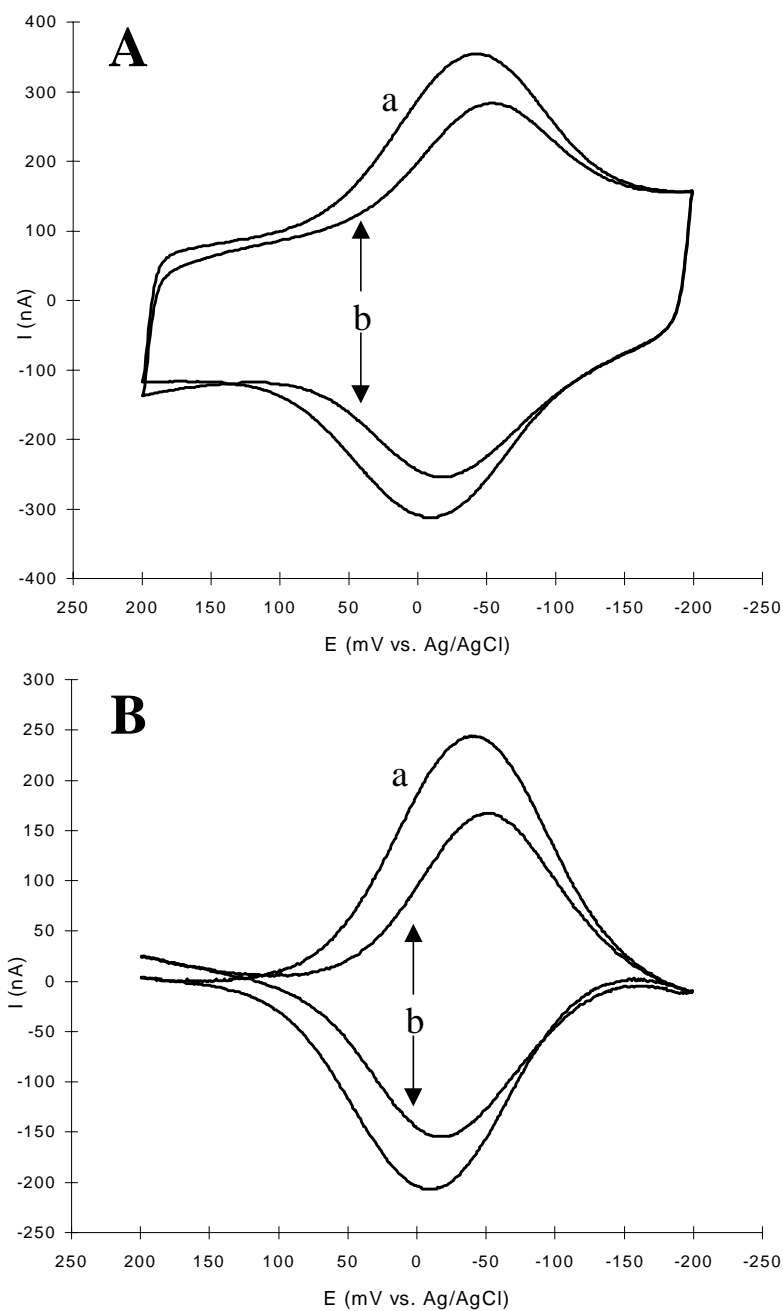


**Figure 4.2.** Cyclic voltammetry (A) and background subtracted cyclic voltammetry (B) of cyt c on  $C_{11}$  acid terminated SAMs that have been traditionally prepared (a) with electrochemically cleaned evaporated gold and normal SAM deposition procedures versus evaporated Au electrodes that have been electrochemically cleaned, modified with a  $C_{11}$  acid SAM and subsequently thermally heated for 1 hour at  $78^\circ\text{C}$  in thiol/ethanolic solutions (b) prior to cyt c adsorption.

**Table 4-1.** Cyt c / C<sub>11</sub>OOH Voltammetry - SAM Thermal Healing Results

System	SAM Prep.	E <sup>o'</sup> (mV) <sup>a</sup>	ΔE <sub>p</sub> (mV) <sup>b,c</sup>	Γ* (pmol/cm <sup>2</sup> ) <sup>b</sup>	FWHM (mV) <sup>b,c</sup>	k <sup>o</sup> et (s <sup>-1</sup> ) <sup>d</sup>
Cyt c / C <sub>11</sub> OOH	Traditional <sup>e</sup>	-35.6 (±3.1)	26 (±5)	12.8 / 11.9 (±2.1 / ±2.6)	134 / 130 (±7 / ±3)	3.1 (±0.6)
Cyt c / C <sub>11</sub> OOH	thermally healed <sup>f</sup>	-36.8 (±2.8)	32 (±9)	6.9 / 7.5 (±1.8 / ±2.0)	116 / 119 (±2 / ±1)	2.5 (±0.7)

<sup>a</sup> E<sup>o'</sup> values were calculated using the average of E<sub>p,a</sub> and E<sub>p,c</sub>.

<sup>b</sup> Measured at 100 mV/sec scan rate.

<sup>c</sup> Cathodic and anodic measurements shown, respectively.

<sup>d</sup> Determined using Laviron's theory for irreversible peak splitting (>200 mV) – (See Ch. 2);

<sup>e</sup> Traditional preparation involves electrochemically cleaning of evaporated gold electrodes, a 72 hour SAM deposition time, and a 1 hour cyt c adsorption, <sup>f</sup> thermal healing involves the same traditional preparation, but the SAM is immersed for 1 hour at ~78°C in a ~5 mM thiol/ethanolic solution (See Experimental Details section).

#### 4.2.2. HMFc Redox Probing of Thermally Healed SAMs

HMFc was used as a redox probe for comparing the permeability of thermally healed SAMs and control SAMs. Although there was no trademark anodic peak potential (E<sub>p,a</sub>) shift indicating a drastic reduction in the density of defects, there was a substantial decrease in faradaic current for the probe molecule. HMFc results are shown in Figure 4.3. The decrease of current on the thermally healed SAMs suggests that some defects have, in fact, been eliminated, although the peak shape clearly indicates that some defects persist.

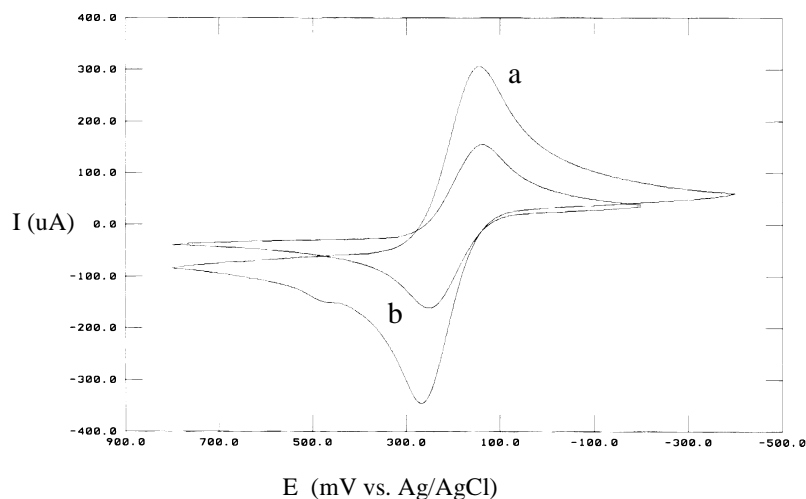


**Figure 4.3.** Cyclic voltammetry of the 2 mM HMFc redox probe at (a) C<sub>11</sub>OOH SAM traditionally prepared and at (b) a thermally healed C<sub>11</sub>OOH SAM. Solution conditions: 0.1 M HClO<sub>4</sub>; scan rate = 100 mV/sec.

Because examples in the literature used only methyl-terminated SAMs, questions arose over the use of acid terminated SAMs for this study. Acid terminated SAMs inherently possess a higher density of defects than methyl terminated SAMs.<sup>6</sup> Therefore, identical experiments were performed on SAMs of dodecanethiol to better assess the results obtained with COOH SAMs. An example is shown in Figure 4.4. As was seen with the acid terminated SAMs, the current from HMFC is also attenuated upon healing of the methyl terminated film. The peak shape indicates greater inhibition for the cathodic process, ostensibly because it is more difficult for  $\text{HMFC}^+$  to penetrate this hydrophobic layer. Results with both types of SAMs on electrochemically pretreated evaporated gold suggest that thermal healing lessens the defect density, but that a significant degree of defects remain.

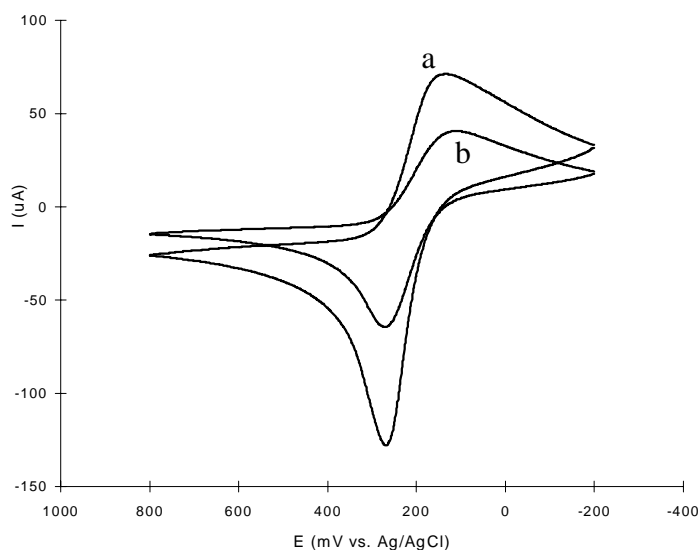


**Figure 4.4.** Cyclic voltammetry of 2 mM HMFC at (a) n-dodecanethiolate SAM, traditionally prepared versus at (b) n-dodecanethiolate SAM, thermally healed (experiments performed with electrochemically cleaned evaporated Au substrates).

#### 4.2.3. SAM Desorption Studies of Thermally Healed SAMs

Thermally healed SAMs were reductively desorbed in basic solution using LSV and compared to controls. Figure 4.5 shows some representative results. The broadened, multiple peak response for the control SAM (Figure 4.5) is typical for COOH SAMs prepared on electrochemically pretreated evaporated Au. This complex response is attributed to the polycrystalline nature of the Au surface as well as the variety of defects found on rougher Au. Upon thermal healing, however, the desorption voltammogram changes significantly. Although multiple peaks are still present, a significant sharpening of one peak occurs at the

expense of another peak and is accompanied by a slight positive shift in potential. The exact meaning of these results is not totally understood but it is thought that they could signify an increase in the ordering of the SAM after thermal healing.

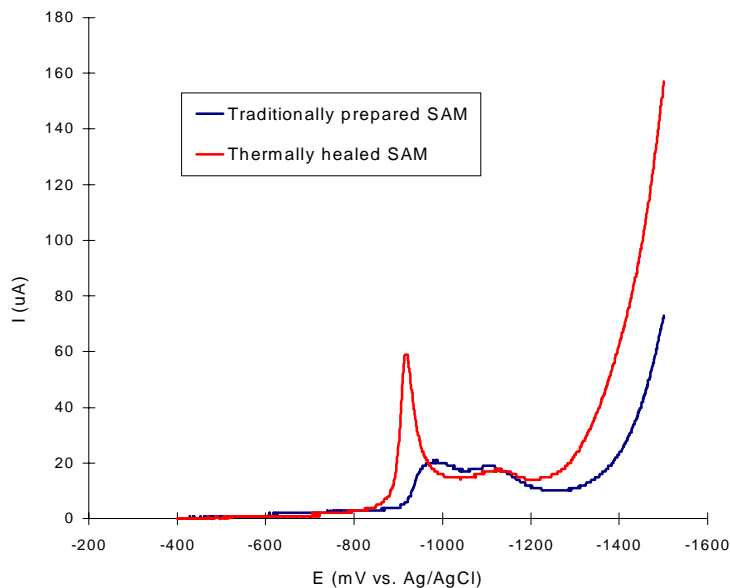


**Figure 4.5.** Linear sweep voltammetry scans of traditionally prepared and thermally healed 11-mercaptoundecanoic acid SAMs. Solution conditions: 0.5 M KOH; Scan rate = 100 mV/sec.

#### 4.2.4. Conclusions and Future Directions for Thermal Healing

Although the results of the thermal healing experiments are somewhat ambiguous, they seem to support the density of defects concept formulated in Chapter 3. Here again, cytochrome c adsorption seems to be favored on more defective surfaces. When the density of defects is reduced by thermal healing treatment, as confirmed by the redox probing and desorption experiments, the cytochrome c response is subsequently reduced as well. The attenuation in the electrochemical response of the protein apparently results from a lower concentration of cytochrome c on the surface, although this has not been independently confirmed, e.g., by XPS.

Why was the thermal healing treatment not more effective at eliminating the defects and why is the cytochrome c response only somewhat decreased? Several possibilities exist to account for these observations. First of all, the acid SAMs on evaporated Au may simply be inherently defective structures, beyond the repair capability of this treatment. If so, the permanent defectiveness of these SAMs can be largely attributed to the rough terrain of the evaporated Au surface in combination with the carboxylic acid headgroups. A more specific

hypothesis is that thermal healing is effective only on gauche conformational defects in the alkyl layer and has a very limited effect on SAM defects whose origins stem from more permanent topographical features (i.e. Au step edges and grain boundaries). Therefore, the ability to reduce defect density in SAMs using thermal healing may very well be more successful on SAMs that modify flatter, single crystal Au. It is recommended, therefore, that future experiments focus on Au substrates whose SAMs present predominantly gauche defects. In any event, the results of this study, while not definitive, are still supportive of the density of defects dependence of cyt c adsorption.

### **4.3 SILVER UNDERPOTENTIAL DEPOSITION BASED SAMs (Ag - UPD)**

In searching for methods to improve the stability and properties of Au/SAM structures for protein electrochemistry, the intriguing possibility of utilizing silver and copper UPD layers on the gold surfaces, prior to modification with  $\omega$ -substituted alkanethiols, was considered. Literature reports describe several improved structural and functional characteristics for SAMs deposited on the Ag and Cu UPD modified Au.<sup>8-12</sup> The immediate goal of this project was to assess the performance of COOH SAM/Ag-UPD/gold as a cyt c adsorption platform. Unfortunately, research priorities, time constraints, and unexpected experimental difficulties truncated this research at a relatively early stage. Still, the initial groundwork has been completed for future pursuit of this worthy objective.

#### **4.3.1. Underpotential Deposition - General Discussion**

The electrochemical deposition of a metal adlayer onto a foreign metal substrate can occur in one of two ways depending on the Gibbs free energy of interaction between the adsorbate and the substrate. If this interaction is weaker than the adsorbate-adsorbate interaction, the deposition will occur at electrochemical potentials lower, or more negative, than the equilibrium potential for bulk deposition. In this case, the adsorbate material will immediately begin to form a three-dimensional crystal structure as deposition commences. If, on the other hand, the adsorbate-substrate interaction is stronger than the adsorbate-adsorbate interaction, deposition will commence at a higher, or more positive potential, than that for bulk deposition. This process is known as underpotential deposition (UPD) and results in a single monolayer or less of deposited metal on the surface of the foreign substrate.

UPD metallic adlayers can be observed using voltammetry with slow scan rates that start at potentials sufficiently positive, where no deposition takes place, and sweep negatively toward deposition potentials before sweeping back again. Current spikes in the voltammetry represent the cathodic deposition and the subsequent oxidative stripping of the UPD layer. These spikes can be integrated for charge to determine amount of UPD coverage on the surface. UPD layers can be inserted into a variety of chemical systems, including SAM technology research.<sup>7</sup>

#### 4.3.2. Silver and Copper UPD Based SAMs on Gold

Although UPD layers of many combinations of metals can be created, Ag and Cu UPD layers on gold are of particular interest in SAM research. It has been reported that Ag and Cu UPD modified Au substrates support the formation of highly ordered and densely packed alkanethiol SAMs.<sup>8,9</sup> As shown in Figure 4.6, the UPD layer is a stable interlayer between the gold surface and the adsorbed thioliates.<sup>8,9</sup> The UPD layer is not etched away during the self assembly process and does not destroy the underlying gold texture.<sup>9</sup> Since these initial reports, a substantial amount of research has focused on studying the unique properties of these SAMs formed on both Ag<sup>8-10</sup> and Cu UPD layers.<sup>11</sup> A brief discussion of these research findings on these specific characteristics of Ag and Cu UPD based SAMs follows.

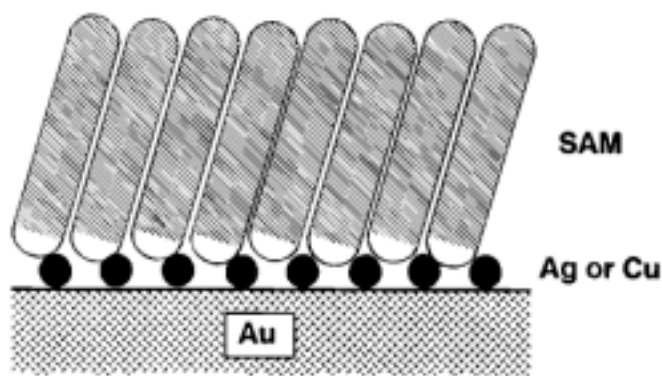


**Figure 4.6.** Schematic illustration of a gold / silver or copper UPD layer / alkanethiolate SAM assembly (Figure from Ref. 8).

The first significant property of UPD based SAMs we consider is their unique structure. The structure of Ag UPD based SAMs is markedly different from the structure of normal Au supported SAMs. The hydrocarbon chains of the UPD-SAM systems, which are

still primarily trans zig-zag in conformation, reside at a tilt angle of approximately  $20^\circ$  from surface normal, in contrast to  $30^\circ$  for alkanethiols on Au, or  $10^\circ$  for those formed on bulk Ag. Thus, the Ag-UPD based SAMs exhibit structural properties intermediate between those of the two parent metals, forming a hybrid SAM of sorts.

Ag and Cu UPD based SAMs have several other intriguing properties that make them attractive for potential cyt c/SAM interface applications. Ag UPD alkanethiol SAMs are extremely resistant to desorption at elevated temperatures and they exhibit much slower kinetics for solution-thiol exchange.<sup>8,9</sup> Considering that exchange kinetics have been linked to the density of defects in a film,<sup>4</sup> this observation suggests that the addition of the Ag-UPD layer may result in less defective SAMs. Along the same lines, addition of a Ag-UPD layer significantly extends the potential window for SAM-coated electrodes.<sup>8</sup> This characteristic results from a more effective electrode passivation by the SAM, a scenario best achieved by the formation of a very low defect, highly ordered SAM. Thus, it appears that these UPD anchored SAMs are more effective at preventing electrolyte solution from penetrating the SAM and accessing the Au surface.

Analogous properties have been discovered for Cu-UPD based SAMs.<sup>11</sup> SAMs formed on Au that is first modified with an adlayer of Cu tend to be extremely resistant toward electrochemical desorption and offer better protection against corrosive chemical attacks. An example from the work of Crooks and coworkers, shown in Figure 4.7, illustrates this enhanced property of Cu-UPD based SAMs. In Figure 4.7, both Au oxidation and Cu oxidation (the oxidation of the Cu UPD layer) have been effectively passivated by the modification with a sufficiently thick alkyl thiol. Furthermore, it is evident from Figure 4.7, that the effective potential window has been expanded by the presence of the Cu UPD layer.

The stability and structure of Ag and Cu UPD based SAMs has been largely attributed to the heightened interaction between the sulfur headgroups of the alkanethiols with the UPD-modified substrates, as well as, a larger degree of van der Waals alkane interactions.<sup>9</sup> However, it has been pointed out that the UPD process is highly dependent upon other experimental factors, most notably the anions present during the electrolyte. As will be seen, this is just one of the many nontrivial concerns to be considered when attempting to deposit UPD layers on metallic surfaces.

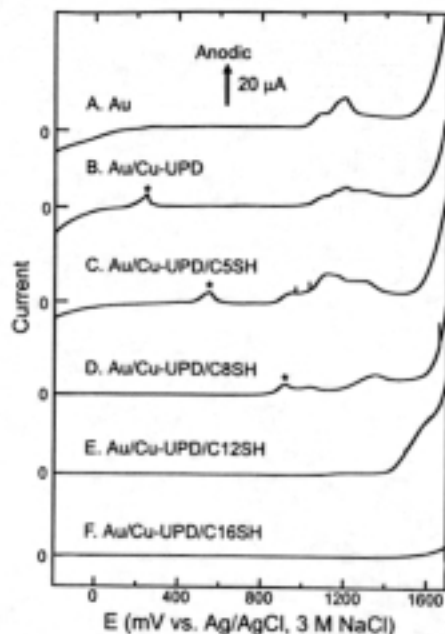


**Figure 4.7.** LSV of (A) Au, (B) Au / Cu-UPD, (C) Au / Cu-UPD / SAM – CH<sub>3</sub>(CH<sub>2</sub>)<sub>4</sub>SH, (D) Au / Cu-UPD / SAM - CH<sub>3</sub>(CH<sub>2</sub>)<sub>7</sub>SH, (E) Au / Cu-UPD / SAM - CH<sub>3</sub>(CH<sub>2</sub>)<sub>11</sub>SH and Au / Cu-UPD / SAM - CH<sub>3</sub>(CH<sub>2</sub>)<sub>15</sub>SH. Solution conditions: 0.1 M HClO<sub>4</sub> ; v = 10 mV/sec. Anodic peaks (\*) in scans B-D results from the oxidation of the Cu-UPD adlayer. Note that the oxidation potential of the Cu-UPD increases with increasing SAM thickness. On even thicker SAMs (scans E & F) neither Cu or Au oxidation is observed (Figure from Ref. 11c).

### 4.3.3. Methods of Depositing UPD Layers

A variety of methods exist for the UPD of Ag on Au and each type was explored before even attempting to involve cyt c in the system. Laibinis and coworkers used a simple cyclic voltammetry technique where the potential of the gold working electrode was scanned from 200 to 650 mV (vs. Ag<sup>0/+</sup> RE) and held for some time at a potential just negative (~50 mV) of the UPD peak.<sup>8,9</sup> In examining a survey voltammogram of a similar system, the choice of the parameters is justified (See Figure 4.8). The potential range is chosen to avoid any significant oxidation of Au (@ > 700 mV) and before the reduction of bulk Ag (@ < -50 mV). By restraining this experiment to this potential window (+0.200 ↔ +0.650) the activity of these reactions is minimized, allowing smaller backgrounds to help elucidate the small, sharp UPD peaks (not shown in Figure 4.8). Work by Gewirth and coworkers demonstrated that scanning the potential beyond these limits results in the loss of sharp UPD features and possible shifts in the UPD peak position, making the UPD peaks much more difficult to identify.<sup>7a</sup>

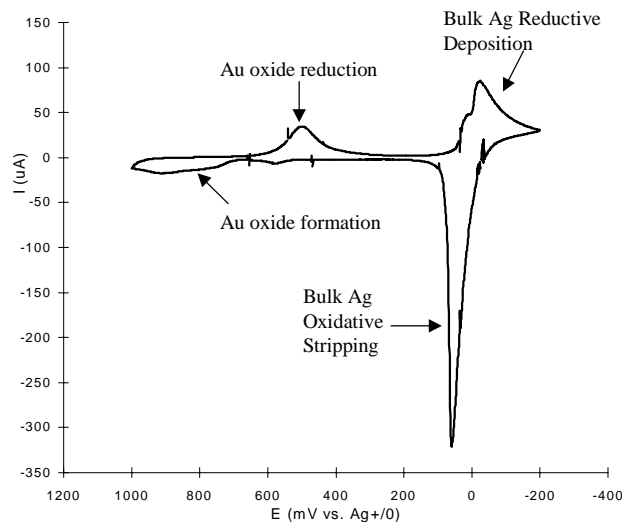


**Figure 4.8.** Survey cyclic voltammetry: 0.6 mM  $\text{Ag}_2\text{SO}_4$  in 0.1 M  $\text{H}_2\text{SO}_4$ ; 20 mV/sec. Potential window for Ag UPD layer redox processes is expected to be between +0.2 and +0.6 V – before bulk Ag redox activity and out of the region where Au-oxide (Au-oxidation) occurs.<sup>7-9</sup>

Researchers in Hawkrige's laboratory,<sup>10</sup> developed a chronocoulometry method for depositing UPD layers on gold in conjunction with a quartz crystal microbalance (QCM). The general waveform, shown in Figure 4.9, involves initially stepping the potential to a point much more negative than the UPD potential, but still positive of the bulk Ag deposition potential, so that the UPD process proceeds extremely fast. The potential is held at this point for some time until the UPD layer is completely formed and then stepped back to an intermediate potential that effectively shuts down the UPD process. This technique is significantly aided with the use of the QCM, which can independently signal the completion of a Ag UPD layer on the Au surface. Without a QCM, it is much more difficult to evaluate the progress of UPD layer formation.

#### 4.3.4. Results and Discussion -- Ag UPD Layers

Experiments were first carried out with the objective of depositing a reproducible Ag UPD layer on the evaporated Au substrates. Unfortunately, many of these experiments were unsuccessful, producing results that were hard to interpret and nearly as difficult to reproduce. The first attempts at producing a Ag UPD layer on Au involved the use of electrochemically cleaned evaporated Au films and a Ag/AgCl reference electrode, but this led to problems with chloride contamination. Based on these results and on literature reports,<sup>8,9</sup> it was decided to utilize a  $\text{Ag}^{+/0}$  reference electrode, a Au wire counter electrode,

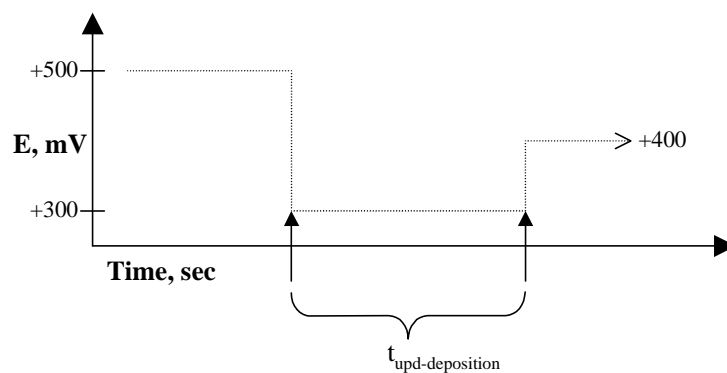


**Figure 4.9.** Waveform of the chronocoulometry experiment depositing Ag-UPD layers on gold.<sup>10</sup> For the experiments in this research, this waveform was used by stepping the potential to a value low enough to induce the UPD process (deposition) at approximately +300 mV, holding the potential at that magnitude for a set amount of time ( $t_{\text{upd-deposition}} = 10\text{-}180$  sec.), and then stepping back to an intermediate or the initial potential, +400 mV or +500 mV, respectively.

and an alternative cleaning procedure, namely piranha cleaning. The use of a  $\text{Ag}^{+/0}$  RE eliminates a source of chloride contamination and the piranha cleaning provides a surface that is free of organic contaminants, as well as chloride. Further experimental aspects are laid out in the Experimental Details Section of this chapter.

Ag UPD is expected to appear in the 500-550 mV (vs.  $\text{Ag}^{+/0}$ ) range as sharp singular peaks, similar to those shown in the literature example in Figure 4.10. In this project, however, the cyclic voltammetry method of depositing Ag UPD layer produced results such as that shown in Figure 4.11. Although cathodic and anodic peaks did appear in approximately the correct potential range, they were inferior to those reported in the literature (Figure 4.10).

Less-than-spectacular results were also achieved using the chronocoulometry method described by Hawkrige and coworkers.<sup>10</sup> To deposit the UPD layer, a potential step to +500 mV was applied for 10 seconds, followed by a potential step to +300 mV for 30 seconds. Afterward, a linear scan toward positive potentials was commenced to oxidatively remove the Ag UPD layer. An anodic spike of current during this type of scan would support the existence of the Ag UPD layer on the Au surface. In many instances, an anodic spike of current was recorded and, based on its size and nature, attributed to Ag UPD oxidation (Results not shown). However, these results were also difficult to repeat and lacked consistency and clarity. Furthermore, the charge passed during the chronocoulometry was noticeably lower than expected, a result also obtained by other researchers.<sup>7a,12</sup>

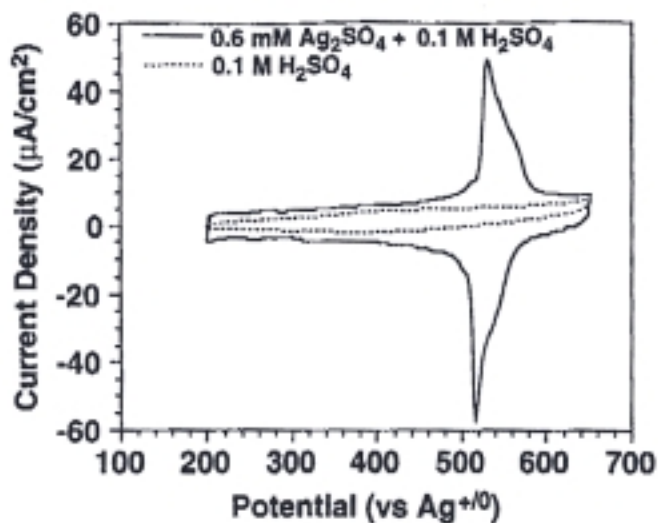


**Figure 4.10.** Example of cyclic voltammetry showing the characteristically sharp peaks of the UPD layer deposition and oxidative stripping (Figure from Ref. 12).

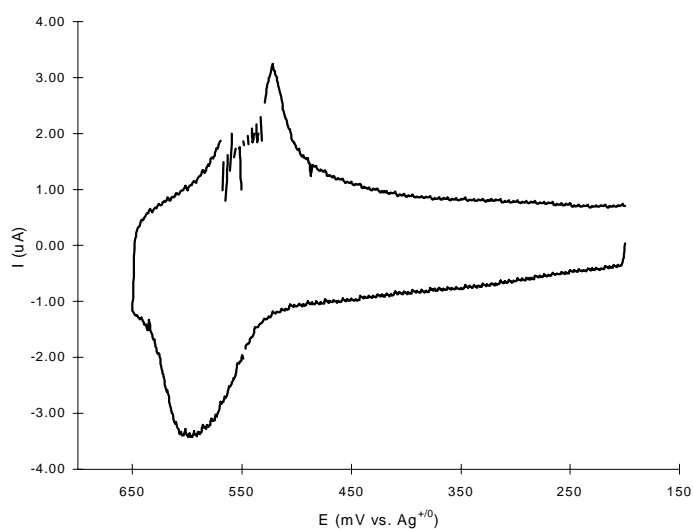


**Figure 4.11.** Cyclic voltammetry of Ag-UPD experiment on piranha cleaned evaporated gold. Peaks centered around +550 mV are suspected to be the result of the Ag-UPD layer being deposited by reduction and oxidized (stripped) off the surface. The peaks, however, appear to be uncharacteristic of UPD voltammetry seen in the literature.<sup>12</sup>

In spite of the difficulties encountered with depositing a reproducible UPD layer, some experiments with SAMs were undertaken and yielded interesting results. The first SAM experiments focused on UPD modified gold, which have previously been described in the literature.<sup>7-10</sup> After repeated application of a chronocoulometric waveform to strip and deposit a Ag UPD layer on the gold, a final UPD layer was deposited with a step to +300 mV for 180 seconds. Afterward, an octanethiol SAM was immediately formed on the UPD

modified surface. Likewise, SAMs without UPD layers were also prepared as a control group. These SAMs were then characterized with redox probe voltammetry and reductive desorption voltammetry. The results of HMFC probing are shown in Figure 4.12. From these results, the SAM atop the Ag-UPD layer exhibits vastly improved blocking ability toward the redox probe than the control SAM.

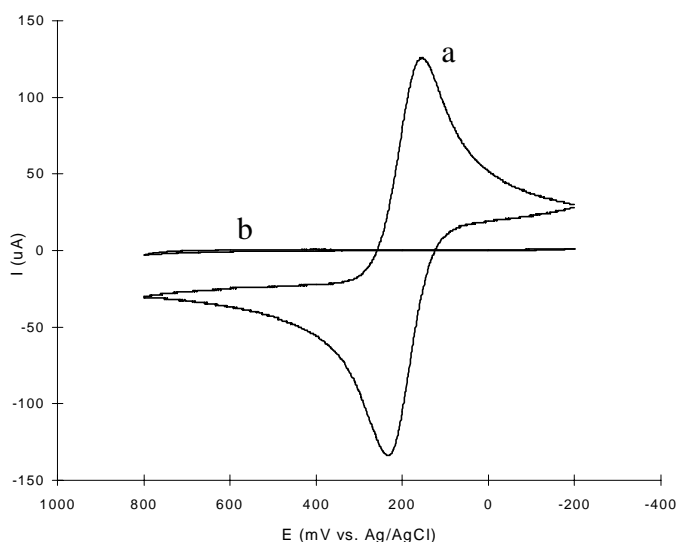


**Figure 4.12.** HMFC (0.2 mM) redox probe voltammetry at a n-octanethiol SAM on evaporated Au (**a**) and at a n-octanethiol SAM on Ag-UPD modified evaporated Au (piranha cleaned) (**b**) – Solution conditions: 0.1 M HClO<sub>4</sub> ; 100 mV/sec.

A reductive desorption sweep for octane thiol/Ag-UPD/gold is shown in Figure 4.13. No significant desorption peaks were detected in contrast to control SAM experiments, which exhibit multiple peaks at -1.0 to -1.2 V (See Figure 4.5). The lack of a desorption wave suggests that the SAM has been stabilized considerably by the presence of the UPD layer. These results seem consistent with the HMFC probe results, and together they indicate that a pure alkyl SAM on a Ag-UPD layer are more ordered with fewer defects than SAMs on Au. Nonetheless, because these UPD experiments were difficult to reproduce, any firm conclusions should wait until additional experiments are performed.

Why were these results so difficult to manufacture, reproduce, and understand? Several reasons for these difficulties became elucidated during this research. First of all, Ag UPD deposition is expected almost 500 mV positive of the bulk Ag reduction (see Figure 4.8). In the case of sulfate electrolytes, which are usually advantageous for Ag-UPD layer formation, it is known that unpredictable anionic discharge can occur.<sup>7a</sup> As a result, the

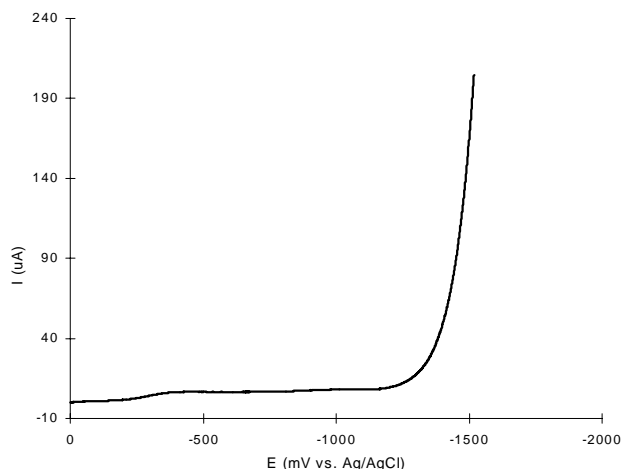


**Figure 4.13.** LSV SAM desorption sweep of an octane thiol SAM on Ag-UPD modified evaporated Au.

charge passed during deposition can be indiscriminate and non-quantitative. The anion discharge phenomenon, which is not well understood, renders the chronocoulometry method of depositing UPD layers much more difficult because the charge passed cannot be correlated to surface coverage. The choice of Au substrate also plays a critical role in forming quality UPD modified Au for supporting SAMs. It has been suggested by Jennings and coworkers that piranha-cleaned Au performs poorly in both UPD and self-assembly experiments. Conversely, freshly evaporated Au, used soon after creation, seems to have a much better reputation in UPD experiments.<sup>12</sup>

Experiments were performed with Au freshly evaporated onto clean glass mounts. The experiments were run only hours after the Au had been evaporated. Using CV, a Ag-UPD layer was deposited on the fresh gold surface and subsequently stripped off, as shown in Figure 4.14. The voltammetry is still not first rate but does come closer to resembling the UPD voltammetry shown in Figure 4.10. This result could not be reproduced after the Au substrate had aged 48 hours, indicating that ambient contamination impacts the Ag-UPD on gold quite significantly.

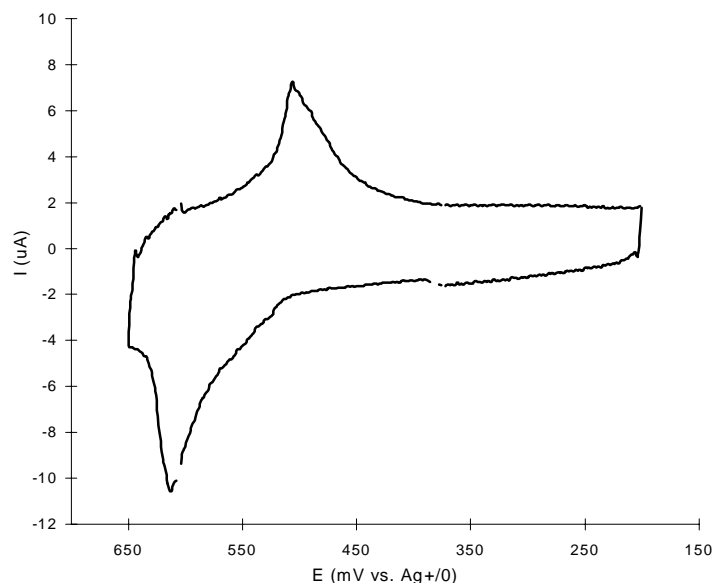


**Figure 4.14.** Stripping / depositing voltammetry of Ag-UPD layer on a freshly prepared evaporated Au film on a glass substrate. Solution conditions: 0.6 mM  $\text{Ag}_2\text{SO}_4$  in 0.1 M  $\text{H}_2\text{SO}_4$ ;  $v = 20$  mV/sec. This figure can be directly compared with Figure 4.10.

#### 4.3.5. Piranha Cleaning vs. Electrochemical Cleaning -- The Cyt c Response

One offshoot of this UPD venture was the implementation of piranha cleaning for Au electrodes. Piranha cleaning is quick, simple, and involves immersing the Au substrate in a solution comprised of concentrated sulfuric acid and hydrogen peroxide (30%) in a ratio of 4:1 for approximately 30 seconds while stirring. Further experimental details for piranha cleaning can be found at the end of this chapter. Piranha cleaning has the additional advantage of not exposing the gold surface to chloride ions. It was of interest to investigate how piranha cleaning of gold alone affected the cyt c response on SAM as compared to the traditional electrochemically cleaned electrodes (Note: there are no UPD layers involved in these experiments). Typical CVs of cyt c adsorbed on  $\text{C}_{11}\text{OOH}$  SAMs modifying both electrochemically and piranha cleaned Au surfaces are shown in Figure 4.15. The electrochemical properties are summarized in Table 4-2. From these results, it seems that there is little difference between the two techniques. The only apparent differences noted are the slightly higher values for FWHM and  $\Delta E_p$  of the piranha cleaned systems. In addition, there appears to be a two-fold increase in  $k_{et}^\circ$  of the cyt c on electrochemically cleaned evaporated gold, a result perhaps due to the roughening effect of this pretreatment. These

results suggest that piranha cleaning, because of its ease and nondestructive nature, should be given serious consideration as an alternative method for cleaning evaporated Au surfaces for cyt c experiments.

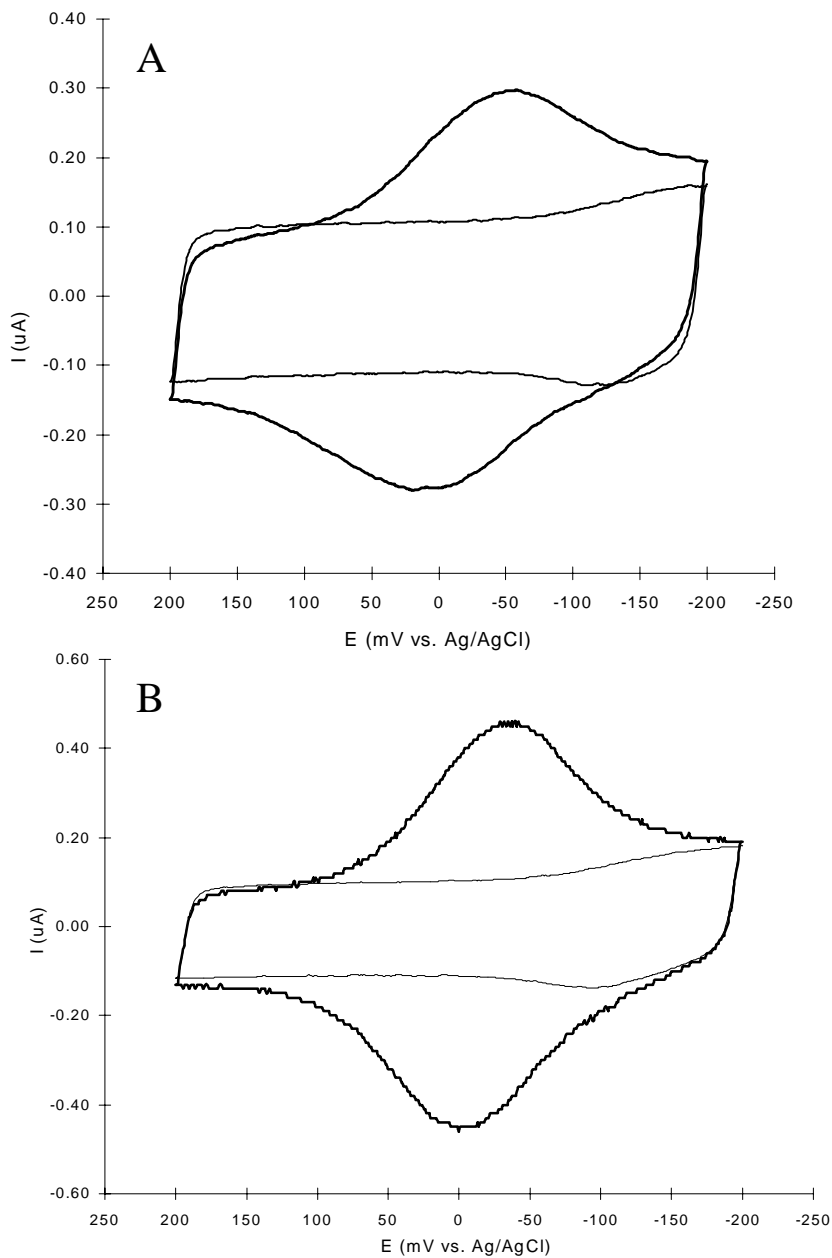


**Figure 4.15.** Cyclic voltammetry of cyt c adsorbed on a C<sub>11</sub>OOH SAM formed on (A) piranha cleaned evaporated gold and on (B) electrochemically cleaned evaporated gold. Voltammetry collected at 100 mV/sec in 4.4 mM KPB (pH=7) and is shown with corresponding SAM background signals, taken in the absence of adsorbed cyt c.

**Table 4-2.** Voltammetry Cyt c / C<sub>11</sub>OOH SAM - Electrochemical Properties (Piranha vs. Electrochemically Cleaned Evaporated Gold)<sup>a</sup>

System	Au Prep.	E <sup>o'</sup> (mV) <sup>b</sup>	ΔE <sub>p</sub> (mV) <sup>b</sup>	Γ* (pmol/cm <sup>2</sup> ) <sup>b,d</sup>	FWHM <sup>c</sup> (mV) <sup>b,d</sup>	k <sup>o</sup> et (s <sup>-1</sup> ) <sup>c</sup>
Cyt c / C <sub>11</sub> OOH	EC	-27.2 (±3.3)	36 (±8)	9.1 / 10.0 (±2.3 / ±2.6)	117 / 131 (±14 / ±22)	9.6 (±1.9)
Cyt c / C <sub>11</sub> OOH	PR	-23.2 (±4.1)	60 (±3)	6.8 / 7.9 (±1.3 / ±1.2)	130 / 153 (±6 / ±11)	5.1 (±0.6)

<sup>a</sup> Results based on a minimum of three experiments (cells) each.

<sup>b</sup> Measured at ≤100 mV/sec scan rate.

<sup>c</sup> Measured using Laviron's theory for irreversible peak splitting (>200 mV) – see Ch. 2.

<sup>d</sup> Cathodic and anodic measurements shown, respectively.

#### 4.3.6. Future Directions - Ag/Cu UPD Layers on Au

Unfortunately, this portion of the research never progressed to the point where Ag-UPD layers on gold were consistently produced with any degree of confidence. Therefore, the effect of these UPD layers on the structure of the SAM, as it relates to the eventual response of adsorbed cyt c on that SAM, remains largely unexplored. A logical next step in this project would be to produce these UPD layers on freshly evaporated Au films, or otherwise identify conditions leading to reproducible results. Many UPD researchers utilize silicon wafers as substrates for evaporated gold films.<sup>8,9,13</sup> To ensure mechanical stability of this type of substrate for UPD experiments, several pretreatments of the silicon wafer have been suggested, especially if the gold is evaporated onto the silicon without co-depositing an adhesion layer. Coating the Si wafer with (3-Mercaptopropyl) trimethoxysilane to act as an adhesive for the Au<sup>14</sup> and electroplating Ni onto freshly evaporated Au on mica and then electrochemically stripping the mica away are both ways of preparing “fresh” gold with stabilized Au(111) character.<sup>15</sup> From the results that have been presented here, it appears that using “fresh” gold provides the best chance at forming successful UPD layers.

Based on the encouraging preliminary results obtained on methyl-terminated SAMs, which indicate more stable and less defective SAMs result from using UPD layers, it would naturally be of interest to extend this work the COOH-type SAMs used for cyt c electrochemistry. The Ag-UPD/Au substrate could prove to be a most worthwhile platform for further exploration of the role of SAM defects on protein electrochemistry.

#### 4.4. FUTURE DIRECTIONS FOR THE SAM/CYT C INTERFACE

The possibilities for experiments that alter the SAM/solution interface are endless. Basically, developing SAM innovations in the literature can be applied to the cyt c/SAM interface in this research. Numerous experiments can be designed to specifically manipulate the density of defects in SAMs or to probe specific interactions between the protein and the surface. One of the more interesting concepts in the SAM literature dealing with defect sites involves blocking a significant amount of the defects in the SAM with a polymer.<sup>16</sup> This type of experiment, when applied to the cyt c system here, may help to divulge further information about the role of defect density in the cyt c electrochemistry. Other defect oriented future experiments may involve the incorporation of electroactive moieties such as ferrocene terminated alkanethiols into SAMs at defect sites.<sup>8,17</sup>

As far as the actual SAM being employed in these studies, SAMs of multiple combinations of chain lengths and endgroups can be employed to emphasize different degrees of hydrophobic, electrostatic, or other surface related intermolecular forces. Mixed SAMs of both Type I and Type II structure can be used to elucidate both defect site effects and interfacial interactions. More specifically, Type II SAMs can be formulated to create nano-sized adsorption sites in the SAM to test cyt c behavior in highly hydrophobic environments, thus elucidating the influence of hydrophobic forces in the system. A similar study involving ferrocene molecules on SAMs where they are encapsulated in hydrophobic environments has already been performed.<sup>18</sup> Additionally, a cyt c study designed to link the protein's adsorption to defect density can be achieved by systematically introducing defects into a uniform SAM as described in an article by Crooks and coworkers.<sup>19</sup>

Along the lines of manipulating defects in the SAM to see how cyt c adsorption is affected, it is proposed that SAMs formed on mercury films should be pursued in the future. SAMs formed on mercury have already been explored by Harrison and coworkers<sup>20</sup> and are of interest in this type of research because they are liquid-like and have no inherent surface structure. Therefore, as a substrate for a SAM, there would be no surface features (step edges, grain boundaries, etc.) to cause defects in the SAM. The electrochemical response of cyt c at these "ideal" Hg based SAMs would be interesting. Considering the results presented throughout this work, the response of cyt c such a platform is expected to be nonexistent, and

preliminary experiments have already supported this expectation.<sup>21</sup> It is further speculated that mixed SAMs on the same mercury films can be introduced to see if cyt c response is regenerated upon the installation of a new, rougher, molecularly textured surface. The interface of the SAM with the solution and how the surface of the SAM interacts with the cyt c remains a lucrative and largely untapped area of research for the future.

#### **4.5 SPECIAL ACKNOWLEDGEMENTS**

Several people contributed greatly to getting these initial experiments started. I would like to thank Melissa Rhoten of Professor Hawkridge's Research Group at VCU and a fellow JMU alumni for many informative and instructional discussions about the chronocoulometric method for depositing Ag UPD layers. Similarly, the UPD project was assisted greatly through repeated correspondence with both Dr. Paul Laibinis of the Massachusetts Institute of Technology and Dr. Kane Jennings of Vanderbilt University. Dr. Jennings was extremely helpful with advice on depositing the Ag UPD layers on gold. Appreciation is given to Mr. Lloyd Carroll of Dr. Gorman's Research Group for assistance with the preparation of "freshly" evaporated Au films.

#### **4.6 EXPERIMENTAL DETAILS**

Electrochemistry was performed as previously described in Chapter 3, using the same potentiostat, cell, solutions, and SAM deposition procedures. Specific differences in procedures and equipment that pertain to this chapter are highlighted below.

##### **4.6.1. Thermal Healing Experiments**

Thermal healing experiments were performed on evaporated Au substrates that were electrochemically cleaned as previously described in a cleaning solution of 0.1 M H<sub>2</sub>SO<sub>4</sub> and 0.01 M KCl. Both 11-mercaptoundecanoic acid and 14-tetradecanoic acid SAMs were prepared as outlined in the Experimental Details section of Chapter 3 for a fixed number of cells. After the normal deposition period of 72 hours, half of the cells were immediately rinsed, exposed to cyt c/KPB (10-25 μM) solution for 1 hour, and subsequently rinsed and tested for cyt c response. These cells were used as controls. The remaining cells were allowed to retain their thiol deposition solution ( 5mM thiol in ethanol) for the thermal

healing process. The cells were connected via their water jackets to a temperature controlled water bath (see Figure 4.16), and a thermometer was used to monitor the solution temperature just above the SAM layer. Prior to being connected to the experimental cells, the water bath was calibrated using a dummy cell equipped with a thermometer.

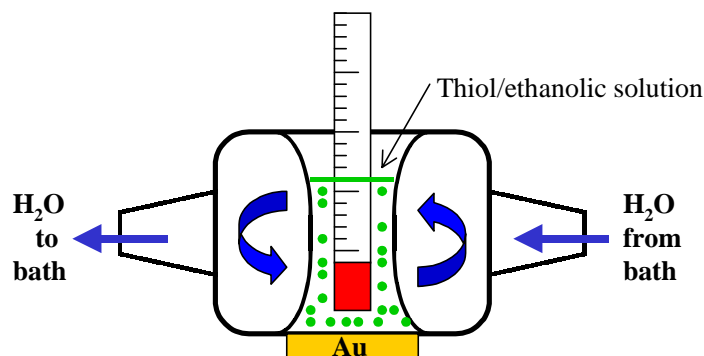


**Figure 4.17.** Experimental apparatus for thermal healing of SAMs in the electrochemical cell. A water bath is connected to the glass jacket of the cell and is allowed to circulate temperature controlled water continuously. By controlling the temperature of the water bath, the temperature within the cell, and subsequently around the SAM, can be manipulated and controlled as seen in Table 4-3. In this manner, the electrochemical cell can be used for temperature controlled (both heating and cooling) experiments on electrochemical systems.

The actual thermal healing process involved heating the deposition solution to 77-78°C and holding the cell at that temperature for one hour. CAUTION: Care is required because the deposition solution tends to evaporate and must be replenished from time to time during the 1 hour procedure. After completion of the thermal healing, the cell was removed from the water bath, rinsed in the usual way (with EtOH and M/Q H<sub>2</sub>O), exposed to cyt c solution in buffer for 1 hour, and tested for cyt c electroactivity.

#### 4.6.2. Ag UPD Experiments

Based on recent literature accounts,<sup>7a</sup> initial Ag UPD experiments were performed as cyclic voltammetry in a 0.6 mM Ag<sub>2</sub>SO<sub>4</sub> in 0.1 M H<sub>2</sub>SO<sub>4</sub> versus an in-house built Ag<sup>+0</sup> reference electrode and utilized a piranha cleaned evaporated Au substrates. Survey scans were performed in a potential window spanning from 1.0 V to -0.200 V. UPD deposition voltammetry involved a much smaller window (+200 to +400 mV) that avoids both bulk Ag redox processes and precedes the Au oxidation region at higher positive potentials.

The second stage of Ag-UPD experiments involved the asymmetric double potential step, chronocoulometry technique described in literature by Hawkrige's laboratory.<sup>10</sup> The actual waveform of this technique is the focus of Figure 4.9. These experiments, like the

previous UPD experiments, all took place on piranha cleaned evaporated Au substrates, utilized the same  $\text{Ag}^{+/0}$  reference as before, as well as, the same Ag solution. The potential was stepped to +300 mV and held there for 90-180 seconds. In some instances, voltammetry was performed immediately after the potential step and step time to voltammetrically strip off the deposited UPD layer. This was largely done to verify the chronocoulometry was successful. Control SAMs and the experimental UPD SAMs were then probed with HMFC and desorbed with LSV as described in Chapter 3.

The last round of Ag-UPD involved voltammetry scans in 0.6 mM  $\text{Ag}_2\text{SO}_4$  and 0.1 M  $\text{H}_2\text{SO}_4$  at freshly evaporated gold on glass substrates. Scanned from +0.200 to +0.650 V, all of the successful UPD experiments on these substrates were performed on the same day as the gold was evaporated.

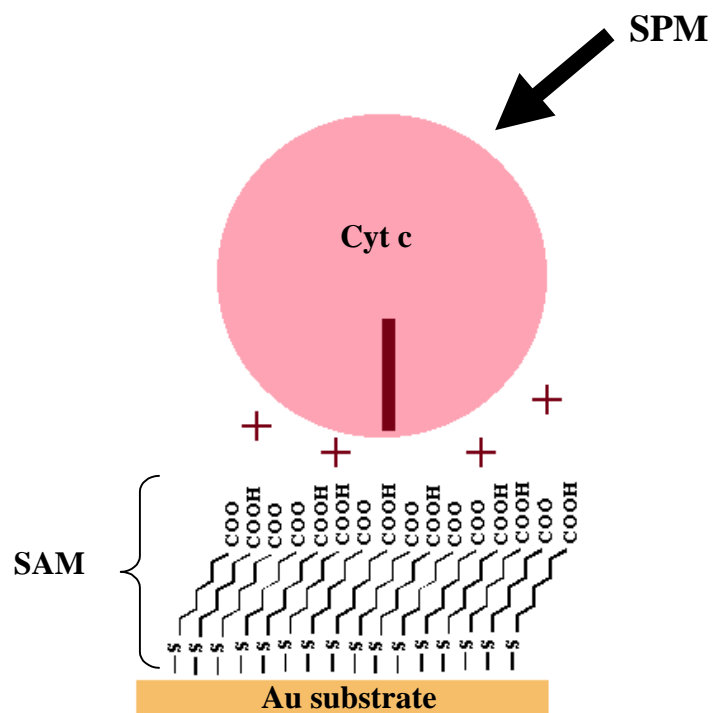
## 4.7 REFERENCES

1. J.P.Bucher, L. Santesson, and K. Kern, "Thermal Healing of Self-Assembled Organic Monolayers: Hexane- and Octadecanethiol on Au(111) and Ag(111)," *Langmuir* **1994**, *10*(4), 980-983.
2. L.A. Bumm, J.J. Arnold, L.F. Charles, T.D. Dunbar, D.L. Allara, and P.S. Weiss, "Creating Molecular Terraces with Molecularly Sharp Boundaries in Organic Thin Films," Preprint submitted to Science.
3. E. Delamarche, H.A. Biebuyck, B. Michel, and C. Gerber, "Golden Interfaces: The Surface of Self-Assembled Monolayers," *Advanced Materials* **1996**, *8*(9), 719-729.
4. a) C.E.D. Chidsey, C.R. Bertozzi, T.M. Putvinski, and A.M. Mujsce, *J. Am. Chem. Soc.* **1990**, *112*, 4301-4306; b) D.M. Collard and M.A. Fox, *Langmuir* **1991**, *7*, 1192-1197.
5. a) G.E. Poirier and E.D. Pylant, "The Self-Assembly Mechanism of Alkanethiols on Au(111)," *Science* **1996**, *272*, 1145-1148; b) G.E. Poirier and M.J. Tarlov, "Molecular Ordering and Gold Migration Observed in Butanethiol Self-Assembled Monolayers Using Scanning Probe Microscopy," *J. Phys. Chem.* **1995**, *99*, 10966-10970; c) C. Schonberger, J.A.M. Sondag-Huethorst, J. Jorritsma, and L.G.J. Fokkink, "What Are the 'Holes' in Self-Assembled Monolayers of Alkanethiols on Gold?," *Langmuir* **1994**, *10*(3), 611-614; d) C. Schonberger, J.A.M. Sondag-Huethorst, and L.G.J. Fokkink, "Formation of Holes in Alkanethiol Monolayers on Gold," *J. Phys. Chem.* **1994**, *98*, 6826-6834.
6. H. O. Finklea, "Electrochemistry of Organized Monolayers of Thiols and Related Molecules on Electrodes," A.J. Bard and I. Rubinstein (Eds.), *Electroanalytical Chemistry - A Series of Advances*, Vol. 19, 108-335, Marcel Dekker: New York, New York, 1996.
7. a) C. Chen, S.M. Vesecky, and A.A. Gewirth, "In Situ Atomic Force Microscopy of Underpotential Deposition of Ag on Au(111)," *J. Am. Chem. Soc.* **1992**, *114*, 450-458; b) W.J. Lorenz, I. Moutzisz, and E. Schmidt, *J. Electroanal. Chem.* **1971**, *33*, 121-133; c) D.P. Sandoz, R.M. Peekema, H. Freund, and C.F. Morrison, "The Deposition and Stripping of Thin Films of Silver at Gold and Platinum Electrodes - A Study of the Multiple Deposition and Stripping Current Peaks," *J. Electroanal. Chem.* **1970**, *24*, 165-174.
8. G.K. Jennings and P.E. Laibinis, "Self-Assembled n-Alkanethiolate Monolayers on Underpotentially Deposited Adlayers of Silver and Copper on Gold," *J. Am. Chem. Soc.* **1997**, *119*, 5208-5214.
9. G.K. Jennings and P.E. Laibinis, "Underpotentially Deposited Metal Layers of Silver Provide Enhanced Stability to Self-Assembled Alkanethiol Monolayers on Gold," *Langmuir* **1996**, *12*, 6173-6175.
10. J.D. Burgess and F.M. Hawkridge, "Octadecyl Mercaptan Sub-monolayers on Silver Electrodeposited on Gold Quartz Crystal Microbalance Electrodes," *Langmuir* **1997**, *13*, 3781-3786.

11. a) M. Nishizawa, T. Sunagawa, and H. Yoneyama, "Underpotential Deposition of Copper on Gold Electrodes Through Self-Assembled Monolayers of Propanethiol," *Langmuir* **1997**, *13*, 5215-5217; b) G.K. Jennings, J.C. Munro, T.-H. Yong, and P.E. Laibinis, "Effect of Chain Length on the Protection of Copper by n-Alkanethiols," *Langmuir* **1998**, *14*, 6130-6139; c) F.P. Zamborini, J.K. Campbell, and R.M. Crooks, "Spectroscopic, Voltammetric, and Electrochemical Scanning Tunneling Microscopic Study of Underpotentially Deposited Cu Corrosion and Passivation with Self-Assembled Organomercaptan Monolayers," *Langmuir* **1998**, *14*, 640-647; d) S.E. Gilbert, O. Cavalleri, and K. Kern, "Electrodeposition of Cu Nanoparticles on Decanethiol-Covered Au(111) Surfaces: An in Situ STM Investigation," *J. Phys. Chem.* **1996**, *100*(30), 12123-12130.
12. Personal correspondence with Dr. Kane Jennings, Vanderbilt University.
13. D. Stamou, D. Gourdon, M. Liley, N.A. Burnham, A. Kulik, H. Vogel, and C. Duschl, "Uniformly Flat Gold Surfaces: Imaging the Domain Structure of Organic Monolayers Using Scanning Force Microscopy," *Langmuir* **1997**, *12*, 2425-2428.
14. C.A. Goss, D.H. Charych, and M. Majda, "Application of (3-Mercaptopropyl) trimethoxysilane as a Molecular Adhesive in the Fabrication of Vapor-Deposited Gold Electrodes on Glass Substrates," *Anal. Chem.* **1991**, *63*, 85-88.
15. P. Samori, J. Diebel, H. Lowe, and J.P. Rabe, "Template-Stripped Gold Supported on Ni as a Substrate for SAMs," *Langmuir* **1999**, *15*, 2592-2594.
16. H.O. Finklea, D.A. Snider and J. Fedyk, "Passivation of Pinholes in Octadecanethiol Monolayers on Gold Electrodes by Electrochemical Polymerization of Phenol," *Langmuir* **1990**, *6*, 371-376.
17. a) C.E.D. Chidsey, C.R. Bertozzi, T.M. Putvinski, and A.M. Majsce, "Coadsorption of Ferrocene-Terminated and Unsubstituted Alkanethiols on Gold: Electroactive Self-Assembled Monolayers," *J. Am. Chem. Soc.* **1990**, *112*, 4301-4306; b) S.E. Creager, L.A. Hockett, and G.K. Rowe, "Consequences of Microscopic Surface Roughness for Molecular Self-Assembly," *Langmuir* **1992**, *8*, 854-861.
18. S.E. Creager and G.K. Rowe, "Redox and Ion Pairing Thermodynamics in Self-Assembled Monolayers," *Langmuir* **1991**, *7*, 2307-2312.
19. O. Chailapakul and R.M. Crooks, "Synthesis and Characterization of Simple Self-Assembling, Nanoporous Monolayer Assemblies: A New Strategy for Molecular Recognition," *Langmuir* **1993**, *9*, 884-888.
20. A. Demoz and D.J. Harrison, "Characterization of Extremely Low Defect Density Hexadecanethiol Monolayers on Hg Surfaces," *Langmuir* **1993**, *9*, 1046-1050.
21. E.F. Bowden, Jim Kelly, and J. Odea, results unpublished.

**THE CYT C/SAM/GOLD SYSTEM ON A MOLECULAR LEVEL:  
A SCANNING PROBE MICROSCOPY STUDY**

**CHAPTER FIVE**



*“God made the solid state, He left the surface to the Devil.” – Enrico Fermi*

## 5. THE CYT C/SAM/Au SYSTEM ON A MOLECULAR LEVEL: A SCANNING PROBE MICROSCOPY STUDY

The final chapter of this dissertation describes efforts direct toward imaging and characterizing cyt c/SAM/Au interfaces with scanning probe microscopy (SPM). SPM techniques such as scanning tunneling microscopy (STM) and atomic force microscopy (AFM) are used to describe the surfaces of the gold substrates, SAMs, and proteins involved with this type of research. SPM provides the unparalleled opportunity to probe these interfaces at a molecular level, illuminating a degree of detail crucial to the overall understanding of this ET model system. Unlike a population experiment, like electrochemistry, SPM is capable of exploring the specific electronic states and topographical features of a surface or interface. Understanding these types of properties in a chemical system is essential to any successful surface science. With SPM, a more detailed molecular understanding of the cyt c/SAM/Au system can be achieved, further defining the ET system and promoting PME as an effective tool for studying ET.

Although SPM has enjoyed a rich amount of research attention in recent years,<sup>1</sup> it is a relatively new direction in the Bowden Research Group. Because of its unprecedented use in the Bowden Laboratory, progress toward established goals has been slow but has made some significant strides. Much of this chapter is dedicated to the research that has been completed to date on this subject, while other major parts of this chapter discuss the reasons for failed results, as well as, prospective experiments for the future. Discussion about how the individual SPM techniques operate is reserved for the Experimental Details Section of this chapter (Section 5.6).

To fully grasp the potential application of SPM to the cyt c/SAM/Au system, a review of some of the specific goals set forth in the Bowden Research Group is appropriate at this time. Beyond the successful imaging of each major surface involved with this system, other research goals involved the accurate determination of cyt c coverage and their spatial distribution on the SAM surface. Much of the proposed work revolves around exploring the adsorption sites of the SAM. SPM imaging of the gold surface, as well as, the surface of the SAM interface with solution provide a means of evaluating the microscopic characteristics of different defect/adsorption sites and will greatly benefit the ultimate determination of their

structure-function relationship.<sup>2</sup> Delineating the microinterfacial environments at specific cytochrome c adsorption sites, such as those localized at defect sites versus sites in highly ordered, defect-free portions of the SAM, is of extreme interest. Eventually, it is foreseen that SPM techniques could be utilized on this system to identify or differentiate between individually adsorbed, electroactive or electroinactive cytochrome c molecules on the surface. SPM experiments are envisioned involving the use of Pcytochrome c in the same capacity as described in Chapter 2, where the microscopy techniques can be used to differentiate between the two adsorbed species, cytochrome c and Pcytochrome c, thereby allowing an assessment of the type of adsorption sites on surface. Achieving these goals has not been a trivial task, as the experimental pitfalls and complications of SPM are numerous. The results of SPM experiments completed on this part of the project are described in subsequent sections, along with corresponding discussion about the problems that were encountered.

### **5.1. SPM: THE GOLD SUBSTRATE**

SPM was performed on several types of Au substrates as part of an effort to define the role of gold topography in cytochrome c voltammetry (Chapter 3). SPM provided microscopic evaluation of surface topography that could be used to supplement electrochemical data. The following paragraphs present SPM imaging of each substrate with a brief description of what each image portrays. Some of the results from this chapter have been incorporated into the structure of the research described in Chapter 3.

STM and AFM experiments were performed on evaporated Au surfaces after being electrochemically cleaned. The resulting images, shown in Figure 5.1, exhibit excellent agreement with literature reports and display what is commonly referred to as “sand dune” topography.<sup>3</sup> Figure 5.2 shows a similar STM image and denotes an area (bottom left of image) for which a mean roughness has been calculated.

In Section 3.3 of Chapter 3, hydrogen flame annealing was explored as a method for altering the gold topography of evaporated gold by reducing the roughness. Evaporated Au films that had been annealed for approximately 30 seconds were imaged with the STM. A representative image, shown in Figure 5.3, may be compared to images of electrochemically cleaned gold (Figure 5.1 & 5.2). The surface has not become overwhelmingly smooth upon

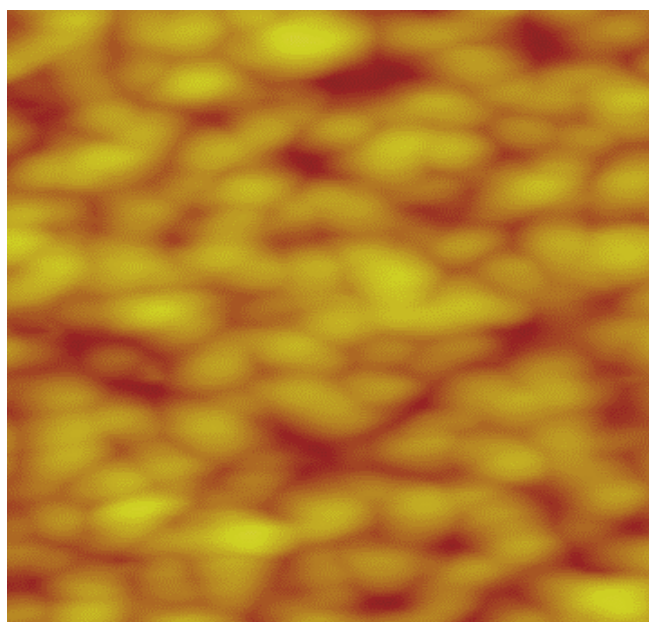
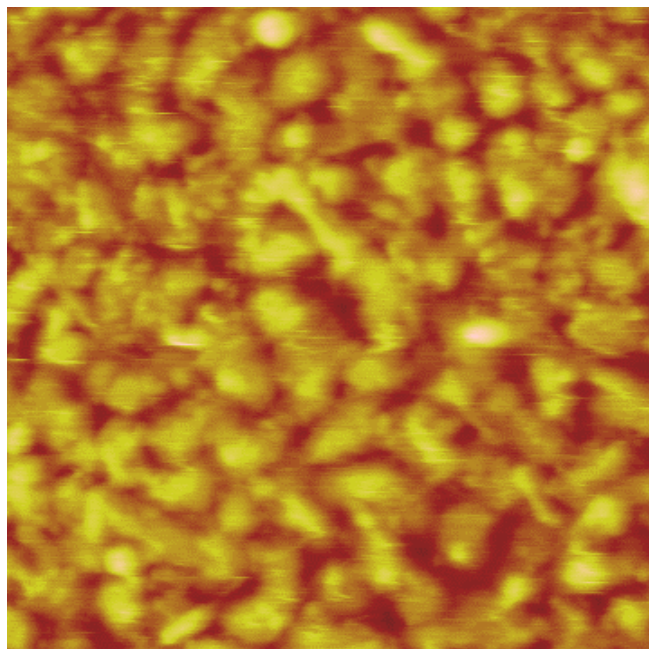


**Figure 5.1.** Contact mode AFM image ( $1\mu\text{m} \times 1\mu\text{m}$ ) of an evaporated Au film electrode (top). Contact mode AFM image ( $1\mu\text{m} \times 1\mu\text{m}$ ) of an evaporated Au film electrode after being “cleaned” by an electrochemical cycling procedure using  $0.1\text{ M H}_2\text{SO}_4$  and  $0.1\text{ M KCl}$  (bottom).

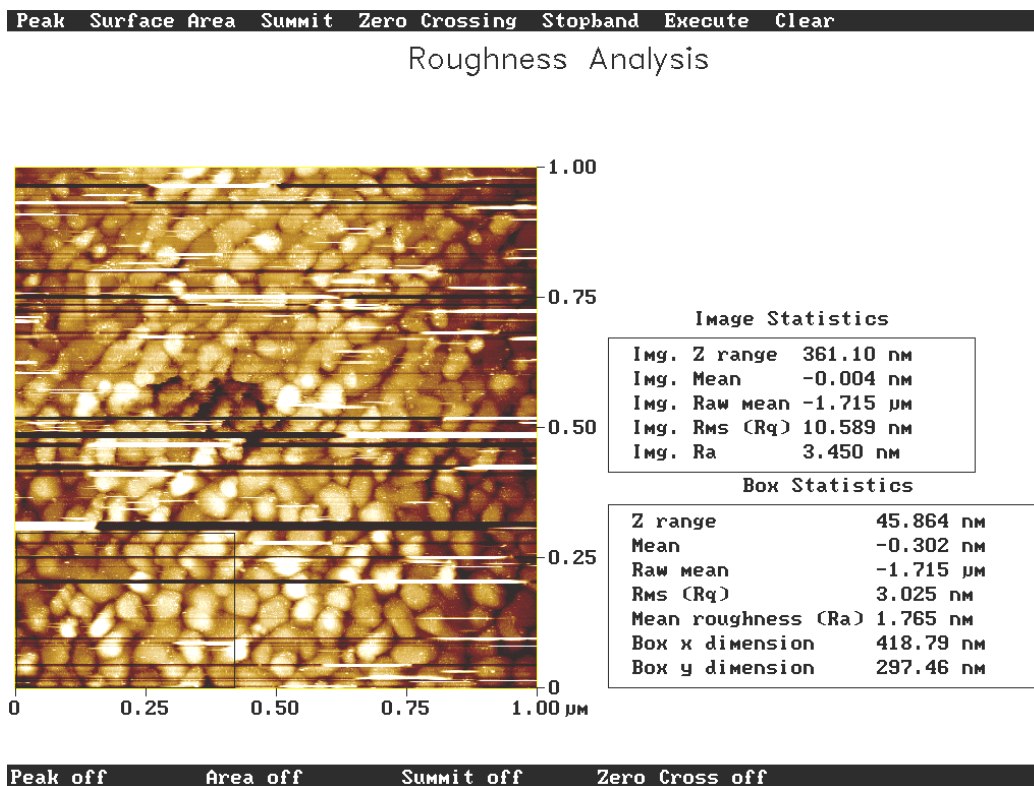


**Figure 5.2.** Roughness analysis of an STM image of evaporated gold that has been electrochemically cleaned. Note the “box statistics” for the outlined part of the image (bottom left corner). The instrument automatically calculates several roughness factors for the surface, including RMS roughness or  $R_q$  as previously described in Chapter 3.

annealing, but does feature significant changes including a difference in the images themselves where the grains are less defined and somewhat larger and a reduction in the calculated mean roughness. In examining these images, however, it is important to remember that, based on reason described in Chapter 3, the annealing of these type of evaporated Au films was discontinued.

SPM images were not obtained for bulk Au samples. Instead, literature reports,<sup>4</sup> especially from Creager’s group,<sup>4a</sup> were used to gain insight into the topography of bulk gold. Optical photomicrographs, shown in Figure 5.4, depict a “splotchy” pattern for aqua regia etched bulk gold, with regions of bright, shiny gold, as well as, regions of yellow and dull orange colored gold. This “particle board” surface structure can be destroyed through abrasive polishing and reinstated through chemical etching (i.e. aqua regia exposure). The different regions of this surface were attributed to single grains of Au in this polycrystalline material.<sup>4a</sup>

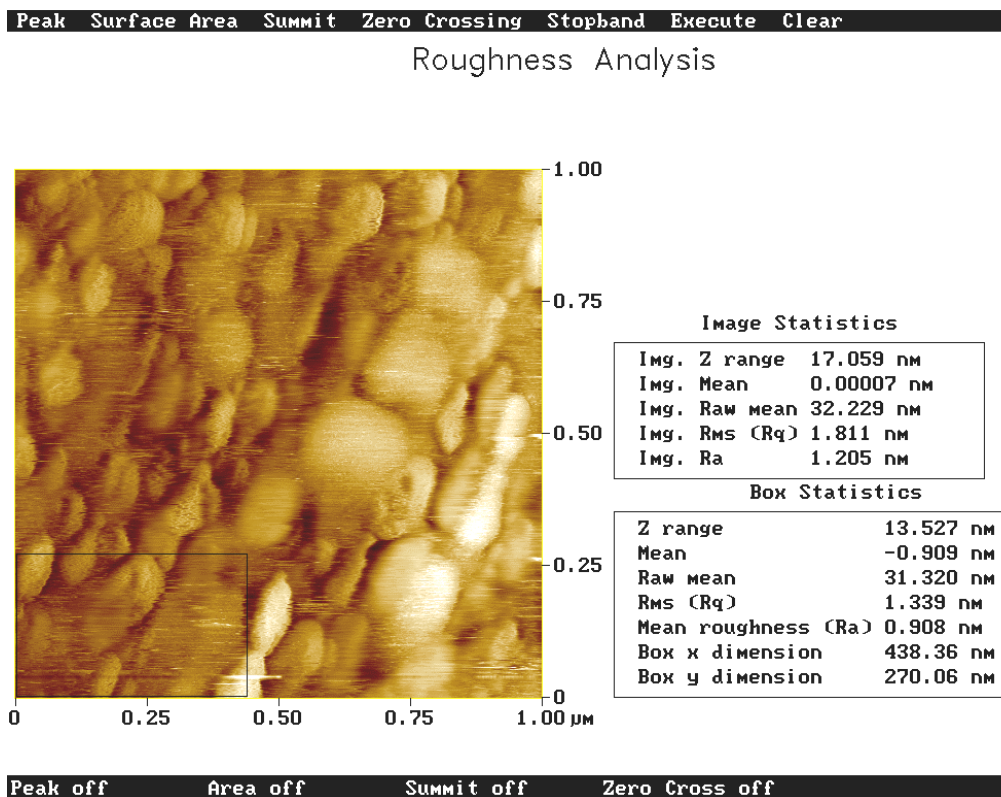


**Figure 5.3.** Roughness analysis of an STM image ( $V_b = 2.0$  V;  $I_t = 2.0$  pA; scan rate = 1 Hz) of evaporated Au that has been electrochemically cleaned and then subsequently hydrogen flame annealed. The mean roughness calculated for the lower left hand corner of the image can be compared to the roughness data on the previous image (Fig. 5.2) – unannealed, electrochemically cleaned evaporated gold. After a smoothing pretreatment like HFA, the surface of the evaporated gold, while exhibiting a lower roughness factor, is still grainy and rough overall.

In spite of the roughness of the aqua regia etched bulk gold surfaces, as displayed in the SEM images of Figure 5.5, the roughness is considered a macroscopic characteristic of the topography. It was suggested by Creager and coworkers that the triangular and rectangular pits, seen in the figure, are the different crystal facets of gold which cause the material to have the “spotty” appearance that is observed. Furthermore, it was proposed that the crystal planes that comprise the angular facets are themselves atomically smooth and single crystalline in nature. Therefore, the aqua regia etched bulk Au surface can be summarized as macroscopically rough, but microscopically smooth.<sup>4a</sup> Unfortunately, this type of surface does not allow for ready imaging via STM/AFM. The large variation in roughness across the area make a SPM experiment prone to crashed tips and obscured image collection. STM imaging, shown in Figure 5.6, compares the surface topography and microscopic roughness of these bulk Au samples to that of evaporated Au films. The bulk

gold sample is clearly rough, but, as shown in Chapter 3, can be thermally annealed to be less rough, especially when compared to evaporated gold substrates. Also, bulk gold contains a high density of grain boundaries due to its polycrystalline nature.

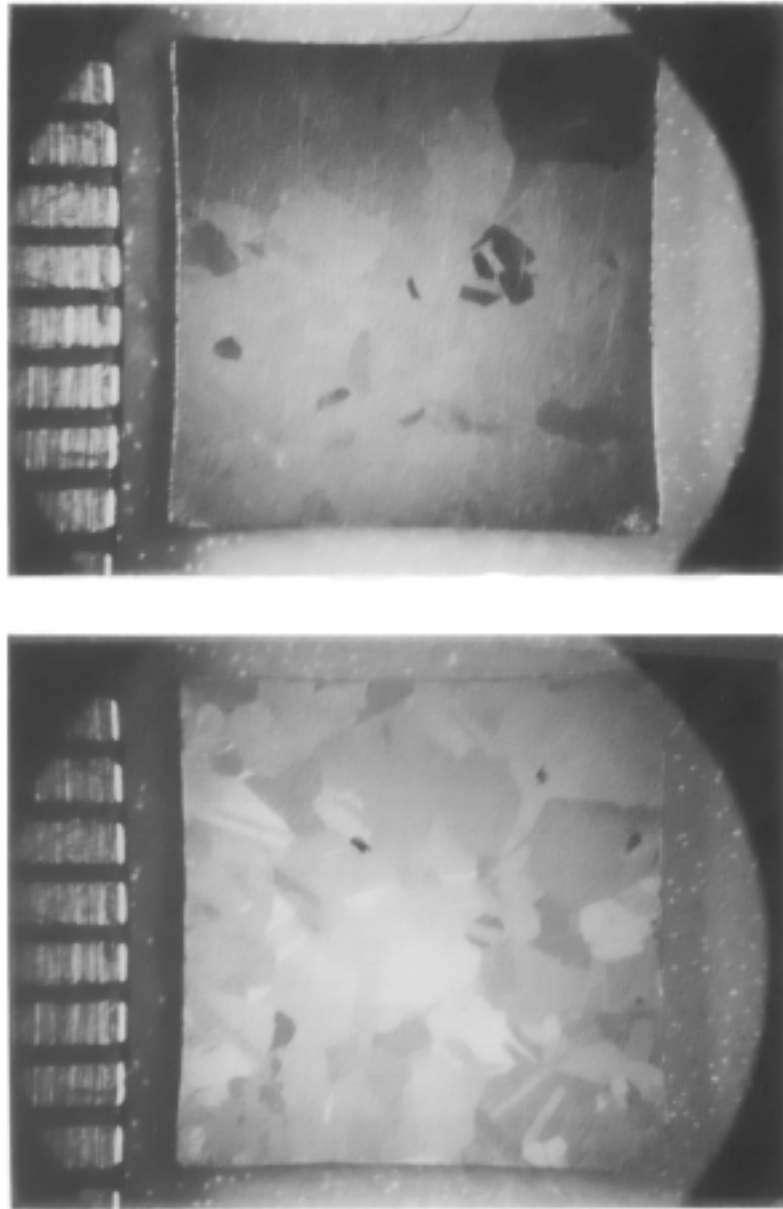


**Figure 5.4.** Optical photomicrograph of bulk gold substrates after etching in dilute aqua regia (top) and after repolishing and re-etching in aqua regia (bottom) – white lines to the left of the image are each 1 mm apart (Figure from Ref. 4a).

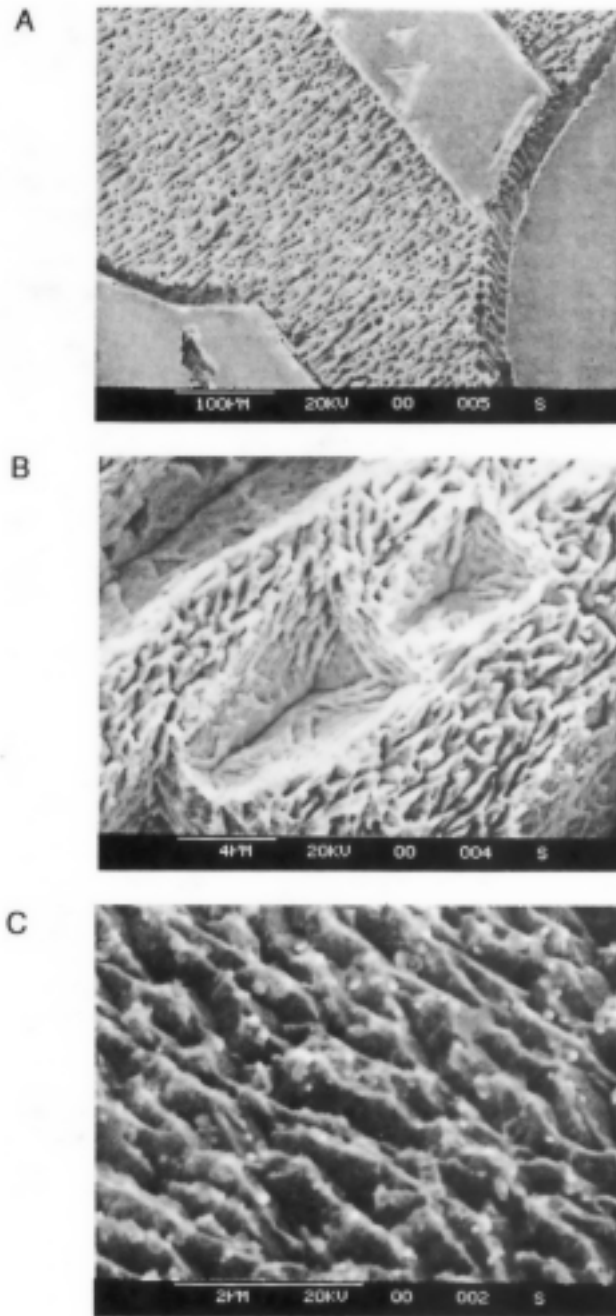


**Figure 5.5.** Scanning electron microscope images of bulk gold electrodes after being etched in aqua regia: A) at low magnification showing etch pits on one crystal face and nominally flat areas on other faces, B) at higher magnification from the center of image (A), and C) at higher magnification from the right side of image (A) – (Figure from Ref. 4a).

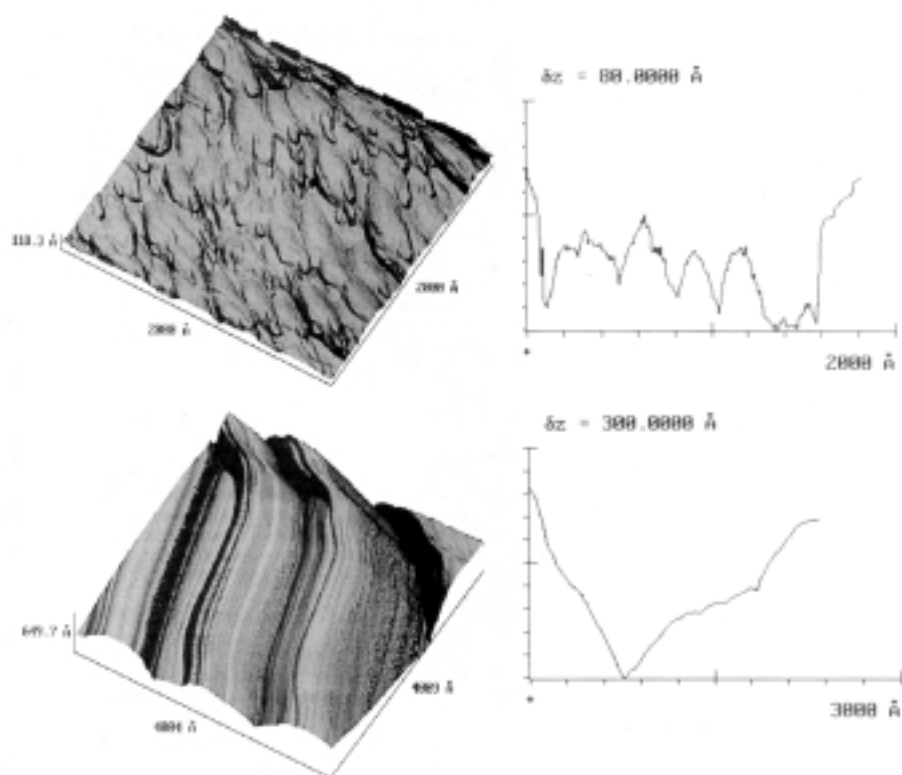


**Figure 5.6.** STM images of evaporated gold substrates (top) compared to bulk gold after chemical etching in aqua regia (bottom). Corresponding cross-sectional analyses are included on the right side of the figure (Figures from Ref. 4a).

SPM imaging of the Au(111) single crystal used in this work was performed by Mike Tarlov and Greg Poirier of NIST prior to the start of this research. The STM imaging is shown in Figure 5.7 and reveals the expected topography of Au(111) - a plateau-laden terrain with a high density of gold step edges (see figure insets), although the number of step edges for a Au(111) can be far fewer. The surface can be “refreshed” by annealing which reforms well defined terraces and step edges and maintains an exclusively Au(111) crystal orientation.<sup>5</sup> Single crystal gold can be summed up as a flat, single crystal material, with a surface comprised of gold terraces and a high density of step edges.

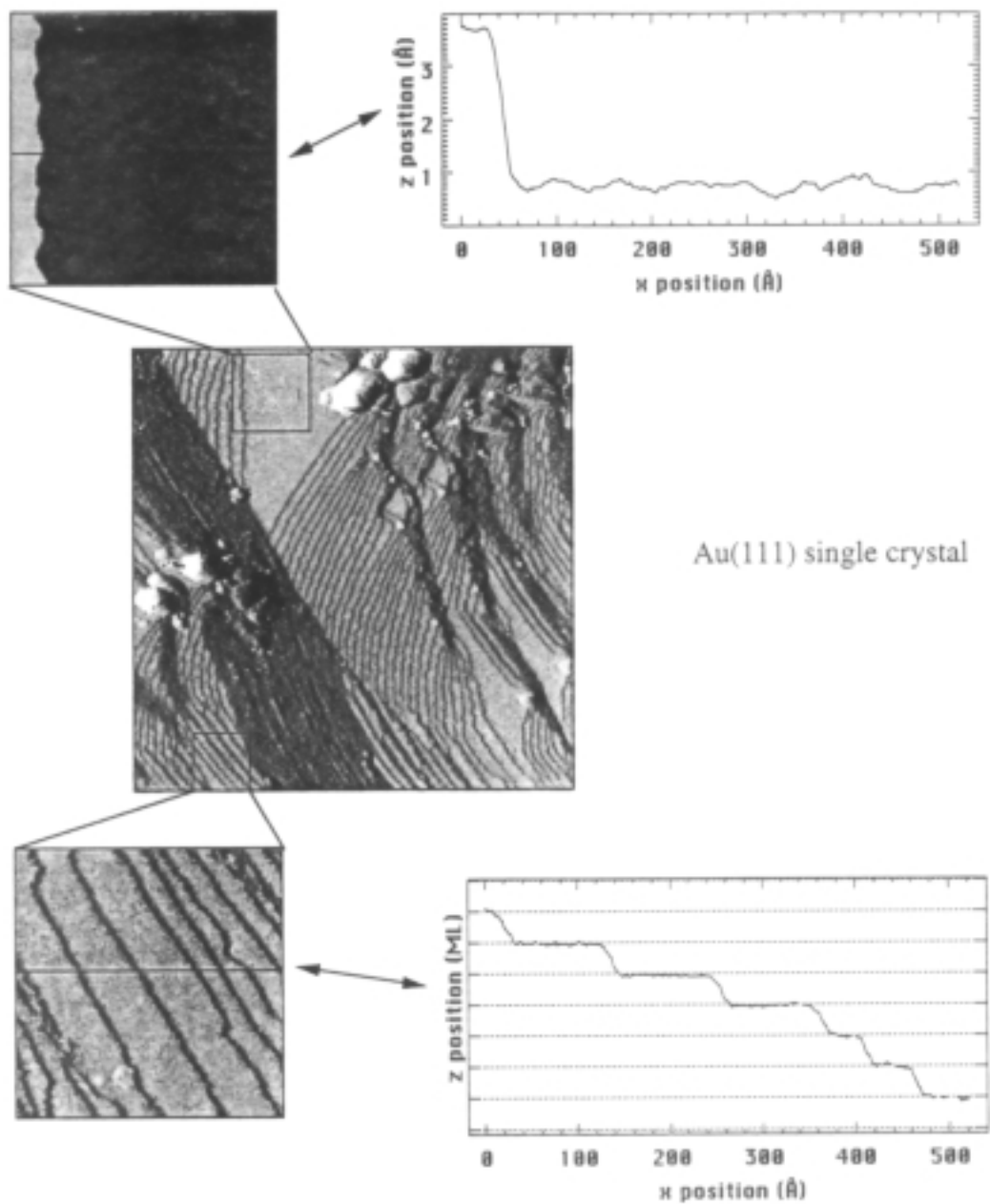


**Figure 5.7.** STM images and cross-sectional analyses of a Au(111) substrate. The central image's dimensions are 3500 Å x 3500 Å. Images taken by Greg Poirer (NIST) – Figure from Rose Clark, Ph.D. Thesis, 1995).

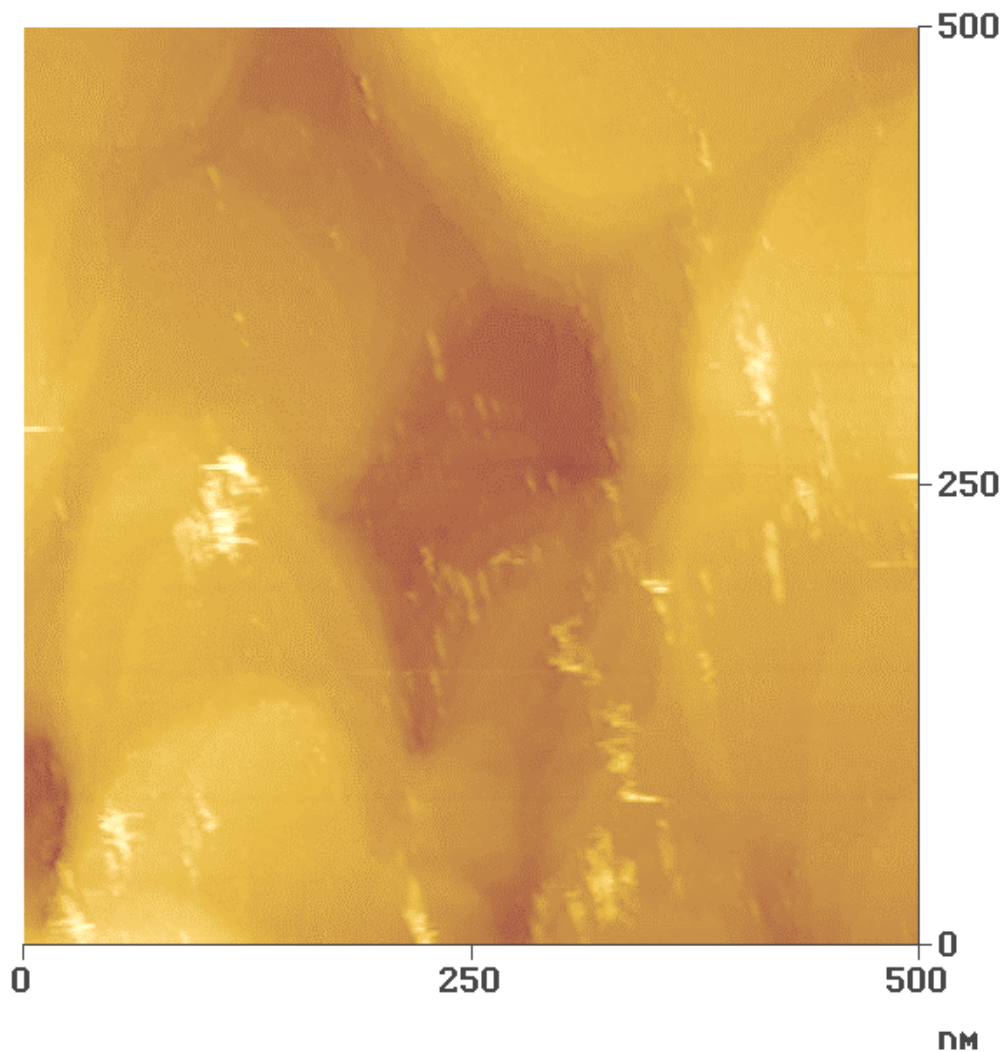


**Figure 5.8.** STM image of gold epitaxially grown on mica substrates. Gold step edges are visible throughout the image and indicate that the surface is extremely flat on these plateau-like areas ( $V_b = 1.0$  V;  $I_t = 5.0$  pA; scan rate = 1.0 Hz). These large flat areas are beneficial when attempting to use gold/mica substrates as a backdrop for imaging adsorbates on a surface.

Because Au epitaxially grown on mica provides the most superior surface for SPM experiments, a great deal of time was devoted to characterizing these surfaces with SPM. A topographical survey, or wide scan, of a Au/mica surface is shown as Figure 5.8 and is in excellent agreement with similar SPM imaging of Au/mica found in the literature.<sup>3a,6</sup> At this image size, plateaus of flat Au are just barely discernible. The flat plateaus are separated, as will be shown, by single Au atomic steps. These rather large, gold atom terraces, combined with a lower density of step edges than the Au(111) single crystal, are the overriding reasons for this substrate's widespread use by SPM scientists. Figure 5.9 shows the same scan with

an area designated for a mean roughness calculation by the instrument. Assuming this sampled area is representative of the entire surface, the mean roughness reflects, especially when compared to evaporated gold, the inherently smooth surface of Au on mica. With flat Au terraces of this size, adsorbates of small dimensions can be imaged with excellent resolution on these surfaces.

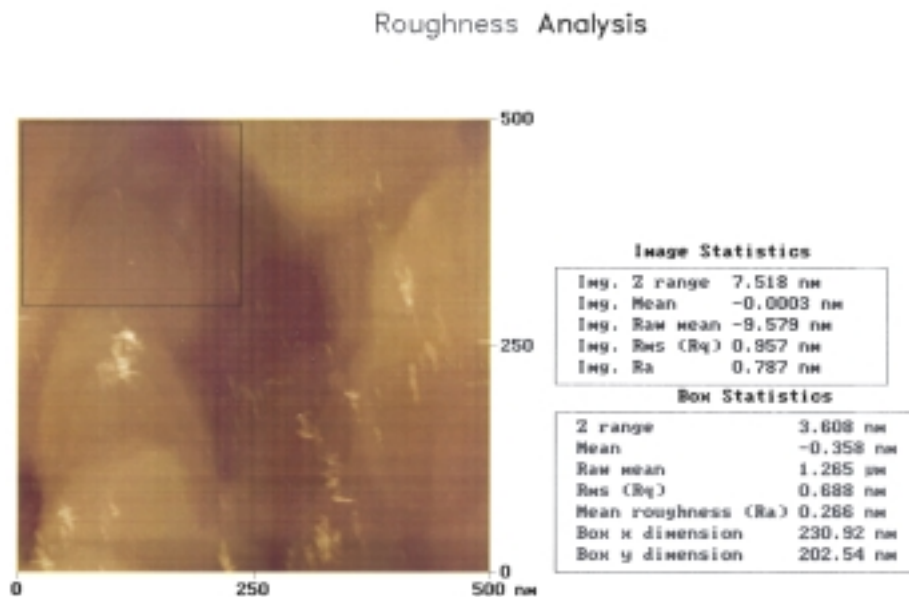


**Figure 5.9.** Roughness analysis of a STM image of Au on mica. The RMS roughness ( $R_q$ ) of the designated area (top left) may be compared to the SPM based roughness factors calculated for Figures 5.2 and 5.3.

STM imaging aimed at characterizing the gold step edges of the Au/mica substrates was carried out. Figures 5.10 and 5.11 show smaller scan size images of two well defined Au step edges. From literature accounts, gold step edges are expected to have an approximate height of 0.2 nm. Accompanying the images in these figures are cross-sectional analyses. The cross section analyzed from each image is marked with a solid black line on the image and displayed in the upper left section of the figure. Colored arrowheads indicate markers for distance measurements, which are listed on the right side of each figure. As shown by the red arrowheads, the height of the step edges of each cross sectional analysis are 0.192 nm and 0.211 nm, respectively. Also of note from these images is the “pitting” seen in some of the images. Au/mica substrates were frequently pretreated with hydrogen flame annealing as recommended by the manufacturer.<sup>7</sup> Some of the substrates were quenched in methanol or exposed at some point to chloride based solutions. The pitting, which was not always present

in the imaging here but is often seen in the literature, is thought to be the result of chemical etching or a natural artifact of the annealing process.<sup>8</sup>

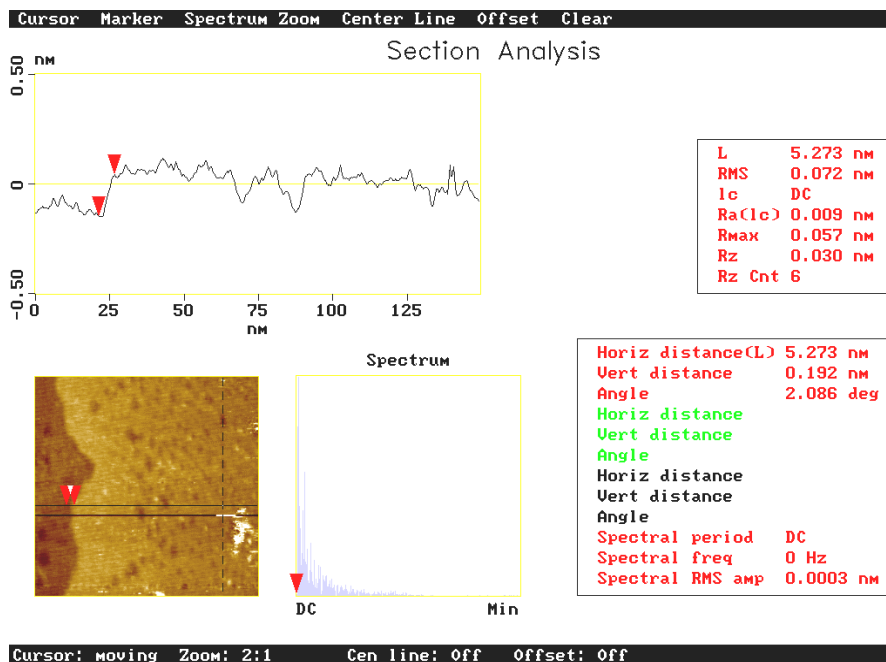


**Figure 5.10.** Sectional analysis of a gold step edge – a prominent surface feature of the gold on mica topography. The cross-section outlined in the top portion of the figure is shown in the STM image (below) with a black horizontal line. Red arrowheads are positioned on both the image and the cross-sectional outline to measure the height of the gold step edge (displayed numerically to the right of the figure).

Step edges are a prevalent feature of the Au/mica topography. The step edges of Au/mica usually separate large, flat plateaus of gold. An example of a gold plateau is shown in Figure 5.12 with corresponding cross sectional analysis. This gold plateau is approximately 50 nm across and is bordered by step edges of about 0.191 nm in height (see figure). This result was one of the first images taken during this research and is nicknamed “Russ’ Island” (see Special Acknowledgments section of this chapter). Plateau topography such as that displayed in Figure 5.12, makes Au/mica a popular choice of substrate for SPM experiments of all kinds.

The low surface roughness of these surfaces originates from the atomically flat mica template on which the gold is grown. In fact it is possible to peel deposited gold off of mica and use the underside (gold surface that was in direct contact with the mica) as an extremely flat substrate for SPM imaging of adsorbates.<sup>9</sup> In summary, Au/mica substrates provide the

flattest gold topography generally available, possessing predominantly Au(111) single crystal character and having a relatively low density of step edges.

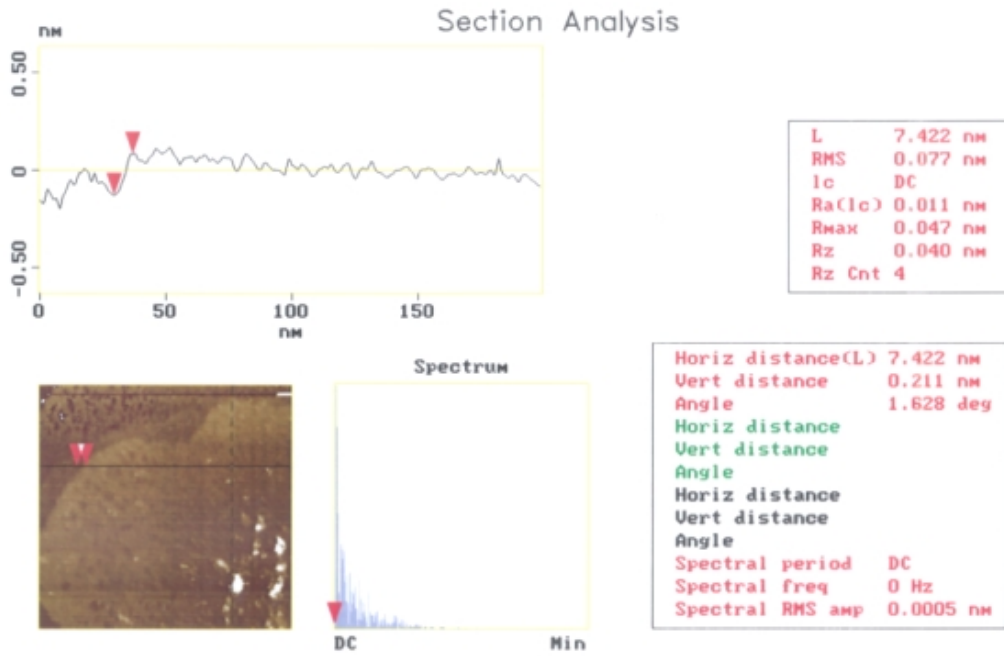


**Figure 5.11.** Sectional analysis of another gold step edge from a STM image of gold epitaxially grown on mica. Gold step edges separating flat, atomic terraces of gold are common to Au/mica topographies.

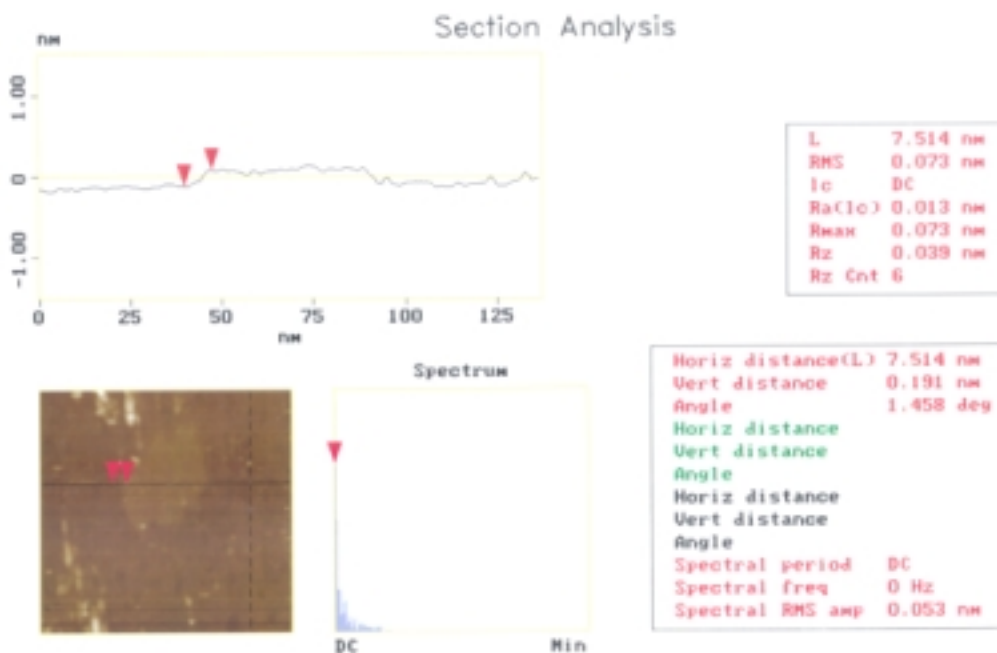


**Figure 5.12.** STM image and cross-sectional analysis illustrating the atomic step plateau topography of gold on mica.

## 5.2 SPM: SAM/SOLUTION INTERFACE

Obviously there is a substantial need to characterize the SAM/solution interface with SPM. Unfortunately, all attempts at imaging gold surfaces modified with carboxylic acid terminated alkane thiols failed. In some cases, the images (not shown) were unable to be interpreted with confidence and, in other cases, experiments often ended with “crashed” probe tips. The difficulties encountered with imaging acid terminated SAMs, however, are not unprecedented in the literature. Methyl terminated SAMs are routinely imaged with molecular resolution by many scientists in the SPM field.<sup>10</sup> This type of surface (hydrophobic/hydrophilic), however, presents a much different imaging interface than the surface of a carboxylic acid SAM (hydrophilic vs. hydrophobic). Although few in number, reports do exist of SPM imaging of hydrophilic, alcohol and acid terminated, SAMs.<sup>11</sup> The huge research effort directed at methyl terminated SAMs has led to improved comprehension of the self-assembly process, as well as atomic resolution images of surface lattice structures.<sup>12</sup> However, since the focus of this research is essentially on COOH terminated SAMs, a lengthy discussion about surface lattice arrangements of methyl terminated SAMs is not warranted.

SPM images of hydrophilic SAMs are much less well-defined in terms of structure and surface lattice. The prevailing rationale is that the difficulty in imaging these interfaces, primarily hydroxy, carboxylic acid, or amine terminated SAM interfaces, originates from the hydrophilic character of the interface itself. Surface hydrophilicity introduces two complicating factors related to SPM imaging: 1) a decrease in the crystallinity which causes the SAM to be less rigid and more fluid-like, especially at the interface and 2) an affinity for the surface to pick up a layer of moisture or other hydrophilic adsorbates. The first factor renders the imaging of such surfaces extremely difficult, especially with the acid terminated SAMs, which have been described as having a liquid-like, dynamic surface state. Methyl terminated SAMs, in comparison, are nearly solid at this same interface, exhibiting highly crystalline, close packed structures, especially noteworthy with SAMs comprised of longer chain length SAMs.

The other factor, foreign hydrophilic materials adhering to the surface, is also a concern. Very low set point currents must be employed in order to successfully image the

SAM/solution interface of carboxylic acid terminated SAMs. The low current is necessary in order to increase the gap resistance, keeping the tip of the STM close enough to the surface to maintain a tunneling current, yet far enough above the surface to prevent it from being dragged through the SAM itself. A common mistake made in trying to image hydrophilic SAMs is using a set point current that is too high, causing the tip to maintain a gap distance that is too small, resulting in tip penetration of the SAM. Under these conditions the sulfur headgroups of the thiol based films are sometimes mistakenly imaged instead of the SAM interface. At low set point currents that place the STM probe tip just at the endgroups of the SAM, there is a risk of tip-adsorbate interactions interfering with the imaging process. This risk is increased if a layer of hydrophilic, foreign material is present on the surface being imaged. This hydrophilic layer, which is sometimes simply a layer of water from the humid atmosphere, can interfere with non-conductive methods of SPM as well. During SFM (AFM) imaging of surfaces covered by an aqueous layer, the cantilevers (probes) can be “snagged” by this water layer or experience shear forces disruptive to successful imaging.<sup>11a,e,13</sup> These complications can be combated by obtaining images in ultra high vacuum (UHV) chambers. Unfortunately, the option of UHV is unavailable for SPM experiments being performed in the NCSU Chemistry Department. Nevertheless, imaging of hydrophilic SAMs, a delicate experiment requiring the experimenter to strike a balance between set point current and gap resistance, has been accomplished in the literature with somewhat controversial results.

#### **-Future Directions for SPM of the COOH SAM/Solution Interface**

Both -OH and NH<sub>2</sub> SAMs have been imaged with more success than COOH terminated SAMs, possibly because of their superior packing order. This task may best be accomplished by first investigating methods of creating more stable acid surfaces. For instance, perhaps the incorporation of mixed SAMs rather than uniform SAMs or the use of Ag or Cu UPD layers beneath the SAM, as described in Chapter 4, will improve the stability of the SAM structure to a point where the SAM interface can be reliably imaged by a SPM technique. Once reproducible and reliable imaging of acid SAMs has been achieved, the SPM aspect of this project can expand toward more of the cyt c/SAM/Au system related

goals. The future of SPM as it relates to that system will be further discussed in a subsequent section.

SPM of mixed SAMs figures to be an important part of future experiments in this area. With increased usage of mixed SAMs in cytochrome electrochemistry, the elucidation of thiol distribution across the gold surface becomes an important goal. Are they phase segregated into domains or are they randomly distributed throughout the film? SPM of mixed films can provide the level of detail necessary to answer these types of questions, as has already been demonstrated.<sup>14</sup> Mixed SAMs can be homogeneously mixed or phase segregated depending on the nature of the two components comprising the SAM. The mixed SAMs of immediate interest here, usually consisting of components separated in length by less than 4 methylene units (Type I structure), are thought to be randomly distributed.

### **5.3. SPM: PROTEINS (CYTOCHROME C)**

During the past decade significant progress has been made with SPM imaging of proteins, enzymes, and other biological entities.<sup>1a</sup> In spite of this intense effort, controversy regarding the exact mechanism of STM imaging of proteins remains vibrant.<sup>1</sup> AFM, an alternative form of SPM with a better understood imaging mechanism, presents other challenges for imaging biological structures. Some AFM methods require a greater degree of probe-adsorbate interaction than STM, risking damage and/or translocation of adsorbates. Furthermore, all SPM techniques require a well defined substrate where the target biological molecule(s) can be adequately immobilized. In light of these complications, successful imaging of proteins by SPM techniques is a nontrivial task.

Most of the published work concerning SPM imaging of proteins has addressed large biomolecule systems<sup>1a,15</sup> such as ferritin. The larger size provides a greater chance of discerning some characteristic internal structure or the overall shape of the biomolecule. More often than not, however, proteins that have appeared in SPM images resemble “fuzzy blobs” accompanied by unrealistic dimensions and little or no scientific analysis. As seen in some of the better biological imaging reports, an image supported by supplemental characterization such as IR spectroscopy or XPS usually carries much greater value.

Known dimensions of biomolecules, often determined by crystallography, are usually used as a means to identify masses in images. However, extreme care should be used when using dimensions to analyze images in this manner. Images of biomolecules are usually skewed to a certain extent. Imaged biomolecules usually appear larger laterally and smaller in height. An example of this effect is shown in Figure 5.13. It has been speculated that this apparent alteration in size is the manifestation of several tip effects including one or more of the following: physical compression of the biomolecule, tip enhanced current (STM only), H<sub>2</sub>O layer effects, or dielectric constant changes. Because of the skewed dimensions, cross sectional analysis of imaged proteins is strongly encouraged. Additionally, spatial volume, rather than strict diameter and height measurements, can sometimes be a useful measurement to compensate for the skewed dimensions. It is believed that the spatial volume of the imaged entity does not change dramatically, even if the dimensions of the mass are skewed.<sup>16</sup>

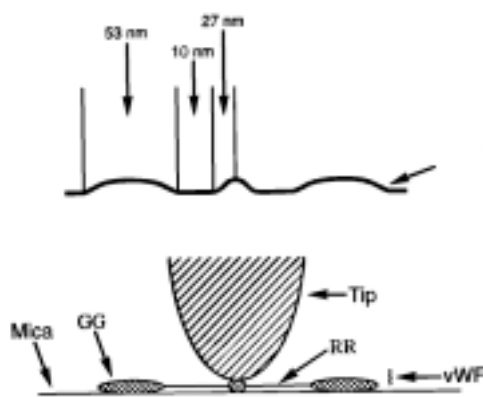


**Figure 5.13.** Illustration depicting how SPM techniques can potentially skew the apparent dimensions of an adsorbate being imaged. In this example, the imaged protein, von Willebrand factor (vWf) is made up of globular domains (GG) that are flanked by fibrillar domains (RR) which surround a central nodule. The SPM profile of this system (top) illustrates that the image of the protein possesses clearly expanded dimensions for the globular domains. If the probe tip is too large, it may even be incapable of imaging the fibrillar domains at all. This phenomenon is a general manifestation of SPM imaging (Figure from Ref. 16).

### 5.3.1. SPM: Cytochrome c on Gold - Experimental Results

Examples of using STM and AFM to study cyt c and similar small proteins are not plentiful<sup>16-19</sup> and quality images of cyt c are even more scarce.<sup>19a,d,e</sup> Table 5-1 lists some examples along with known dimensions and imaged dimensions. In several instances, spatial volumes have been calculated for comparison as well. Cyt c is known from crystallographic

reports, to be globular in nature with an ellipsoidal shape and an approximate diameter of 3.0-3.4 nm.

**Table 5.1.** Comparison of Known Protein Dimensions to Experimental SPM Determined Dimensions

<b>Protein System (protein / surface)</b>	<b>Known Dimensions<sup>a</sup></b>	<b>SPM Dimensions<sup>b,c</sup></b>
Cyt c <sub>551</sub> / Au / mica <sup>19d</sup>	a = 2.9 nm ; b = c = 4.9 nm diameter = 3 nm V <sub>s</sub> = 14 x 10 <sup>3</sup> Å <sup>3</sup>	6.9 x 4.4 x 0.9 nm <sup>3</sup> diameter = 4.0-4.4 nm height = 1.0-1.2 nm V <sub>s</sub> = 14 <sub>(±2)</sub> x 10 <sup>3</sup> Å <sup>3</sup>
Cyt c <sub>3</sub> / Au / mica <sup>19d</sup>	a = 5.3 nm ; b = 6.8 nm ; c = 3.5 nm ; d = 3.4nm V <sub>s</sub> = 2 x 10 <sup>4</sup> Å <sup>3</sup>	diameter = 6-7 nm height = 1.0-1.2 nm V <sub>s</sub> = 1.8 <sub>(±2.2)</sub> x 10 <sup>4</sup> Å <sup>3</sup>
Ferritin / Au foil <sup>15d</sup>	diameter = 12 nm	diameter = 11.5 <sub>(±1.5)</sub> nm height = 10.1 <sub>(±1.3)</sub> nm
Hemoglobin / HOPG <sup>17b</sup>	6.4 x 5.5 x 5.0 nm <sup>3</sup>	6.4 x 5.4 x 6.8 nm <sup>3</sup>
Lysozyme / mica <sup>18e</sup>	3.5 x 3.5 x 5.0 nm <sup>3</sup>	diameter = 20 nm height = 6-8 nm
G-Actin / mica <sup>18e</sup>	diameter = 5.5 nm height = 6 nm	diameter = 15 nm height = 10-14 nm
Cyt c / Evap. Au <sup>19a</sup>	diameter = 3.0-3.4 nm	diameter = 3.3 <sub>(±0.5)</sub> nm height = 0.5 <sub>(±0.1)</sub> nm

<sup>a</sup> Known dimensions designated by letters were determined using crystallography; others were determined using a variety of techniques including computer modeling and simulations (see individual literature reports for more details).

<sup>b</sup> Experimental dimensions determined by some form of SPM including both STM and AFM techniques.

<sup>c</sup> Spatial volume (V<sub>s</sub>) is sometimes used to compensate for the skewed dimensions that SPM may present.

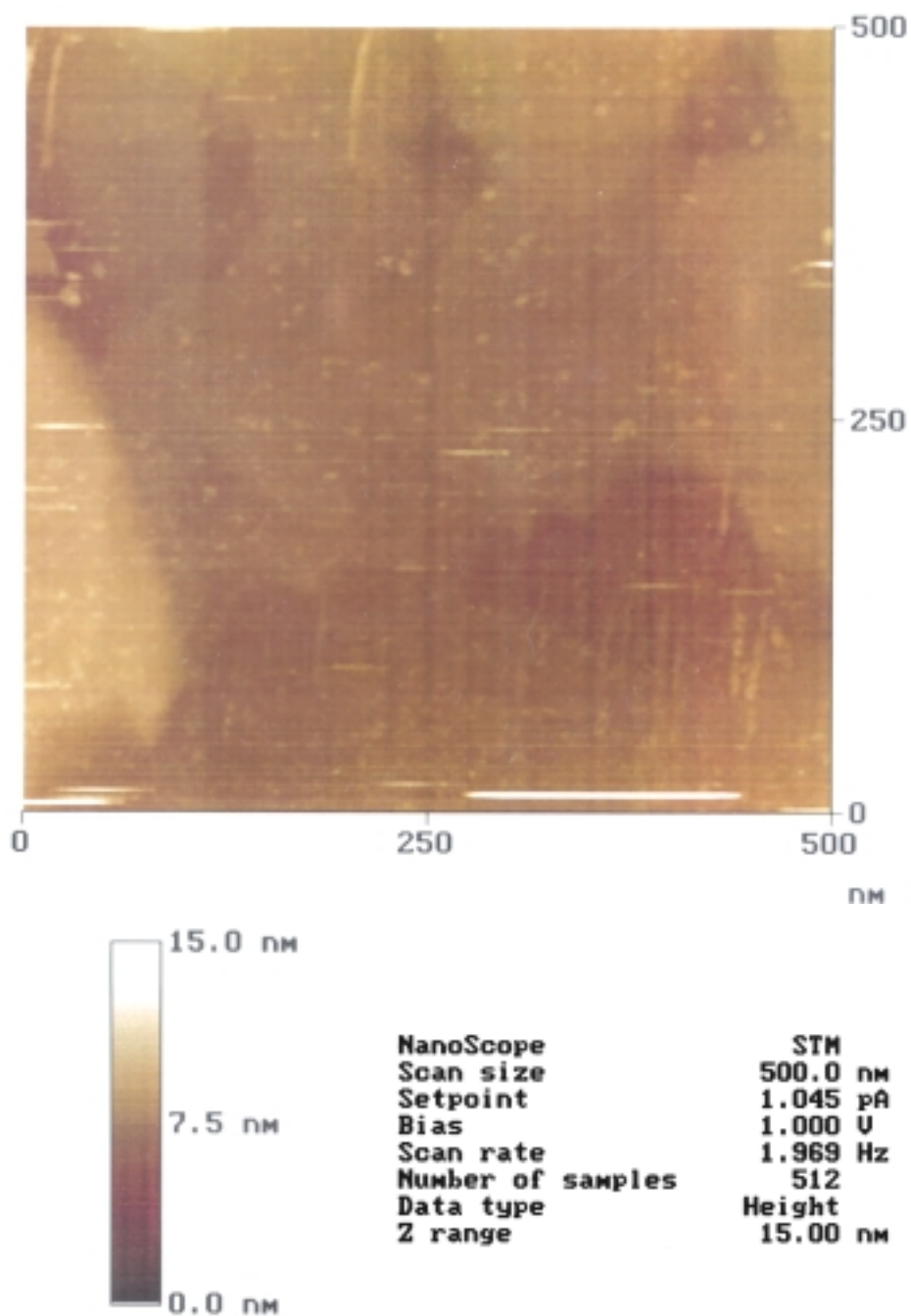


**Figure 5.14.** STM image (survey scan) of cyt c proteins on gold on mica – imaged in air (See Experimental Details Section for more details). Note the small dots representing individual proteins on this surface compared to the surface shown in the image in Figure 5.8.

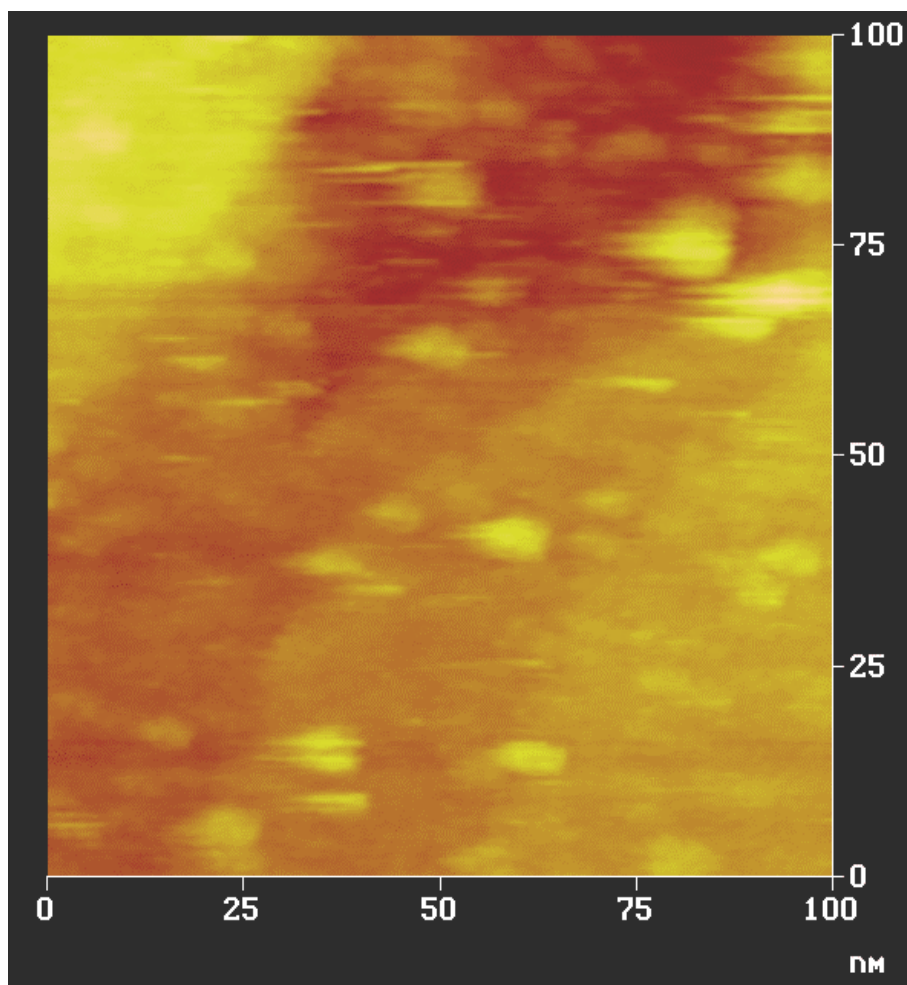


**Figure 5.15.** STM image of apparent single molecules of cyt c protein adsorbed onto a gold on mica surface. Notice that both the adsorbed cyt c molecules and the gold step edges are discernable in the image ( $V_b = 1.0$  V;  $I_t = 1.0$  pA; scan rate = 2.0 Hz).

Cyt c molecules were dispersed on a previously annealed Au/mica substrate according to the procedure laid out in the Experimental Details section of this chapter. Figure 5.14 shows a survey STM image of the surface following protein deposition. Small globular bodies are discernible and are suspected to be cyt c molecules since they are conspicuously absent from the image of bare Au/mica (Figure 5.8). Ideally, SPM images should show a clearly defined adsorbate and, at the same time, some discernible feature of the surface that is characteristic to that particular type of surface (i.e. step edges, lattice pattern, etc.). The image of cyt c/Au/mica, shown in Figure 5.15, captures both of these topographical features: individual cyt c molecules and step edges of the Au/mica surface. Dimensional analysis, performed by taking cross sections of the image, is given in Figure 5.16. The lateral

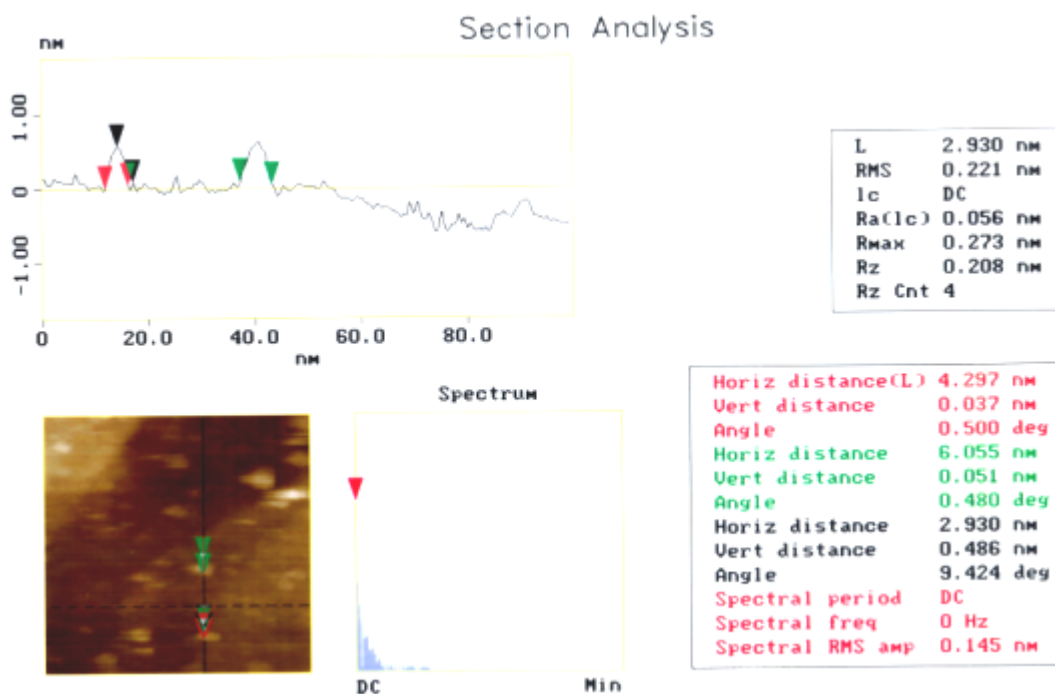


**Figure 5.16.** Sectional-analysis of two apparent cyt c from the image in Figure 5.15. Red and green arrowheads mark diameter measurements while the black arrowheads are for height determinations. Cyt c is expected to have a diameter of 3.0 nm.<sup>19a</sup>

dimensions of the imaged cyt c molecules in this study are in excellent agreement with values found in the literature for other imaged cyt c diameters (See Table 5-1).<sup>19a,d,e</sup> In all of these reports and as expected, the lateral dimensions are slightly enlarged from crystallographic measurements, most likely due to the imaging process itself (STM) and the hydrated nature of the protein. Another possibility for the larger than normal dimensions may be that the protein is slightly denatured, having spent a significant amount of time ( $\geq 0.5$  hrs) on a bare gold surface. The image in Figure 5.17 shows four individual cyt c molecules, of which one appears to be damaged, perhaps from the motion of the STM tip being dragged across that particular protein. In any event, the quality of these STM images of individual cyt c molecules equals or exceeds the best known images that have been published.<sup>2,19a,d,e</sup> While quality imaging of proteins, especially of small size, is still a novel accomplishment, it is much more interesting to use SPM as a scientific tool to learn about the cyt c/SAM/Au system on a molecular level. The remainder of this chapter will focus on the presentation of future experiments/projects that are designed to unlock the potential of SPM by applying it to the cyt c/SAM/Au ET system, using it in a more significant manner to map out topographical information and relate protein adsorption to specific characteristics of SAM structure.

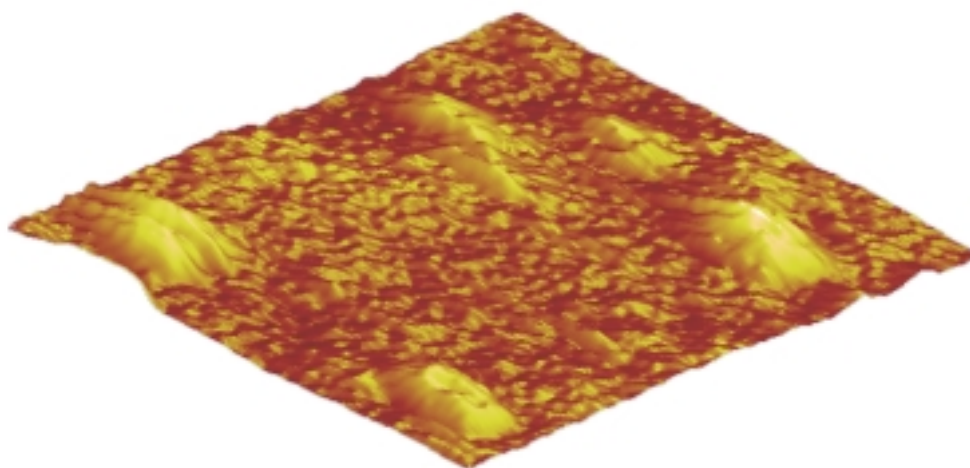
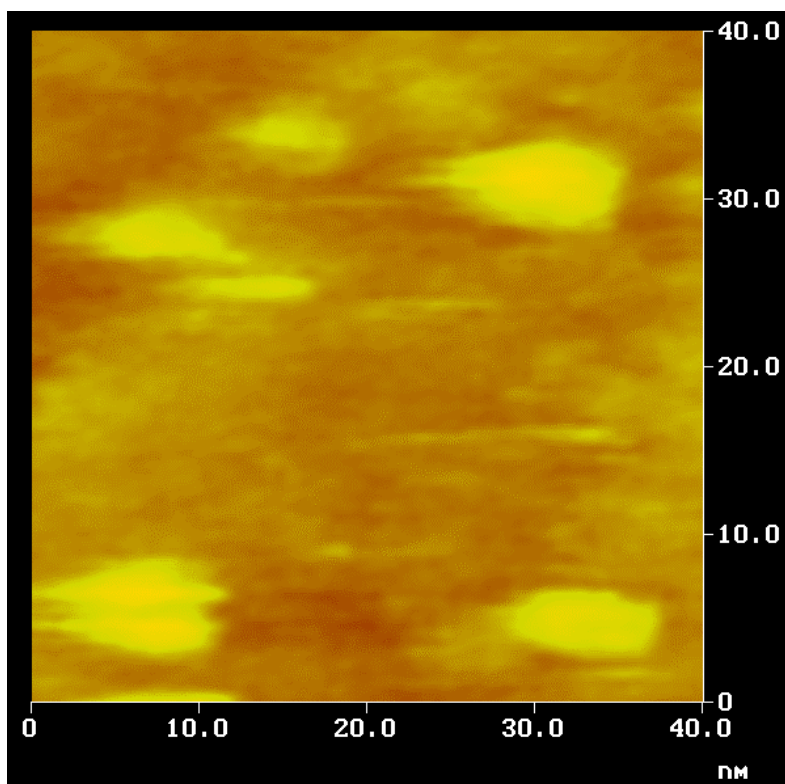


**Figure 5.17.** STM image (top) of individual cyt c molecules adsorbed onto a gold on mica substrate ( $V_b = 1.0$  V;  $I_t = 0.2$  pA). The image shows four individual cyt c molecules with the upper left protein seemingly having been damaged by tip-adsorbate interaction. Three dimensional view (below) of the same four cyt c molecules at 40 nm x 40 nm.

#### **5.4. SPM: THE CYT C/SAM/Au SYSTEM - CONCLUSIONS AND FUTURE DIRECTIONS**

SPM imaging of the complete cyt c/SAM/Au system has not been achieved yet due largely to the difficulties associated with well resolved imaging the SAM itself. There is much, however, that could be done using this technique. This section is devoted to possible future experiments, including a fairly detailed description of a possible resonant tunneling study. Of major interest is an assessment of whether cyt c adsorption sites can be correlated with specific defect features of the SAM that could arise at step edges, crystal grain boundaries, or etch pits.<sup>2</sup> Based on results in Chapter 3, SPM could be a good approach to determine whether cyt c adsorbs on atomically flat terraces. Accomplishing these tasks would involve being able to routinely and effectively image gold substrates, SAM modified gold substrates, and cyt c monolayers adsorbed to those gold substrates. This type of imaging would have to be performed in careful stages and is envisioned as a primarily *ex situ* project.

##### **-Electrochemical SPM (ECSPM)**

*In situ* SPM experiments performed under potential control, also known as electrochemical scanning probe microscopy (ECSPM),<sup>1c,20</sup> should also be pursued because of its potential usefulness in gaining insight into surface electrochemistry. Successful imaging using ECSPM is expected to be challenging, but feasible. *In situ* ECSPM is potentially a powerful method of identifying specific cyt c adsorption sites at active interfaces and may possibly allow for single molecule characterization and manipulation. *In situ* ECSPM experiments of this nature present several formidable obstacles that will have to be addressed, including the need for specialized probes. For electrochemical scanning tunneling microscopy (ECSTM), for example, high quality insulated tips are required to minimize extraneous currents and to increase the probability that current flow arises from electron tunneling to or from the surface bound cyt c molecules. Several procedures for preparing coated tips of this nature are available in the literature.<sup>21</sup>

##### **-Advanced ECSPM Experiments (Resonant Tunneling)**

Successful ECSPM imaging of the cyt c/SAM/Au system would serve as the basis for more advanced experiments that more fully utilize the potential of SPM as a scientific tool. Even the most impressive protein images are usually subject to severe criticism due to the nature of the imaging process. As stated previously, many SPM images show proteins simply

as “fuzzy blobs” with little or no supporting evidence to support interpretations. More credible SPM papers include supplemental evidence from other techniques to bolster interpretations made with regard to the protein images. Unfortunately, this approach usually involves manipulating a single substrate with bioadsorbates through multiple characterization techniques, a nontrivial task when one of the techniques is *ex situ* SPM which increases the probability of natural degradation of the protein unless the environment is rigorously controlled. One criticism of this approach is that it involves the assumption that the entire experimental substrate is realistically portrayed by the small area imaged by SPM. It must be assumed that the image is characteristic of the surface of the entire substrate, as well as, nearly identical to the substrates being tested by other techniques. Considering the substrate to substrate variation witnessed with gold surfaces, the propensity for defects in SAMs, the variation of SAM structure that can exist, and the sensitivity of the cyt c/SAM/Au system to different preparation and pretreatment procedures, this is not always a safe assumption to make. When faced with this situation, a SPM technique or experiment that can perform the imaging process while simultaneously and unambiguously distinguishing chemical identity is an extremely attractive idea. To this end, an exciting set of experiments are proposed that not only address this exact dilemma, but also encompass most of the objectives of this research.

Recently, the phenomenon of resonant tunneling (RT) has been used in STM experiments to chemically identify single types of molecules adsorbed onto surfaces.<sup>20a,22</sup> Resonant tunneling experiments are performed by having a redox species adsorbed onto a substrate that is under potential control. Traditionally, a bipotentiostat, capable of independently controlling the potential of two electrodes, is used for RT experiments. As a form of ECSPM, one of the two working electrodes is the substrate, while the other is the STM tip itself. The substrate’s Fermi level, via the bipotentiostat, is “tuned” to the reaction potential of the adsorbed molecules. Thus, this “tuning” effectively aligns the energy levels of the substrate with the LUMO energy levels (redox orbitals) of the adsorbed molecules.<sup>22b,d</sup> This is most easily accomplished by adjusting the substrate’s potential to formal potential of the adsorbed redox species as determined from electrochemistry. When this alignment is scanned with the STM tip with a fixed tip-substrate voltage bias, the energy levels of the tip, adsorbate, and substrate are aligned or brought into resonance with each other. This overlap

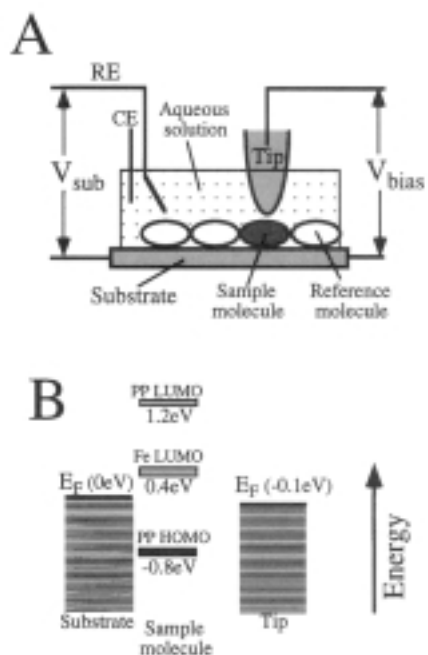


**Figure 5.18.** (A) Schematic of a resonant tunneling ECSTM experiment showing sample molecules and reference molecules on a substrate being probed by a STM tip.  $V_{\text{sub}}$  and  $V_{\text{bias}}$  are the substrate potential (with respect to the reference electrode) and the tip-substrate bias voltage, respectively - both of which are controlled via a biopotentiostat. (B) Energy diagram of the resonant tunneling experiment showing the Fermi level of Fe(III) - protoporphyrin IX in relation to the Fermi levels of the substrate and tip. Note the alignment of the energy levels of the tip and substrate with the LUMO of the Fe(III) - protoporphyrin.<sup>22a</sup>

of redox orbitals results in a sudden and slight increase in orbital-mediated tunneling current.<sup>22b</sup> With a fixed tip-substrate bias, the increase in tunneling current is a manifestation of the unoccupied orbital pathway that has been created by aligning the energy levels of the tip, adsorbate's redox orbitals and the substrate. This pathway only exists when the substrate/adsorbate has been effectively tuned to align the energy levels of the three components. Tunneling current usually exists anyway between the tip and substrate and, with resonant tunneling, is simply mediated with a orbital pathway. To compensate for this sudden change in current, the STM will react to change the tunneling current back to its set-point magnitude. This is most easily accomplished by STM tip movement until the set point current is again achieved. Thus, resonant tunneling is perceived by the STM as an apparent increase in height of the imaged molecules, thereby causing the molecules to “light up” in the actual image.

The phenomenon of resonant tunneling is best illustrated by experiments by Tao and coworkers.<sup>22a</sup> Tao successfully performed resonant tunneling on Fe-protoporphyrins IX. His experimental apparatus and an example of resonant tunneling are shown as Figures 5.18 and 5.19, respectively. Fe-protoporphyrin IX is an ideal choice for resonant tunneling, considering it can be readily immobilized on a flat graphite surface, undergoes fast ET reactions, and has an excellent reference molecule to serve as its electroinactive compliment.

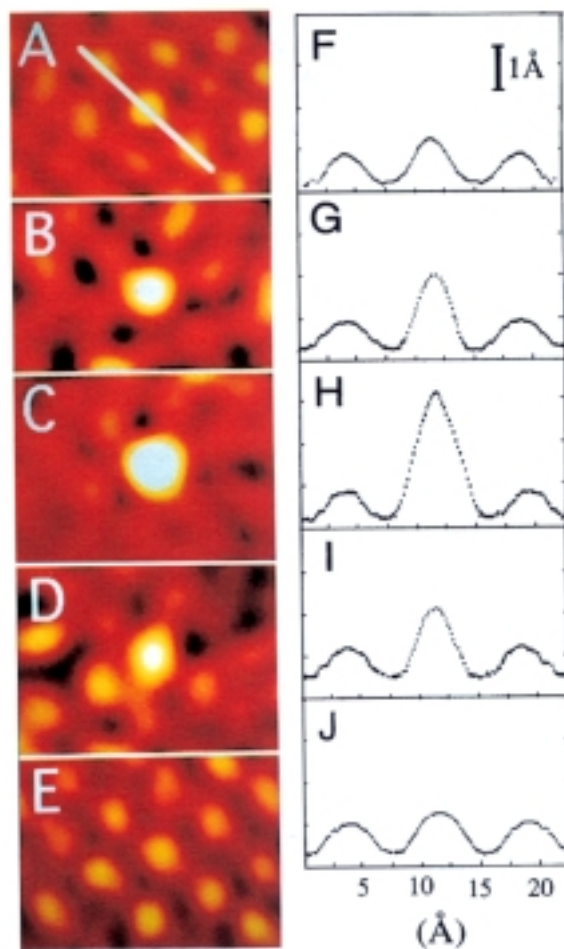


**Figure 5.19.** STM images of a Fe-protoporphyrin IX embedded in an ordered array of protoporphyrin (reference) molecules while the potential of the substrate is held at a A)  $-0.15$ , B)  $-0.30$ , C)  $-0.42$ , D)  $-0.55$ , and E)  $-0.65$  V, respectively. Corresponding cross-sectional analyses are shown for each image (Figure from Ref. 22a).

Fe-protoporphyrin IX can be imaged along with protoporphyrin IX, a molecule with the same structure but lacking the redox active Fe core (shown in Figure 5.20). In this manner, mixtures of different ratios of the two molecules could be used in resonant tunneling experiments, allowing for the electroactive molecules to light up while the electroinactive molecules remained dormant. This type of experiment would allow the Fe-protoporphyrin IX / protoporphyrin IX ratios to be visualized in the resonant tunneling experiment by observing the molecules that are lit up and those that are not. This result is borne out by Tao's research in Figure 5.21 along with corresponding cyclic voltammograms that are supplied as further evidence of the system being imaged. Figure 5.22 illustrates the apparent height increase found for molecules in the resonant tunneling condition. The height increase is shown in this

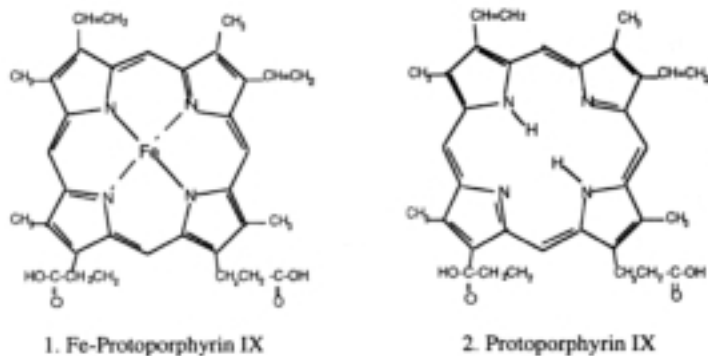


**Figure 5.20.** Sample (left) and reference molecule (right) studied by Tao's resonant tunneling experiments (Figure from Ref. 22a).

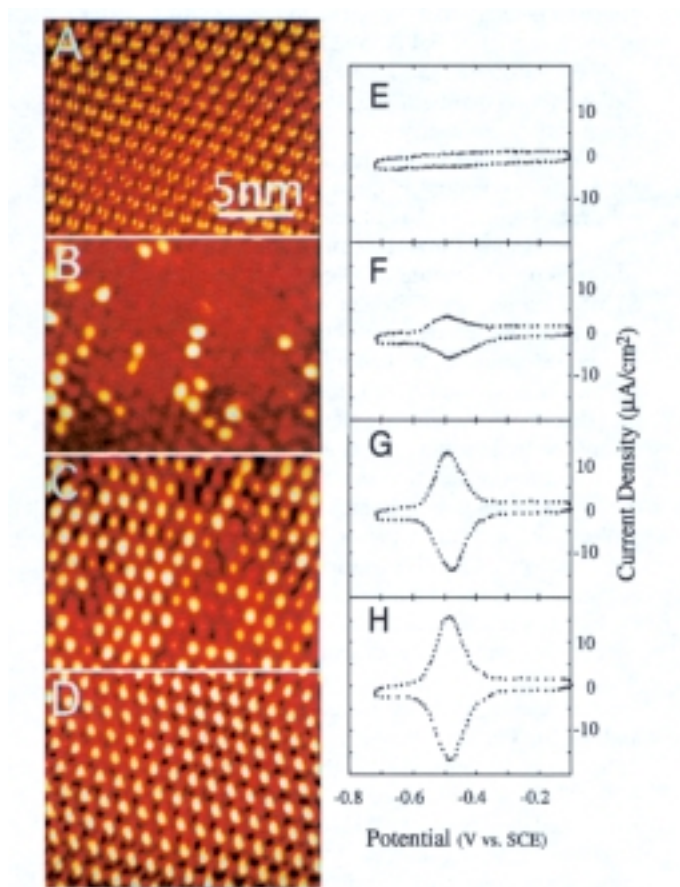


**Figure 5.21.** STM images and corresponding cyclic voltammetry of Fe-protoporphyrin (sample molecules) and protoporphyrin (reference molecules) adsorbed at a graphite substrate in 0.05 M  $\text{Na}_2\text{B}_4\text{O}_7$  solutions at a ratio of A) 0:1, B) 1:4, C) 4:1, and D) 1:0. All of the images were taken with the substrate potential set to  $-0.41$  V (the redox potential for Fe-protoporphyrin), a tunneling current of 30 pA, and a tip-substrate bias of  $-0.1$  V. The voltammetry shown was collected at 200 mV/sec (Figure from Ref. 22a).

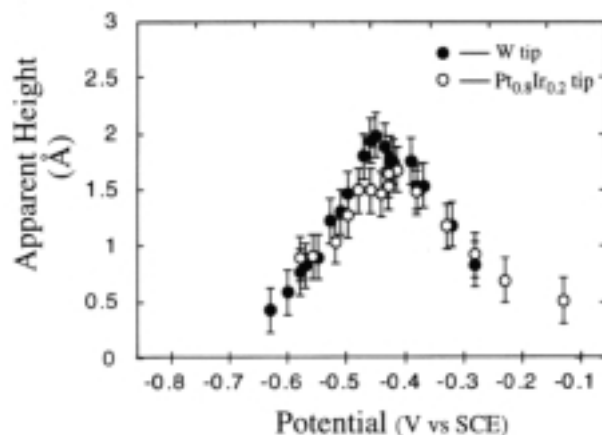
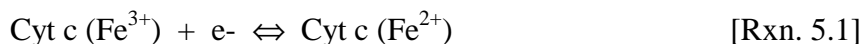


**Figure 5.22.** Apparent height, as measured by the STM resonant tunneling experiments, of the imaged Fe-protoporphyrin relative to the protoporphyrin. Data is shown for two different types of STM probes (W and Pt/Ir STM probe tips) – (Figure from Ref. 22a).

figure as a function of applied potential to the substrate, further substantiating that the resonant tunneling phenomenon occurs at the formal (redox) potential of the adsorbate, in this case -0.48 V vs. SCE.<sup>22a</sup> For the cyt c system being studied here, it is proposed that an analogous experiment to the one just described may prove successful.

The cyt c system has several advantageous aspects that increase the probability that resonant tunneling experiments would be possible. In order to achieve similar resonant tunneling results for cyt c, the protein must first be imaged to molecular resolution. As shown earlier in this chapter, this first obstacle is already being overcome (see Figure 5.17). Resonant tunneling also requires an adequate reference molecule. In the work by Tao, protoporphyrin IX served this purpose. For the cyt c system, porphyrin cyt c (Pcyt), as produced by Vanderkooi and Erecinska<sup>23</sup> and previously described by Rose Clark for research efforts in our group (see Chapter 2), is an obvious reference molecule in the context of resonant tunneling. Pcyt c is cyt c which has had the electroactive iron atom has been removed. Thus, Pcyt c has no metal center to provide unoccupied orbitals for tunneling current. In all probability, its molecular orbitals are at very different energy levels than the Fermi levels of the tip and substrate.<sup>22a</sup> Therefore, even when the substrate is “tuned” to the redox potential of cyt c, the energy levels of the Pcyt will still be effectively unaligned and unavailable for resonant tunneling activity. Pcyt c, therefore, essentially plays the same role in these proposed experiments as the protoporphyrin played in Tao’s experiments.

Another encouraging aspect of the proposed resonant tunneling of cyt c molecules is that the porphyrin core of HH cyt c is identical to the Fe-protoporphyrin used by Tao. Thus, the protein environment may simply hinge on gaining access to this same porphyrin ring inside the cytochrome's protein shell. The redox orbitals of adsorbed cyt c are already routinely accessed during traditional voltammetry experiments performed with the cyt c/SAM/Au system:



Thus it seems possible that, by setting the applied voltage of the substrate to the formal redox potential of adsorbed cyt c, the probability of accessing these redox orbitals during a resonant tunneling STM experiment may be significant. With this in mind, a possible experimental set-up of the proposed experiment is shown in Figure 5.23. Upon examination of this experimental apparatus, it bears a striking resemblance to the peak broadening experiments described in Chapter 2, making the resonant tunneling form of the experiment highly applicable and potentially very fruitful for understanding this system. It is hopeful that this experiment can show the same phenomena Tao showed with the porphyrin system. Resonant tunneling of cyt c, therefore, should be a major long term goal of the Bowden research effort.

The proposed cyt c resonant tunneling experiments are not without some major hurdles. Experimentally, resonant tunneling of cyt c will require highly insulated STM tips with extremely low leak currents ( $< 1$  pA).<sup>21,22a</sup> Additionally, the resonant tunneling experiment is best performed with a bipotentiostat as a three electrode experiment, including a reference electrode. Resonant tunneling experiments can, however, be conducted in a more modest manner, with a two electrode set up, lacking a reference electrode. This type of experiment is accomplished by simply ramping the voltage and monitoring the current output.<sup>22c</sup> If resonant tunneling occurs in this type of experiment, the corresponding current response to the ramped potential change should also contain an additional spike of current from the resonant tunneling affect. A hypothetical example of such a result is shown in Figure 5.24. Unlike the four electrode experiment, however, the positioning (potential) at which this current spike occurs will be arbitrary and undefined from the lack of a reference electrode in the experiment. Still, the experiment is valid, if at least to illustrate the viability of more advanced experiments into resonant tunneling.

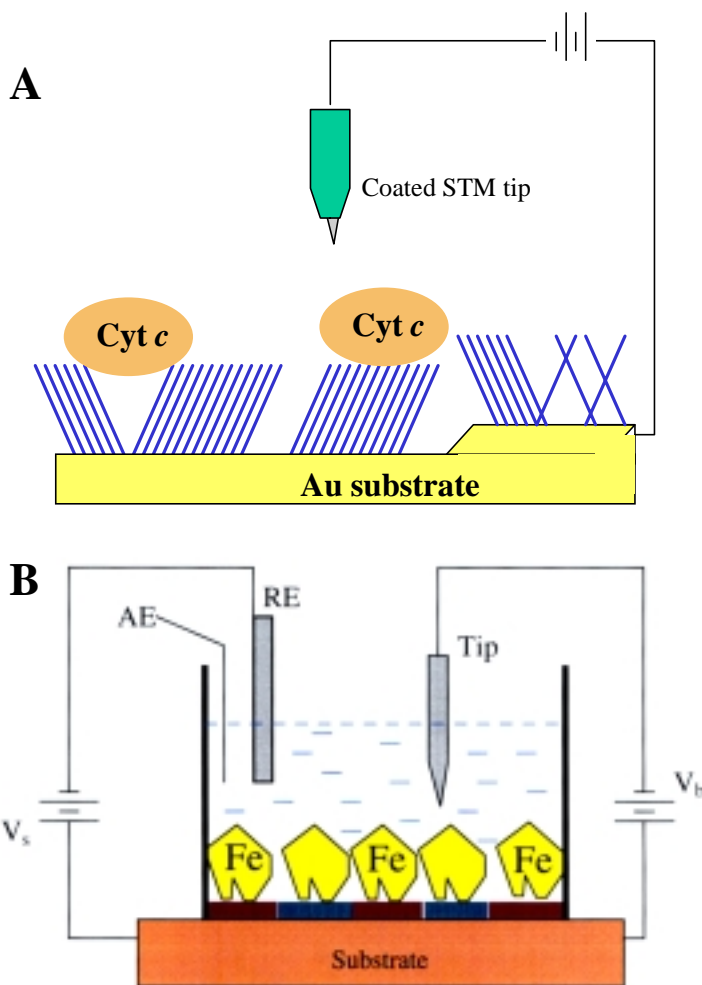


**Figure 5.23.** A) Hypothetical ECSTM experiment on cyt c molecules adsorbed at both defect sites and ordered domains of a SAM on gold and B) a proposed resonant tunneling experiment for cyt c and porphyrin cyt c. SPM experiments under potential control figure to be a major aspect of future experiments on this project.

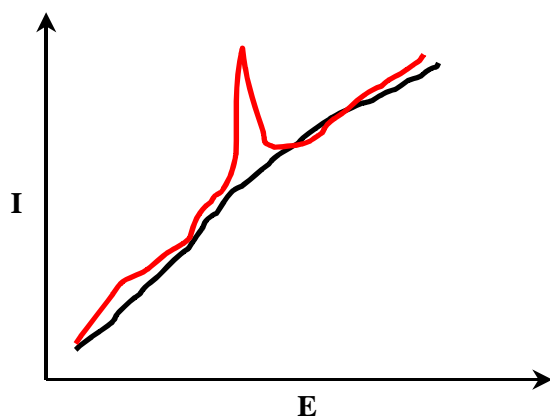


**Figure 5.24.** Hypothetical sketches of potential - current plots for a two electrode resonant tunneling experiment where the potential is ramped and the current response is measured: *black* - reference molecules (electroinactive) and *red* - sample molecules (electroactive).

Perhaps the most substantial obstacle to achieving resonant tunneling of cyt c molecules is the fact the STM imaging mechanism of proteins is not well established and it is not clear that an experiment of this nature would, in fact, work. It is believed that the cytochrome's protein shell will defeat the resonant tunneling process by inducing metal center-solvent separation, providing a fluctuating barrier to tunneling current, or altering the accessibility of the current to the heme group.<sup>20a</sup> Clearly, the answer to such speculation is to perform actual experiments. Considering that resonant tunneling is theoretically possible on material up to 100 Å thick, a range which cyt c falls well within, the experiments seem justified.<sup>22</sup> All in all, the resonant tunneling of cyt c, while a difficult project, is viewed by this researcher as having a definite probability, albeit possibly small, of being successful.

If initial experimentation on the resonant tunneling of cyt c fails, poor access of the tunneling current to the insulated heme may be the reason for the unsuccessful results. If this is the case, some alternative steps can be taken. The overall idea of these alternative experiments is still to achieve the first known example of resonant tunneling on a protein system. This may be best accomplished by simply increasing the probability that the tunneling current can access the redox core. This probability, it is proposed, can be increased by three different means: altering the position of the protein's redox active sites, altering the number of redox active sites per protein, or decreasing the extent of the protein shell around the porphyrin redox core. All three of these alternatives seek to simply allow greater access to the redox center of the protein, increasing the probability of a resonant tunneling effect taking place.

To alter the number of redox sites, multi-heme cytochromes such as cytochrome  $c_3$ , which has three heme groups could be used. To alter the position of the heme group, yeast cyt c may be employed as seen in Saavedra's work,<sup>24</sup> where the protein is immobilized on a gold surface by a covalent bond at the cysteine 102 position. Being anchored at this position effectively reverses the natural binding orientation, which normally places the heme crevice directly against the substrate surface. Thus, with covalent attachment, the heme crevice will be situated in a more exposed position, facing out towards the solution, as depicted in Figure 5.25. It is conceivable that this type of orientation may provide the STM tip with greater access to the protein's electroactive core. To decrease the extent of the protein shell, very

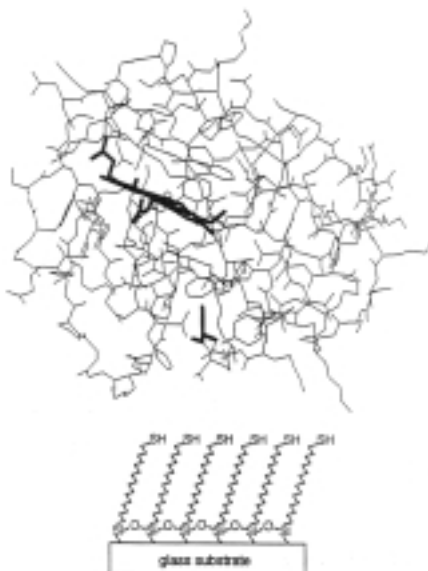


**Figure 5.25.** Yeast cyt c (wild type) may be covalently bonded via a disulfide bond between the SAM and a cysteine amino acid group in position 102. The porphyrin (Fe heme group) and the relevant cysteine residue at position 102 are shown in bold (Figure from Ref. 24).

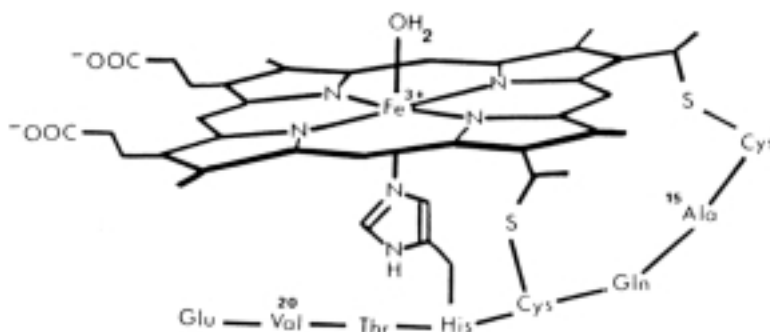


**Figure 5.26.** Microperoxidase may be used in future experiments for initial tests of resonant tunneling of proteins (Figure from Ref. 25).

small heme proteins such as microperoxidase, shown in Figure 5.26, could be used. Microperoxidase is a cyt c protein whose protein shell has been enzymatically digested until only eight amino acids remain attached to the porphyrin center.<sup>25</sup> If the protein shell was interfering with the resonant tunneling process on normal cyt c molecules, microperoxidase offers an improved chance of observing the phenomenon. If resonant tunneling is successful with microperoxidase and not with cyt c, it would strongly suggest that the protein shell is acting as the main barrier to the process. In summary, resonant tunneling of proteins is

clearly a risky venture, but one well worth consideration because of the valuable information that can be gained from such research.

Resonant tunneling serves the ultimate objectives of this research well. Resonant tunneling of cyt c, if successful, would provide the unprecedented ability to image cyt c adsorbed to electrode surfaces, as well as, differentiate between native/denatured or electroactive/electroinactive forms of the cytochrome molecules, all while maintaining potential control at the interface. Combinations of Pcyt c and cyt c could be used to identify strong and weak adsorption sites and correlate them with surface structure. Once molecular comprehension of the surface aspects of protein monolayer electrochemistry become available through research such as that described here, applied research in bioanalytical chemistry will benefit. The availability of accurate molecular adsorption models and well-defined ET mechanisms should lead to practical and clinically useful biosensors with performance that is currently unattainable.

## **5.5. SPECIAL ACKNOWLEDGEMENTS**

I am extremely grateful to the people that went out of their way to help me out with SPM experiments. Both Professor Chris Gorman and Dr. Igor Touzov, a Gorman Research Group postdoctoral associate, helped me out a great deal with SPM explanations, tutorials, and suggestions on my experiments. Most of all, however, I would like to thank my good friend and roommate of many years, Mr. Russell Miller. Without Russ, I never would have gotten the results that have been presented in this chapter. My only regret is that I didn't have more time to pursue the SPM goals, which, in my opinion are very exciting, achievable, and have the potential to be extremely insightful.

## **5.6. EXPERIMENTAL DETAILS**

### **5.6.1. STM Experiments**

STM experiments were conducted with a Digital Instruments Nanoscope III Multimode Scanning Probe Microscope operating in a low current STM mode. Images were collected at a constant current, using Pt/Ir mechanically cut STM tips (Digital Instruments). Tip shape is an extremely important aspect of imaging as it can distort reality by obscuring

the dimensions of imaged adsorbates, the number of molecules in the images, and the pattern of imaged materials (“ghost images”). To this end, many STM scientists systematically etch W tips. For this research, however, mechanically cut Pt/Ir tips, whose tip-to-tip quality varied significantly, were predominantly used. All measurements were carried out in a dry atmosphere of pre-purified helium with a relative humidity of < 1% as measured by a digital hygrometer (Fisher Scientific). Set point currents and voltage biases during imaging were usually in the range of 1-10 pA and 1-2 V, respectively. Wherever possible, these parameters have been included in the figures of the images or in their captions.

Gold substrates were pretreated and used as described in Chapter 3. All materials and equipment was handled with lint-free clean room gloves and/or stainless steel forceps to minimize contamination. Cyt c/gold samples were prepared by first hydrogen flame annealing gold on mica (Molecular Imaging, Inc.) as described by technical support from both Molecular Imaging and Digital Instruments.<sup>5,7</sup> Cyt c solution (0.25  $\mu$ M Horse Heart cyt c in 4.4 mM KPB) was then dispersed in the form of several drops via a disposable glass pipette, onto the cooled, dry gold surface. The cyt c was allowed to adsorb before the solution was very gently blown off the surface with a steady stream of dry Ar. The substrates were then imaged immediately over the next few hours.

### **5.6.2. AFM Experiments**

All AFM imaging was performed with a Digital Instruments Nanoscope III Multimode Scanning Probe Microscope. Cantilever deflections were detected optically a typical photodiode array detections system common to AFM instrumentation. In such an apparatus, a laser is deflected off the back of the cantilever and onto a position-sensitive photodetector. Images of gold surfaces were collected using contact mode AFM with an equiforce setting. This type of experiment was selected based on the stable structure of the Au substrate. Cantilevers of silicon nitride were used as received from Digital Instruments as 100 or 200  $\mu$ m isosceles triangular probes with both narrow and wide legs. The spring constants for the 100  $\mu$ m narrow and wide legs were 0.38 and 0.58 N/m, respectively, and 0.06 and 0.12 N/m for the 200  $\mu$ m cantilevers.

## 5.7 REFERENCES

1. a) O. Marti and M. Amrein, *STM and SFM in Biology*, Academic Press Inc.: New York, 1993. b) H.J. Guntherodt, and R. Wiesendanger, Eds., *Scanning Tunneling Microscopy I*; Springer Series in Surface Sciences 20; Springer-Verlag: Berlin, 1992; c) H.J. Guntherodt, and R. Wiesendanger, Eds., *Scanning Tunneling Microscopy II*, Springer Series in Surface Sciences 28; Springer-Verlag: Berlin, 1992; d) C. Bai, *Scanning Tunneling Microscopy and its Application*, Springer Series in Surface Sciences 32; Springer-Verlag: Berlin, 1995; e) S. Magonov, S. and M.H. Whangbo, *Surface Analysis with STM and AFM: Experimental and Theoretical Aspects of Image Analysis*, VCH: New York, 1996; f) L.A. Bottomley, J.E. Coury, and P.N. First, *Anal. Chem.* **1996**, *68*, 185R-230R; g) R.J. Hamers, "Scanned Probe Microscopies in Chemistry," *J. Phys. Chem.* **1996**, *100*, 13103-13120; h) M.D. Ward and H.S. White, "Scanning Tunneling and Atomic Force Microscopy of Electrochemical Interfaces," In *Modern Techniques in Electroanalysis*; P. Vanysck, Ed., Chemical Analysis Series; John Wiley and Sons Inc.: 1996; Vol. 139, Chapter 3.
2. Supplemental Proposal to NSF Grant (CHE-9307257).
3. a) C.R. Clemmer and T.P. Beebe, "A Review of Graphite and Gold Surface Studies for Use as Substrates in Biological Scanning Tunneling Microscopy Studies," *Scanning Microscopy* **1992**, *6*(2), 319-333; b) J. Vancea, G. Reiss, F. Schneider, and H. Hoffman, "Substrate Effects on the Surface Topography of Evaporated Gold Films - A Scanning Tunneling Microscopy Investigation," *Surface Science* **1989**, *218*, 108-126.
4. a) S.E. Creager, L.A. Hockett, and G.K. Rowe, "Consequences of Microscopic Surface Roughness for Molecular Self-Assembly," *Langmuir* **1992**, *8*, 854-861; b) S. Manne, J. Massie, V.B. Elings, P.K. Hansma, and A.A. Gewirth, "Electrochemistry on a Gold Surface Observed With the Atomic Force Microscope," *J. Vac. Sci. Technol. B* **1991**, *9*(2), 950-954.
5. Personal correspondence with B.C. Schardt of Digital Imaging Corporation, 1996.
6. a) J. Kang and P.A. Rowntree, "Molecularly Resolved Surface Superstructure of Self-Assembled Butanethiol Monolayers on Gold," *Langmuir* **1996**, *12*, 2813-2819; b) D.J. Trevor, C.E.D. Chidsey, and Dominic N. Loiacono, "In Situ Scanning-Tunneling-Microscope Observation of Roughening, Annealing, and Dissolution of Gold(111) in an Electrochemical Cell," *Physical Review Letters* **1989**, *62*(8), 929-932.
7. Personal communication with technical support at Molecular Imaging Corporation.
8. a) G.E. Poirier, M.J. Tarlov, "Molecular Ordering and Gold Migration Observed in Butanethiol Self-Assembled Monolayers Using Scanning Tunneling Microscopy," *J. Phys. Chem.* **1995**, *99*, 10966-10970; b) C. Schonberger, J.A.M. Sondag-Huethorst, J. Jorritsma, and L.G.J. Fokkink, "What Are the 'Holes' in Self-Assembled Monolayers of Alkanethiols on Gold," *Langmuir* **1994**, *10*(3), 611-614; c) C. Schonberger, J.A.M. Sondag-Huethorst, and L.G.J. Fokkink, "Formation of Holes in Alkanethiol Monolayers on Gold," *J. Phys. Chem.* **1994**, *98*, 6826-6834.
9. a) M. Hegner, P. Wagner, and G. Semenza, "Ultralarge Atomically Flat Template-Stripped Au Surfaces For Scanning Probe Microscopy," *Surface Science* **1993**, *291*, 39-46; b) N.G. Woodard

and G.P. Lafyatis, "Fabrication and Characterization of Extremely Smooth Large Area Gold Surfaces," *J. Vac. Sci. Technol. A* **1996**, 14(2), 332-335.

10. a) G.E. Poirier, *Langmuir* **1997**, 13, 2019-2026; b) M.J. Poirier and E.D. Pylant, "The Self-Assembly Mechanism of Alkanethiols on Au(111)," *Science* **1996**, 272, 1145-1148; c) C.A. Alves, E.L. Smith, M.D. Porter, "Atomic Scale Imaging of Alkanethiolate Monolayers at Au Surfaces with Atomic Force Microscopy," *J. Am. Chem. Soc.* **1992**, 114, 1222-1227; d) R. Yamada and K. Uosaki, "In-Situ, Real Time Monitoring of the Self-Assembly Process of Decanethiol on Au(111) in Liquid Phase. A Scanning Tunneling Microscopy Investigation," *Langmuir* **1997**, 13, 5218-5221; e) J. Pan, N. Tao, and S.M. Lindsay, "An Atomic Force Microscopy Study of a Self-Assembled Octadecyl Mercaptan Monolayer Adsorbed on Gold (111) Under Potential Control," *Langmuir* **1993**, 9, 1556-1560; f) C.B. Ross, L. Sun, R.M. Crooks, "Scanning Probe Litography. 1. Scanning Tunneling Microscope Induced Lithography of Self-Assembled n-Alkanethiol Monolayer Resists," *Langmuir* **1993**, 9, 632-636.
11. a) M. Sprik, E. Delamarche, B. Michel, U. Rothlisberger, M.L. Klein, H. Wold, and H. Ringsdorf, "Structure of Hydrophilic Self-Assembled Monolayers: A Combined Scanning Tunneling Microscopy and Computer Simulation Study," *Langmuir* **1994**, 10, 4116-4130; b) K. Hu and A.J. Bard, "Use of Atomic Microscopy for the Study of Surface Acid-Base Properties of Carboxylic Acid-Terminated Self-Assembled Monolayers," *Langmuir* **1997**, 13, 5114-5119; c) M.P.L. Werts, E.W. van der Vegte, and G. Hadziioannou, "Surface Chemical Reactions Probed with Scanning Force Microscopy," *Langmuir* **1997**, 13, 4939-4942; d) J.T. Woodward and D.K. Schwartz, "In Situ Observation of Self-Assembled Monolayer Growth," *J. Am. Chem. Soc.* **1996**, 118, 7861-7862; e) U. Durig, O. Zuger, B. Michel, L. Haussling, and H. Ringsdorf, "Electronic and Mechanical Characterization of Self-Assembled Alkanethiol Monolayers by Scanning Tunneling Microscopy Combined With Interaction Force Gradient Sensing," *Physical Review B* **1993**, 48(3), 1711-1717; f) J.L. Wilbur, H.A. Biebuyck, J.C. MacDonald, and G.M. Whitesides, *Langmuir* **1995**, 11, 825-831; g) M. Lestelius, B. Liedberg, and P. Tengvall, *Langmuir* **1997**, 13, 5900-5908.
12. a) N. Camillone, C.E.D. Chidsey, G. Liu, and G. Scoles, "Superlattice Structure at the Surface of a Monolayer of Octadecanethiol Self-Assembled on Au(111)," *J. Chem. Phys.* **1993**, 98(4), 3503-3511; b) G.E. Poirier and M.J. Tarlov, "The c(4x2) Superlattice of n-Alkanethiol Monolayers Self-Assembled on Au(111)," *Langmuir* **1994**, 10(9), 2853-2857; c) G.E. Poirier, H.E. Rushmeier, and M.J. Tarlov, "Two-Dimensional Liquid Phase and the  $p \times \sqrt{3}$  Phase of Alkanethiol Self-Assembled Monolayers on Au(111)," *Langmuir* **1994**, 10, 3383-3386; d) N. Camillone, P. Eisenberger, T.Y.B. Leung, P. Schwartz, and G. Scoles, "New Monolayer Phases of n-Alkane Thiols Self-Assembled on Au(111): Preparation, Characterization, and Imaging," *J. Chem. Phys.* **1994**, 101, 11031-11036; e) C. Schonberger, J. Jorritsma, J.A.M. Sondag-Huethorst, and L.G.J. Fokkink, "Domain Structure of Self-Assembled Alkanethiol Monolayers on Gold," *J. Phys. Chem.* **1995**, 99, 3259-3271.
13. Digital Instruments Nanoscope® III Multimode Scanning Probe Microscope, Instruction Manual, Manual Version 1.5, November 12, 1993.
14. a) L.A. Bumm, J.J. Arnold, L.F. Charles, T.D. Dunbar, D.L. Allara, and P.S. Weiss, "Creating Molecular Terraces With Molecularly Sharp Boundaries in Organic Thin Films," submitted to *Science*; b) E. Delamarche, B. Michel, H.A. Biebuyck, and C. Gerber, "Golden Interfaces: The Surface of Self-Assembled Monolayers\*\*," *Adv. Mater.* **1996**, 8(9), 719-729; c) S.J. Stranick,

- A.N. Parikh, T.-T. Tao, D.L. Allara, and P.S. Weiss, "Phase Separation of Mixed Composition Self-Assembled Monolayers Into Nanometer Scale Molecular Domains," *J. Phys. Chem.* **1994**, *98*, 7636-7646.
15. a) H. Arakawa, K. Umemura, and A. Ikai, "Protein Images Obtained by STM, AFM, and TEM," *Nature* **1992**, *358*, 171-173; b) S. Karrasch, R. Hegerl, J.H. Hoh, W. Baumeister, and A. Engel, "Atomic Force Microscopy Produces Faithful High-Resolution Images of Protein Surfaces in an Aqueous Environment," *Proc. Natl. Acad. Sci. USA* **1994**, *91*, 836-838; c) F. Caruso, D.N. Furlong, and P. Kingshott, "Characterization of Ferritin Adsorption Onto Gold," *Journal of Colloid and Interface Science* **1997**, *186*, 129-140; d) A. Mosca, R. Paleari, P. Arosio, A. Cricenti, M.A. Scarselli, R. Generosi, S. Selci, and E. Rovida, "Direct Observation of Human Liver Ferritin by Scanning Tunneling Microscopy," *J. Vac. Sci. Technol. B* **1994**, *12*(3), 1486-1489; e) S. Ohnishi, M. Hara, T. Furuno, and H. Sasabe, "Imaging the Ordered Arrays of Water-Soluble Protein Ferritin with the Atomic Force Microscope," *Biophys. J.* **1992**, *63*, 1425-1431; f) S. Ohnishi, M. Hara, T. Furuno, and H. Sasabe, "Direct Visualization of Polypeptide Shell of Ferritin Molecule by Atomic Force Microscopy," *Biophys. J.* **1993**, *65*, 573-577; J. Yang, K. Takeyasu, A.P. Somlyo, and Z. Shao, "Scanning Tunneling Microscopy of an Ionic Crystal: Ferritin Core," *Ultramicroscopy* **1992**, *45*, 199-203.
16. S.J. Eppell, F.R. Zypman, and R.E. Marchant, "Probing the Resolution Limits and Tip Interactions of Atomic Force Microscopy in the Study of Globular Proteins," *Langmuir* **1993**, *9*(9), 2281-2288.
17. a) Q. Chi, J. Zhang, S. Dong, and E. Wang, "Direct Observation of Native and Unfolded Glucose Oxidase Structures by Scanning Tunneling Microscopy," *J. Chem. Soc. Faraday Trans.* **1994**, *90*(14), 2057-2060; b) J.D. Zhang, Q. Chi, S.J. Dong, and E. Wang, "High Resolution Imaging of Native Hemoglobin by Scanning Tunneling Microscopy," *J. Electroanal. Chem.* **1994**, *379*, 535-539; c) R. Guckenberger, M. Heim, G. Cevc, H.F. Knapp, W. Wiegrabe, and A. Hillebrand, "Scanning Tunneling Microscopy of Insulators and Biological Specimens Based on Lateral Conductivity of Ultrathin Water Films," *Science* **1994**, *266*, 1538-1540; d) F.-R. F. Fan and A.J. Bard, "STM on Wet Insulators: Electrochemistry or Tunneling?," *Science* **1995**, *270*, 1849-1851; e) M.E. Welland, M.J. Miles, N. Lambert, V.J. Morris, J.H. Coombs, and J.B. Pethica, "Structure of the Globular Protein Vicilin Revealed by Scanning Tunneling Microscopy," *Int. J. Biol. Macromol.* **1989**, *11*, 29-32; f) D.C. Dahn, M.O. Watanabe, B.L. Blackford, M.H. Jericho, and T.J. Beveridge, "Scanning Tunneling Microscopy Imaging of Biological Structures," *J. Vac. Sci. Technol. A* **1988**, *6*(2), 548-552; g) M.A. Voelker, S.R. Hameroff, J.E. He, R.S. McCuskey, C.W. Schneiker, T.A. Chvapil, L.S. Bell and L.B. West, "STM Imaging of Molecular Collagen and Phospholipid Membranes," *J. Mol. Biology* **1988**, *152*(2), 557-566.
18. a) P. Wagner, P. Kernén, M. Hegner, E. Ungewickell, G. Semenza, "Covalent Anchoring of Proteins onto Gold-Directed NHS-terminated Self-Assembled Monolayers in Aqueous Buffers: SFM Images of Clathrin Cages and Triskelia," *FEBS Letters* **1994**, *356*, 267-271; b) A.B. Maunsbach and K. Thomsen, "Atomic Force Microscopy of Crystallized Na<sup>+</sup>/K<sup>+</sup> - ATPase," In *The Sodium Pump. Structure Mechanism, Hormonal Control, and its Role in Disease*, E. Bamberg and W. Schonert, Eds. Steinkopff Verlag, Darmstadt 1994, 342-345; c) J.E.T. Andersen, E. Friis, L.L. Madsen, P. Moller, and J. Ulstrup, "The Behavior of P. Aeruginosa Azurin and its Ser26Cys Mutant at Gold Surfaces, Investigated by Cyclic Voltammetry and AFM," conference abstract; d) J.D. Burgess, V.W. Jones, and M.D. Porter, "Tapping Mode Scanning Force Microscopy Images of Cytochrome c Oxidase Immobilized in an Electrode Supported Lipid

- Bilayer Membrane,” submitted to *Nature*, **1998**; e) M. Fritz, M. Radmacher, J.P. Cleveland, M.W. Allersma, R.J. Stewart, R. Gieselmann, P. Janmey, C.F. Schmidt, and P.K. Hansman, “Imaging Globular and Filamentous Proteins in Physiological Buffer Solutions with Tapping Mode Atomic Force Microscopy,” *Langmuir* **1995**, *11*, 3529-3535; f) A.P. Quist, L.P. Bjorck, C.T. Reimann, S.O. Oscarsson, B.U.R. Sundqvist, “A Scanning Force Microscopy Study of Human Serum Albumin and Porcine Pancreas Trypsin Adsorption on Mica Surfaces,” *Surface Science* **1995**, *325*, L406-L412.
19. a) J.E.T. Andersen, P. Moller, M.V. Pedersen, and J. Ulstrup, “Cytochrome c Dynamics at Gold and Glassy Carbon Surfaces Monitored by *In Situ* Scanning Tunneling Microscopy,” *Surface Science* **1995**, *325*, 193-205; b) P. Connolly, J. Cooper, G.R. Moores, J. Shen, and G. Thompson, “Development of Molecular Patterning and Immobilization Techniques for Scanning Tunneling Microscopy and Atomic Force Microscopy,” *Nanotechnology* **1991**, *2*, 160-163; c) P. Connolly et al., *Nanobiology* **1993**, *2*, 43-53; d) Z. Nawaz, T.R.I. Cataldi, J. Knall, R. Someleh, and J.B. Pethica, “STM Imaging of Molecules: Factors Affecting Their Reliable Imaging,” *Surface Science* **1992**, *265*, 139-155; e) E. Delamarche, H. Biebuyck, B. Michel, G. Sundarababu, H. Sigrist, H. Wolf, and H. Ringsdorf, In *Procedures in Scanning Probe Microscopies*; Colton et al. Eds.; John Wiley and Sons Inc.: Chichester, UK, 1995; f) Z. Liu, A. Manivannan, H. Inokuchi, and H. Yanagi, *J. Vac. Sci. Technol. B* **1993**, *11*(5) 1766-1773; g) Z. Liu, A. Manivannan, H. Inokuchi, M. Ashida, A. Fujishima, and H. Yanagi, *Surface Science Letters* **1993**, *284*, L411-L415; h) B. Zhang and E. Wang, “Tip Induced Dynamic Characterization of Multilayers and Variable Morphologies of Cyt c Molecules on Highly Ordered Pyrolytic Graphite Revealed by *In Situ* Scanning Tunneling Microscopy,” *J. Chem. Soc., Faraday Trans.* **1997**, *93*(2), 327-331; i) E.P. Friis, J.E.T. Andersen, L.L. Madsen, P. Moller, R.J. Nichols, K.G. Olesen, and J. Ulstrup, “Metalloprotein Adsorption on Au(111) and Polycrystalline Platinum Investigated by *In Situ* Scanning Tunneling Microscopy with Molecular and Submolecular Resolution,” *Electrochimica Acta* **1998**, *43*(19-20), 2889-2897; j) J.D. Burgess, V.W. Jones, and M.D. Porter, “Tapping Mode-Scanning Force Microscopy Images of Cytochrome c Oxidase Immobilized in an Electrode-Supported Lipid Bilayer Membrane,” submitted to *Nature*.
20. a) J.E.T. Andersen, A.A. Kornyshev, A.M. Kuznetsov, L.L. Madsen, P. Moller, and J. Ulstrup, “Electron Tunneling in Electrochemical Processes and *In Situ* Scanning Tunnel Microscopy of Structurally Organized Systems,” *Electrochimica Acta* **1997**, *42*(5), 819-831; b) J.E.T. Andersen, J. Ulstrup, and P. Moller, “Electrode Surfaces in Metalloprotein Electrolytes Investigated by *In Situ* STM,” conference abstract.
21. a) L.A. Nagahara, T. Thundat, S.M. Lindsay, “Preparation and Characterization of STM Tips for Electrochemical Studies,” *Rev. Sci. Instrum.* **1989**, *60*(10), 3128-3130; b) L. Libioulle, Y. Houbion, J.M. Gilles, “Very Sharp Platinum Tips for Scanning Tunneling Microscopy,” *Rev. Sci. Instrum.* **1995**, *66*(1), 97-100; c) C.E. Bach, R.J. Nichols, W. Beckmann, H. Meyer, A. Schulte, J.O. Besenhard, and P.D. Jannakoudakis, “Effective Insulation of Scanning Tunneling Microscopy Tips for Electrochemical Studies Using an Electropainting Method,” *J. Electrochem. Soc.* **1993**, *140*(5), 1281-1284.
22. a) N.J. Tao, “Probing Potential-Tuned Resonant Tunneling Through Redox Molecules With Scanning Tunneling Microscopy,” *Physical Review Letters* **1996**, *76*(21), 4066-4069; b) K.W. Hipps and U. Mazur, “Unoccupied Orbital Mediated Tunneling: Resonance-like Structures in the Tunneling Spectra of Polyacenes,” *J. Phys. Chem.* **1994**, *98*, 5824-5829; c) J. Campbell, S. Li, D. Gust, T. Moore, A. Moore and S.M. Lindsay, “Probing Electron Transfer in Single Molecules

- with the STM,” presented at STM 95, Snowmass, CO, July 23-28 (1995); d) K.W. Hipps and U. Mazur, “Resonant Tunneling Bands and Electrochemical Reduction Potentials,” *J. Phys. Chem.* **1995**, *99*, 6684-6688; e) S.M. Lindsay, O.F. Sankey, Y. Li, C. Herbst, and A. Rupprecht, “Pressure and Resonant Effects in Scanning Tunneling Microscopy of Molecular Adsorbates,” *J. Phys. Chem.* **1990**, *94*, 4655-4660; f) S.M. Lindsay, Y. Li, J. Pan, T. Thundat, L.A. Nagahara, P. Oden, J.A. DeRose, U. Knipping, and J.W. White, “Studies of the Electrical Properties of Large Molecular Adsorbates,” *J. Vac. Sci. Technol. B* **1991**, *9*(2), 1096-1101; g) S.M. Lindsay, L. Lyubchenko, Y. Li, N.J. Tao, J. Pan, P. Oden, and J.A. DeRose, “Scanning Tunneling Microscopy and Atomic Force Microscopy Studies of Biomaterials at a Liquid-Solid Interface,” *J. Vac. Sci. Technol. A* **1993**, *11*(4), 808-815.
23. J.M. Vanderkooi and M. Erecinska, *Eur. J. Biochem.* **1975**, *60*, 199-207.
24. S. Saavedra, *J. Am. Chem. Soc.* **1997**, *119*, 560-576.
25. M. Adam, A.K. Brimah, R.D. Fischer, Li Xing-Fu, “Cyclic Voltammetry of Imidazolemicroperoxidase-8: Modeling the Control of the Redox Potential of the Cytochromes,” *Inorg. Chem.* **1990**, *29*, 1597-1599.
26. R.L. Miller, “Investigating the Effects of the Incorporation of Functional Elements Into Adlayer,” Master’s of Science Thesis, 1997.
27. a) S.N. Magonov and M.H. Whangbo, “Interpreting STM and AFM Images\*\*,” *Advanced Materials* **1994**, *6*(5), 355-371; b) D.M. Eigler, P.S. Weiss, N.D. Lang, and E.K. Schweizer, “Imaging Xe with a Low-Temperature Scanning Tunneling Microscope,” *Physical Review Letters* **1991**, *66*(9), 1189-1192; c) I.A. Rauf, “A Comparison of Scanning Tunneling Microscopy With Conventional and Scanning Transmission Electron Microscopy Using Tin-Doped Indium Oxide Thin Films,” *Surface Science* **1995**, *325*, L413-L419; d) R. Heinz and J.P. Rabe, “Scanning Tunneling Microscopy Investigation of Sulfide and Alkanethiolate Adlayers on Ag(111),” *Langmuir* **1995**, *11*, 506-511; e) J.P. Song, K.A. Morch, K. Carneiro, and A.R. Tholen, “STM Investigations of Solid Surfaces in Water and Air,” *Surface Science* **1993**, *296*, 299-309; f) M.F. Crommie, C.P. Lutz, and D.M. Eigler, “Confinement of Electrons to Quantum Corrals on a Metal Surface,” *Science* **1993**, *262*, 218-220; g) *Physics Today*, August **1986**; h) P.K. Hansma, V.B. Elings, O. Marti, and C.E. Bracker, “Scanning Tunneling Microscopy and Atomic Force Microscopy: Application to Biology and Technology,” *Science* **1988**, *242*, 209; i) Bruce Schardt, S.L. Yau, F. Rinaldi, “Atomic Resolution of Adsorbates on Metal Surfaces in Air: Iodine Adsorption on Pt(111),” *Science* **1989**, *243*, 1050-1053; j) Y. Zhang, X. Gao, and M.J. Weaver, “Scanning Tunneling Microscopy of C60 and C70 on Ordered Au(111) and Au(110): Molecular Structure and Electron Transmission,” *J. Phys. Chem.* **1992**, *96*, 510-513.
28. a) B. Drake, C.B. Prater, A.L. Weisenhorn, S.A.C. Gould, T.R. Albrecht, C.F. Quate, S. Cannell, H.G. Hansma, P.K. Hansma, *Science* **1989**, *243*, 1586-1589; b) N.A. Burnham and R.J. Colton, “Force Microscopy,” Chapter 7 of *Scanning Tunneling Microscopy and Spectroscopy*, 191-249; c) M. Salmeron, G. Neubauer, A. Folch, M. Tomitori, D.F. Ogletree, and P. Sautet, *Langmuir* **1993**, *9*, 3600-3611; d) S.E. Roark, D.J. Semin, and K.L. Rowlen, *Anal. Chem.* **1996**, *68*, 473-480; e) W. Han, S.M. Lindsay, T. Jing, “A Magnetically Driven Oscillating Probe Microscope for Operation in Liquids,” *Appl. Phys. Lett.* **1996**, *69*(26), 4111-4113; f) C.B. Prater, P.G. Maivvald, K.J. Kjoller, and M.G. Heaton, “Tapping Mode Imaging - Applications and Technology,” *Digital Instruments Brochure*.

## **SOLVENTLESS ELECTROCHEMISTRY OF METALLODENDRIMERS**

### **APPENDIX A**

*“For every expert, there is an equal and opposite expert.” – Late 20<sup>th</sup> Century folklore*

## A. SOLVENTLESS ELECTROCHEMISTRY OF METALLODENDRIMERS

### A.1. INTRODUCTION -- NANOTECHNOLOGY

As technology becomes more and more integrated into people's everyday lives, the demand for faster computers, capable of storing enormous amounts of information, is becoming greater. Coupled with this concept is the continuing need and desire of society to make computing and communication circuitry as small as possible while still maintaining the device's operational function or its ability to successfully encode information (Figure A.1).<sup>1</sup> Chemists are focusing on developing materials that can serve as ultra-miniature electrical components, commonly referred to as molecular electronics. Indeed, with the advent of scanning probe microscopy, as well as recent advances in synthetic, characterization, and self-assembly techniques, the idea of single molecules acting as nanoscale electronic devices is starting to be realized. Over the years, many researchers have proposed or created molecular structures supposedly capable of serving as electrical components such as wires, capacitors, switches, or diodes.<sup>2</sup> However, few of these materials were presented with evidence of functional behavior,<sup>3</sup> and researchers are only now beginning to provide true molecular devices with demonstrated functionality. Research into molecular electronics and the development of nanotechnology remains at the forefront of engineering, as well as, chemical, physical, and materials research.

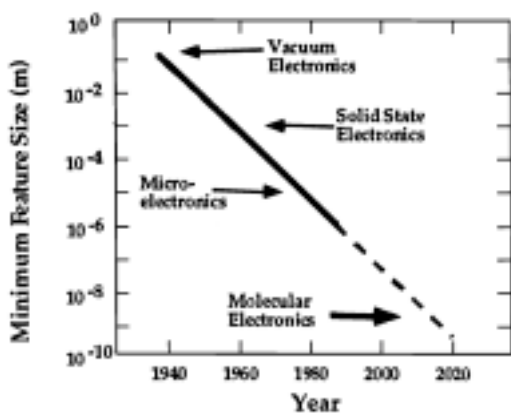


**Figure A.1.** Miniaturization of electronic devices – past, present, and future (Figure from Ref. 1).

### A.2. THE INFORMATION BEARING UNIT (IBU)

One aspect of molecular electronics is the development of a molecular switch or information bearing unit (IBU). Essentially, a molecule acting as an IBU would behave as a nanoscale sized computer bit. After all, information storage in computers is simply made up of many series of bits or bytes (a collection of switches representing ones and zeros). Like

the traditional bit, a successful IBU molecule would be capable of existing in two stable states or positions: an “on” position and an “off” position, a one or zero, respectively. Additionally, the IBUs would need to be spatially controlled on a surface and easily accessible or readable with respect to their information states. Spatial manipulation on the molecular and atomic scale is already a commonplace phenomenon in the research lab, advanced greatly in recent years by the proliferation of superior scanning probe microscopy (SPM) technologies.<sup>4</sup> It is then conceivable that arrays of these molecular switches, each bearing an independent unit of binary information, could potentially exist in a computer system capable of storing immense amounts of data in a minute amount of space relative to today’s standards. To this end, researchers are now focused on creating, isolating, and characterizing molecules that are promising candidates to act as molecular switches.

One approach to developing a functional IBU molecule is to utilize a stable redox molecule, employing its inherent oxidation states as a form of binary information. Encoding information in the form of molecular oxidation states is a promising but formidable task, one that has yet to be demonstrated and is not without significant complications. For instance, stable redox molecules must be controllably immobilized and positioned on a surface without disrupting their ability to undergo redox reactions. More importantly, each IBU must be sufficiently isolated from one another in order to prevent intermolecular electron transfer (ET) processes from altering assigned oxidation states. If it occurs, intermolecular ET between two IBUs in close proximity is, in effect, a loss of encoded information. This is an unacceptable side effect of molecular IBUs and therefore, molecules designed to hold information must account for this possibility. Therefore, the most realistic aspirations of advancing this type of technology start with researchers developing stable redox species that have the appropriate characteristics and behavior to act as an IBU.

### **A.3. THE GORMAN RESEARCH PROJECT – METALLODENDRIMERS**

Research in the Gorman Group at NCSU revolves around the development of IBUs using electroactive inorganic cores that are systematically encapsulated by dendritic ligands. Taken literally, the term dendritic or dendrimer is derived from the Greek word *dendro-*, meaning treelike or branching. In terms of chemistry, a dendrimer possesses a specific type

of structure, illustrated in Figure A.2.<sup>5</sup> Dendrimers are compounds with a hyperbranching molecular architecture that can create very unique three dimensional molecular structures. Metal core based dendrimers, called metallodendrimers, represent the creation of interesting inorganic/organic hybrid molecules and have recently become the subject of much interest in both the dendrimer and nanoelectronic research communities. In fact, several excellent review articles are available with in depth discussions of the synthesis, characterization, structural diversity, and potential applications of this unique class of supramolecules.<sup>6</sup>

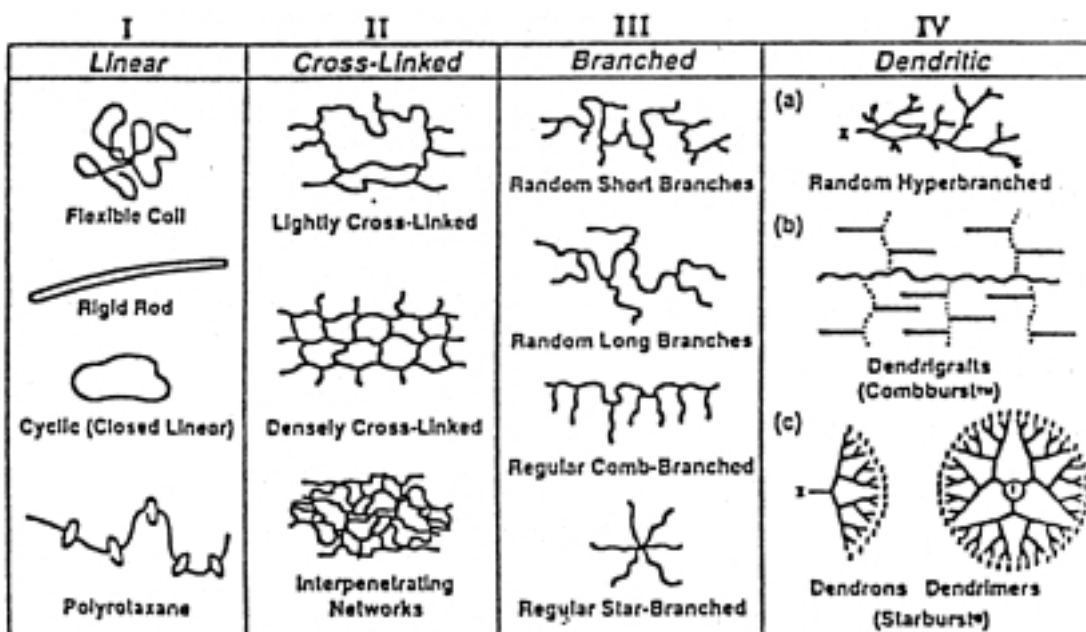


**Figure A.2.** Main classes of macromolecular architecture - dendrimers (lower right) have a specifically ordered branched structure (Fig. from Ref. 5).

The hyperbranching structure of metallodendrimers is what makes these compounds especially attractive as potential IBUs. Given the right type of synthetic design, a dendrimer can act as an encapsulating shell around smaller molecules or even around its own core.<sup>7</sup> Effectively, this encapsulating dendritic material should act as a type of electrical insulator, creating a unique microenvironment within the molecule and attenuating the reactivity of the electroactive core. Thus, it is hopeful that the encapsulated redox moiety can act as a charge storage device. As shown in Figure A.3,<sup>8</sup> the dendritic encapsulation of a redox center is expected to prevent facile intermolecular ET and, in the case of an IBU, reduce the possibility of losing stored information. With this in mind, the general objective of the Gorman Research Group is to develop metallodendrimers with a molecular structure - property

relationship where the degree of hyperbranching in the dendritic ligands can be related to the attenuation of the ET properties of the core.

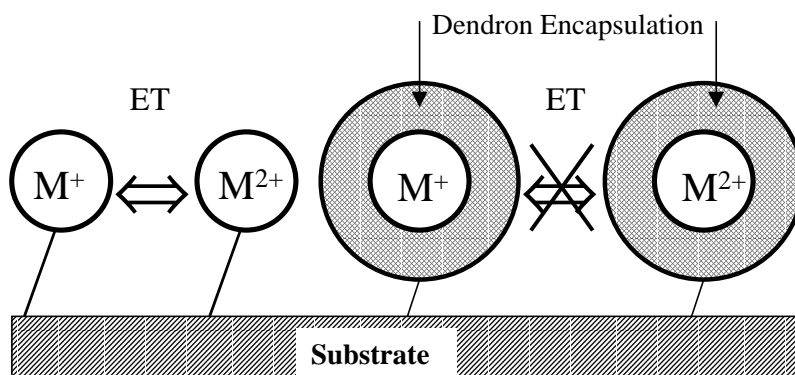


**Figure A.3.** Dendritic encapsulation should prevent facile ET between redox centers  $M^+$  and  $M^{2+}$  (Fig. from Ref. 8).

### A.3.1 Fe - S Based Dendrimers

Researchers in the Gorman group have been successful at synthesizing and characterizing potential IBU dendrimers based on the modification of an iron-sulfur core.<sup>9</sup> The tertiary butyl thiolated iron sulfur core, shown in Figure A.4, is an excellent redox center for a metallodendrimer functioning as an IBU for several reasons. Not only does the core exist in two primary oxidation states, an essential requirement for a potential molecular switch, but it also is the same redox center that is found in many redox active proteins, some of which function as ET and charge storage entities in biological systems.<sup>10</sup> Additionally, the core is synthetically accessible and it undergoes facile ligand exchange with macromolecules such as dendrons, making it an easily tailored redox center.<sup>7</sup> The thiol based ligating points bound to the iron corners of the cluster allow for the use of well documented synthetic processes, and the tetrahedral nature of the core is more conducive to global encapsulation of dendritic ligands around the core than some other spatial arrangements. The electrochemical behavior of this Fe-S core has been well characterized and establishes a standard to which the electroactivity of any derivatives of this cluster can be compared.<sup>4</sup>

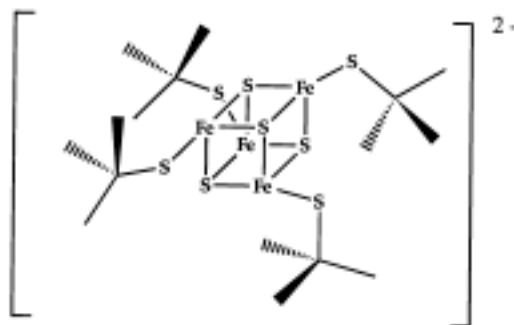


**Figure A.4.** The tertiary butyl thiolated iron-sulfur core  $[\text{Fe}_4\text{S}_4(\text{S}-t\text{-Bu})_4]^{2-}$  – the redox center of the metallodendrimers synthesized in the Gorman Research Group. This Fe-S core is readily accessible to potential ligands, undergoing facile exchange with macromolecules, making it ideal for dendritic encapsulation. Similar redox centers, or Fe-S “cubes” can be found in certain proteins, ferredoxins and rubredoxins for example, that function as ET and storage sites in biological systems.<sup>10</sup> (Fig. from Ref. 8)

Depending on the type of ligand attached to the Fe-S core, two main families of metallodendrimers have been synthesized in the Gorman research group: flexible IBUs, utilizing valerate based ligands, and rigid IBUs, consisting of phenylacetylene ligands. The designation of the flexibility of the structures is derived from the degrees of torsional rotation that exist in the flexible dendrimers as compared to the lack of conformational freedom found in the rigid structure. Molecular modeling studies done by the Gorman Group show that the overall disposition of the flexible dendrimers is globular, although not completely symmetrical about the core. On the other hand, the more rigid structure was found to adhere to a disk-like shape. These two types of dendrimers and their hyperbranching are illustrated as Figure A.5 and A.6 respectively.<sup>8</sup>

These two types of metallodendrimers are designed with one to four branching points in their dendritic ligands. In describing these compounds, the number of branching points creating the periphery is considered the molecule’s generation. For example, a flexible dendrimer with three branching points is referred to as a third generation flexible dendrimer or, in an abbreviated fashion, as “G3 flex.” This type of structural based nomenclature is portrayed with the flexible dendrimers in Figure A.5. For both the flexible and rigid molecules, the generations of hyperbranching are radially distributed throughout the interior of the macromolecule. Thus, a mental image of these molecules with the branches intertwined and folded in on each other can be visualized.<sup>11,12a</sup> As far as the core’s electroactivity is concerned, it was hypothesized that as the number of branches in the

dendron ligands around the core increased there would be a substantial and systematic change in the kinetics of ET.

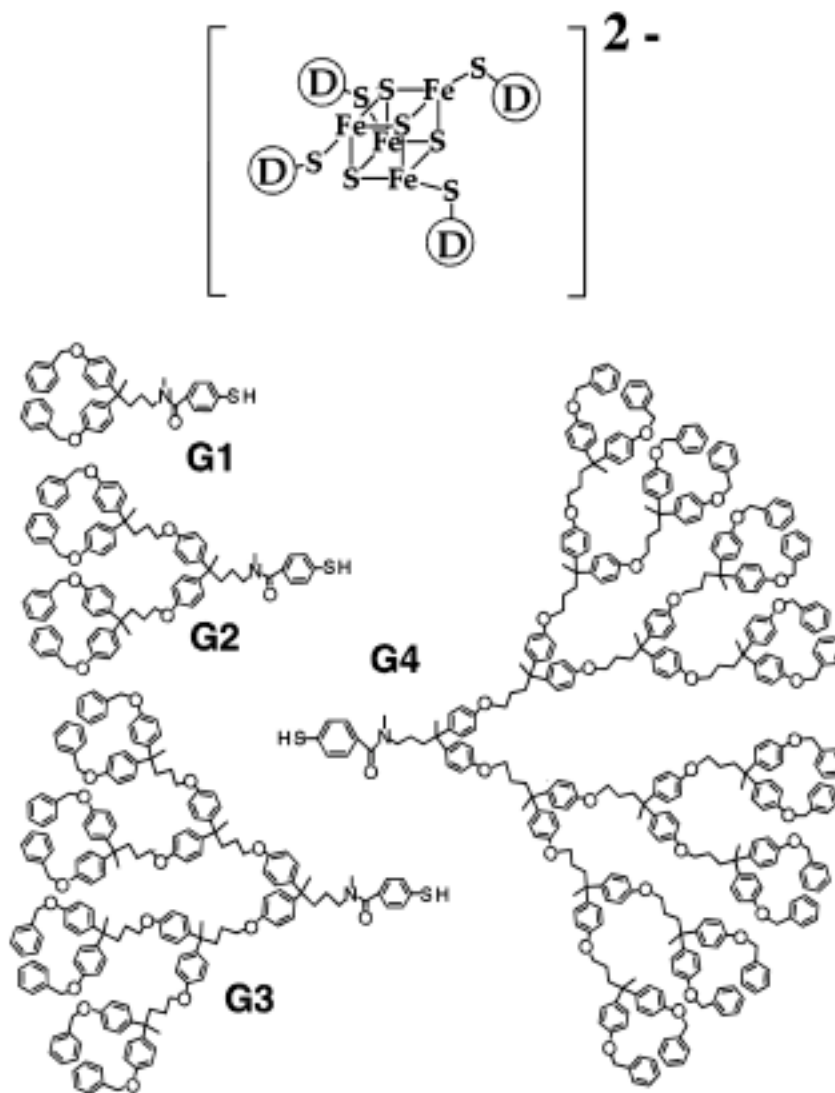


**Figure A.5.** Flexible IBU metallodendrimers; each type (generation) of dendritic ligand (G1-G4) that can be connected to the redox core is shown. The counter ions of these molecules are two tetrabutyl ammonium ions  $[(\text{CH}_3\text{CH}_2\text{CH}_2\text{CH}_2)_4\text{N}^+]$  (Fig. from Ref. 8).

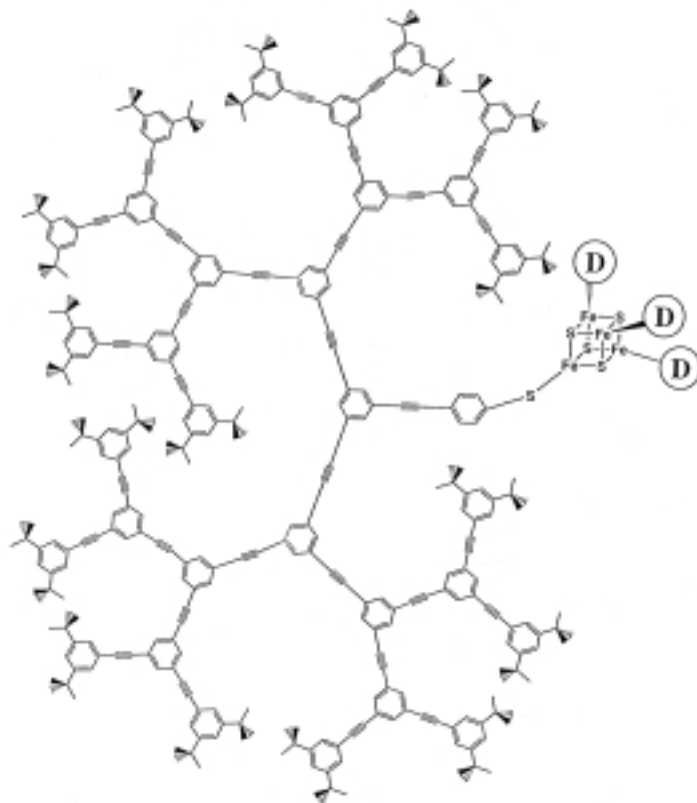


**Figure A.6.** An example of a fourth generation (G4 - rigid) rigid-type metallodendrimer with phenylacetylene ligands (Fig. from Ref. 8).

In general, previously performed electrochemical research on the dendrimers in organic solvent supported the hypothesis, showing an attenuation of ET properties with increasing generations of hyperbranching.<sup>12b</sup> All of the solution electrochemistry on these systems was performed in an inert atmosphere (glove box) because of the core's inherent instability in the presence of oxygen and/or water. As shown in Figure A.7, and summarized in Table A-1, the results of cyclic voltammetry and chronoamperometry experiments confirm the expected trend with increased branching and encapsulation of the redox center. Most of the dendrimers tested displayed ideally shaped voltammograms indicative of a freely diffusing species with quasi-reversible kinetics for a one electron transfer redox reaction. The results are consistent with the idea that as the size and number of branching points in the ligands are increased, both kinetics and thermodynamics are affected, as evidenced by the change in the separation of oxidizing and reducing peak potentials ( $\Delta E_p$ ) and by the shift in the reduction potential ( $E_{1/2}$ ) values, respectively. Thus, with increasing generations of hyperbranching, the molecules became more difficult to oxidize and reduce, clear evidence

**Table A-1.** Electrochemical Data Previously Obtained<sup>a</sup> for Metallo dendrimers<sup>7,9,12b</sup>

Generation (Ligand Branching)	Structure	$E_{1/2}^b$ (mV)	$\Delta E_p^c$ (mV)	$D_{\text{coeff}}^{f,g}$ ( $\text{cm}^2/\text{s}$ ) $\times 10^{-6}$	$k_{\text{et}}^h$ ( $\text{cm}/\text{s}$ ) $\times 10^{-3}$
0	flex	-1352 (3)	76 (6)	4.14(0.12)	8.63(0.83)
1	flex	-1360 (6)	80 (6)	3.47(0.16)	8.36(0.89)
2	flex	-1366 (10)	101 (11)	2.51(0.38)	3.59(0.33)
3	flex	-1371 (19)	148 (69) <sup>c</sup>	2.02(0.49)	0.51(0.22)
4	flex	-- <sup>d</sup>	-- <sup>d</sup>	--	-- <sup>i</sup>
0	rigid	-1354 (4)	80 (5)	4.75(0.42)	8.95(0.96)
1	rigid	-1323 (16)	80 (6)	2.17(0.46)	5.13(1.11)
2	rigid	-1329 (13)	111 (7)	1.89(0.37)	2.13(0.36)
3	rigid	-- <sup>e</sup>	-- <sup>e</sup>	-- <sup>e</sup>	-- <sup>e</sup>
4	rigid	-- <sup>e</sup>	-- <sup>e</sup>	-- <sup>e</sup>	-- <sup>e</sup>

<sup>a</sup> Data collected by Jennifer Smith, Gorman Research Group.

<sup>b</sup> From cyclic voltammetry experiments of 1mM dendrimer in dimethyl formamide (DMF) at 100mV/sec, with 100mM nBu<sub>4</sub>NPF<sub>6</sub> as the supporting electrolyte; measured versus a Ag<sup>+0</sup> reference electrode at a platinum working electrode.

<sup>c</sup> All values of  $\Delta E_p$  were measured at 100mV/sec with the exception of G4 flex which was only measurable at extremely slow scan rates ( $\leq 5$  mV/sec).

<sup>d</sup> Value undetermined due to poor voltammetric response (irreversible).

<sup>e</sup> DMF solubility problems existed with the higher generation rigid dendrimers.

<sup>f</sup> Values measured via chronoamperometry experiments.<sup>12b</sup>

<sup>g</sup> Similar results were obtained with pulsed field gradient NMR experiments (results not shown).

<sup>h</sup> Kinetic analysis using Nicholson cyclic voltammetry method ( $\alpha = 0.5$ ).

<sup>i</sup> Quantitative data eventually obtained using Osteryoung Square Wave Voltammetry fit to an irreversible model.<sup>12b</sup>

Note: Values in parentheses denote the 90% confidence intervals of each result.

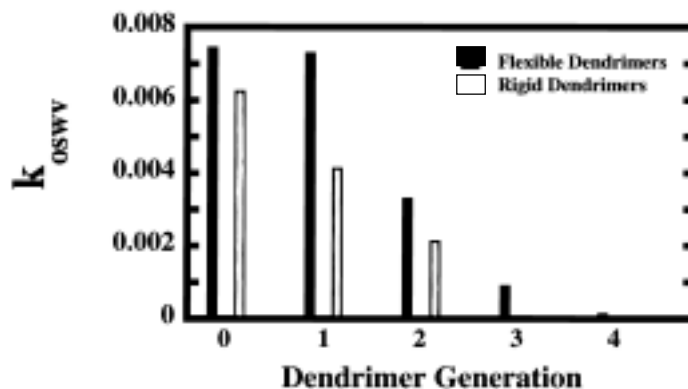


**Figure A.7.** Data illustrating the effective encapsulation of the metallo dendrimers and its effect on the ET rate constant. Experiments were performed in solution at Pt macroelectrodes. Note that data was unattainable under these experimental conditions higher generation molecules (Data collected by Jennifer Smith; Figure from Ref. 12b).

supporting the hypothesis that the dendritic periphery effectively encapsulates and insulates the electroactive core. The highest generation flexible dendrimer (G4-flex), however, showed very poor voltammetric behavior, with no clear reoxidation wave present in the cyclic voltammetry (See Table A-1 for more details). While this result suggests that the electroactive core may be completely insulated in the G4-flex molecule, it is unfortunate from a quantitative analysis and comparison standpoint. Quantitative determination of redox potential, ET rate constants, diffusion coefficients, and peak separation was unattainable, leaving an incomplete set of data for the flexible IBUs. Likewise, a complete data set could not be collected for some of the rigid molecules because the higher generation forms of this dendrimer were not very soluble in most solvents (See Table A-1). In spite of these problems, the collected data provide promise that this type of dendritic encapsulation is an effective means to kinetically “trap” a molecule in a specific redox state and, in doing so, create a legitimate model for an IBU.

### **A.3.2. Gorman / Bowden Collaboration Project**

In an effort to more fully characterize the ET properties of these molecules and advance progress on this project, a research collaboration was formed between the Gorman Research Group and the Bowden Research Group. The collaboration is a naturally synergistic relationship considering research in the Bowden Group is primarily directed at studying the ET properties of the charge carrier protein, cytochrome *c*. As alluded to earlier, the dendritic IBU molecules synthesized by the Gorman Group are not only models for information/charge storage, but have many features comparable to actual proteins.<sup>1,11</sup> Therefore, in addition to being potential molecular switches, the dendrimers may also serve as synthetic models for certain biomolecules.

As will be explained, the parallel between the research of these two groups includes a mutual interest in self-assembled monolayers (SAMs). In the Bowden Group, the ET properties of surface confined *cyt c* molecules are studied by electrostatically immobilizing the protein on carboxylic acid terminated SAMs (See Figure A.8a).<sup>11</sup> In a similar fashion, the Gorman group hopes to physisorb their metallodendrimers to alkanethiol based SAMs and demonstrate adsorbed molecular behavior in these compounds similar to that seen in solution (Figure A.8b). This type of experiment represents a significant step toward their overall

research goal, a surface bound IBU. The analogous chemical systems allow for both groups to work together toward project goals with mutual interest. The research presented here is due to a collaborative effort with Dr. Jennifer Smith in the Gorman Research Laboratory.

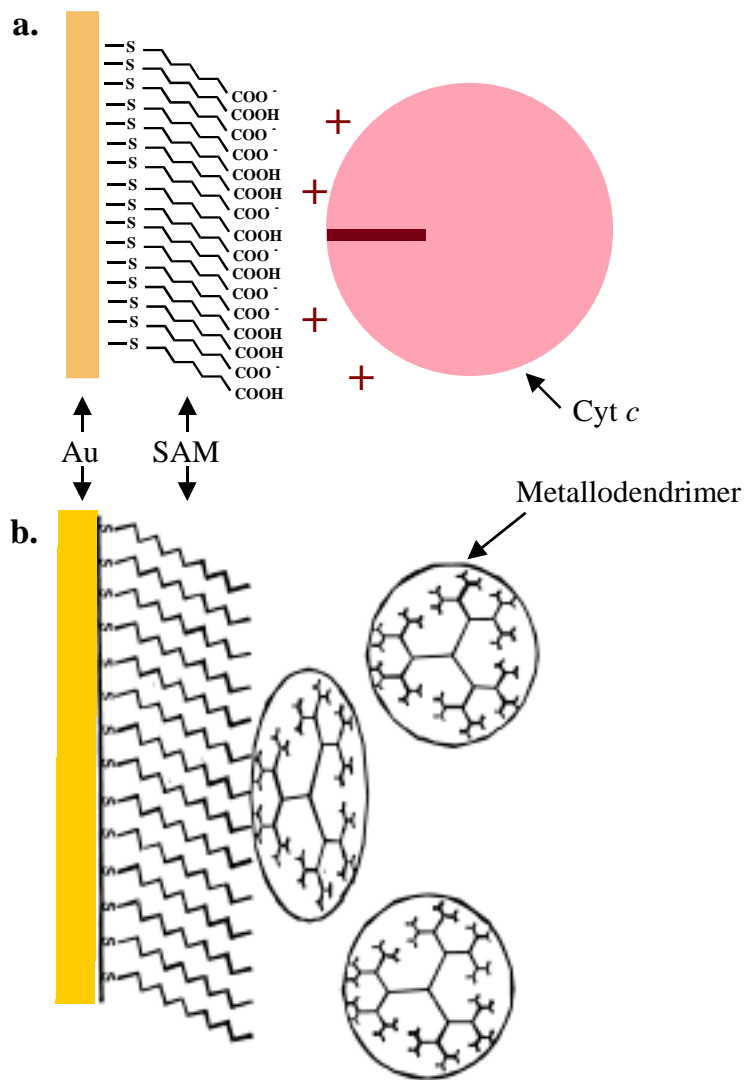


**Figure A.8.** Illustrative models showing the similarities of the ET systems being researched in the a) Bowden Research Group (cyt c/SAM/Au) and b) the Gorman Research Group (metallodendrimer/SAM/Au). (Fig. 8b from Ref. 11)

### **A.3.3. Research Objectives**

Eventually, any macromolecules being considered as potential IBUs or molecular switches will have to be specifically tailored to render the molecules switchable, addressable, and able to be organized on a surface. A large challenge of reaching this goal is to simply immobilize the molecule on any surface and gain the ability to control the IBU/surface interaction. Furthermore, each IBU must be confined to a designated space and position on that surface while maintaining the ability to effectively store charge. SAM technology, in conjunction with lithographic techniques, seems to hold great promise with regard to achieving this type of control over this chemical system. SAMs can be created with a variety of structures and properties, enlisting both hybrid combinations of mixed monolayers with different chain lengths and functional groups, as well as, micro-contact printing of patterned SAMs. Examples of using mixed monolayers to effectively immobilize dendritic molecules on surfaces have already been seen in the literature.<sup>13</sup> Scanning tunneling microscopy (STM) based lithography is not only capable of designing specifically tailored SAM surfaces, but can also accommodate the nanometer resolution spatial manipulation required for eventually addressing individual IBUs.<sup>4</sup> Both SAMs and SPM allow for unprecedented order and localized spatial definition on the molecular level, clearly beneficial for the proposed type of work.

Most scientific research progresses in very small increments; the Gorman/Bowden collaboration on the metallodendrimer project is no different. Before attempting work on the advanced goals depicted in the previous paragraph, the collaborative effort of the two groups focused on first simply finding an experimental medium conducive to testing the electrochemical behavior of all of the dendrimers. Therefore, quantifying the electrochemical properties of all eight IBUs is the first objective of this research. Secondly, and possibly in conjunction with the first objective, it was desired to successfully immobilize the IBU on a SAM and begin characterizing the ET of surface bound dendrimer assemblies.

### **A.4. PRELIMINARY EXPERIMENTS**

Upon inspection of the properties of the dendrimers, it appears that, by taking advantage of their relatively hydrophobic nature, they could be reasonably adsorbed to methyl

terminated SAMs in polar solutions. How polar the solvent had to be to facilitate this interaction remained a focal point of the search for an adequate experimental environment. In addition to all the dendrimers being soluble in it, the solvent used for this electrochemistry must also be able to dissolve the supporting electrolyte and possess an adequate polarity. Finding a solvent with all of these properties is not a minor task, especially when dealing with organic solvents. Although aqueous experiments have been performed on the dendrimers (data not shown or discussed in detail) and was beneficial toward the formation and stability of the SAMs, the dendrimers used in these aqueous environments ultimately suffered from oxygen exposure, which induced degradation of the molecules in only a brief amount of time. Additionally, dendrimers exposed to oxygen usually showed poor voltammetric behavior and sporadic results. All previous electrochemistry was performed in dimethylformamide (DMF) with ammonium-borate based supporting electrolyte, usually tetrabutylammonium hexafluoroborate ( $n\text{Bu}_4\text{NPF}_6$ ).<sup>4,9,12b</sup> With the success of this system already established, it seemed like a logical place to begin experimentation and simply tweak the system to find an appropriate combination of experimental conditions. One of the more important aspects of this testing, considering the very negative redox potentials of the dendrimers ( $\sim -1300$  mV vs.  $\text{Ag}^{+/0}$ ), was to choose a solvent with a potential window far enough negative to accommodate the redox reactions. Some solvents showed adequate solubility toward the dendrimers and the electrolytes, but simply did not have “clean” background electrochemistry that far into the negative potential window ( $\text{CH}_2\text{Cl}_2$ , toluene, pyridine). Thus, yet another restriction had to be considered when choosing a solvent/electrolyte combination. If, eventually, a maximum of a monolayer of physisorbed dendrimer occupies the SAM, the background signal or noise of the system must be sufficiently low enough to resolve the dendrimer signal. Table A-2 summarizes many of the tested solvents and lists each solvent’s inherent problem in the proposed experimental scheme. With all of the restrictions imposed by the desired system including the solubility of the dendrimers and electrolyte in the solvent, the solvent’s potential window, the signal to noise ratio, the negative thermodynamic reduction potentials of the metallodendrimers, and their air sensitivity (See Experimental Details section), a formidable task emerged to simply establish the experimental conditions.

**Table A-2.** Summary of Solvent / Electrolyte / Potential Window Testing

Solvent	Potential Window (V) <sup>a</sup>	Polarity <sup>b</sup> (Dielectric constant)	Problem(s)
Water	~1.0 to -1.0 <sup>c</sup>	78.4	-Dendrimer degradation (solvent would have to be degassed) -Potential Window
DMF	1.3 to -2.4	36.7	-Clean B/G signal -High generation solubility (Rigids) -Low generation too soluble (not adequate non-solvent)
ACN	1.3 to -2.5	37.5	-High generation solubility (Rigids and Flexibles) -Clean B/G signal
THF		7.6	-Electrolyte solubility -Polarity - not a non-solvent
CH <sub>2</sub> Cl <sub>2</sub>		8.9	-Clean B/G signal
Pyridine		12.4	
PC	1.5 to -2.3	64.4	-High generation solubility (Rigids)

Note: DMF = Dimethyl formamide; ACN = Acetonitrile; THF = tetrahydrofuran; CH<sub>2</sub>Cl<sub>2</sub> = Methylene chloride; PC = Propylene carbonate.

<sup>a</sup> Measured versus a Ag<sup>+0</sup> reference electrode; <sup>b</sup> Dielectric constants taken from Ref. 14.

<sup>c</sup> Potential window may vary based on electrolyte, RE (shown vs. SCE), and working electrode material.

#### A.4.1. Exploratory Electrochemistry in Propylene Carbonate

In spite of some dendrimer solubility problems, propylene carbonate (PC) seemed to be an excellent candidate for this type of experimentation, especially with regard to immobilizing the dendrimer on the SAM. PC displays a relatively flat background throughout most of its very wide potential window (1.5V ↔ -2.3V vs. Ag<sup>+0</sup>). Sometimes referred to as “organic water” because of its extremely high polarity for an organic solvent, PC also appeared to be an excellent solvent for inducing a hydrophobic interaction between dendrimer and SAM. Additionally, the use of PC in conjunction with alkanethiolate SAMs is preceded in literature reports by Creager and coworkers.<sup>15</sup> Although experiments done in PC successfully formed SAMs on gold, the use of PC as a solvent for the desired system ultimately failed, exposing a dramatic realization that affected the entire outlook of this project.

Evidence for the SAM's formation and existence in PC was readily available, and the process of allowing for hydrophobic interaction between dendrimer and SAM could have been carried out. However, actual physisorption of the dendrimer onto the SAM may or may not have occurred. No electrochemical data gathered using cyclic voltammetry supported the existence of any surface-confined dendrimers on the SAM. Instead, the cyclic voltammetry seemed to break down during the scanning in the negative potential region where the reduction/oxidation waves for the dendrimers were expected to occur. The result of these negative sweeps was the electrochemical desorption of the SAM from the Au substrate. Linear sweep voltammetry (LSV) was performed to specifically illustrate this phenomenon. Figure A.9 and Table A-3 both summarize the results of the LSV experiments, where eventually the reductive potential applied to the working electrode (WE) facilitated a breakdown in the covalently bonded thiols (reductive desorption). Upon further examination, this phenomenon was also supported by capacitance measurements done on SAMs in PC by Creager and coworkers.<sup>15</sup>

The ramification of these results was that electrochemistry on these particular metallodendrimers bound to a SAM, because of their extremely negative redox potentials, would be extremely difficult without completely destroying the SAM or severely altering the experiment to accommodate for reductive desorption. One option for altering the experiment is an in depth investigation into the creation of more stable SAMs. SAMs with higher stability can better withstand negative potentials, resisting desorption until much more negative potentials. The SAMs tested, mercaptohexane, mercaptodecane, mercaptotetradecane, and a mixture of mercaptotetradecane and mercaptodecane, did, after all, behave according to convention, with the more stable long chain SAM and the mixed SAMs desorbing at progressively more negative potentials.<sup>16</sup> Altering solution conditions, like pH, and changing SAM terminal groups might have offered more SAM stability and, in turn, expanded the working potential window. At this point in the project, however, the fact that one would have to extend the window several hundred millivolts more negative was a major deterrent to this proposal. Both researchers agreed that, based on the results, the development of a new method for analyzing the dendrimers was a much more appropriate course of action.

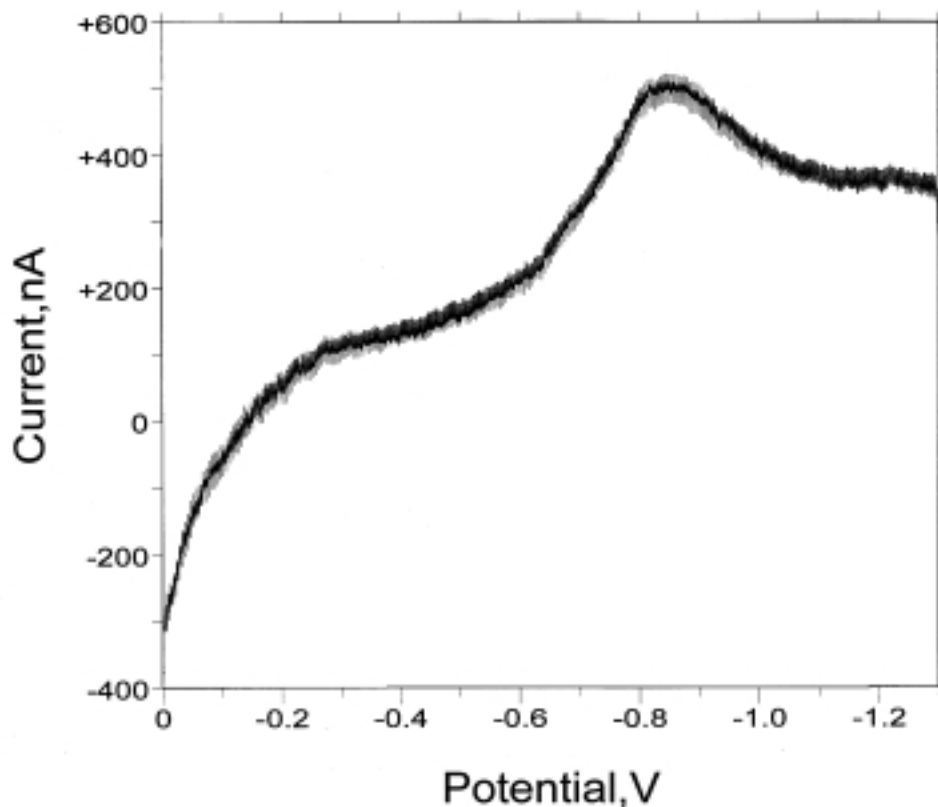


**Figure A.9.** LSV desorption scan of a tetradecane thiol ( $\text{CH}_3(\text{CH}_2)_{13}\text{SH}$ ) SAM on Au in propylene carbonate with 100 mM tetraethylammonium tetrafluoroborate ( $\text{TEABF}_4$ ). SAM desorbs as current peaks at approximately -0.85 V (vs.  $\text{Ag}^{+/0}$  RE).

**Table A-3.** Linear Scan Voltammetry - SAM Desorption Results

SAM	$C_{dl}$ ( $\mu\text{F}/\text{cm}^2$ ) <sup>a</sup>	$E_{\text{desorp}}$ (mV) <sup>b</sup>
Bare Evaporated Au <sup>c</sup>	43.3	---
-S(CH <sub>2</sub> ) <sub>5</sub> CH <sub>3</sub>	5.6	-645
-S(CH <sub>2</sub> ) <sub>9</sub> CH <sub>3</sub>	4.3	-785
-S(CH <sub>2</sub> ) <sub>13</sub> CH <sub>3</sub>	2.7	-855
-S(CH <sub>2</sub> ) <sub>13</sub> CH <sub>3</sub> & -S(CH <sub>2</sub> ) <sub>9</sub> CH <sub>3</sub>	3.1	-854

Solution conditions: 100 mM tetraethyl ammonium tetrafluoro borate in propylene carbonate. Experimental conditions: XX mV/sec sweep rate from 0 to -1300 mV vs.  $\text{Ag}^{+/0}$ .

<sup>a</sup> Double layer capacitance determined using cyclic voltammetry and measured at 50mV vs.  $\text{Ag}^{+/0}$ .

<sup>b</sup>  $E_{\text{desorp}}$  assumed to be where  $i_{p,c}$  of reductive desorption redox activity occurred.

<sup>c</sup> Gold substrate tested after being electrochemically cleaned.

## A.5. SOLVENTLESS ELECTROCHEMISTRY

Since the primary objective of this research project is to obtain electrochemical data for all of the generations of rigid and flexible dendrimers, a new experimental medium had to be chosen. Based on the previous experimental results and the observed solubility complications with the dendrimers, an attractive option is to eliminate the solvent from the entire system and, thus, completely alleviate any solubility concerns. While this doesn't seem practical experimentally, it was this line of thinking that led to the possibility of using "solventless" electrochemistry to achieve the research goals.

Professor Royce Murray at the University of North Carolina, Chapel Hill, routinely performs solventless electrochemistry, also known as solid state voltammetry. Dr. Murray uses the technique to measure rates of diffusion of solute molecules. The coined names of his techniques, solventless electrochemistry and solid-state voltammetry, are actually misnomers and do not accurately depict the entire picture. Solventless electrochemistry essentially utilizes a polymeric medium, laden with a lithium based salt, as its "solvent" and electrolyte, respectively. The polymer, officially referred to as being in the "solid-state," houses not only the supporting electrolyte, but also the electroactive species under investigation. The Li electrolyte dissolved in the polymer allows for ionic conductivity throughout the material, enabling electrochemistry to be performed on the electroactive solute dispersed in the polymer. In a more practical sense, electrochemistry on this type of a system is better described as a study of electron transport in an undiluted polymer melt.

### A.5.1. Polymer Salts

The effectiveness of solventless electrochemistry stems from the fact that certain polymers readily dissolve particular electrolytic salts via the following reaction:



where MX is the metal salt and -RY- is the polymer's repeat unit.<sup>17</sup> More specifically, polyether based polymers are known to effectively complex with alkali metal salts, their dominant interaction being between the oxygen atoms of the ethers and the alkali metal cations. The reaction between these two components is thermodynamically favored because the Gibbs solvation energy of the salt by the polymers exceeds the lattice energy of the solid

salt.<sup>17</sup> The result is a homogeneous polymer-salt blend (polymer electrolyte) that is conductive enough to promote both ion and electron transport through the polymer.

The conductivity of the polymer melt is greatly enhanced by the excellent ion mobility throughout the material. The ion mobility in the polymer is a consequence of the internal movement of the poly-ether chains which, because of their inherent flexibility, are known to undergo large amplitude motions. Increased motion in the polymer induces mobile ions which either “hop” between energetically favorable sites in the polymer lattice or promote the ions to experience a diffusional fluidity through the polymer.<sup>17</sup> In both cases, the consequences of the activity is a conductive polymer melt and a potential system for unique electrochemical experiments.

Accordingly, as the length of the polymer chain increases, the properties of the melt are altered. Polymeric electrolytes based on longer polymer chains tend to be more crystalline in nature and thus have attenuated ion mobility. Subsequently, as the morphology of the polymer changes, the formation of the cation-polymer complex is more energetically disfavored and the resulting melts are less conductive overall. Because of this phenomenon, short chain poly-ethers are the most common polymer used in these materials. Short chain polymers have a greater degree of inherent motion and, therefore, have more satisfactory conductance properties. The extent of the polymer branch motion and a high concentration of polar or basic functional groups along the polymer chain are the two basic criteria for creating highly conductive polymer melts.<sup>17</sup> The most popular method to make these polymeric electrolytes is to 1) dissolve the salt in a solvent, typically methanol (MeOH) or acetonitrile (ACN), 2) add the selected polymer, 3) stir, and 4) remove the solvent via vacuum evaporation to create a “solventless” mixture. These polymer electrolytes are used both as bulk materials or as thin films placed on an electrode. Thin polymer films coated on electrode platforms are employed for the research presented here.

Electrolytic polymers are of great interest as a component of a high energy density battery where the electrolyte is capable of conforming to any solid electrode. Other applications for polymer electrolytes are for the development of electrochemical devices such as electrochromic displays or windows, solid-state photoelectrochemical cells, and electrochemical sensors.<sup>17</sup> In this study, however, the polymer electrolytes will be employed

on a much more basic level as a convenient media for novel electrochemical experiments on the metallodendrimers.

#### **A.5.2. Solventless Electrochemistry at Microelectrodes – Royce Murray Research**

Research on these undiluted redox melts is ongoing and has already resulted in a plethora of publications.<sup>18</sup> Solventless electrochemistry is performed primarily with microelectrodes.<sup>18a</sup> Microelectrodes exhibit unique advantages including favorable background current and compatibility with highly resistive environments that would be unsuitable for traditional macroelectrodes. With normal macroelectrodes under resistive conditions, the uncompensated resistance effects (iR effects) are problematic for any potential experiments. These same iR effects are effectively minimized or eliminated by using microelectrodes, whose dimensions are minute enough to diminish the iR effects. Therefore, microelectrodes are routinely used for varied cyclic voltammetry experiments designed to study ET kinetics and electrode reaction mechanisms,<sup>19</sup> including *in vivo* measurements in rat brains<sup>20</sup> and in single nerve cells.<sup>21</sup> Considering the modest conductivity of the polymeric melts, microelectrodes, with their ability to minimize the iR effects, are a perfect tool for solventless electrochemistry experiments.

The basic concept of the Murray experiment is to use the microelectrode as a platform for a polymer electrolyte film. A common experimental apparatus is shown in Figure A.10.<sup>18p</sup> A large number of experiments by Murray and coworkers use polyethylene oxide (PEO) or polyethylene glycol (PEG) polymers with dissolved lithium perchlorate as the electrolyte. Within this type of medium, a variety of redox species, usually some type of ferrocene or viologen derivative, have been tested.<sup>18</sup> As mentioned above, the supporting electrolyte material, LiClO<sub>4</sub>, is first dissolved in MeOH and the polymer and redox species are added afterward. This slurry of material is deposited as a thin, visible film on the microelectrode platform which is then sealed in a vacuum cell where the MeOH can be pumped out of the polymer (See Figure A.10).

The technique is advertised as a means of voltammetrically measuring ultraslow diffusion coefficients ( $D_{\text{coeff}}$ ). Literature reports show diffusional rate coefficients on the order of  $10^{-12}$  cm<sup>2</sup>/sec being routinely measured for species in a polymeric media.<sup>18a</sup> This

technique rivals other methods of measuring very small diffusional parameters as shown in Table A-4.

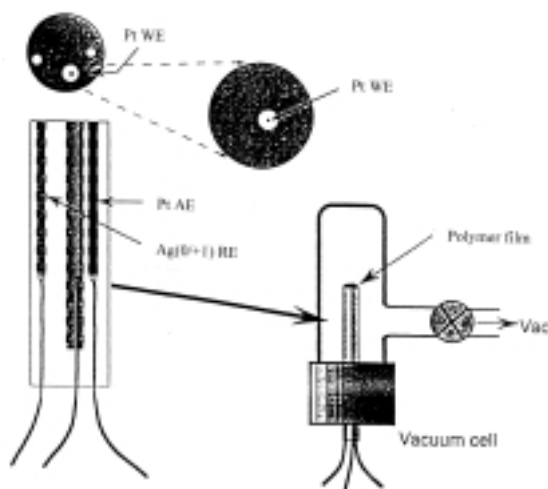


**Figure A.10.** Experimental apparatus used by the Royce Murray Research Group for performing solventless electrochemistry at a platform microelectrode. A similar vacuum cell and microelectrode assembly, encased in a Faraday cage, were used for performing solventless electrochemistry on the metallodendrimers (Fig. from Ref. 18p).

**Table A-4.** Methods Capable of Measuring Very Slow Diffusion Rates<sup>18a</sup>

Method	Limit of Diffusional Measurement (cm <sup>2</sup> /sec)
NMR Relaxation	≥ 10 <sup>-15</sup>
Radiotracer Techniques	≥ 10 <sup>-10</sup>
Pulsed Field Gradient NMR	≥ 10 <sup>-7</sup>
Photobleaching Relaxation	≥ 10 <sup>-10</sup>
Low Frequency AC Impedance	<10 <sup>-10</sup>
Voltage Relaxation	<10 <sup>-10</sup>
DC Polarization	<10 <sup>-10</sup>
Solid State Voltammetry	~ 10 <sup>-12</sup>

### A.5.3. Apparent Diffusion Coefficients ( $D_{app}$ )

Cyclic voltammetry (CV) and chronoamperometry (CA) are usually performed to extract diffusion coefficients ( $D$ ) for a chemical species. The former method is used to learn about the overall processes taking place at the electrode surface whereas the latter method is used for quantitative determinations of  $D$ .<sup>18a</sup> The current response observed with both of these techniques is dependent on several factors, one of which is the diffusion geometry at the

electrode. Within these polymer films several factors can affect the diffusion geometry including the following: temperature, type of polymer (presence of ordered regions, homogeneity, crystallinity, etc.), use of a plasticizing agent, and presence of electron hopping. When physical diffusion rates are slow, as is the case with solute molecules dispersed in these polymers, electron exchange (electron hopping) between the electroactive molecules becomes more significant. Larger  $D$  values are found in polymer systems with low molecular weights, elevated temperatures, or when the film is plasticized with a solvent saturated gas. In these cases, electron hopping is most likely a minimal contributor to overall diffusional rates. However, with dry films composed of higher molecular weight polymers, which are partially crystalline in nature at room temperature, electron hopping becomes much more significant. Both physical diffusion and electron exchange contribute to the overall diffusion rates. The coefficient describing that rate is known as the “apparent” diffusion coefficient ( $D_{app}$ ).<sup>22</sup> In normal diffusing electrochemical systems, physical diffusion ( $D_{phys}$ ) dominates and the effect of electron exchange between the molecules is negligible. In the polymer films, however, both factors are significant and are accounted for in the Dahms-Ruff equation describing  $D_{app}$ .<sup>18c,23</sup>

$$D_{app} = D_{phys} + \frac{k_{ex}\xi C}{6} \quad [\text{Eqn. A.1}]$$

where  $k_{ex}$  is the electron exchange rate constant between solute molecules,  $\xi$  is the average redox center to center distance, and  $C$  is the total concentration of analyte in the film.

#### A.5.4. $D_{app}$ and Diffusion Geometry

Cyclic voltammetry (CV) on redox molecules dispersed throughout the polymer electrolyte will reveal one of three diffusion geometries: radial, linear, or mixed radial-linear diffusion. In the first case, the voltammetry may show a steady-state response in the form of a sigmoidal wave shape, a clear sign that radial diffusion is present at the microelectrode. If that is the case,  $D_{app}$  may be directly derived from the equation for limiting current at a disk-shaped microelectrode:<sup>24</sup>

$$I = 4nFrDC \quad [\text{Eqn. A.2.}]$$

where  $I$  is the total steady state current,  $n$  is the number of electrons being transferred in the electrochemical reaction,  $F$  is the Faraday constant,  $r$  is the radius of the electrode,  $D$  is the diffusion coefficient (in this case  $D_{app}$ ), and  $C$  is the bulk concentration of redox species.

In the second case, cyclic voltammetry showing semi-infinite linear diffusion may be observed. This type of voltammetric behavior can be harnessed in two ways to extract a measurement of  $D_{app}$ . A series of CVs acquired at varying scan rates allows for a plot of the peak current ( $i_p$ ) versus the square root of the scan rate ( $v^{1/2}$ ). The relationship between these two variables is linear for a reversible redox couple according to the Randles-Sevcik equation:<sup>24</sup>

$$I_{p,c} = -2.69 \times 10^5 n^{3/2} A D_o^{1/2} C_{ox} v^{1/2} \quad [\text{Eqn. A.3}]$$

where  $I_{p,c}$  is the peak current of the cathodic wave,  $n$  is the number of electrons transferred,  $A$  is the area of the electrode,  $D_o$  is the diffusion coefficient ( $D_{app}$  in this case),  $C_{ox}$  is the bulk concentration of the oxidant species, and  $v$  is the sweep rate of the experiment. From the slope of this plot,  $D_{app}$  can be calculated.

The second approach to the semi-infinite linear diffusion case uses chronoamperometry (CA) to step the potential far beyond the redox potential of the electroactive species and then measure the decaying current response. If the response is diffusion controlled, known as a Cottrellian response, the current is described by the Cottrell equation:<sup>24</sup>

$$I(t) = \frac{nFAD^{1/2}C_{\infty}}{(\pi t)^{1/2}} \quad [\text{Eqn. A.4}]$$

where  $n$  is the number of electrons transferred,  $F$  is the Faraday constant,  $A$  is the area of the electrode,  $D$  is the diffusion coefficient (in this case referred to as  $D_{app}$ ),  $C_{\infty}$  is the bulk concentration of the electroactive species, and  $t$  is time. Using this relationship, a Cottrell plot of current versus the inverse square root of time can be constructed and a value of  $D_{app}$  can be obtained from the slope of the curve. When in the polymeric media, the CA approach for calculating  $D_{app}$  is favored because it is less prone to  $iR$  effects.<sup>18a</sup>

The preceding two cases represent limiting diffusional behaviors, both of which extremely simplify any data analysis involved with determining  $D_{app}$  values. Diffusion, however, may occur via a combination of radial and linear diffusion geometries. The

analysis required for a mixed diffusion geometry is complicated and the subject of ongoing studies in many research groups. Although it is beyond the scope of this discussion, it is worth mentioning that the solution to the mixed diffusion geometry involves modeling the total current at a microelectrode. Solutions presented for this purpose involve digital simulations based on “hopscotch” algorithms<sup>25</sup> and equations derived through a process called convolutive forecasting.<sup>26</sup> In spite of these efforts, most researchers using the polymer film systems usually adjust their experimental parameters until the electrode behavior is represented by one of the limiting cases.

#### **A.5.5. Relevant Experimental Results from the Murray Group**

Over the years, many different polymers and a vast number of redox species have been tested and examined by Murray and coworkers. What will be discussed here, however, are the results obtained that are relevant to the metallodendrimer project at hand. In 1992, a paper by Murray’s group outlined some practical experimental aspects of solid state voltammetry performed with polymeric electrolytes.<sup>18d</sup> Different polymers were tested with respect to their molecular weight, structure, and morphology. Also considered were the electrochemical effects of temperature and plasticization with solvent saturated vapor. For each polymeric electrolyte, cyclic voltammetry was used to test the background signal and establish a signature potential window. The results of these experiments, background voltammograms of several polymer-electrolyte combinations, are presented in Figure A.11. Of particular interest, with respect to the dendrimer research being discussed, are the first three background scans of poly(ethylene glycol) dimethyl ethers (MePEG) with dissolved LiClO<sub>4</sub> (Figure A.11a-c). These scans are noteworthy because of their large negative potential limit and low background signal, which led us to believe that these polymers might provide adequate signal-to-noise ratios at extremely negative potentials to accommodate electrochemistry on the metallodendrimers.

Polyethylene glycol with methyl terminated end groups (MePEG) is described based on the following formula:<sup>18d</sup>



where X=CH<sub>3</sub>, Y=H and the repeat unit of the polymer is defined as -CH<sub>2</sub>CH<sub>2</sub>O-. This hygroscopic polymer is commercially available in several molecular weights (MW) [250, 400, 1000, 2000] which span a wide range of bulk structure at room temperature from viscous liquids (low MWs) to solid waxes (higher MWs). The MePEGs dissolve LiClO<sub>4</sub> and have been extensively studied by the Murray researchers as potential candidates for solventless electrochemical experiments.

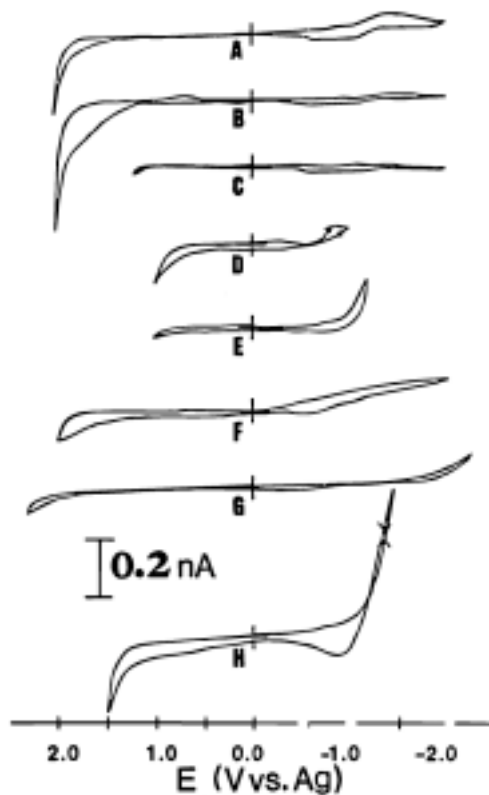


**Figure A.11.** Solventless electrochemistry at microelectrodes - background cyclic voltammograms of various polymer melts: (A) Me<sub>2</sub>PEG-400/LiClO<sub>4</sub> (16:1); (B) Me<sub>2</sub>PEG-1000/LiClO<sub>4</sub>(16:1); (C) Me<sub>2</sub>PEG-2000/LiClO<sub>4</sub>; (D) PPO-4000/LiClO<sub>4</sub> (25:1); (E) PEO-600,000/LiCF<sub>3</sub>SO<sub>3</sub> (15:1); (F) network PEO/LiClO<sub>4</sub> (50:1); (G) MEEP/LiCF<sub>3</sub>SO<sub>3</sub> (4:1); (H) PEUU/LiClO<sub>4</sub> (55:1). Ratios represent the O:Li status of each polymer melt. Backgrounds A-F and H were collected at 25°C with G collected at 60°C. Most of the voltammetry was run with the vacuum cell filled with dry N<sub>2</sub> (D was collected in air; E with acetonitrile saturated N<sub>2</sub>). (Figure from Ref. 18d)

In addition to studying the potential window limitations and the background currents of the polymers, Murray also used each of the polymers in a solventless electrochemical experiment where each polymer electrolyte was intermixed with a simple redox species and solid state voltammetry was performed to determine the apparent diffusion coefficients. The

relevant experiment to this discussion involved carboxylic acid ferrocene dispersed throughout the MePEG polymers.<sup>18d</sup> Thin films of the material were placed on the microelectrode platform and voltammetry was performed. Figure A.12 displays the voltammetric responses obtained from the ferrocene derivative in three different MWs. From this figure, one can easily ascertain the influence of the different diffusion geometries, previously discussed, that can exist. The shortest chain polymer, the MePEG(400), is a viscous liquid with the greatest degree of internal mobility. The ion movement within the MePEG(400) causes the film to have a high conductivity which, in turn, culminates in a sigmoidal shaped current response with steady state characteristics (Fig. A.12c). Thus, the  $D_{app}$  of carboxylic acid ferrocene in this medium can be determined using the steady state current approach (Eqn. A.2), discussed in the previous section.

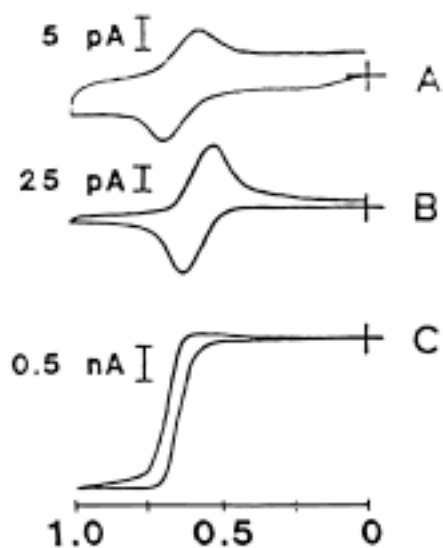


**Figure A.12.** Cyclic voltammetry of 5 mM carboxylic acid ferrocene films at the microelectrode assembly in A) Me<sub>2</sub>PEG-2000/LiClO<sub>4</sub>; B) Me<sub>2</sub>PEG-1000/ LiClO<sub>4</sub>; C) Me<sub>2</sub>PEG-400/ LiClO<sub>4</sub>. Experimental conditions: O:Li = 16 at 25°C in dry N<sub>2</sub> and a sweep rate of 10 mV/sec (Figure from Ref. 18d).

Also shown in Figure A.12a and b, are CVs obtained with higher MW MePEGs. The results reveal very differently shaped voltammograms. With the MePEG(1000) and especially the MePEG(2000), both of which are solid waxes at room temperature, the voltammetry takes on a diffusional or Cottrellian shaped response. These experiments require a Cottrellian analysis based on linear diffusion to extrapolate the  $D_{app}$  values. In these cases, electron hopping is a significant contributor to the overall diffusion of the ferrocene. The shape of the voltammograms, due to very unique diffusion geometry at the microelectrode, is drastically altered by changing the specific polymer that houses the electroactive species. Although it is not shown here, it should be noted that similar effects can be seen by altering

the melt's temperature, varying the scan rate of the experiment, or introducing a solvent saturated gas.<sup>18d</sup>

## A.6. SOLVENTLESS ELECTROCHEMISTRY – METALLODENDRIMERS

At this point in the discussion, it may be advantageous to review the benefits of solventless electrochemistry that endeared it as a potential technique for testing the metallodendrimers. Using the MePEG/LiClO<sub>4</sub> polymeric media as a medium for the metallodendrimers, not only are the concerns over solvent solubility quenched but the potential window is expanded far enough negative to easily accommodate the expected reduction potentials of the dendrimers. Furthermore, considering the low background current for MePEG in this negative region, only a few nanoamps of faradaic current generated by the metallodendrimers would suffice for a measurable signal. Noting the excellent electrochemical behavior of most of the dendrimers in solution,<sup>12b</sup> several nanoamps of current would seem to be easily achievable. If successful, solventless electrochemistry of the dendrimers would provide several pertinent results: 1) electrochemical data on all the dendrimers, rigid and flexible, as well as the higher generations without regard to solubility; 2) a series of  $D_{app}$  values for increasing generations; 3) the first documented data of surface-confined metallodendrimers of this type, a key element to the development of the overall IBU behavior for these structures, and 4) an indirect measure of the electron exchange rate constant ( $k_{ex}^{\circ}$ ) or electron hopping between dendrimers, the very intermolecular property these macromolecules were designed to inhibit at high generations.

The most serious problem anticipated was that the MePEG is hygroscopic. This is usually not a problem, but when taken in conjunction with the metallodendrimer's air sensitivity, a polymer that readily absorbs moisture represents a nontrivial complication to the solventless electrochemistry approach. The water absorbed into the polymer most likely will have dissolved air in it as well and will require further degassing. The presence of both water and/or air in the polymer film is a significant detriment to the background signal of the negative window, with both contaminants expected to have redox activity in the -1.0 V (vs. Ag<sup>+0</sup>) region. Additionally, if the polymer itself adsorbs enough water or is exposed to the atmosphere too long, the dendrimers immersed in the film will also be exposed to the contaminants. To this end, a great deal of time was devoted to simply reproducing the

background signals seen in Figure A.11. Related to that goal, time was also spent finding a suitable polymer film preparation procedure (see Section A.10) both that minimizes air/H<sub>2</sub>O exposure and protects the structural integrity and functionality of the dendrimers. Most of the results from these endeavors are not included in this report, but an example of a satisfactory background voltammogram, with an extremely small background current, is shown in Figure A.13.

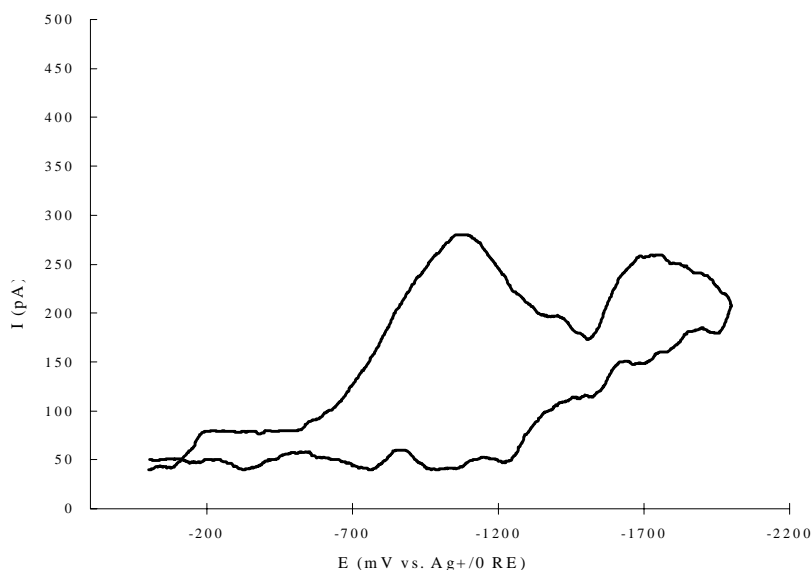


**Figure A.13.** Cyclic voltammogram of background signal of Me<sub>2</sub>PEG(250)/LiClO<sub>4</sub> after extensive pretreatment to remove H<sub>2</sub>O, O<sub>2</sub>, and other contaminants (See Experimental Details Section). {10 mV/sec; 25°C} Flat backgrounds such as those obtained by the Murray researchers were extremely difficult to reproduce and were never achieved during the research project, although backgrounds like this example were deemed sufficient if enough faradaic current from the analyte (dendrimers) could be generated (data smoothed by a 13 point sliding average).

#### A.6.1. N.C. State Versus UNC

It should be noted and is described in detail in the experimental section of the chapter (Section A.10), that these polymers, when used for this particular application, require such an extensive preparation procedure that these experiments are rendered extremely challenging. Even though Murray advertises solventless electrochemistry as a method conducive to operating at large negative potentials, his own research seems to avoid the negative potential regime altogether. Only very recently has Professor Murray tested a solute in this range.<sup>27</sup> However, this report shows no background of the system and includes no details of the preparation procedure with regard to water and air contamination. Traditionally, Murray

performs his experiments on the benchtop without regard to contamination. Other differences in the experimental protocols used by our group, as opposed to the procedures used by Murray, are pointed out in subsequent paragraphs.

#### **A.6.2. Preliminary Results - Carboxylic Acid Ferrocene / MePEG(250)**

To test the behavior of the microelectrode assembly and ensure the viability of this technique, the carboxylic acid ferrocene experiment was repeated. A polymer melt of MePEG(250), a viscous liquid at room temperature, with dissolved  $\text{LiClO}_4$  was prepared via the procedure described in the Experimental Details (Section A.10). An important difference between the preparation procedure used in the Gorman/Bowden research collaboration and the Murray experiments was that no solvent, either to aid in the dissolution of the Li salt or for use as a plasticizing agent, was ever introduced into the system. Because of this, no solvent had to be removed from the melt after it was prepared. This experiment was successful and results are presented as Figure A.14. Scans at different sweep rates revealed that the electrode behaves as a microelectrode, showing a steady state response at low scan rates and diffusion controlled response at higher scan rates.<sup>24</sup> These results are consistent with the results shown in Figure A.12 and validated our execution of this type of solventless electrochemistry. The next experiments incorporated metallodendrimers into the MePEG electrolyte films.

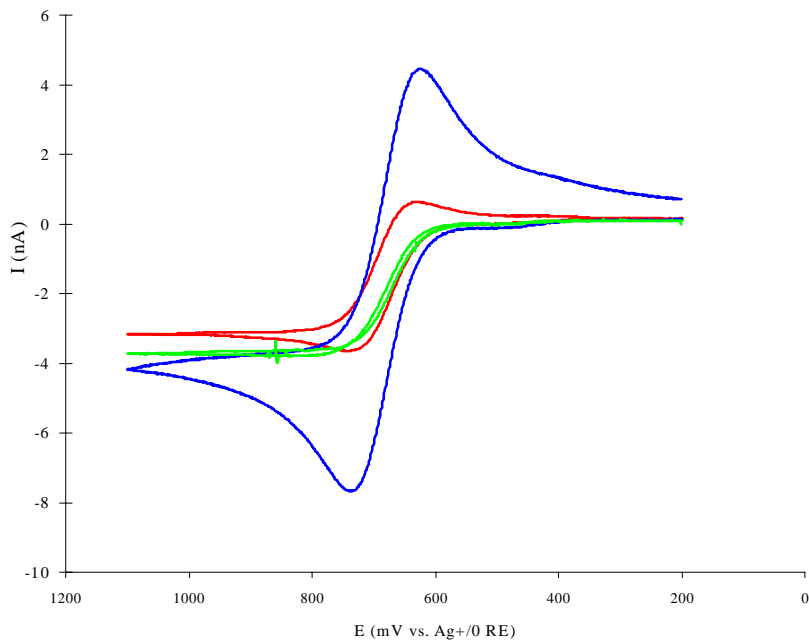


**Figure A.14.** Cyclic voltammetry of carboxylic acid ferrocene (5 mM) in Me<sub>2</sub>PEG(250) with LiClO<sub>4</sub>. Voltammograms shown were collected at 2 mV/sec (green), 10 mV/sec (red), and 100 mV/sec (blue) and illustrate typical scan rate dependent behavior at microelectrodes, sigmoidal shaped voltammetry at low scan rates and diffusional shaped voltammetry at higher scan rates.

### A.6.3. Flexible IBUs / MePEG(250) Results

The first solventless electrochemistry experiments on the metallodendrimers were performed on the low generation (G0, G1, & G2), flexible series of molecules in MePEG(250). Both the G0 flexible dendrimer and the low MW polymer, MePEG(250), were chosen for the initial experiments because they offered the greatest chance of success. The dendrimers, it was feared, would be too bulky and insulating to undergo facile ET of any kind in the higher MW, long chain polymers. Although the results are not shown here, experiments with dendrimers in higher MW polymer were attempted and showed very poor results in accordance with this line of thought. Additionally, the longer chain polymers were much more difficult to prepare clean and anhydrous. After a tremendous amount of effort and repeated trials, experiments with GO were eventually successful.

Electrochemistry on the flexible IBUs required both an extensive preparation procedure for the polymer and a specific polishing procedure for the microelectrode assembly. Both of these procedures are outlined in the Experimental Details section at the

end of this appendix. Cyclic voltammetry on the first three flexible generations of dendrimer afforded the voltammograms shown in Figure A.15. Background scans of the polymer electrolyte alone were devoid of the peaks. Data collected from both CV and CA experiments are summarized in Table A-5. The only significant trends shown in Table A-5 involve the peak separations ( $\Delta E_p$ ) and the peculiar FWHM values. Because of the dramatic decrease in the peak currents ( $i_{p,c}$  &  $i_{p,a}$ ) from the G1(flex) to the G2(flex) scans (Figures A.15b & A.15c), experiments with higher generations were not attempted.

**Table A-5.** Solventless Electrochemical Properties of Metallo dendrimers

IBU	$E^{\circ}$ (mV) <sup>a</sup>	$\Delta E_p$ (mV) <sup>b</sup>	$\Gamma^*$ (fmol/cm <sup>2</sup> ) <sup>b</sup>	FWHM <sup>c</sup> (mV) <sup>b</sup>	$k^{\circ}et$ (s <sup>-1</sup> ) <sup>d</sup>	$k^{\circ}et$ (s <sup>-1</sup> ) <sup>b</sup>	Dapp <sup>e</sup> (cm <sup>2</sup> /sec)
GO	-1100	475	102/94	334/372	3.8 E-3	6.9 E-3	3.0 E-7
G1	-1200	588	62/63	409/405	3.6 E-3	3.0 E-3	2.0 E-7
G2	-1000	672	104/87	400/521	4.1 E-5	5.0 E-3	6.6 E-8

<sup>a</sup>  $E^{\circ}$  values are calculated using the average of  $E_{p,a}$  and  $E_{p,c}$ .

<sup>b</sup> Measured at 50 mV/sec scan rate versus a  $Ag^{+/0}$  pseudo reference electrode.

<sup>c</sup> Anodic and cathodic measurements shown, respectively.

<sup>d</sup> Measured at several scan rates:  $\leq 100$  mV/sec that significantly increased  $\Delta E_p$ .

<sup>e</sup> Measured via a Cottrellian analysis (Chronoamperometry- PW=400sec; Step E= -1.8V).

Note: Only measurements from electrode assembly #6 shown; variation in data not shown but exceeded 100% in some cases.

## A.7. DISCUSSION

The most pertinent information that can be ascertained from the voltammetry of the flexible dendrimers, reiterated in Figure A.16, is the distinct kinetic effect displayed in the voltammograms. A clear qualitative trend in the kinetics can be inferred from the peak splitting and peak shape of each successive generation. Indicative of the ET attenuation for which these molecules were designed, the results show each generation insulating the redox core and hampering the intermolecular electron exchange. With each added generation, the peak splitting, a function of the kinetics, increased significantly. Moreover, the attenuation present in the ET function of the G2(flex) is so severe that the signal is poorly resolved and barely discernible from the background. Peak splitting of this nature in CV is most often seen as a sign of highly irreversible ET kinetics. Normal, diffusional voltammetry in solution of irreversible kinetics usually has a peak splitting of at least 200 mV.

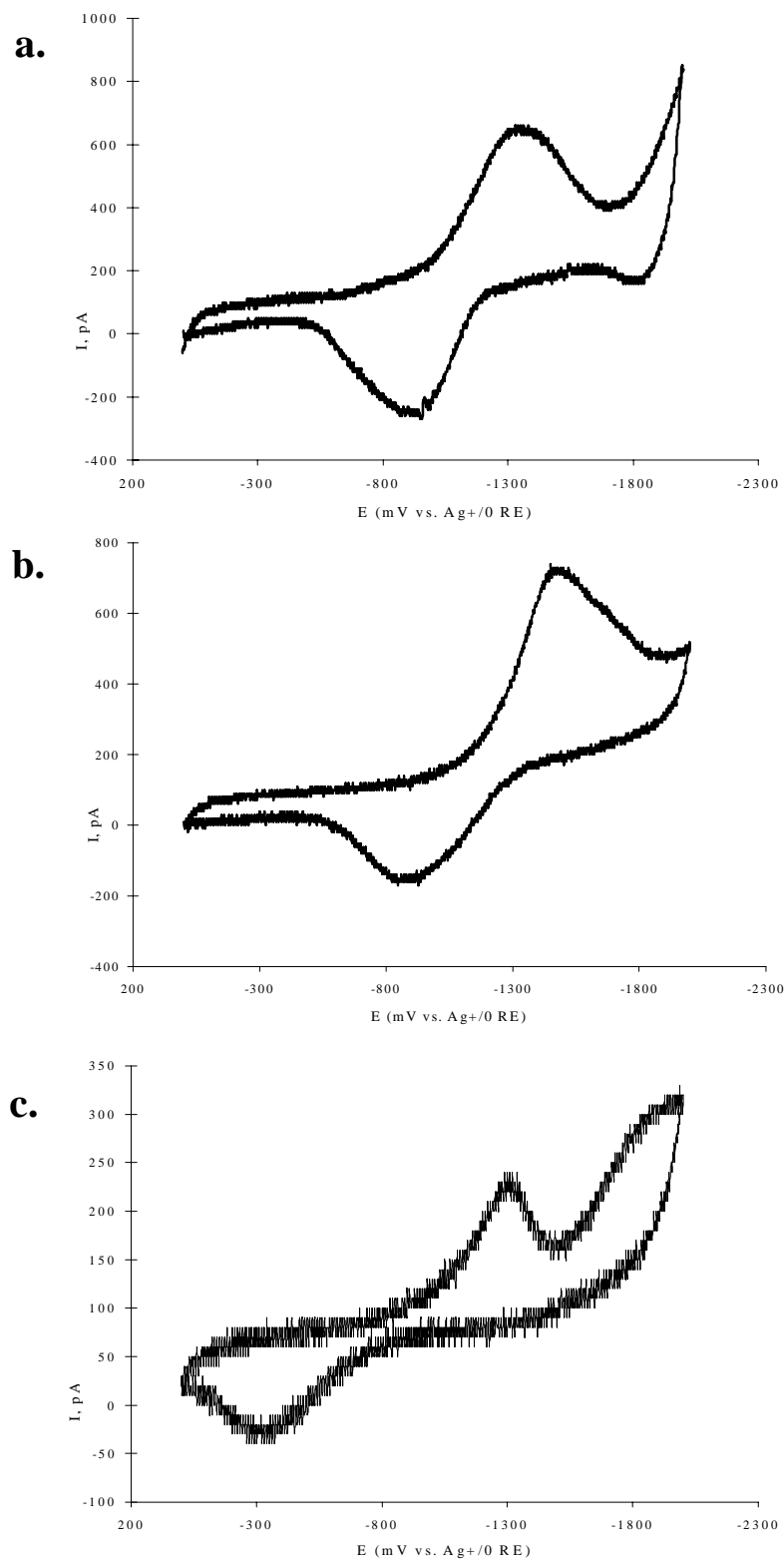


**Figure A.15.** Cyclic voltammograms of first three generations of the flexible IBU molecules (5 mM) in Me<sub>2</sub>PEG(250) with LiClO<sub>4</sub>: a) GO; b) G1, and c) G2.

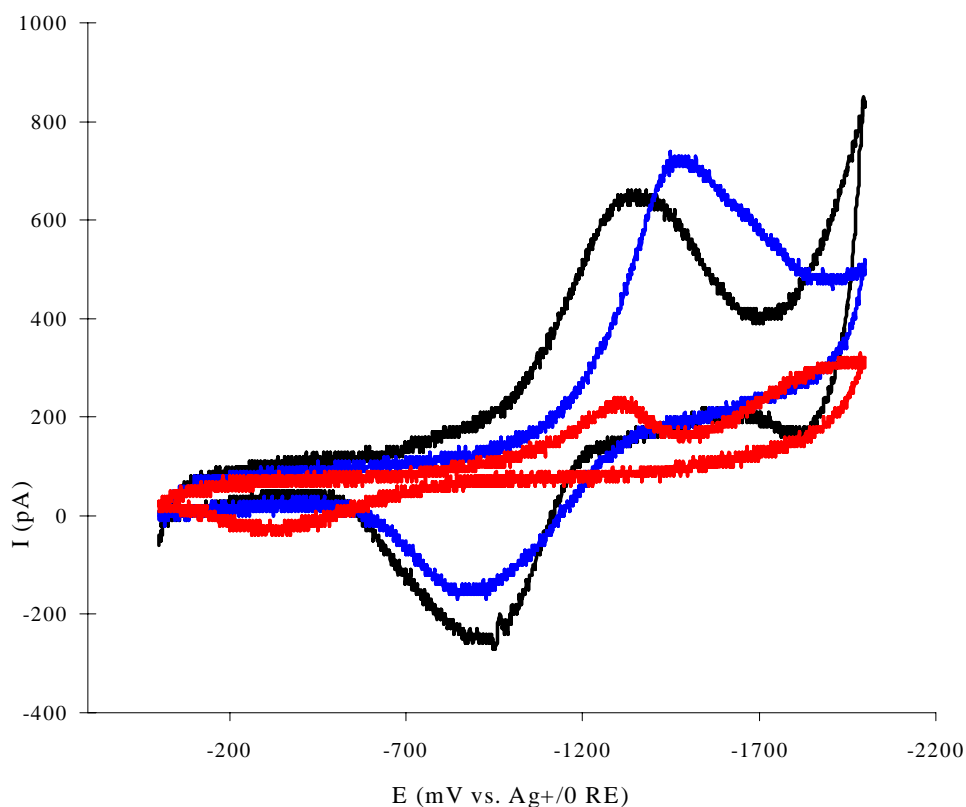


**Figure A.16.** Cyclic voltammetry results comparison between GO-flex(black), G1-flex(blue), and G2-flex(red). Note the decrease in current and increase in peak splitting with increasing generations of metallodendrimers.

Unfortunately, the quantitative analysis of these experiments is not as definitive. All measurements of ET rate constants ( $k_{app}^{\circ}$ ) and diffusion coefficients ( $D_{app}$ ) on the dendrimer systems resulted in inconsistent values showing no trend and a large degree of variability. The results of these calculations are shown in Table A-5. It is believed that the quantitative measurements ultimately failed because all of the calculations required the application of an accurate model describing the nature of the dendrimer-polymer films. All of the models applied to this system thus far are believed to be inaccurate or lacking in some dimension.

These films are difficult to define. The peak shapes of the voltammetry appear to be diffusionless in nature, especially the oxidative waves. The voltammetry seems to return to baseline after the dendrimer redox activity, devoid of any diffusion limited current. This type of peak shape contrasts sharply with the solventless electrochemistry performed by Murray, which is clearly diffusional.

To evaluate the idea that the dendrimer electrochemistry is surface confined, the impact scan rate was probed for GO. If the molecule's behavior is adsorbed in nature, the peak currents should be linearly related to the scan rate of the experiments according to equation A.3. Voltammograms at varying scan rates for GO(flex) are shown in Figure A.17. The corresponding plots of  $i_{pa}$  and  $i_{pc}$  versus scan rate are presented in Figure A.18 Attempts to fit the same data to a diffusing system model (Eqn. A.3:  $i_p$  vs.  $v^{1/2}$ ) were not successful. Clearly, these result support the notion that the dendrimers in the polymer melt behave similarly to surface confined molecules.

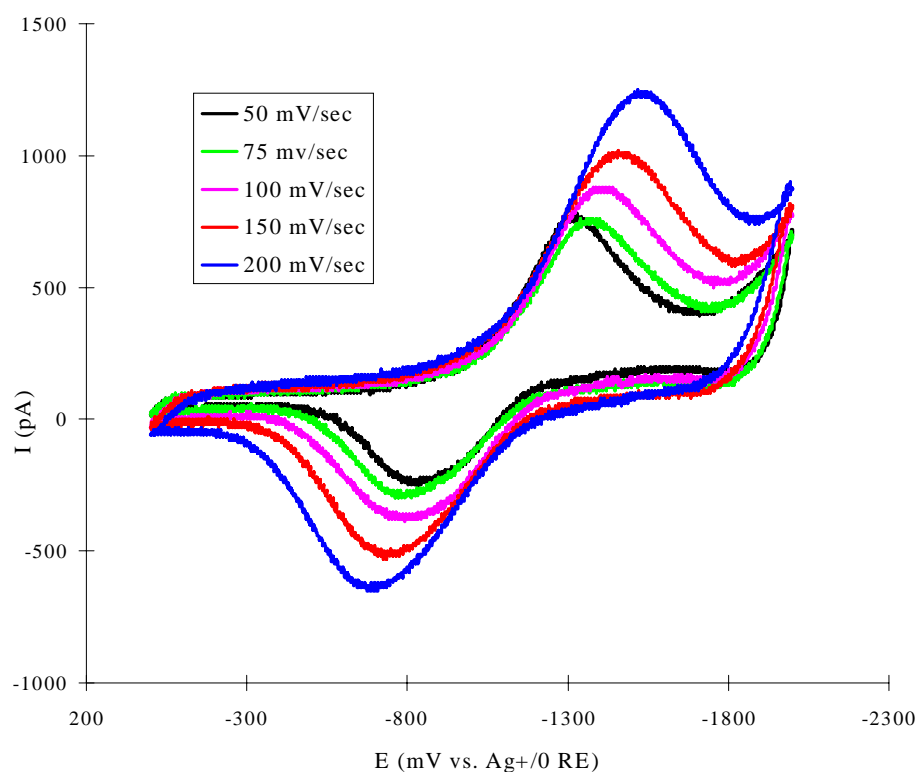


**Figure A.17.** Cyclic voltammograms at varying scan rates of GO-flex in Me<sub>2</sub>PEG(250)/ LiClO<sub>4</sub>.

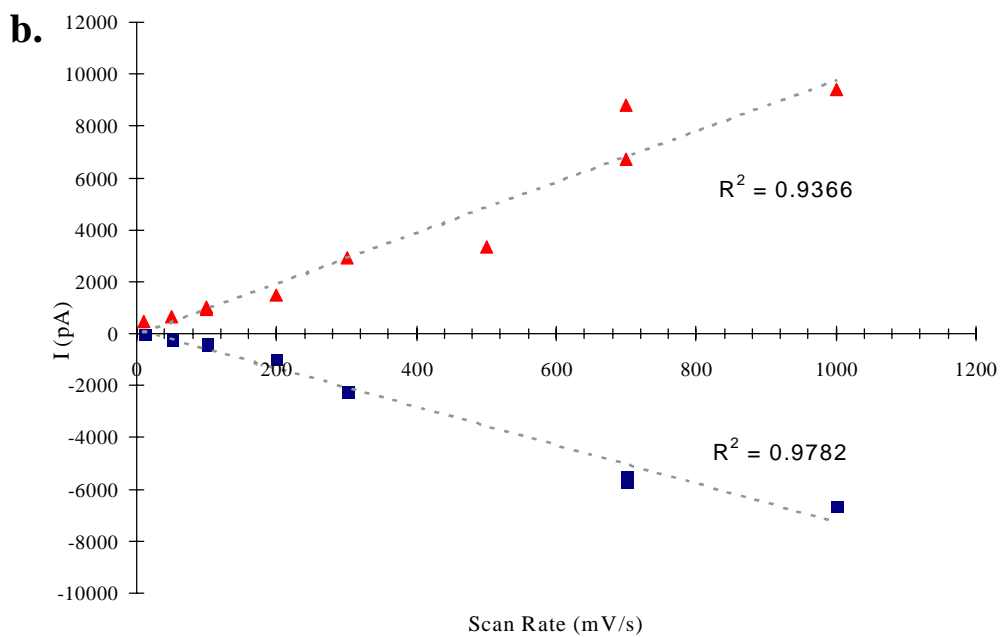
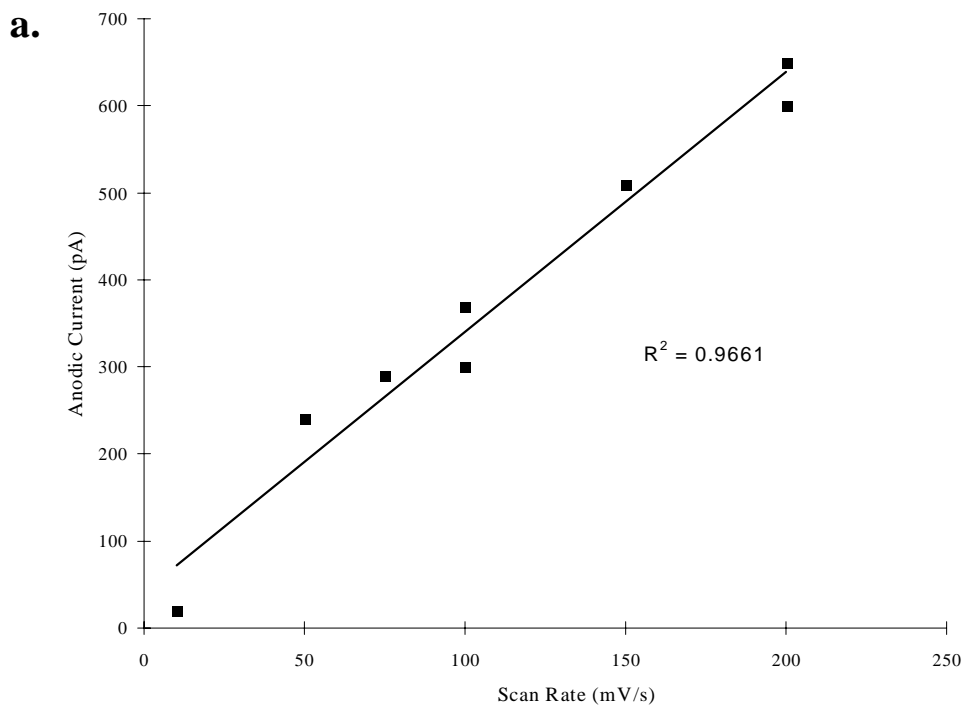


**Figure A.18.** Scan rate ( $\nu$ ) dependence plots of GO-flex in Me<sub>2</sub>PEG(250)/ LiClO<sub>4</sub>: a) anodic current vs.  $\nu$  and b) cathodic/anodic current ( $\pm i$  vs.  $\nu$ ). Correlation coefficients ( $R^2$ ) values are provided to show the degree of linearity inherent in the data; high  $R^2$  values indicate the strong adsorbed behavior of the system.

One particularly interesting property of the dendrimers' solid-state voltammetry is the unusually large FWHM values. Ranging from 300 to 500 mV, these FWHM values are exceptionally large and indicative of the complex nature of this system. The reasons for the broadened peaks are unknown, although non-diffusional broadened peaks of this magnitude have been seen in conjunction with surface effects<sup>28</sup> and in thin-layer voltammetry.<sup>24</sup>

If thin-layer behavior is indeed taking place, the charge passed during the scans would be inclusive of all the electroactive molecules in the entire film. By integrating the area under the voltammetric curves, the charge passed during the actual experiment can be directly compared to the theoretical charge passed if the film is completely electrolyzed. To calculate the theoretical charge passed, several assumptions about the system have to be made. The first assumption is that the polymer electrolyte-dendrimer films are evenly distributed across the microelectrode platform. Secondly, it is accepted that the hard sphere, molecular radii of the dendrimers (See Table A.6a) is accurately approximated by independent molecular modeling computer simulations. Third, it is assumed that only dendrimers above the working electrode were able to be electrolyzed. Thus, any radial derived current in these experiments is essentially neglected. Finally, as displayed in Figure A.19, it is assumed that the IBU molecules are in close contact within the polymer film, adopting a simple cubic packing order. Because both dispersion and aggregation of the dendrimers in these films remain viable and equally plausible possibilities, this last assumption suggests that the theoretical value calculated will be an estimation of the upper limit of dendrimers that may be electrolyzed. In any event, these assumptions, along with the information in Table A-6a, Table A-6b, and the model depicted in Figure A.19, were used to determine the theoretical upper limit of electrolyzed molecules.

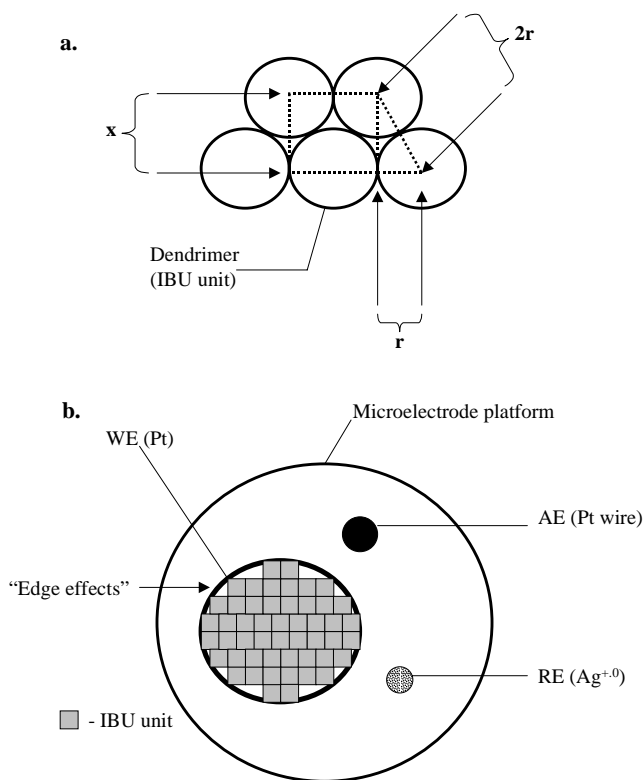


**Figure A.19.** a) Hypothetical model used for charge calculations aimed at determining the number of IBUs being electrolyzed; b) "edge effects" were assumed to be negligible for all of the calculations

**Table A-6a.** IBU Parameters and Properties

IBU	Radius ( $\text{\AA}$ ) <sup>a</sup>	X ( $\text{\AA}$ ) <sup>b</sup>	Unit Area ( $\text{\AA}^2$ )	Unit Area ( $\text{cm}^2$ )
GO (flex)	6	10.4	124.8	$1.25 \times 10^{-14}$
G1 (flex)	8	13.9	222.4	$2.22 \times 10^{-14}$
G2 (flex)	11	19.1	420.2	$4.20 \times 10^{-14}$

<sup>a</sup> Determined by molecular computer simulations performed by Jennifer Smith, Gorman Research Group.

<sup>b</sup> Parameter of length defined by the model depicted in Figure A.19.

**Table A-6b.** Microelectrode Assembly Parameters and Properties

Electrode	WE radius <sup>c</sup> ( $\mu\text{m}$ )	WE area ( $\text{cm}^2$ )	Platform Area ( $\text{cm}^2$ ) <sup>d</sup>
E6	14.2 <sub>4</sub>	$6.4 \times 10^{-6}$	0.196
EB	14.4 <sub>9</sub>	$6.5 \times 10^{-6}$	0.283
EA	19.2 <sub>9</sub>	$1.1 \times 10^{-5}$	0.196

<sup>c</sup> Radius of working electrode determined by Royce Murray Research Group using an inverted optical microscope.

<sup>d</sup> Platform area calculated from platform diameter and radius ( $A=\pi r^2$ ) as measured with calipers.

To determine the corresponding experimental values, knowledge of the total number of molecules deposited on the entire electrode platform is required. This amount also requires a few significant assumptions. Considering that the film is placed on the electrode via the inefficient and imprecise method of dropcoating from a microsyringe, the volume of material deposited is not accurately known. Therefore, it is estimated that the volume of material placed on the microelectrode platform was approximately 1-2  $\mu\text{L}$  of polymer. In this manner, theoretical values are reported with high and low calculations to designate a range of possible values. The results of these calculations are shown in Tables A-7. While not totally complete, the experimental data that can be compared to theoretical numbers shows that, in almost all the cases, only a maximum of 33% of the dendrimer films is being electrolyzed during the voltammetry. This result contradicts typical thin layer behavior and leaves the specific nature of these films and their electrochemistry largely a mystery.

#### **A.8. CONCLUSIONS AND FUTURE DIRECTIONS**

Even though the results shown here are significant, the future of solventless electrochemistry on these metallodendrimers is uncertain at best. A positive aspect of these results is their support, at least on a qualitative level, of the dendritic encapsulation property of the metallodendrimers. The changing kinetics of the different generation dendrimers is the exact structure-function relationship being sought in this project. Unfortunately, this technique apparently can not elucidate these properties in higher order generations and has failed to yield useful quantitative data in the lower generation molecules. There is definitely science to be wrought here, however, as solventless electrochemistry remains a largely untapped and potentially useful technique with many applications. In fact, it might serve as an excellent method of recording previously unachieved data on the rigid IBUs, which were never tested in this medium.

Solventless electrochemistry is not a side project. The extreme difficulty of the measurements involved, as well as the time consuming nature of the required preparation procedures, render electrochemistry of metallodendrimers a clear candidate for a full doctoral project. Before proceeding with a full solventless electrochemistry project

**Table A-7.** Dendrimer - Polymer Film – Number of Molecules Electrolyzed  
(Based on Theoretical and Experimental Charge Passed on Three Different Electrode Assemblies)

Electrode	Parameter	GO	G1	G2
<b>E6</b>	$N_{\text{exp}} \rightarrow$ anodic/cathodic	$1.40 \times 10^{10} / 1.59 \times 10^{10}$	$1.29 \times 10^{10} / 1.22 \times 10^{10}$	$1.19 \times 10^{10} / 9.63 \times 10^9$
	$\pm \sigma_{N_{\text{exp}}}$	$(3.96 \times 10^9) / (2.99 \times 10^9)$	$(3.26 \times 10^9) / (3.44 \times 10^9)$	$(6.19 \times 10^9) / (6.33 \times 10^9)$
	$N_{\text{theor}} \text{ range} \rightarrow$	$2.04 \times 10^{12} - 1.02 \times 10^{12}$	$1.97 \times 10^{11} - 9.85 \times 10^{10}$	$1.96 \times 10^{11} - 9.85 \times 10^{10}$
	$\% N_{\text{elec. range}} \rightarrow$	1.6% to 0.7%	13.1% to 6.2%	12.1% to 4.9%
<b>EB</b>	$N_{\text{exp}} \rightarrow$ anodic/cathodic	--- / ---	--- / ---	$1.30 \times 10^{10} / 2.34 \times 10^{10}$
	$\pm \sigma_{N_{\text{exp}}}$	--- / ---	--- / ---	$(6.18 \times 10^9) / (6.98 \times 10^9)$
	$N_{\text{theor}} \text{ range} \rightarrow$	$1.41 \times 10^{11} - 7.02 \times 10^{10}$	$1.41 \times 10^{11} - 7.04 \times 10^{10}$	$1.40 \times 10^{11} - 7.02 \times 10^{10}$
	$\% N_{\text{elec. range}} \rightarrow$	---	---	33.4% to 9.2%
<b>EA</b>	$N_{\text{exp}} \rightarrow$ anodic/cathodic	--- / $7.49 \times 10^9$	$5.62 \times 10^9$ / ---	--- / ---
	$\pm \sigma_{N_{\text{exp}}}$	--- / $(1.35 \times 10^9)$	$(1.15 \times 10^9) / (---)$	--- / ---
	$N_{\text{theor}} \text{ range} \rightarrow$	$3.59 \times 10^{11} - 1.79 \times 10^{11}$	$3.60 \times 10^{11} - 1.80 \times 10^{11}$	$3.60 \times 10^{11} - 1.80 \times 10^{11}$
	$\% N_{\text{elec. range}} \rightarrow$	4.2% to 2.1%	3.1% to 1.6%	---

- $N_{\text{exp}}$  is the number of molecules electrolyzed as determined from the charge passed.
- $\sigma_{N_{\text{exp}}}$  is the standard deviation of the  $N_{\text{exp}}$ .
- Number of measurements in most cases was 4-12.
- $N_{\text{theor}}$  is the number of molecules electrolyzed as determined theoretically by model in Figure A.19 and the geometry characteristics of the microelectrode.
- $\% N_{\text{elec.}}$  is the percentage of the dendrimers in the film that are electrolyzed:  

$$\% N_{\text{elec.}} = N_{\text{exp}} / N_{\text{theor}} \times 100$$
 -where the high % = larger experimental number / low theoretical number and,  
 the low % = smaller experimental value / highest theoretical value.

however, it is advisable to first pursue the research objectives of the Gorman group by other means. Both interdigitated arrays and specifically designed synthesis of new dendrimer species offer excellent alternatives to this approach.<sup>29</sup> Synthetically creating more robust dendrimers with qualities more conducive to experimental measurements, such as water and air stable molecules capable of aqueous electrochemical treatment, is an interesting prospect. Research in the Gorman group is already underway to design dendrimers with a charged periphery, allowing for possible electrostatic immobilization of the dendrimers on the SAMs, a process already extensively studied in bioanalytical research.<sup>30</sup> Additionally, Gorman and coworkers have implemented the synthesis of polymer ligand based IBUs. Molecules of this nature are even more analogous to compounds Murray has used recently for solventless

electrochemistry experiments.<sup>29b</sup> Thus, any of these advancements in the dendrimer project could easily resurrect solventless electrochemistry as a potential experimental technique for elucidating ET properties of metallodendrimers. The work that has been presented here represents the pioneering effort into the realm of solventless electrochemistry on metallodendrimers and has been made available for possible future collaborations with the Gorman Research Group.

## **A.9. SPECIAL ACKNOWLEDGEMENTS AND AUTHOR'S NOTES**

This work was completed with the dedication and effort of my coworker from Dr. Gorman's group, Jennifer Smith - my partner in crime, a good friend and an excellent scientist. I very much enjoyed working on this project with both Jen and Dr. Gorman. I am appreciative of Dr. Gorman for offering me the opportunity to undertake this project and only wish I could have completed the experiments with a greater degree of overall success. This is a natural collaboration for researchers in the Bowden group and I would hope that future students consider working on this project. With that said, I must also sincerely thank Dr. Bowden for allowing me to participate in this interesting side project. This work provided me with valuable experience in different areas of chemistry, expanded my knowledge of science, and represents one of the more challenging episodes of my graduate career.

Additionally, I would like to thank Dr. Susan Hendrickson of the Royce Murray group at UNC, Chapel Hill (presently an assistant professor at Davidson College) for providing two senior graduate students with the microelectrodes used in this project, thereby sparing us the task of making our own. I would also like to acknowledge Jan Singhaus for making our vacuum cells, a pivotal part of the experimental apparatus.

## **A.10. EXPERIMENTAL DETAILS**

### **A.10.1. Equipment / Materials / Procedures**

#### **-General**

Cyclic voltammetry (CV), chronoamperometry(CA), and linear sweep voltammetry(LSV) were performed using either an EG&G PAR 263 potentiostat or a Bioanalytical BAS-50W voltammetric analyzer. Each instrument was used with its

accompanying software, the PAR 270 software being operated in Ramp Mode, generating a staircase applied voltage waveform with a 0.5 mV step height. The current response of all scans under 100 mV/sec were filtered with a built-in 5.3 Hz. low pass filter. To ensure reproducibility, a minimum of 3 CV cycles were collected at any given scan rate with the final scan being saved. CA experiments were run in duplicate for repeatability.

The metallodendrimers used for each experiment were all previously synthesized and physically characterized with elemental analysis by members of the Gorman Research Group.<sup>9</sup> Atmospheric control around these molecules was maintained with a N<sub>2</sub> purged glove box, as well as, a variety of Schlenck flasks and vacuum lines. Exposure of the dendrimers to the atmosphere was minimal if at all throughout the experiments.

### **A.10.2. SAM Experiments & LSV Desorption**

#### **-Equipment/Materials**

An electrochemical cell previously described was used for all the aqueous or wet electrochemistry. The working electrode(WE) and substrate for the SAMs was an evaporated Au mirror electrode, 1000-4000Å Au / 50Å Ti / glass (Evaporated Metal Films, Ithaca, NY). The predominant RE used throughout these experiments was an in house built, non-aqueous, silver (Ag<sup>+0</sup>) wire, pseudo reference.<sup>14</sup> The silver wire was housed in a glass sheath that was filled with solvent containing a small amount of dissolved AgNO<sub>3</sub>. A platinum wire was used as the AE and wrapped around the outside of the glass barrel of the RE. The entire apparatus was then placed in the cell as close to the gold WE as possible to minimize solution resistance. Since organic solvents were employed with these electrochemical cells, Kalrez™ o-rings were used in place of the traditional Viton™ o-rings. The Kalrez™ o-rings are more resistant to chemical attack and degradation.

The thiols used to form the SAM on the gold surface were previously synthesized, purified, and characterized by Linderman and co-workers<sup>31</sup> or used as received from Aldrich Chemical Company (11-mercaptoundecanoic acid). The thiols were generally used as 5 mM solutions in ethanol (EtOH). The ammonium-borate salts were purchased in anhydrous form from Aldrich Chemical Company(St. Louis, MO) and used as received after drying and occasionally recrystallizing by standard procedures.<sup>32</sup> All solvents were purchased anhydrous or used directly from a still with air sensitive techniques (i.e. cantellation;

Schlenk flasks). Freeze-pump-thaw (F-P-T) cycles using liquid nitrogen and a heat gun were applied as needed to the organic solvents, The small percentage of aqueous experiments were done with Milli-Q filtered deionized water. All open transfers of materials or chemicals took place inside the glove box under inert atmosphere.

### **-Procedure**

Gold electrodes were cleaned with fresh Piranha solution (1:4 H<sub>2</sub>O<sub>2</sub>(30%) / H<sub>2</sub>SO<sub>4</sub>(conc.)) by immersing the electrode into the solution and stirring for 30 seconds. After the 30 second exposure, the Piranha solution was removed and the electrodes were rinsed thoroughly with copious amounts of Milli-Q water. CAUTION: Piranha solution is extremely dangerous and can react violently with organic compounds; extreme care should be used when handling or using Piranha solution! The electrodes were then rinsed several times with EtOH before being exposed to 900  $\mu$ L of the 5 mM alkanethiol ethanolic solutions. After several minutes, the electrodes were rinsed with pure EtOH, dried under a dry Ar gas stream, and packed in jars with dry Ar. These jars were then pumped into the glove box where they were assembled into the electrochemical cells.

For the actual experiments, the cells were filled with propylene carbonate (PC) containing 100 mM tetraethylammonium tetrafluoroborate. CV scans were made for C<sub>d1</sub> measurements and LSV was performed from 0.0V to -1.3V to facilitate the reductive desorption of the SAM.

### **A.10.3. Solventless Electrochemistry**

#### **-Materials/Equipment**

Microelectrode assemblies were borrowed from Royce Murray's Research Group and were used in conjunction with a vacuum cell designed in this lab and built by the NCSU glassblower. The experimental apparatus, shown in Figure A.20, was housed in a homemade faraday cage. The microelectrodes were polished on a wheel with successively smaller grain alumina paste micropolish (Buehler Inc.). The microelectrode was polished two times each with each size alumina paste (1.0, 0.3, & 0.05  $\mu$ m). The final polishing step was to polish the electrode by hand using the 0.05  $\mu$ m sized alumina, forming a "figure 8" with both hands.

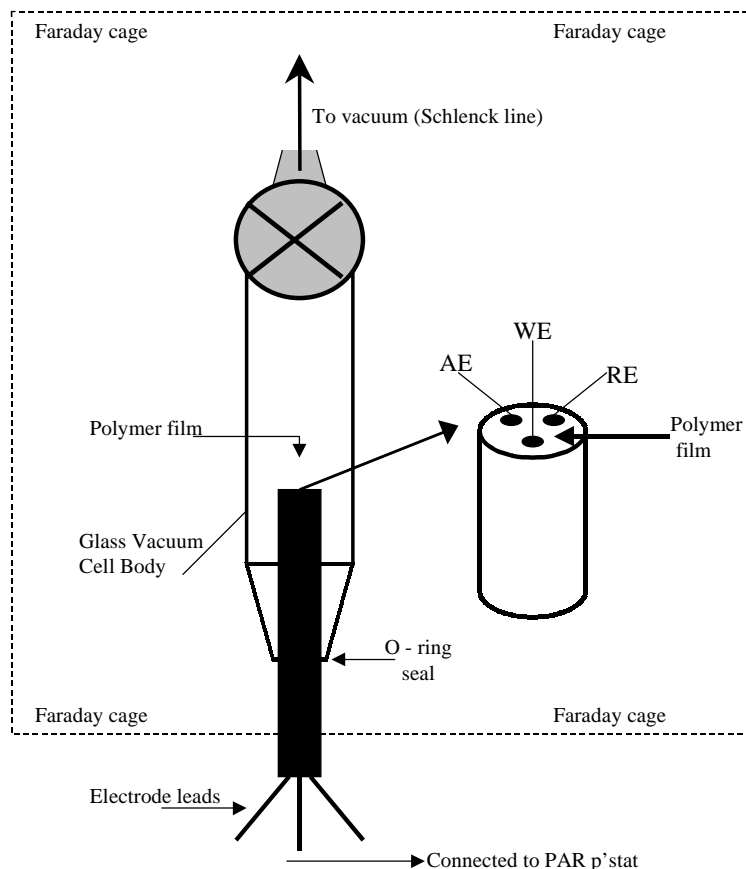


**Figure A.20.** In-house built experimental apparatus used for solventless electrochemistry of the metallodendrimers.

The polymers were purchased from either Aldrich Chemical Company or Polysciences Inc.. The starting polymer material was measured out in the glove box and transferred to a Schlenk flask. All glassware was kept in the oven for at least 48 hours prior to use and was flame dried with a methane Bunsen burner before use. The polymer was treated with several F-P-T cycles until bubbles ceased to form during the process. The flask with the polymer was then kept under vacuum and stirred with an internal magnetic stir bar. The flask was heated to 60-70°C via an oil bath. The polymer was kept under these conditions for at least 48 hours. At the end of this treatment, activated 3Å molecular sieves were added to the polymer while it was under a jet stream of dry N<sub>2</sub>. [Note: the sieves were activated by heating in a vacuum oven (-90 psi.) at 150°C.] This slurry of material was then heated at 60-70°C and slowly stirred overnight. [Note: the slurry was stirred extremely slowly so as to not damage the molecular sieves.]

Simultaneously, the  $\text{LiClO}_4$  solid was purchased as an anhydrous salt and was further dried in a vacuum oven at  $>100^\circ\text{C}$  for at least 3 days prior to initial use. The  $\text{LiClO}_4$  was kept in the vacuum oven at this temperature for the duration of the solventless electrochemistry project and used as needed. [Note: It is imperative to dry the salt before using it since the Li salts readily adsorb moisture.<sup>17</sup>

The dried  $\text{LiClO}_4$  and the dry MePEG, which was cantilated away from the molecular sieves into another vacuum flask, were both pumped into the glove box where they were combined. The Li salt was quantitatively added the polymer by measuring out enough to maintain a ratio of ether oxygen to Li of 16:1.<sup>18d</sup> The combination of these two materials, contrary to literature reports,<sup>18</sup> were not readily miscible. Instead the mixture required being returned to the vacuum pump for at least overnight stirring and heating ( $60\text{-}70^\circ\text{C}$ ).

Finally, for the solventless electrochemistry experiments themselves, the polymer electrolyte was transferred back to the glove box and mixed with the dendrimer in an approximate concentration of 5mM IBU. Several drops of this material were placed, via a glass microsyringe, on the microelectrode platform. The entire microelectrode tip was then sealed into a vacuum cell and returned to the vacuum line. The thin film of material was pumped on in this manner for at least 3 days before any testing was attempted. After the third day of pumping, the films were tested daily until the voltammetry became consistent. It was believed that the consistent signal was a sign that moisture had been completely removed from the film and stabilized the signal. The films, which were very thin and uniform but visible to the naked eye, were watched closely for any signs of “cracking,” an indication that they were excessively dry. Overly dry films have a greater propensity for iR effects to be present in the electrochemistry. CV experiments were performed first, followed by CA testing. CV scans were performed from 0.0V to -2.0V (vs.  $\text{Ag}^{+/0}$ ) at varying scan rates, typically less than 100 mV/sec. CA experiments were performed with step potentials of -1.5 to -2.0V and a pulse width of 10, 400, or 1000 seconds.

## A.11. REFERENCES

1. C.B. Gorman, "The Need for Potentiostatic Control in Imaging and Lithography with Nanoscale Electronic Devices," DURIP Proposal [AFOSR MURI F49620-96-1-0035], 1998.
2. a) Various Authors, "The Man Who Dared to Think Small," *Science*, **1991**, 28, 1300-1324. b) J.M. Lehn, "Perspectives in Supramolecular Chemistry - From Molecular Recognition Towards Molecular Information Processing and Self-Organization," *Angew. Chem. Int. Ed. Engl.* **1990**, 29, 1304-1319. c) *Molecular Electronics - Science and Technology*; American Institute of Physics: New York, 1991. d) *Molecular Electronics, Materials, and Methods*, Kluwer Academic Publishers; Topics in Molecular Organization and Engineering, 1991. e) J.S. Schumm, D.L. Pearson, and J.M. Tour, "Iterative Divergent / Convergent Approaches to Linear Conjugated Oligomers by Successive Doubling of Molecular Length: a Rapid Route to 128Å - Long Potential Molecular Wire," *Angew. Chem. Int. Ed. Engl.* **1994**, 33, 1360-1363.
3. a) M.A. Reed, C. Zhou, C.J. O'Muller, T.P. Burgin, and J.M. Tour, "Conductance of a Molecular Junction," *Science* **1997**, 278, 252. b) S. Prathapan, T.E. Johnson, J.S. Lindsay, "Building-block Synthesis of Porphyrin Light-harvesting Arrays," *J. Am. Chem. Soc.* **1993**, 115, 7519. c) D.L. Klein, P.L. McEuen, J.E. Katari, R. Roth, and A.P. Alivisatos, "An Approach to Electrical Studies of Single Nanocrystals," *Appl. Phys. Lett.* **1996**, 68, 2574. d) A. Credi, V. Balzani, S.J. Langford, and J.F. Stoddart, "Logic Operations at the Molecular. An XOR Gate Based on a Molecular Machine," *J. Am. Chem. Soc.* **1997**, 119, 2679-2681. e) P.G. Collins, A. Zettl, H. Bando, A. Thess, and R.E. Smalley, "Nanotube Nanodevice," *Science* **1997**, 278, 100-103.
4. C.B. Gorman, B. Parkhurst, K. Chen, W. Su, M. Hager, and I. Touzov, "A Model for Single-Information Storage," in *Fourth International Conference on Frontiers of Polymers and Advanced Materials*, P.N. Prasad, J.E. Mark, S.H. Kandil, and Z. Kafafi, Eds.: Plenum Press.
5. Donald Tomalia, personal communication.
6. a) C.B. Gorman, "Metallo-dendrimers: Structural Diversity and Functional Behavior," *Adv. Mater.* **1998**, 10(4), 295-309. b) G.R. Newkome, H. He, and C.N. Moorefield, "Suprasuper-molecules with Novel Properties: Metallo-dendrimers," *Chem. Rev.* **1999**, 7, 1689-1746. c) A.W. Bosman, H.M. Janssen, and E.W. Meijer, "About Dendrimers: Structure, Physical Properties, and Applications," *Chem. Rev.* **1999**, 7, 1665-1688.
7. C.B. Gorman, "Encapsulated Electroactive Molecules," *Adv. Mater.* **1997**, 9(14), 1117-1119.
8. Used with permission from the Gorman Research Group, North Carolina State University.
9. C.B. Gorman, B.L. Parkhurst, W.Y. Su, and K. Chen, "Encapsulated Electroactive Molecules Based Upon an Inorganic Cluster Surrounded by Dendron Ligands," *J. Am. Chem. Soc.* **1997**, 119, 1141-1142.
10. J.J.R. Frausto da Silva and R.J.P. Williams, *The Biological Chemistry of the Elements - The Inorganic Chemistry of Life*, Clarendon Press: Oxford, 1991.

11. C.B. Gorman, D. Feldheim, and D.W. Brenner, "An Interdisciplinary Approach to Nanotechnology: Combining Synthesis, Fabrication, and Computation to Establish Functional Behavior at the Nanoscale," NSF Proposal [98-20], 1998.
12. a) C.B. Gorman and J.C. Smith, "Effect of Repeat Unit Flexibility on Dendrimer Conformation as Studied by Atomistic Molecular Dynamic Simulation," *Polymer* **2000**, *41*, 675-683 b) C.B. Gorman, J.C. Smith, M.W. Hager, B.L. Parkhurst, H. Sierzputowska-Gracz, and C.A. Haney, "Molecular Structure – Property Relationships for Electron-Transfer Rate Attenuation in Redox-Active Core Dendrimers," *J. Am. Chem. Soc.* **1999**, *121*, 9958-9966.
13. H. Tokuhisa, M. Zhao, L.A. Baker, V.T. Phan, D.L. Dermody, M.E. Garcia, R.F. Peez, R.M. Crooks, T.M. Mayer, "Preparation and Characterization of Dendrimer Monolayers and Dendrimer-Alkanethiolate Mixed Monolayers Adsorbed to Gold," *J. Am. Chem. Soc.* **1998**, *120*, 4492-4501.
14. D.T. Sawyer, A. Sobkowiak, J.L. Roberts, *Electrochemistry for Chemists*, 2<sup>nd</sup> Ed., John Wiley and Sons: New York, 1995.
15. K.A. Groat and S.E. Creager, "Self-Assembled Monolayers in Organic Solvents: Electrochemistry at Alkanethiolate-Coated Gold in Propylene Carbonate," *Langmuir* **1993**, *9*, 3668-3675.
16. a) D.E. Weisshaar, M.M. Walczak, and M.D. Porter, "Electrochemically Induced Transformations of Monolayers Formed by Self-Assembly of Mercaptoethanol at Gold," *Langmuir* **1993**, *9*, 323-329. b) M.W. Walczak, D.D. Popenow, R.S. Deinhammer, B.D. Lamp, C. Chung, and M.D. Porter, "Reductive Desorption of Alkanethiolate Monolayers at Gold: A Measure of Surface Coverage," *Langmuir* **1991**, *7*, 2687-2693.
17. a) M.A. Ratner and D.F. Shriver, "Ion Transport in Solvent-Free Polymers," *Chem. Rev.* **1988**, *88*, 109-124. b) D.F. Shriver, B.L. Papke, M.A. Ratner, R. Dupon, T. Wong, and M. Brodwin, "Structure and Ion Transport in Polymer-Salt Complexes," *Solid State Ionics* **1981**, *5*, 83-88.
18. a) M.L. Longmire, M. Watanabe, H. Zhang, T.T. Wooster, and R.W. Murray, "Voltammetric Measurement of Ultraslow Diffusion Rates in Polymeric Media with Microdisk Electrodes," *Anal. Chem.* **1990**, *62*, 747-752. b) E.F. Dalton and R.W. Murray, "Viologen(2+/1+) and Viologen(1+/0) Electron-Self-Exchange Reactions in a Redox Polymer," *J. Phys. Chem.* **1991**, *95*, 6383-6389. c) M. Watanabe, T.T. Wooster, and R.W. Murray, "Electron-Self-Exchange Reactions in Solid State Voltammetry. The Radical Anion of 7,7,8,8-Tetracyanoquinodimethane in Polymer Electrolytes. 1," *J. Phys. Chem.*, **1991**, *95*, 4573-4579. d) M.L. Longmire, M. Watanabe, H. Zhang, T.T. Wooster, and R.W. Murray, "Experimental Aspects of Solid-State Voltammetry," *Anal. Chem.* **1992**, *64*, 1132-1140. e) J.C. Brumfield, C.A. Goss, E.A. Irene, and R.W. Murray, "Preparation and Characterization of Laterally Heterogeneous Polymer Modified Electrodes Using in Situ Atomic Force Microscopy," *Langmuir* **1992**, *8*, 2810-2817. f) N.A. Surridge, M.E. Zvanut, F.R. Keene, C.S. Sosnoff, M. Silver, and R.W. Murray, "Effects of Mixed-Valent Compositions and Bathing Environment on Solid-State Electron Self-Exchanges in Osmium Bipyridine Redox Polymer Films," *J. Phys. Chem.* **1992**, *96*, 962-970. g) M. Watanabe, T.T. Wooster, and R.W. Murray, "Long Range Electron Transfers Between Very Slowly Diffusing Tetracyanoquinodimethane and its Radical Anion in Poly(ether) Solutions," *J. Phys. Chem.* **1992**, *96*, 5886-5893. h) H. Zhang and R.W. Murray, "Polymer Solvent Dynamic Effects

on an Electron Transfer Cross Reaction Rate at a Redox Polymer / Polymer Solution Interface,” *J. Am. Chem. Soc.* **1993**, *115*, 2335-2340. i) C.S. Velazquez, J.E. Hutchison, and R.W. Murray, “Electrochemical Reactions and Charge Transport in Undiluted Room Temperature Melts of Oligo(ethylene glycol) - Based Electron Carriers,” *J. Am. Chem. Soc.* **1993**, *115*, 7896-7897. j) M.G. Sullivan and R.W. Murray, “Solid-State Electron Self-Exchange Dynamics in Mixed Valent Poly(vinylferrocene) Films,” *J. Phys. Chem.* **1994**, *98*, 4343-4351. k) J.N. Richardson, J. Harvey, and R.W. Murray, “Heterogeneous Electron-Transfer Dynamics of Decamethylferrocene from 130 to 181 K,” *J. Phys. Chem.* **1994**, *98*, 13396-13402. l) M.W. Poupert, C.S. Velazquez, K. Hassett, Z. Porat, O. Haas, R.H. Terrill, and R.W. Murray, “Limit of Slow Diffusion to Electrodes: Molecular-Scale Diffusion Paths in a Redox Melt,” *J. Am. Chem. Soc.* **1994**, *116*, 1165-1166. m) C.S. Velazquez and R.W. Murray, “Synthesis and Voltammetry of a Tetrathiafulvalene Polymer Electrolyte Melt,” *Journal of Electroanalytical Chemistry* **1995**, *396*, 349-357. n) R. Pyati and R.W. Murray, “Voltammetry and Conductivity of a Polyether-Pyridinium Room Temperature Molten Salt Electrolyte and of Its Polymer Electrolyte Solutions in Polydimethylsiloxane,” *J. Electrochemical Society*, **1996**, *143*(2), 401-405. o) J.W. Long, C.S. Velazquez, and R.W. Murray, “Electron Self-Exchange Dynamics of an Iron Bipyridine Complex Redox Polyether Hybrid in Its Room Temperature Melt,” *J. Phys. Chem.* **1996**, *100*, 5492-5499. p) T. Hatazawa, R.H. Terrill, and R.W. Murray, “Microelectrode Voltammetry and Electron Transport in an Undiluted Room Temperature Melt of an Oligo(ethylene glycol) - Tailed Viologen,” *Anal. Chem.* **1996**, *68*, 597-603. q) J.W. Long, I.K. Kim, and R.W. Murray, “Hybrid Redox Polyethers: Molecular Melts of Metalloporphyrins,” *J. Am. Chem. Soc.* **1997**, *119*, 11510-11515. r) F. Emmenegger, M.E. Williams, and R.W. Murray, “Redox Polyether Hybrid Copper Bipyridine Complex Molten Salts,” *Inorg. Chem.* **1997**, *36*, 3146-3151. s) M.E. Williams, H. Masui, J.W. Long, J. Malik, and R.W. Murray, “Electron and Mass Transport in Hybrid Redox Polyether Melts: Co and Fe Bipyridines with Attached Polyether Chains,” *J. Am. Chem. Soc.* **1997**, *119*, 1997-2005.

19. A.C. Michael and R.M. Wightman, “Microelectrodes,” in *Laboratory Techniques in Electroanalytical Chemistry*, 2<sup>nd</sup> edition, P.T. Kissinger and W.R. Heineman Eds., Marcel Dekker, Inc.: New York, 1996.
20. a) R.M. Wightman, L.J. May, and A.C. Michael, “Detection of Dopamine Dynamics in the Brain,” *Anal. Chem.* **1988**, *60*, 769A. b) R.M. Wightman, D.J. Michael, “Electrochemical Monitoring of Biogenic Amine Neurotransmissions in Real-Time,” *Journal of Pharmaceutical and Biomedical Analysis* **1999**, *19*(1-2), 33-42. c) R.M. Wightman and Q. Xin, “Simultaneous Detection of Catecholamine Exocytosis and Ca<sup>2+</sup> Release From Single Bovine Chromaffin Cells Using a Dual Microsensor,” *Anal. Chem.* **1998**, *70*(9), 1677-1681.
21. a) R.A. Wallingford and A.G. Ewing, “Capillary Zone Electrophoresis With Electrochemical Detection in 12.7-MU-M Diameter Columns,” *Anal. Chem.* **1988**, *60*, 1975. b) P.D. Curry, R.A. Wallingford and A.G. Ewing, “Chemical Analysis of Single Cells With Capillary Zone Electrophoresis,” *Abstracts of Papers of the American Chemical Society* **1988**, 196:177-ANYL.
22. C.R. Martin and C.A. Foss, “Chemically Modified Electrodes,” in *Laboratory Techniques in Electroanalytical Chemistry*, 2<sup>nd</sup> edition, P.T. Kissinger and W.R. Heineman Eds., Marcel Dekker, Inc.: New York, 1996.
23. a) I. Ruff, “Experimental Evidence of Electronic Conduction in Aqueous Solutions,” *Electrochimica Acta* **1970**, *15*, 1059. b) I. Ruff, V.J. Friedrich, K. Demeter, and K. Csillag,

- “Transfer Diffusion: Kinetics of Electron Exchange Reaction Between Ferrocene and Ferricinium Ion in Alcohols,” *J. Phys. Chem.* **1971**, 75(21), 3303-3309. d) L. Botar and I. Ruff, “Effect of Exchange Reaction on Transport Processes: Fick’s Second Law for Diffusion on Lattice Points,” *Chemical Physics Letters* **1986**, 126(3,4), 348-351. e) I. Ruff and I. Korosi-Odor, “Application of Diffusion Constant Measurement to the Determination of the Rate Constant of Electron-Exchange Reactions,” *Inorganic Chemistry* **1970**, 9(1), 186-188. f) H. Dahms, *J. Phys. Chem.* **1968**, 72, 362. g) E. Laviron, *J. Electroanal. Chem.* **1980**, 112, 1.
24. C.M.A. Brett and A.M.O. Brett, *Electrochemistry: Principles, Methods, and Applications*, Oxford University Press: Oxford, 1994.
25. D. Shoup and A. Szabo, “Chronoamperometric Current at a Finite Disk Electrode,” *J. Electroanal. Chem.* **1982**, 140, 237-245.
26. C.G. Zoski, A.M. Bond, C.L. Colyer, J.C. Myland, and K.B. Oldham, “Near Steady State Cyclic Voltammetry at Microelectrodes,” *J. Electroanal. Chem.* **1989**, 263, 1-21.
27. E. Dickinson, M.E. Williams, S.M. Hendrickson, H. Masui, and R.M. Murray, “Hybrid Redox Polyether Melts Based on Polyether-Tailed Counterions,” *J. Am. Chem. Soc.* **1999**, 121, 613-616.
28. a) R.A. Clark and E.F. Bowden, “Voltammetric Peak Broadening for Cytochrome c / Alkanethiolate Monolayer Structures: Dispersion of Formal Potentials,” *Langmuir* **1996**, 13, 559-565. b) M.C. Leopold and E.F. Bowden, manuscript in preparation.
29. a) H. Nishihara, F. Dalton, and R.W. Murray, “Interdigitated Array Electrode Diffusion Measurements in Donor / Acceptor Solutions in Polyether Electrolyte Solvents,” *Anal. Chem.* **1991**, 63, 2955-2960. b) R.H. Terrill, T. Hatazawa, and R.W. Murray, “Electron Transport and Frozen Concentration Gradients in a Mixed Valent Viologen Molten Salt,” *J. Phys. Chem.* **1995**, 99, 16676-16683.
30. S. Song, R.A. Clark, M.J. Tarlov, and E.F. Bowden, “Characterization of Cytochrome c / Alkanethiolate Structures by Self-Assembly on Gold,” *J. Phys. Chem.* **1993**, 97(24), 6564.
31. T.M. Nahir, D. Tiani, D. Miller, R.J. Linderman, and E.F. Bowden, manuscript in preparation.
32. D.D. Perrin and W.L.F. Armarego, *Purification of Laboratory Chemicals*, 3<sup>rd</sup> Ed., Pergamon Press: New York, 1988.

## **INTERESTING ELECTROCHEMISTRY AT INDIUM OXIDE ELECTRODES**

### **APPENDIX B**

*“There is no crisis to which academics will not respond with a seminar.” - Anonymous*

## **B.1. INTRODUCTION**

This appendix describes research performed as part of a collaboration with Dr. Ashley Bush and coworkers in the Laboratory of Oxidation Biology in the Department of Psychiatry and Neurology - Genetics and Aging Unit at the Harvard Medical School and Massachusetts General Hospital. The research is focused on using electrochemistry as a complementary technique to explore drug pathways and delineate the pathology behind age related degradation of function and neurological disease. Although this research collaboration is in its early stages, it appears as though electrochemistry may be useful in understanding some of these disorders. What follows is a brief synopsis of the electrochemistry performed as part of this research collaboration. The following discussion is not intended to be a detailed description of the current state of neurological disease and age related illnesses. Instead, the discussion attempts to provide a glimpse of how electrochemistry has been and can be utilized to assist in biomedical research of this nature. The accounts of this research effort discuss recent successful ventures using electrochemistry in biomedical studies as well as specific complications that clearly warrant future electrochemical experiments in this area. This appendix is provided as part of this dissertation, not only to register an account of the research activity, but to hopefully inspire future researchers to consider work in this exciting, new collaboration.

## **B.2. NEUROLOGICAL DISEASE<sup>1</sup>**

Age related illnesses and neurological diseases are some of the worst ailments affecting human beings today. Alzheimer's disease (AD), for example, causes a progressive loss of memory and mental capabilities in elderly people, eventually leaving people afflicted with this disease confused and incompetent to care for themselves. The disease can render its victims helpless to recognize and remember even their closest loved ones and friends. AD affects 5-10% of all people over the age of 65, some 4 million persons in North America. Other examples of the more prominent neurological diseases affecting the elderly are Huntington's disease (HD) and Parkinson's Disease (PD). Huntington's disease affects one in ten thousand individuals, about 30,000 people in North America alone, and caused its victims to make involuntary movements, become cognitively impaired, and eventually

mentally disturbed. One million people in North America suffer from PD, a condition which eventually results in serious dementia. Not very well understood, these diseases continue to affect people around the world and are met with non-optimal medical treatments that are only able to slow, not halt, the degenerative process of the disease. Thus, scientists aim research efforts at understanding the pathology of these diseases in order to develop more successful and effective means of treating and preventing the onset of the diseases. Several hypothetical mechanisms for these diseases have been proposed including oxidative stress, free radical activity, excitotoxicity, accumulation of intracellular aggregates, mitochondrial dysfunction, and apoptosis. These ideas and more are being pursued throughout the biomedical field in search of a better understanding of how these diseases occur and, more importantly, how they can be treated or prevented.

### **B.3. METAL OXIDE ELECTRODES**

For this research, the pathology of several age related illnesses, neurological diseases, and drug pathways, were investigated using voltammetry, at metal oxide electrodes. Metal oxide electrodes have been used previously for electrochemical experiments both in the general literature<sup>2</sup> and in this research group.<sup>3</sup> Metal oxides such as tin oxide and indium tin oxide (ITO) provide stable (unreactive), conductive surfaces for electrochemical experiments. These semi-metallic electrodes are comprised of a conductive, transparent film of tin-doped indium oxide on a glass substrate. Their transparent nature renders these substrates useful in spectroscopic studies and their acid/base surfaces allow for control of surface ionization with solution pH. Although their interfacial properties are not completely understood, ITO electrodes have been used exclusively for this research effort. ITO electrodes exhibit a very wide potential window in aqueous solution and are less prone to fouling due to material irreversibly adsorbing on their surface. Metal electrodes such as gold, while superior in other electrochemical experiments, are extremely reactive toward foreign material and therefore have a tendency to promote surface adsorption/contamination. If the material is biological in nature, such as the case in some of this work, the materials may irreversibly adsorb to the gold and subsequently become denatured on the surface. Most of the research involving ITO electrodes also utilized copper solutions whose redox activity occurs at positive potentials

which are easily accommodated by the ITO. For these reasons, ITO was chosen to act as the working electrode in all of the following studies.

#### **B.4. THE KYNURENINE PATHWAY - A CATARACT STUDY**

A major portion of this research focused on the amino acid tryptophan's catabolic reaction, or kynurenine pathway. This pathway is found throughout most of the tissue in the human body and is illustrated in Figure B.1. In this pathway, a number of toxic intermediates including 3-hydroxykynurenine (3HK) and 3-hydroxyanthranilic acid are produced. Multiple research efforts have implicated the kynurenine pathway and its toxic intermediates as playing a role in a number of neurological, inflammatory, and age related diseases including: HD, PD, HIV infection, bladder cancer, cerebral malaria, poliomyelitis, fetomaternal tolerance, and animal multiple sclerosis and viral pneumonia.<sup>4,5</sup> The toxic intermediates 3HK and 3HAA cause neuronal cell death with apoptotic features in cultures.<sup>4</sup>

The kynurenine pathway and the subsequent derivatives of the reaction are also active in the epithelial cells of the ocular lens. In the lens, 3HK interacts with lysyl residues of the lens proteins, such as  $\alpha$ -crystallin, and may function as a short wavelength ultraviolet light filter for the eye.<sup>6</sup> Recent work performed on the kynurenine pathway component 3HK has shown that the amount of 3HK bound to lenticular proteins increases with age and eventually fosters protein aggregation. This aggregation is speculated to contribute to the opaque nature of cataractous lens.<sup>4,6</sup>

Protein aggregation leading to cataract formation is also characterized by oxidative stress damage. Numerous studies<sup>4</sup> have shown that the process is accompanied by both a decrease in antioxidant defense enzymes and an increase in hydrogen peroxide. Additionally, there have been accounts of a raised level of Cu(II) in the cataractous lens, which has been implicated as a cofactor in generating potentially damaging reactive oxygen species, such as peroxide and superoxide, which may also foster protein aggregation.<sup>4</sup> Taken together, these findings suggest that oxidative stress, initiated by the combination/reaction of 3HK and other related kynurenine catabolites with redox active copper and other metals may participate in age related cataract formation.

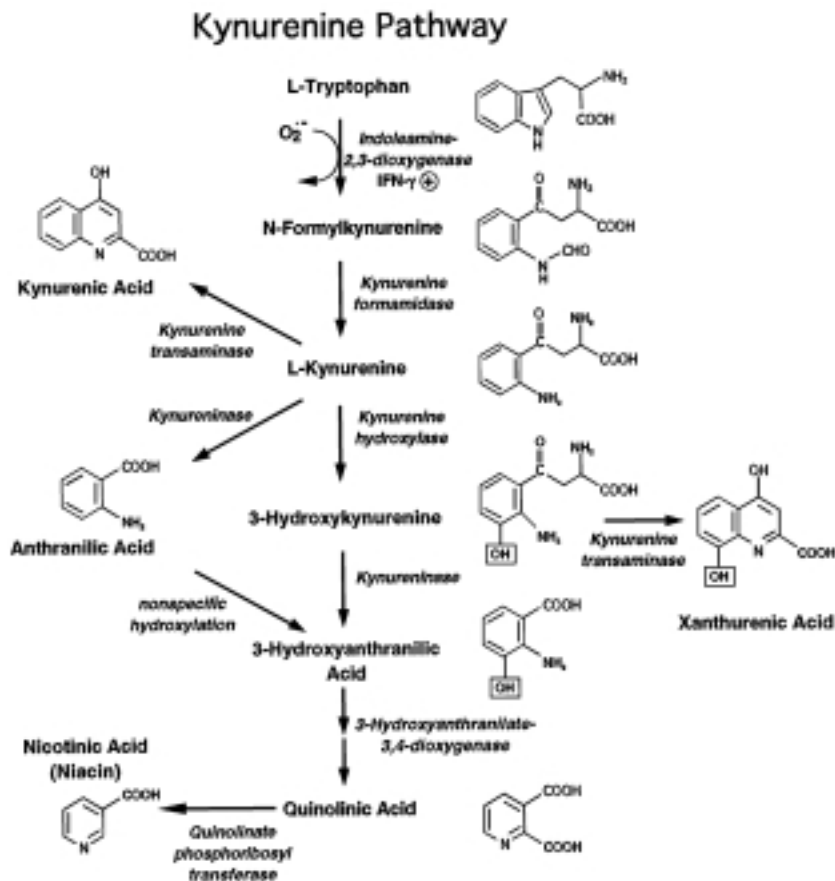


**Figure B.1.** Tryptophan metabolism through the kynurenine pathway. Enzymes catalyzing reactions are indicated in italics. The phenolic hydroxyl group is noted by a box on the compounds that reduce Cu(II) to Cu(I) and generate hydrogen peroxide (3HK, 3HAA, and XA).<sup>4</sup>

In this research, the possibility is considered that the interactions between the two phenolic kynurenine derivatives, 3HK and 3HAA, and redox active Cu(II) contribute to the generation of reactive oxygen species, ultimately oxidative stress, and the aggregation of crystallins. This interaction initially involves the reduction of the Cu(II) through Fenton chemistry before the ultimate generation of hydroxyl radicals, peroxides, and superoxides.<sup>7</sup> Research on the kynurenine catabolites, performed by Bush and coworkers, involving metal reduction, hydrogen peroxide, and superoxide assays (results not shown) suggest that the ortho-aminophenol kynurenine derivatives, 3HK and 3HAA, but not their nonhydroxylated precursors, kynurenine (KYN) and anthranilic acid (ANA), effectively reduce Cu(II) and Fe(III) at physiological pH, subsequently setting the stage for the generation of hydrogen peroxide and, in the case of 3HAA, superoxide. To further explore this proposal, cyclic voltammetry was employed for further characterization. Electrochemistry has been

performed previously on kynurenine catabolites,<sup>8</sup> but their electrochemistry in the presence of metal species is largely unexplored.

Data from the Bush laboratory indicated that 3HK and 3HAA were the strongest Cu(II) reducing agents in the kynurenine pathway. Therefore, as a means of confirming this apparent redox activity of 3HK and 3HAA, cyclic voltammetry was used to study the interaction of these catabolites with Cu(II). This study, illustrated in Figure B.2, compared 3HK and 3HAA to their non-phenolic analogs, KYN and ANA, in aqueous solutions of Cu(II) at pH 7.41. Cyclic voltammetry of the four catabolite compounds in the absence of Cu(II) (data not shown) revealed no significant redox activity in the +0.15 to -0.4 V potential window compared to the phosphate buffer solution (PBS) background (scan a). At potentials above +0.15 V, the catabolites undergo direct irreversible oxidation, a reaction that is not considered further at this point. Cyclic voltammetry of Cu(II) in PBS yielded a current response at approximately 100 mV due to the reduction of the metal ion (scan b). In the presence of either KYN or ANA, the Cu(II) reduction wave remained largely unaffected (scan c) although KYN appears to show some slight reactivity. This result suggests that most of the Cu(II) remains uncomplexed and available for reduction in the presence of the two catabolites. The Cu(II) reduction wave was nearly abolished (scan c) in the presence of 3HK, and markedly decreased in the presence of 3HAA. These results indicate that, for the experimental conditions used (see Experimental Details), loss of electrochemically active Cu(II) by complexation and/or reduction occurs readily in the presence of 3HK and 3HAA, but not in the presence of KYN or ANA. These findings are consistent with the proposed reduction of Cu(II) by 3HK and 3HAA, supporting the scenario laid out by the Bush research.

While supporting the hypothesis of the Bush laboratory, these results are not without their own complications and clearly require further investigation to fully understand the situation. As can be noted from Figure B.2, the scans of the catabolites KYN, 3HK, and 3HAA with copper (scan c of Figure B.2), all show an apparent rise in background cathodic current starting at approximately -0.225 V, which may be residual dioxygen reduction or an initial sign of a solvent related redox process. Since Bush's group showed that the reaction of copper with reactive metabolites in the presence of dioxygen led to hydrogen peroxide

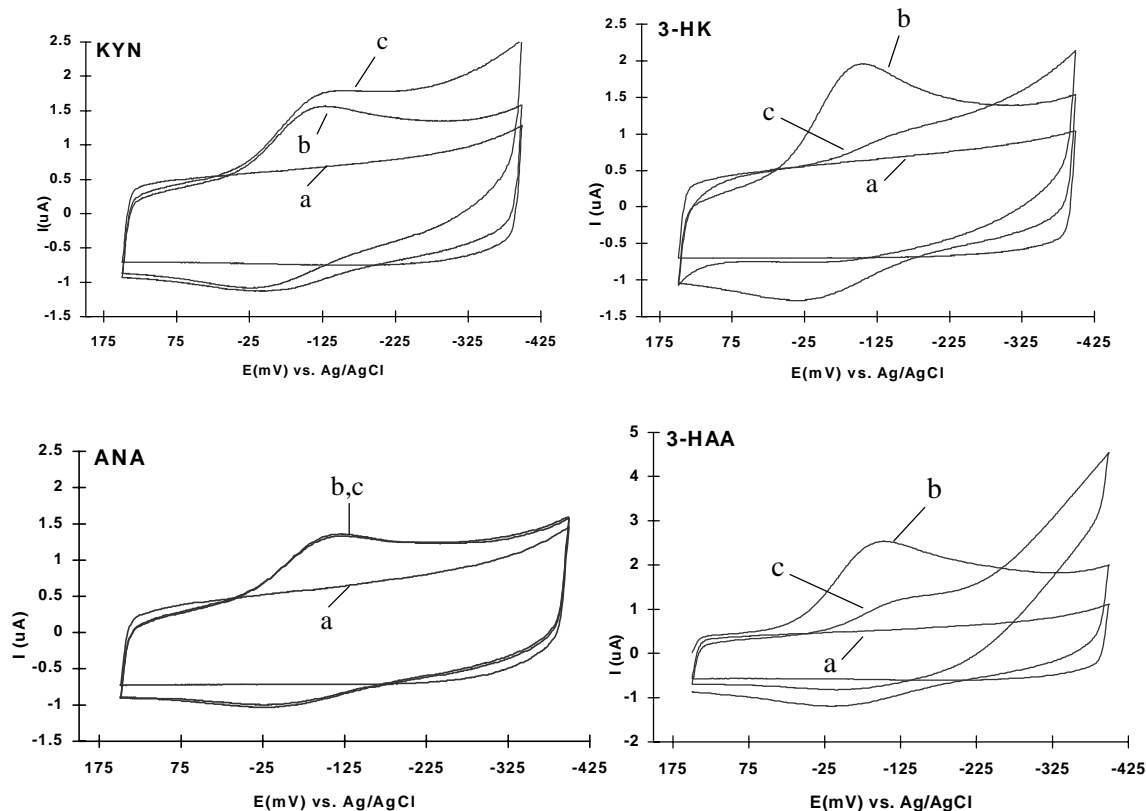


**Figure B.2.** Electrochemical analysis by cyclic voltammetry of kynurenine pathway catabolites in the presence of Cu(II). Cyclic voltammetry was conducted on phosphate buffered saline solutions (PBS) at pH = 7.4 of copper (II) chloride (25  $\mu$ M) in the presence and absence of 100  $\mu$ M L-kynurenine (KYN), 3-hydroxykynurenine (3-HK), anthranilic acid (ANA), and 3-hydroxyanthranilic acid (3-HAA). In each panel, voltammograms are shown of (a) background current in PBS, (b) Cu(II) in PBS, and (c) Cu(II) in the presence of the designated catabolite.

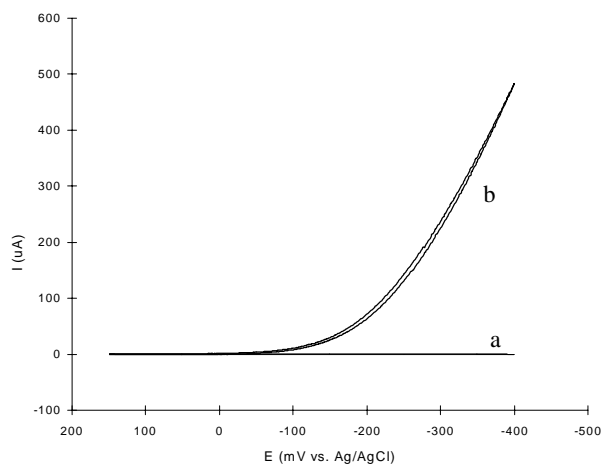


**Figure B.3.** Cyclic voltammetry of (a) PBS background and (b) PBS background with added  $\text{H}_2\text{O}_2$ .

production, it was speculated that the rise in background current was the result of peroxide formation and its subsequent reduction. To test this hypothesis, a blank scan of PBS in this same potential window was compared with PBS with added  $\text{H}_2\text{O}_2$  and is shown in Figure B.3. It appears from these results that the rise in background current is the result of peroxide reduction.

The results in Figure B.2 were obtained using ITO electrodes that were “activated” by an electrochemical pretreatment. Activation of ITO electrodes, in this case, involved cycling the electrode potential scan range to high values (+1.2 to -0.4 V). The results obtained on ITO electrodes depended significantly on this activation step, as first discovered during some of the catabolite system voltammetry where there seemed to be an unusual potential window dependence in the results. An example of this phenomenon is shown as Figure B.4 with 3HAA in the presence of copper ion. Voltammetry of Cu(II) in the presence of 3HAA at an activated ITO electrode has already been shown (Figure B.2C) and depicts only weak copper redox activity when the ITO at an activated surface. This is the result consistent with the proposed hypothesis of complexation and/or metal reduction processes taking place. However, without activation, i.e. when the same system is scanned in a small potential window, the initial scan (Fig. B.2A) clearly shows a copper signal largely unaffected by the presence of 3HAA. When the potential is cycled to more positive potentials, the Cu signal disappears, consistent with the proposed reaction mechanism with 3HAA. It also appears from this figure that there exists a threshold potential, possibly where the catabolite begins to be forcibly oxidized by the applied potential, where a substantial, yet unknown, effect occurs to change the voltammetry. Similar potential window anomalies were witnessed with some of the other kynurenine based systems as well. It is believed that this effect is a property of the ITO surface itself, but at this early stage in the research the influence of concentration and reaction mechanisms involving the oxidized forms of these catabolites that are generated at these higher positive potentials cannot be unambiguously ruled out as contributing factors. Furthermore, all of the kynurenine pathway catabolites readily autooxidize. For these reasons, voltammetry experiments dedicated to this current study focusing on copper reactivity were isolated to a narrow potential window, performed as quickly as possible, on ITO electrodes that had previously been activated.

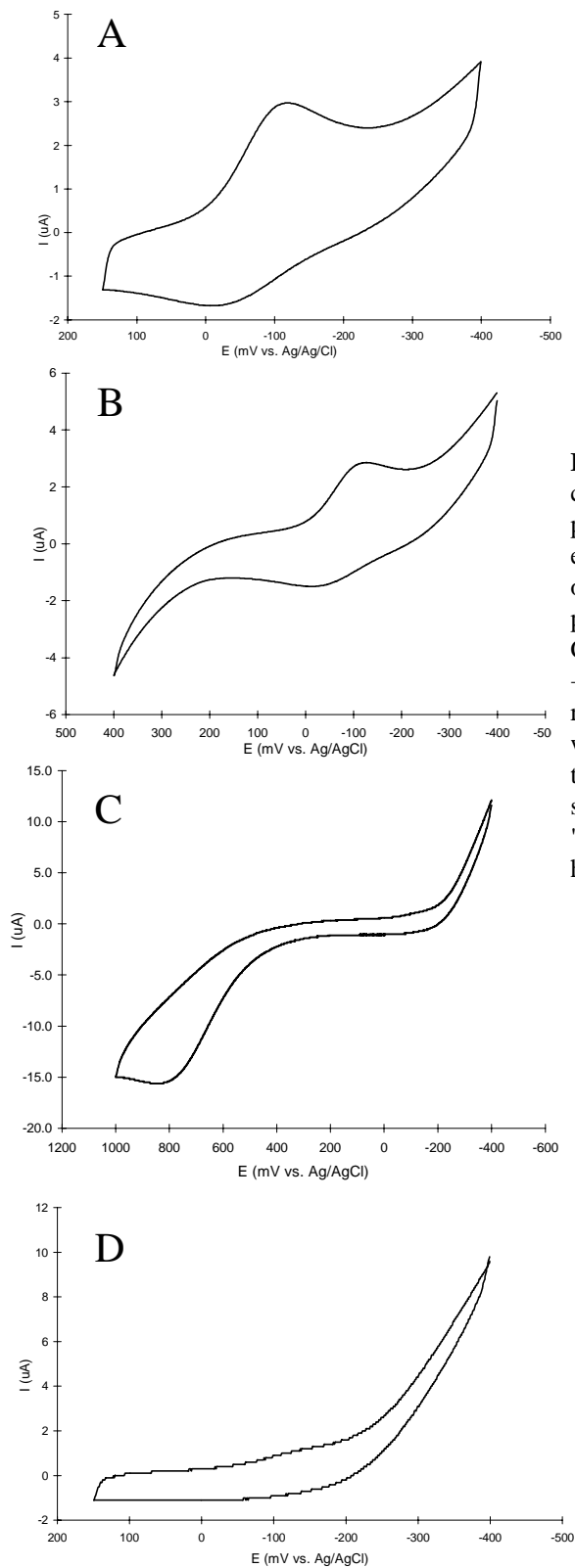


**Figure B.4.** Cyclic voltammetry of copper (II) chloride ( $25\ \mu\text{M}$ ) in the presence of 3HAA ( $100\ \mu\text{M}$ ) at an ITO electrode: A) initial potential window of  $+0.15\text{ V} \leftrightarrow -0.4\text{ V}$ ; B) a larger potential window of  $+0.4\text{ V} \leftrightarrow -0.4\text{ V}$ ; C) an extended potential window of  $+1.0\text{ V} \leftrightarrow -0.4\text{ V}$ ; and subsequently returning to the original potential window of  $+0.15\text{ V} \leftrightarrow -0.4\text{ V}$ . Notice that the copper signal at  $-100\text{ mV}$  is substantial until the electrode is "activated" by scanning to potentials of higher positive values (C & D).

Some of the strongest evidence for this potential window dependence being a function of the ITO electrode itself and independent of the presence of specific catabolites is the voltammetry collected for the copper standard. Figure B.5 shows several voltammetric scans of Cu(II) in PBS in various potential windows. The potential window dependence of the system is very evident. With each expansion of the potential window, the copper signal is enhanced. This trend was observed regardless of degassing, although higher copper currents did result from degassed samples. Even though the activation mechanism and the potential cycling mechanism are not known, activation did lead to reproducible results for experiments. This is not an unusual situation in electrochemistry for the early stages of a solid electrode investigation. In light of these results, however, further investigation of the ITO “activation” mechanism is clearly needed. Additionally, the future of this particular project could entail electrochemical analysis on the ocular protein,  $\alpha$ -crystallin, to see how its electroactivity is affected by the presence of these kynurenine pathway catabolites.

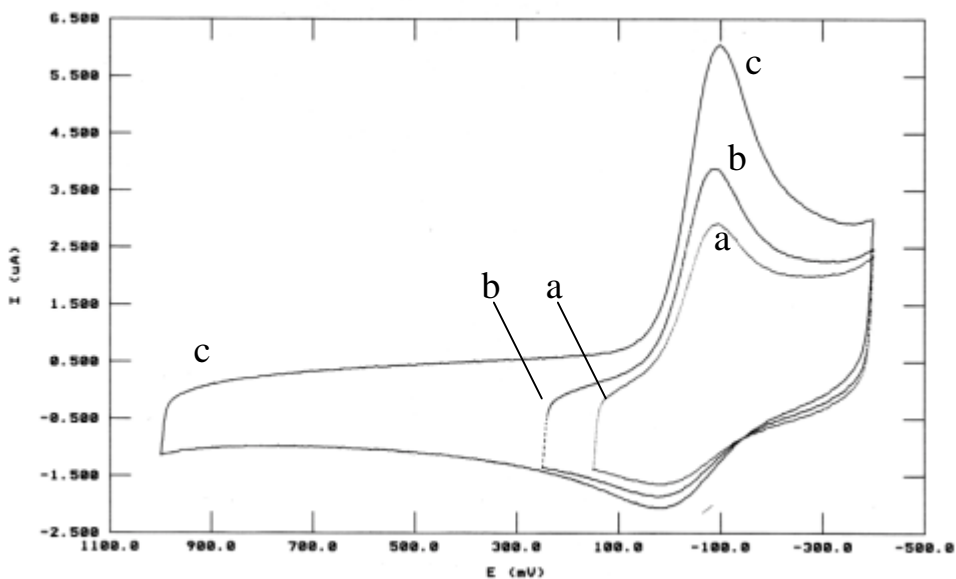


**Figure B.5.** Cyclic voltammetry of 25  $\mu$ M copper (II) chloride in PBS (pH 7.3) scanned sequentially in the following potential windows: (a) +0.15  $\leftrightarrow$  -0.4 V; (b) +0.4  $\leftrightarrow$  -0.4 V; (c) +1.0  $\leftrightarrow$  -0.4 V. Note the apparent increase in the Cu signal at -100 mV with each enlargement of the scanned potential window toward more positive potentials. Scanned at 100 mV/sec ; Ag/AgCl (1M KCl) reference electrode.

## B.5. THE A $\beta$ PEPTIDE AND ALZHEIMER'S DISEASE

Redox metal based oxidative stress mechanisms have been targeted as playing a vital role in the pathogenesis of Alzheimer's disease (AD). Early biological events that signal the start of AD involve enzymes attacking a neuron based protein called APP (see Figure B.6).

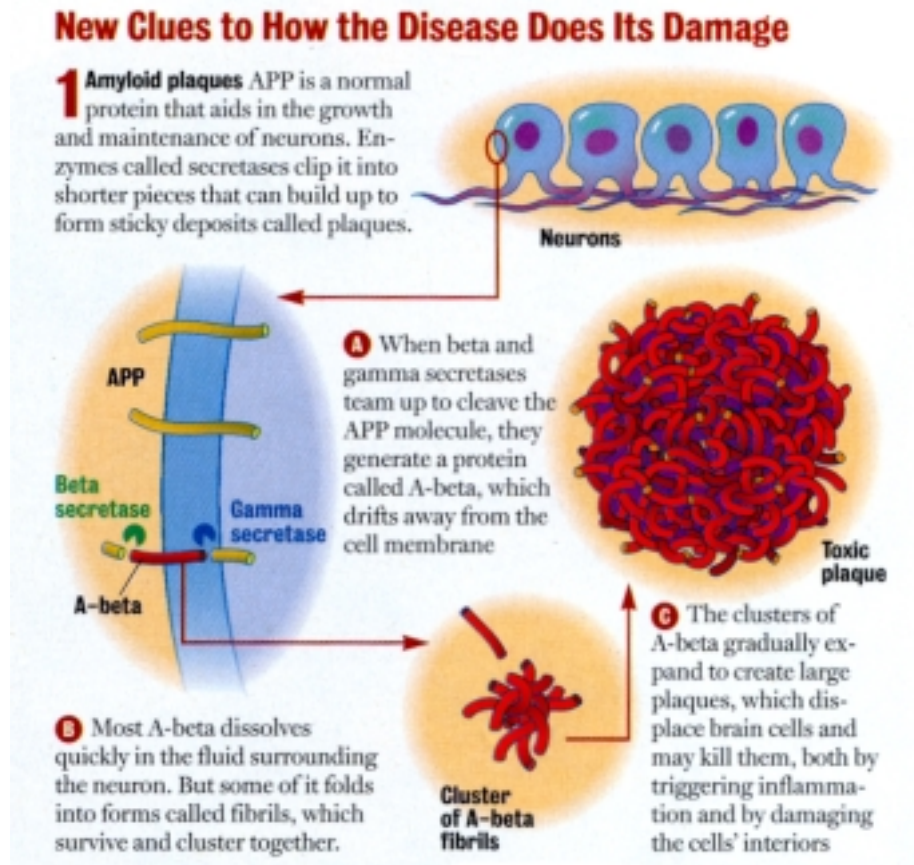


**Figure B.6.** Illustration of how Alzheimer's attacks the brain (Figure from Ref. 1e).

Normally APP functions as a growth and maintenance protein. However, at the onset of Alzheimer's, the APP proteins are attacked by secretase enzymes (both beta and gamma) that dice the protein into shorter pieces, including a protein fragment called A-beta ( $A\beta$ ). Most of the  $A\beta$  peptides dissolve quickly in the fluid surrounding the neuron cells. Some of the  $A\beta$ , however, drifts away from the cell membrane and forms clusters with other  $A\beta$  strands, called fibrils. The fibrils eventually enlarge into masses called toxic plaques which subsequently displace brain cells, sometimes destroying them and sometimes triggering an inflammation reaction. In response to the inflammation, the human body will release toxic agents in the form of free radicals which attack the infection. This response usually ends up

destroying the neurons in an attempt to rid the organism of the fibrils and plaques. Eventually the neuron cell's interior is severely damaged and no longer can function. Victims of AD have an increased concentration of these A $\beta$  peptides in their brains, which are literally littered with sticky plaque lesions. Thus, much AD research has focused on studying the A $\beta$  peptides and their role in this process in order to understand the pathology of this disease and possibly learn of a possible intervention treatment.<sup>1</sup>

Specific A $\beta$  peptides have been shown to have a neurotoxicity linked to metal reduction and subsequent hydrogen peroxide generation, although the mechanism is unknown. Evidence has recently been reported that supports a proposed mechanism in which specific A $\beta$  peptides react with redox metals to produce a Fenton-like reaction, the by-product of which is hydrogen peroxide.<sup>9</sup> This reaction scheme is displayed as Figure B.7. This finding is interesting in that abnormally high concentrations of Cu(II) and Fe(II) have been found in the amyloid plaques and AD-infected neuropile. Additionally, there is evidence in the literature that suggests that copper binds to the A $\beta$  peptides.<sup>1,10</sup> Copper selective chelators have been shown to dissolve A $\beta$  deposits from AD inflicted brain tissue, increasing suspicion that the presence of local redox metals may play an important role in this disease.<sup>1,11</sup> Consequently, copper chelating and antioxidant chemical treatments on patients with AD have significantly slowed both the onset and progression of AD and other neurological diseases.

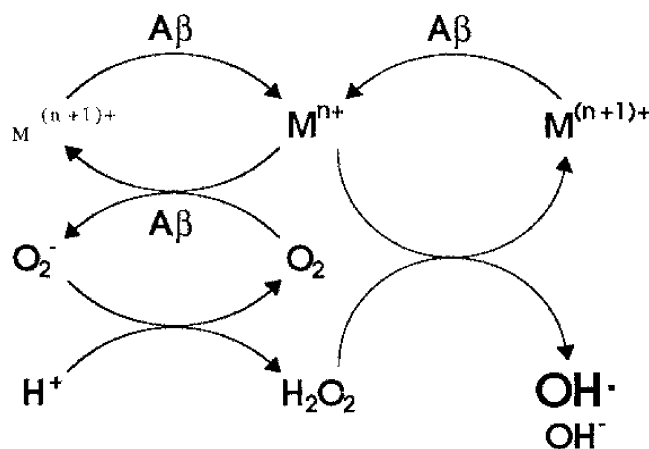


**Figure B.7.** Model for the generation of reduced metal ions,  $O_2^-$ ,  $H_2O_2$ , and  $OH\cdot$  by A $\beta$  peptides. Note that A $\beta$  facilitates two consecutive steps in the pathway: the reduction of metal ions and the reaction of  $O_2$  with reduced metal ions.<sup>9,11</sup>

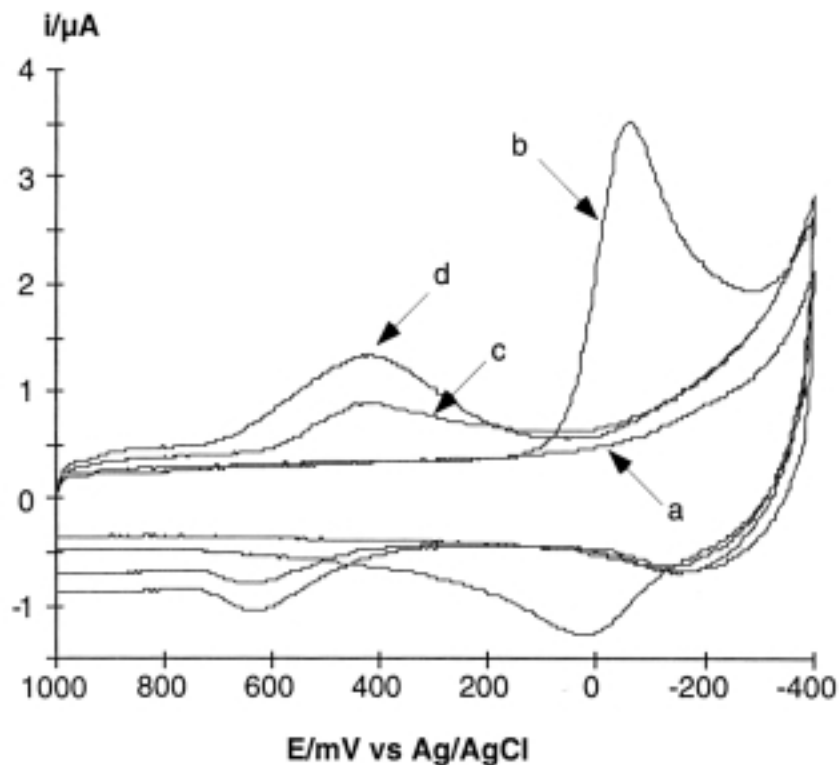


**Figure B.8.** Electrochemical characterization of a complex formed between A $\beta$ 1-42 and copper. Electrochemical analysis by cyclic voltammetry of A $\beta$ 1-42 with and without added Cu(II). Response obtained from (a) Dulbecco's PBS, pH=7.3; (b) Cu(II) (17  $\mu$ M) in buffer; (c) A $\beta$ 1-42 (100  $\mu$ M) in buffer, and (d) A $\beta$ 1-42 (100  $\mu$ M) with added Cu(II) (17  $\mu$ M) in buffer. All cyclic voltammograms were obtained at an ITO electrode with a scan rate of 100 mV/sec.<sup>11</sup>

In this study, electron paramagnetic resonance (EPR) and metal reduction assays performed by Bush and coworkers indicated that the A $\beta$  peptide, known as A $\beta$ 1-42, had a strong tendency to bind and reduce Cu(II).<sup>9,11</sup> To help corroborate this finding, cyclic voltammetry was performed by researchers in the Bowden laboratory. Again, the electrochemical behavior of Cu(II) was assessed in the presence and absence of the A $\beta$  peptide in question. The results of these experiments are displayed in Figure B.8. Included in this figure are scans of PBS alone and with Cu(II) (scans a & b). The PBS was found to routinely possess approximately 0.1  $\mu$ M Cu background contamination. Scan c of Figure B.8 shows the voltammetry of A $\beta$ 1-42 in the Cu contaminated buffer. The peak seen in scan c at  $\sim$  +500-550 mV is thought to be the redox activity of a Cu- A $\beta$  complex. The high positive potential displayed by the complex suggests that the copper is in a +1 oxidation state that is stabilized by the peptide binding. To support this hypothesis and determine whether A $\beta$

interaction with Cu metal in the PBS is responsible for the electrochemical response observed, Cu(II) in the form of CuCl<sub>2</sub> was added to the mixture. Adding Cu(II) to the solution increased the magnitude of the response at +500-550 mV (scan d in Figure B.8), a response consistent with the electrochemical response being characteristic of a copper- A $\beta$  complex. As noted from the figure, the Cu(II) response at -80 mV (scan b) is completely abolished in the presence of the A $\beta$  peptide, an indication that no free copper is available when the A $\beta$  is present. Thus, the cyclic voltammetry results support the hypothesis that the A $\beta$ 1-42 peptide binds and reduces Cu(II) and may be an integral part of the Fenton chemistry that eventually leads to the production of hydrogen peroxide and ultimately to oxidative stress, a proposed mechanism of AD.

A complete understanding of the pathology of AD remains elusive. One current focus is a mutant form of the A $\beta$  peptide, called the Dutch type or Q22, which has been targeted as playing a significant role in amyloidogenic disease.<sup>12</sup> Similar metal reduction/peroxide formation mechanisms are thought to be responsible in this case and, thus, a key need for exploring these possibilities is monitoring the reduction of Cu(II). A popular method of monitoring Cu(II) reduction is through the use of a specific colorimetric ligand for Cu(I), bathocuproine disulfonate (BC). BC's ability to complex both Cu(II) and Cu(I), however, is the subject of debate in the literature and welcomes future experiments aimed at delineating the processes involved with BC-copper interactions. Perhaps, electrochemistry, having shown promising results in these projects, can be used to clarify the exact relationship between BC and copper species.<sup>13</sup> In any event, applying electrochemistry to study neurological diseases and age related illness appears to be a challenging, yet potentially rewarding, emerging field of study.

## **B.6. CYTOCHROME C AT ITO ELECTRODES**

As noted in a previous section, the surface ionization of ITO, due to its inherent number of acid/base surface sites, can be adjusted via solution pH manipulation. The fact that the surface can be made negative at near neutral pH encouraged the use of the ITO substrate as an electrostatic binding partner for cyt c molecules. If successful, the ET of cyt c adsorbed on ITO may be studied without the use of a surface modifier or SAM. Thus, a

project arose with the objective of basic electrochemical characterization of cyt c adsorbed at ITO electrodes.

Considerable work has been performed with cytochrome monolayers on SnO<sub>2</sub> electrodes,<sup>3</sup> but the adsorption of cyt c at ITO electrodes, whose conductivity is higher than SnO<sub>2</sub>, is relatively uncharted territory.<sup>15</sup> In this current study, cyt c molecules were successfully adsorbed to the ITO. An example of a cyclic voltammogram of adsorbed cyt c at ITO is shown as Figure B.9. The electrochemical response of cyt c, shown in the figure, is stable for several days and the native form of the adsorbed protein seems to persist, unlike at bare metal electrodes. As with tin-oxide electrodes, the hydrophilic and negatively charged, ionic surface of the ITO causes the hindered denaturation of the protein. Both HH cyt c and yeast C102T cyt c were successively immobilized and electrochemically characterized on the ITO. Table B.1 shows the results of these experiments. The data were collected solely from voltammetry experiments because all attempts to duplicate the data with electrochemical impedance spectroscopy (EIS) have been, up to this point, unsuccessful. The reasons for the failure of EIS are unknown and require additional investigation.

In the evaluation of these systems, a curious and somewhat familiar trend emerged concerning a scan rate dependent rate constant. Theoretically, the electron transfer rate constant should show no dependence on the scan rate. A plot of scan rate versus ET rate constant, shown as Figure B.10, indicates otherwise. From the plot, it is clear that at low sweep rates, the ET rate constant undergoes a dramatic change. A nonlinear trend for this system is also noted, as shown in Figure B.11, for the peak splitting ( $\Delta E_p$ ) versus the scan rate. Previous work with HH cyt c adsorbed at tin oxide electrodes showed similar phenomena.<sup>3c</sup> The reasons behind these results are still being investigated. Research on this project is now geared toward understanding these trend and establishing an adsorption model, possibly a square scheme mechanism, which effectively describes the cyt c/ITO system.

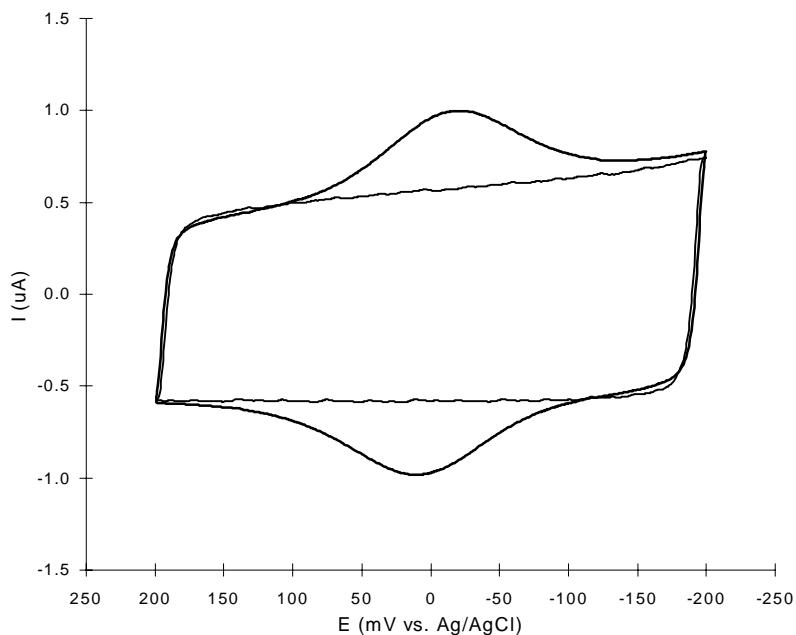


**Figure B.9.** Cyclic voltammetry of HH cyt c adsorbed to ITO. Shown with background (Data collected by Ryan Gallagan).

**Table B-1.** Cyt c / ITO Voltammetry<sup>a</sup>

System	$E^{\circ'}$ (mV)	$\Gamma^*$ (pmol/cm <sup>2</sup> ) <sup>d</sup>	FWHM (mV) <sup>d</sup>	$k^{\circ et}$ (s <sup>-1</sup> ) <sup>e</sup>
HH Cyt c <sup>b</sup>	-6.2 (±4.0)	14.5 (±2.1)	108.3 (±1.1)	15.9 (±4.6)
Yeast C102T Cyt c <sup>c</sup>	-9.7 (±4.9)	8.7 (±1.3)	103.4 (±1.3)	7.3 (±8.5)

<sup>a</sup> Data collected by Ryan Gallagan.

<sup>b</sup> Values calculated from 10 different cells; <sup>c</sup> Values calculated from 5 cells.

<sup>d</sup> Measured using voltammetry at 100 mV/sec.

<sup>e</sup> Rate constants determined by Laviron's Theory for quasi -reversibility (500 mV/sec  $\leq v \leq$  2000 mV/sec for the HH cyt c and 10 mV/sec  $\leq v \leq$  1000 mV/sec for the Yeast cyt c) – See Ch. 2.

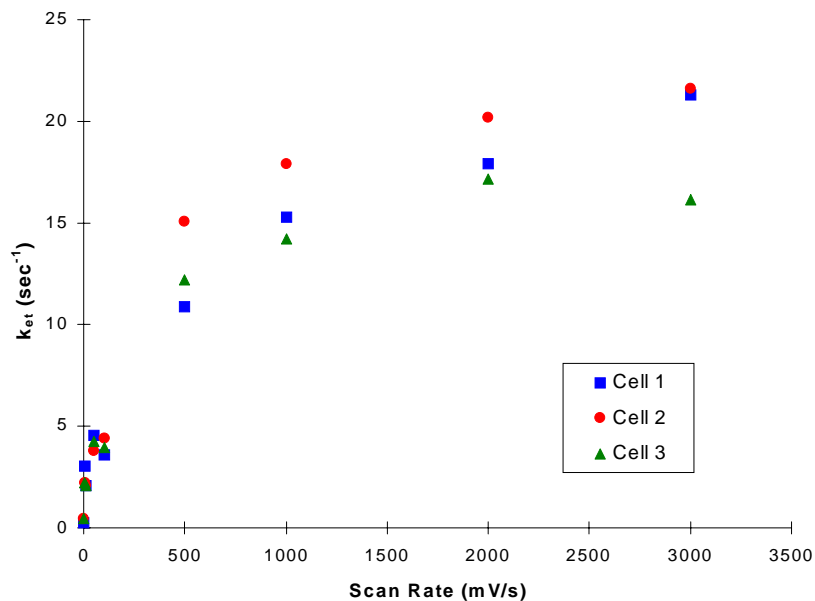


**Figure B.10.** Plot of scan rate versus electron transfer rate constant for the HH cyt c / ITO system showing data from three different cells (Data collected by Ryan Gallagan).

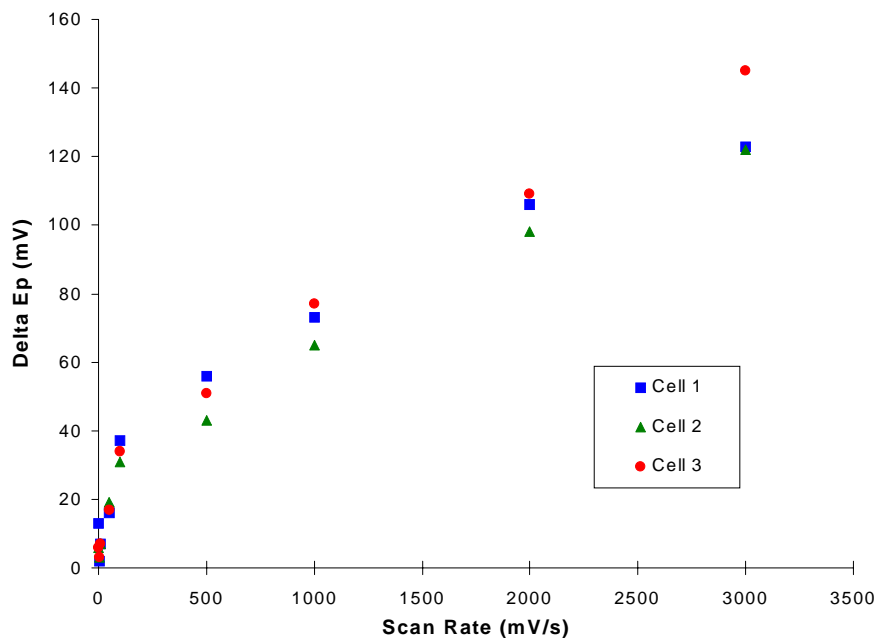


**Figure B.11.** Plot of scan rate versus peak splitting for the HH cyt c / ITO system showing data from 3 different cells (Data collected by Ryan Gallagan).

## **B.7. SPECIAL ACKNOWLEDGEMENTS**

I must thank Dr. Bowden for first introducing me to the Bush research collaboration. I really loved the applied nature of this work and enjoyed something different from the traditional research performed in the Bowden Laboratory. I am very appreciative to Dr. Lee Goldstein at Massachusetts General Hospital for numerous e-mails, faxes, and telephone discussions about the A $\beta$  and 3HK research. I hope that in the future there is another opportunity to work with Lee. I would also like to thank Karen Stokes, a former Bowden research who performed the initial experiments with the A $\beta$ . Additionally, I must acknowledge Dr. Asma El Kasmi (Al Akhawayn University, Ifrane, Morocco), a visiting professor in our group who was the first person to adsorb cyt c to the ITO electrode and has now engaged in current experiments to explain the rate constant trend. Finally, I must acknowledge Ryan Galligan, my undergraduate researcher, who, in spite of my sinus surgery and thesis writing, became one of the best and hardest working undergraduate researchers I've encountered. Thanks Ryan and good luck in the future.

## **B.8. EXPERIMENTAL DETAILS**

### **B.8.1. Kynurenine Pathway Experiments**

Cyclic voltammetry was performed at room temperature ( $22\pm 2^\circ$  C) on ambient solutions using an EG&G PAR potentiostat, Model 273. The potentiostat was operated in Ramp Mode, generating a potential staircase waveform with a 0.25 mV step height. The potential window of +0.15 to -0.4 V, in which Cu(II) is electroactive but the catabolites are not, was scanned in both directions at a rate of 100 mV/sec. The current response was passed through a 5.3 Hz low pass filter. A minimum of three cycles were collected for each scan, ensuring the stability of the electrochemical response. The electrochemical cell consisted of an indium/tin oxide working electrode (Delta Technologies) with an active area of 0.32 cm<sup>2</sup>, a Pt wire auxiliary electrode and a Ag/AgCl (1 M KCl) reference electrode (Microelectrodes Inc.). Both the auxiliary and reference electrodes were positioned in the cell in close proximity to the working electrode. The working electrodes were pretreated with successive 10 minute sonications in Alconox (~ 8 g/L), 95% ethanol, Milli-Q purified H<sub>2</sub>O (2X), and PBS (Sigma - Dulbecco's Phosphate Buffer; pH=7.41), followed by an overnight soak in

PBS (pH=7.41). The ITO electrodes were subsequently “activated” immediately prior to use by successive cycling in PBS for three cycles in each of the following potential windows: +0.15↔-0.4 V, +0.4↔-0.4 V, and +1.0↔-0.4 V. Cupric chloride (25μM) (Allied Chemical) was used as the Cu(II) source. Background voltammograms were obtained on each new electrode before testing the kynurenine pathway cataobolites, 100 μM KYN, 3HK, ANA, and 3HAA (Sigma Chemical Company), by themselves in PBS, and in the presence of Cu(II) (25μM) in PBS. Each experiment also included a scan of Cu(II) (25μM) in PBS without added test compound. All solutions were tested within minutes of being prepared. Each test was repeated to ensure the reproducibility of the results.

### **B.8.2. Aβ Experiments**

Cyclic voltammograms were obtained at room temperature (22±2° C) on air equilibrated solutions using an EG&G PARC potentiostat, Model 263A. The electrochemical cell incorporated an indium/tin oxide (ITO) working electrode (Donnelly Corporation) of 0.32 cm<sup>2</sup> area, a platinum auxiliary electrode, and a Ag/AgCl (1 KCl) reference electrode. The working electrodes were pretreated with successive 30 minute sonications in Alconox (~ 8 g/L), 95% ethanol, Milli-Q purified H<sub>2</sub>O, and PBS (Sigma - Dulbecco’s Phosphate Buffer; pH=7.3), followed by an overnight soak in PBS (pH=7.3). The peptide solution was prepared by first dissolving Aβ1-42 with sonication in deionized water to 300 μM, after which the peptide solution was added to Dulbecco’s phosphate buffered saline without Ca or Mg (Sigma) to a final concentration of 100 μM. Background voltammograms were first acquired in buffer on each new electrode used, followed by examination of Aβ1-42 (100 μM) in buffer, CuCl<sub>2</sub> (17 μM) in buffer, and Aβ1-42 (100 μM) with CuCl<sub>2</sub> (17 μM) in buffer. The possibility that the formal potentials measured were for surface adsorbed complexes cannot be excluded, and, in fact, the wave shapes (Figure B.8 lines c & d) of the copper signals are suggestive of involvement by adsorbed species. Further investigation is warranted to resolve this issue.

### **B.8.3. Cyt c / ITO Experiments**

Cyclic voltammetry was performed at room temperature (22±2° C) on ambient solutions using an EG&G PAR potentiostat, Model 273. The potentiostat was operated in Ramp Mode, generating a potential staircase waveform with a 0.25 mV step height. The

current response was passed through a 5.3 Hz low pass filter. A minimum of three cycles were collected for each scan, ensuring the stability of the electrochemical response. The electrochemical cell consisted of an indium/tin oxide working electrode (Delta Technologies) with an active area of 0.32 cm<sup>2</sup>, a Pt wire auxiliary electrode and a Ag/AgCl (1 M KCl) reference electrode (Microelectrodes Inc.). Both the auxiliary and reference electrodes were positioned in the cell in close proximity to the working electrode. The working electrodes were pretreated with successive 10 minute sonications in Alconox (~ 8 g/L), 95% ethanol, Milli-Q purified H<sub>2</sub>O (2X), and PBS (pH=7), followed by an overnight soak in PBS (pH=7). The PBS was made (as described in Chapter 3 - Experimental Details) from mono and dibasic potassium phosphate salts and Milli-Q purified H<sub>2</sub>O. Pre-prepared ITO electrodes were often stored for several days at the Milli-Q water step prior to use. The storage time of the ITO electrodes in the water seemed to have a negligible effect on the results of the experiments. To avoid contamination of the ITO surfaces, new surface were used for each surface and used ITO substrates were discarded.

HH Cyt c was purified based on the procedure given in the Experimental Details section of Chapter 3 and C102T yeast cyt c was purified via the procedure described in reference 14. Deposition procedures and voltammetric testing was carried out as described in Chapter 3 (Experimental Details) and were, for the most part, identical to the deposition and testing of cyt c on SAM modified gold.

## B.9 REFERENCES

1. a) S.M. Hurtley, "Neurodegeneration," *Science* **1999**, 282, 1071; b) I. Shoulson, "Experimental Therapeutics of Neurodegenerative Disorders: Unmet Needs," *Science* **1999**, 282, 1072-1074; c) J. Hardy and K. Gwinn-Hardy, "Genetic Classification of Primary Neurodegenerative Disease," *Science* **1999**, 282, 1075-1078; d) D.L. Price, S.S. Sisodia, and D.R. Borchelt, "Genetic Neurodegenerative Disease: The Human Illness and Transgenic Models," *Science* **1999**, 282, 1079-1083; e) A. Underwood, "Alzheimer's - Unlocking the Mystery," *Newsweek*, January 31, 2000.
2. a) M. Tominaga, T. Kumagai, S. Takita, and I. Taniguchi, "Effect of Surface Hydrophilicity of an Indium Oxide Electrode on Direct Electron Transfer of Myoglobins," *Chemistry Letters* **1993**, 1771-1774; b) J. Strojek and T. Kuwana, "Electrochemical Spectroscopy Using Tin-Oxide Coated Optically Transparent Electrodes," *J. Electroanal. Chem.* **1968**, 16, 471-483.
3. a) J.L. Willit and E.F. Bowden, "Adsorption and Redox Thermodynamics of Strongly Adsorbed Cytochrome c on Tin Oxide Electrodes," *J. Phys. Chem.* **1990**, 94, 8241-8246; b) M. Collinson and E.F. Bowden, "UV-Visible Spectroscopy of Adsorbed Cytochrome c on Tin Oxide Electrodes," *Anal. Chem.* **1992**, 64, 1470-1476; c) J.L. Willit and E.F. Bowden, *J. Electroanal. Chem.* **1987**, 221, 265-274.
4. L.E. Goldstein, M. Hartshorn, M. Leopold, X. Huang, C. Atwood, A. Saunders, J. Lim, K. Faget, R. Scarpa, L. Chylack, E. Bowden, and A. Bush, "3-Hydroxykynurenine and 3-Hydroxyanthranillic Acid Generate Hydrogen Peroxide and Promote  $\alpha$ -Crystallin Crosslinking by Metal Ion Reduction," in press, *Biochemistry*.
5. a) S. Okuda, N. Nishiyama, H. Saito, and H. Katsuki, "Hydrogen Peroxide-Mediated Neuronal Cell Death Induced by an Endogenous Neurotoxin, 3-Hydroxykynurenine," *Proc. Natl. Acad. Sci., USA*, **1996**, 93, 12553-12558; b) T. Ishii, H. Iwahashi, R. Sugata, and R. Kido, "Oxidation of 3HK Catalyzed by Methemoglobin with Hydrogen Peroxide," *Free Radical Biology and Medicine*, **1992**, 13, 17-20; c) M. Manthey, S.G. Pyne, and R.J.W. Truscott, "Mechanism of Reaction of 3HAA with Molecular Oxygen," *Biochimica et Biophysica Acta* **1990**, 1034, 207-212.
6. a) A.M. Wood and R.J. Truscott, "Ultraviolet Filter Compounds in Human Lenses: 3-Hydroxykynurenine Glucoside Formation," *Vision Res.* **1994**, 34(11), 1369-1374; b) R.J.W. Truscott and A.M. Wood, "Gourami Lenses Convert Tryptophan Into 3HK," *Ophthalmic Res.* **1994**, 26, 214-218; c) S.J. Atherton, J. Dillon, and E.R. Gaillard, "A Pulse Radiolysis Study of the Reactions of 3-Hydroxykynurenine and Kynurenine with Oxidizing and Reducing Radicals," *Electrochimica et Biophysica Acta* **1993**, 1158, 75-82.
7. D.T. Sawyer, *Oxygen Chemistry*, Oxford University Press: New York, 1991.
8. A.M. Bond, D. Dakternieks, Z. Qing, D.J. Tucker, and D.E. Rivett, "New Aspects of the Chemistry and Mechanism of Electrochemical Reduction of Kynurenine at Mercury Electrodes in Aqueous Media," *J. Electroanal. Chem.* **1991**, 309, 173-197.

9. X. Huang, C.S. Atwood, M.A. Hartshorn, G. Multhaup, L.E. Goldstein, R.C. Scarpa, M.P. Cuajungco, D.N. Gray, J. Lim, R.D. Moir, R.E. Tanzi, and A.I. Bush, "The A-Beta Peptide of Alzheimer's Disease Directly Produces Hydrogen Peroxide Through Metal Ion Reduction," *Biochemistry* **1999**, 38(24), 7609-7616.
10. J.H. Viles, F.E. Cohen, S.B. Prusiner, D.B. Goodin, P.E. Wright, and H.J. Dyson, "Copper Binding to the Prion Protein: Structural Implications of Four Identical Cooperative Binding Sites," *Proc. Natl. Acad. Sci. USA* **1999**, 96, 2042-2047.
11. X. Huang, C.S. Atwood, J.D.A. Tyndall, G. Hanson, K.C. Stokes, M.C. Leopold, M.A. Hartshorn, G. Multhaup, L.E. Goldstein, R.C. Scarpa, A.J. Saunders, C. Glabe, C.L. Masters, D.P. Fairlie, R.E. Tanzi, M.P. Cuajungco, D.N. Gray, J. Lim, R.D. Moir, R.E. Tanzi, and A.I. Bush, "Cu(II) Potentiation of Alzheimer A $\beta$  Neurotoxicity: Correlation with Cell-Free Hydrogen Peroxide Production and Metal Reduction," *J. Biol. Chem.* **1999**, 274(52), 37111-37116.
12. a) C.S. Atwood, R.D. Moir, X. Huang, R.C. Scarpa, N. Michael, E. Bacarra, D.M. Ramanos, M. Hartshorn, R.E. Tanzi, and A.I. Bush, "Dramatic Aggregation of Alzheimer A $\beta$  by Cu(II) Is Induced by Conditions Representing Physiological Acidosis," *J. Biol. Chem.* **1998**, 273(21), 12817-12826; b) J. Davis and W.E. Van Norstrand, "Enhanced Pathologic Properties of Dutch-Type Mutant Amyloid  $\beta$ - Protein," *Proc. Natl. Acad. Sci. USA* **1996**, 93, 2996-3000; c) E.M. Castano, F. Prelli, C. Soto, R. Beavis, Etsuro Matsubara, M. Shoji, and B. Fraggione, "The Length of Amyloid  $\beta$  in Hereditary Cerebral Hemorrhage with Amyloidosis, Dutch Type," *J. Biol. Chem.* **271**(50), 32185-32191; d) P.E. Fraser, J.T. Nguyen, H. Inouye, W.K. Surewicz, D.J. Selkoe, M.B. Podlisny, D.A. Kirschner, "Fibril Formation by Primate, Rodent, and Dutch-Hemorrhagic Analogues of Alzheimer Amyloid  $\beta$  Protein," *Biochemistry* **1992**, 31, 10716-10723.
13. a) L.M. Sayre, "Alzheimer's Precursor Protein and the Use of Bathocuproine for Determining Reduction of Copper(II)," *Science* **1996**, 274, 1933-1934; b) F. Wang and L.M. Sayre, "Kinetics and Mechanism of Aliphatic Amine Oxidation by Aqueous (batho) $_2$ Cu $^{II}$ ," *J. Am. Chem. Soc.* **1992**, 114, 248-255; b) F. Wang and L.M. Sayre, "Oxidation of Tertiary Amine Buffers by Copper(II)," *Inorganic Chemistry Communications* **1989**, 28(2), 169-170; c) A.G. Lippin, M.P. Youngblood, and D.W. Margerum, "Electron-Transfer Reactions of Copper(I) and Copper (III) Complexes," *Inorg. Chem.* **1980**, 19, 407-413.
14. J. M. Wallace, Ph.D. Thesis, North Carolina State University, 2000.
15. a) E.F. Bowden, *J. Electroanal. Chem.* **1984**; b) E.F. Bowden and S. Song, unpublished results; c) E.A. Kasmi, R. Galligan, M.C. Leopold, and E.F. Bowden, unpublished results.